Durham E-Theses

Geochemistry of volcanic rocks from the Sunda Arc

DEMPSEY, SCOTT,ROBERT

How to cite:

Use policy

Academic Support Office, Durham University, University Office, Old Elvet, Durham DH1 3HP
e-mail: e-theses.admin@dur.ac.uk Tel: +44 0191 334 6107
http://etheses.dur.ac.uk

Geochemistry of volcanic rocks from the Sunda Arc

A thesis presented for the degree of Doctor of Philosophy

By

Scott Robert Dempsey

Department of Earth Sciences

Durham University

2013

Declaration

No part of this thesis has previously been submitted for a degree at this or any other University. The work described in this thesis is entirely that of the author, except where reference is made to previously published or unpublished work.

Abstract

Geochemical analyses of igneous rocks can provide valuable information about processes, element fluxes, and rock lithologies not evident at the surface. This is particularly important in subduction zone settings where complex interactions between the subducting plate, mantle wedge and arc crust cannot yet be measured by alternative methods.

The Sunda arc, in SE Asia, provides an ideal opportunity to study the effects of subduction in a complex tectonic setting where the basement is poorly exposed and understood. However, in order to do so, magma compositions modified during differentiation in the arc crust must be effectively distinguished from those modified at the source. This study includes a detailed major- and trace element and isotopic (Sr-Nd-Hf-Pb) examination of volcanoes from west Java (Papandayan, Patuha and Galunggung), Central Java (Sumbing), east Java (Kelut) and Bali (Agung), the result of which provides greater insights into petrogenesis both across and along the arc.

Contamination in the arc crust is more extensive than previously recognised, particularly in west and central Java where few volcanoes can be used in order to identify subduction and source contributions. In west Java, volcanoes such as Papandayan and Patuha show significant enrichments in isotope ratios above mantle values (e.g. $^{87}Sr/^{86}Sr \sim 0.706$, $^{143}Nd/^{144}Nd \sim 0.5125$, $^{208}Pb/^{204}Pb \sim 18.91$ and $^{176}Hf/^{177}Hf \sim 0.2827$) which indicates a terrigneous crustal contaminant. At Sumbing volcano, most magma compositions are similar to those at Merapi and Merbabu, and show strong evidence for the assimilation of carbonate-rich lithologies with some magmas becoming enriched in CaO, Sr and $^{87}Sr/^{86}Sr$.

Differentiation in volcanoes from east Java and the western part of the Lesser Sunda Islands (Bali, Lombok and Sumbawa) is dominantly controlled by fractional crystallisation, which provides better controls on source compositions. At Kelut, one group of samples show the most 'depleted' magma compositions yet discovered on Java, which contain MORB-like values for $^{143}Nd/^{144}Nd$ and $^{176}Hf/^{177}Hf$ (0.5130 and 0.2831 respectively). These samples represent the depleted (asthenospheric) mantle and are situated towards the front of the arc in east Java. It is likely that the progressive enrichment further back on the arc (i.e. Leucititic compositions at Ringgit-Besar) include more of an enriched (lithospheric) mantle (SCLM) component derived from the NW margin of Australia during the breakup of Gondwana.

Acknowledgments

Chapter Contents

Chapter 1: Introduction

Chapter 2: A Trace Element and Sr-Nd-Hf-Pb Isotopic Study of Kelut Volcano, East Java

Chapter 3: Carbonate Assimilation and Melting Variations between Pyroclastic Deposits and Lavas at Sumbing Volcano, Central Java

Chapter 4: Magma Evolution by Fractional Crystallisation at Agung Volcano, Bali

Chapter 5: A regional and tectonic framework for magmatism in the Sunda Arc, SE Asia: A Summary and Conclusions

Figure Contents

Chapter 1: Introduction

Chapter 2: A Trace Element and Sr-Nd-Hf-Pb Isotopic Study of Kelut Volcano, East Java

Chapter 3: Carbonate Assimilation and Melting Variations between Pyroclastic Deposits and Lavas at Sumbing Volcano, Central Java

Chapter 4: Magma Evolution by Fractional Crystallisation at Agung Volcano, Bali

Chapter 5: A regional and tectonic framework for magmatism in the Sunda Arc, SE Asia: A Summary and Conclusions

Table Contents

Chapter 1

Introduction

1.1. General Introduction

Since the acceptance of the plate tectonic theory over 50 years ago, subduction has remained enigmatic. The complexity of processes involved during the transfer of material at convergent margins makes this a challenging and rapidly evolving part of earth science, but a particularly important one for understanding the growth of continents and destruction of ocean lithosphere (e.g. Rudnick and Fountain, 1995; Rudnick and Gao, 2003). Much of what we know about subduction zones comes from the volcanoes situated above them, as they represent the physical manifestation of this recycling process.

Most generalised models suggest that the subducting plate provides the impetus for melting above subduction zones by releasing volatiles into the mantle wedge and lowering the solidus (Gill, 1981; Tatsumi *et al.,* 1986; McCulloch and Gamble, 1991; Hawkesworth *et al.,* 1993). The resulting melts then traverse through the upper plate on the way to the surface. Therefore, this process has the potential to provide useful information on the nature of all three components; the subducting plate, the mantle asthenosphere or lithosphere, and the arc crust.

Magmatism can provide a valuable probe into several aspects of the tectonic evolution of an area and offer information on processes which are not evident at the surface. However, for the chemistry of arc magmas to provide reliable and informative information about a particular tectonic environment, element and isotope budgets must be identified and quantified for each of the contribution's shown in figure 1.1 (*a* and *b*). Figure 1.1*b* shows three key areas which are critical to understanding genesis of arc magmatism. These include:

1)   The differentiation of magmas in the arc crust.

This involves one or a combination of fractional crystallisation, magma mixing and crustal contamination and will act to modify a mantle source from its primary composition. It is a prerequisite to identify and eliminate any magmas which have been modified during magma mixing or crustal contamination prior to discussing source compositions because they will alter trace element and isotope ratios (Thirlwall and Graham, 1984; Davidson, 1987; Davidson *et al.,* 1987; Thirlwall *et al.,* 1996; Davidson *et al.,* 2005; Handley *et al.,* 2008; Davidson and Wilson, 2011).

1

Schematic Representations of Subduction Components
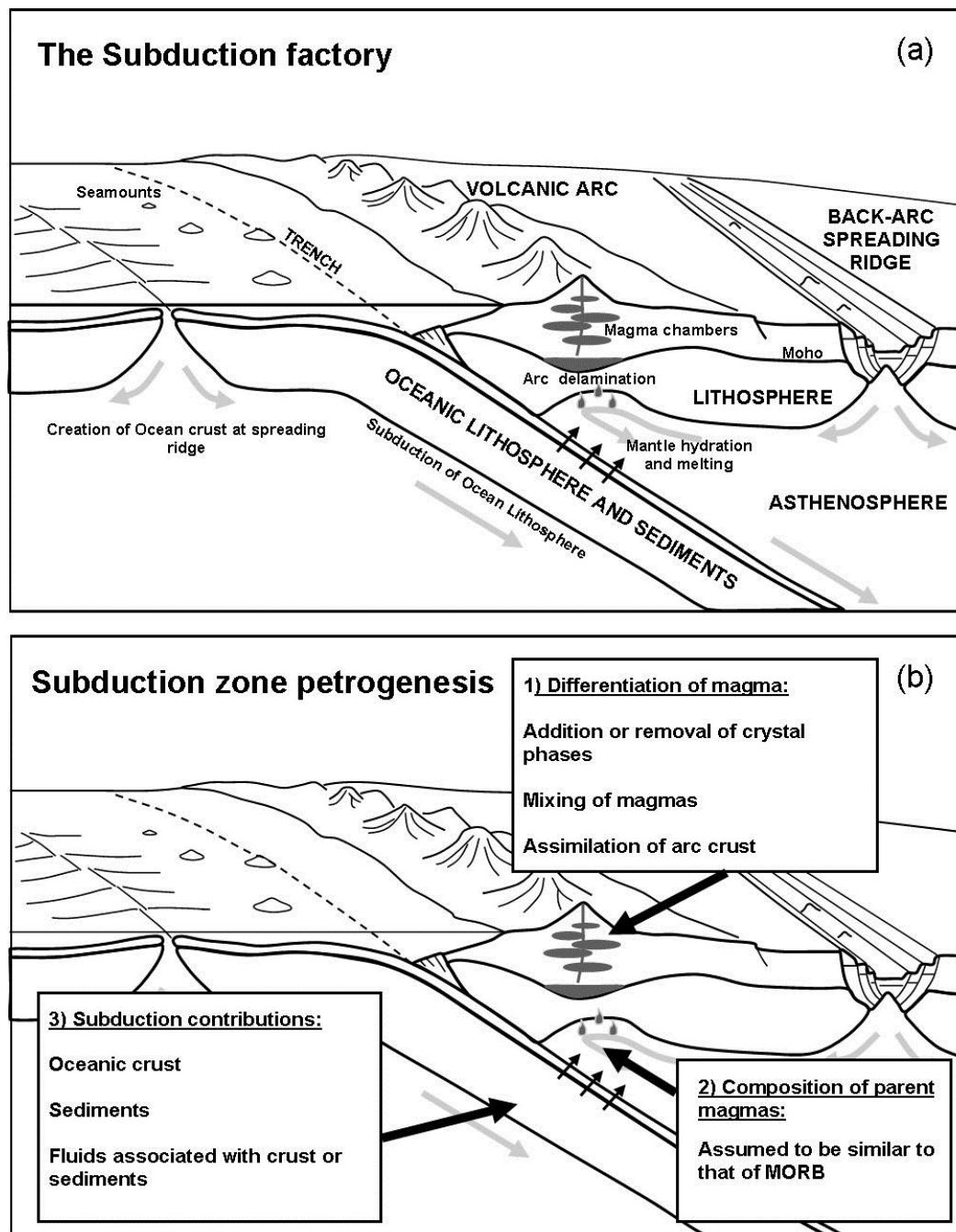
Fig. 1.1. (a) Schematic diagram showing the geological components involved in subduction zones. Grey arrows display hypothetical asthenosphere flow patterns away from the spreading ridges. In some mature arcs this flow can ablate the base of the lithosphere creating delamination and upwelling (see Macpherson, 2008). Many of these components can be highly variable in arcs worldwide (e.g. Thirlwall *et al.,* 1996; Elliot *et al.,* 1997; Handley *et al.,* 2011; and Nebel *et al.,* 2011). **(b)** Shows some of the most commonly cited variables in subduction zone petrogenesis (McCulloch & Gamble, 1991; Saunders *et al.,* 1991; and Davidson, 1987). A volcanoes chemical signature can record the contributions from the subducting and overriding plates. Within a single arc, combinations or relative contributions of these processes can change on a volcano basis. Volcanoes must therefore be analysed in detail on an individual basis to identify changes in these process along or across arcs.

2) Pre-subduction mantle source compositions.

Primary arc magmas are rarely discovered without having been modified by fluids and/or sediments derived from the subducting plate, or during differentiation in the arc crust. Therefore, pre-subduction source compositions are not well known. Above arcs built on thin crust, isotope ratios and relatively immobile trace elements contain values similar to mid-ocean ridge basalts (MORB). This suggests that the pre-subduction compositions of some mantle sources are similar to MORB (Pearce and Parkinson, 1993; Woodhead *et al.,* 1993; Hochstaedter *et al.,* 2000; Workman and Hart, 2005; Woodhead *et al.,* 2012).

3) Subduction components.

Mantle source compositions are commonly modified by fluids and/or sediments derived from the subducting plate. The relative contributions of these components can vary significantly depending on the setting of the arc and tectonic factors such as the amount and type of sediment being subducted. Isotope ratios which are displaced away from MORB and have not been modified during differentiation are typically used to trace the identity of the slab component (Elliot *et al.,* 1997; Plank and Langmuir, 1998; Turner and Foden, 2001; Turner *et al.,* 2009; Handley *et al.,* 2011; Straub and Zellmer, 2012).

The strength of each particular contribution is largely reflected by the tectonic setting of an arc. For example, where the subduction of ocean lithosphere occurs beneath thick continental crust, differentiation and processes in the arc crust tend to be the most strongly associated with the geochemistry of the rocks. This is because magmas will spend a longer residence time within the arc crust and, therefore, be more likely to inherit a geochemical fingerprint from such a component. The most obvious example of this is in the Andes, where compositional variations in arc magmatism strongly reflect changes in the crust through space and time (Hildreth and Moorbath, 1988; Mamani *et al.,* 2010).

While this type of volcanic arc can provide excellent details about the nature of the crust, the source of magmatism and contributions from the subducting plate are largely erradicated by geochemical overprinted in the crust. Geochemical enrichments in such environments can also involve the lithosphere, or sub-continental lithosphere situated at the base of the crust. In these circumstances the asthenosphere can be partially, or completely, excluded from the sub-arc region and melting may be confined to the lithosphere (Saunders *et al.,* 1991).

In contrast to continental arcs, oceanic arcs are built above thinner oceanic and immature volcanic basement. As a result, magmas from these environments are more rarely modified

by processes in the arc crust and are commly used to evaluate source and subduction contributions. Island arcs such as Tonga, New Britain and Izu-Bonin are partcilculry associed with young, depleted, mantle asthenosphere (Ewart and Hawkesworth, 1987; Turner et *al.,* 1997; Woodhead *et al.,* 1998; Hochstaedter *et al.,* 2000). Therefore, they provide better constraints on flux rates into the mantle wedge.

1.2. Why the Sunda Arc?

The Sunda arc is is unique with respect to the archetypal continental and oceanic-type arcs because it appears to contains a transitional character somewhere between the two. Due to a lack of basement exposure in SE Asia and beneath the Sunda arc it is still unclear which parts are built on continental crust and which are on oceanic crust. This has made arc petrogenesis particularly problematic in terms of identifying which chemical signatures are inherited through subduction and which signatures are inherited in the crust (Edwards *et al.,* 1993; Gasparon and Varne, 1998; Turner and Foden, 2001; Handley, 2006).

Many of the previous works studying magmatism from the Sunda Arc have done so on the basis that continental crust is only located in western regions and becomes progressively oceanic towards the east (Hamilton, 1979; Curray *et al.,* 1977). However, a number of recent reappraisals have suggested that continental basement is more widespread than previously thought. Figure 1.2 shows a recent reconstruction of the distribution of continental crust and continental growth of SE Asia since the Mesozoic (Hall and Sevastjanova, 2012). Comparisons between inherited Archaean and Proterozoic zircon ages from east Java, west Sulawesi and Borneo with northwest Australia, and similarities in the deep structure between the two regions, suggest that a number of rifted fragments derived from Australia are present beneath SE Asia (Smyth *et al.,* 2007; van Leeuwen *et al.,* 2007; Granath *et al.,* 2011; Hall, 2011).

Previous geochemical studies have drawn attention to the resemblance between alkaline igneous rocks from Java and South Sulawesi and also to the similarity between mafic potassic rocks in the eastern Sunda arc and those from NW Australia (Edwards *et al.,* 1994; Varne,

SE Asia Basement Reconstructions
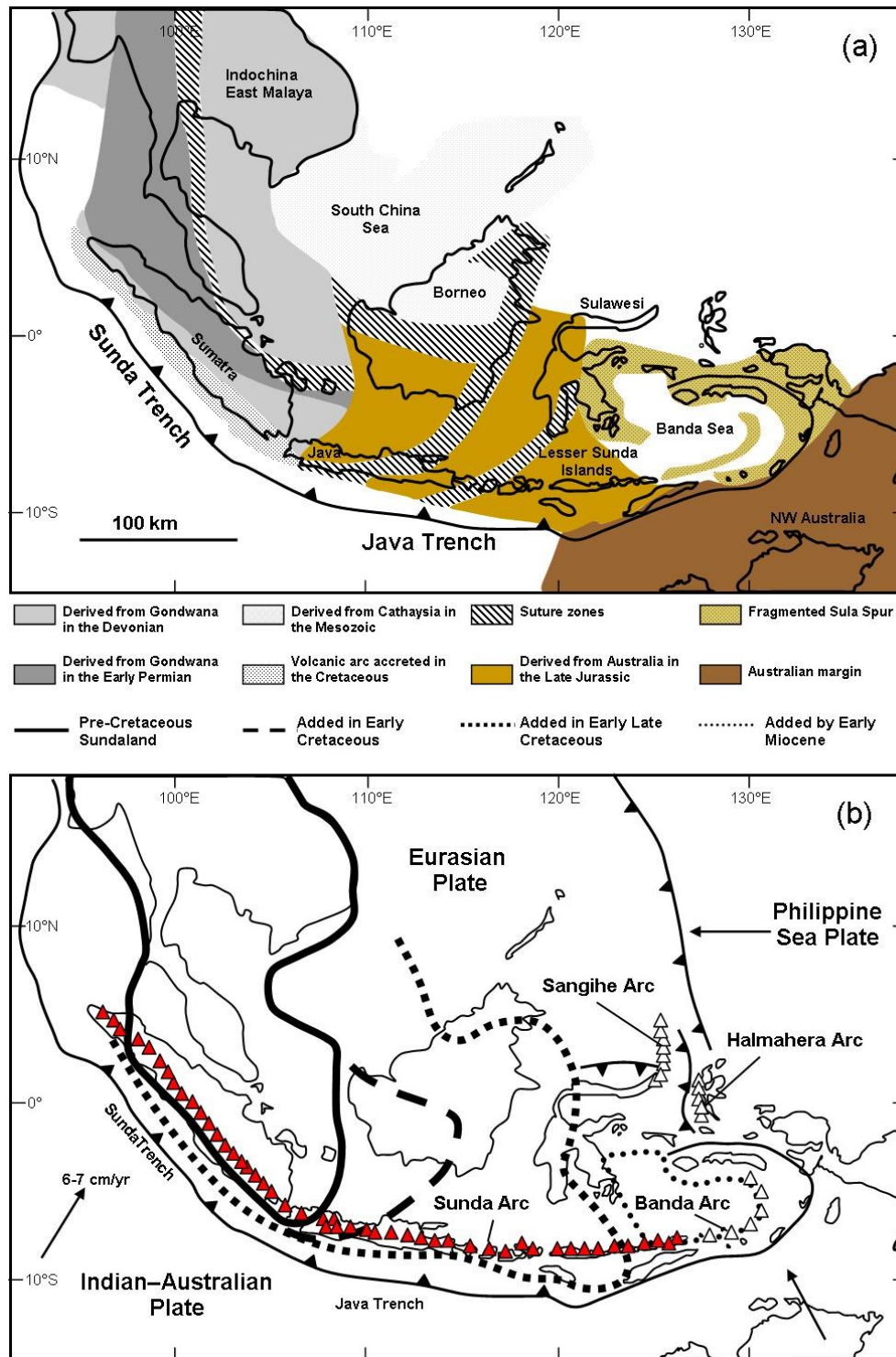
Fig 1.2. (a) Tectonic reconstruction of the main continental blocks in SE Asia, after Hall & Sevastjanova (2012). Grey fragments are those thought to derive from Gondwana, while brown blocks are thought to originate from NW Australia. The pre-Cretaceous Gondwanan terranes are modified after Metcalfe (1996, 2011a, 2011b) and Barber *et al.* (2005). The striped terranes represent suture zones. See text for details. **(b)** Shows the proposed growth of Sundaland since the Mesozoic after Hamilton (1979), Hall (2008), Hall & Wilson (2000), Hall *et al.* (2008) and modified by Hall & Sevastjanova (2012). Arrows indicate the direction of plate movement relative to other plates. Red trianges highlight Sunda Arc volcanoes. Other Arcs are shown with white triangles.

1985; Leterrier *et al.,* 1990). However these rocks tend to be associated with back-arc positions and not be influenced by subduction. There are currently no rocks from the Sunda arc (outside of the region in collision with the NW Australian margin) which show evidence for the presence of ancient continental material. This suggests that either the magmas are not sampling the continental material or that is is not present beneath the arc.

1.3. Geological Background

Detailed tectonic reconstructions of Indonesia are given by Hamilton (1979); Hutchinson (1982); Hall (1996, 2002, 2012). An overview of the geology is given here and regional tectonic settings are discussed during each Chatper.

1.3.1. The Sunda Arc

The Sunda arc is one of four volcanic arcs which are focused around the plate boundaries between the Eurasian, the Indian Australian and the Pacific plates (fig 1.2*b*). The Sunda arc includes ~ 80% of the Indonesia's active volcanoes and includes the Andaman Islands, Sumatra, Java and the Lesser Sunda Islands (Hall and Smyth, 2008) where Subduction has been continuous at the Java trench since the mid Eocene (~ 45 Ma) due to the northward propagation of the Indo-Australian plate beneath the Eurasian plate at a rate of ~ 6/7 cm/yr^{-1} (Tregoning *et al.,* 1994; Hall, 2002). Beneath Sumatra, subduction is oblique and poorly constrained belief zones can only be traced to depths of ~ 200 km (Curray, 1989). In contrast, there is almost normal subduction beneath Java and the seismic zone extends to depths in excess of 600 km where the north-dipping slab steepens (to ~ 60°) below depths of 100 km (Whitford, 1979; Curray, 1989). The eastern part of the Sunda arc has been in collision with the Australian margin since ~ 3 Ma.

1.3.2. Continental SE Asia

SE Asia is a heterogeneous mosaic of continental blocks joined by suture zones (Hall, 2008; Hall, 2009). Western Indonesia consists of Gondwanan fragments brought together by the

6

closure of numerous Tethyan Oceans. These fragments now represent the Sundaland continental core of SE Asia and have been in there present position since the Triassic (Hall, 2012). This region includes Sumatra and west Java from the Sunda arc which are situated on the Sundaland margin and includes widespread Cretaceous post-collisional granites which were emplaced following the collision of continental blocks (Hamilton, 1979; Gasparon and Varne, 1995). This is the only part of the Sunda arc where continental-like magmatism in evident (outside of the Australia – east Indonesia collision).

The exposed basement east of Sundaland is limited to few narrow distributions of Cretaceous arc, ophiolite and melange rocks in Jiwo Hills and Luk Ulo, Central Java and also in SE Borneo (Hamilton, 1979; Parkinson *et al.,* 1998; Wakita, 2000). This is suggested to be a continuous NE-SW ophiolite belt which runs through west Java and into the Meratus Mountains of SE Borneo which marks one of potentially many suture zones in SE Asia (Hamilton, 1979; Hall, 2012). It is now thought that much of Borneo, west Sulawesi and Java are located above Australian continental blocks which were rifted from the NW Australian margin during the Jurassic. This crust is also suspected to be located beneath most of Lesser Sunda (Hall and Sevastjanova, 2012).

1.3.3. Magmatism

Magmatism in the Sunda Arc extends back to the Mesozoic in Sumatra while the oldest rocks in the Lesser Sunda Islands are of Miocene age (McCourt *et al.,* 1996). Pleistocene-to-recent volcanism in the Sunda Arc has been the focus of many studies (e.g. Whitford, 1975; Whitford & Nicholls, 1976; Whitford *et al.,* 1979; Whitford & Jezek, 1982; Nicholls & Whitford, 1976; Whitford & White, 1981; Nicholls *et al.,* 1980; Wheller *et al.,* 1987; Hilton & Craig, 1989; Hilton *et al.,* 1991; Edwards *et al.,* 1990; Gasparon *et al.,* 1994; Alves *et al.,* 1999; Turner & Foden, 2001; Gertisser and Keller, 2003 Handley *et al.,* 2009) and contains the widest range of magma compositions known from any other arc or orogenic setting (Wheller *et al.,* 1987). Lavas range from tholeiitic through to highly alkaline leucititic.

The most abundant rocks are calc-alkaline basaltic-andesites and andesites, with an average silica content of 55 wt. %, characteristic of many other island arcs (Whitford 1975; Nicholls & Whitford 1976). However, uniformly low abundances of Mg, Ni and Cr indicate that very few, if any, lavas represent primary mantle melts, and that most have undergone varying

degrees of differentiation (Nicholls & Whitford, 1976; Nicholls *et al.,* 1980; Wheller *et al.,* 1987; Handley *et al.,* 2009).

Volcanism in Sumatra is different from elsewhere in the arc, and contains the highest number of felsic intrusive rocks with radiogenic $^{87}Sr/^{86}Sr$ and un-radiogenic $^{143}Nd/^{144}Nd$. These are suspected to have been contaminated in Sumatran crust (Gasparon and Varne, 1995, 1998). There is no evidence for the same type of crustal material in Java, and felsic rocks are far less common. One suggestion is that the relatively basic magma compositions simply reflect a less mature basement, and that any contaminant has an isotopic signature similar to those of the ascending magmas, making assimilation difficult to detect (Handley, 2006; Handley *et al.,* 2008, 2009). As a result, many studies have implicated the importance of a subducted component and source heterogeneity to explain chemical and isotopic anomalies in Java (Whitford & Jezek, 1982; Edwards *et al.,* 1991; Turner & Foden, 2001; Alves, 1999; Handley *et al.,* 2008, 2009; Sendjaja *et al.,* 2009).

1.4. Thesis aims and objectives

The main aims of this thesis are:

1. To produce a detailed mineralogical and geochemical study of three Quaternary volcanoes across the Sunda Arc and identify the processes which occur in the crust during differentiation, the composition of the mantle source, and components added to the mantle source from the subducting slab.

2. Combine the results from these volcanoes with other published sources of data to build a profile of changes along and across the arc and examine how magmatism is linked to the tectonic setting of a particular region.

3. To identify the character of unseen source and basement rocks, particularly in relation to modern tectonic reconstructions. This will help to evaluate the use of geochemical proxies to understand tectonic process not evident at the surface.

Sunda Arc volcanoes included in this study
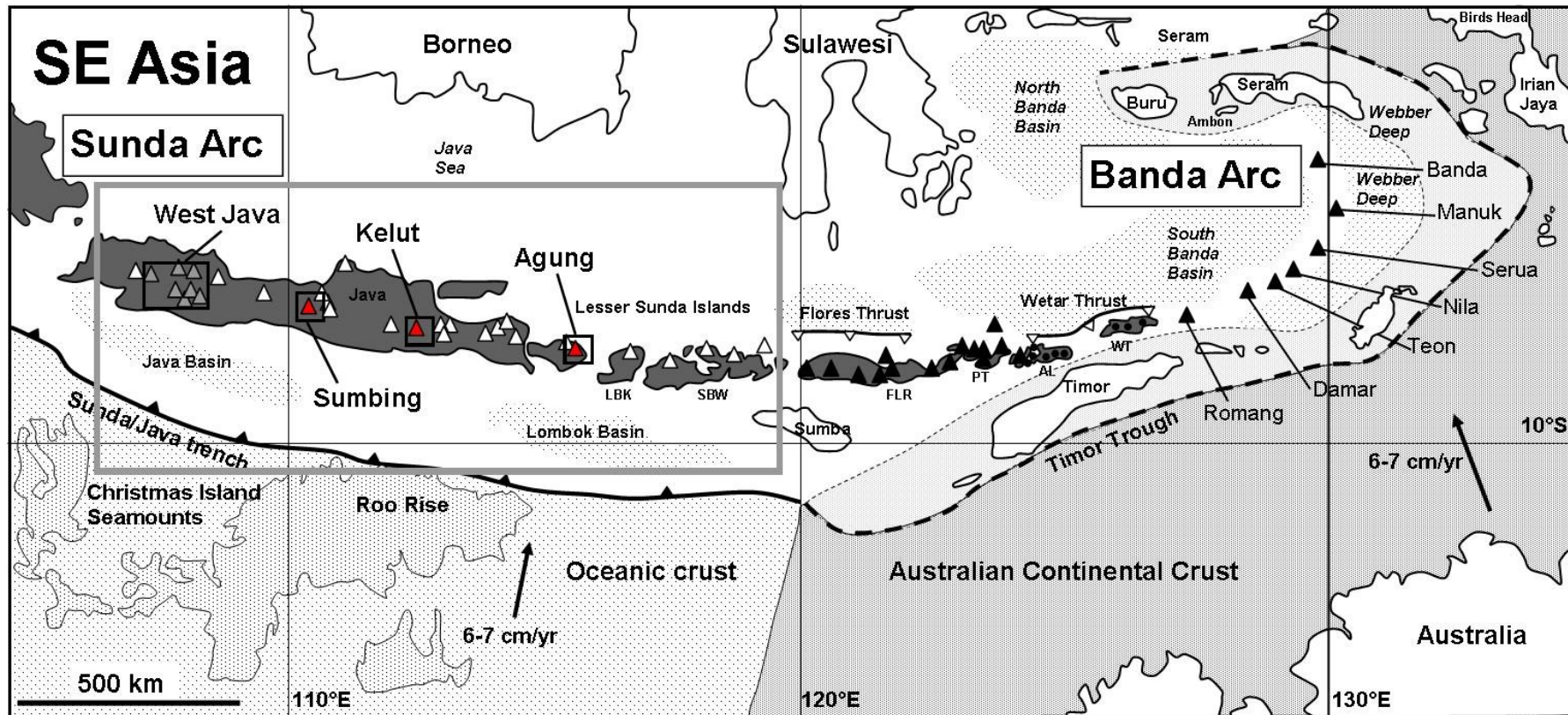
Fig. 1.3. Schematic diagram of the east Sunda and Banda volcanic arcs. Volcanoes in this region run continuously from west Java to Banda Api. Banda arc volcanoes include Romang, Damar, Teon, Nila, Serua, Manu and Banda, for more details see Vroon *et al.,* (1993, 1995, 2001) and Nebel *et al.,* (2010, 2011). Sunda arc volcanoes shown here only include those with published data and stretch from west Java to Wetar. The main area of this study include those volcanoes inside the grey box; where, red triangles show volcanoes for which a full dataset is obtained and discussed here in significant detail, grey triangles show volcanoes where data was collected and is discussed in the relevent sections, and white triangles are discussed based on data from previous studies. In most cases, the data collected from the west Java volcanoes only act to supplement pre-existing datasets, for which studies already exist (Gerbe *et al.,* 1992; de Hoog et *al.,* 2001; Handley *et al.,* 2008, 2010; Sendjaja *et al.,* 2009). A more detailed insert map is shown in figure 2.3. Volcanoes outside the main study area are shown in black, either as triangles (which indicate that they are active), or as circles (which indicate that they are no longer active). The magmas from these volcanoes are all assumed to have a strong influence from the colliding Australian continent (Elburg *et al.,* 2002, 2004, 2005; Elburg & Kamenetsky, 2008; Hoogewerff *et al.,* 1997; and Shulgin *et al.,* 2009). Note the heterogeniety of the subducting plate from east to west. See text for more details.

Region	Volcano	Summit altitude (m)	Arc Position	Latitude	Longitude	(Syracuse & Geoffrey 2006)	(Hutchison 1982)	(Whitford 1975)
W. Java	Salak	2211	FA	6.72°S	106.73°E	91	157	140
	Gede	2958	FA *(RA)*	6.78°S	106.98°E	102		
	Patuha	2434	FA	7.160°S	107.40°E	89		
	Tangkuban Perahu	2084	RA	6.77°S	107.60°E	148	182	170
	Papandayan	2665	FA	7.32°S	107.73°E	91	142	130
	Guntur	2249	FA *(RA)*	7.143°S	107.840°E	118	159	150
	Tampomas	1684	RA	6.77°S	107.95°E	172		
	Galunggung	2168	FA	7.25°S	108°058°E	117	155	150
	Cereme	3078	RA	6.892°S	108.40°E	183	186	
C. Java	Slamet	3428	RA	7.242°S	109.208°E	170	172	
	Sumbing	3371	RA *(FA)*	7.384°S	110.070°E	174	173	200
	Ungaran	2050	RA	7.18°S	110.33°E	205	179	240
	Merbabu	3145	RA	7.45°S	110.43°E	173		
	Merapi	2968	RA *(FA)*	7.542°S	110.442°E	161	169	190
E. Java	Wilis	2563	FA	7.808°S	111.758°E	141	118	
	Kelut	1731	FA	7.93°S	112°308°E	133	153	180
	Semeru	3676	FA	8.108°S	112.92°E	133	143	170
	Tengger (Bromo)	2329	RA	7.942°S	112.95°E	154	161	200
	Lamongan	1651	RA *(FA)*	7.979°S	113.342°E	160	166	190
	Argopuro	3088	RA	7.97°S	113.57°E	170		
	Ijen	2799	RA *(FA)*	8.058°S	114.242°E	177	169	180
Bali	Batur	1717	RA	8.242°S	115.375°E	175	165	
	Agung	3142	RA *(FA)*	8.342°S	115.508°E	162	160	
Lombok	Rindjani	3726	RA *(FA)*	8.42°S	116.47°E	150	164	
Sumbawa	Tambora	2850	RA *(FA)*	8.25°S	118.00°E	151	182	
	Sangeang Api	1949	RA *(FA)*	8.20°S	119.07°E	152	192	

Table 1A. Estimated depths to the Wadati-Benioff zone beneath Java and Lesser Sunda volcanoes. All values are in km's after Whitford (1975); Hutchinson (1982); and Syracuse *et al.,* (2006). The arc position refers to the volcanoes relative position compared with other volcanoes on the arc. FA = Front arc, RA = Rear arc. Where a second position is given (in italics) it refers to criteria from Syracuse and Geoffrey (2006). Front arc volcanoe in this study are shown in grey and < 150 km according to the criteria of Syracuse and Geoffrey (2006) and < 160 km according to the criteria of Hutchinson (1982). A volcanoes position relative to the trench is also considered.
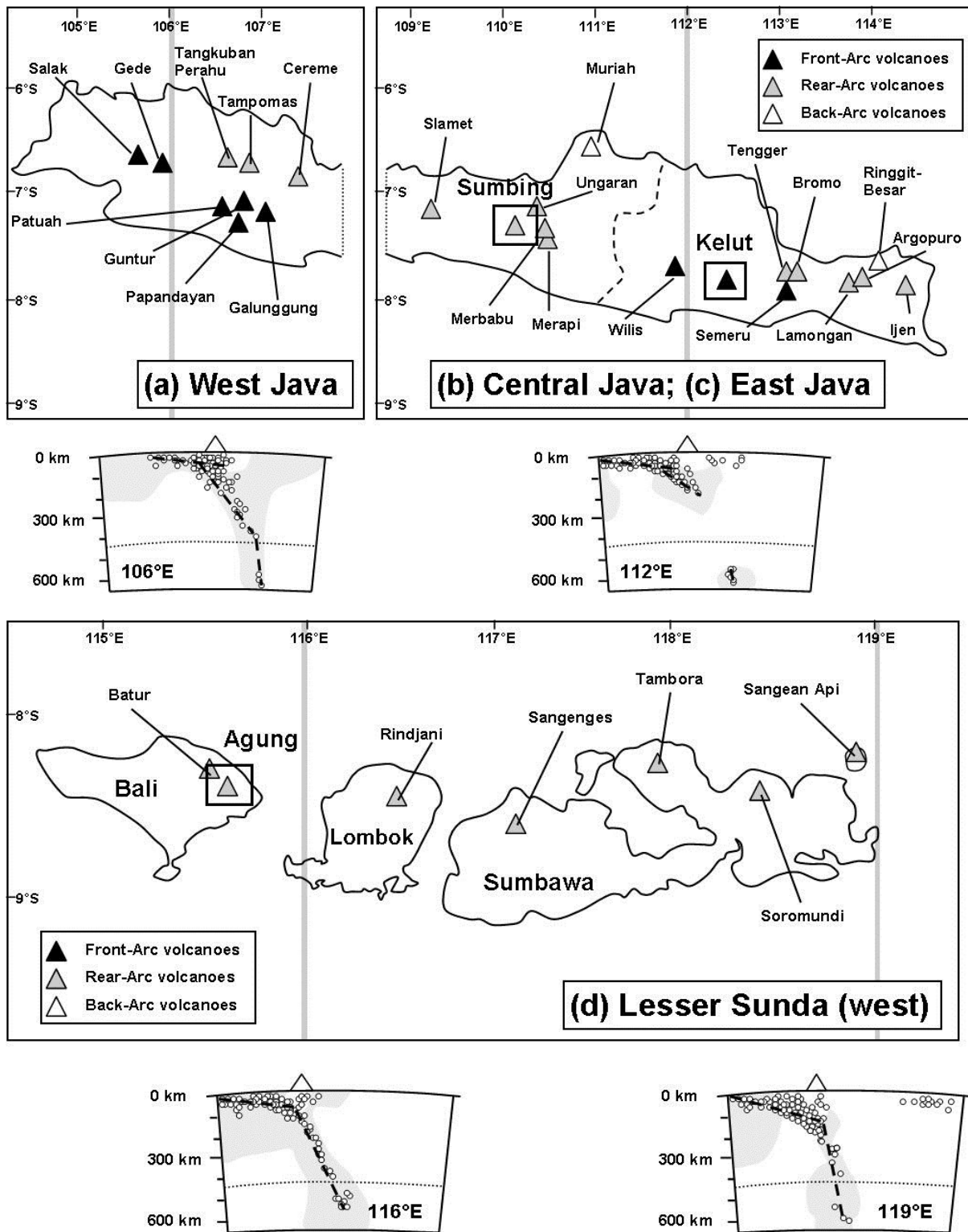
Fig. 1.4. (a-c) Schematic map showing the locations of west, central and east Java volcanoes. Only volcanoes with recent datasets are included. Volcanoes are classified according to their positions on the arc and depth to the Benioff zone as either Front-Arc (black triangles), Rear-Arc (grey triangles), or Back-Arc (white triangles). The front and rear-arc locations represent the active Quaternary volcanoes, while the back-arc represents the extinct Pleistocene volcanoes (Edwards *et al.,* 1991, 1994). The subdivision between central and east Java is marked with a dashed line. Slab profiles are shown for west and east Java, represented by the grey bands. The profiles are modified from (Widiyantoro *et al.,* 2011) and highlight a significant slab-gap section in east Java. **(d)** shows a similar map for the western Lesser Sunda Islands which include Bali, Lombok and Sumbawa. Slap profiles are also given. The black boxes indicate the volcano chapters in this study.

Figure 1.3 shows the locations of volcanoes which are examined during this study. The red triangles show volcanoes for which a detailed study has been produced. These include:

- Chapter 2: Kelut (east Java).
- Chapter 3: Sumbing (central Java)
- Chater 4: Agung (Bali)

Each of these volcanoes are examined on the basis of major and trace elements, mineral data and the radiogenic isotopes $^{87}Sr/^{86}Sr$, $^{143}Nd/^{144}Nd$, $^{176}Hf/^{177}Hf$, $^{206}Pb/^{204}Pb$, $^{207}Pb/^{204}Pb$ and $^{208}Pb/^{204}Pb$. The grey triangles show the location of volcanoes for which a less detailed study has been conducted, but the data has contributed toward the understanding of a region. This includes:

- Chapter 5: (West Java)

Chapter 5 discusses the geochemistry on a more regional scale by combining all of the previous conclusion from chapters 2-4. The grey box in figure 1.3 shows the scope of this thesis. Eastern parts of the Sunda arc are reffered to, but they are not the focus of this study.

Table 1A shows a list of estimated depths for easch volcano to the Wadati Benioff zone (WBZ) through a number of studies. These are reffered to in order to highlight a volcanoes relative poistion on the arc (or away from the trench). This is important in a regional study because the chemical character of volcanoes in the Sunda arc has been suggested to correlate with increasing depth to the WBZ (e.g. Whitford and Nicholls, 1976; Whitford *et al.,* 1979).

Figure 1.4 shows the location of the volcanoes in this study and their position on the arc which can broadly be subcategorised according to the criteria of (Hutchinson, 1982; Syracuse and Geoffrey, 2006). There are problems in presenting the data this way. For example, Syracuse and Geoffrey (2006) have shown that there is an along-strike shift of ~ 70 km either side of west Java (~ 108 °E). This appears at overlapping ends of two volcanic chains and suggests that there is a more complex structural control of volcanism in Java. This precludes across arc variational comparisons between west Java and central and east Java without considerable caution. However, these WBZ estimates provides a basic framework with which volcano behaviour can be examined across the arc. Seismic profiles are also included, after (Widiyantoro *et al.,* 2011) which provide details of the structure of the subdcuting plate.

Chapter 2

A Trace Element and Sr-Nd-Hf-Pb Isotopic Study of Kelut Volcano, East Java, Indonesia. Implications for Crustal Contamination, Mantle Fertility and Fluid Enrichment

2.1. Introduction

Understanding the composition of a mantle source prior to the addition of subduction-related contributions or modification in the arc crust is critical. It provides a reference point with which to measure and quantify changes through these latter processes (Woodhead, 1989; Hochstaedter *et al.,* 2000; Woodhead *et al.,* 2012). A popular way of identifying the composition of pre-subduction mantle sources beneath volcanic arcs is to utilise groups of elements which are less mobile in the presence of fluids. Experiments suggest that the high-field strength elements (HFSE) and heavy-rare earth elements (HREE) are considerably less mobile in aqueous fluids than large-ion lithophile elements (LILE) or light-rare earth elements (LREE) and are also lower in arc magmas (Tatsumi *et al.,* 1986; Brenan *et al.,* 1994, 1995; Keppler, 1996; Ayers *et al.,* 1997; Kogiso *et al.,* 1997; Ayers, 1998).

In volcanic rocks from Java, concentrations of HFSE and ratios such as Zr/Nb suggest that pre-subduction mantle source compositions are similar or slightly more enriched than MORB (Gerbe *et al.,* 1992; Gertisser and Keller, 2003; Handley *et al.,* 2007, 2010). However, they have significantly higher concentrations of HFSE and lower LILE/HFSE and LILE/LREE ratios than in a number of oceanic arcs (Hawkesworth *et al.,* 1993; Woodhead *et al.,* 1993; Hochstaedter *et al.,* 2000). A number of these arcs such as Tonga, Izu-Bonin and New Britain contain depleted front-arc magmas to which a strong fluid signature is appearent in high Ba/La, Ba/Th, Sr/Nd and slightly elevated $^{87}Sr/^{87}Sr$ (Ewart and Hawkesworth, 1987; Turner and Hawkesworth, 1997; Hochstaedter *et al.,* 2001; Straub *et al.,* 2010).

At present similar magmas have not been discovered in Java and suggest that either: *(1)* the pre-subdction mantle source is inherently more enriched that for many oceanic arcs (i.e. there is a contribution from the lithosphere); *(2)* the back-arc is not well-developed enough (because depletion is usually associated with significant back-arc spreading); or, *(3)* that volcanoes situated at the front of the arc are limited. It is also unclear at present whether the lack of a similar fluid signature (i.e. elevated LILE/HFSE and LILE/LREE) in magmas from Java are buffered by a subducted sediment or an enriched mantle contribution.

This Chapter presents an Sr-Nd-Hf-Pb isotope, and major and trace element study of Kelut volcano. This provides an excellent opportunity to investigate the nature of a the mantle source beneath Java and therefore subduction contributions added to this mantle. Because it located at the front of the Quaternary arc in east Java, south of Pleistocene back-arc volcanism, it will help address some of the issues outlined above.

2.2 Geological, Tectonic, and magmatic Framework

There are a number of important tectonic factors to consider for east Java which may have a control on the composition of the magmas. This section details four areas of the regional geology which are critical to understanding the processes involved at Kelut volcano.

2.2.1. Volcano Location

Kelut is located west of the Tengger and Kawi-Butak volcanic massifs and southwest of Arjuno-Welirang volcano (fig. 2*a*). It is situated in a unique position for two reasons: firstly, it is closer to the trench than any other volcano in central or east Java, with an estimated depth to the Wadati-Benioff zone (WBZ) of 133 km (Syracuse and Geoffrey, 2006); and secondly, it marks the eastern continuation of Quaternary volcanism along the arc following a largely extinct sector between Merapi and Kelut (fig. 2*a*). The transition east of Merapi is thought to reflect a major structural division from central to east Java represented by the Muriah-Progo lineament and is associated with a number of stratigraphic, tectonic and magmatic changes. The reader is referred to Hall *et al.* (2007) and Clements *et al.* (2009) for more information on the structure of Java. From this point forward, east Java will refer to the region east of the Muriah-Progo lineament.

2.2.2. Stratigraphy and basement

East Java consists of four main provinces which run parallel to the arc and are defined based upon their structure and stratigraphy (after van Bemmelen, 1949; Smyth *et al.,* 2008).

The Rembang Zone

The northernmost province in east Java is known as the Rembang Zone, which extends from the Muriah-Progo lineament in the west to Madura Island east (Smyth, 2005). This area was elevated throughout much of the Cenozoic and covered in clastic marine and carbonate sediments which now reside in fault-controlled basins (Smyth *et al.,* 2005, 2008). The Eocene to Pliocene shelf edge and carbonate sediments vary in thickness from 2000 m to 6000m and rest unconformably on Pre-Cenozoic arc and ophiolitic basement. While the basement is not exposed at the surface it is speculated that it may be a continuation of the basement exposed

at Karangsambung and Luk Ulo in central Java and the Meratus ophiolite belt which runs up through eastern Borneo (Hamilton, 1979; Parkinson *et al.,* 1998; Hall, 2012).

Most of the Rembang zone is of low relief, composed of modern volcanic and alluvial deposits. In the northwest, the low relief is punctuated a major ENE-WSW trending ridge, known as the Rembang high, and an extinct volcanic highland (Smyth, 2005; Smyth *et al.,* 2008). The Pliocene-Pleistocene volcanoes situated here (e.g. Muriah and Lasem) are distinctive by their location, 100 km north from the axis of the Quaternary volcanic arc, and their character, which is ultrapotassic to leucititic (Edwards, 1990; Edwards *et al.,* 1991; Leterrier *et al.,* 1990). Magmas with a leucititic character are also located 150 km further ENE-WSE from Muriah on Bawean Island (Leterrier *et al.,* 1990). It is proposed that extension in the Bawean Trough, and a continuation of the major fault system in the Rembang zone, may provide the catalyst for such magmatism through decompression melting of a phlogopite-rich metasomatic layer situated in the lithosphere (Edwards, 1990; Leterrier *et al.,* 1990). However, it is unclear to what extent, if any, subduction zone processes play in their genesis.

The Kendeng Zone

The Kendeng zone is situated south of the Rembang Zone and immediately north of the Quaternary volcanic arc. It is a deep basin filled predominantly with volcanogenic material derived from the southern mountains and modern arc. The basin deposits are poorly exposed and comprise up to 8000 m of Eocene and Miocene sediment which records a deepening of the basin with time caused by the progressive loading of the volcanic arc (de Genevraye and Samuel, 1972; Smyth, 2005; Waltham *et al.,* 2008). The entire Kendeng basin is marked by a prominent negative Bouguer gravity anomaly of more than -580 μm-2 (fig. 2.1*b*) which is abruptly terminated at the Muriah-Progo lineament, but continues east into the straits of Madura and north of Bali (Smyth *et al.,* 2008). Today, the northern part of the Kendeng basin is an east-west trending thrust belt (Smyth *et al.,* 2005). No basement is exposed within the Kendeng zone.

The Modern Arc

The modern volcanic arc consists exclusively of Quaternary volcanoes which, in east Java, are situated on top of the Kendeng Zone. Between Merapi and Kelut magmatism is sparse, where only fumarolic activity is present at Lawu and Wilis volcano. Following this 200 km

Regional Geological Features
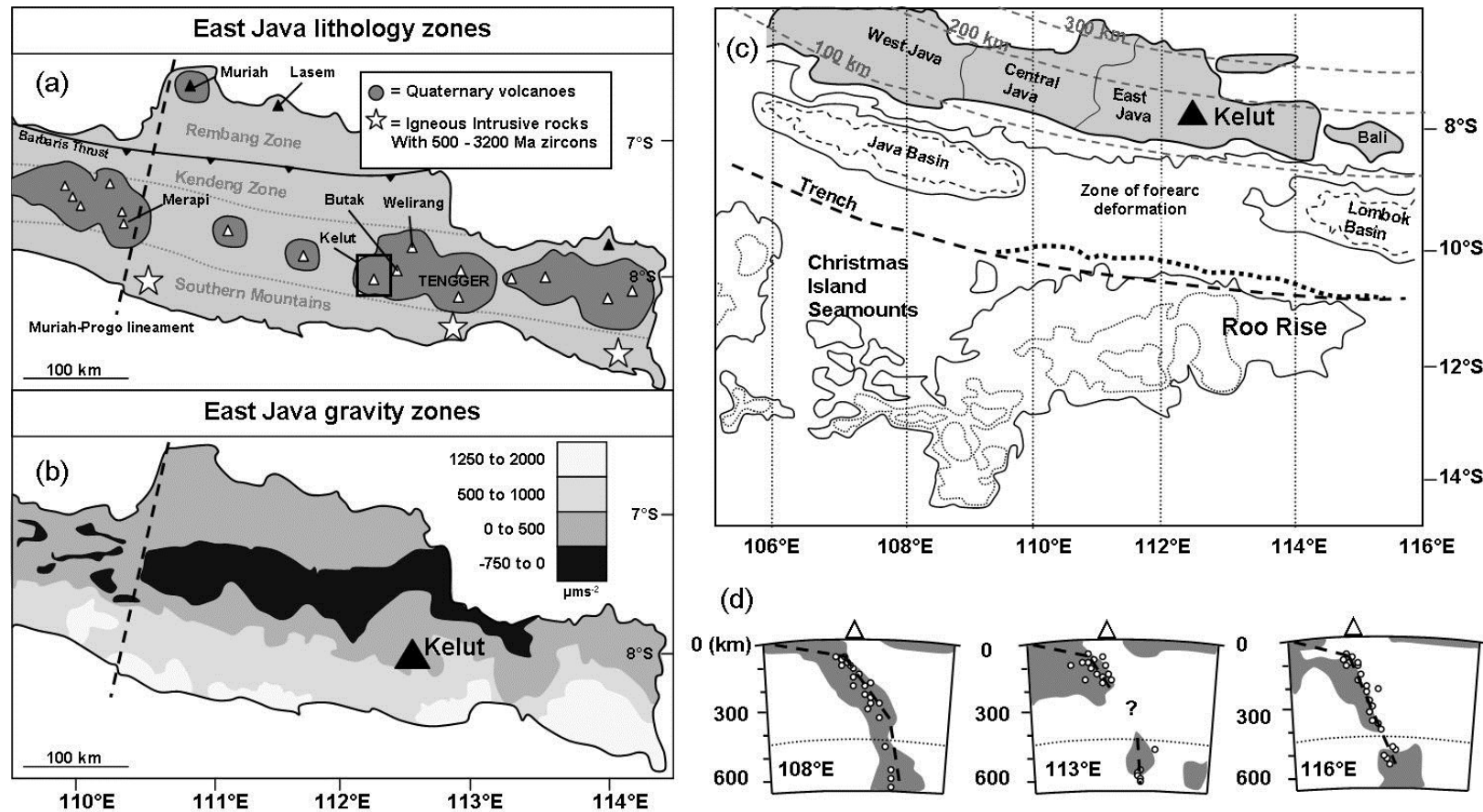
Fig. 2.1. (a) Shows a subdivision of structural provinces (grey dotted lines) east of the Muriah-Progo lineament (dashed black line). Also shown is the location of igneous intrusive rocks containing Cambrian to Archaean zircons (white stars) in the Southern Mountains, Quaternary volcanoes (white triangles) in the modern arc and the Pliocene and Pleistocene extinct volcanoes (black triangles) located in the Rembang Zone. The division between the Rembang and Kendeng zones is marked by the Barbaris thrust. After Smyth (2005). **(b)** Shows gravity data for east Java, after Smyth *et al.* (2008). **(c)** A schematic representation of the Roo Rise collision at the Java trench, redrawn after Kopp *et al.* (2006)**. (d)** Seismic profiles along Java, after Widiyantoro *et al.* (2011). Note the gap in the slab at 113°E.

hiatus, Kelut marks a return to more frequent volcanism (Wheller *et al.,* 1987) and the spacing between volcanoes along the rest of east Java is ~ 25 m apart. Setijadji (2010) shows that the diminished section of volcanic activity is associated with a prominent area of low heat flow terminated by the Barbaris Thrust between the Kendeng and Rembang zones. The character of the magmatism from this section of the arc will be discussed in the following sections.

The Southern Mountains

The Southern Mountains represent the southernmost province in east Java and an older Eocene to Miocene volcanic arc. A detailed account of the Southern Mountains stratigraphy is reported in Smyth (2005). This volcanic arc is currently situated ~ 50 km south of the modern arc but has been thrust north onto the volcaniclastic sequences in the Kendeng basin (Hall *et al.,* 2007; Clements *et al.,* 2009). Upper Oligocene to lower Miocene volcaniclastic deposits suggest that the termination of volcanism was associated with explosive eruptions and magmas of an intermediate and acidic composition. The products of which are know found extensively in the Kendeng basin. This contrasts with the modern arc where very few evolved compositions have been discovered.

The nature of the basement beneath the Southern Mountains has recently been reviewed following a number of studies by Smyth *et al* (2005, 2007, 2008) who discovered that many of the zircons from igneous rocks yielded Cambrian to Archaean ages. Similar age ranges have also be recorded in the Milano metamorphic basement complex in western Sulawesi (e.g. van Leeuwen *et al.,* 2007) which is associated with widespread acidic magmatism containing isotopic characteristics typical of an old crustal source (Bergman *et al.,* 1996; Polve *et al.,* 1997; Polve *et al.,* 2001). Hall *et al*. (2009) and Hall and Sevastjanova (2012) now interpret the deep crust in east Java and west Sulawesi to be part of the same continental block (the Argo block), which rifted from the Australian continental margin during the Jurassic. Such a model is supported by deep basement structures in Indonesia and NW Australia (Granath *et al.,* 2011; Hall, 2011) and zircon populations from east Java, west Sulawesi and NW Australia (Smyth *et al.,* 2007; van Leeuwen *et al.,* 2007; Southgate *et al.,* 2011). However, to date, there has been little evidence for the existence of such continental material outside of the Southern Mountains in east Java.

2.2.3. Seamount Collision at the Java Trench

Since the Asian Tsunami in 2004, much work has been done to increase understanding of the processes which occur along the Sunda and Java trenches. Papers which document the seismic structure, subduction erosion and material transfer beneath the Java margin provide a clearer picture of the geodynamic constraints under which magmatism may have occurred.

In a geophysical study along the Java trench Kopp *et al*. (2006) state that " subduction processes off central Java are dominated by the collision of the Roo Rise with the forearc between 109°E and 115°E". Fig. 2.1*c* shows a schematic representation of the Roo Rise seamount colliding with the trench offshore central and eastern sections of Java. Bathymetric data shows that that the Roo Rise is ~ 70 km into the trench at its most northern point which suggests that it subduction of the plateau started at between 1.1 and 1.3 Ma (Shulgin *et al.,* 2011). This has caused significant uplift and deformation to the forearc between the west Java and Lombok basins and a deflection of the trench on average of 40 km from its normal curvature (Kopp *et al.,* 2006). Kelut is one of a few volcanoes clearly within this zone of deformation and therefore provides a good candidate for examining the effects of such significant changes along the trench. Offshore central and east Java the trench is reported to be devoid of any sediment other than localised ponds (Kopp, 2011; Masson *et al.,* 1990).

2.2.4. The subducting plate: Seismic Profiles

A tear, or gap, in the slab beneath east Java has been imaged by high resolution P-wave tomography and been linked to the previous subduction of a buoyant plateau (similar to the present day Roo Rise) at ~ 8 Ma (Hall *et al.,* 2009; Widiyantoro *et al.,* 2011). The gap, now in the mid-upper mantle, is thought to have resulted from trench migration southwards after collision and slab break-off. Resumed subduction, behind the accreted plateau, would presumably have pulled the gap further into the mantle until its present-day position at between ~ 250 km and 550 km depth. An analogous example of slab-tear is decribed beneath the Izu-Bonin-Mariana arc, where changes in slab morphology and seismicity are related to collisions of oceanic pleateaus at the trench (Fryer & Smoot, 1985; Widiyantoro *et al.,* 2011). Fig. 2.1*d* shows three sesimic profiles across Java after Widiyantoro *et al.* (2011). It shows that Kelut volcano is situated on a section of the arc beneath which there is a significant gap in the subducting plate related to collisional processes at the trench.

2.3. Kelut: Volcanic history, Sample Selection, and Petrography

Historically, Kelut is one of the most active and dangerous volcanoes in Java because of its close proximity to low lying cities such as Kediri and Blitar. There have been more than 30 recorded eruptions in the historical record. Since 1500 AD, a reported 15,000 lives have been lost, about 5000 of them during an explosive pyroclastic eruption in February 1990 (Sudradjat, 1991). During an eruption in 2007 a new lava dome emerged, replacing the crater lake during a series of violent eruptions (Hidayati *et al.,* 2009).

During a field season in May 2009, more than 20 samples were collected from the volcano flanks, the crater and the new lava dome (fig. 2.2*a* and *b*). The material collected is presumed to be from the most recent eruption; however, no dating has been done to verify this. Detailed reports of the stratigraphic units at Kelut are documented in (Wirakusumah, 1993). No other studies have been published regarding petrogenesis, geochemistry or petrology. The rocks detailed in this study include 19 fresh lavas (LOI < 0.54) and three crustal cumulates.

2.3.1. Lavas

Lava compositions and mineral components are summarised in table 2A and fig. 2.5. The groups identified to best represent Kelut are based on their major and trace element geochemistry and isotope ratios and in this study are subdivided into a high-Zr (HZR) and low-Zr (LZR) group. These are discussed in section 4.

The two groups are largely indistinguishable on the basis of their petrography and contain a basic mineralogy of plagioclase, clinopyroxene, orthopyroxene and titanomagnetite. The basaltic andesites are porphyritic with a predominantly glassy (vitrophyre) groundmass. Most of these lavas contain more than 50% phenocrysts with occasional cumulophyric clots and aggregates of minerals which appear to have been scavenged from plutonic cumulates. Olivine is absent in all but one sample, where it constitutes < 1% of the sample.

Plagioclase is the most common phenocryst and measured compositions from a LZR group basaltic andesite range from An90 (anorthite) to An70 (bytownite). Like many other lavas in Java, crystals shown signs of textural disequilibrium such as resorbed or rounded cores and rims, oscillatory zoning, reverse zoning and sieve-textured cores (e.g. Handley, 2006).

Sample Localities
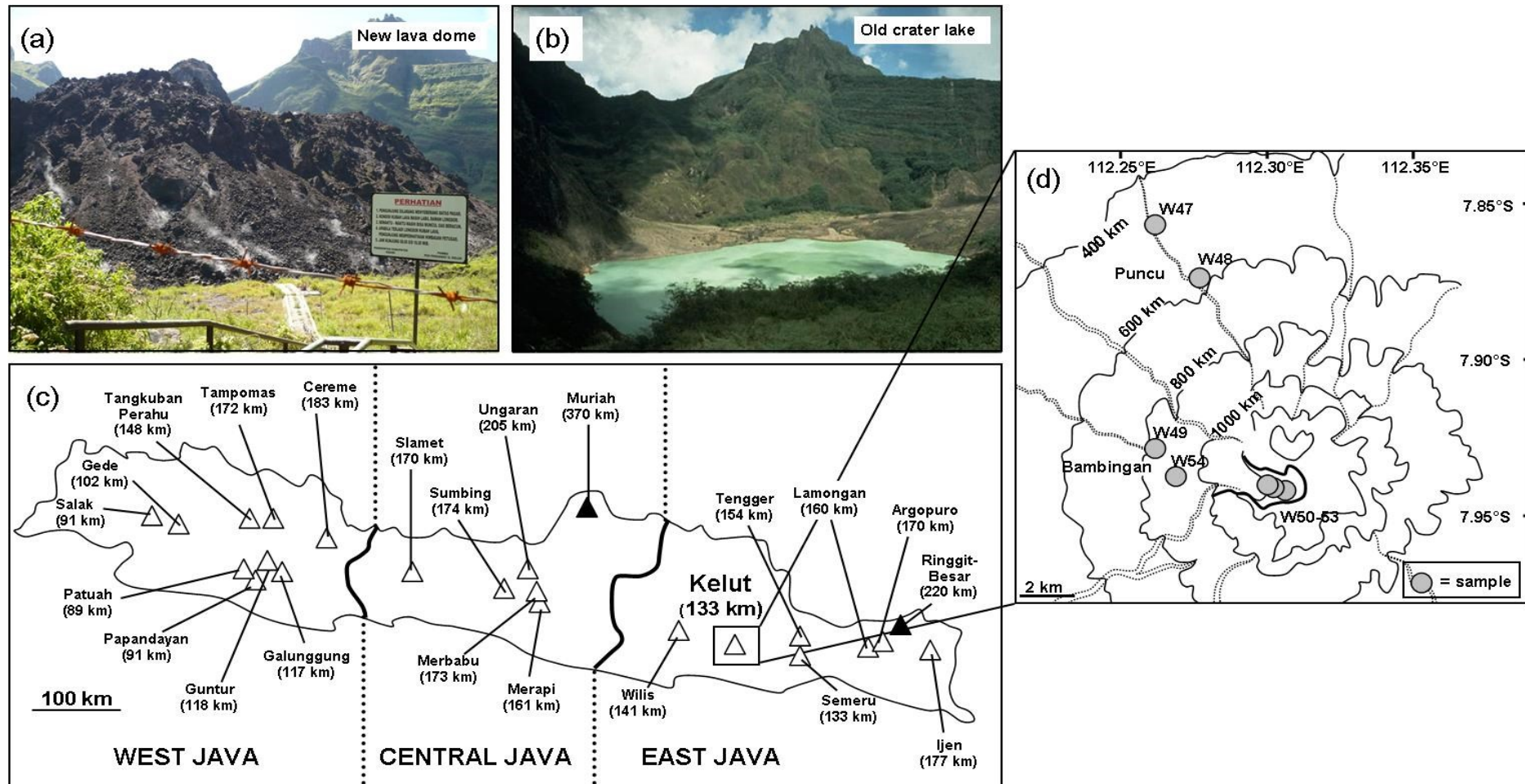
Fig. 2.2. (a) Photo of the new lava dome taken during the 2009 field season. **(b)** Photo of the pre- 2007 crater lake from http://www.geographic.org/photos/volcanoes. **(c)** Schematic map of Java volcanoes with published geochemical data. WBZ depths after Syracuse and Geoffrey (2006). Quaternary volcanoes with low, medium and high-K associations are shown in white and Pliestocene leucititic and ultrapotassic volcanoes in black. **(d)** Insert map shows the sample locations for Kelut lavas analysed during this study shown with a grey circle. The bold black line shows an outline of the crater. W = waypoint localities corresponding to the rock samples reported in table 2A.

Clinopyroxene phenocrysts are typically subhedral and can range significantly in size from a millimetre to a centimetre scale. Phenocryst compositions show a restricted range (En 41.1-42.7, Fs 15.6-17.1, Wo 41.3-42.2) and are also resorbed in places. Orthopyroxene phenocrysts are slightly less abundant than clinopyroxene. These tend to be euhedral or subhedral and contain a narrow range of compositions (En 64.5-67.0, Fs 30.2-32.7, Wo 2.5-2.9). Together with titanomagnetite, these ferromagnesian minerals are commonly clustered together.

Most of the samples between $\sim$ 56 and 57.5 wt. % SiO_2 contain amphibole, which is absent in the more mafic basaltic-andesites and also in the andesites with SiO_2 > 57.5 wt.%. The presence of amphibole is apparent in both groups and usually as an additional phase to the basic plagioclase-clinopyroxene-orthopyroxene-titanomagnetite assemblage, although it is sometimes at the expense of clinopyroxene. Some of the amphiboles are very large in size (> 5 cm) and often enclose smaller minerals such as plagioclase. This type of ophitic texture is common in some of the amphibole-rich cumulates collected at Kelut. Most of the smaller phenocrysts (i.e. < 1 mm) are euhedral to subhedral and are commonly resorbed or embayed in the centres and around the edges of the crystals.

The more evolved andesites (> 57.5 wt.%) which do not contain amphibole are all microcrystalline with a groundmass of microlitic plagioclase feldspar, titanomagnetite-magnetite and small amounts of clinopyroxene (and occasionally minor orthopyroxene). Cumulophyric clots of larger plagioclase crystals, or ferromagnesian clusters of clinopyroxene, orthopyroxene and titanomagnetite are also common, as are large (> 10 mm). In the HZR group, one sample (Kel12) contains a large (> 5 cm), possibly xenocrystic, plagioclase contains a cluster of smaller (< 0.5 mm) minerals around its rim. The plagioclase is euhedral and zoned around its rim. The smaller minerals include rounded quartz grains, tabular plagioclase laths, subhedral clinopyroxene and opaques.

Plagioclase compositions for the HZR and LZR group andesites show similar compositions (Kel60 = An 37-89, Ab 10.4-58.2, Or 0.02-4.73 and Kel12 = An 50-82, Ab 17.1-48.1, Or 0.06-1.55) with the latter containing a slightly wider range. Clinopyroxene and orthopyroxene could not be analysed in Kel60, due to the scarcity in the rock. However, in Kel12 compositions range from En 37.0 to 42.5, Fs 13.6 to 17.2 and Wo 41.0 to 46.3 for clinopyroxene and En 63.4 to 66.6, Fs 31.0 to 34.1, and Wo2.3 to 2.7 for orthopyroxene, which are not dissimilar to the compositions of the basaltic andesites.

Table 2A. Kelut rock summary

sample	waypoint	SiO$_2$ (wt.%)	MgO (wt.%)	Mg#	texture	mineral components	composition
High-Zr Group (HZR)							
Kel56	54	54.16	4.31	49.20	porphyritic	plag, cpx, opx, Fe-Ti oxide, ol	
Kel26	48	55.91	3.48	46.14	porphyritic	plag, cpx, Fe-Ti oxide, opx, amph	
Kel27	48	56.66	3.33	45.95	porphyritic	plag, cpx, Fe-Ti oxide, opx, amph	
Kel50	51	55.38	3.63	47.31	porphyritic	plag, cpx, opx, Fe-Ti oxide	
Kel61	54	57.03	3.23	46.21	porphyritic	plag, cpx, opx, Fe-Ti oxide	
Kel22	47	57.14	3.07	44.93	porphyritic	plag, amph, Fe-Ti oxide	
Kel12	47	59.04	2.79	44.14	porphyritic/xenocrystic plag/qtz	plag	An$_{(50-82)}$, Ab$_{(17.1-48.1)}$, Or$_{(0.06-1.55)}$
						cpx	En$_{(37.0-42.5)}$, Fs$_{(13.6-17.2)}$, Wo$_{(41.9-46.3)}$
						opx	En$_{(63.4-66.6)}$, Fs$_{(31-34.1)}$, Wo$_{(2.3-2.7)}$
						Fe-Ti oxide	Fe$^{+2}_{(0.8-1.26)}$, Fe$^{+3}_{(1.18-1.75)}$, Ti$_{(0.04-0.36)}$
Low-Zr Group (LZR)							
Kel25	48	53.53	3.58	44.49	porphyritic/vitrophyre	plag, cpx, opx, Fe-Ti oxide	
Kel40	49	54.43	3.89	46.94	porphyritic/vitrophyre	plag, cpx, opx, Fe-Ti oxide	
Kel48	50	54.92	3.77	46.61	porphyritic/vitrophyre	plag, cpx, opx, Fe-Ti oxide	
Kel51	52	54.98	3.80	46.88	porphyritic/vitrophyre	plag	An$_{(70-90)}$, Ab$_{(9.7-28.7)}$, Or$_{(0.1-0.5)}$
						cpx	En$_{(41.1-42.7)}$, Fs$_{(15.6-17.1)}$, Wo$_{(41.3-42.2)}$
						opx	En$_{(64.5-67.0)}$, Fs$_{(30.2-32.7)}$, Wo$_{(2.5-2.9)}$
						Fe-Ti oxide	Fe$^{+2}_{(1.07-1.13)}$, Fe$^{+3}_{(1.37-1.40)}$, Ti$_{(0.23-0.25)}$
Kel45	49	55.25	3.39	44.23	seriate	plag, cpx, Fe-Ti oxide, minor opx	
Kel34	48	56.99	2.83	42.64	porphyritic/xenocrystic amph	plag, amph, Fe-Ti oxide, minor cpx, opx	
Kel43	49	57.29	2.64	41.59	porphyritic	plag, amph, cpx, opx, Fe-Ti oxide	
Kel59	54	58.89	2.12	39.15	porphyritic/microcrystalline	plag, Fe-Ti oxide + minor cpx	
Kel23	47	58.90	2.07	38.52	porphyritic/microcrystalline	plag, Fe-Ti oxide + minor cpx	
Kel64	54	58.96	2.11	38.76	porphyritic/microcrystalline	plag, Fe-Ti oxide + minor cpx	
Kel60	54	59.01	2.11	38.95	porphyritic/microcrystalline	plag	An$_{(37-89)}$, Ab$_{(10.4-58.2)}$, Or$_{(0.02-4.73)}$
						Fe-Ti oxide	Fe$^{+2}_{(1.21-1.26)}$, Fe$^{+3}_{(1.25-1.36)}$, Ti$_{(0.30-0.34)}$
						cpx*	
Kel14	47	59.69	1.80	38.04	porphyritic/microcrystalline	plag, cpx, opx, Fe-Ti oxide	

Table 2A. Summary table for the Kelut rock samples. Data includes the waypoint localities, major elements (SiO_2 and MgO) used for differentiation indices, Mg# calculated as $100*((MgO)/((MgO+FeOtot)))$, rock texture, mineral components and compositions (where analysed). Grey shading indicates samples from the HZR group (see section 4 for details). Plag = plagioclase, cpx = clinopyroxene, opx = orthopyroxene, Fe-Ti oxide = titanomagnetite, amph = amphibole, ol = olivine.

sample	waypoint	SiO_2 (wt.%)	MgO (wt.%)	Mg#	texture	mineral components	composition
Gabbro							
Kel37	48	41.68	5.48	58.90	cumulate	plag, cpx, opx, Fe-Ti oxide, ol	
Hornblende Gabbro							
Kel38	48	43.66	6.33	52.83	cumulate	plag, amph, cpx, opx, Fe-Ti oxide	
Hornblendite							
Kel53	53	41.03	11.91	58.72	othocumulate	amph, Fe-Ti oxide (interstitial plag, cpx, opx)	

Table. 2B. Summary table for cumulate rocks recovered from Kelut. Criteria as for table 2A.
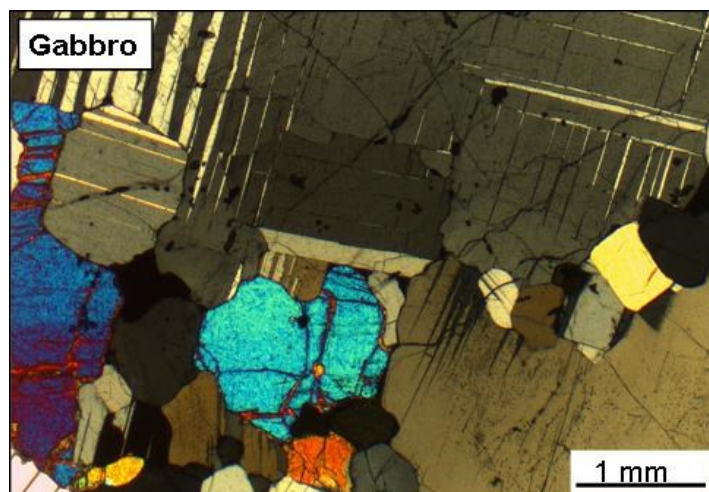
Fig. 2.3. Representative photomicrograph (crossed-polarised light) of the Plag-cpx-opx-ol gabbro cumulate (Kel37). See text for details.
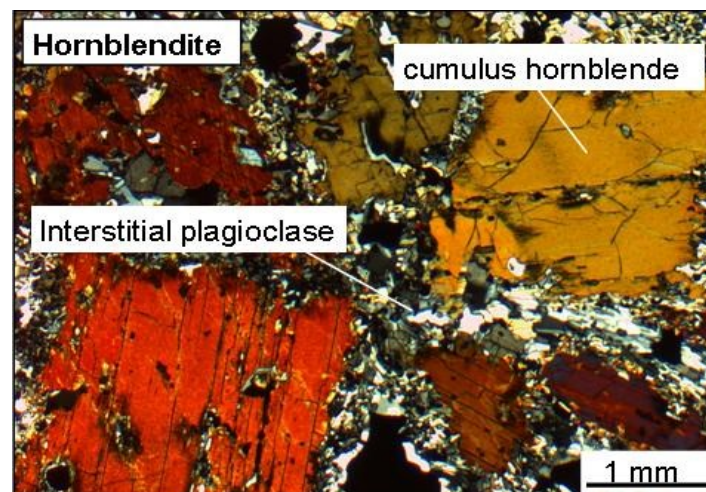
Fig. 2.4. Representative photomicrographs (crossed-polarised light) of the hornblendite cumulate (Kel53). See text for details.

Mineral Compositions
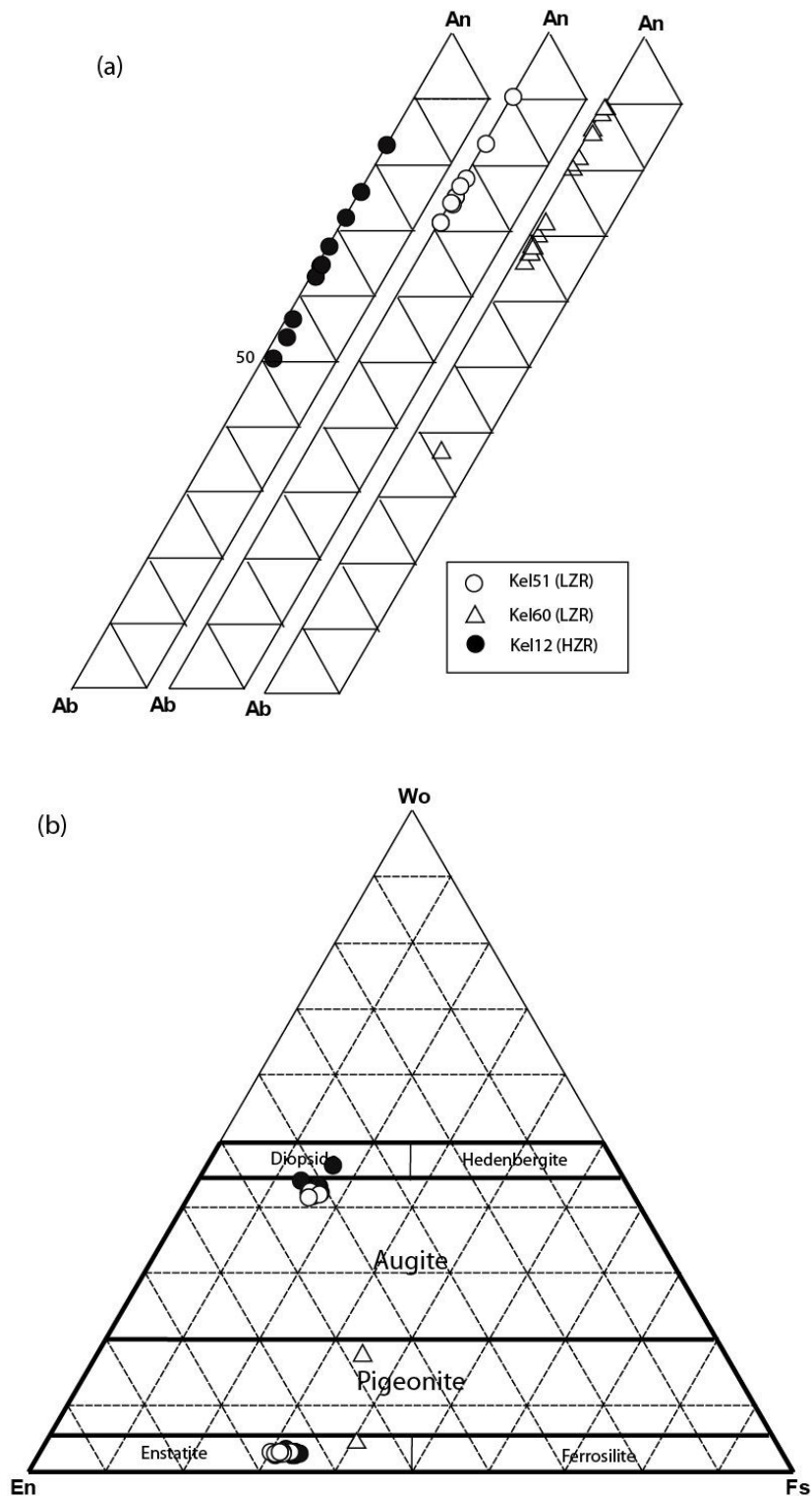
Fig. 2.5. Analyses of **(a)** Plagioclase phenocrysts and **(b)** pyroxene phenocrysts in three of the Kelut samples. Dashed lines represent 10% increments. An = Anorthite, Ab = Albite, En = Enstatite, Fs = Ferrosilite, Wo = Wollastonite. See text for details.

2.3.2. Cumulate xenoliths

Three cumulates were analysed in addition to the lavas (table 2B). The first two were collected in a quarried flank section by the town of Puncu (see fig. 2.2*d*). These cumulates are gabbro's of different composition. The first is composed of plagioclase, clinopyroxene, orthopyroxene and olivine (fig. 2.3) and the second is a hornblende gabbro, which largely consists of plagioclase and amphibole. The final cumulate was collected by the new lava dome. This ultramafic rock is a hornblendite (fig. 2.4). The composition of this cumulate is primarily hornblende (80-90%) and Fe-Ti oxides. Between the larger cumulate crystals are patchy regions of interstitial plagioclase.

2.4.   Geochemistry

The Kelut volcanic rocks are classified by the Total Alkali-Silica (TAS) and K_2O against SiO_2 schemes, together with other published data for east Java, in figures 2.6 *(a)* and *(b)*. According to these criteria the lavas at Kelut consist of low- to medium-K basaltic-andesites and andesites. Compared to the other volcanoes in east Java, the Kelut magmas show the lowest alkali concentrations for a given SiO_2 contents with other volcanoes showing medium-K (Semeru and Wilis), high-K (Lamongan, Tengger and Ijen), or Leucititic (Ringgit-Besar) affinities.

To highlight the trends in magma evolution major and trace elements and isotopic ratios are described here against MgO (wt.%). Differentiation is typically measured against either SiO_2 (wt.%), MgO (wt.%) or Mg# as an index, and SiO_2 is commonly used for highly differentiated rocks (Davidson *et al.,* 2005; Davidson and Wilson, 2011). MgO is preferred here; firstly because of the small variation in SiO_2 between the most evolved and least evolved rocks at Kelut; and secondly, because it enables for fractionation corrections, typically for at a given MgO, when evaluating source characteristics (e.g. Woodhead *et al.,* 1993). Discussion focuses on the individual variations between rock suites at Kelut, and those rocks in context with other volcanoes from east Java (e.g. Tengger, after van Gerven & Pichler, 1995; Wilis, after Hartono, 1996; Lamongan, after Carn & Pyle, 2001; and Ijen, after Handley *et al.,* 2007). The volcanoes have been subcategorised by their position relative to the trench, where Kelut Wilis and Semeru are all situated in front arc positions closest to the trench (bold outlines), and Tengger, Lamongan and Ijen are positioned further back on the arc

Classification Diagrams
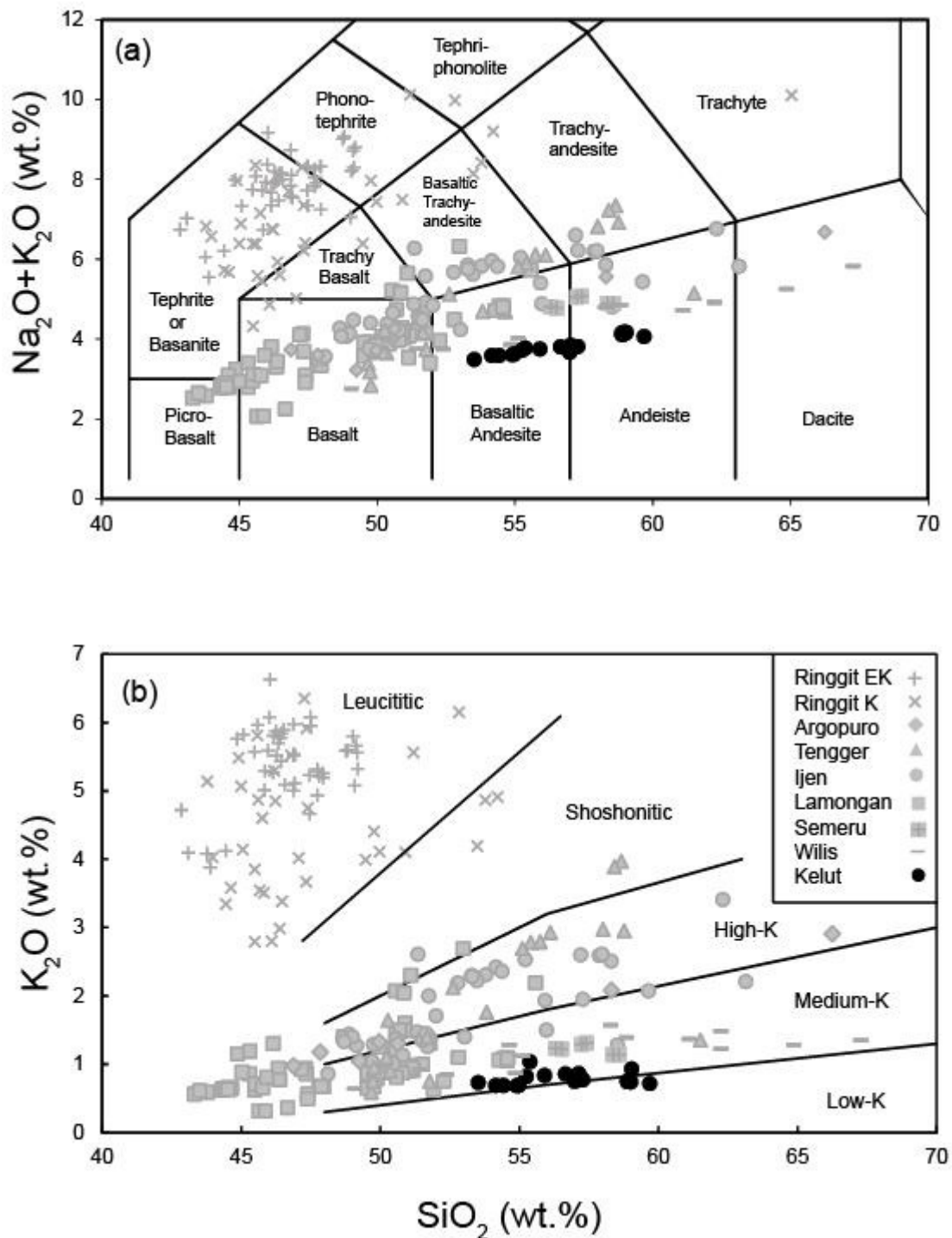
Fig. 2.6. (a) The Total Alkali-Silica (TAS) and **(b)** K_2O against SiO_2 classification schemes for east Java volcanic rocks, after Le Bas *et al*. (1986), Peccerillo & Taylor (1976) and Wheller *et al*. (1987). Kelut samples are highlighted as black circles. Additional data after Edwards (1990), Edwards *et al*. (1991, 1994); van Gerven & Pichler (1995); Hartono (1996); Carn & Pyle (2001); and Handley *et al*. (2007). See text for details.

(dashed line). The reader is referred to fig. 2.2*c* for volcano positions and WBZ depth estimations.

2.4.1. Major elements

Major element concentrations against MgO (wt.%) for the Kelut lavas and cumulate xenoliths are shown in fig. 2.7 (*a-p*), along with fields for Tengger Volcanic field (TVF), Wilis (WIL), Lamongan Volcanic Field (LVF), Semeru (S), and Ijen (IJ) (left).

In section 2.3.1, two rock suites were introduced for Kelut. These can be defined by contrasting geochemical trends, which are particularly notable for a number of incompatible trace elements including Zr. On this basis the groups are termed a high-Zr series (HZR) and low-Zr series (LZR). The LZR series can also be distinguished from the HZRs series by their low-K (< 0.8 wt.%) and tholeiitic affinities with respect to FeO*/MgO against SiO_2 (not shown).

TiO_2, Fe_2O_3 and CaO all decrease with decreasing MgO contents and for these elements there are little variation between the LZR and HZR series which appear to project back toward the hornblendite cumulate (at ~ 12wt.% MgO). Al_2O_3 remains relatively constant, at between 18.5 and 19 (wt.%), as does P_2O_5 in all but the most evolved andesites which show elevations. The LZR and HZR show variations between the alkalis, particularly in K_2O, which remains constant with increasing differentiation in the former and is elevated in the latter, although concentrations for both series are low (generally < 1 wt.%). SiO_2 also becomes progressively higher in the HZR series with differentiation compared to the LZR series (see fig. 2.7*p*).

In comparison with other volcanic rocks from east Java, the Kelut samples contain relatively low MgO contents (all < 5 wt.%) and mostly plot within fields for Wilis and Semeru. The LZR samples, in particular, have low concentrations of K_2O for a given MgO content compared to other volcanic rocks. The rocks with the highest concentrations of MgO come from Lamongan Volcanic Field. With the exception of TiO_2 and Fe_2O_3, most of the major element compositions for Lamongan project back towards the values for the hornblendite cumulate.

Major Element Geochemical Plots against MgO
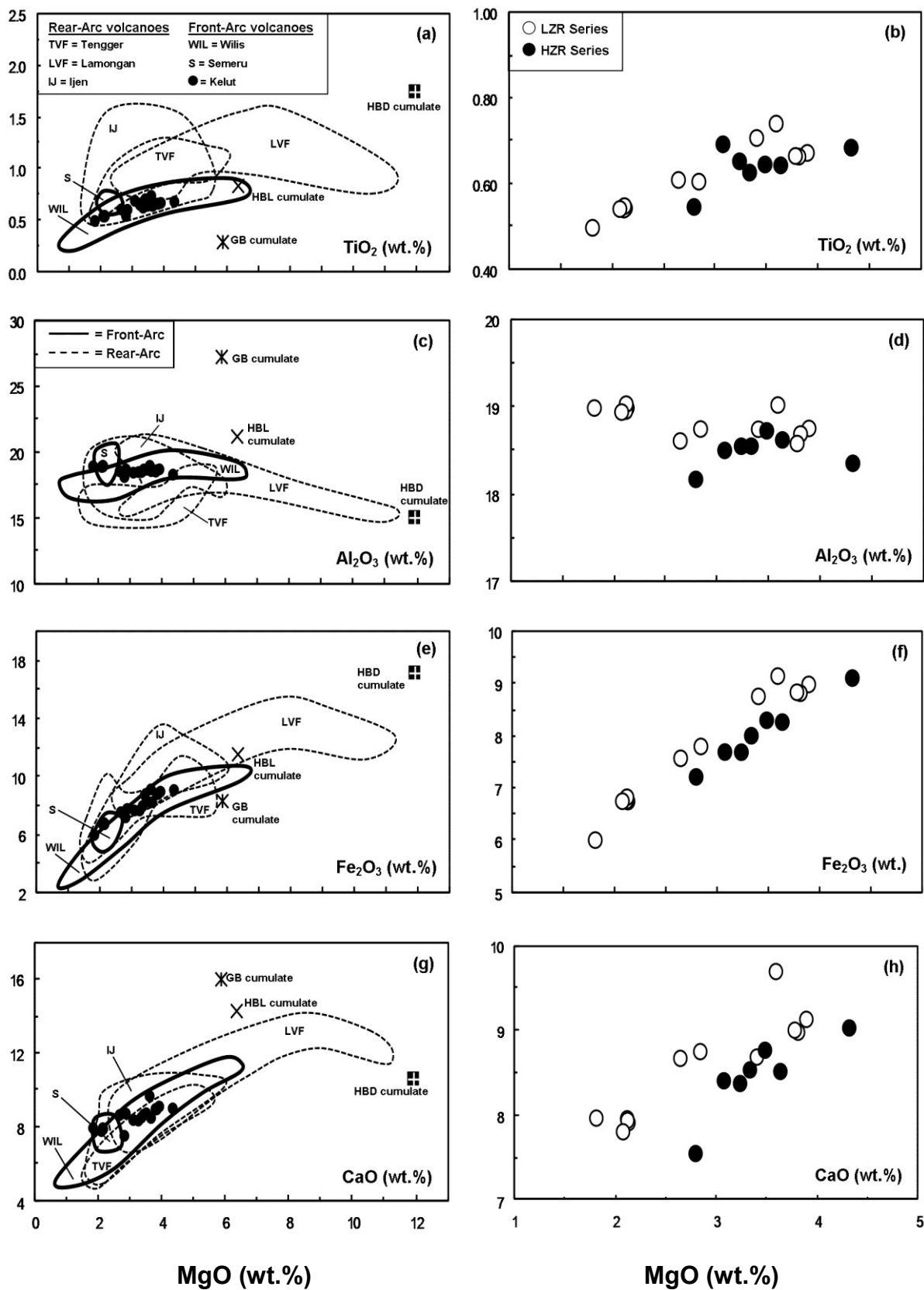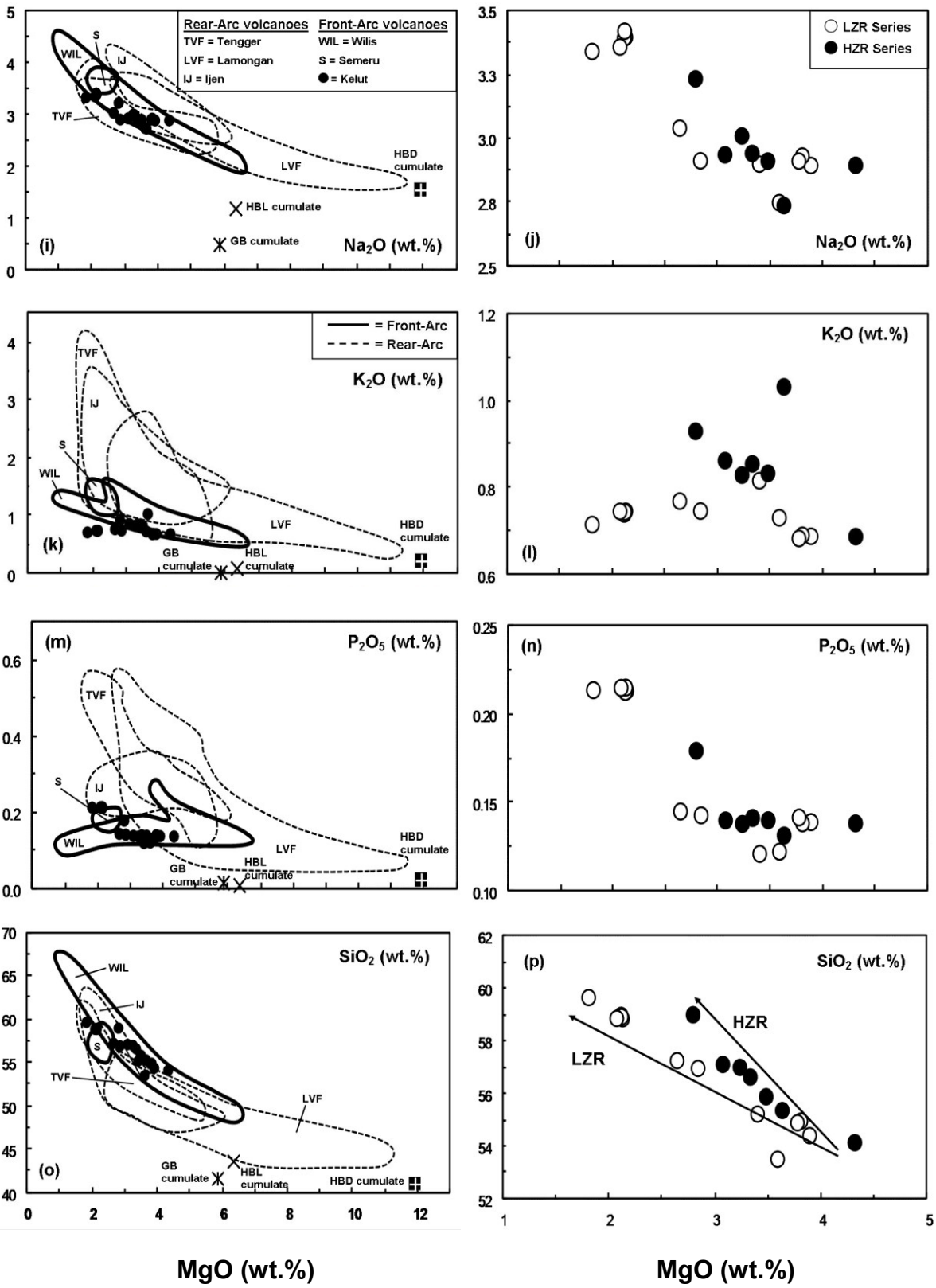
Fig. 2.7. (a-p) Major elements plotted against MgO (wt.%). Figures (a, c, e, g, i, k, m and o) show the Kelut samples (black circles) and cumulates in relation to other volcanoes from east Java. HBD = hornblendite cumulate, HBL = hornblende gabbro cumulate, and GB = gabbro cumulate. Data fields from the east Java volcanoes shown in text. Figures (b, d, f, h, j, l, n and p) show variations between two rock suites at Kelut; a Lower-Zr Series (white circles) and Higher-Zr Series (black circles).

30

2.4.2. Trace elements

Trace element concentrations are discussed here on the basis of groups of elements with similar behaviour in basaltic magmas. For example, those elements which behave compatibly can be distinguished from those which are incompatible but readily mobilised in aqueous fluids, and those which are incompatible and considered to be relatively immobile (e.g. Tatsumi *et al.,* 1986). The additional fields are the same as for those above.

2.4.2.1.   Compatible trace elements *(Ni, Cr, V and Sc)*

Compatible trace element concentrations against MgO (wt.%) are shown in fig. 2.8 (*a-h*). For this group of elements the two series of rocks are indistinguishable. Ni and Cr contents are low (< 20 ppm and < 30 ppm respectively) and patterns mirror one another. V and Sc are also relatively low (< 200 ppm and 30 ppm), with identical patterns. All of the volcanic rocks in east Java show a trend of decreasing Ni, Cr, V and Sc with decreasing MgO.

2.4.2.2.   Large-Ion Lithophile Elements *(LILE; Cs, Rb, Ba, K, Sr Pb and U)*

The group of elements known as Large-Ion Lithophile Elements (LILE) are those with a high ionic radius and a low ionic charge and, as a result, a high solubility in aqueous fluids (e.g. Tatsumi *et al.,* 1986). These elements are generally the ones considered to be most readily transported to the mantle wedge by fluids during dehydration of the subducting slab (e.g. Brenan *et al.,* 1995; Ayers *et al.,* 1997; Kogiso *et al.,* 1997; Ayers, 1998). In most arc magmas the LILE are most elevated related to Mid-Ocean Basalt (MORB) compositions which is inferred to result from the subduction component (McCulloch and Gamble, 1991).

Rb, Ba, Sr and Pb against MgO are shown in fig 2.9 (*a-h*), and K_2O against MgO is shown in fig. 2.7*k*. A pattern between all of the LILE is not apparent. Both of the Kelut series have particularly low Rb and K_2O compared to the other volcanoes in east Java (and also compared to most other rocks in Java). For these elements the HZR samples contain progressively higher concentrations for similar MgO. The low LZR samples only become slightly more enriched in Rb and K_2O with decreasing MgO. In contrast, Sr concentrations in the LZR andesites are extremely high (fig. 2.9*e* and *f*), exceeding values for other volcanoes

Compatible Trace Element Geochemical Plots against MgO
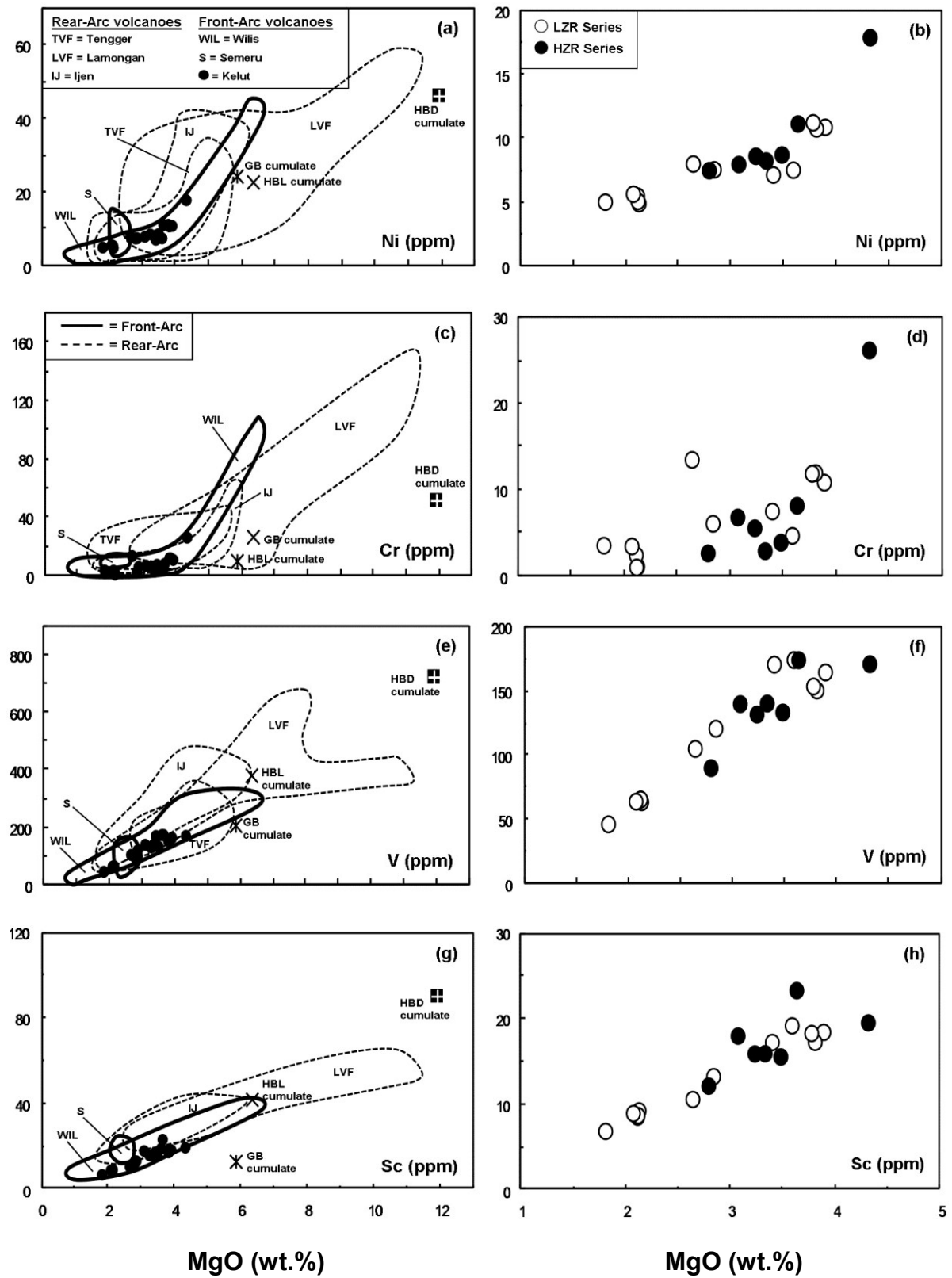
Fig. 2.8. (a-h) Trace Elements showing compatible behaviour plotted against MgO. Note the low concentrations of Ni and Cr even in the most primitive rocks. Fields are the same as for fig. 2.7.

Fluid-Mobile Trace Element Geochemical Plots against MgO
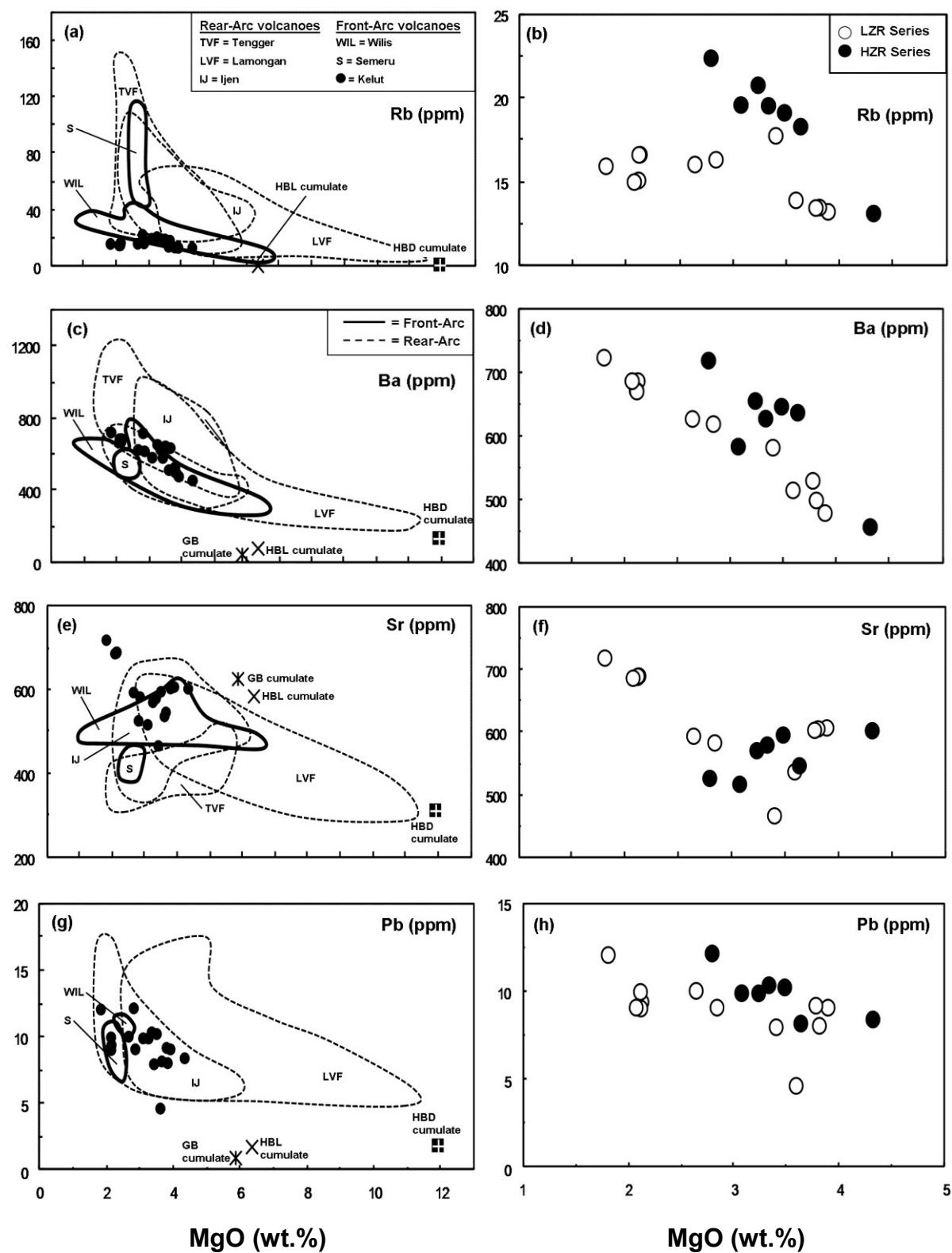
Fig. 2.9. (a-h) Trace elements considered to be some of the most fluid-mobile (Tatsumi *et al.,*1986) plotted against MgO. Fields are the same as for fig. 2.7.

Fluid Immobile Trace Element Geochemical Plots against MgO
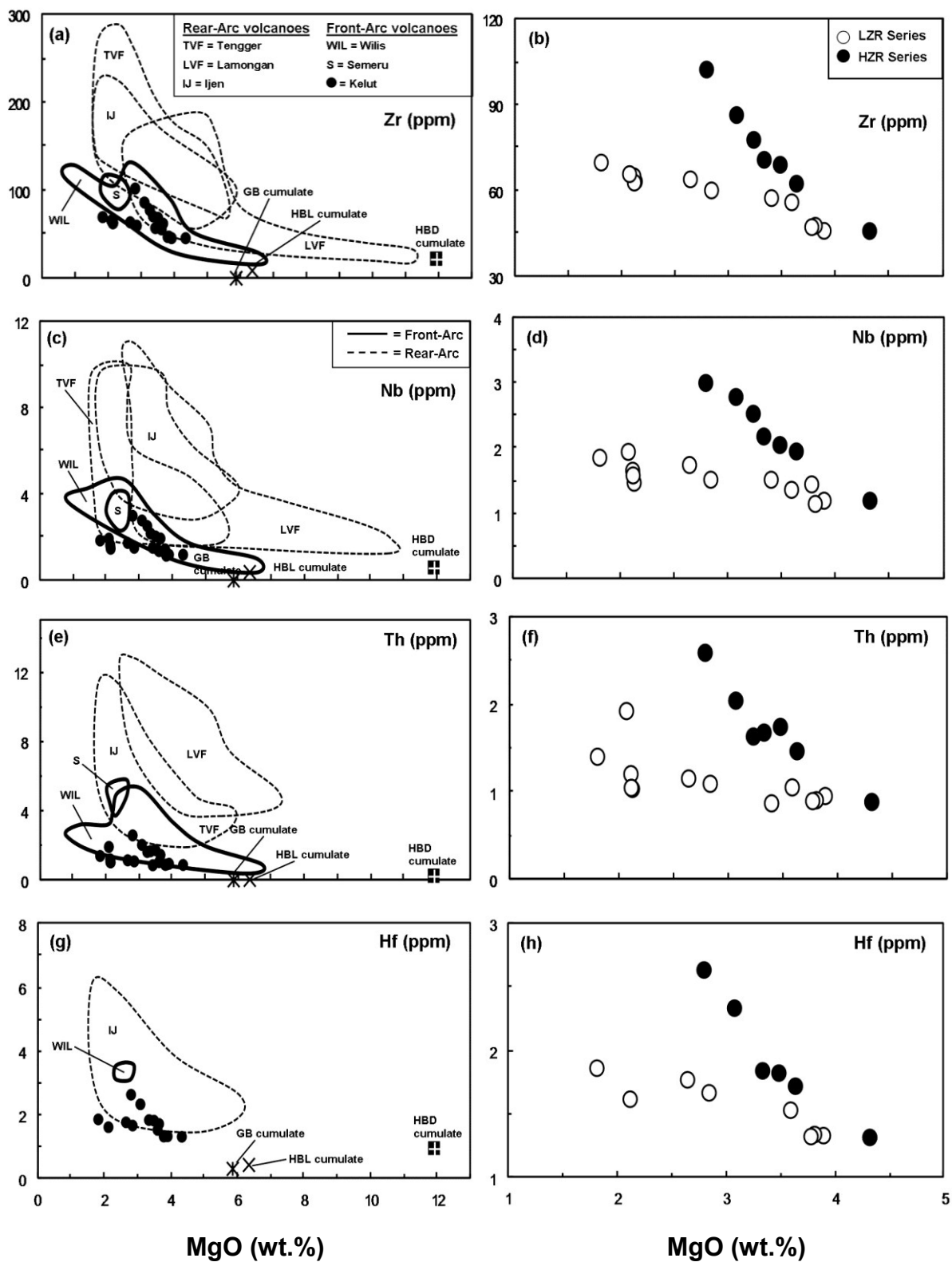
Fig. 2.10. (a-h) Trace elements considered to be the least fluid-mobile (Tatsumi *et al.,* 1986) plotted against MgO. Note the low concentration s in Kelut lavas and variation between series. Fields are the same as for fig. 2.7.

with similar MgO in east Java. This is one of the few examples where the concentration of an element becomes more enriched in the LZR relative to the HZR during differentiation.

Ba and Pb show slight differences between the Kelut series, but are similar in concentrations to the other volcanoes. In a similar fashion to the major and compatible trace elements the east Java fields, and in particular Lamongan, appear to project back towards the hornblendite cumulate. The other cumulates do not plot within profiles for the volcanic rocks.

2.4.2.3. High Field-Strength Elements *(HFSE; Nb, Ta, Zr and Hf)*

This group of elements typically have lower concentrations in arc magmas compared to LILE. They have a high ionic charge and low ionic potential which makes them much less soluble in aqueous fluids and, therefore, more likely to reflect a source prior to the addition of a subduction component (e.g. Woodhead *et al.,* 1993; Brenan *et al.,* 1994).

HFSE against MgO are show in fig. 2.10 (*a-h*). The Kelut samples all have very low concentrations of these elements, particularly compared to magmas from the volcanoes further away from the trench (i.e. Tengger, Lamongan and Ijen). Semeru and Wilis also contain relatively low abundances of these elements compared to rear-arc equivalents. Trends of Zr, Hf, Nb, Ta and Th all mirror those of Rb and K for the LZR and HZR samples. For all of these elements the HZR series become more enriched with decreasing MgO compared to the LZR series. A similar distinction between groups is shown for Wilis volcano. All of these profiles show that significant elevations occur in the HFSE in rocks which contain < ~ 5 wt.% MgO, particularly for those volcanoes sitauted behind the front of the arc.

2.4.3. Isotope Geochemistry

Isotopic ratios are show against MgO to highlight how they may have been modified in the crust during differentiation. Subsequent plots of isotope against isotope are evaluated during the discussion.

$^{87}Sr/^{86}Sr$, $^{143}Nd/^{144}Nd$, $^{176}Hf/^{177}Hf$ and $^{206}Pb/^{204}Pb$ against MgO are shown in fig. 2.9. The HZR and LZR can be clearly distinguished by these isotope plots. The HZR samples show increasing values for $^{87}Sr/^{86}Sr$ and $^{206}Pb/^{204}Pb$ and decreasing $^{143}Nd/^{144}Nd$ and $^{176}Hf/^{177}Hf$.

Radiogenic Isotope Geochemical Plots against MgO
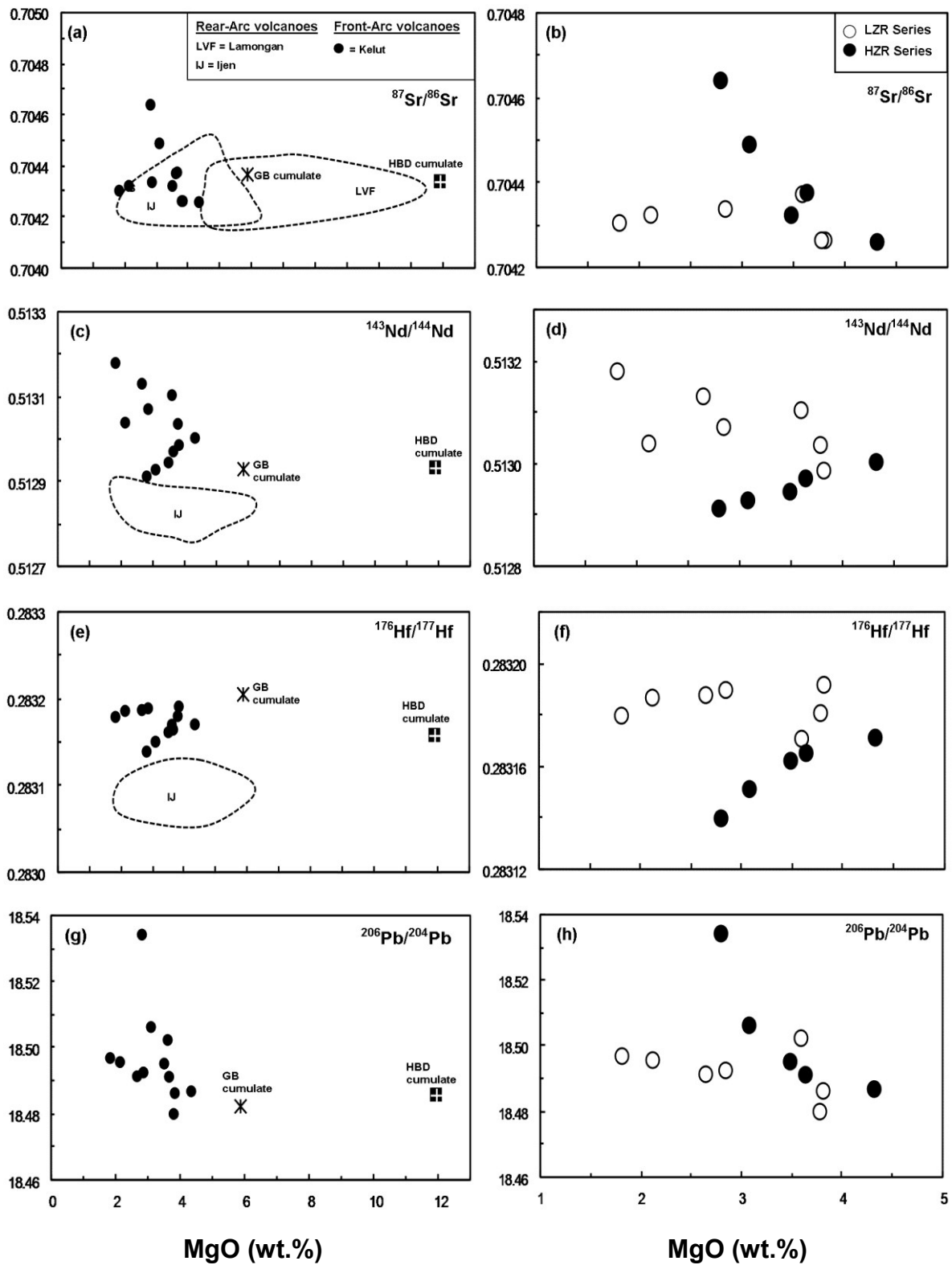
Fig. 2.11. (a-h) Radiogenic isotopes plotted against MgO. Note the slightly enriched trends produced by the Kelut HZR lavas in comparison to the flat profiles of the LZR lavas. Fields are the same as for fig. 2.7.

In contrast the LZR samples show no variation for the isotope ratios with decreasing MgO concentrations. Ratios of $^{143}Nd/^{144}Nd$ and $^{176}Hf/^{177}Hf$ for this group are high and similar to mantle values (e.g. Chauvel & Blichert-Toft, 2001; Janney *et al.,* 2005).

Isotopic data from other volcanoes in east Java is sparse. However, the LZR series contain higher $^{143}Nd/^{144}Nd$ and $^{176}Hf/^{177}Hf$ than Ijen, and similar $^{87}Sr/^{86}Sr$ to Ijen and Lamongan. The HZR samples extend to higher $^{87}Sr/^{86}Sr$ ratios than the Ijen-Lamongan field at lower MgO concentrations. The hornblendite and gabbro cumulate have ratios very similar to the least evolved for both series (Kel56).

2.4.4. N-MORB Normalised Incompatible Trace Elements

Normalised variation diagrams are used to evaluate the concentrations of selected incompatible trace elements against a reference, in this case Normal Mid-Ocean Ridge Basalt (N-MORB). N-MORB is typically used as an index against subduction-related magmas in order to highlight enrichments in groups of fluid mobile elements such as LILE and LREE over less mobile groups of elements such as HFSE and HREE (McCulloch and Gamble, 1991; Elliot *et al*., 1997; Turner and Hawkesworth, 1997; Handley *et al*., 2007). Because the HFSE and HREE concentrations from subduction zone magmas are usually similar to MORB, it is commonly inferred that the pre-subduction mantle source is of a similar composition (e.g. Woodhead, 1989; Woodhead *et al.,* 1993).

Figure 2.12 *a* presents a plot of the Kelut samples normalised against MORB. A number of Indian MORB (I-MORB) samples are also shown because Sunda arc magmas are commonly inferred to have a slightly more 'enriched' source similar to these compositions (Gertisser and Keller, 2003; Macpherson *et al.,* 2003; Handley *et al.,* 2010). The HZR series shows a similar profile to the LZR with slight enrichments in Th, Nb, Ta, Zr and Nb. These enrichments were discussed in section 2.4.2.3. The general profile shows an increase in element concentrations from Lu to Cs, punctuated by some large positive anomalies at Sr, Pb, K and Ba. An equally significant negative anomaly is shown for Nb and Ta. Most of the HFSE and HREE in the Kelut magmas are slightly lower in concentration than N-MORB.

Figures 2.12 *(b)* and *(c)* Shows the Kelut samples compared to other Quaternary magmas from Java and the hornblendite cumulate. A couple of significant points can be taken from these plots. Firstly, the Kelut volcanic rocks contain a very similar trace element profile to the

hornblendite cumulate with peaks in Ba, K, Pb and Sr. Secondly, the Ba positive anomaly is significantly higher than for any other volcano in Java. This is coupled with the lowest values for Nb and Ta. The next section will discuss the observations from this data.

2.4.5. Chondrite normalised Rare-Earth Elements

Chondrite normalised REE plots are shown in figure 2.13. Figures *(a)* and *(b)* shows the Kelut volcanic rocks compared to the medium- and high-K and leucititic data for east Java, and N-MORB. The Kelut low-Zr magmas are shown in figure *(a)* and in more detail in *(c)* and the low-Zr magmas are shown in *(b)* and in more detail in *(d)*.

In the low-Zr group, the basaltic-andesites contain LREE ~ 20-25 times Chondrite and HREE ~ 10-15 times Chondrite. The andesites show greater enrichment in LREE (~ 35 times Chondrite) and slightly higher HREE (~15 times Chondrite) than the basaltic-andesites. The high-Zr shows similar REE trends to the low-Zr group, with the exception of the sample Kel12. This andesite contains significantly greater LREE (~45 times Chondrite) than for equivalent low-Zr andesite compositions (see dashed lines in fig. 2.13*d*).

Compared to N-MORB, the Kelut samples display lower, slightly concave up, MREE- to HREE; and higher LREE. However, they show ubiquitously lower REE than all of the other medium- to high-K arc volcanic rocks from east Java which contains up to 100 times Chondrite LREE and 25 times Chondrite HREE. The leucititic volcanic rocks have between 200 and 700 times Chondrite LREE and as low as 5 times Chondrite HREE.

Fig. 2.12. (a-d) Multi-element diagrams normalised to N-MORB (Sun and McDonough, 1989). **(a)** Shows the Kelut HZR and LZR series against a range of I-MORB values (Janney *et al.,* 2005). **(b)** Shows Kelut against the hornblendite cumulate and the east Java data from section in section. **(c)** Shows Kelut magmas against west Java data from Tangkuban Perahu (Sendjaja *et al.,* 2009; this study), Tampomas (Sendjaja *et al.,* 2009), Cereme (Sendjaja *et al.,* 2009; Edwards, 1990), Salak (Handley *et al.,* 2008), Gede (Handley *et al.,* 2010; this study), Guntur (Edwards, 1990; Sendjaja *et al.,* 2009), Papandayan (Sendjaja *et al.,* 2009; this study), Patuha (this study) and Galunggung (Sendjaja *et al.,* 2009; Turner & Foden, 2001; this study). **(d)** Shows Kelut against Central Java data from Slamet (Vukadinovic and Sutawidjaja, 1995), Ungaran (Claproth, 1989), Merbabu (Handley *et al.,* 2011), Merapi (Gertisser and Keller, 2003), and Sumbing (this study).

N-MORB Normalised Multi-Element Diagrams

39
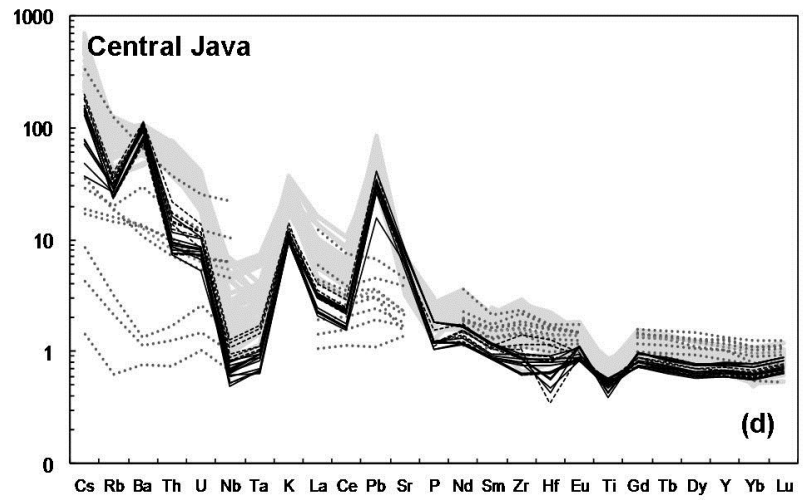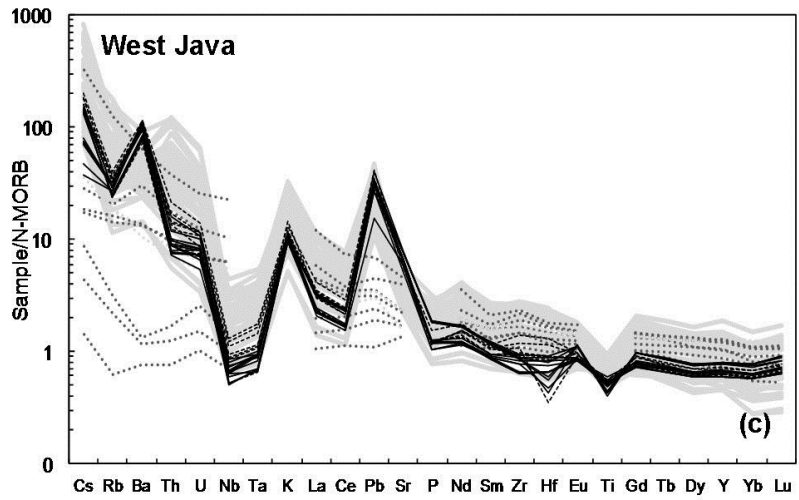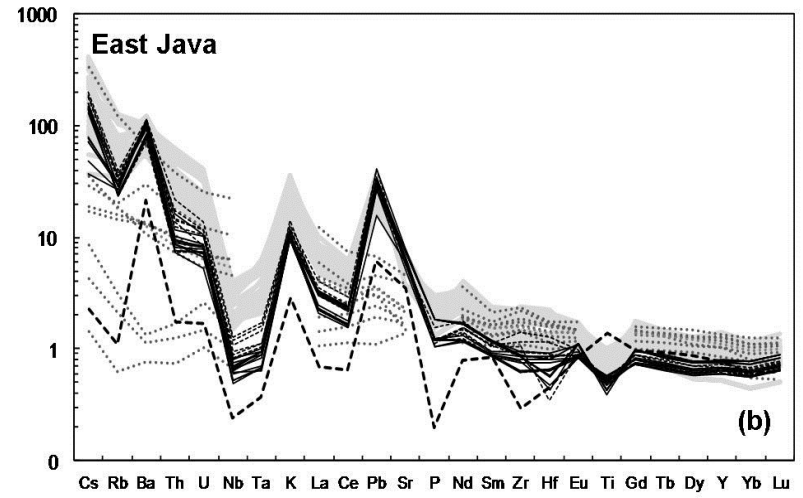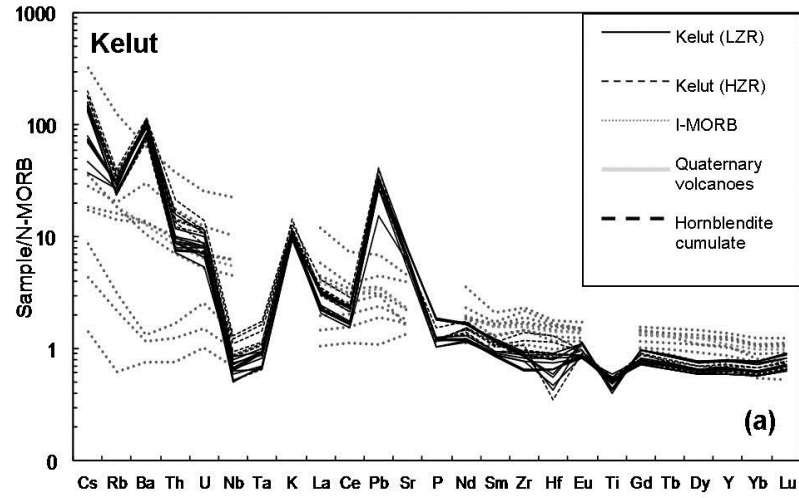
Chondrite-Normalised REE Diagrams
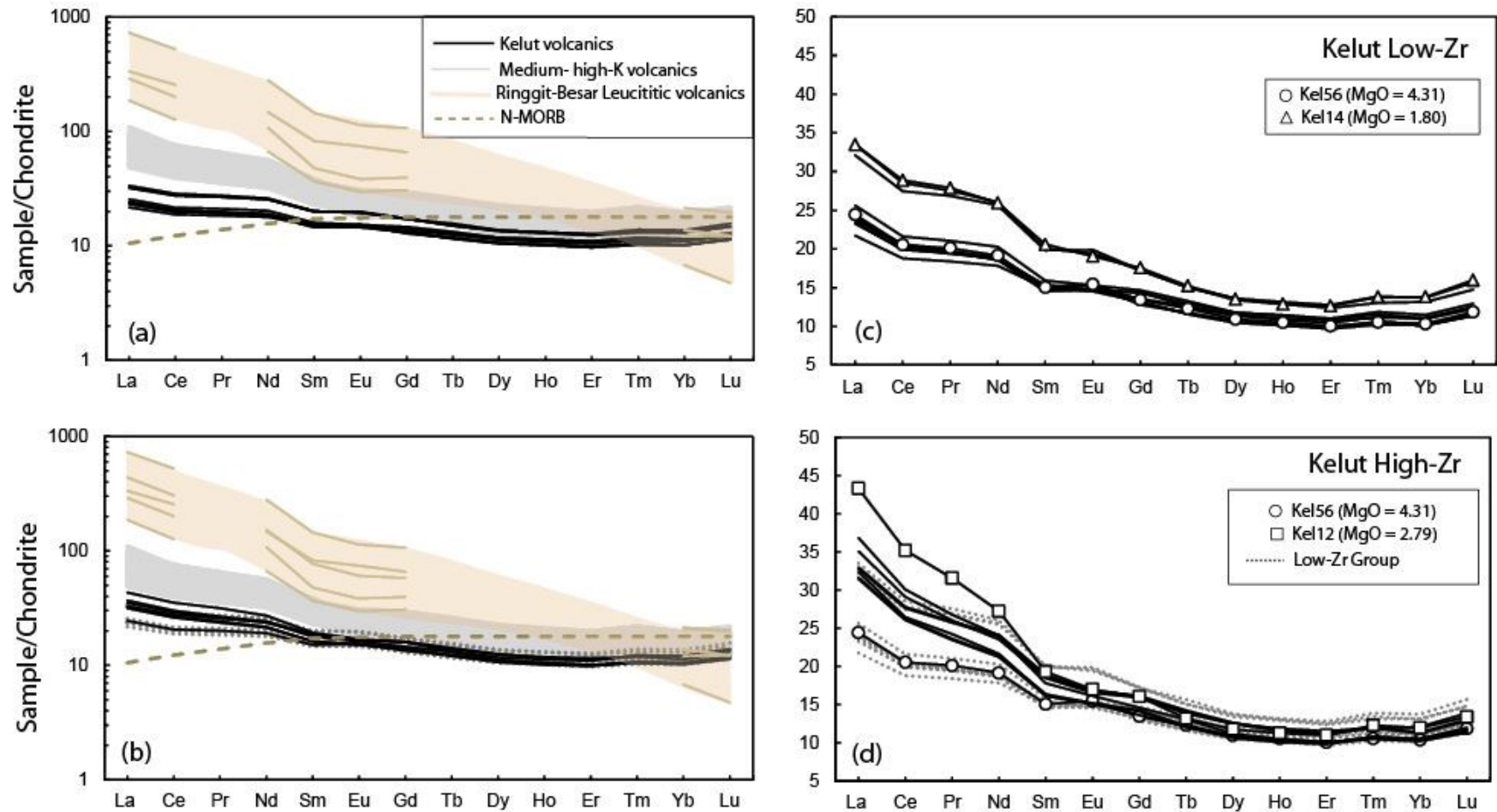
Fig. 2.13. Chondrite-normalised REE plots for **(a)** and **(c)**, the Kelut low-Zr group; and **(b)** and **(d)** the Kelut high-Zr group. Figures **(a)** and **(b)** include other data from east Java (references as for figure 2.6). The symbols in figures **(c)** and **(d)** show the most primitive and most evolved samples within the groups.

2.5. Discussion

2.5.1. Magmatic differentiation in the crust: constraints from cumulate xenoliths

In recent years the role of amphibole in the evolution of arc magmas has become increasingly important in modelling processes which operate within the crust. The widespread occurrence of amphibole-rich plutonic rocks and xenoliths suggests that crystallisation in deep- to-mid crustal levels is prevalent beneath island arcs (Davidson *et al.,* 2007; Alonzo-Perez *et al.,* 2009; Larocque and Canil, 2010; Davidson and Wilson, 2011; Tiepolo *et al.,* 2011).

The presence of amphibole in the lavas and cumulates at Kelut suggests that it is an important mineral phase during the differentiation of magmas. Both rock suites identified at Kelut appear to converge towards a common parent (or source) at higher MgO, and most major and trace element compositions project back towards the hornblendite cumulate. It is therefore important to establish if a co-genetic relationship exists between the hornblende-rich cumulates and basaltic andesite lavas and hence if the former was removed during a liquid line of decent. To understand the controls on differentiation beneath Kelut three approaches are taken here:

1) Trace-element modelling of the cumulate rocks.

2) Least Squares modelling of all mineral phases in the lavas.

3) Trace-element modelling of the lavas using the Rayleigh fractionation equation.

2.5.1.1. Trace-element modelling of the cumulate rocks

The first aim is to identify whether amphibole was removed during differentiation. This can be achieved using the hornblendite cumulate for which it can be assumed has a similar bulk-rock composition to a single amphibole (because it is primarily composed of it). Experimental studies show that Fe/Mg partitioning between amphibole and basaltic melt ($Kd^{amph/liq}$) ranges between 0.29 and 0.47, with an average of 0.38 (Sisson and Grove, 1993b; Pichavant and Macdonald, 2007; Alonzo-Perez *et al.,* 2009; Larocque and Canil, 2010). By adopting this approach (i.e. cumulate $Mg\#/Kd^{amph/liq}$ Mg#) it can be calculated that the Xmg of the melt in equilibrium with the hornblendite is ~ 0.48.

Figure 2.14 shows the calculated composition of melt in equilibrium with the hornblendite at an Xmg of 0.48. Kelut lavas with Xmg values between 0.46 and 0.49 are included for comparison, as is the whole-rock hornblendite. Trace element concentrations from the cumulate are normalised to experimentally determined $Kd^{amph/liq}$ coefficients from Tiepolo *et al.* (2007) at 1015°C and 1.4 Gpa which appears to be a good estimate for basaltic-andesite liquids. Because the hornblendite does contain some interstitial plagioclase, only trace elements whose budget will be largely controlled by amphibole are used (e.g. the HFSE and mid- heavy REE). Elements such as Sr, La and Eu are more likely to be affected by the plagioclase.

There is an excellent correlation between the calculated melt and the basaltic-andesite lavas with an Xmg ~ 0.48. This suggests that the parental melts at Kelut where in equilibrium with the hornblendite. It is likely that the inter-cumulus plagioclase between the cumulate hornblende crystals represents trapped residual melt. This provides strong evidence for a co-genetic relationship between primitive melts and the cumulate.

The gabbro cumulates do not show evidence for a significant influence on magmatic evolution which is not a surprise considering the lack correlation between these cumulates and the lavas on differentiation plots (see figures 2.7-2.11). Amphibole-rich cumulates typically contains less silica than gabbroic (ol-cpx-plag) assemblages and much lower Ni and Cr concentrations. As a result, the removal of the hornblende is effectively more efficient at driving residual liquids towards more evolved compositions (e.g. Davidson *et al.,* 2007).

2.5.1.2. Least Squares modelling

Now that amphibole has been shown to have a significant effect during crystal fractionation within the deep crust, it is important to quantify the additional mineral phases which may have been removed, or added, during differentiation. The phenocrysts observed in almost every sample were plagioclase, clinopyroxene, orthopyroxene and titanomagnetite; a common mineral assemblage from arc magmas from Java (Handley, 2006). Low concentrations of compatible elements (Ti, Fe, Mg, Ni, Cr, V and Sc) would suggest that removal of these minerals may have had a significant effect on magma compositions. In an attempt to quantify this, an XLFRAC least squares model (after Stormer & Nicholls, 1978) was applied to major element and mineral concentrations to determine the probability of

Primitive-Mantle Normalised Multi-Element Diagram
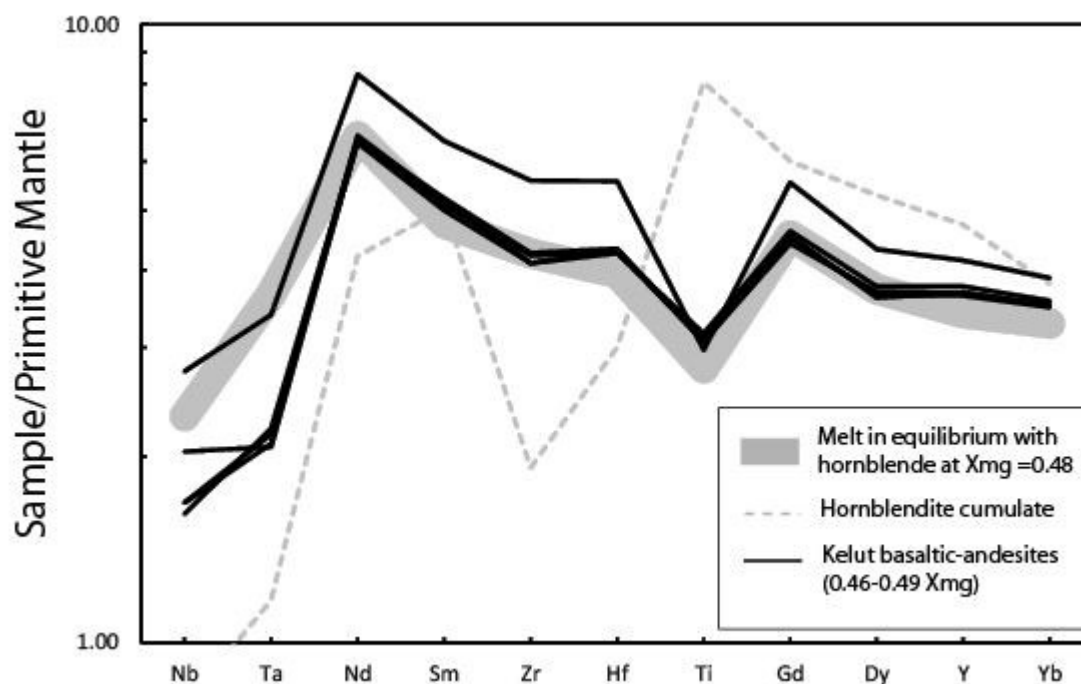
Fig. 2.14. Chondrite normalized multi-element plot showing a calculated melt from the hornblendite at an Xmg of 0.48 (assumes that whole rock is similar to one hornblende). Concentrations were calculated using the values in table 5.1. Note the similarity between the melt (grey line) and the basaltic-andesite lavas from Kelut with Mg# ranging from 46 to 49. Similarity between melt and magmas at the same Xmg suggests the melt was in equilibrium with the cumulate in the crust.

Table 2C. Model Parameters

	Hornblendite (a)	Kd$^{amph/liq}$ (b)	Calculated melt (c)	Kel56 (d)	Kel50	Kel40	Kel51	Kel48
Mg#	58.72		48.00	49.20	47.31	46.94	46.88	46.61
Nb	0.56	0.34	1.66	1.20	1.96	1.20	1.15	1.45
Ta	0.05	0.32	0.15	0.09	0.14	0.09	0.09	0.09
Nd	5.71	0.64	8.92	8.94	11.23	8.69	8.82	8.78
Sm	2.24	1.06	2.11	2.30	2.88	2.22	2.32	2.26
Zr	21.46	0.45	47.69	45.95	62.56	46.02	47.80	47.32
Hf	0.93	0.76	1.22	1.32	1.72	1.33	1.34	1.32
Ti	10475.76	2.90	3612.33	4109.30	3861.15	4035.08	3983.28	3992.15
Gd	3.58	1.32	2.71	2.76	3.30	2.69	2.64	2.71
Dy	3.90	1.42	2.75	2.78	3.19	2.68	2.72	2.66
Y	21.55	1.39	15.51	17.15	18.88	16.56	16.70	16.75
Yb	1.88	1.16	1.62	1.76	1.92	1.72	1.74	1.72

Table 2C. Values used in modelling. Solid/liquid partition coefficients for amphibole determined experimentally (Tiepolo *et al.,* 2007, 2011) at 1015°C and 1.4 GPa. Primitive Mantle values after (Sun and McDonough, 1989).

producing final (daughter) magma composition from an initial (parent) magma. Daughter compositions can be derived by either adding, or subtracting mineral phases, which, in a good solution minimises the $\sum r^2$ to values typically < 0.5.

Results of the modelling are shown in in Table 2D. For most of the models, Kel56, the least evolved sample analysed, was used as a parent composition for both series. However, models were also produced between the subdivisions highlighted previously. For example, using an intermediate basaltic-andesite as a parent composition opposed to a mafic basaltic andesite. This is to identify whether the trends observed between compositions from the LZR and HZR represent two liquid lines of decent. The mineral phases used in the modelling included plagioclase, amphibole, clinopyroxene, orthopyroxene, and Fe-Ti oxide. Because of the lack of olivine in Kelut lavas it is assumed that it was removed at an earlier stage and therefore is not modelled.

The models all produced acceptable values of < 0.19 and agree with a fractional crystallisation sequence of plagioclase, amphibole, orthopyroxene, Fe-Ti oxide and clinopyroxene with a removal of ~ 30% of crystals to produce the andesite compositions from the mafic basaltic andesite (Kel56). As expected, amphibole was removed at an early stage. This is shown by the necessity to add a small amount of amphibole to successfully model an andesitic composition from an intermediate basaltic-andesite in the LZR Series, while models between the mafic basaltic-andesites and more evolved compositions require significant removal of amphibole.

2.5.1.3. Trace element modelling

The final aim is to identify whether the trace element variations between the LZR and HZR series can result from fractional crystallisation. For this purpose, the results from XLFRAC least squares models can be utilised to test trace element concentrations during fractional crystallisation by using the Raleigh fractionation equation defined as $C_l/C_o = F^{(D-1)}$, where C_l is the concentration of an element in the daughter (final) liquid, C_o is the concentration of an element in the parent (initial) liquid, F is the melt fraction remaining , and D is the bulk distribution coefficient. The degrees of crystallisation and phase proportions are used from the least squares analyses and distribution coefficients selected from the GERM database. Due to the ambiguity of some Kd values, particularly for amphibole, the same figures are

XLFRAC Least Squares Modelling Results for Kelut Magmas

Plag+amph+opx+Fe-Ti oxide+cpx

Model	Group	Parent (initial)	Daughter (final)	$\sum r^2$	Phases					Removed (%)	Added (%)	Total (%)
No.	Daughter	MgO (wt%)	MgO (wt.%)		plag	amph	opx	Fe-Ti oxide	cpx			
1	HZR (mafic BA)	Kel56 (4.31)	Kel50 (3.63)	0.19	-4.73	-1.15	-2.16	-2.16	-2.15	-12.35	0.00	-12.35
2	HZR (intermediate BA)	Kel56 (4.31)	Kel22 (3.07)	0.11	-8.73	-6.10	-3.63	-1.68	-0.68	-20.82	0.00	-20.82
3	HZR (Andesite)	Kel56 (4.31)	Kel12 (2.79)	0.06	-13.85	-8.00	-3.65	-2.44	-2.17	-30.11	0.00	-30.11
4	HZR (intermediate BA)	Kel26 (3.48)	Kel 22 (3.07)	0.03	-5.93	0.08	-2.34	-0.95	-0.61	-9.83	0.61	-9.22
5	HZR (Andesite)	Kel26 (3.48)	Kel12 (2.79)	0.01	-11.81	-2.04	-2.39	-1.81	-2.32	-20.37	0.00	-20.37
6	LZR (mafic BA)	Kel56 (4.31)	Kel45 (3.39)	0.04	-3.66	-3.90	-2.43	-0.31	-1.03	-11.33	0.00	-11.33
7	LZR (intermediate BA)	Kel56 (4.31)	Kel43 (2.64)	0.07	-9.00	-7.20	-5.30	-1.56	0.54	-23.06	0.54	-22.52
8	LZR (Andesite)	Kel56 (4.31)	Kel14 (1.80)	0.10	-13.72	-7.98	-6.79	-2.99	-1.76	-33.24	0.00	-33.24
9	LZR (intermediate BA)	Kel34 (2.83)	Kel43 (2.64)	0.00	-3.47	2.41	-2.23	-0.41	-0.40	-6.51	2.41	-4.10
10	LZR (Andesite)	Kel59 (2.12)	Kel14 (1.80)	0.03	-1.77	-0.69	-1.48	-1.48	0.91	-5.42	0.91	-4.51

Table 2D. Results of least squares modelling. Small $\sum r^2$ values indicate good agreement between model and daughter composition. BA = basaltic andesite, (%) removed = sum of the mineral phases removed during fractional crystallisation between parent and daughter compositions, (%) added = sum of the mineral phases added during fractional crystallisation between parent and daughter compositions. Plag = plagioclase, amph = amphibole, opx = orthopyroxene, Fe-Ti oxide = titanomagnetite, cpx = clinopyroxene.

Trace Element Modelling
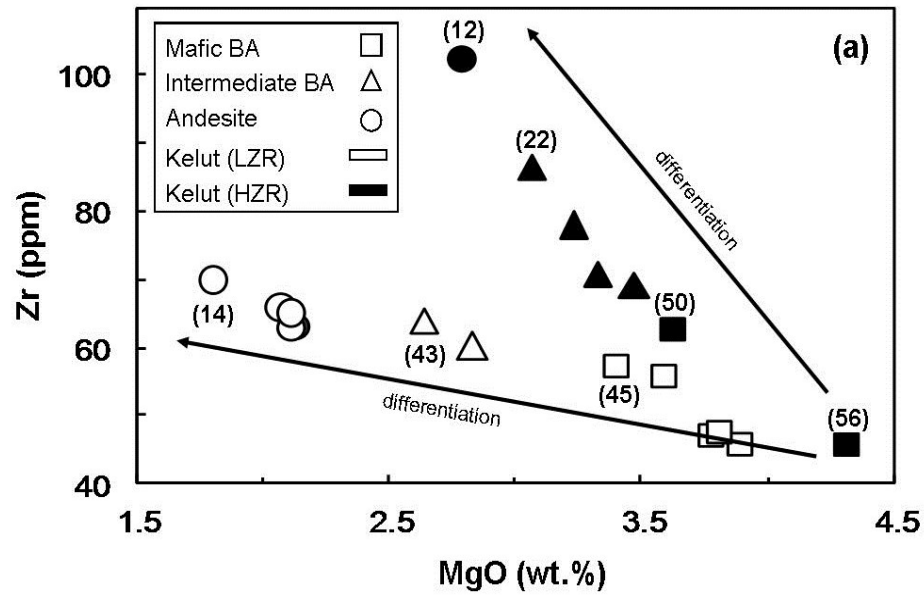
Table 2E.

	plagioclase	amphibole	orthopyroxene	Ti-Fe Oxide	clinopyroxene
Rb	0.113	0.400	0.022	0.150	0.033
Ba	0.440	0.460	0.072	0.183	0.038
Th	0.059	0.500	0.048	0.235	0.035
K	0.178	0.960	0.017	0.045	0.010
Sr	2.512	0.510	0.048	0.110	0.139
Y	0.076	0.900	0.343	0.322	0.860
Yb	0.052	0.200	0.423	0.218	0.661
U	0.112	0.100	0.008	0.110	0.016
La	0.183	0.045	0.068	0.150	0.130
Nb	0.275	0.800	0.351	0.837	0.168
Zr	0.098	0.700	0.061	0.727	0.197
Hf	0.031	1.533	0.101	0.353	0.297
Ta	0.057	0.380	0.079	1.113	0.123
Ti	0.052	7.960	0.423	9.500	0.350

46
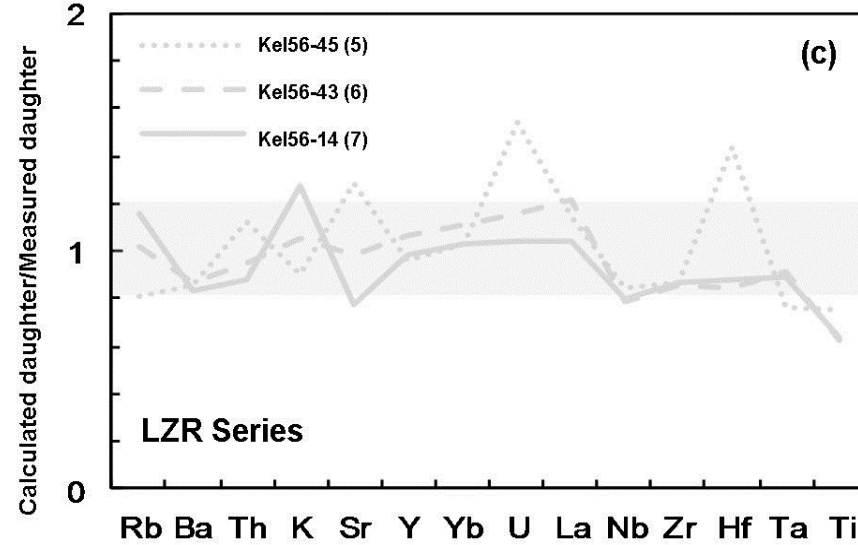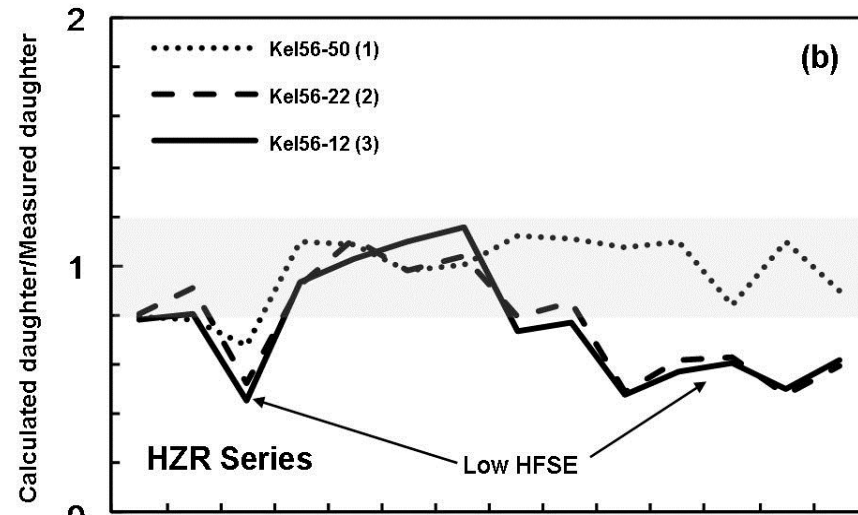
Fig. 2.15. (a) Shows the trends produced by differentiation for the HZR and LZR series and the samples used in the modelling (in brackets). **(b)** Shows the calculated values for trace element modelling of the HZR series. The grey shading shows a limit for acceptable results. Note that the HFSE are particularly low. **(c)** Shows trace element modelling results for the LZR series. Note that most calculated concentrations fall within the grey shaded area. **Table 2E** Shows the Kd values used during modelling.

used as for the cumulate modelling above (Tiepolo *et al.,* 2007, 2011).

The results of forward modelling are shown in fig. 2.15. Models were essentially the same daughter and parent compositions as for the least squares models. These are shown in fig. 2.15*a*. To produce an acceptable result the calculated daughter compositions (C$_l$), must be close to the concentrations which have been measured for that rock; and therefore plot close to 1 on the normalised plot. Most of the LZR group are within 20% of this line, and where outside of this range the elements are generally very low in concentration (e.g. U and Hf), and more susceptible to discrepancies between calculated and measured compositions.

In contrast to the LZR, the HZR Series show very poor agreements for Th, Nb, Zr, Hf, Ta and Ti. This is particularly the case for models involving the mafic basaltic-andesite parent (Kel56) and the more evolved compositions (Kel22 and Kel12) from that group. A systematic underestimation of these elements suggests that they have been enriched by a process that was not simple fractional crystallisation.

To summarize the models:

1) The basaltic andesite magmas were co-genetic with hornblende deep in the crust, before early fractional crystallisation removed the amphibole and stored them as cumulates.

2) Fractional crystallisation of plagioclase, amphibole, orthopyroxene, titanomagnetite and clinopyroxene are responsible for driving differentiation in the LZR Series.

3) Simple fractional crystallisation cannot explain the elevations in some trace element concentrations in the HZR Series, particularly some of the HFSE and Th. These magmas require an additional process to explain their different chemistry.

2.5.2. Assimilation of the arc crust

It is clear that open-system processes play a fundamental and important role in the petrogenesis of arc magmas (e.g. Davidson *et al.,* 2005). These processes are becoming more evident on Java through mineral and whole-rock studies (Gasparon and Varne, 1998; Reubi *et al.,* 2002; Chadwick *et al.,* 2007; Handley *et al.,* 2008; Deegan *et al.,* 2010). Furthermore, most, if not all, rocks show strong evidence for magma-crystal disequilibrium which is a likely result of open-system behaviour.

Trace element modelling showed that enrichments in some elements with differentiation in the HZR group are not caused by fractional crystallisation alone. Therefore, the higher concentrations of Th, Nb, Zr and Hf may have been inherited from a contaminant. A particularly useful way to identify crustal contamination in magmas is to plot a number of radiogenic isotopes (e.g. $^{87}Sr/^{86}Sr$, $^{143}Nd/^{144}Nd$, $^{206}Pb/^{204}Pb$ and $^{176}Hf/^{177}Hf$) against indices for differentiation (e.g. SiO_2, MgO and Mg#). This is because isotope ratio values will not be modified during 'closed system' processes such as fractional crystallisation (Handley *et al.,* 2007).

Figure 2.11 (*a-h*) shows isotope ratios for $^{87}Sr/^{86}Sr$, $^{143}Nd/^{144}Nd$, $^{206}Pb/^{204}Pb$ and $^{176}Hf/^{177}Hf$ in the LZR series do not change significantly with decreasing MgO. In contrast, isotope ratios in the HZR series magmas become higher for $^{87}Sr/^{86}Sr$ and $^{206}Pb/^{204}Pb$ and lower for $^{143}Nd/^{144}Nd$ and $^{176}Hf/^{177}Hf$. This suggests that crustal contamination has contributed to the chemistry of the HZR magmas, possibly in association with fractional crystallisation (AFC).

It is difficult to produce a quantifiable model for AFC in the HZR series magmas because the changes in isotope ratios are quite small. This suggests that either crustal contamination involved a second component with a similar composition to the HZR series magmas, or that only small quantities of the second component were assimilated. The second option is presented as the preferable model here because elevations in particular groups of elements such as the HFSE, Th and SiO_2 with MgO suggest that a detrital, terrigneous or acid volcanogenic contaminant would be most plausible. It is unlikely that another basic igneous rock or clay and carbonate sediment lithologies would produce such enrichments. Meta-sedimentary and plutonic xenoliths collected at Kelut suggest that some of the magmas have been contaminated in the upper crust probably within the deep sediment filled basin beneath the volcano (Smyth *et al.,* 2007, 2008).

2.5.3. Mantle source components

Having examined the effects of differentiation and how the lavas at Kelut have been modified in the crust, the mantle source components can be identified. For most arc magmas this usually involves a combination of the mantle wedge, slab-derived fluids and/or sediments, and a lithospheric component beneath continental arcs (McCulloch and Gamble, 1991; Saunders *et al.,* 1991; Plank and Ludden, 1992).

One way to assess the relative contributions of source and subduction components is to utilise trace-element ratios which minimise the effects of fractional crystallisation and partial melting and can therefore highlight 1) variations in mantle sources, 2) fluid enrichments, and 3) sediment enrichments. Contributions of these specific components can be complicated further through mantle fertility, the composition of the subducting plate including the overlying sediment, and changes in slab dynamics. To address these issues, the petrogenesis of an individual volcano must also be placed in the context of the variations along the arc, and if possible in comparison to other arcs (Churikova *et al.,* 2001).

On Java, there has long been dispute over the relative significance between contributions from the crust and those from the subducting plate (Wheller *et al.,* 1987; Hilton and Craig, 1989; Gasparon *et al.,* 1994; Gasparon and Varne, 1998; Turner and Foden, 2001). Furthermore, while some authors argue for a homogeneous subduction component (Edwards *et al*., 1993), others suggest variations in the amount and type of sediment subducted between west Java and east Java (Handley, 2006). In order to clarify this, trace-element ratio and isotopic variations at Kelut will be compared with those from other volcanoes along Java and included in the discussion.

Selected trace-element ratios for the two Kelut Series and the hornblendite cumulate are shown in table 2F (top row), together with upper and lower limits from west Java, central Java, east Java, and the ultrapotassic associations from Muriah and Ringgit-Besar. The data from Muriah and Ringgit-Besar only include the HK and EK groups which represent mantle compositions which have not been modified in the crust (Edwards, 1990). Data sources are given in fig. 2.12 and table 2F. Only the ratios from Kelut LZR will be discussed here because of contributions from the crust in the HZR Series.

As highlighted in section 2.4, the LILE show significant enrichment relative to the other elements. This is emphasised by the elevated Ba/La, Ba/Th and Sr/Nd ratios compared to the

Trace Element Ratios associated with Geodynamic changes
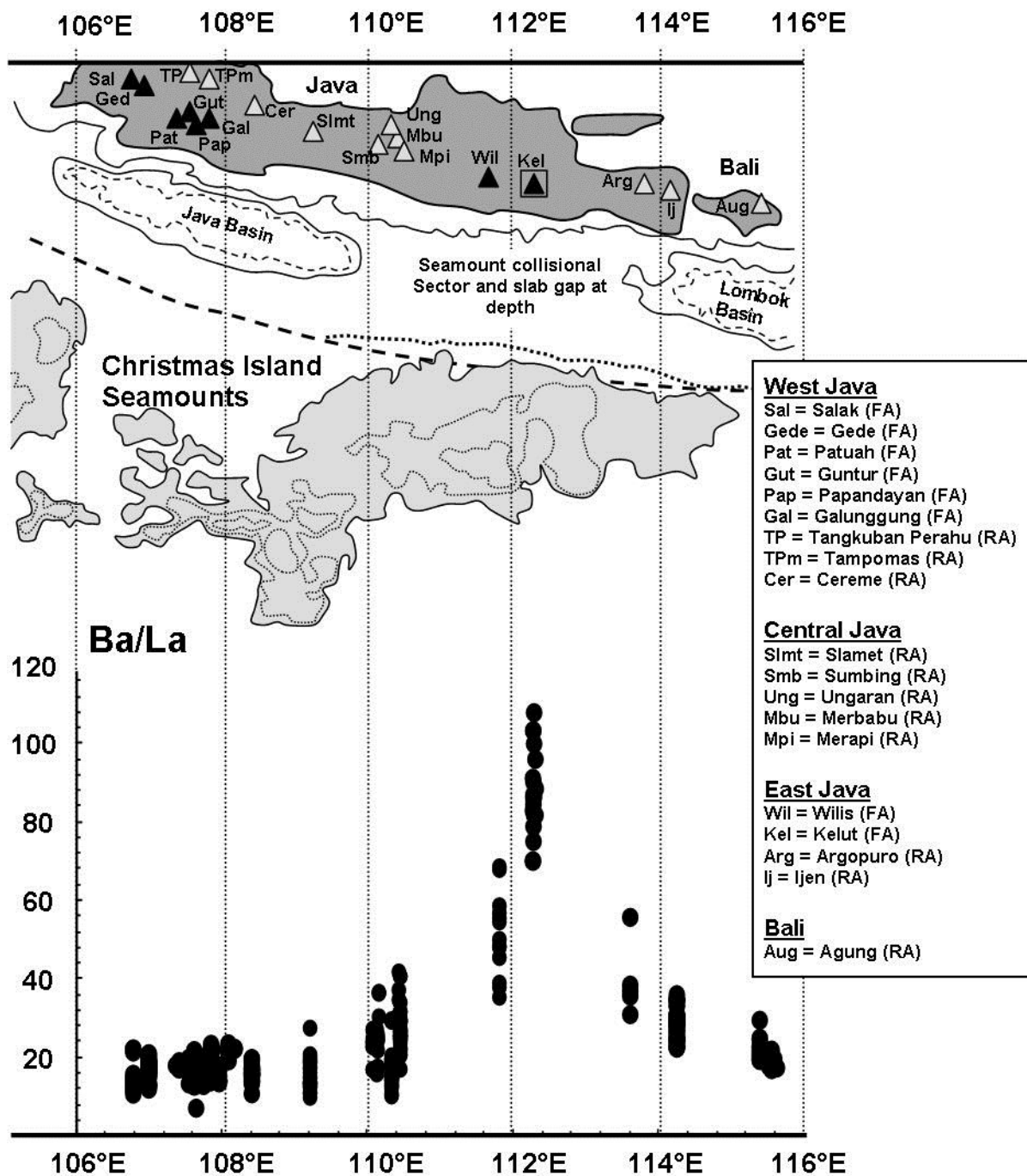
Fig. 2.16. Schematic diagram showing the variation of Ba/La ratios in volcanoes from Java and Bali against a longitudinal section of the arc and offshore seamount provinces. Values along the x-axis refer to longitude coordinates. Note a significant correlation between elevated Ba/La and the deformation to the Java fore-arc which peaks at Kelut. This point represents the central region of fore-arc deformation and subduction erosion resulting from collision of the Roo Rise. Figure modified from (Kopp *et al.,* 2006). Data sources from Java volcanoes as for fig. 2.12. Includes data from Agung (Bali) analysed in this study. Volcanoes located at WBZ depths < 140 km are shown in black, and those > 140 km in grey (after Syracuse and Geoffrey, 2006).

Table 2F. Trace Element Ratios for Java Volcanoes, Potential Source Components, sediments, and Oceanic Arc Volcanoes

Java

	Kelut (LZR)	Kelut (HZR)	Hornblendite	West Java	Central Java	East Java	S. Mountains	High-K (Muriah)	High-K (EK Ringgit)
Ba/La	87 - 108	70 - 87	77	7 - 24	10 - 42	36 - 69	18	3 - 16	23 - 76
Ba/Th	356 - 668	277 - 514	639	20 - 160	27 - 115	110 - 307	151	7 - 88	184 - 452
Sr/Nd	56 - 70	41 - 68	55	5 - 42	12 - 52	27 - 51	11	13 - 30	13 - 27
Rb/Ba	0.02 - 0.03	0.03	-	0.07 - 0.29	0.02 - 0.20	0.03 - 0.08	0.04	0.1 - 0.65	0.05 - 0.13
Zr/Nb	34 - 41	31 - 38	38	9 - 42	10 - 35	24 - 46	59	1 - 8	2 - 7

Sources and sediments

	I-MORB	I-MORB (DUPAL)	N-MORB	I-OIB	AOC	CSS	CSS (av.)	SSS	SSS (av.)
Ba/La	1 - 32	13 - 20	1 - 13	9 - 11	6 - 44	0.52 - 73	14	1 - 107	25
Ba/Th	42 - 94	172 - 332	20 - 130	46 - 278	126 - 778	12 - 288	60	15 - 585	82
Sr/Nd	9 - 37	11 - 49	7 - 18	4 - 33	10 - 33	45 - 97	75	1 - 12	5
Rb/Ba	0.03 - 0.37	0.04 - 0.07	0.09 - 0.11	0.02 - 0.14	0.1 - 2.12	0.05 - 0.32	0.14	0.03 - 0.36	0.10
Zr/Nb	11 - 75	10 - 19	8 - 79	5 - 15	47 - 71	1 - 18	15	8 - 27	12

Oceanic (fluid-dominated) Arcs

	Tonga (FA)	Tonga (BA)	Izu-Bonin (FA)	Izu-Bonin (RA)	Mariana (FA)	New Britain (FA)	New Britain (BA)	Kamchatka (FA)	S. Sandwich
Ba/La	29 - 139	7 - 9	28 - 115	20 - 42	29 - 60	32 - 86	3 - 16	25 - 75	28 - 76
Ba/Th	254 - 1175	128 - 142	293 - 1027	104 - 257	294 - 673	396 - 888	35 - 201	197 - 752	103 - 920
Sr/Nd	26 - 116	14 - 18	17 - 73	3 - 39	18 - 49	31 - 98	7 - 12	12 - 46	9 - 58
Rb/Ba	0.02 - 0.10	0.06 - 0.10	0.02 - 0.06	0.05 - 0.11	0.04 - 0.08	0.03 - 0.12	0.07 - 0.22	0.03 - 0.11	0.02 - 0.14
Zr/Nb	20 - 311	23 - 31	73 - 130	11 - 45	42 - 86	60 - 124	16 - 18	25 - 103	39 - 168

Table 2F. Selected trace element ratios for volcanoes in Java, Indian Mid- Ocean Ridge Basalts (I-MORB), Atlantic and Pacific Mid- Ocean Ridge Basalts (N-MORB), Kerguelen Ocean Island Basalt (I-OIB), Altered Oceanic Crust (AOC), Calcareous Sunda Sediment (CSS), Silicic Sunda Sediment (SSS) and selected oceanic arcs (FA = Front Arc positions, RA = Rear Arc and BA = Back-Arc). Data sources for west Java, central Java and east Java as for fig. 2.12. Southern Mountains data from this study, Muriah high-K (Edwards *et al.,* 1991), Ringgit-Besar (EK) (Edwards *et al.,* 1994), I-MORB (Price *et al.,* 1986; Rehkamper and Hofmann, 1997; Chauvel and Blichert-Toft, 2001; Janney *et al.,* 2005;), I-MORB (DUPAL) (Janney *et al.,* 2005), N-MORB (Chauvel and Blichert-Toft, 2001), I-OIB (Yang *et al.,* 1998), AOC (Staudigel *et al.,* 1995), CSS and SSS (Gasparon and Varne, 1998; Othman *et al.,* 1989; Plank and Ludden, 1992), Tonga (Turner *et al.,* 1997), Izu-Bonin (Straub *et al.,* 2010; Taylor and Nesbitt, 1998), Mariana (Elliot *et al.,* 1997), New Britain (Woodhead *et al.,* 1998), Kamchatka (Churikova *et al.,* 2001), and South Sandwich (Pearce *et al.,* 1995). See text for discussion.

rest of Java. Figure 2.16 shows the along-arc variations of Ba/La from west Java to Bali and a significant rise in the ratio from ~ 110°E, which "climaxes" at Kelut and "falls back" to the west Java values at ~ 115°E. None of these values show correlation with SiO_2 or MgO which suggests that it is a source characteristic. Furthermore, the changes show a remarkable resemblance to the limits of trench deformation caused by subduction of the Roo Rise, and with that the associated change in mass transfer between accretion and erosion from ~ 109°E to ~ 115°E (Kopp *et al.,* 2006; Kopp, 2011; Shulgin *et al.,* 2011). The seismic data also shows that the gap in the subducting plate between ~ 250 km and ~ 550 km depth is also most evident at ~ 113°E (Widiyantoro *et al.,* 2011).

Elevations in the Ba/La ratio are commonly attributed to an aqueous fluid contribution from the slab (McCulloch and Gamble, 1991). Experimental data have shown that Ba, K, Sr, Pb and U are highly mobile in oxidising aqueous fluids whereas HFSE (Nb, Ta, Zr and Hf) together with Th and REE are thought to be much less readily transported in fluids (Tatsumi *et al.,* 1986; Brenan *et al.,* 1995; Keppler, 1996). Hermann *et al.* (2006) suggests that at 15-25 kbar and 500-600°C, aqueous fluids are liberated from eclogite facies ultramafic rocks. They propose that these fluids only release moderate amounts of LILE, Sr and Pb and that a second dehydration phase at 700-750°C (and subarc depths of 100-150 km) is required to elevated LILE element mobilities within the subducted oceanic crust. The conclude by suggesting that above 750°C the subduction component is most likely to be from a hydrous melt.

A strong fluid signature is common of many oceanic arcs were flux rates are better constrained due to their lack of thick crust and lithosphere (e.g. Elliot *et al.,* 1997; Lin *et al.,* 1990; Pearce *et al.,* 2005; Churikova *et al.,* 2001). This is particularly true for volcanoes situated at the front of volcanic arcs where presumably shallower depths to the subducting slab favour a component rich in aqueous fluids at lower temperatures.

Table 2F shows selected trace-element ratios for a number of oceanic arcs and I-MORB, Indian-type Ocean Island Basalt (Kerguelen OIB), AOC, and Silicic and Calcareous Sediment (SSS and CSS) analysed from ocean drilling projects offshore Java. I-MORB (DUPAL) refers to a type of enriched I-MORB which will be discussed at a later point. FA, RA and BA refer to the volcanoes relative position on the arc, so in trimodal volcanic suites these are front-arc, rear-arc and back-arc respectively. The table shows the similarity between ratios such as Ba/La, Ba/Th and Sr/Nd from the Kelut LZR series and most and volcanoes situated in the front-arc at oceanic arcs such as Tonga, New Britain and Mariana. These ratio values appear to be too high to be explained by a by a sediment melt.

In an attempt to map specific slab contributions in the Mariana arc Pearce *et al*. (2005) suggested that the high Ba/Th characterises the lower-temperature fluid component because both elements are mobilised in melts but only Ba is mobilised in fluids. At higher temperatures, deeper subduction components are characterised by sediment melts which mobilise both Ba and Th the wedge. A similar conclusion was suggested for the Banda Arc (Vroon, 1992).

If a similar hypothesis were applied here, it would imply that across Java a more fluid-dominated component is apparent between ~ 110°E and 115°E, "climaxing" around the longitude of Kelut at between 112°E and 113°E (fig. 2.16). There are a number of strong arguments for this. Firstly, Ba concentrations at Kelut are no higher than for other volcanoes along Java, but Th and La are lower. One reason for this could be a smaller sediment contribution (which would elevate Th and La). Also, the bathymetric data of Kopp *et al*. (2006), Kopp (2011), and Shulgin *et al*. (2011) suggest that very little sediment is going down the trench in this part of Java. There is clearly a strong correlation between higher Ba/La ratios, the collision of the Roo Rise and a seismic gap in the subducting plate at depth.

A distinctive relationship between elevated LILE/HFSE ratios and the nature of the mantle wedge has been identified for most of the oceanic arcs listed in table 2F (e.g. Pearce and Parkinson, 1993; Woodhead *et al.,* 1993, 1998; Turner *et al.,* 1997). Correlations between ratios such as Ba/La and Zr/Nb have been used to show that fluid contributions are best developed in magmas which are chemically depleted (Hawkesworth *et al.,* 1993; Macpherson *et al.,* 2003). Therfore, an evaluation into the nature of the mantle wedge along Java is a pre-requisit to understanding the cause of these trace-element ratio patterns.

2.5.3.1.   Pre-subduction mantle characteristics and partial melting

Some oceanic arcs such as Tonga and New Britain show significant mantle depletion, with HFSE concentrations lower than MORB (Ewart and Hawkesworth, 1987; Woodhead *et al*., 1998). Most authors suggest that this type of depletion takes place through a previous melt extraction (Pearce and Parkinson, 1993; Woodhead *et al.,* 1993; Pearce, 2005). One particular method through which this is though to be accomplished is by extracting a melt fraction from the back of the arc where the remaining refractory material is transported to the melting column by convection. Therefore, back-arc spreading is inexorably linked to depletion of incompatible trace elements in many environments (Woodhead *et al.,* 1993). Table 2F highlights the difference in trace-element ratios between front-arc and back-arc for Tonga, Izu-Bonin and New Britain. In each case the front arc magmas contain higher Ba/La and Zr/Nb ratios than the back-arc equivalents.

Most continental arcs such as Sunda also show some evidence for spatial variations across the arc (Whitford and Nicholls, 1976; Stolz *et al.,* 1990; Edwards *et al.,* 1991; Edwards *et al.,* 1994), but with two significant differences to those from oceanic arcs. Firstly, the chemically 'enriched' nature of the ultrapotassic volcanoes behind the arc such as Muriah and Ringgit-Besar far exceeds those in oceanic settings (see table 2F). Secondly, the HFSE-depleted tholeiitic magmas associated with front arc volcanism in Tonga and New Britain (Woodhead *et al.,* 1998) is not apparent along the Sunda Arc. The most obvious reason for such a difference is the involvement of the lithosphere in the Sunda Arc (Varne, 1985; Edwards, 1990).

Model 1: Pearce and Parkinson (1993)

To test mantle fertility along Java, and ultimately identify if the elevations in Ba/La, Ba/Th and Sr/Nd at Kelut are linked to variations of the source, a model by Pearce & Parkinson (1993) is employed. For this purpose, the term 'depleted mantle' refers to fertility and previous extraction events, not variations between N-MORB and I-MORB. The model utilises a number of elements not thought to be significantly affected by subduction and ranks them in order of compatibility. During melting, the Very Highly Incompatible elements (VHI) are the first to leave the mantle and enter the melt; thereby depleting the residue in these elements. A subsequent melting event will therefore be lower in VHI elements than the group of Highly and Moderately Incompatible (HI and MI) elements. Conversely, enriched

Source Variation Diagrams
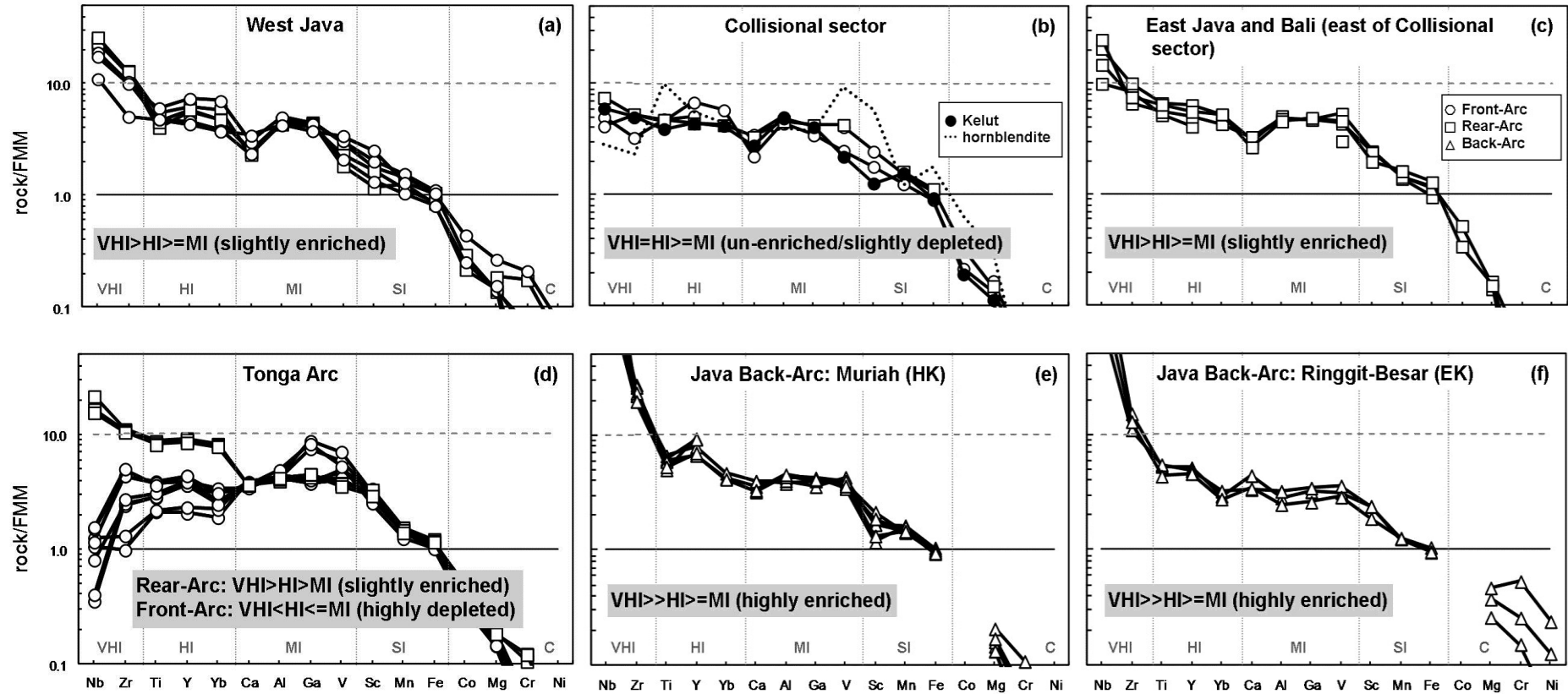
Fig. 2.17. (a-f) The results of source enrichment modelling after Pearce and Parkinson (1993). All rocks used in modelling > 5 wt.% MgO to reduce effects from mineral fractionation and normalised to fertile MORB mantle (FFM). FA = Front Arc volcanoes (circle symbols), Ra = Rear Arc volcanoes (square symbols) and BA = Back Arc volcanoes (triangle symbols). Elements used are thought to be relatively immobile in aqueous fluids and can be categorised as Very Highly Incompatible (VHI), Highly Incompatible (HI), Moderately Incompatible (MI), Slightly Incompatible (SI) and Compatible (C) in FFM. Volcanoes used in modelling include; West Java: (RA) Gede (Handley *et al.,* 2010), Tangkuban Perahu (this study), Cereme (Edwards, 1990); (FA) Guntur low-K (Edwards, 1990), Patuha (this study) and Galunggung (this study); Collisional sector (includes those volcanoes inside the area of forearc deformation from fig. 2.16.): (RA) Merbabu (Handley *et al.,* 2011); (FA) Wilis (Claproth, 1989), Southern Mountains (this study), **Kelut** and **hornblendite cumulate** (this study); East Java and Bali: (RA) Tengger Volcanic Field (van Gerven and Pichler, 1995), Argopuro (Edwards *et al.,* 1994), Ijen (Handley *et al.,* 2007) and Agung (this study); Tonga Arc (Turner *et al.,* 1997); Muriah HK (Edwards *et al.,* 1991), Ringgit-Besar (Edwards *et al.,* 1994). Criteria in the grey shaded areas after Pearce and Parkinson (1993). See text for discussion.

sources will have VHI>>HI. Different degrees of partial melting can also affect the model, with smaller melt fractions represented by steeper profiles. In this scenario VHI>HI>MI>SI>C for small degrees of partial melting; however, this is unlikely to be the case for arc magmas where larger degrees of melt and therefore flatter profiles are expected (Pearce and Parkinson, 1993).

To test for variations both across and along the arc, volcanoes are categorised into the regions: west Java (low LILE/HFSE volcanoes between 106°E and 110°E); collisional sector (which refers to volcanoes between 110°E and 114°E with significant elevations in LILE/HFSE, including Kelut); and the east Java/Bali sector (low LILE/HFSE volcanoes between 114°E and 116°E). For this purpose, only volcanoes containing > 5 wt.% MgO are used, so that any effects of crystal fractionation are limited (with the exception of Kelut, although the hornblendite cumulate provides a good proxy for magmas compositions at ~ 12 wt.% MgO).

In order to identify spatial patterns across the arc, front-arc volcanoes have been assigned circle symbols, rear-arc volcanoes square symbols, and back-arc volcanoes triangle symbols. These controls are in accordance with the model of Hermann *et al*. (2006). For Java front arc volcanoes are situated between the 100-150 km transition (above the depth for hydrous melting) and should therefore be dominated by a fluid component. Volcanoes sitauted at WBZ > 150 km are classified as rear-arc, and the ultrapotassic volcanoes Muriah and Ringgit-Besar represent the back-arc. For perspective, Tonga back arc and front arc magmas are also shown in fig. 2.17. However, it must be stressed that these are not directly comparible with Java because the front arc volcanoes (Tofua and Tafahi) are situated considerably closer to the WBZ (between 57 and 89 km) than most Java volcanoes, although the backarc representative (Nivafo'ou) is within the range of Muriah and Ringgit-Besar (308 km compared with 370 and 200 km repectively).

A couple of significant points can be taken from these models. Under the criteria of Pearce and Parkinson (1993), volcanoes positioned in west Java and the east Java-Bali sector show similar element profiles. This suggests that mantle sources for these regions contain similar element concentrations and are slightly more fertile than FMM. The volcanoes positioned within the collisional sector all show lower concentrations of VHI elements. There are two possibilties for this; either the collision (and or the gap in the slab) is affecting the source compositions beneath these volcanoes, or it is just a reflection that most of these volcanoes

are situated in the front of the arc and so are slightly more depleted (c.f. Tonga). Figures 2.17 *(e)* and *(f)* show that the ultrapotassic volcanoes from Java are considerablty more enriched in VHI than the backarc island of Niuafo'ou. Therefore, while a similar process of backarc enrichment may be applicable in Java and Tonga there are clearly different source compositions involved.

Model 2: K-Zr/Nb relationships

In order to understand the nature of source variations in Java the relationship between mantle source depletion and enrichment must be constained. At this stage the term 'enrichment' just refers to elevated concentrations of a particular element relative to a MORB composition. The nature of the enrichment, either through a subduction component or a contribution from the lithosphere, will be discussed in the next section.

In this particular model poassium is used because of the well documented spatial relationship between potassium and position of the volcano relative to the trench and/or WBZ (e.g. Whitford and Nicholls, 1976), Although these generalised models have been disputed (Arculus and Johnson, 1978). In contrast the Zr/Nb ratio is often used as a proxy for previous melt extraction episodes and depletion of a MORB source because high values cannot be obtained through direct melting of this type of peridotite (Elliot *et al.,* 1997; Macpherson *et al.,* 2003).

Figure 2.18*a* shows K_2O against SiO_2 for six volcanoes which best represent source compositions in Java. This includes the Kelut LZR series and Galunggung from the front of the arc, Ijen and Argopuro from behind the arc front (but within the Quaternary volcanic arc) and Ringgit-Besar and Muriah from the back of the arc. Because the Kelut LZR series contain no samples with > 5 wt.% MgO, or < 50 wt.% SiO_2, the hornblendite cumulate has been added to show where less differentiated magmas may have project back to. Detailed studies on all of these volcanoes show that none of these volcanoes have been contaminated in the arc crust and in some cases (e.g. Galunggung, Muriah and Ringgit-Besar) contains mantle-like MgO, Ni and Cr contents (Edwards, 1990; Gerbe *et al.,* 1992; Handley, 2006). However, because only Galunggung is represented from outside of east Java it inhibits, to some degree, an evaluation of source variations along the arc in this model.

Figure 2.18*a* shows that at low SiO_2 (i.e. 45-50 wt.%) there is a clear distinction between

Source Modelling using SiO$_2$, K$_2$O and Zr/Nb Relationships
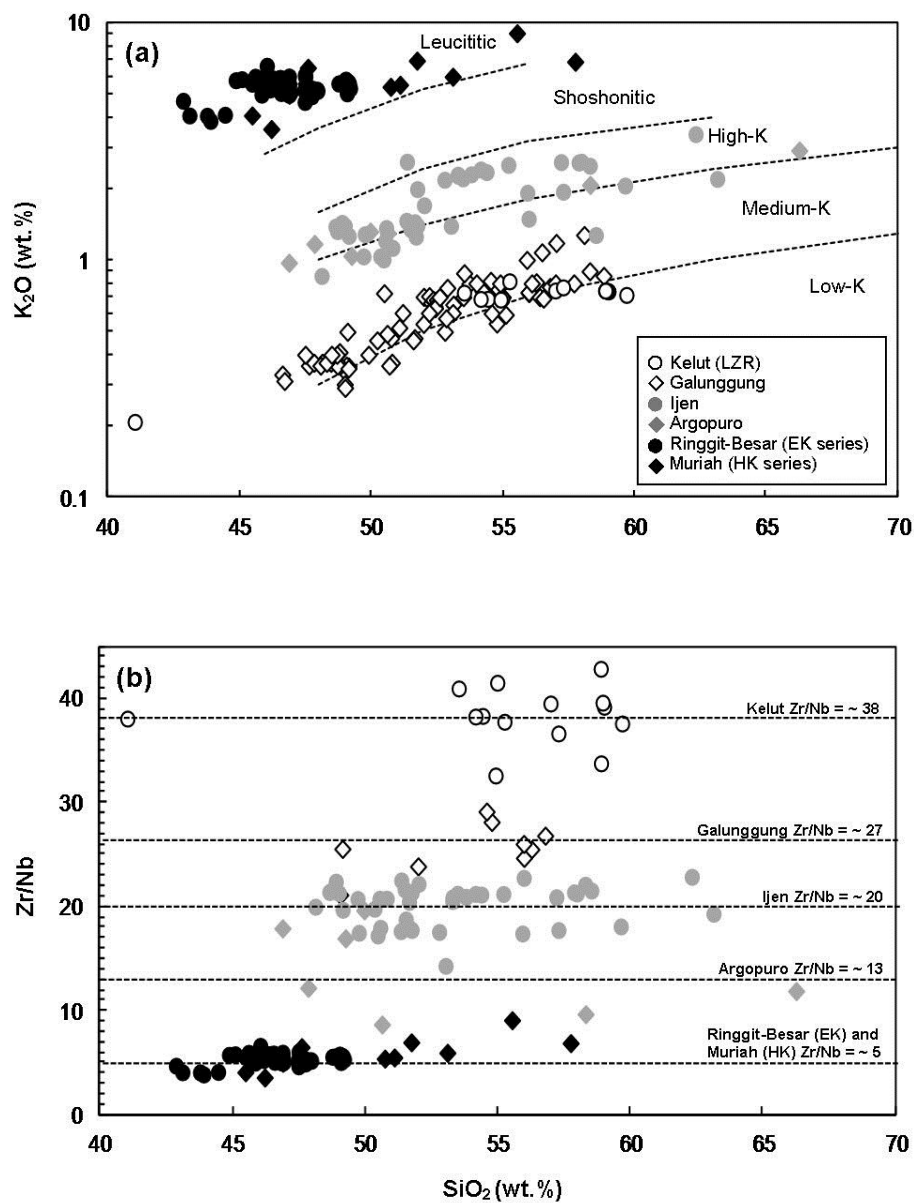
Fig 2.18. (a) Shows K$_2$O against SiO$_2$ for volcanoes which best represent source compositions. White symboles show volcanoes located in the front of the arc, grey symboles show volcanoes located behind the front of the arc, and black symboles show back arc volcanoes. Volcano data after Edwards (1990), Handley (2006) and this study. K$_2$O-SiO$_2$ subdivisions after Peccerillo and Taylor (1976) and Wheller *et al.* (1987). **(b)** shows Zr/Nb against SiO$_2$ for the same criteria. Note the difference between K$_2$O and Zr/Nb for these volcanoes. See text for discussion.

the volcano position and the K_2O concentration of the magmas. The subdivisions used are after Peccerillo and Taylor (1976) and Wheller *et al.* (1987) and show that Galunggung and Kelut (LZR series) contain low-medium-K affinities, Ijen and Argopuro contain high-K affinities and Ringgit-Besar (EK series) and Muriah (HK series) contain leucititic affinities. Based on potassium enrichment alone no other distinction can be made between the samples.

Figure 2.18*b* shows Zr/Nb for the same group of volcanoes. For this ratio, there is still a broad correlation between the groups of volcanoes; however, the Kelut LZR series magmas contain significantly higher ratios to Galunggung. Likelwise, many of the Argopuro magmas contain lower Zr/Nb than Ijen. These ratios are clearly not modified during differentiation so the only alternative is that they come from a variably depleted and enriched sources. While enrichment is more evident towards the back of the arc, Kelut (at 133 km above the WBZ) has higher Zr/Nb ratios to those at Galunggung (at 118 km above the WBZ). This suggests the more depleted source at Kelut cannot be related to the volcano position alone.

To summarise this section:

1) The Kelut LZR series magmas provide useful information about mantle source processes because they have not been contaminated in the arc crust or show signs for significant 'open-system' behavoir during differentiation.

2) Trace element ratios commonly used to infer fluid contributions, such as Ba/La, are significantly higher in the at Kelut than in other volcanoes on Java and resemble those from oceanic settings. Elevations in such ratios appear to correlate with collision at the Java trench offshore central and east Java.

3) Based on potassium enrichment, there are three distinguishable types of source character in Java, those that produce low to medium-K magmas, those that produce high-K magmas and those which are leucititic. The enrichment of such sources becomes progressively higher away from the trench

4) Another source distinction can be made using Zr/Nb. This broadly correlates with volcano position away from the trench by does show variations between volcanoes with the same potassium contents. The Kelut LZR series contain the lowest Zr/Nb values which suggest that the mantle source may have been previously depleted.

2.5.3.2. Isotopic constraints on slab contributions

Radiogenic isotopes such as $^{87}Sr/^{86}Sr$, $^{143}Nd/^{144}Nd$, $^{176}Hf/^{177}Hf$, $^{208}Pb/^{204}Pb$, $^{207}Pb/^{204}Pb$ and $^{206}Pb/^{204}Pb$ can be particularly useful tracers of material which has been added to the mantle source during subduction (Straub and Zellmer, 2012). This is usually suggested to be either as fluid component (Pearce *et al.,* 1995; Taylor and Nesbitt, 1998; Woodhead *et al.,* 1998; (Dorendorf et al., 2000; Hochstaedter *et al.,* 2001; Churikova *et al.,* 2001), recycled subducted sediment (Vroon *et al.,* 1995; Macpherson *et al.,* 2003; Handley *et al.,* 2011), and in in many cases a combination of both (Elliot *et al.,* 1997; Turner and Hawkesworth, 1997; Turner *et al.,* 1997; Taylor and Nesbitt, 1998; Ishikawa and Tera, 1999; Lin *et al.,* 1990; Trollstrup *et al.,* 2010).

High trace element ratios of Ba/La, Ba/Th and Sr/Nd in the Kelut LZR series magmas suggest that a fluid component may have elevated LILE against LREE and HFSE. This is particularly common in some of the Pacific oceanic arcs such as Tonga, New Britain, Izu-Bonin and Kamchatka, where LILE/HFSE ratios are best developed in the most depleted (i.e. the highest Zr/Nb) arc rocks (e.g. Hawkesworth *et al.,* 1993; Woodhead *et al.,* 1998; Hochstaedter *et al.,* 2000, 2001), but are not common in the Sunda Arc. Therefore, the aim of this section is to firstly, identify the nature of the subduction component; and secondly, to identify if there is a common link between the high LILE/HFSE ratio patterns at Kelut and some of the oceanic arcs.

Lead isotopes

Lead isotopes are commonly suggested to provide the most powerful radiogenic isotope tracer for identifying subducted sediment in the genesis of arc magmas (Elliot *et al.,* 1997; Plank and Langmuir, 1998; Macpherson *et al.,* 2003). This is because, more than any other isotope, the Pb in upper continental crust and sediment is significantly enriched over values for primitive mantle which make it particularly sensitive to even very small amounts (Hemming and McLennan, 2001; Straub and Zellmer, 2012). On Java, there is relatively co-linear relationship between $^{207}Pb/^{204}Pb$ and $^{208}Pb/^{204}Pb$ against $^{206}Pb/^{204}Pb$ ratios from Indian Ocean sediments and magma compositions from west and central Java volcanoes (Gertisser and Keller, 2003; Turner and Foden, 2001). However, little is known from the Quaternary volcanoes in east Java. Figure 2.19 shows *(a)* $^{207}Pb/^{204}Pb$ against $^{206}Pb/^{204}Pb$ and *(b)* $^{208}Pb/^{204}Pb$ against $^{206}Pb/^{204}Pb$ for Kelut together with the volcanoes used in fig. 2.18 and

^{206}Pb/^{204}Pb against ^{207}Pb/^{204}Pb and ^{208}Pb/^{204}Pb
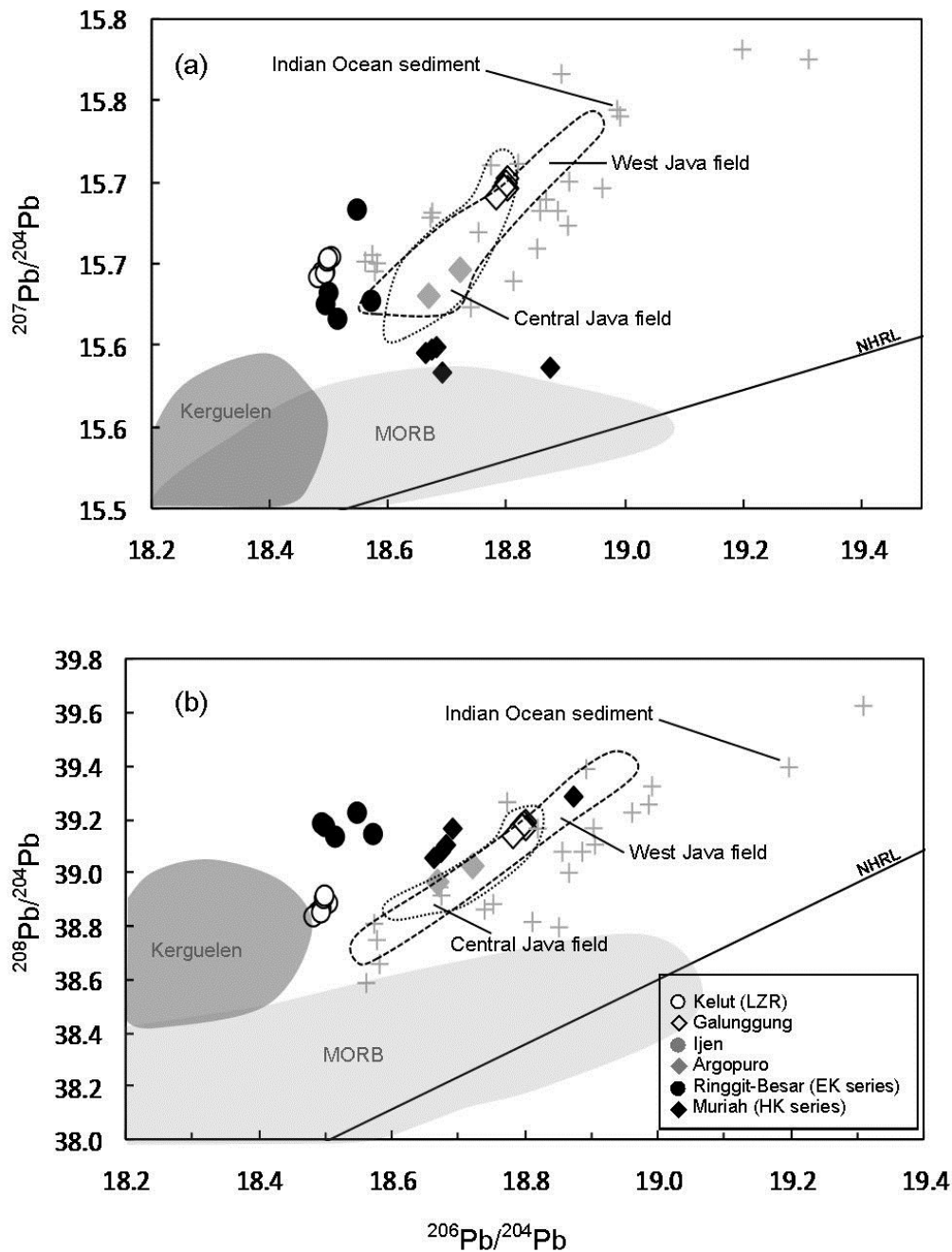
Fig 2.19. (a) ^{207}Pb/^{204}Pb against ^{206}Pb/^{204}Pb and **(b)** ^{208}Pb/^{204}Pb against ^{206}Pb/^{204}Pb for the volcanoes outlined in fig 5.5 compared with fields for west and central Java, Indian Ocean sediment, MORB and the Kerguelen Ocean Island basalt. Data sources include: MORB, after Price *et al. (*1986), Ito *et al.* (1987), Rehkamper and Hofmann, (1997), Chauvel and Blichert-Toft (2001) and Janney *et al.* (2005); Kerguelen OIB, after (Yang *et al.* (1998); Indian Ocean Sediment, after Plank and Ludden (1992) and Gasparon and Varne (1998); Northern Hemisphere Reference Line (NHRL), after Hart (1984). References for the west and central Java fields as for fig. 2.12. Note the displacement of Kelut away from the Java field towards lower ^{206}Pb/^{204}Pb.

fields for west Java, central Java, MORB, Kerguelen (Indian Ocean Island basalt) and Indian Ocean sediment. The sediment was analysed from a number ODP and DSDP drilling sites around the northeast Indian Ocean, and does not distinguish between silicic and calcareous-organogenic compositions (Gasparon and Varne, 1998; Plank and Ludden, 1992).

The figures show that, while a strong case can be argued for the involvement of sediment in the Quaternary volcanoes from west and central Java, mixing between a MORB source and this sediment cannot be argued for the Kelut magmas, or for the Ringgit-Beasr (EK series) and Muriah (HK series). In particular, Kelut and Ringgit-Besar are displaced towards lower $^{206}Pb/^{204}Pb$ ratios against $^{207}Pb/^{204}Pb$ and $^{208}Pb/^{204}Pb$ towards the Kergulen OIB. However, this does not provide a satisfactory source composition for the Kelut magmas because of their higher Zr/Nb, Ba/La, Ba/Th and Sr/Nd than would be expected for OIB (see table 2F for comparison).

Hafnium and Neodymium isotopes

In recent years isotopes of hafnium and neodymium have been used to identify a sediment contribution to arc magmas in spite of the fact that their trace elements are used to identify pre-subduction source compositions (Elliot *et al.,* 1997; Handley, 2006; Turner *et al.,* 2009). It is suggested that because Hf and Nd are relatively immobile during the transport of aqueous fluids, $^{176}Hf/^{177}Hf$ and $^{143}Nd/^{144}Nd$ ratios displaced away from MORB provide unique perspective of sediment contributions from the subducting slab (Woodhead *et al.,* 2001; Handley *et al.,* 2011). However, it has also been demonstrated that $^{176}Hf/^{177}Hf$ and $^{143}Nd/^{144}Nd$ ratios can provide insights into the nature of the "ambient mantle" prior to subduction (Woodhead *et al.,* 2012).

In order to assess each of these ideas, $^{143}Nd/^{144}Nd$ and $^{176}Hf/^{177}Hf$ have first been plotted against Zr/Nb in fig 2.20 *(a)* and *(b)*. In figure 2.20, the magmas used in figs 2.18 and 2.19 have been plotted against a field for MORB. Zr/Nb has been used because there is clearly a source control to this ratio (as shown in fig. 2.18). For both figures the isotope ratios correlate with the trace element ratios across the suite of volcanoes. These correlations are unlikely to be reconciled by the addition of subducted sediment, particularly in the case of Ringgit-Besar (EK series) and Muriah (HK series), for which there is strong evidence to suggest that they are not influenced by a recent subduction component (Edwards *et al.,* 1991, 1993, 1994) and contain Zr/Nb ratios significantly lower than Indian Ocean sediment. The same is true for the

^{143}Nd/^{144}Nd, ^{176}Hf/^{177}Hf and Zr/Nb Relationships
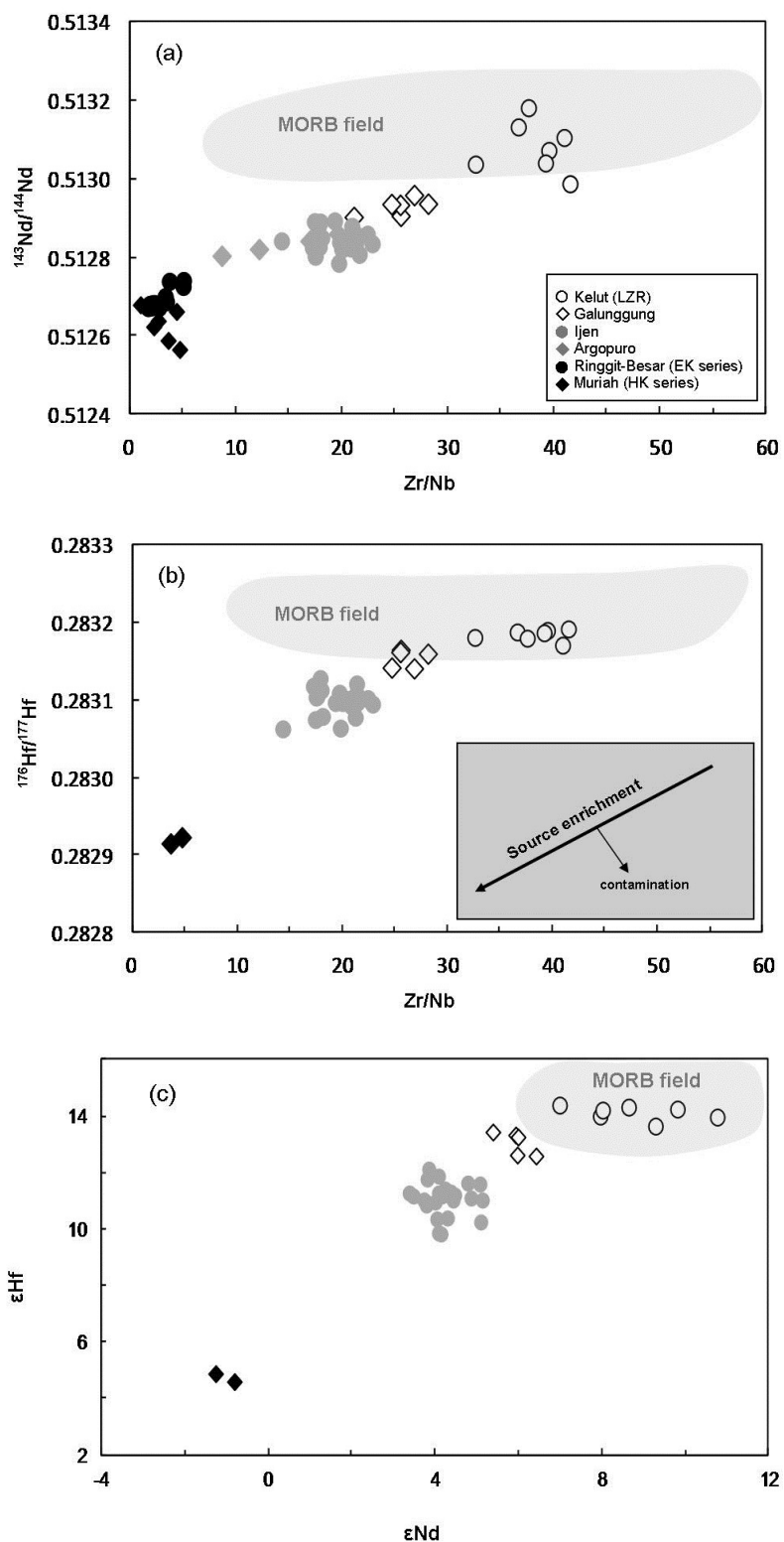
Fig 2.20. (a) ^{143}Nd/^{144}Nd and **(b)** ^{176}Hf/^{177}Hf against Zr/Nb, and **(c)** εHf against εNd for the volcanoes used in fig. 2.18 and 2.19 agaist a field for MORB. Data sources for MORB as for fig.2.19 and includes Nowell *et al.* (1998). See text for details.

Kelut LZR magmas which are within the fields for MORB and contain mantle-like $^{176}H/^{177}Hf$ and $^{143}Nd/^{144}Nd$ ratios (fig. 2.20c).

Fitton *et al*. (2003) show a similar correlation between $^{143}Nd/^{144}Nd$ and Nb/Zr beneath the Icelandic plume, which they explain in terms of dynamic melting. The idea is that in a heterogenous source, composed of enriched plums within a more refractory matrix, small degrees of melt will preferetially extract the more fusable parts (i.e. the enriched plums). Once a melt has been extracted a depleted residue will be left behind. Therefore, the most depleted basalts will contain the highest $^{143}Nd/^{144}Nd$ and $^{176}Hf/^{177}Hf$.

This type of melting could create the type of chemical zonation common to spreading ridges and arcs, where the most depleted rocks are useually located in the areas prone to higher degrees of melting (i.e. at the ridge and the front of the arc). It is also common in these setting for the most enriched, often alkaline basalts to be associated away from the spreading axis or in the back of the arc. These type of melting patterns are advocated here in preference to a sedimentary component derived from the subducting slab for this group of particular magmas. On this basis, it is plausible that Ringgit-Besar (EK series) and Muriah (HK series) best represent an enriched mantle component beneath Java which has been progressively depleted. The Kelut LZR series represent a refractory MORB-like source which has encountered progressive stages of melt extraction.

Strontium and Neodymium isotopes

Having discounted a major role for subducted sediment, fluid contributions from the slab can be contrained. Strontium isotope ratios coupled with neodymium will provide a unique perspective in this respect because while $^{143}Nd/^{144}Nd$ has been shown to be relatively immobile and controlled by source variations (in the volcanoes described above), $^{87}Sr/^{86}Sr$ is highly fluid mobile and enriched in AOC (Staudigel *et al.,* 1995; Kelly *et al.,* 2003).

Figure 2.21*a* shows $^{143}Nd/^{144}Nd$ against $^{87}Sr/^{86}Sr$ for the Kelut LZR samples and other volcanoes used in figs 2.18 to 2.20 against other fields for Java. The dashed line represents a mantle array which is defined in the caption. The Kelut LZR lavas produce an almost straight, vertical line perpendicular to representative samples from AOC. This line is continued to lower $^{143}Nd/^{144}Nd$ at Muriah, whose magmas contain a similar $^{87}Sr/^{86}Sr$ to Kelut.

Source Variation and Fluid Enrichment
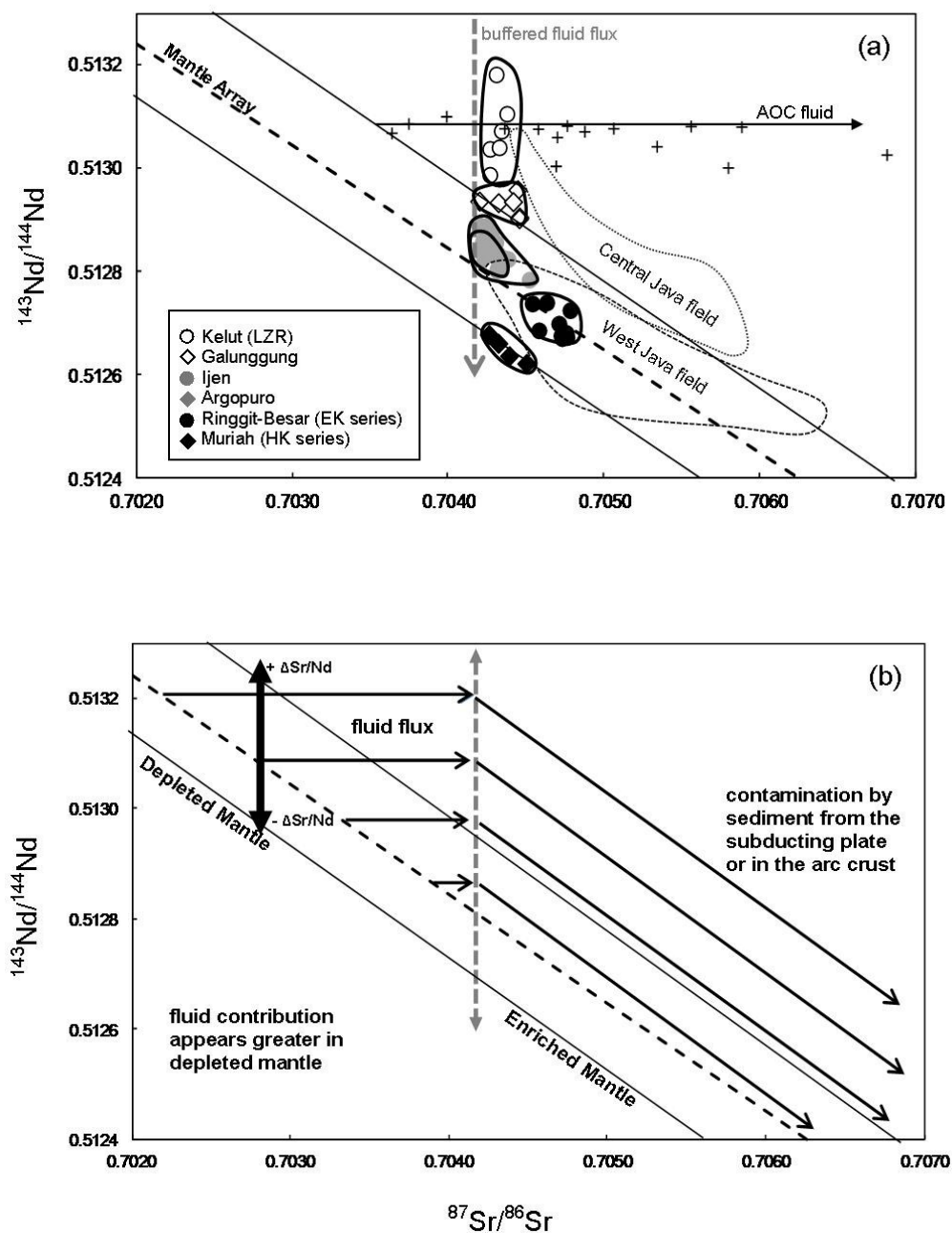
Fig. 2.21. (a) ^{143}Nd/^{144}Nd versus ^{87}Sr/^{86}Sr for the volcanoes used in figs 2.15, 2.16 and 2.17 including fields for central and west Java. The mantle array is defined by ^{143}Nd/^{144}Nd=0.19823(^{87}Sr/^{86}Sr)+0.6524 and determined by MORB and OIB data after, Price *et al.* (1986); Ito *et al.* (1987); Dosso *et al.* (1988); Rehkamper & Hofmann (1997); Yang *et al.* (1998); Chauvel & Blichert-Toft (2001); Janney *et al.* (2005); Workman & Hart (2005). AOC fluid data after Staudigel *et al.* (1995). Data sources for west and central Java after fig. 2.12. **(b)** shows a schematic representation of the data where most of the volcanoes used for source modelling define an ^{87}Sr/^{86}Sr line for Java at changing ^{143}Nd/^{144}Nd.

Figure 2.21*b* shows an interpretation of this data. In this interpretation, the vertical line from Kelut to Muriah represents a buffered fluid modification of variably fertile mantle. This supports the idea that $^{143}Nd/^{144}Nd$ highlights the variation in source fertility, while $^{87}Sr/^{86}Sr$ provides a constant value (~0.7042) for the ratio of fluid being fluxed from the slab into the mantle. Most sediments and upper crustal material are significantly higher in $^{87}Sr/^{86}Sr$ and lower in $^{143}Nd/^{144}Nd$ to suggest that magma contamination involving these materials would systematically alter both ratios as is the case for many of the west and central Java volcanoes.

2.5.3.3. Quantifying fluid contributions

Having isotopically identified that the Kelut LZR series magmas are derived from a fluid-modified depleted mantle source it should be possible to model this process. In order to achieve this, trace element data is applied because there is a large quantity of experimental data available (Tatsumi *et al.,* 1986; Brenan *et al.,* 1994, 1995; Ayers *et al.,* 1997; Kogiso *et al.,* 1997). The aim is to replicate the trace element composition of the most primitive Kelut LZR sample (i.e. Kel56) through adding AOC derived fluid to a depleted mantle composition. The starting composition of the mantle which produced the Kelut magmas must require a more depleted mantle composition than N-MORB because concentrations of HFSE are generally lower, even after melting.

The the results of the model are shown in fig. 2.22. To create the fluid modified mantle composition, 2% AOC fluid was added to the depleted mantle composition after (Salters and Stracke, 2004). This vaule is similar to the one used by Handley (2006) to model fluid contributions at Ijen. The fluid was calculated by applying mobility data from Kogiso *et al.* (1997) to the AOC composition presented in table 2G (after Staudigel *et al.,* 1995 and Kelly *et al.,* 2003). The profile of the fluid-modified mantle in this model produces a good match for the hornblendite and Kel56. In this case the hornblenite may provide a good reference because it is thought that slab deried fluids may interact with hydrous rocks at, or below the forearc (Tatsumi and Kogiso, 1997).

Batch melts of the modelled mantle composition were then carried out for 5, 15 and 25% melting. It is unlikely in reality that batch melting can explain the mantle depletion and potentially episodes of previous melt extraction required at Kelut. However, they provide an approximation, which suggests that between 15 and 25% melting is required to replicate the

Quantifying Fluid Enrichments at Kelut
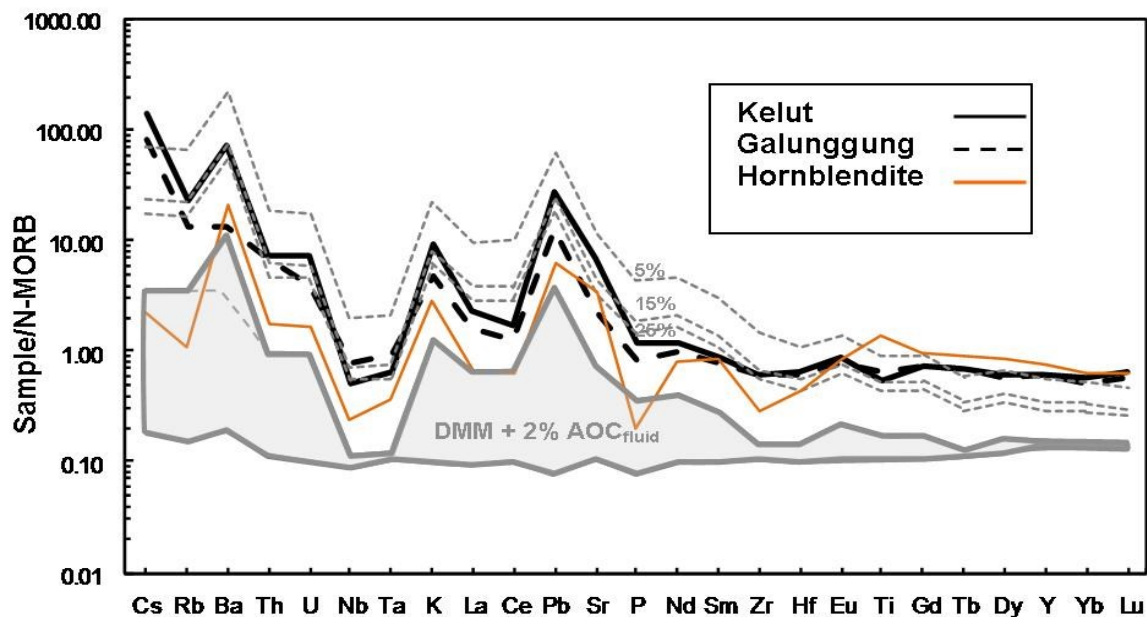
Fig 2.22. Shows the results of mixing 2% AOC fluid with depleted MORB mantle using the criteria in Table 2G. The fluid composition is calculated using mobility data from Kogiso *et al.* (1997) and an AOC composition after Staudigel et al. (1995). Ba and Sr concentrations are modified within the ranges of Kelly *et al.* (2003) for altered basalts. Grey dashed lines show batch melts of 5, 15 and 25% using the mineral components show in Table 2G and distribution coefficents, either by calculation or interpolation, after Pearce and Parkinson (1993); McDade *et al.* (2003); Salters and Stracke (2004); Janney *et al.* (2005). DDM composition after Salters and Stracke (2004).

Table 2G. Parameters used in Model 2.22.

	DMM	AOC	fluid	ol	opx	cpx	Sp
Cs	0.00132	0.04	1.20	0.0000	0.0000	0.0000	0.0000
Rb	0.088	2.21	92.82	0.0002	0.0006	0.0110	0.00001
Ba	1.2	109.30	3533.33	0.0001	0.0010	0.0058	0.0010
Th	0.0137	0.20	5.07	0.0001	0.0001	0.0060	0.0010
U	0.0047	0.10	1.93	0.0001	0.0001	0.0070	0.0010
Nb	0.211	1.30	3.12	0.0006	0.0049	0.0350	0.0010
Ta	0.0139	0.10	0.10	0.0006	0.0049	0.0350	0.0010
K	60	1079.26	35975.33	0.0000	0.0001	0.0070	0.0000
La	0.234	1.29	69.44	0.0005	0.0090	0.0800	0.0100
Ce	0.772	6.36	204.68	0.0005	0.0050	0.0800	0.0100
Pb	0.023	1.00	56.67	0.0001	0.0010	0.0720	0.0010
Sr	9.8	69.00	2788.00	0.0002	0.0070	0.0670	0.0001
P	40.7	523.68	6982.40	0.0001	0.0090	0.1780	0.0006
Nd	0.713	6.58	114.05	0.0001	0.0100	0.1900	0.0100
Sm	0.27	2.51	23.43	0.0002	0.0270	0.1800	0.0100
R	7.94	63.40	152.16	0.0033	0.0360	0.2040	0.0010
Hf	0.199	1.91	4.58	0.0010	0.0360	0.3440	0.0100
Eu	0.107	0.94	5.95	0.0016	0.1410	0.2960	0.0100
Ti	798	6772.09	26185.41	0.0400	0.0240	0.4500	0.1500
Gd	0.395	3.72	12.40	0.0011	0.0065	0.3500	0.0100
Tb	0.075	0.73	0.68	0.0040	0.0600	0.3800	0.0015
Dy	0.531	4.61	11.06	0.0017	0.0600	0.6900	0.0100
Y	4.07	28.20	9.40	0.0010	0.0600	0.7380	0.0010
Yb	0.401	2.87	2.68	0.0015	0.0920	0.7130	0.0010
Lu	0.063	0.44	0.09	0.0015	0.1190	0.7180	0.0100
Mode				0.50	0.30	0.12	0.08
Melt cont.				0.25	0.25	0.36	0.14

Global Fluid-Dominated Arc Magmas
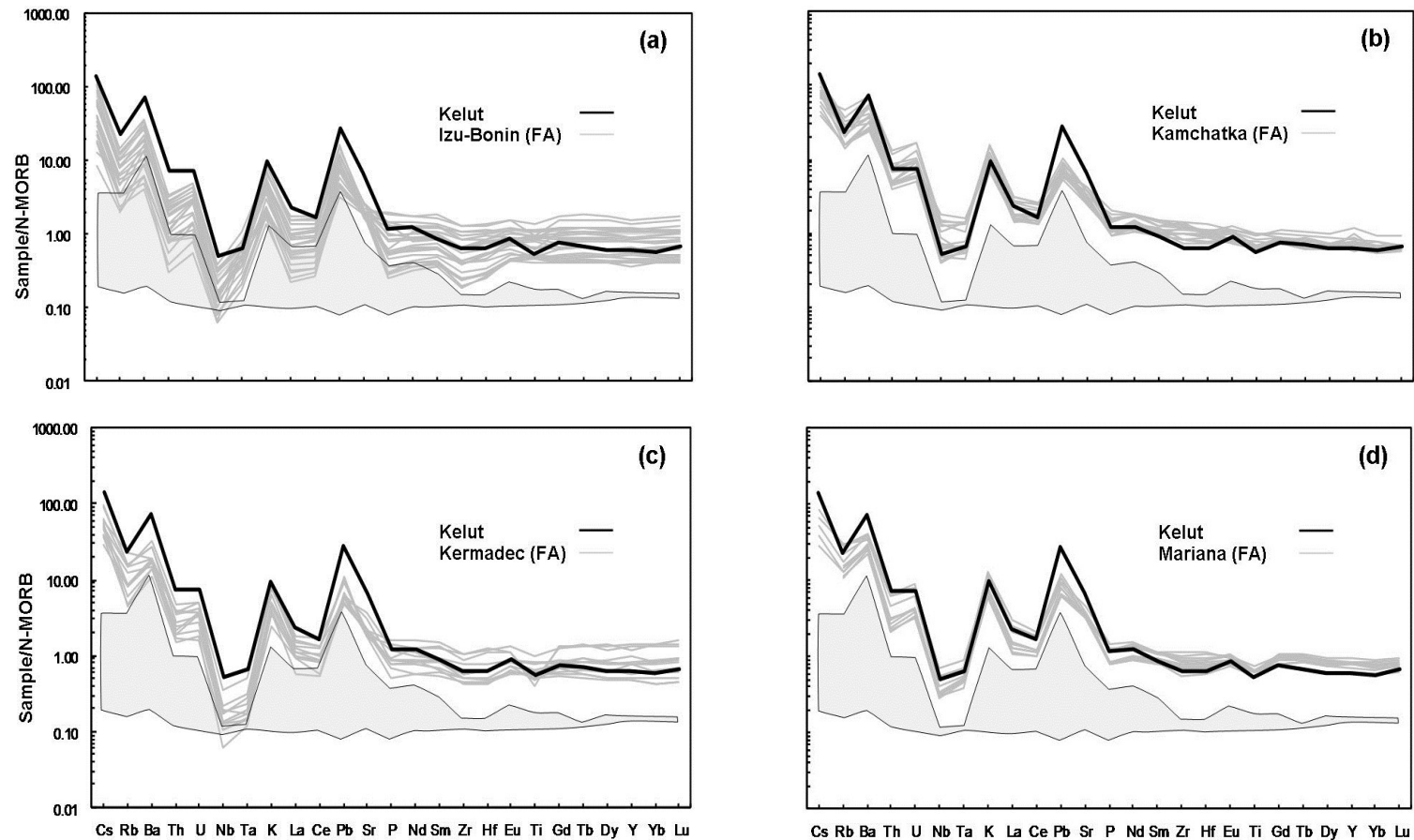
Fig 2.23. Shows Kelut and the fluid modified mantle composition against some Pacific Oceanic arcs. Data after (Elliot *et al.,* 1997; Turner *et al.,* 1997; Taylor and Nesbitt, 1998; Churikova *et al.,* 2001).

trace element concentrations for Kel56. In this model, the HREE are lower than would should be expected, but this may be resolved with small modifications to the mobility data, or the kd values used in table 2G. In conclusion, the trace element concentrations at Kelut can be well replicated using basic fluid mobility data and melting models. This suggest that the addition of subducted sediment is not required in these magmas.

In comparison to other arc magmas suspected to be influenced by the introduction of fluids into the mantle wedge, the trace element profile of Kelut compares well. Figure 2.23 shows Kel56 and the fluid modified mantle against front arc magmas from *(a)* Izu-bonin, *(b)* Kamchatka, *(c)* Kermadec and *(d)* Mariana. It is clear, that irrspective of the greater depletion of HFSE at Izu-Bonin and Kermadec, the profiles are very similar. Figure 2.12 shows that this is not true of any other volcanoes from Java, which contain higher HFSE and lack the Ba positive anomaly show by the Kelut magmas. The evidence from this study suggests that this is due to a combination of factors. In the magmas not contaminated in the arc crust, the fluid signature becomes progressively buffered through more enriched mantle source components across the arc. In magmas which have been contaimniated in the arc crust such as those from central Java and west Java (e.g. Gasparon and Varne, 1998; Chadwick *et al.,* 2007; Handley *et al.,* 2008; Deegan *et al.,* 2010), the fluid signature is also lost, presumably in the crust.

2.6. Chapter Conclusions

Kelut contains two series of magmas, the HZR and LZR, which can be distinguished by variations in major and trace elements during differentiation. The HZR magmas have elevated concentrations of HFSE, Th and SiO_2, and higher $^{87}Sr/^{86}Sr$, $^{206}Pb/^{204}Pb$ and lower $^{143}Nd/^{144}Nd$, $^{176}Hf1^{77}Hf$ than the LZR series which is a result of contamination in the arc crust. The preferential enrichments in elements such as Zr, Hf, Th and SiO_2 suggest that the contaminent was of a detrital, terrigneous, or acid igneous composition. A plausible origin for this material is the Kendeng Basin, which is filled with volcanogenic sands from the Southern Mountains.

The LZR series magmas show little evidence for contamination in the crust and contain isotope ratios which do not change with differentiation. These magmas are unique in terms of there high low HFSE concentrations, high Zr/Nb and mantle-like $^{143}Nd/^{144}Nd$ ratios. Compared with other uncontaminated magmas these provide a depleted end-member in

which fluid contributions are most pronounced. In magmas derived from progressively enriched sources this signature becomes buffered as is less evident.

To speculate, there is clearly a correlation between Ba/La, Ba/Th and Sr/Nd and the collisional processes at the central and east Java trench. This suggests that the mantle depletion at Kelut is related to the changing tectonic environment in which other volcanoes, such as Wilis and Lawu have become volcanically extinct. More work is required in order to address the effects of collisional processes in Java on arc magmatism.

Chapter 3

Carbonate Assimilation and Melting Variations between Pyroclastic Deposits and Lavas at Sumbing Volcano, Central Java, Indonesia. A Major and Trace Element, and Isotopic (Sr, Nd, Pb and Hf) Evaluation

3.1. Introduction

Crustal contamination of primitive arc magma is believed to be an important process in modifying the composition at many island arc localities (Thirlwall & Graham, 1984; Thirlwall *et al.,* 1996; Davidson *et al.,* 1987; Davidson, 1987; Ellam & Harmon, 1990; Macpherson *et al.,* 1998; Peccerillo *et al.,* 2004; Hildreth & Moorbath, 1988) including in the Sunda arc (Gasparon *et al.,* 1994; Gasparon & Varne, 1998; Edwards *et al.,* 1991; Handley *et al.,* 2008; Turner *et al.,* 2003). On Java, isotopic ratios are notably more radiogenic in volcanoes from the west and central part of the island, which was thought reflect the thickness of the crust (Curray *et al.,* 1977; Gasparon & Varne, 1998) prior recent studies (Granath *et al.,* 2011; Kopp, 2011).

Elevated isotopic ratios and high concentrations of LILE and LREE in arc magmas from Java are often considered as being more consistent with source contamination due to their lack of correlation with indices of differentiation (Edwards *et al.,* 1993; Turner & Foden, 2001; Gertisser & Keller, 2003; Handley *et al.,* 2010). On this basis, some authors discounted the idea that assimilation had a major influence on their geochemistry (Turner & Foden, 2001; Gertisser & Keller, 2003). However, for differentiation to drive magma towards intermediate and silicic compositions a contaminant has to be distinct (both in trace element concentrations and isotopic ratios) from the ascending magmas (e.g. Davidson *et al.,* 2005; Handley, 2006).

Recently, a number of studies from Merapi have identified that the magmas are interacting with calc-silicate lithologies in the sub-volcanic basement (Chadwick *et al.,* 2007; Deegan *et al.,* 2010). Most of the evidence for this originated from mineral studies and the effect on whole-rock magma geochemistry appears to be subtle but may have profound effects on the CO_2 budget beneath the volcano (Troll *et al.,* in press). At present, there are no other volcanoes on Java which show evidence for the assimilation of carbonate lithologies. However, few detailed studies have been done on neighbouring volcanoes situated around Merapi which are presumably built upon similar basement.

This Chapter presents a major and trace element and Sr-Nd-Hf-Pb isotope analysis of Sumbing volcano, located < 50 km east of Merapi. The main objective is to identify what effect, if any; upper crustal processes have had on this large volcano.

3.2. Sumbing geological background and sample selection

At 3,371 meters in elevation, Gunung Sumbing is the third highest volcano on Java, exceeded only by Semeru (3,676 m) and Slamet (3,428 m). The volcano dominates the landscape between the Cities of Wonosobo and Yogyakarta in central Java, but is relatively unknown due to its dormancy since 1730. Sumbing is the southernmost volcano in a NNW chain consisting of Gunung Sundoro and the Dieng Plateau and is situated ~ 175 km above the northward dipping seismic Benioff Zone (Hutchinson, 1982). Figure 3.1 shows the NNW-SSE volcanic chain and a parallel volcanic succession extending from Ungaran to Merapi situated around 50 km west of Sumbing which are the subject of this study.

Cretaceous and Tertiary basement is exposed close to the south-west flank of Sumbing in a mountainous region at Karangsambung (see figure 3.1). This is one of few regions in Java where basement can be observed showing fault-bounded slivers of ophiolitic and arc-type lithologies overlain by Eocene-Miocene sedimentary successions (Wakita & Munasri, 1994; Smyth, 2005). Further east, Sumbing is bordered by the West Progo Mountains; a series of carbonates, marls and volcanic remnants, known as the 'Old Andesites' (Van Bemmelen, 1949; Smyth, 2005). The mountains are eroded volcanic cores which represent the initial phase of volcanism in the Southern Mountains which erupted during the Oligocene and Miocene and these are surrounded by the low-land sediments (West Progo Beds) (Van Bemmelen, 1949; Lelono, 2000; Lunt, 2000).

Sumbing Volcano presents a particularly interesting study for a number of reasons. Firstly, it has very limited data, in contrast to Merapi, which is very well documented (e.g. Hammer & Voight, 2000; Gertisser & Keller, 2003; Debaille *et al.,* 2006; Chadwick *et al.,* 2007; Deegan *et al.,* 2010). Sumbing is also situated close to a proposed transition zone, where basement character and zircon ages suggest spatial variations from west to east (Curray *et al.,* 1977; Handley, 2006; Hall, 2009; Hall & Smyth, 2008; Hall *et al.,* 2009; Granath *et al.,* 2011; Smyth *et al.,* 2007, 2008). The aims of this study are therefore *1)* to understand the petrogenesis at Sumbing for which little is known; *2)* examine the magmatism at Sumbing in a regional context, for both central Java and the growing database for Java (e.g. Edwards, 1990; van Gerven & Pichler, 1995; Vukadinovic & Sutawidjaja, 1995; Carn & Pyle, 2001; Gertisser & Keller, 2003; Handley, 2006; Chadwick *et al.,* 2007; Sendjaja *et al.,* 2009;

Central Java Volcanoes, Basement and Stratigraphic Zones
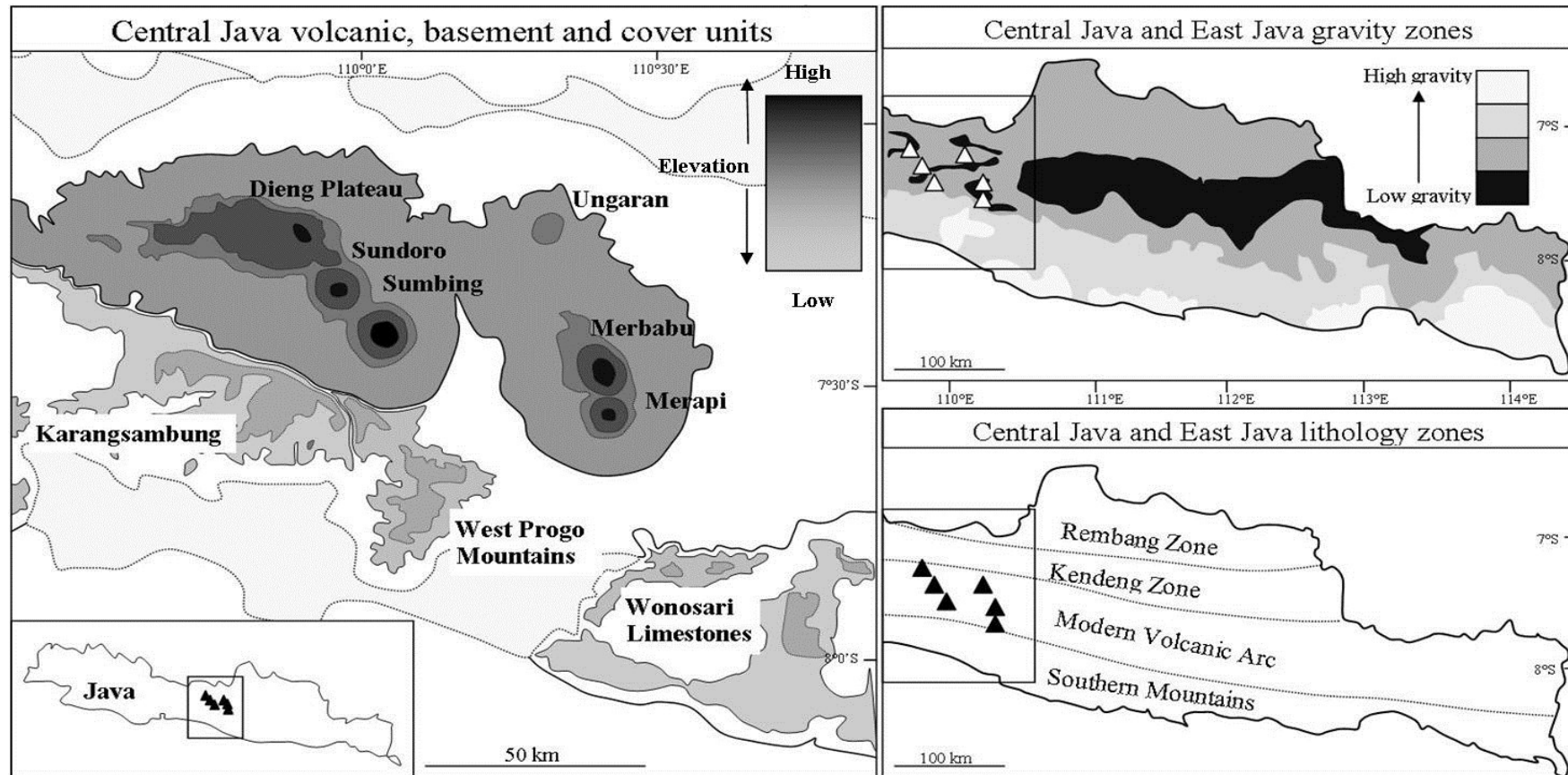
Fig. 3.1. Left: Schematic map showing the two NNW-SSE trending volcanic chains in Central Java (Dieng, Sundoro and Sumbing in the west; Ungaran, Merbabu and Merapi in the east) in relation to local basement (Karangsambung) and sediment cover (West Progo Mountains and Wonosari Limestones). Darker grey shading denotes higher topographic regions. Insert map shows the location of the volcanic chains. Top right: Gravity zones for central and east Java based on Bouguer Anomaly Quadrangle Maps of Java, produced by the Geological Research and Development Centre, Bandung (after Smyth, 2005). The low gravity region in the Kendeng Zone shows strong negative bouguer anomalies which indicate up to 10 km of basin sediment fill (Smyth et al 2008). White triangles display the two volcanic chains from central Java, shown left. Bottom right: The van Bemmelen (1949) zonation scheme for central and east Java shows the east-west trending stratigraphic and structural zones. Black triangles show the positions of the volcanoes discussed in text.

Deegan *et al.,* 2010); *3)* identify the basement lithologies which magmas may have interacted at depth.

3.2.1. Sample Selection

A total of 20 fresh samples were collected primarily from five localities around the volcano flank. These can be categorised in two obvious groupings; pyroclastic deposits and lava flows which are shown in figure 3.2. More detail about the geology is available in Sukhyar (1989).

3.2.2. Pyroclastic Deposits

Pyroclastic rocks are abundant on the lower regions of the volcano flanks. Extensive pyroclastic flows and lahars on the northeast flank are accompanied by an 800 m-wide horseshoe shaped crater at the summit. Therefore, it is likely (although undocumented) that at least one flank collapse sent debris avalanches down the northern and eastern flanks. In addition, there are elevations on the eastern flank (at Windu Sari) and on sections of the southern flank. It is unclear whether these are remnants of historical dome collapse, or an edifice of previous volcanic episodes, as deposits on the south flank are referred to as 'Old Sumbing Deposits' by GRDC base maps from the Geological Survey at Bandung, West Java. Either way, they are a likely result of an older period of volcanism.

The samples located within this group are all basaltic andesites, with a very restricted range in composition. On the north flank, a large quarry at Kwandungan is cut into the base of the volcano displaying a section through the pyroclastic flows. Most of the angular clasts are suspended in a lahar deposit ranging in size from meter-sized blocks to cm-sized fragments. Two of the samples (sumb69 and 71) collected at the quarry have been included in the analyses. A second locality on the extreme southern flank was selected for additional sample collection due to its close proximity to the Southern Mountains. These rocks (Sumb94-99) appear to have a similar composition to those in the north.

3.3.1.2.　Lavas

The remaining samples are all located at greater elevations on the volcano and comprise the impressive lava flows which fill deep incised valleys around the cone. Abundant porphyritic

Sample Localities
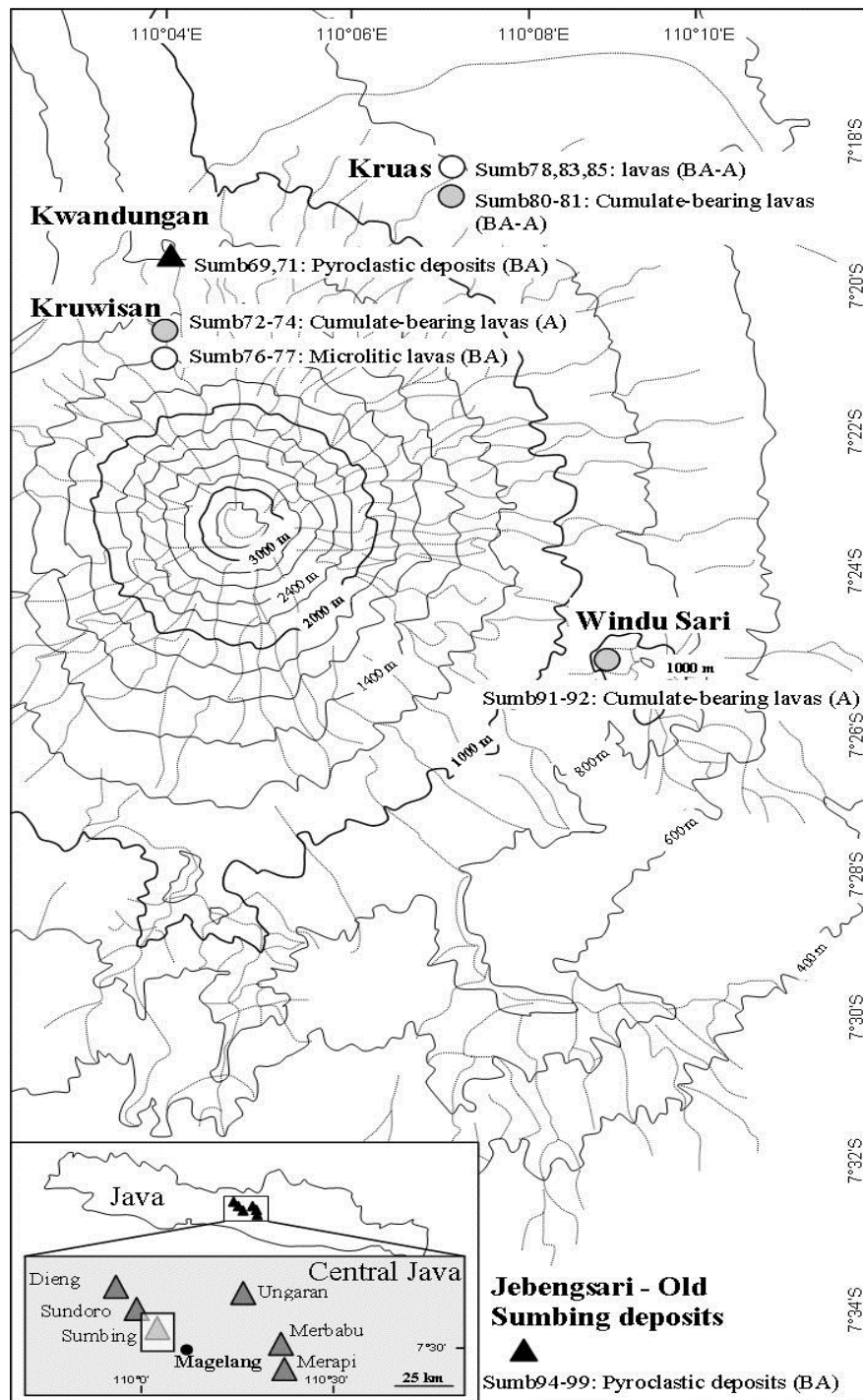
Fig. 3.2. Topographic sketch map of Sumbing volcano. Black triangles show pyroclastic rock samples, grey circles show cumulate-bearing lavas and white circles show basaltic-andesite and andesite lavas with no evident cumulate minerals. Symbols also used in subsequent figures. The dashed (lighter) lines show drainage patterns away from the volcano and the bold lines represent topographic discontinuities. Insert map displays the location of Sumbing (inside the shaded square) relative to other selected volcanoes in Central Java which produce two parallel NNW-SSE trending volcanic chains.

andesites, typified by those located at the village of Kruwisan on the north flank contain hydrous minerals such as amphibole and biotite. These rocks (Sumb72-74) display a number of interesting features and textures including coarse-grained xenoliths (of dioritic and hydrous-mineral bearing cumulates), flow banding, and lens-shaped pockets of mafic magma entrained within the host rock. In addition to these are a group of dense basaltic andesites (Sumb76-77) which show an idomorphic granular fabric of well-orientated plagioclase minerals.

A stream exposure close to the village of Kruas on the NE flank displayed basaltic andesite compositions similar to those at Kruwisan. These rocks also contain mixed bands of lighter and darker layers and are also very dense. Five rocks, including two of the basaltic andesites (sumb78 and 81) and three andesites (sumb80, 83 and 85) are all discussed in this chapter. The final locality is the elevated terrain of Windu Sari on the east flank. Two amphibole-rich porphyritic andesites (sumb91 and 92) were collected. These rocks had been classified as 'crystal tuffs' by the Geological Society of Indonesia and may also represent a phase of older volcanism.

3.3. Petrology and mineral chemistry

In common with many other volcanoes on Java, rock compositions at Sumbing display a restricted range from basaltic andesite to andesite. All of the rocks have a standard mineral assemblage of plagioclase, pyroxene and titanomagnetite, and most are porphyritic containing megacrysts, phenocrysts, microphenocrysts and cumulophyric clots. Hydrous accessory phases include amphibole and biotite which appear to be inherited from cumulates and/or xenocrysts. The samples are described based upon groups of similar eruptive products, provenance, mineral assemblage and chemistry.

3.3.1. Pyroclastic Deposits (Sumb69, 71 & 94-99)

The pyroclastic deposits are summarised in figures 3.3 (*a-c*). These rocks all have a basaltic andesite composition and phenocryst phases are dominated by plagioclase, clinopyroxene and titanomagnetite. Three of the samples (including the two from Kwandungan) contain phenocrysts which are set in a brown glassy matrix with irregular vesicles containing glass inclusions. They are moderately porphyritic, with phenocryst

Pyroclastic Deposits

Fig. 3.3 (a) Field photograph showing the pyroclastic deposits which are exposed on the lower flanks of Sumbing. The volcanic clasts range from meter-sized blocks to centimetre-sized fragments and are basaltic andesite in composition.
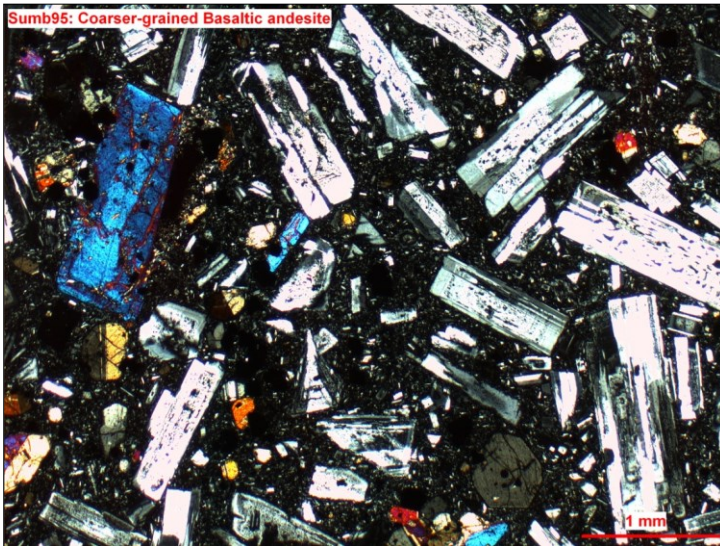
Fig. 3.3 (b) Photomicrograph of a pyroclastic basaltic andesite (Sumb95) showing the highly porphyritic nature of these rocks. Samples have high modal proportions of plagioclase and clinopyroxene phenocrysts with textures indicative of melt disequilibrium such as inclusions, resorption and oscillatory zoning (in plagioclase minerals).
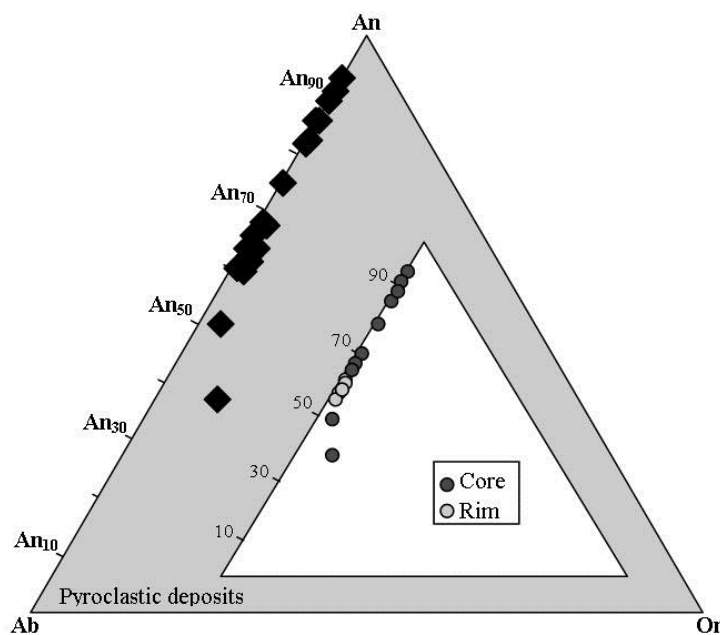
Fig. 3.3 (c) Plagioclase analyses of the pyroclastic deposits (Sumb69 and 94) show a wide distribution in Anorthite (An) compositions. Insert displays core and rim mineral analyses for the plagioclase phenocrysts. An = Anorthite, Ab = Albite and Or = Orthoclase.

contents up to 50%, the largest of which are around 2 mm in length. The other samples (all from the southern flank) are more phenocryst-rich (up to 80%) and set in a fine-medium grained groundmass of plagioclase, clinopyroxene and titanomagnetite (fig. 3.3*b*). These rocks have higher proportions of clinopyroxene and titanomagnetite, which are often clustered together, or in cumulophyric clots with plagioclase. In addition to the higher proportion of crystals, phenocryst sizes tend to be larger in the latter, with many in excess of 1 mm.

3.3.1.1. Pyroclastic Phenocryst Phases

Plagioclase is by far the most dominant phenocryst phase in all samples. Crystals are commonly subhedral to euhedral laths, but can also be rounded or fragmented and display ubiquitous evidence of melt disequilibrium. Textures including normal, reverse or oscillatory zoning, concentric core-to-rim melt inclusions, resorption and partial replacement to clinopyroxene are prevalent, particularly in the more crystalline samples where these features tend to be more prominent.

The phenocrysts from this group display a large range in compositions (fig. 3.3*c*), from An 36 to An 92, with the highest values located in the cores. Within a single plagioclase phenocryst, anorthite content can range from An 60 to An 92 in the Old Sumbing Deposits and An 61 to An 90 in Kwandungan. This is not a characteristic observed in all feldspars, with many crystals exhibiting a more restricted range within the labradorite field. The most sodic plagioclase has an orthoclase content of ~10%, a value far higher than for any of the lavas.

Clinopyroxene phenocrysts are ubiquitous in the pyroclastic deposits, and account for a significant proportion of the modal rock volume, particularly in the more crystalline rocks (up to ~10% of the total rock volume). Clinopyroxene is the most dominant ferromagnesian mineral occurring as phenocrysts, microphenocrysts, aggregates (commonly with titanomagnetite) and intergrowths (usually in other partially resorbed minerals). Euhedral to subhedral crystals range in size from less than 0.1 mm to over 1 mm, and are often twinned and less frequently zoned. All of the phenocrysts are classified as augites (fig. 3.5), with a restricted range in compositions (En_{40-45}, Fs_{14-19}, Wo_{40-44}). However, the more crystalline samples contain slightly higher wollastonite content ($Wo_{41.3-43.7}$) compared to the glassy samples ($Wo_{39.8-41.8}$), which correspond with a higher abundance of clinopyroxene in these rocks.

The minor mineral phases include titanomagnetite, orthopyroxene, apatite and amphibole. Amphibole is not evident in all samples and is often partially (or completely) resorbed and/or replaced by clinopyroxene. A single megacryst of amphibole in Sumb98 exceeds 0.5 cm and is rimmed by small plagioclase, orthopyroxene and Fe-Ti oxides which suggests that it was grown under different magmatic conditions and possibly represents an inherited mineral.

Titanomagnetite and orthopyroxene are phases in all of the basaltic andesites, often occurring as clots of ferromagnesian minerals. The former are generally small subhedral and account for 2 to 5% of the modal rock volume. Exsolution patterns are visible in the oxides through a 10 μm electron microprobe beam, exhibiting the separation between magnetite and illmenite although the ulvospinel content for these has not been quantified. The orthopyroxene is sparse and frequently mantled by clinopyroxene and/or partially resorbed in the highly crystalline samples. Crystal sizes are generally small (< 0.5 mm) with a restricted range in composition (En_{62-65}, Fs_{33-34}, and Wo_{3-4}).

3.3.2. Cumulate-Bearing Lavas (Sumb72-74, 80-81 & 91-92)

This group of lavas are summarised in fig. 3.4 (*a-c*). They comprise the most evolved samples at Sumbing and show evidence for the mixing, or mingling, of two distinct types of magma and/or magma-cumulate interaction (fig. 3.4*a* and *b*). Field evidence clearly displays mixing of coarse and fine-grained material and magmas of different compositions, and this is verified in thin-section. These andesites show more phenocryst heterogeneity than rocks from the other groups, primarily due to the variable incorporation of amphibole and biotite.

3.3.2.1. Lava Phenocryst Phases

In common with all of the rocks at Sumbing, plagioclase is the dominant phenocryst phase. These include microphenocrysts and phenocrysts which are mostly less than 1mm and tabular. They all show the textural evidence for disequilibrium as outlined for the pyroclastic deposits, although probably to a lower degree due to the less extensive resorption, melt inclusions and sieve patterns. Furthermore, an anorthite content of between 37 and 59 is far more restricted than for the pyroclastic rocks, with all phenocrysts falling into labradorite and andesine fields (fig.3.4*c*).

Cumulate-Bearing Lavas
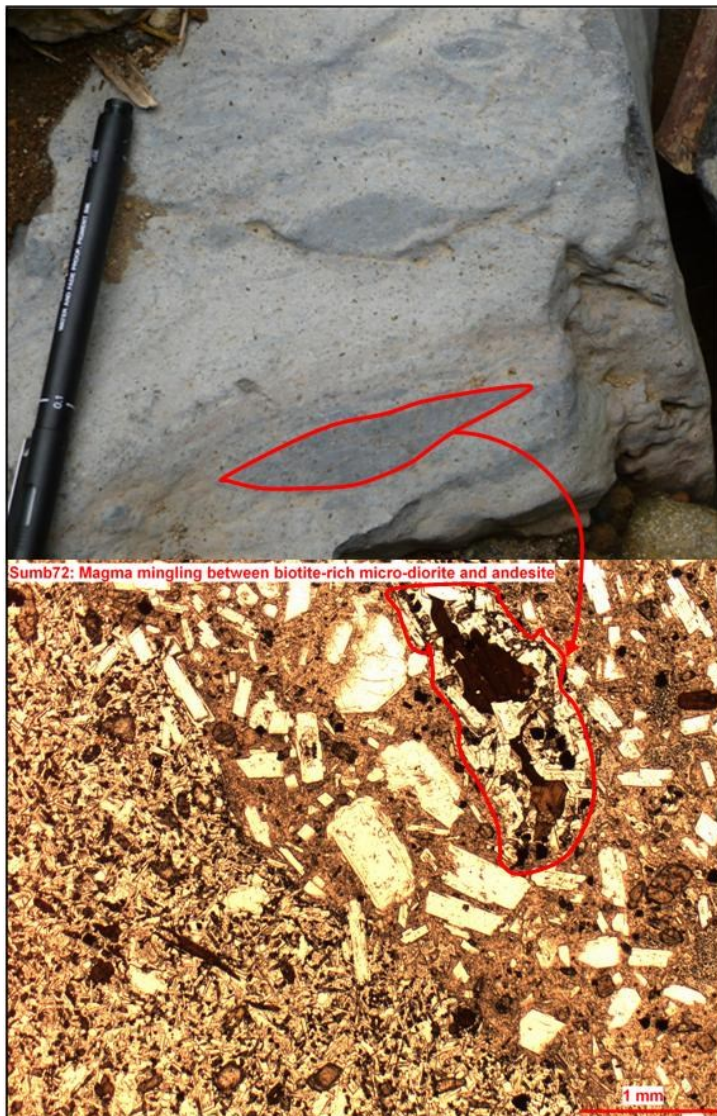
Fig. 3.4 (a) Field photograph showing mingled andesite magmas at Kruwisan (Sumb72-74).

Fig. 3.4 (b) Photomicrograph of Sumb72 showing mingling between a diorite cumulate of plagioclase, clinopyroxene, orthopyroxene, Fe-Ti oxide, amphibole, biotite and apatite and a host rock. Fragments of the diorite have evidently broken away from the main crystal body. Photomicrograph in plane-polarised light
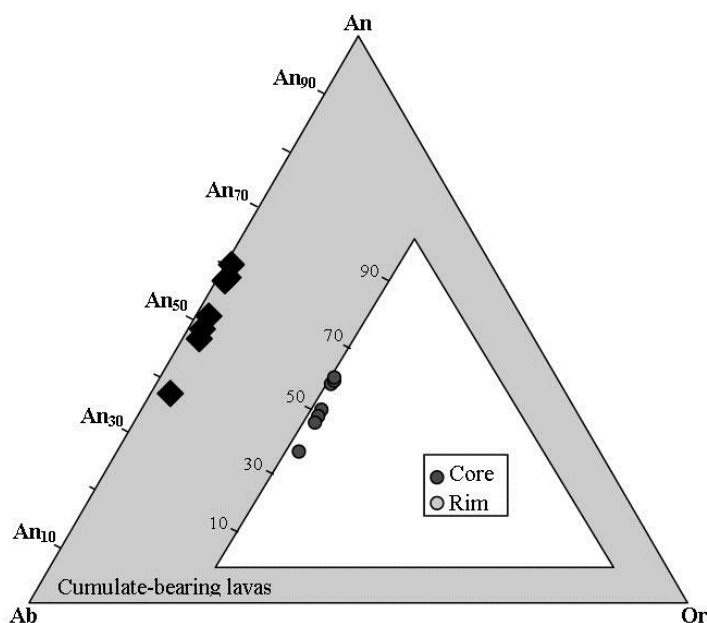
Fig. 3.4 (c) Plagioclase analyses of Sumb74 shows a more restricted range in compositions than for the pyroclastic deposits. Core compositions for the plagioclase phenocrysts analysed do not exceed 60% mol. An = Anorthite, Ab = Albite and Or = Orthoclase.

Pyroxene Mineral Compositions
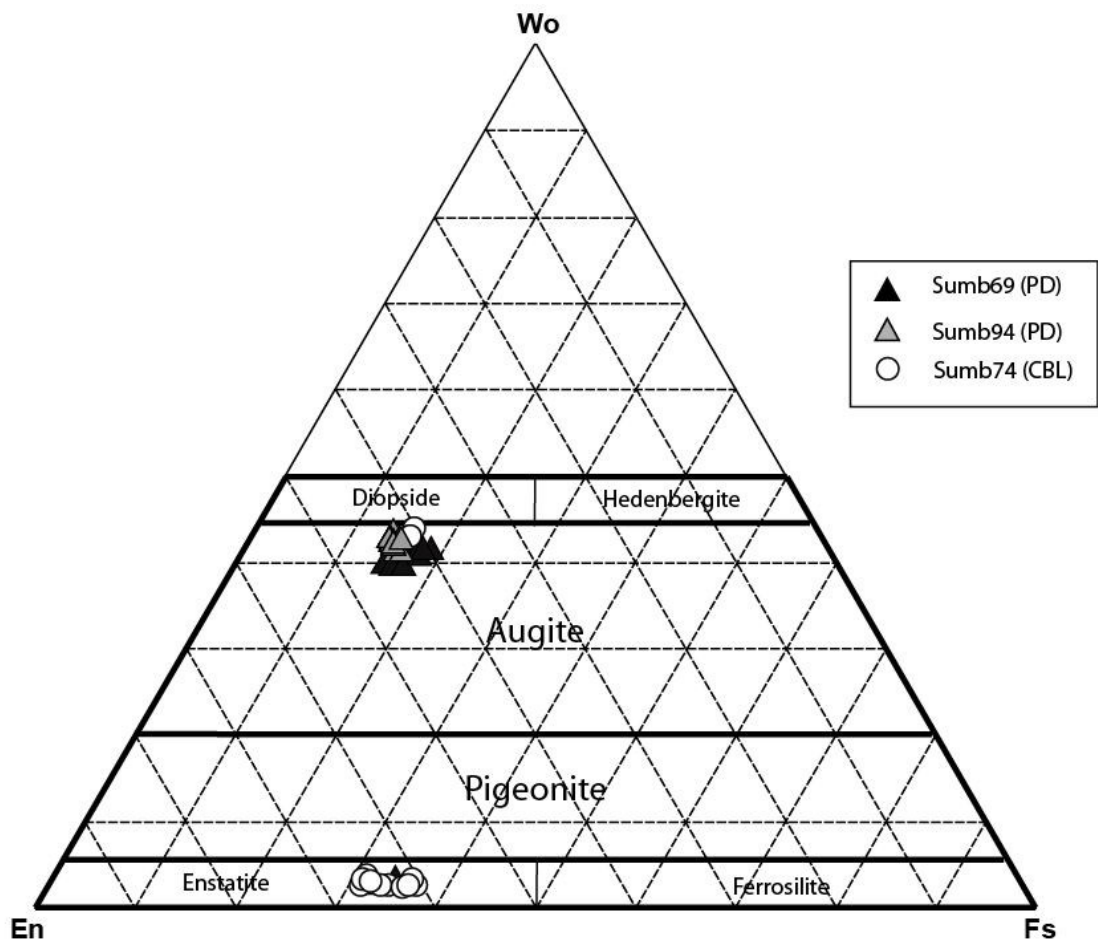
Fig. 3.5. Analyses of pyroxene phenocrysts in three of the Sumbing samples. Triangles represent the pyroclastic deposits (PD) and circles the cumulate-bearing lavas (CBL). Dashed lines represent 10% increments. En = Enstatite, Fs = Ferrosilite, Wo = Wollastonite. See text for details.

In samples Sumb72-74, orthopyroxene is the dominant ferromagnesian phenocryst. Both types of pyroxene occur mostly as euhedral to subhedral microphenocrysts with a few clustered mineral aggregates which also include plagioclase and titanomagnetite. The composition of orthopyroxene (En_{61-66}, Fs_{31-37}, Wo_{2-4}) covers a slightly larger range than for the pyroclastic rocks (see fig. 3.5). The clinopyroxene compositions (En_{40-41}, Fs_{16}, Wo_{43-44}) are slightly more restricted, albeit similar to the pyroclastic deposits. The final ferromagnesian mineral, titanomagnetite, is smaller (< 0.1 mm) and less prominent than in the previous samples.

The three samples all contain a hydrous micro-diorite of plagioclase orthopyroxene, clinopyroxene, Fe-Ti oxide, amphibole and biotite which has been mingled into a host rock. The diorite is composed of acicular fine to medium grains surrounding a few solitary phenocrysts of plagioclase, amphibole and biotite. The boundary between diorite and host is very clear, as are the additional fragmented crystal aggregates which have drifted away from the main body and been severely resorbed. The amphibole is more euhedral and generally smaller than the biotite (which is up to 3mm long) and can be classified as pargasite on the basis of Si, Na and K concentrations (Deer *et al.,* 1992).

Sumb80 has a similar bulk rock composition to Sumb72, 73 and 74, but with a different type of cumulate which lacks amphibole and biotite. The diorite in this rock is medium to coarse-grained with generally more rounded minerals of subhedral plagioclase, clinopyroxene, orthopyroxene, and Fe-Ti oxide. Minerals are severely affected by alteration and surrounded by patches of amorphous brown oxide. The plagioclase is highly zoned and partially resorbed in the cores and melt inclusions of glass and clinopyroxene are evident on the larger minerals. The clinopyroxene, orthopyroxene and Fe-Ti oxides are grouped together in a mix of various shapes and sizes, often with irregular fragments of glass. Clustered ferromagnesian minerals appear smaller and less affected by alteration than the individual minerals where clinopyroxene commonly mantles subhedral orthopyroxene, a feature noted in other in other volcanoes from Java (e.g. Vukadinovic and Sutawidjaja, 1995; Carne and Pyle, 2001; Handley, 2006).

The final type of andesite was located at Windu Sari, on the east flank of Sumbing. These rocks have similar bulk mineralogy to Sumb72, 73, 74 and 80 although clinopyroxene is the dominant ferromagnesian mineral and phenocryst sizes are larger and less abundant (~55% of the total rock volume). The rock is composed primarily of plagioclase and clinopyroxene

with minor orthopyroxene and titanomagnetite which are mostly restricted to small cumulophyric clots. The groundmass contains a highly variable black and brown isotropic glass with no identifiable minerals, although unlike the previous samples a major cumulate phase is not obvious. However, heavily fragmented amphibole and biotite minerals, which are often partially resorbed or completely replaced by clinopyroxene, are a likely consequence of the magma-diorite interaction noted for the previous samples and as a result are included within the cumulate-bearing group.

3.3.3. Basaltic-andesite and andesite Lavas (Sumb78, 83, 85 & 76-77)

Figure 3.6 (*a* and *b*) shows representative lavas from Sumbing. This group of rocks cover a larger range of compositions and do not show any evidence for mixing or mingling with magmas and cumulates of different source regions and/or growth conditions. One of these samples (Sumb78) is very similar to the pyroclastic samples described from Kwandungan. It is moderately porphyritic, with minerals set in an isotropic brown glassy groundmass. Plagioclase and clinopyroxene are the dominant phenocryst phases, with minor orthopyroxene and titanomagnetite.

The other samples (Sumb83 and 85) are the least porphyritic lavas at Sumbing with phenocryst contents ranging from 40 to 50% of the modal rock volume. Phenocrysts and microphenocrysts of plagioclase, clinopyroxene, orthopyroxene and titanomagnetite are accompanied by very occasional amphibole in the more evolved samples. However, with the exception of a few large feldspars, minerals are less severely resorbed and fragmented than observed in the pyroclastic deposits or the cumulate-bearing lavas. No mineral compositions have been measured for these rocks.

3.3.3.1. Microlitic Lavas

The microlitic lavas are shown in figure 3.7 (*a* and *b*). These rocks appear less affected by textures indicative of disequilibrium. They are primarily composed of small elongated plagioclase feldspar microlites which have which appear to contain a well-oriented fabric. Most of the sparse phenocryst phases are also of plagioclase, which do display oscillatory and normal zoning. Clinopyroxene, orthopyroxene and titanomagnetite make up a very small proportion of these rocks, primarily as part of the medium-grained groundmass where

Basaltic-Andesite and Andesite Lavas

Fig. 3.6. (a) Field photograph of a lava flow at Kruas.
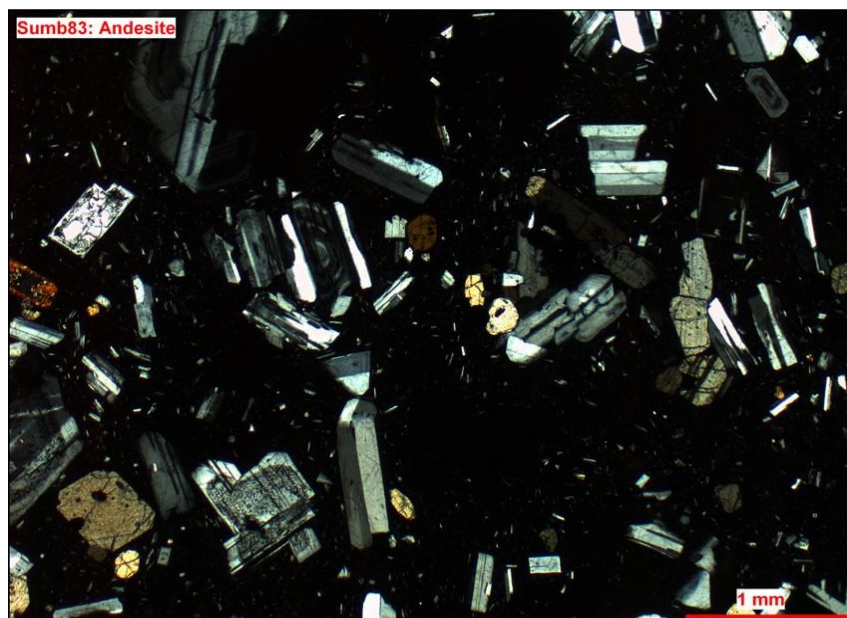
Fig. 3.6. (b) Photomicrograph of andesite Sumb83 showing a less porphyritic texture than displayed in pyroclastic deposits and cumulate-bearing lavas. Plagioclase and orthopyroxene phenocrysts display a lower severity of disequilibrium textures such as resoption and melt inclusions with only minor zoning in some feldspars.

Microlitic lavas

Fig. 3.7. (a) Field photograph of flow banding and mineral alignment in basaltic andesite rocks (Sumb76-77) at Kruwisan.
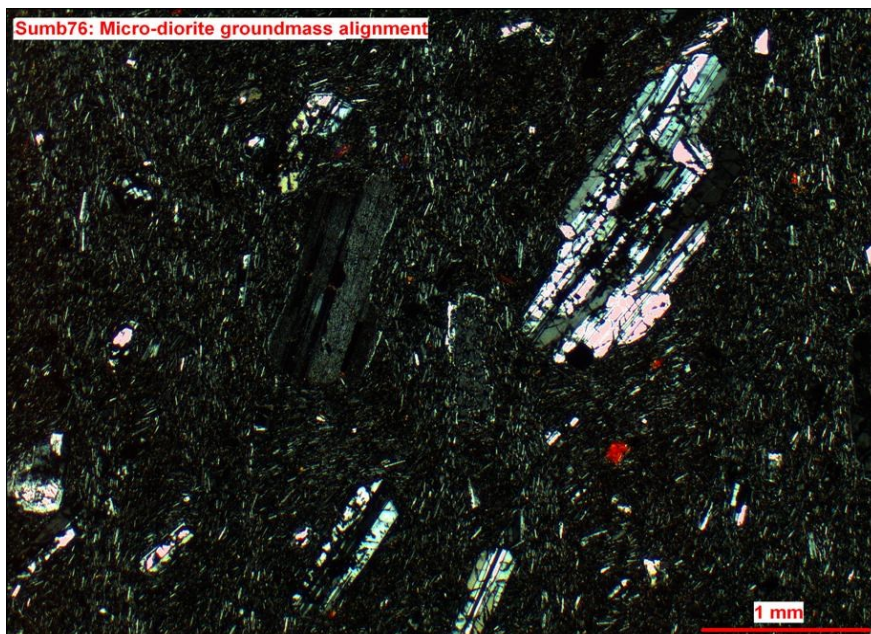
Fig. 3.7. (b) Photomicrograph of a microlitic lava (Sumb76) at Sumbing. The fine-grained groundmass shows alignment of plagioclase microlites around larger phenocrysts. Plagioclase has a very high modal abundance in these samples.

minerals are ~ 0.1 to 0.2 mm long. This subgroup will be discussed as part of the basaltic-andesite and andesite lavas in future sections.

To summarise the major observation differences between pyroclastic and lavas at Sumbing:

- The Pyroclastic samples are all highly porphyritic basaltic andesites. Phenocryst phases are dominantly plagioclase and clinopyroxene with titanomagnetite. Minor mineral phases include orthopyroxene, amphibole and apatite. Many phenocrysts show high degrees of zoning, resorption and melt inclusions with highly variable plagioclase anorthite contents (An = 92 to 36).

- The lavas are basaltic-andesite and andesite compositions. A number of the lavas contain cumulate composed of amphibole and apatite ± biotite. Phenocryst phases include plagioclase, orthopyroxene, clinopyroxene and titanomagnetite with various degrees of disequilibrium textures. Groundmass is predominantly glassy, and rarely microlitic. Plagioclase An-contents are more restricted (An = 59 to 37).

3.4. Geochemistry

The Sumbing volcanic rocks are classified by the Total Alkali-Silica (TAS) and K_2O against SiO_2 schemes, together with other published data for central Java, in figures 3.8 *(a)* and *(b)*. The Sumbing lavas plot within fields for medium-K basaltic-andesites and andesites. In contrast, most of the pyroclastic deposits show a high-K affinity and could be classified as basaltic trachy-andesites. From the other volcanoes in central Java, Merapi and Merbabu contain similar compositions to Sumbing, ranging from medium- to high-K; and Ungaran has high-K to shoshonitic magma compositions. Muriah shows Leucititic (HK) and shoshonitic (K) magma compositions similar to Ringgit-Besar in Chapter 2.

All major and trace element concentrations and isotope ratios presented below are plotted against SiO_2 (wt.%) as indices for differentiation. The discussion includes individual groups at Sumbing and their relationship with other volcanoes from central Java (e.g. Claproth, 1989; Edwards *et al.*, 1991; Gertisser & Keller, 2003; Handley *et al.,* 2011).

Classification Diagrams
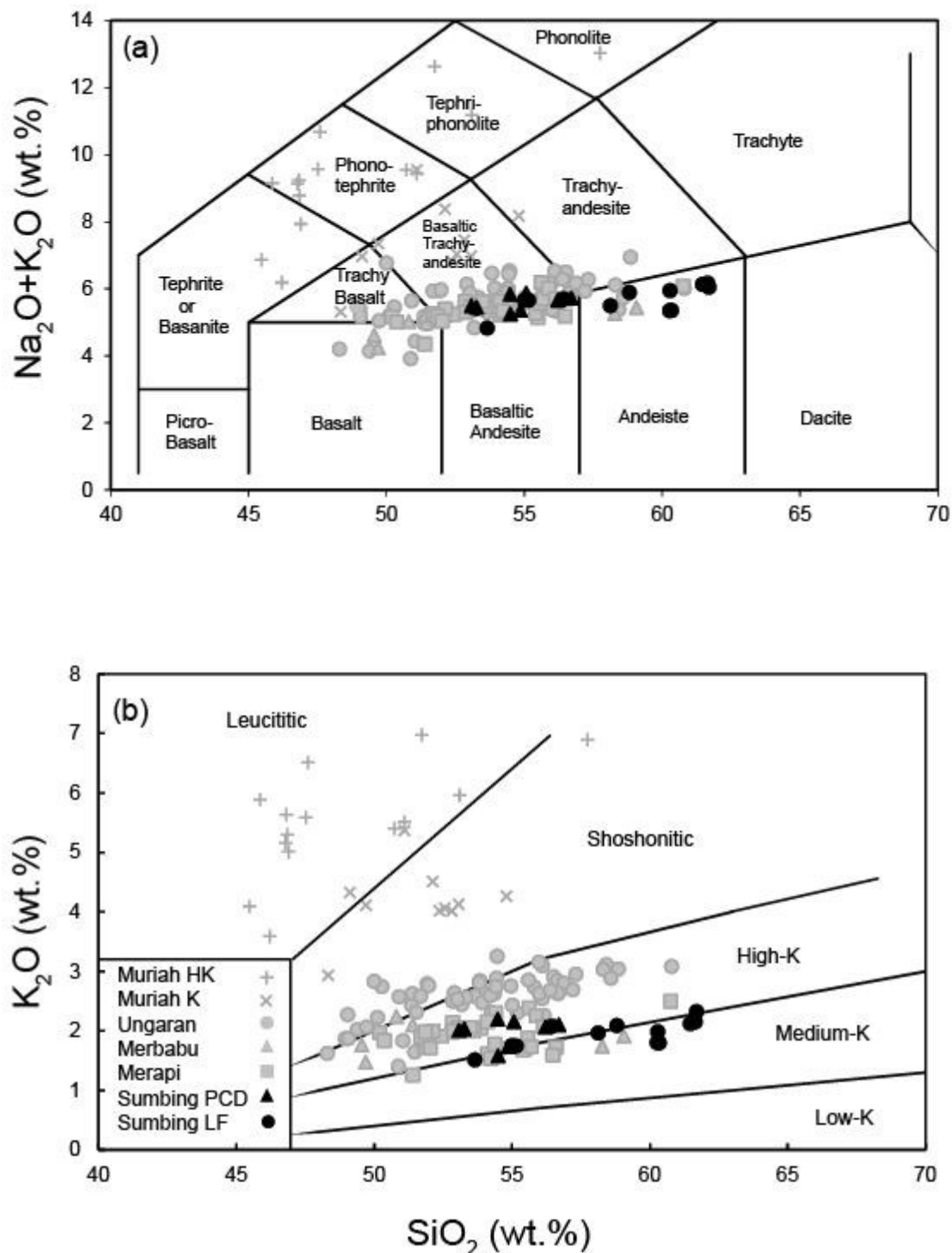
Fig. 3.8. (a) The Total Alkali-Silica (TAS) and (b) K_2O against SiO_2 classification schemes for east Java volcanic rocks, after Le Bas *et al*. (1986), Peccerillo & Taylor (1976) and Wheller *et al*. (1987). Sumbing samples are highlighted in black, where triangles represent pyroclastic deposits (PCD) and circles represent lava deposits (LD). Additional data after Claproth (1988); Edwards (1990), Edwards *et al*. (1991); Vukadinovic & Sutawidjaja (1995); Turner & Foden (2001); Gertisser & Keller (2003); Handley *et al*. (2011). See text for details.

3.4.1. Major Element Concentrations

Major element concentrations against SiO_2 for Sumbing are shown in figure 3.9 (*b, d, f, h, j, l, n,* and *p*), and compared to fields for Merapi, Merbabu and Ungaran in figure 3.9 (*a, c, e, g, i, k, m,* and *o*). TiO_2, Al_2O_3, Fe_2O_3, MgO and CaO decrease with increasing SiO_2 in all Sumbing groups. Na_2O becomes slightly elevated and there is poor correlation between K_2O and SiO_2. The andesites at Sumbing represent some of the most evolved rocks in central Java with low TiO_2, Al_2O_3 and Fe_2O_3 and high SiO_2 and Na_2O.

3.4.2. Trace Element Concentrations

The trace elements are evaluated here by their characteristic behaviour in basaltic and andesitic magmas and grouped accordingly.

3.4.2.1. Compatible Trace Elements (Ni, Cr, V and Sc)

Compatible trace-element concentrations are plotted against SiO_2 in Figures 3.10 (*a-h*). All rocks contain low concentrations of Ni (< 12 ppm) and Cr (<25 ppm) with little correlation against SiO_2. V and Sc are also low in concentration (< 210 ppm and < 30 ppm respectively) and decrease with increasing SiO_2 in both groups of lavas. The pyroclastic deposits contain slightly lower Sc contents than lava equivalents and similar V. The limited data for central Java show a broad decrease in all compatible trace element concentrations with differentiation.

3.4.2.2. Large-Ion Lithophile Elements (Rb, Ba, Sr and Pb)

Collectively, the group of elements known as Large-Ion Lithophile Elements (LILE) are considered to be the most readily mobilised in aqueous fluids. Some of these elements (such as Cs, Rb and Ba) are also among the most incompatible in basaltic magmas (Tatsumi *et al.,* 1986; Brenan *et al.,* 1995; Keppler, 1996). As a result, concentrations in arc magmas can be significantly elevated during partial melting, dehydration of subducting oceanic crust, melting of subducted sediments, or during differentiation in the crust (Hawkesworth *et al.,* 1993; Staudigel *et al.,* 1996; Elliot *et al.,* 1997; Davidson *et al.,* 2005).

Major Element Geochemical Plots against SiO_2 (1)
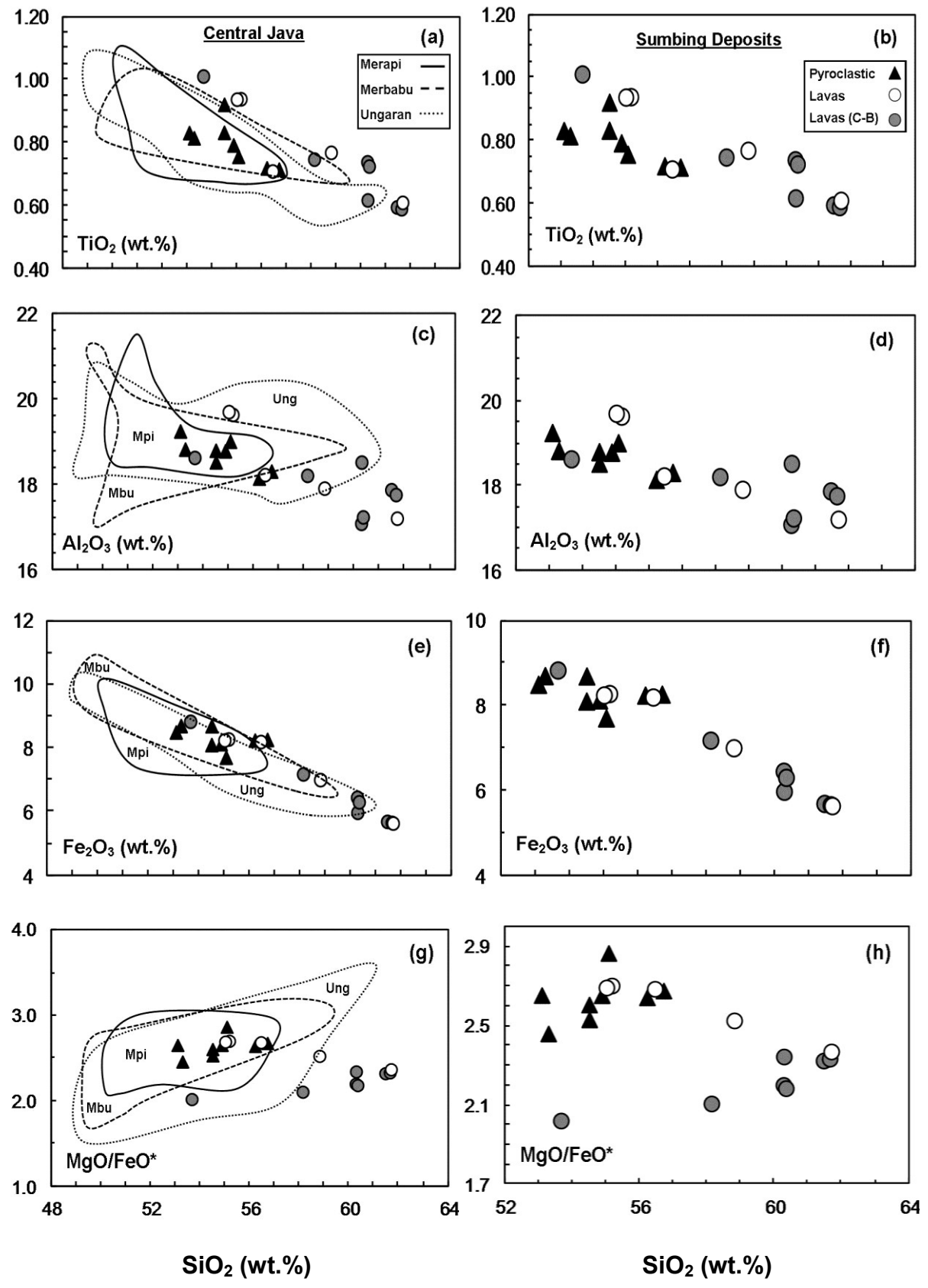
Major Element Geochemical Plots against SiO$_2$ (2)
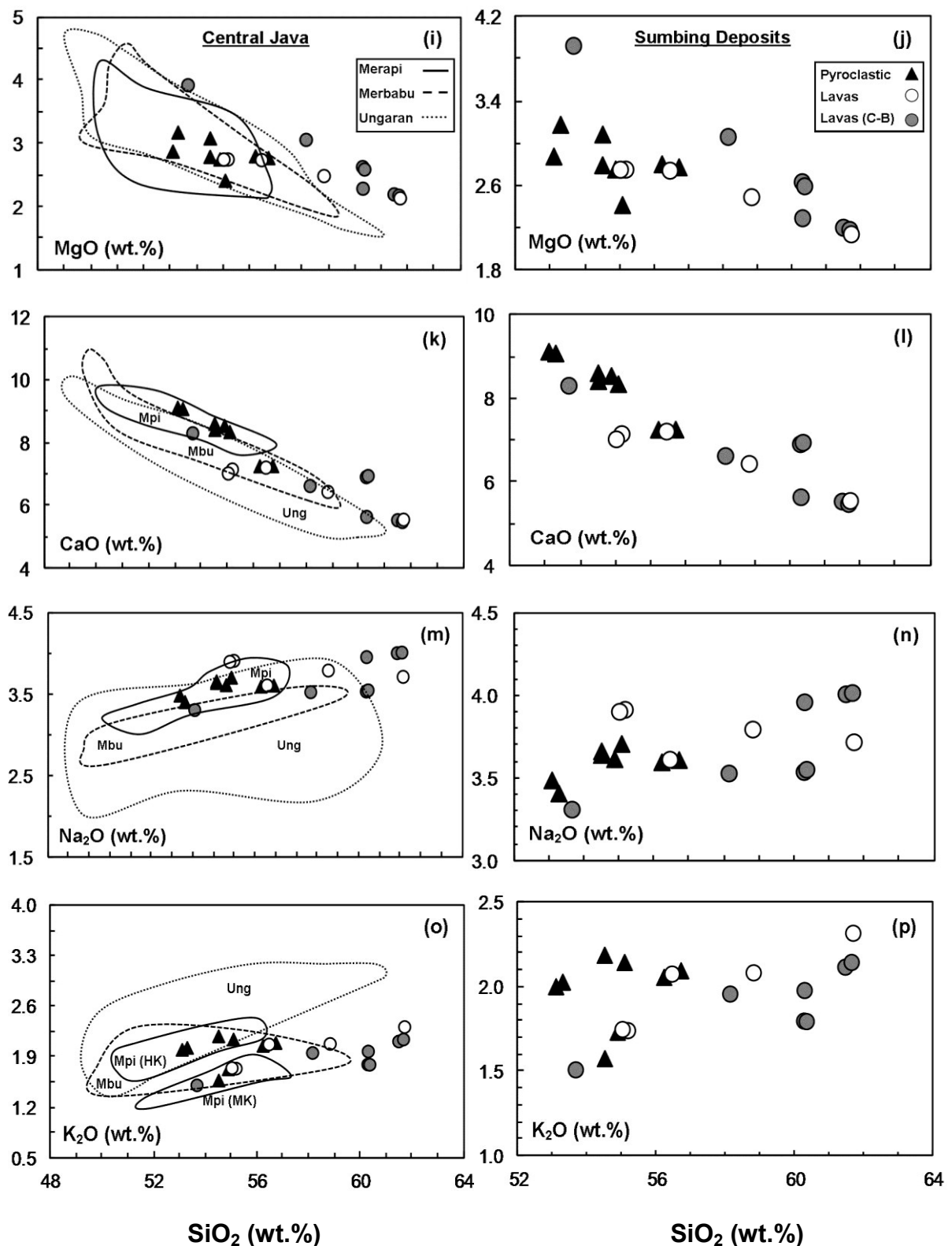
Fig. 3.9. (a-p) Major elements plotted against SiO$_2$ (wt.%). Figures on the left show major element concentrations for the Sumbing pyroclastic deposits (black triangles) and lavas (grey and white circles) relative to other volcanoes from central Java. Central Java data fields include: Merapi (Gertisser & Keller, 2003), Merbabu (Handley *et al.,* 2011) and Ungaran (Claproth, 1989). Figures on the right show major element concentrations between groups at Sumbing.

91

Compatible Trace Element Geochemical Plots against SiO_2
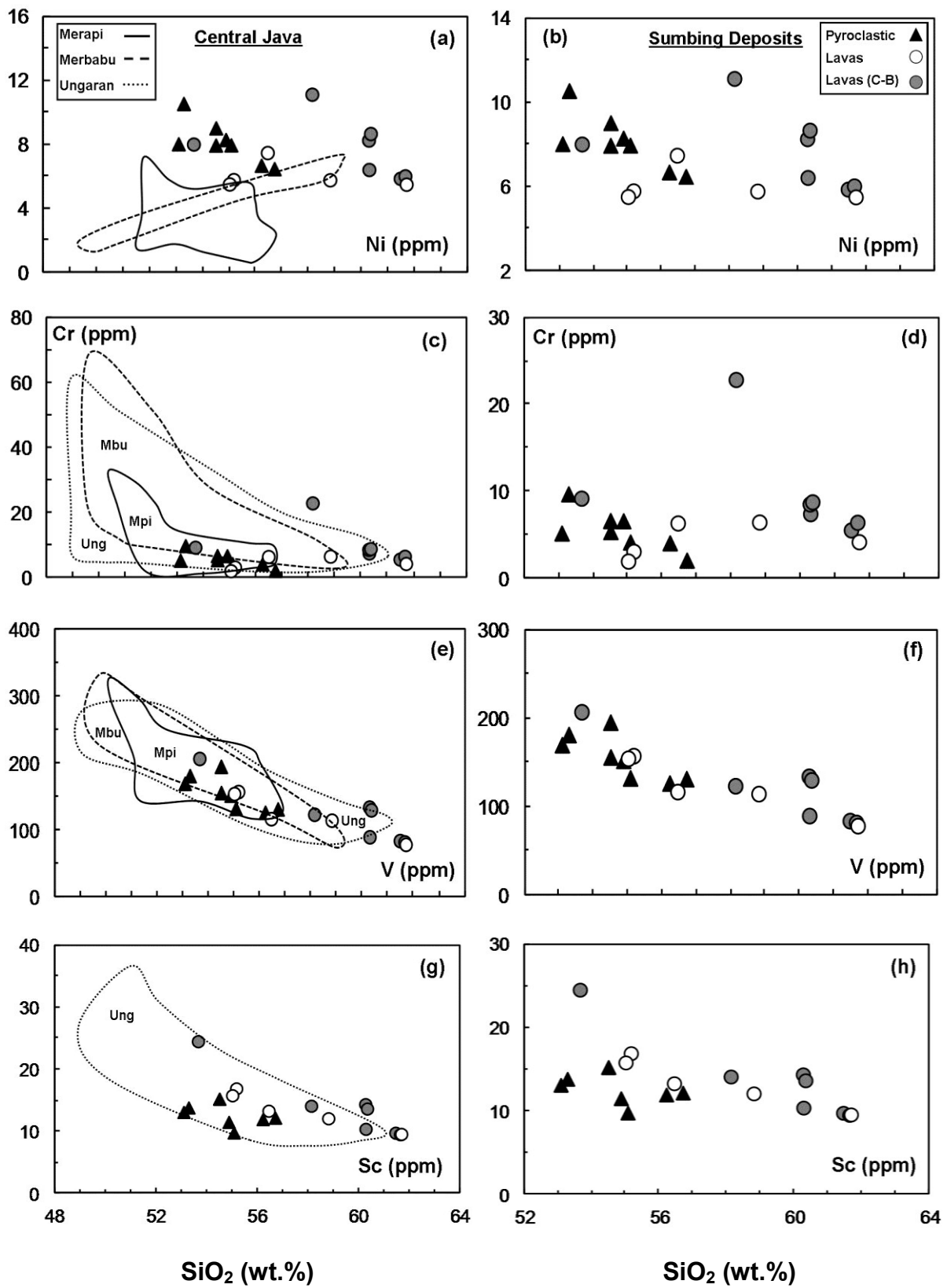
Fig. 3.10. (a-h) Trace elements showing compatible behaviour plotted against SiO_2 (wt.%). Left shows fields for central Java and right shows Sumbing groups. Note the low concentrations in Ni, Cr.

Mobile Trace Element Geochemical Plots against SiO$_2$
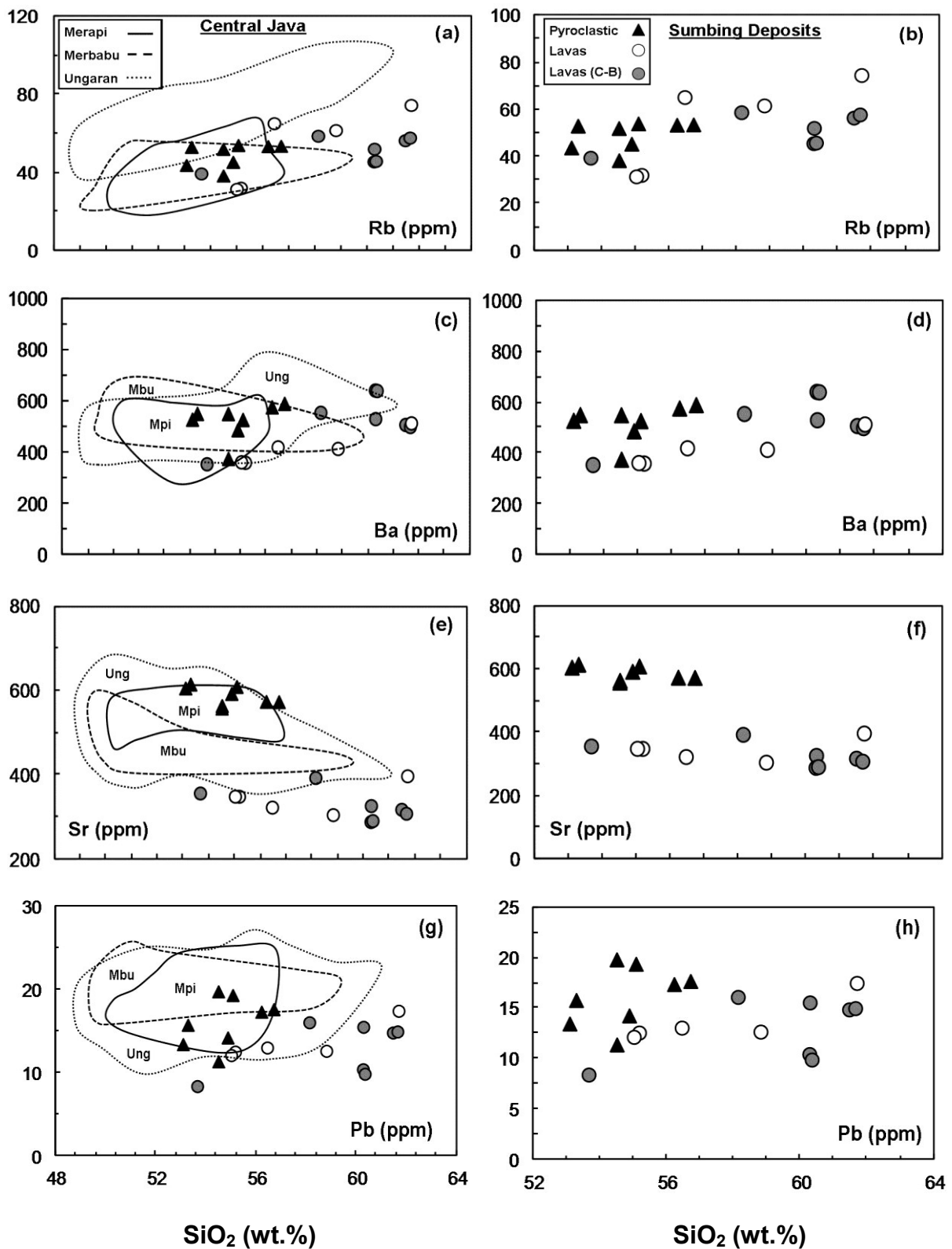
Fig. 3.11. (a-h) A group of trace elements considered to be the most fluid-mobile (e.g. Tatsumi *et al.,* 1986) plotted against SiO$_2$ (wt.%). Note the variation in Sr concentrations between pyroclastic deposits and lavas. Fields as for figure 3.9.

ImmobileTrace Element Geochemical Plots against SiO_2
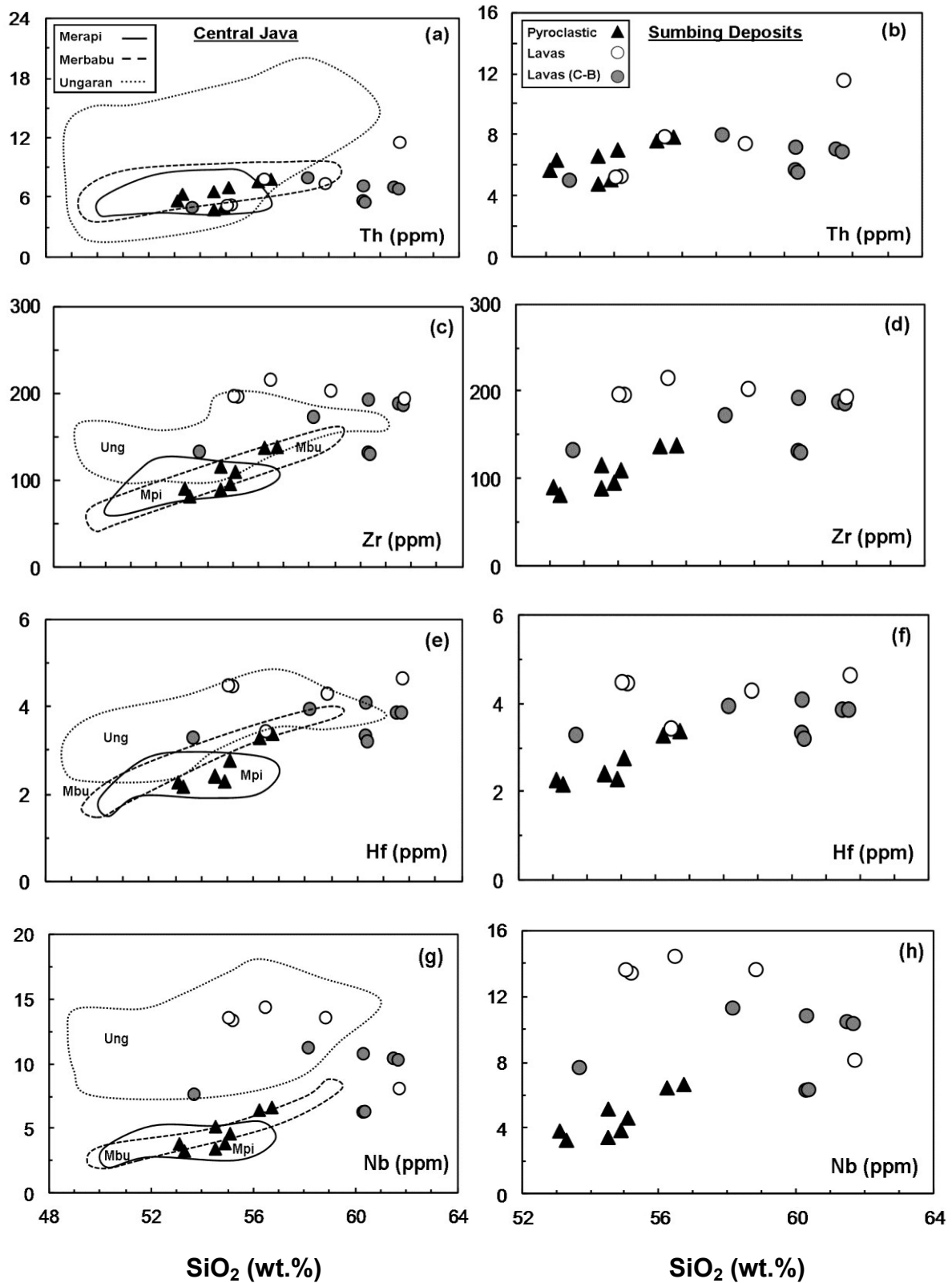
Fig. 3.12. (a-h) A group of trace elements considered to be the least readily mobilised in aqueous fluids against SiO_2 (wt.%). Note the high concentrations of HFSE in lavas (and Ungaran) relative to pyroclastic deposits (Merapi and Merbabu). Data fields as for figure 3.9.

LILE against SiO$_2$ are shown in figures 3.11 (*a-h*). Concentrations of Rb, Ba and Pb are indistinguishable for the Sumbing pyroclastic deposits and lavas and show little variation with SiO$_2$. On the other hand, Sr concentrations are considerably higher in the pyroclastic deposits (558 to 615 ppm) than in the lavas (288 to 397 ppm). Concentrations of LILE in the pyroclastic deposits plot inside the fields for Merapi for all examples.

3.4.2.3. High-Field Strength Elements (Th, Zr, Hf and Nb)

In contrast to the LILE, High-Field Strength Elements (HFSE) are considered to be much less readily mobilised in fluids and are less abundant in continental crust and sediments. For this reason, the HFSE are frequently used to investigate source compositions beneath island arcs (Pearce & Parkinson, 1993; Woodhead *et al.,* 1993; Handley *et al.,* 2011).

Th, Zr, Hf and Nb are plotted against SiO$_2$ in figures 3.12 (*a-h*). Concentrations of HFSE are typically higher in both groups of lavas relative to the pyroclastic deposits. Nb and Ta (not shown) show particularly evident disparities between the gropus of rocks at Sumbing. The pyroclastic deposits show more obvious elevations in Zr, Hf and Nb against SiO$_2$, and again plot within fields for Merapi. The lavas have compositions of Zr, Hf, Nb and Ta more similar to Ungaran which have Nb contents up to 18 ppm.

3.4.2.4. Rare-Earth Elements (La, Nd, Eu and Dy)

Selected Rare-Earth Elements (REE) against SiO$_2$ are shown in figures 3.13 (*a-h*). The basaltic-andesite and andesite lavas have higher concentrations of La, Nd, Eu and Dy than the cumulate-bearing lavas. These rocks display increasing La and Nd with increasing SiO$_2$ with little change in Eu and Dy (with the exception of two basaltic-andesites). The cumulate-bearing lavas show slight decrease in Eu and Dy which is not evident in the Light REE (LREE). Pyroclastic rocks show little variation of REE with differentiation. Compared to the other data in central Java REE concentrations at Sumbing are similar to Merapi and Merbabu. Based on the limited data for Ungaran, it appears to have elevated LREE relative to the other volcanoes with La/Yb ratios up to 28 (compared to Sumbing, mostly between 6 and 10).

REE Geochemical Plots against SiO$_2$
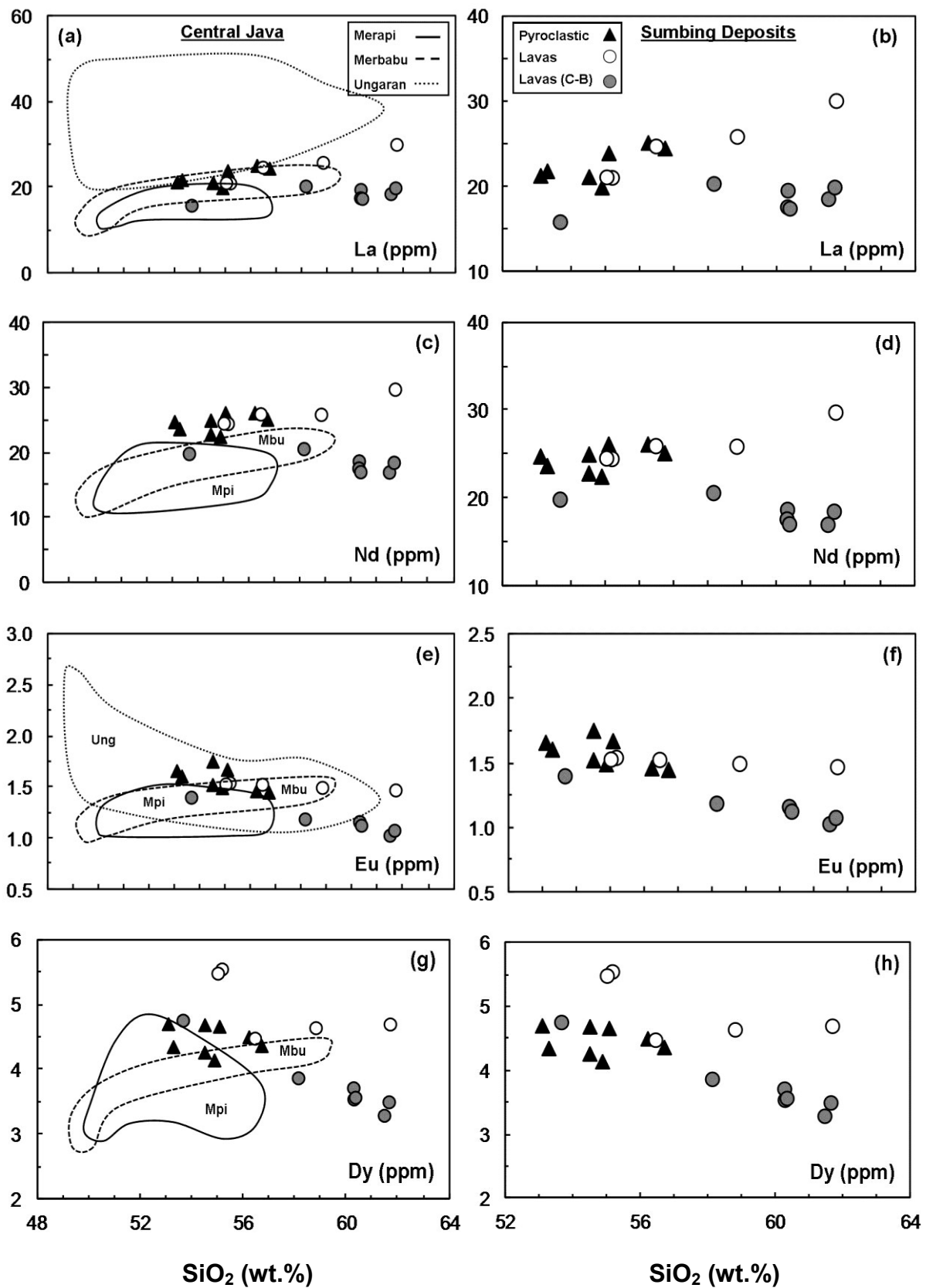
Fig. 3.13. (a-h) Selected Rare-Earth Elements plotted against SiO$_2$ (wt.%). Data fields as for figure 3.9.

3.4.3. Normalised Trace Element Concentrations

Trace element concentrations normalised to Normal Mid-Ocean Ridge Basalt (N-MORB) display the typical enrichments of LILE and LREE relative to HFSE and HREE as described for many volcanic arc rocks, including those from Java (Vukadinovic & Sutawidjaja, 1995; Gasparon & Varne, 1998; Turner & Foden, 2001; Gertisser & Keller, 2003; Handley, 2006). The similarity between trace element patterns in arc magmas and sediment analysed at Ocean drilling sites are commonly attributed to a subduction component (Plank & Ludden, 1992; Turner & Foden, 2001), although this is disputed beneath Java on the basis of limited sediment entering the trench and similarity to continental crust (Gasparon & Varne, 1998; Kopp *et al.,* 2006; Kopp, 2011). Nevertheless, normalised diagrams are often a useful tool for highlighting subtle variations between groups of elements which are not always obvious in element-element plots.

3.4.3.1. MORB-Normalised multi-element group variations

Normalised trace element plots for Java are show for Sumbing in figure 3.14 (*a-c*) relative to other volcanoes in central Java and a range of compositions for I-MORB. The I-MORB compositions range from a relatively depleted N-MORB, to a more enriched OIB-like composition and highlights the difficultly in constraining potential magma sources in Java. The most prominent variations are between the lavas (both groups) and the pyroclastic deposits, particularly for Sr (which are more elevated in the latter) and Nb, Ta, Zr, Hf (which are more elevated in the former). Patterns between group samples are not always parallel to each other, particularly for the LILE. The lavas show the most elevated concentrations of elements relative to MORB (excluding Ba, Pb, Sr and P) in this part of central Java (which for locality reasons does not include Slamet).

3.4.3.2. Chondrite-normalised rare earth elements

Chondrite-normalised REE plots for Sumbing samples are shown in figure 3.15. These include the pyroclastic deposits *(a)* and lavas *(b)* together with other central Java arc volcanoes and N-MORB; and more detailed plots of the pyroclastic deposits *(c)* and lavas *(d)*. The pyroclastic samples contain LREE between 84 and 106 times Chondrite and HREE

MORB-Normalised Multi-Element Diagrams
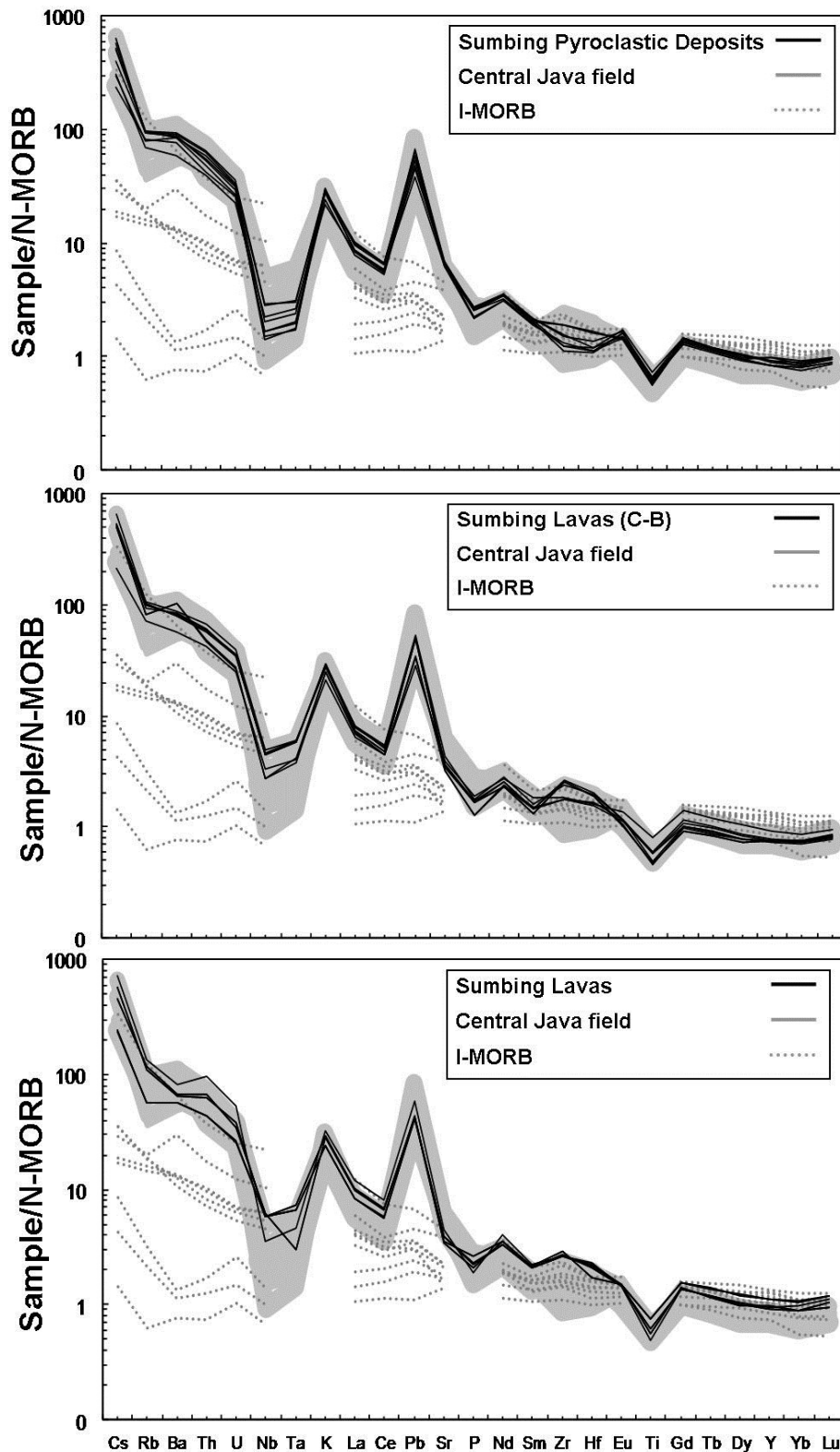
Fig. 3.14. Multi-element diagrams normalised to N-MORB (Sun & McDonough, 1989). Black lines show compositions for Sumbing pyroclastic deposits (top), cumulate-bearing lavas (middle) and lavas (bottom) relative to data from other data from central Java (grey line) and a representative range of I-MORB compositions (dashed grey lines). Data sources from central Java include: Merapi (Gertisser & Keller, 2003); Merbabu (Handley *et al.,* 2011); and Ungaran (Claproth, 1989). Data sources for I-MORB from Janney *et al.* (2005).

Chondrite-Normalised REE Diagrams
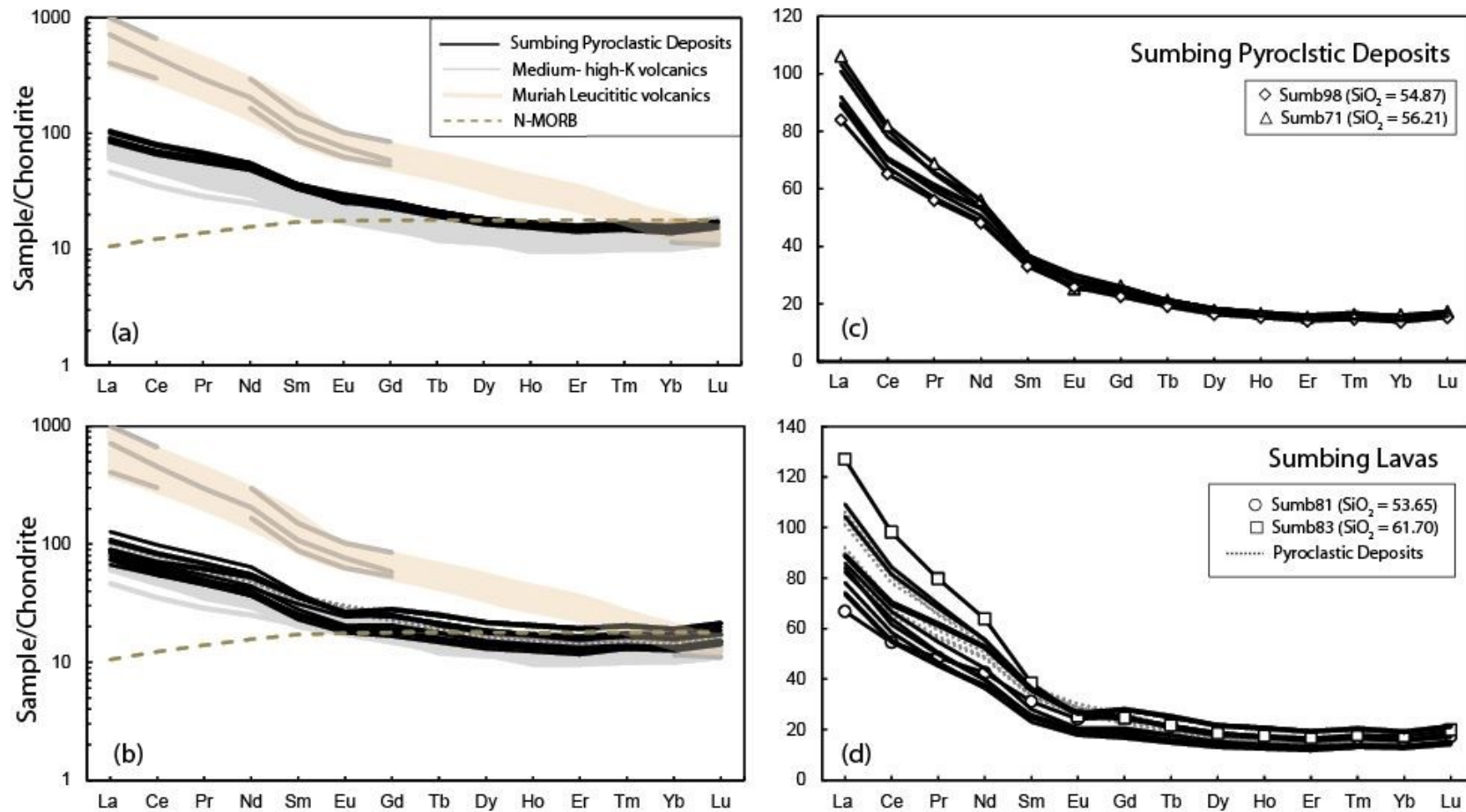
Fig. 3.15. Chondrite-normalised REE plots for **(a)** and **(c)**, the Sumbing pyroclstic deposits; and **(b)** and **(d)** the Sumbing lavas. Figures **(a)** and **(b)** include other data from central Java (references as for figure 3.8). The symbols in figures **(c)** and **(d)** show the most primitive and most evolved samples within the groups.

between 15 and 17 times Chondrite. The lavas have lower average LREE which range from 73 to 127 and HREE from 14 to 23.

Compared to other arc volcanoes in Java, Sumbing magmas show similar REE profiles with MORB-like HREE and higher LREE. In contrast, the leucititic magma compositions from Muriah display significantly higher LREE of between 400 and 1000 times Chondrite values for La.

3.4.4. Isotope Geochemistry

In this section isotope ratios are plotted against SiO_2 to show how they may have been modified during differentiation. Additional isotope-element, isotope-trace element ratio and isotope-isotope plots are shown in the discussion

$^{87}Sr/^{86}Sr$, $^{143}Nd/^{144}Nd$, $^{206}Pb/^{204}Pb$ and ^{176}Hf /^{177}Hf isotope data against SiO_2 are shown in figures 3.16 (*a-h*). The $^{87}Sr/^{86}Sr$ ratios at Sumbing have a wide range from 0.704458 to 0.705759, similar to other volcanoes in central Java (e.g. Claproth, 1998; Gertisser & Keller, 2003; Handley *et al.,* 2011). A distinction between the pyroclastic deposits and lavas are well defined by the more radiogenic values of the latter.

For the pyroclastic deposits, all samples exceed 0.705118 and become less radiogenic with increasing SiO_2. In contrast, the lavas are less radiogenic (< 0.704789), with the exception of one sample at 0.705108, and contain little variation between the groups. $^{143}Nd^{144}Nd$ ratios range from 0.512784 to 0.513059 with less distinction between groups although the pyroclastic rocks have generally lower values than the lavas.

$^{206}Pb/^{204}Pb$ shows a similar distinction between pyroclastic deposits and lavas. The single lava with more radiogenic Sr and less radiogenic Nd, also displays more radiogenic values for Pb. Sumbing pyroclastic deposits have $^{206}Pb/^{204}Pb$ values (18.75-18.78), similar to those at Merapi (18.73-18.78) and higher than the lavas (18.61-18.71). $^{176}Hf^{177}Hf$ ratios display the most restricted range (0.283096 to 0.283169 for all samples) and have values similar to Merapi (Handley *et al.,* 2011) with no change against SiO_2.

To summarise the major chemical differences between pyroclastic and lavas at Sumbing:

Isotopic Ratios against SiO$_2$
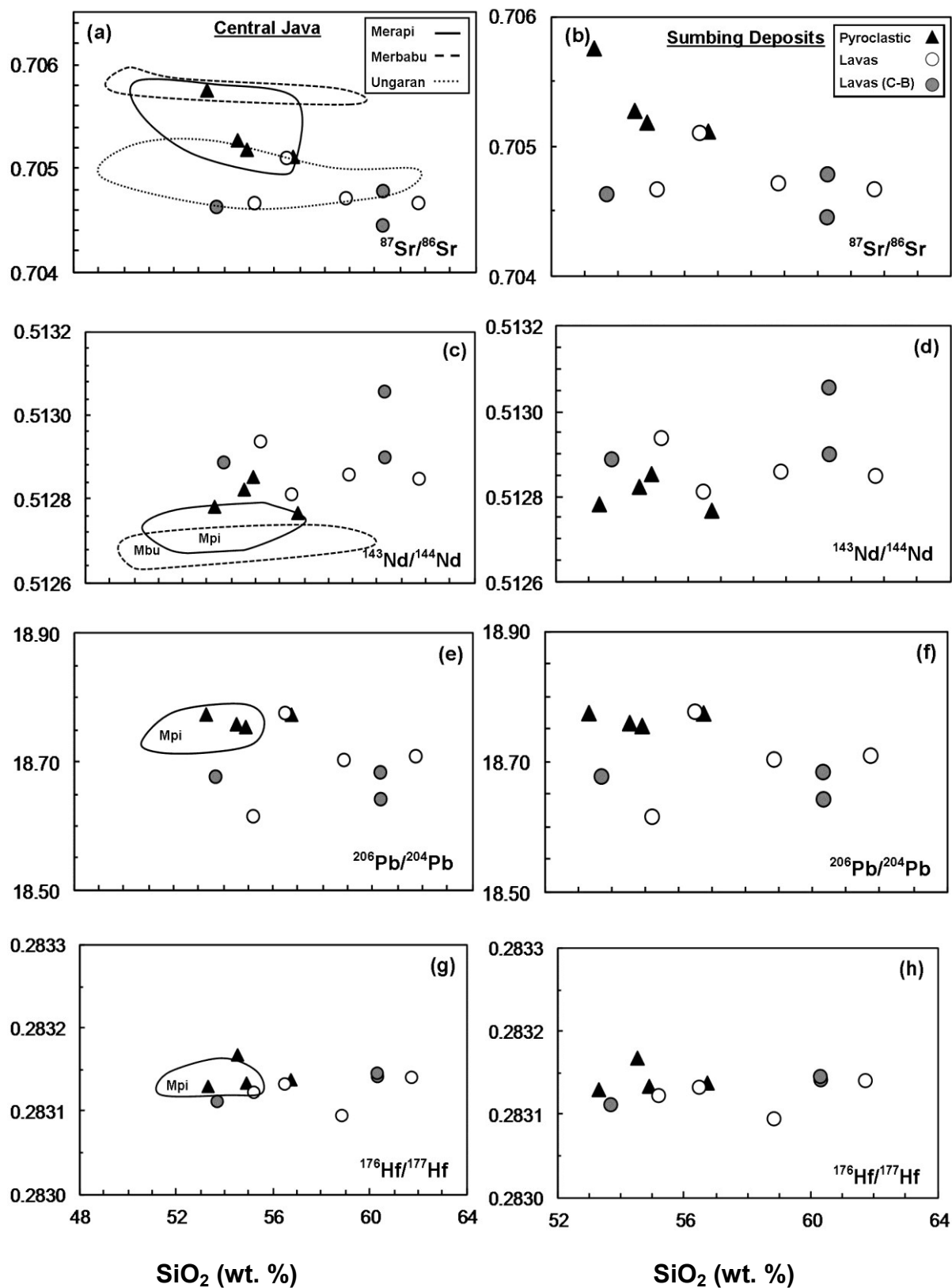
Fig. 3.16. (a-h) Selected radiogenic isotopes plotted against SiO$_2$ (wt.%). Data fields as for figure 3.9. Note elevations in ^{87}Sr^{86}Sr for Sumbing pyroclastic deposits (Merapi and Merbabu) relative to the lavas (and Ungaran).

- The Pyroclastic Deposits contain major and trace element and isotopic ratios very similar to Merapi. This includes notably higher Sr (ppm), $^{87}Sr/^{86}Sr$ and $^{206}Pb/^{204}Pb$ and lower HFSE and $^{143}Nd/^{144}Nd$ than the lavas. $^{87}Sr/^{86}Sr$ ratios become progressively higher in samples with lower SiO_2 (wt.%)

- The lavas are more heterogeneous in their chemistry with variable MgO/FeO*, Ni, Cr and La/Yb, lower $^{87}Sr/^{86}Sr$ and $^{206}Pb/^{204}Pb$, higher $^{143}Nd/^{144}Nd$, and similar $^{176}Hf/^{177}Hf$ compared to the pyroclastic rocks. Elevated HFSE contents in the lavas resemble those at Ungaran. There is little variation between isotope ratios and differentiation, other than lava Sumb78, which contain ratios similar to the pyroclastic deposits.

The aim of the next section is to examine the processes which are capable of causing the magmatic variation between the groups described above.

3.5. Discussion

3.5.1. Discriminating between Pyroclastic Deposits and Lavas through upper crustal processes

The absence of primitive rock compositions at Sumbing suggest that the magmas were modified from an original mantle source as they rose through the crust. It is therefore important to establish the nature and extent of the processes that occur via differentiation in crustal reservoirs to see if they are capable of creating the decoupling of elements between magmatic groups. Island arc magmas are rarely emplaced at the surface without having experienced some degree of fractional crystallisation, mixing between magmas of different compositions or growth conditions, and/or assimilation of the arc crust (Davidson, 1987; Gasparon *et al.,* 1994; Handley, 2006; Deegan *et al.,* 2010).

Evidence for upper crustal processes typically includes textural signs of disequilibrium in minerals, incorporation of crustal and cumulate xenoliths, and systematic element variations against indices of differentiation with low concentrations of compatible elements (e.g. Davidson *et al.,* 2005). It is also suggested that dominance of intermediate compositions in volcanic arcs may reflect mixed hybrids, where reservoirs with slowly evolving melts are

replenished by an influx of primitive mafic magma prior to eruption (Sudradjat, 1991; Reubi *et al.,* 2002). Petrographic observations suggest that mixing between compositionally distinct magmas are common beneath Sumbing, and minerals which have experienced different growth conditions have also been mixed together. The question is; to what extent does this modify the chemistry of the lava?, does it affect all of the rocks?, and are any other open system processes in operation?

Simple binary mixing between two magmas would be expected to produce near linear relationships on element-element plots, or hyperbolic arrays on ratio-element plots (Langmuir *et al.,* 1978; Vogel, 1982; Flood *et al.,* 1989). This type of geochemical trend is not obvious in the element-element plots shown in figures 3.9 to 3.13. However, the addition of plutonic xenoliths, and mingling between magmas and distinct crystal residues, would create disturbances in magmatic trends by the addition (or removal) of mineral phases (Luhr & Haldar, 2006). This provides a more realistic process for some groups at Sumbing.

The pyroclastic samples at Sumbing show a highly porphyritic appearance with abundant clinopyroxene and plagioclase phenocrysts. Plagioclase core-to-rim compositions (An_{36-90}) are particularly variable in these rocks compared to the lavas. A wide range in anorthite content is not an unusual feature in Sunda arc volcanoes (e.g. Handley, 2006; Chadwick *et al.,* 2007). However, the wide range is limited to the pyroclastic rocks.

The lava deposits show a restricted range of anorthite contents which do not exceed $An_{59.}$ It is evident that mineral chemistry and petrography in addition to chemistry can distinguish two groups of rocks at Sumbing which have potentially had different pre-eruptive histories. It is also evident that both groups have experienced differentiation prior to emplacement. To address these issues in greater detail, the two groups are evaluated on an individual basis below.

3.5.1.1. Differentiation of magmas 1: Fractional Crystallisation

The most notable variation in chemistry between the pyroclastic rocks and lavas are the concentrations in Sr and HFSE. Strontium is characteristically compatible in plagioclase, where it readily substitutes for calcium. Therefore, one way of producing the distinction between groups could be to either accumulate plagioclase in the pyroclastic rocks, or remove plagioclase from the lavas.

Higher concentrations of CaO, Al$_2$O$_3$, Ba and Eu for a given SiO$_2$ and MgO contents in the pyroclastic samples add support this idea. To quantify this hypothesis, modelling has been applied to both groups using the XLFRAC Least Squares modelling technique (after Stormer & Nicholls, 1978).

Least Squares Modelling

The model requires an initial (parent) and final (daughter) magma (whole-rock oxide values), together with a number of phases representative of mineral compositions. It works by calculating the probability of adding or subtracting the phases in order to derive the daughter from the parent, in which a good solution minimises the sum of all residuals ($\sum r^2$). For this model, 8 oxides are used and the five phases present in most rocks; plagioclase, amphibole, clinopyroxene, orthopyroxene and titanomagnetite. The objectives are firstly, to determine whether pyroclastic deposits and lavas can be derived from the addition and/or removal of plagioclase; and secondly, the plausibility of fractional crystallisation as a driving force between group compositions.

Results of the modelling are shown in table 3A (*1-14*). For each sample, SiO$_2$ and Mg# values are given, together with the mineral phases required to be removed or added during differentiation. Models 1-7 use lava Sumb81 as a parent magma composition because it is the least evolved rock on the basis of SiO$_2$ and Mg#. Because there are no obvious liquid lines of decent (based upon geochemistry), daughter derivatives from a number of the lavas have been calculated (see figure 3.17*a*).

Models 1-7 produce acceptable results with $\sum r^2$ values of between 0.06 and 0.26 in accordance with a crystallisation assemblage of plagioclase + amphibole + opx + cpx + Fe-Ti oxide. Results show that between 21.80% and 55.68% crystallisation of the minerals are required to produce the daughter compositions from Sumb81. Models 1 to 3 use CBL's as daughter compositions with progressive elevations in SiO$_2$ and decreases in Mg#. This series of rocks do not form a liquid line of decent because of inconsistencies in the removal of amphibole and clinopyroxene. Similarly, the same is true for models between Sumb81 and the lavas (4-7). For this case the only inconsistency is in model 6, where Sumb78 requires less clinopyroxene removal than adjacent lavas.

XLFRAC Modelling Results for Sumbing Magmas

Plag+amph+cpx+opx+Fe-Ti oxide

Model Number	Group Parent	SiO$_2$	Mg#	Group Daughter	SiO$_2$	Mg#	$\sum r^2$	Phases plag	amph	cpx	opx	Fe-Ti oxide	Removed (%)	Added (%)	Total (%)
1	Sumb81 (Lava C-B)	53.65	47.69	Sumb80 (Lava C-B)	58.13	46.64	0.06	-21.83	-8.66	-3.37	-1.10	-2.69	-37.65	0.00	-37.65
2	Sumb81 (Lava C-B)	53.65	47.69	Sumb92 (Lava C-B)	60.35	45.75	0.24	-28.07	-12.59	-0.01	-2.98	-3.25	-46.90	0.00	-46.90
3	Sumb81 (Lava C-B)	53.65	47.69	Sumb73 (Lava C-B)	61.65	44.12	0.26	-32.14	-9.93	-4.52	-3.31	-3.80	-53.70	0.00	-53.70
4	Sumb81 (Lava C-B)	53.65	47.69	Sumb83 (Lava)	61.70	43.74	0.21	-34.74	-8.52	-4.00	-4.55	-3.87	-55.68	0.00	-55.68
5	Sumb81 (Lava C-B)	53.65	47.69	Sumb85 (Lava)	58.81	42.17	0.16	-27.79	-7.44	-3.50	-3.95	-2.86	-45.54	0.00	-20.37
6	Sumb81 (Lava C-B)	53.65	47.69	Sumb78 (Lava)	56.45	40.68	0.08	-20.45	-6.46	-2.14	-3.58	-1.58	-34.21	0.00	-34.21
7	Sumb81 (Lava C-B)	53.65	47.69	Sumb76 (Lava)	55.16	40.53	0.11	-9.73	-3.51	-5.65	-2.01	-0.90	-21.80	0.00	-21.80
8	Sumb78 (Lava)	56.45	40.68	Sumb85 (Lava)	58.81	42.17	0.16	-11.11	-1.52	-2.06	-0.54	-1.95	-17.18	0.00	-17.18
9	Sumb78 (Lava)	56.45	40.68	Sumb83 (Lava)	61.70	43.74	0.27	-21.65	-3.18	-2.81	-1.45	-3.48	-32.57	0.00	-32.57
10	Sumb81 (Lava C-B)	53.65	47.69	Sumb99 (Pyroclastic)	53.28	42.82	0.25	-8.17	3.59	1.70	-7.98	-0.06	-16.21	5.29	-10.92
11	Sumb81 (Lava C-B)	53.65	47.69	Sumb97 (Pyroclastic)	55.07	39.12	0.12	-16.64	-0.48	-0.98	-8.11	-1.37	-27.58	0.00	-27.58
12	Sumb97 (Pyroclastic)	55.07	39.12	Sumb99 (Pyroclastic)	53.28	42.82	0.24	11.84	5.56	3.73	0.21	1.83	0.00	23.17	23.17
13	Sumb99 (Pyroclastic)	53.28	42.82	Sumb97 (Pyroclastic)	55.07	39.12	0.14	-10.83	-3.77	-3.3	-0.64	-1.57	-20.11	0.00	-20.11
14	Sumb80 (Lava C-B)	58.13	46.64	Sumb85 (Lava)	58.81	42.17	0.07	-9.14	1.59	-0.1	-4.34	-0.26	-13.84	1.59	-12.25

Table 3A. Results of least squares modelling. Small $\sum r^2$ values indicate good agreement between model and daughter composition. BA = basaltic andesite, (%) removed = sum of the mineral phases removed during fractional crystallisation between parent and daughter compositions, (%) added = sum of the mineral phases added during fractional crystallisation between parent and daughter compositions. Plag = plagioclase, amph = amphibole, opx = orthopyroxene, Fe-Ti oxide = titanomagnetite, cpx = clinopyroxene.

Three other models (8, 9 and 14) use only lava compositions; 8 and 9 uses Sumb78 as a parent composition and produces unsatisfactory results using other lavas (85 and 83) as daughter compositions. This is not surprising because the latter contain higher SiO_2 and higher Mg# than Sumb78, which would not be expected if the daughter compositions were produced through fractional crystallisation. Finally, model 14 has a very acceptable $\sum r^2$ value of 0.07. However, the CBL Sumb80 requires the addition of amphibole to produce lava 85, which is again, not consistent with simple fractional crystallisation.

The results of Least Squares modelling show that the lavas cannot be produced by either, fractional crystallisation within groups, or between the CBL and lava compositions; which supports the petrographic observations and geochemical data. In addition to these examples, four models are shown which include the pyroclastic samples. Models 10 and 11 show that much smaller quantities of plagioclase and larger quantities of orthopyroxene are removed parent Sumb81, and that amphibole and clinopyroxene are added in model 10.

The addition of clinopyroxene, and to a lesser extent amphibole, with removal of orthopyroxene is consistent with the petrography of these rocks, which have higher quantities of clinopyroxene and amphibole phenocrysts and little visible orthopyroxene. The final two models calculate between pyroclastic parent and daughter compositions (see models 11 and 12).

The pyroclastic rocks were also analysed without amphibole as a crystallising mineral phase (not shown) because it is unclear whether amphibole phenocrysts are xenocrystic in nature. Also clinopyroxene and orthopyroxene appear to show significant variations in abundance, the former becoming more concentrated in the lower SiO_2 samples, while the latter becomes less abundant.

Models which involve a lower silica parent and higher silica daughter yield good results, with $\sum r^2$ values of 0.03, but show significant removal of clinopyroxene, moderate removal of plagioclase and minor removal of titanomagnetite; with addition of orthopyroxene. These results appear to be completely inconsistent with petrographic observations. When reversed (i.e. high SiO_2 parent to low SiO_2 daughter), the model provides a similarly good result ($\sum r^2$ values of 0.03), but requires the addition of clinopyroxene and plagioclase which would appear more plausible considering the high abundance of these minerals, particularly in the lower SiO_2 samples. Furthermore, $^{87}Sr/^{86}Sr$ ratios increase from high-silica, to low-silica

samples which suggest that differentiation may be driving magma compositions to lower SiO$_2$ and higher ^{87}Sr/^{86}Sr.

To summarise; the highly porphyritic nature of the pyroclastic deposits composed of clinopyroxene (often clearly replacing other mineral phases) and plagioclase, suggest that it is plausible that these samples were becoming progressively silica-depleted, opposed to silica-enriched. In which case, the modelling shows that to produce the daughter magma (Sumb96 at 53.08 wt.% SiO$_2$), the parent (Sumb69 at 56.71 wt.% SiO$_2$) requires an additional 50% clinopyroxene, 14% plagioclase and 3% titanomagnetite, balanced by the removal of 45% orthopyroxene. This will be discussed in greater detail in section 3.5.1.2.

Trace Element Modelling

Least Squares modelling suggest that fractional crystallisation alone cannot account for major element variations in the CBL and lavas at Sumbing; also, that the pyroclastic samples may be differentiated towards more silica-depleted compositions. To further test these ideas, trace element models are applied to the same 14 models and shown in figures 3.17 (*b-f*). In these models, the results from XLFRAC least squares models are used to calculate the degrees of crystallisation and phase proportions. Element concentrations during fractional crystallisation are calculated using the Raleigh fractionation equation, which is defined by the equation $C_l/C_o = F^{(D-1)}$; where C_l is the concentration of an element in the daughter (final) liquid, C_o is the concentration of an element in the parent (initial) liquid, F is the melt fraction remaining , and D is the bulk distribution coefficient.

Each of the figures in 3.17 includes a grey band which represents 20% variation from a 1 line. An acceptable model solution will plot within the band for each element, and good models fit close to 1. Elements which plot above this band show that a particular element calculated during modelling is too high; and therefore, the measured (true) value is lower than expected from fractional crystallisation. Conversely, elements which plot below the line contain higher than expected concentrations.

Figure 3.17*b* shows models for the CBL; which, in agreement with Least Squares models, show poorer solutions for 2 and 3, and a good solution for 1. In general most elements are lower than expected. One reason for this may be the high degrees of crystallisation predicted

Trace Element Modelling Results
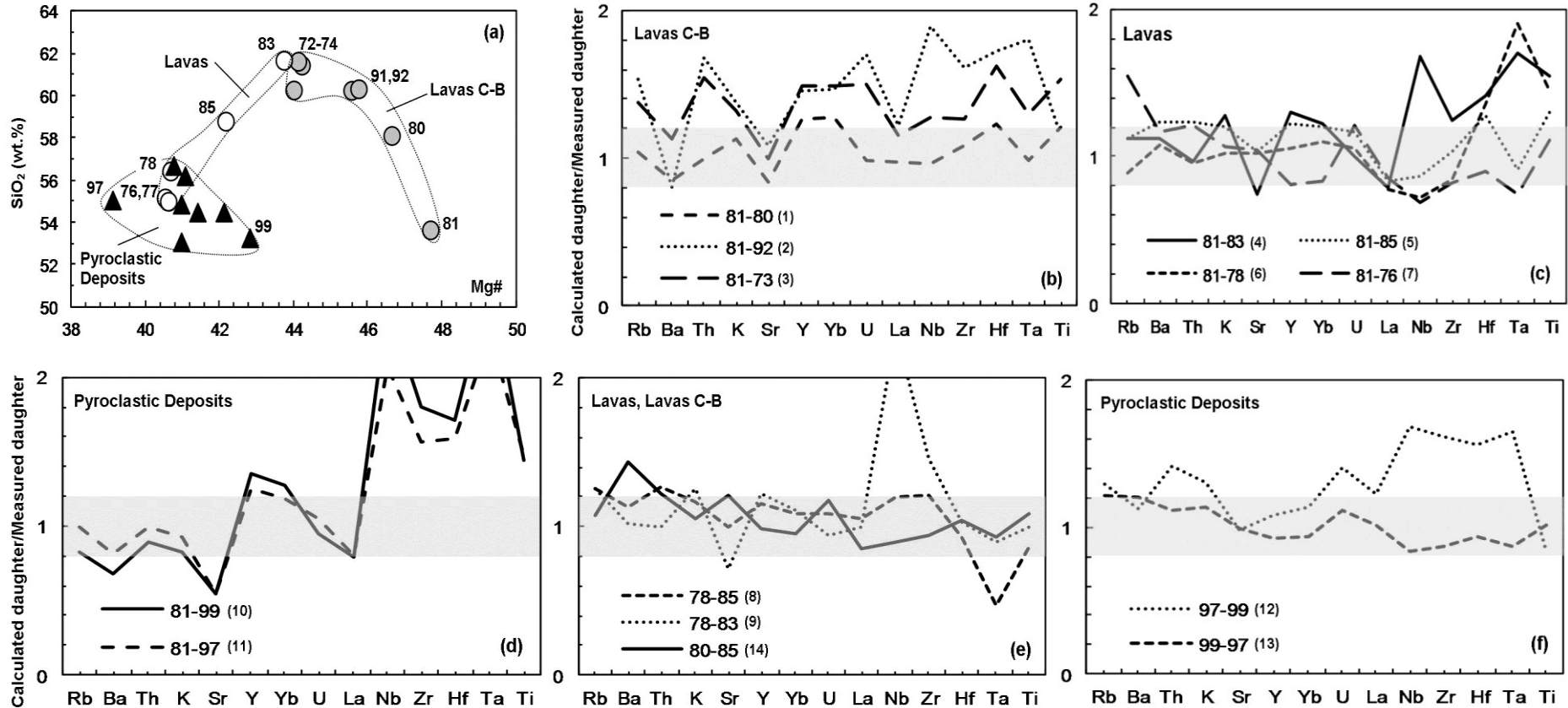
Fig. 3.17. Results of trace element modelling. **(a)** Shows the samples selected for modelling and their SiO₂ concentrations and Mg#'s. **(b)** The probability that cumulate-bearing lavas are derived through fractional crystallisation of Sumb81. Small numbers represent corresponding XLFRAC Least Squares Model. Elements which provide a satisfactory solution are closer to 1and the grey line represents within 20% error. **(c)** The probability that lava trace element concentrations can be produced through fractional crystallisation of Sumb81. **(d)** The probability that trace element concentrations in the pyroclastic deposits can be produced through fractional crystallisation of Sumb81. **(e)** A model involving other potential parent lava compositions. (f) Modelling between two pyroclastic deposits. Mineral phases and degree of crystallisation used from least square models above. Partition coefficients used from selected basaltic-andesites and andesites from http://earthref.org/GERM/index.html.

from the XLFRAC models, which are probably unrealistic considering the small variations in SiO$_2$ and Mg# values (figure 3.17*a*).

Figure 3.17*c* shows models 4-7 which produce slightly better solutions, but with variable predicted HFSE concentrations. Again, there may be a number of reasons for this. In particular, kd values for HFSE can vary dramatically depending on residual phases such as amphibole, in which HFSE may be more compatible. However, this problem can be applied to all of the models, most of which show variable HFSE. This is highlighted in figure 3.17*e* (8 and 9), which shows relatively good model solutions for all elements other than Nb and Ta.

Figure 3.17*d* shows the trace element modelling between lava Sumb81 and the pyroclastic deposits. This shows particularly poor solutions for Sr, which is higher in the samples than calculated by the models; and HFSE which are significantly lower than predicted by the models. Similar variations in Sr and HFSE are noted between pyroclastic deposits and lavas in fig. 3.11. Ba is also low in these rocks, which suggests that the addition (or accumulation) of plagioclase may be responsible. Figure 3.17*f* (12) shows a similar profile between the high SiO$_2$ pyroclastic sample (parent composition) and low SiO$_2$ pyroclastic sample; albeit mostly above the 1 line (compare profiles of 3.17*d* (10 and 11) with 3.17*f* (12)).

Major and Trace Element Summary between groups

- A combination of observational evidence, geochemistry and modelling suggest that differentiation is driving the Pyroclastic Deposits towards lower SiO$_2$ with higher ^{87}Sr/^{86}Sr contents, accumulating plagioclase and clinopyroxene.

- Fractional crystallisation cannot account for the difference between the lavas and pyroclastic samples, or within group variations. Sr and to a lesser extent Ba are higher in these samples than would be expected from simple fractional crystallisation, and HFSE's are lower.

- Lavas produce slightly better modelling solutions, although fractional crystallisation is unable to account for variations between the CBL and other lava samples. Some trace element model profiles resemble those for the pyroclastic rocks.

3.5.1.2. Differentiation of magmas 2: Contamination of the Arc Crust

Major and trace element modelling shows that additions, as well as removal, of mineral phases is important at Sumbing; and that simple closed-system evolution produced by fractional crystallisation does not fully account for the geochemistry of samples. While this type of semi-quantitative modelling provides some important information about magma differentiation, it does not distinguish between fractional crystallisation, magma mixing and assimilation or assimilation and fractional crystallisation (AFC). Therefore, other types of differentiation must be examined.

It was noted in section 3.5.1, that simple binary mixing should produce linear relationships between elements and hyperbolic arrays between elements and ratios which are not obvious in any of the Sumbing groups. Therefore, this section will address crustal contamination. For simplicity, the lavas will be discussed as one group because they contain very similar isotopic ratios compared to the pyroclastic rocks.

Continental xenoliths have not been discovered at Sumbing to provide direct evidence of the lithologies through which the magmas may interact at lower and mid-crustal levels. However, recently erupted calc-silicate xenoliths at Merapi provide considerable evidence for interaction between the magmas and local carbonate-rich upper crust (Chadwick *et al.,* 2007; Deegan *et al.,* 2011; Troll *et al.,* in press). The xenoliths contain skarn-type mineralogy of wollastonite and diopside with vesicular reaction rims from interaction with the basaltic andesite (Deegan *et al.,* 2011). Similar magma-carbonate interactions have also been reported from Vesuvius and the Alban Hills, Italy (Del Moro *et al.,* 2001; Gilg *et al.,* 2001; Dallai *et al.,* 2004), and Popocatepetl, Mexico (Goff *et al.,* 2001; Schaaf *et al.,* 2005), and is often accompanied by high CO_2 fluxes and explosive eruptions similar to those at Merapi (Deegan *et al.,* 2010; Troll et *al.,* in press).

The upper crust beneath Merapi is reported to be a 2 km thick succession of limestone, marl and volcaniclastic units which may extend to depths of up to 11 km in the Kendeng basin, (van Bemmelen, 1949; Smyth, 2005; Deegan *et al.,* 2010). This is likely to be similar for Sumbing, which is located about 50 km west of Merapi and bordered to the south by carbonates, marls and volcanic remnants from the West Progo Beds. So the magmas have, at least the potential to interact with similar rocks at shallow levels.

Experimental studies suggest that basaltic magma which incorporates sedimentary carbonates will result in silica-depleted (and under-saturated) residual melt, as a consequence of favoured Ca-Al rich silicic phases such as Ca-rich plagioclase and clinopyroxene, at the expense of other mineral phases. Increasing carbonate interaction will also increase the degree of crystallisation in a magma and generate CO_2-rich fluid phases in the reactions:

$$CaCO_3 + MgO^{melt} + 2SiO_2^{melt} \rightarrow CaMgSi_2O_6^{cpx} + CO_2^{fluid}$$

$$2CaCO_3 + 3SiO_2^{melt} + Mg_2SiO_4^{olivine} \rightarrow 2CaMgSi_2O_6^{cpx} + 2CO_2^{fluid}$$
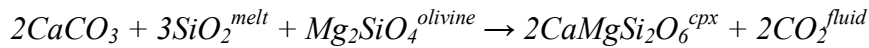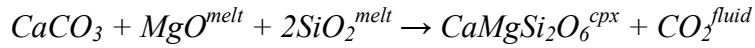
This provides one possible explanation for the XLFRAC modelling results and mineralogy of pyroclastic deposits, particularly the idea of magmas becoming progressively silica-depleted and the highly crystalline, plagioclase and clinopyroxene-rich, nature of the rocks. It also poses an interesting question about the volcanic nature of the deposits, as they are all composed of pyroclastic (i.e. more explosive) samples, while the lavas represent more effusive lava flows?

Although considerable study at Merapi provides much better temporal magmatic constraints (Hammer *et al.,* 2000; Gertisser & Keller, 2003), the similarity in chemistry between Merapi and Sumbing, and their close proximity and trench position, suggest that similar processes may be involved in their petrogenesis. Unfortunately no age constraints can be placed on the Sumbing magmas, so the only distinction which can be made is by petrology and chemistry.

To test the hypothesis that Sumbing magmas have undergone assimilation by carbonate-bearing rocks, two approaches are taken here:

1) Silica saturation modelling, using CIPW normative calculations, and

2) Trace element modelling, using Sr/HFSE ratios.

Silica saturation and CIPW normative calculations

To test the idea of subduction-related magmas becoming progressively silica undersaturated, CIPW normative contents of quartz, hypersthene and diopside are shown in Table 3B, together with selected major and trace elements, trace element ratios and isotope ratios for the lavas and pyroclastic deposits.

Normative minerals are hypothetical end-member solutions, where silica is allocated relative to the oxides in the rock. These calculations can be utilised to examine the degree of silica saturation by reassigning silica into the end-member minerals (Best, 2003). They also enable a user to differentiate between magmas of varying alkali contents for a particular value of SiO_2 (wt.%). For example, using silica as a standard index for differentiation, the reader is unable to differentiate between basalt and a phonotephrite, even though the latter is a more silica undersaturated rock.

Normative minerals for Sumbing are calculated assuming 20% of Fe as Fe^{+3}, a conservative estimate for the Fe-oxidation state of subduction zone magmas (Kelly & Cottrell, 2009). All samples for Sumbing are plotted on a Ne-Ol-Di-Hy-Qz tetrohedron, together with a field for Merapi, in figure 3.18*a*. The two planes, between Di and Hy and Di and Ol, represent divisions for silica saturated rocks and silica undersaturated rocks repectively. The lavas show a strongly silica saturated character, with larger proportions of normative quartz and hypersthene. In contrast, the pyroclastic deposits move into a field for Merapi, and appears to becoming progressively less silica-saturated (i.e. away from quartz-hypersthene and towards diopside-hypersthene). These samples move into a field for Merapi, which are mostly within the triad for silica saturated rocks.

For changes in silica saturation at Sumbing to be attributed to interaction with carbonate at crustal levels, the variations must be controlled by differentiation. For example, suites of highly silica undersaturated and silica saturated lavas at Muriah are not thought to be a function of fractionation, rather mixing between parental magmas of alkaline and silica-saturated affinities, and/or variable degrees of partial melting (Edwards *et al.,* 1991). To address this issue, figure 3.18*b* shows SiO_2, Sr/Nb and $^{87}Sr/^{87}Sr$ against the sum of normative diopside (Di) and hypersthene (Hy) and normative quartz (Qz).

If silica saturation is controlled by differentiation, the concentrations and ratios should change with progressive increases or decreases in the normative minerals. Sr/Nb was choosen because firstly, calculated trace element models show that the pyroclastic magmas contain elevated Sr and low HFSE's; and secondly, that carbonates (and calc-silicates) contain high concentrations of Sr and very little Nb (Chadwick *et al.,* 2007). Therefore, Sr/Nb ratios of carbonate-rich sediments are higher than silicic or volcanogenic sediments (Plank & Ludden, 1992; Vroon *et al.,* 1995; Gasparon & Varne, 1998).

.

Selected Major and Trace Element Concentrations, Ratios, Isotope Ratios and Normative Values for Sumbing Magmas

Pyroclastic Deposits

	SUMB 96	SUMB99	SUMB 94	SUMB 95	SUMB98	SUMB97	SUMB 69	SUMB 71
SiO_2 (wt.%)	53.08	53.28	54.49	54.50	54.87	55.07	56.71	56.21
Mg#	40.97	42.82	41.41	42.12	40.97	39.12	40.76	41.07
CaO (wt.%)	9.14	9.09	8.62	8.43	8.55	8.36	7.27	7.26
Sr (ppm)	605.90	615.08	558.17	564.18	592.80	609.50	573.38	574.01
Nb (ppm)	3.88	3.32	3.49	5.21	3.91	4.66	6.70	6.49
Sr/Nb	156.23	185.26	159.83	108.28	151.67	130.68	85.57	88.41
$^{87}Sr/^{86}Sr$		0.705759		0.705278	0.705187		0.705118	
Quartz (wt.%)$_N$	0.48	0.72	1.68	3.36	3.76	3.01	5.97	5.78
Hypersthene(wt.%)$_N$	10.75	11.49	9.97	12.15	10.73	9.56	12.77	12.84
Diopside (wt.%)$_N$	10.78	11.29	10.89	9.01	9.40	9.20	5.79	5.97

Lavas (C-B)

	SUMB 81	SUMB80	SUMB 74	SUMB 91	SUMB 92	SUMB 72	SUMB 73
SiO_2 (wt.%)	53.65	58.13	60.29	60.27	60.35	61.47	61.65
Mg#	47.69	46.64	44.00	45.56	45.75	44.22	44.12
CaO (wt.%)	8.32	6.63	5.65	6.92	6.95	5.54	5.48
Sr (ppm)	356.56	393.32	326.68	288.69	291.08	317.84	308.36
Nb (ppm)	7.73	11.33	10.87	6.36	6.39	10.51	10.39
Sr/Nb	46.13	34.70	30.07	45.39	45.56	30.24	29.67
$^{87}Sr/^{86}Sr$	0.704636		0.704789	0.704458			
Quartz (wt.%)$_N$	3.11	9.09	11.64	13.01	13.01	12.91	13.13
Hypersthene(wt.%)$_N$	15.27	13.49	11.91	9.77	9.59	10.56	10.39
Diopside (wt.%)$_N$	7.19	3.19	0.12	6.85	6.69	1.68	1.85

Lavas

	SUMB 76	SUMB 77	SUMB 78	SUMB 85	SUMB 83
SiO_2 (wt.%)	55.16	55.01	56.45	58.81	61.70
Mg#	40.53	40.62	40.68	42.17	43.74
CaO (wt.%)	7.16	7.03	7.22	6.45	5.56
Sr (ppm)	348.79	348.96	322.99	305.18	397.42
Nb (ppm)	13.45	13.66	14.47	13.66	8.17
Sr/Nb	25.93	25.55	22.33	22.34	48.63
$^{87}Sr/^{86}Sr$	0.704673		0.705108	0.704720	0.704674
Quartz (wt.%)$_N$	3.64	3.69	6.02	9.48	14.52
Hypersthene(wt.%)$_N$	13.97	14.33	12.81	11.33	9.92
Diopside (wt.%)$_N$	2.64	1.93	5.65	4.21	2.63

Table 3B. Selected Major and trace element concentrations, trace element ratios, isotopic ratios and calculated normative compositions which may be modified through assimilation of carbonates.

Classification of Sumbing Rocks according to Degree of Silica Saturation

(a)

Fig. 3.18. (a) Sumbing pyroclastic deposits and lavas plotted according to degree of silica saturation. Ne = normative Nepheline, Ol = normative olivine, Di = normative diopside, Hy = normative hypersthene, and Qz = normative quartz Silica under-saturated rocks typically contain higher proportions of normative olivine (Ol) and normative Nepheline (Ne), while silica oversaturated rocks have higher normative quartz (Qz). Note that the pyroclastic deposits with the least normative quartz have the lowest SiO_2 and highest Sr/Nb and $^{87}Sr/^{86}Sr$ ratios. **(b)** SiO_2, Sr/Nb and $^{87}Sr/^{86}Sr$ plotted against the sum of normative diopside (Di) and hypersthene (Hy) (left) and normative quartz (Qz) for the pyroclastic deposits and lavas. Note the change in Sr/Nb and $^{87}Sr/^{86}Sr$ with increasing Di+Hy and decreasing Qz in the pyroclastic samples compared to the lavas which show little variation.

114

The pyroclastic deposits show decreasing SiO_2, and increasing Sr/Nb and $^{87}Sr/^{86}Sr$ with increasing Di+Hy and decreasing Qz which suggests that the most silica-undersaturated (or least silica-oversaturated) rocks are those with the highest Sr/Nb and $^{87}Sr/^{86}Sr$ and lowest SiO_2. In contrast, the lavas show little change in Sr/Nb or $^{87}Sr/^{86}Sr$ with Di+Hy or Qz. This shows that pyroclastic rocks are either differentiating towards higher SiO_2, with more silica-saturated compositions and progressively lower Sr/Nb and $^{87}Sr/^{86}Sr$, or that they are being driven towards lower SiO_2, increasing silica-undersaturation and higher Sr/Nb and $^{87}Sr/^{86}Sr$. Based on the evidence presented above, and from experimental studies at Merapi (Chadwick *et al.,* 2007; Deegan et *al.,* 2010; Troll et al. in press), the latter is preferred here; in which reactions between the pyroclastic magmas and crustal carbonate have produced progressively silica-undersaturated, high Sr/Nb, high $^{87}Sr/^{86}Sr$ deposits.

The geochemical similarities between rocks erupted at Merapi and the Sumbing pyroclastic deposits (see figures 3.9 to 3.13) are particularly striking. Deegan *et al.* (2011) show that assimilation with calc-silicate skarns occurs largely in the upper 10 km of crust beneath Merapi, generating a Ca-rich, high $^{87}Sr/^{86}Sr$ melts. Xenocrystic plagioclase phenocrysts are thought to be inherited from the calc-silicates with low FeO and MgO and highly anorthic radiogenic $^{87}Sr/^{86}Sr$ cores (Chadwick *et al.,* 2007). In addition to this, they also note that physical mingling occurs between contaminated and unaffected melts.

Mineral analyses at Sumbing suggest that a similar process is plausible for the pyroclastic deposits and the lavas where physical mingling is very apparent. For one example, the pyroclastic deposits have a very wide range of plagioclase phenocrysts anorthite compositions, up to An92 mol%; while the range of lava plagioclase compositions do not exceed An60 mol% (fig. 3.3 and 3.4).

Trace element modelling, using Sr/HFSE ratios

To help understand the relationship between the lavas and pyroclastic samples, and the Sumbing rocks in the broader context of central Java, figure 3.19 (*a-d*) shows Sr/Nb and $^{87}Sr/^{86}Sr$ against other rocks in Java. In figure 3.19 *b*, a clear distinction can be made between the Sumbing pyroclastic rocks, Merapi and Merbabu, which all have elevated Sr/Nb with decreasing SiO_2; and the Sumbing lavas and Ungaran, which show little variation of Sr/Nb

Sr/Nb and $^{87}Sr/^{87}Sr$ against SiO$_2$ for Sumbing and other Volcanoes in Central Java
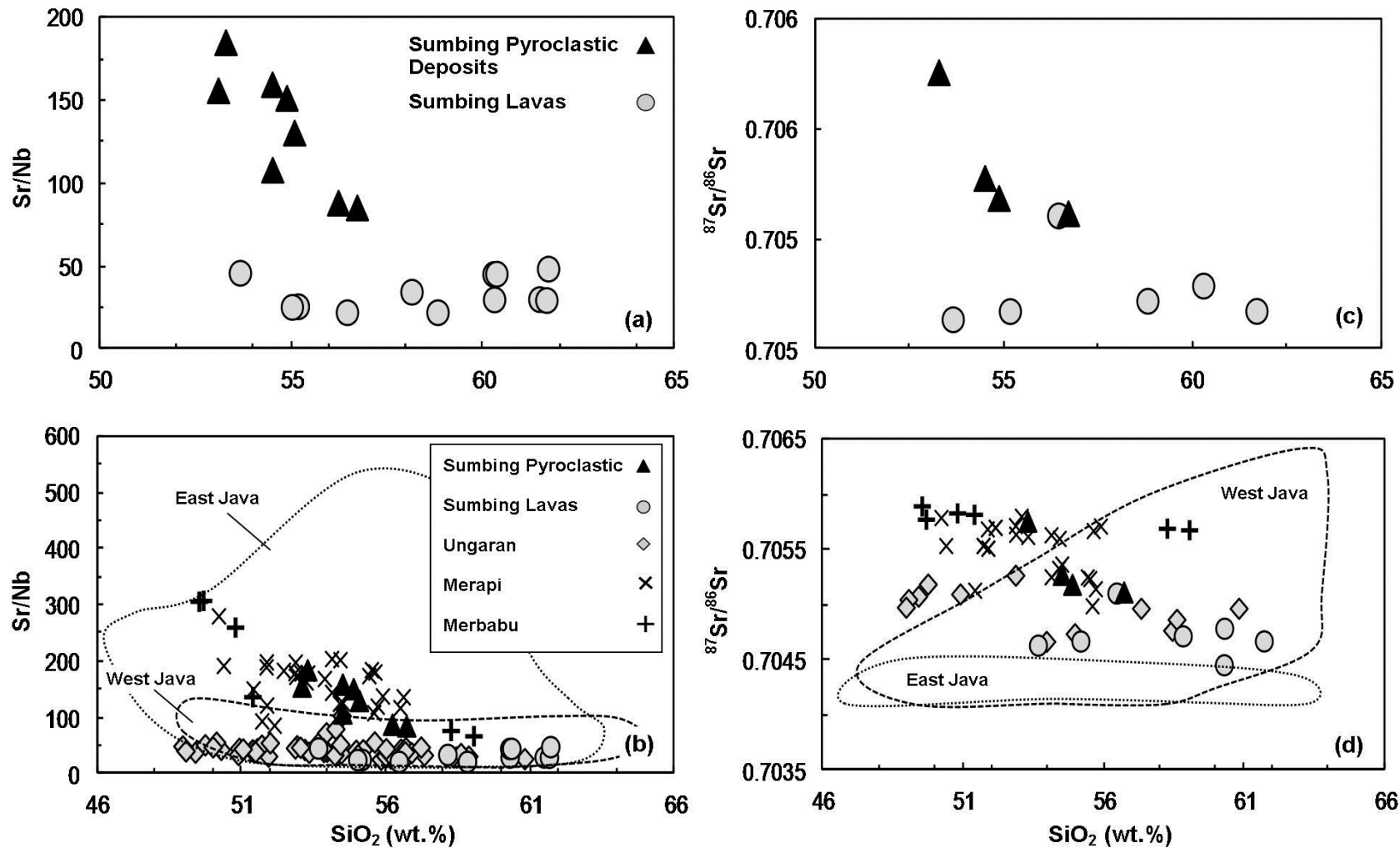
Fig. 3.19. Sr/Nb and $^{87}Sr/^{86}Sr$ against SiO$_2$ (wt.%) for Sumbing (**a** and **c**), central Java and fields for east and west Java (**b** and **d**) . Note the increasing Sr/Nb and $^{87}Sr/^{86}Sr$ ratios with decreasing SiO$_2$ for Sumbing pyroclastic deposits, Merapi and Merbabu and relatively constant ratios of Sumbing lavas and Ungaran. See data sources below.

Sr/Nb against $^{87}Sr/^{86}Sr$
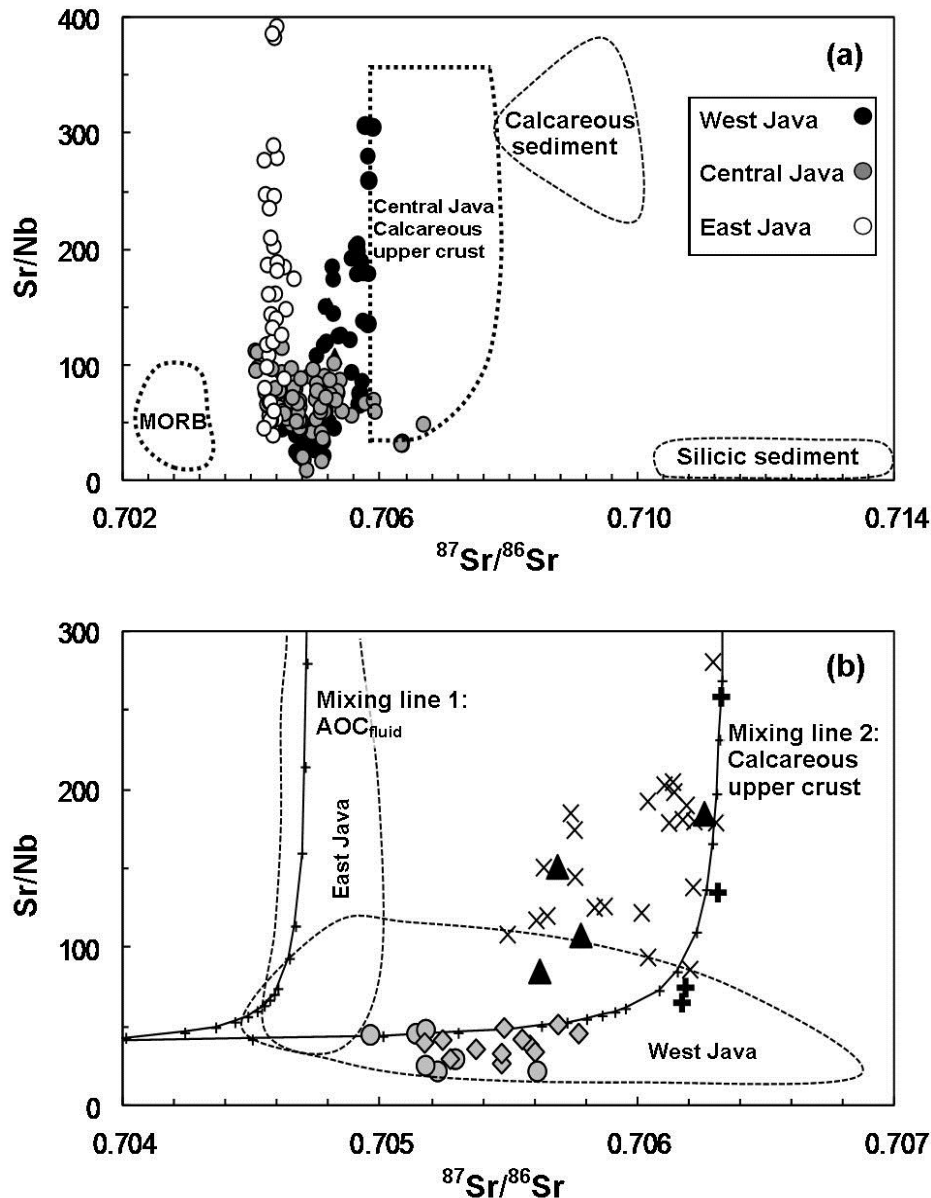
Fig. 3.20. Sr/Nb against $^{87}Sr/^{86}Sr$ showing **(a)** central Java, east Java and west Java fields with respect to MORB, central Java calcareous upper crust, calcareous sediment and silicic sediment; and **(b)** individual volcanoes from central Java used in this study. Mixing line 1 illustrates a hypothetical fluid end-member assumed to have $^{87}Sr/^{86}Sr$ = 0.704230, Sr = 1000 ppm, Nb = 1 ppm. Mixing line 2 uses data from calc-silicate xenoliths erupted from Merapi (after Chadwick et al. 2007; Deegan et al. 2010); WR $^{87}Sr/^{86}Sr$ = 0.705842, calc-silcate rim Sr = 710 ppm and Nb = 2 ppm. I-MORB values (after Janney et al. 2005), assuming 10% melting; $^{87}Sr/^{86}Sr$ = 0.7029, Sr = 12 ppm, Nb = 3 ppm. Symbols as for figure 5.3b. Data sources from west Java include: Tangkuban Perahu (Sendjaja *et al.,* 2009; this study), Tampomas (Sendjaja *et al.,* 2009), Cereme (Sendjaja *et al.,* 2009; Edwards, 1990), Salak (Handley *et al.,* 2008; this study), Gede (Handley *et al.,* 2010; this study), Guntur MK (Edwards, 1990; Sendjaja *et al.,* 2009), Papandayan (Sendjaja *et al.,* 2009; this study), Patuha (this study) and Galunggung (Sendjaja *et al.,* 2009; Turner & Foden, 2001; this study). Data sources from central Java include: Ungaran (Claproth, 1989), Merbabu (Handley *et al.,* 2011), Merapi (Gertisser & Keller, 2003), and Sumbing (this study). Data sources from East Java include: Lamongan Volcanic Field (Carn & Pyle 2001), Ijen (Handley et al. 2007), Argopuro (Ringgit-Bear CA group after Edwards *et al.,* 1994) and Kelut (this study). Other data sources include MORB (I-MORB after Chauvel & Blichert-Toft 2001; Janney *et al.,* 2005), central Java calcareous upper crust (Gertisser & Keller, 2003), calcareous sediment (Ben Othman *et al.,* 1989; Gasparon & Varne, 1998; Vroon, *et al.,* 1995), and silicic sediment (Ben Othman *et al.,* 1989; Gasparon & Varne, 1998; Vroon *et al.,* 1995).

117

with SiO_2. Available data from west Java volcanoes all show a similar relationship to the the lavas and Ungaran, while east Java volcanoes contain high Sr/Nb with little correlation to SiO_2. Figure 3.19*d*, shows that the reverse is true for east and west Java against $^{87}Sr/^{86}Sr$ against SiO_2.

The east Java volcanoes, show no change in $^{87}Sr/^{86}Sr$ with SiO_2, compared to west Java, where contamination in the upper crust has elevated $^{87}Sr/^{86}Sr$ in some volcanoes (Edwards, 1990; Handley *et al.*, 2008). The volcanoes in central Java show a similar profile to figure 3.19*b*, with elevated $^{87}Sr/^{86}Sr$ and decreasing SiO_2 in Sumbing pyroclastic rocks, Merapi and Merbabu, compared to little variation in $^{87}Sr/^{86}Sr$ with SiO_2 in the Sumbing lavas and Ungaran.

Regional variations for these particular ratios become more apparent in figure 3.20*a*, where Sr/Nb is plotted against $^{87}Sr/^{86}Sr$. Here, distinct regional varitions in both Sr/Nb and $^{87}Sr/^{86}Sr$ are characterised by source variations and crustal contamination. For comparison, average MORB values, calcareous and silicic sediment values and a calc-silicate (calcareous upper crust) field are shown.

The high Sr/Nb ratios of Kelut and some of the other volcanoes from east Java are inherited from source compositions; where a fluid subduction component has fluxed a refractory mantle wedge (see Chapter 2). Near constant $^{87}Sr/^{86}Sr$ and little correlation between Sr/Nb and SiO_2 testify to this. In contrast, the volcanoes from west Java show elevated $^{87}Sr/^{86}Sr$ that do correlate with SiO_2, but maintain low Sr/Nb. This suggests that crustal contamination in this region involves a contaminant with little carbonate and a more continental character.

The central Java array is defined by increasing Sr/Nb and $^{87}Sr/^{86}Sr$, towards the field for central Java upper crust and calcareous sediment. The overwhelming evidence from Sumbing pyroclastic rocks and Merapi (Chadwick *et al.*, 2007; Deegan *et al.*, 2010; Troll *et al.*, in press) suggest that these ratios are modified in the crust, opposed to at the mantle source (Gertisser & Keller, 2003). Furthermore, there are very few rocks > 5 % MgO in this part of central Java compared with west and central Java, which suggests that most are highly differentiatied from their source compositions (Claproth, 1989; Edwards *et al.*, 1994; Gasparon *et al.*, 1994; Gasparon & Varne, 1998; Carn & Pyle, 2001; Gertisser & Keller, 2003; Handley, 2006; Sendjaja *et al.*, 2009).

Merbabu contains one of few samples to exceed 5 wt.% MgO (MB-2 = 5.75 MgO wt.%, Handley *et al.,* 2011), which provides evidence for the nature of source compositions (Pearce & Parkinson, 1993; Woodhead *et al.,* 1993). This is discussed in detail during the next section. However, at Merbabu $^{87}Sr/^{86}Sr$ values do not change with differentiation, and appear to be 'buffered' at ~ 0.706. Sumbing and Merapi rocks also do not exceed this value (see figure 3.20*a*). There are two possibilties for this: *1)* source compositions at Merbabu have $^{87}Sr/^{86}Sr$ values of 0.7058, and differentiation has subsequently lowered Sr/Nb ratios towards the field for west Java, Ungaran and pryroclastic lavas; or *2)* that assimilation of carbonatious upper crust is raising Sr/Nb, lowering SiO_2 and buffering $^{87}Sr/^{86}Sr$, similar to Sumbing and Merapi. The first would require considerable differences in source compositions and differentiation processes from Sumbing and its twin volcano Merapi, which is unlikely. So latter is considered here.

Modelling of the central Java rocks, between I-MORB and calcareous upper crust, are shown by mixing line 2 in figure 3.20*b*. The calc-silicate end-member used here is based upon a consrvatiove whole-rock value for $^{87}Sr/^{86}Sr$ (0.705842) and the high end of Sr/Nb ratios (Sr = 710 ppm, Nb = 2 ppm) after Chadwick, *et al.* (2007). These ratios are likely to be highly variable, depending on carbonate and silicate portions throughout the sediment pile. Nevertheless, the mixing line provides a good fit for the central Java data. Furthermore, it shows that this type of mixing can create a buffering of $^{87}Sr/^{86}Sr$ by the calc-silcates, similar to a fluid component shown by mixing line 1. This is largely because of the greater Sr concentrations in carbonates and fluids relative to HFSE, and and Sr/HFSE partitioning in silicate-carbonate melts ($D^{carbonate/silicate}Sr = 4.1$, $D^{carbonate/silicate}Nb = 0.503$), and fluid-silicate melts ($D^{fluid/silicate}Sr = 4.3$, $D^{fluid/silicate}Nb = < 0.3$) (Keppler, 1996; Veksler *et al.,* 1998).

3.5.2. Mantle Source characteristics and Partial Melting

Having shown that processes in the upper crust have a significant impact on the chemistry of rocks at Sumbing, the nature of the mantle must be discussed. Most of the rocks have undergone substantial differentiation, including contamination in arc crust, and therefore do not present ideal samples for an examination of parental mantle compositions. Nevertheless, high $^{143}Nd/^{144}Nd$ in the least evolved lavas suggest that the lavas may represent relatively good examples of the pre-modified source. Large variations in mantle source compositions are highlighted in Indian MORB compositions (Ito *et al.,* 1987; Rehkamper & Hofmann,

1997; Chauvel & Blichert-Toft, 2001; Janney *et al.,* 2005) and depleted to enriched mantle characteristics beneath the Sunda Arc (Wheller *et al.,* 1987; Edwards 1990; Stolz *et al.,* 1990; Edwards *et al.,* 1991; Edwards *et al.,* 1994) and Java (Edwards, 1990; this study).

3.5.2.1. Identifying mantle sources and contamination trends

HFSEs and HREEs are considered to be particularly useful when attempting to identify mantle source compositions at subduction zones because of their low solubility in aqueous fluids (Tatsumi *et al.,* 1986; ; McCulloch and Gamble, 1991; Pearce and Parkinson, 1993; Woodhead *et al*., 1993; Brenan *et al.,* 1995). Unlike Sr and Pb, Hf and Nd isotopic ratios are thought to remain relatively unaffected by hydrothermal alteration in mid-ocean-ridge basalts (White & Patchett, 1984; Nowell *et al.,* 1998; Chauvel & Blichert-Toft, 2001). Therefore, mantle wedge Hf and Nd-isotopic compositions beneath Island Arcs are less affected by dehydration processes involving subducting oceanic crust, and/or sediments compared to Sr and Pb (Salters & Hart, 1991; Woodhead *et al.,* 2001; Handley *et al.,* 2011).

Because of their similar characteristics, Hf and Nd isotopic ratios behave analogously in most mantle and crustal reservoirs (Vervoort *et al.,* 1999; Chauvel & Blichert-Toft, 2001; Nowell *et al.,* 1998). However, fractionation of Lu relative to Hf, or Sm relative to Nd can cause a decoupling between Hf and Nd isotopes. The most obvious cases of this are in pelagic sediments, which tend to contain greater Nd/Hf (Vervoort *et al.,* 1999; Handley *et al.,* 2011), melting in the presence of garnet (which is strongly HREE compatible), or melting of mantle metasomatised by carbonated or hydrous fluids (in which HFSE are more insoluble) (Nelson *et al.,* 1998; Vervoort *et al.,* 1999; Janney *et al.,* 2005). Therefore, this also provides an opportunity to examine Hf-Nd isotope behavior for magmas that have interacted with carbonates and should favour high Nd/Hf ($D^{carb/melt}Nd = 0.92$, $D^{carb/melt}Hf = 0.0093$, (Veksler, *et al.,* 1998).

Figure 3.21 (*a-c*) shows Hf, Nd and Sr-isotope variations for central Java compared to other Java fields. For all figures, the volcanoes highlighted in bold (Kelut, Galunggung and Ijen) are those which represent variations in the mantle source beneath Java, without the added complications of crustal contamination (see Chapter 2). Figure 3.*21a* shows εHf against $^{87}Sr/^{86}Sr$ for Java, which displays a similar distinction for the fields shown in figure 3.21 between central Java (symbols), east Java (bold line) and west Java (dashed line).

Hf, Nd & Sr Isotopes: Source and Contaminantion Variations
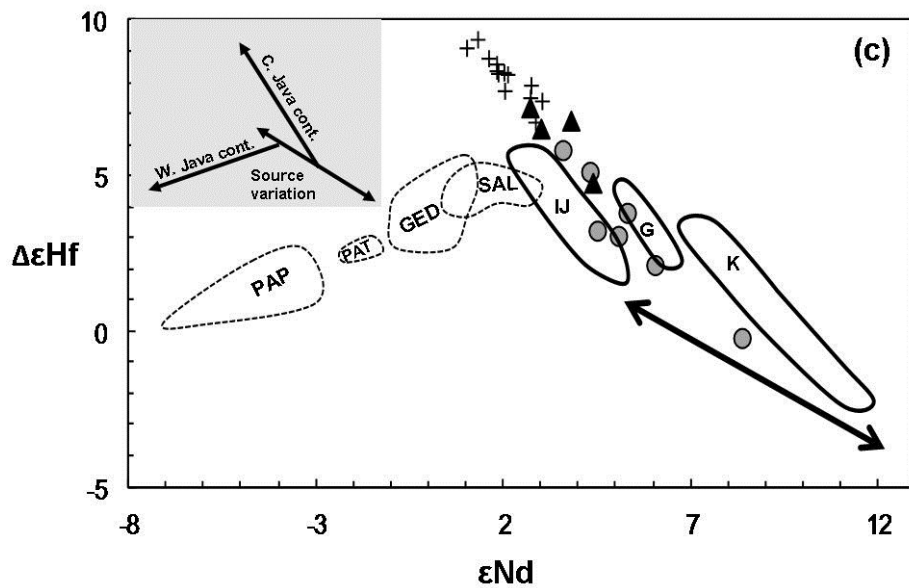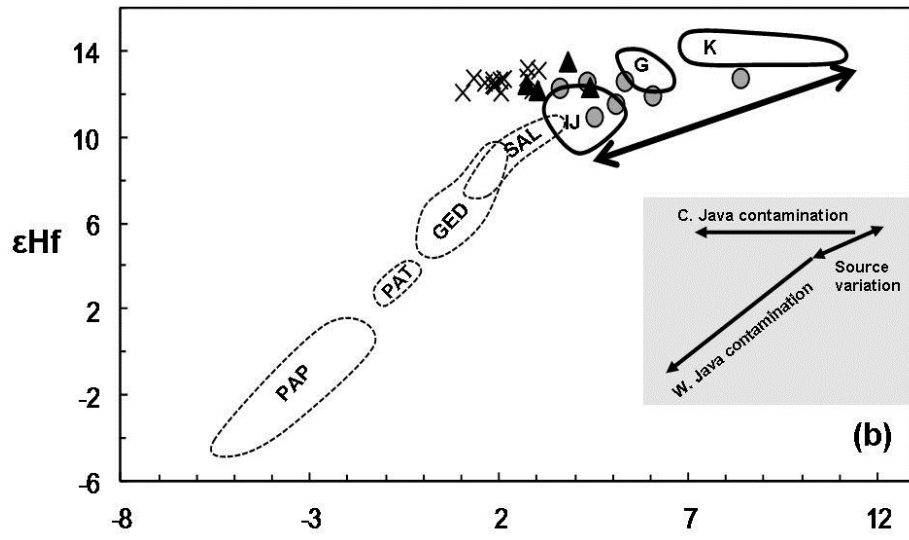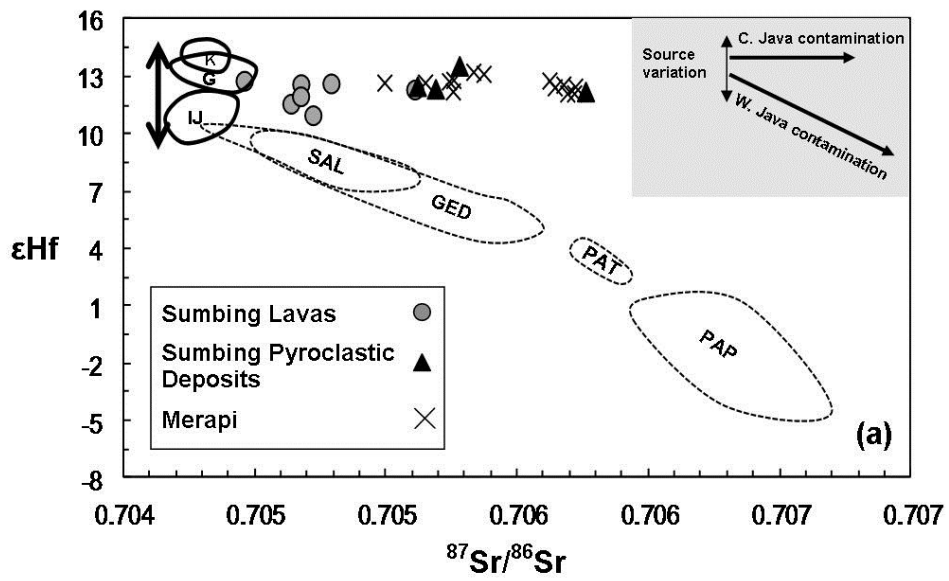
Fig. 3.21. (a) εHf against $^{87}Sr/^{86}Sr$ for rocks in central Java in comparison to equivalent rocks from east and west Java. Bold fields represent volcanoes for which contamination by subducted sediment and/or arc crust is minimal; K = Kelut (LZR), G = Galunggung, IJ = Ijen. West Java volcanoes are show as dashed lines: includes, SAL = Salak, GED = Gede, Pat = Patuha and PAP = Papandayan. The grey box shows an interpretation of the data. **(b)** εHf against εNd and **(c)** ΔεHf against εNd for the same fields described above. ΔεHf describes the deviation from the εHf against εNd mantle array (after Vervoort et al. 1999). Data sources include: Ijen (Handley *et al.,* 2007), Salak (Handley *et al.,* 2008), Gede (Handley *et al.,* 2010), Merapi (Gertisser & Keller 2003) Kelut (LZR), Galunggung, Patuha and Papandayan from this study. εNd = $((Nd_{sample})/(0.51263)-1*10000$, εHf = $((Hf_{sample})/(0.282785)-1*10000$. See text for details.

Kelut, Galunggung and Ijen all parallel MORB εHf compositions, while being displaced to higher $^{87}Sr/^{86}Sr$. As discussed in Chapter 2, this is likely to represent a fluid-fluxed mantle which has elevated $^{87}Sr/^{86}Sr$, but not εHf (or εNd). Therefore the latter are representative of a pre-subduction mantle. Central Java and west Java form two distinct arrays similar to $^{143}Nd/^{144}Nd$ against $^{87}Sr/^{86}Sr$. However, for central Java there is little change in εHf with elevated $^{87}Sr/^{86}Sr$. This is probably because contamination with carbonate-rich sediments or melts is unlikely to drive silicate melts towards less radiogenic Hf than MORB. All of the central Java rocks project back towards a more depleted mantle, than those in west Java, which show the slightly enriched characteristics of I-MORB (Ito *et al.,* 1987; Rehkamper & Hofmann, 1997; Chauvel & Blichert-Toft, 2001; Janney *et al.,* 2005).

Figure 3.21*b* shows εHf against εNd for the Java fields. As expected, Kelut lies within the field for depleted MORB, while Galunggung and Ijen are slightly displaced toward lower εHf and εNd. The profile for Java fields mirrors that of figure 3.21*a* with west Java trending towards lower εHf and εNd, while central Java has lower εNd for unchanged εHf, similar to MORB.

This has been previously interpreted as a change in subducted sedimentary material with a terrigneous character in west Java, to a pelagic character in central and east Java (Handley 2006; Handley *et al.,* 2011). However, additional data from Chapter 2 and this study suggest that this is unlikely because it does not explain all of the isotopic and trace-element charcateristics. The lower εHf in a few of the Sumbing lavas suggest that there may be a slight mixing of sources, as this could not be caused by fractional crystallisation, partial melting or contamination with calc-silicate. This would not be surprising considering the heterogeneity of these samples, and the petrographic evidence for magma mingling.

The final panel (3.21c) shows ΔεHf against εNd. This highlights the deviation from the Nd/Hf mantle array (Vervoort *et al.,* 1999). Again, Kelut plots within the field for depleted

mantle, while Galunggung and Ijen are slightly displaced towards higher $\Delta\varepsilon Hf$ and εNd. In this plot, central Java data becomes progressively elevated in $\Delta\varepsilon Hf$ with lower εNd, which shows an elevation in isotopic Nd/Hf with increasing contamination (εNd).

Merapi and the Sumbing pyroclastic deposits contain the highest $\Delta\varepsilon Hf$ values, which suggest that decoupling between Nd/Hf is strongly affected by carbonate assimilation, a conclusion similar to that reached by Nelson *et al.* (1998) for carbonatites. This figure also shows that the lavas fall mostly within the mantle array for Nd and Hf, between depleted mantle and the Sumbing pyroclastic deposits. This suggests that the source region beneath Sumbing is more similar to front-arc volcanoes such as Kelut and Galunggung, while the rest of west Java has a more enriched IMORB-type source similar to Ijen (Handley *et al.,* 2007).

3.5.2.2. Partial melting variations between pyroclastic rocks and lavas

Assuming that both lavas and pyroclastic deposits at Sumbing originate from a similar source, and that they mostly fall along a trend between depleted MORB mantle and central Java upper crust (carbonate-calc-silicate), a couple of trace-element variations have yet to be addressed. In particular, significant variations in Sr and HFSE concentrations between the two groups are not explained by fractional-crystallisation, mixing or AFC. Therefore, in this section partial melting at Sumbing will be examined.

Although all of the HFSE in the lavas are elevated compared to the pyroclastic deposits, Nb concentrations are particularly high (up to 15 ppm). Figure 3.22*a* shows Zr/Nb against εNd, which clearly defines fields for source variations and contamination trends. Zr/Nb is useful because it can be used as a tracer for previous melt depletion, which raises the ratio beyond MORB values (Woodhead, 1989; Pearce & Parkinson, 1993; Macpherson *et al.,* 2003). This is highlighted by Kelut in figure 3.22*a*; where, conversely the high-K back arc volcanoes form a low Zr/Nb end-member, indicative of an enriched source (see Chapter 2).

Melt variations between the front-arc and the back-arc may explain this disparity. For example, smaller melt fractions in the back-arc, which escapes significant slab fluxing may preferentially tap into enriched parts of the mantle below Java (e.g. Edwards *et al.,* 1991, 1994). Higher degrees of partial melting, triggered by metasomatism in the front arc, may swamp this signature and begin to melt more refractory mantle. This process is documented by Macpherson *et al.* (2010) for high-and low-Nb basalts from the Sulu Arc, and a similar

Zr/Nb, Nb/Y and εNd: Source characteristics and partial melting
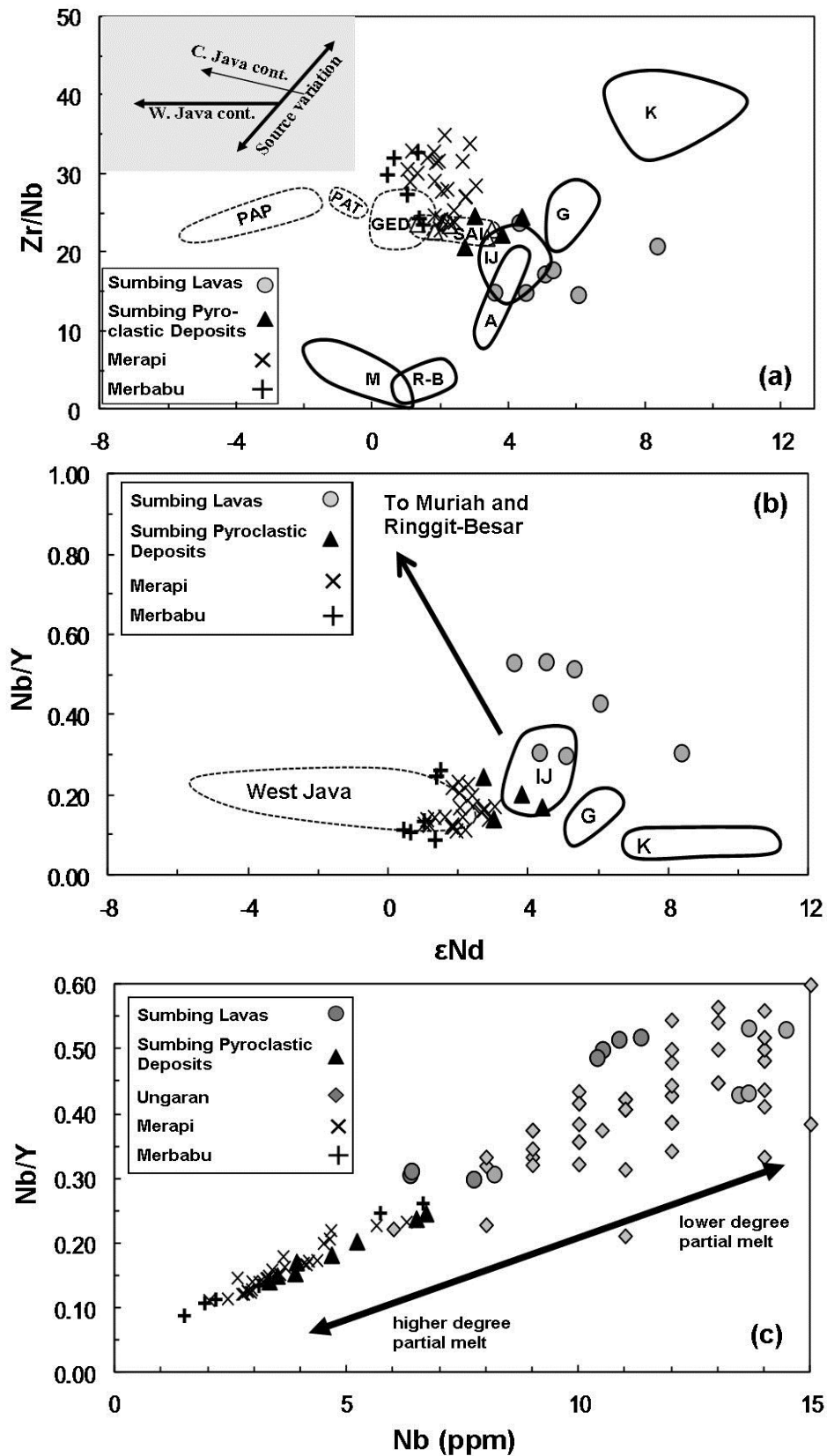
Fig. 3.22. (a) Zr/Nb against εNd, **(b)** Nb/Y against εNd, and **(c)** Nb/Y against Nb for Java fields. See fig. 3.9 and fig. 3.20 for volcano data sources and descriptions. See text for details.

model can be applied to Java where elements such as Nb and La are systematically in volcanoes further away from the trench. This was first noted by Whitford *et al*. (1979) for K and some of the other LILE variations in Java and Bali.

In figure 3.22*a* the volcanoes highlighted in bold all plot within a range of depleted-enriched MORB compositions (Chauvel & Blichert-Toft, 2001; Janney *et al.,* 2005), which further supports the ideas of Macpherson *et al.* (2010). Central Java and west Java volcanoes whose magmas have been contaminated in the arc crust project to lower εNd and slightly higher Zr/Nb. However, the lavas from Sumbing show lower Zr/Nb than would be expected from the source modelling in the previous section. These rocks possess isotopic ratios consistant with relatively depleted mantle (note high εNd). This is because of the high Nb concentrations lowering the Zr/Nb ratio of the lavas, which are not consistent with other volcanoes for Java.

Figure 3.22*b* shows Nb/Y ratios against εNd, which suggests a similar issue. The Sumbing lavas have higher Nb/Y for there εNd compared to other volcanoes. One reason for this anomaly might be a change in the degree of partial melting between volcanoes, as shown for the high-and low-Nb lavas from the Sulu Arc (Macpherson *et al.,* 2010), particularly because the other volcanoes which show depleted mantle signatures are those from the front of the arc.

Figure 3.22*c* shows Nb/Y against Nb (ppm) for all of the volcanoes in Central Java, including Ungaran which is toward the back-arc. This shows a clear distinction between the Sumbing lavas and Ungaran, with high Nb and Nb/Y, compared to Merapi, Merbabu and the Sumbing pyroclastic deposits. Because this cannot be accounted for by any of the upper crustal processes discussed, or variations in the mantle, these variations are probably related to partial melting, where the higher values are from the magmas with the lowest degrees of partial melt.

To examine this concept on a regional scale figure 3.23 shows a number of the volcanoes discssed during this chapter. For each volcano Nb/Y is measured against an estimated depth from volcano to the Benioff Zone (Hutchinson, 1982). This shows that Nb/Y is significantly elevated with progressive depths to the Benioff Zone, where there is evidence for melting of more enriched sections of mantle. In central Java, Merapi, Merbabu and the Sumbing lavas show lower Nb/Y than should be expected, according to the projection. One can speculate

Nb/Y against depth to Benioff Zone
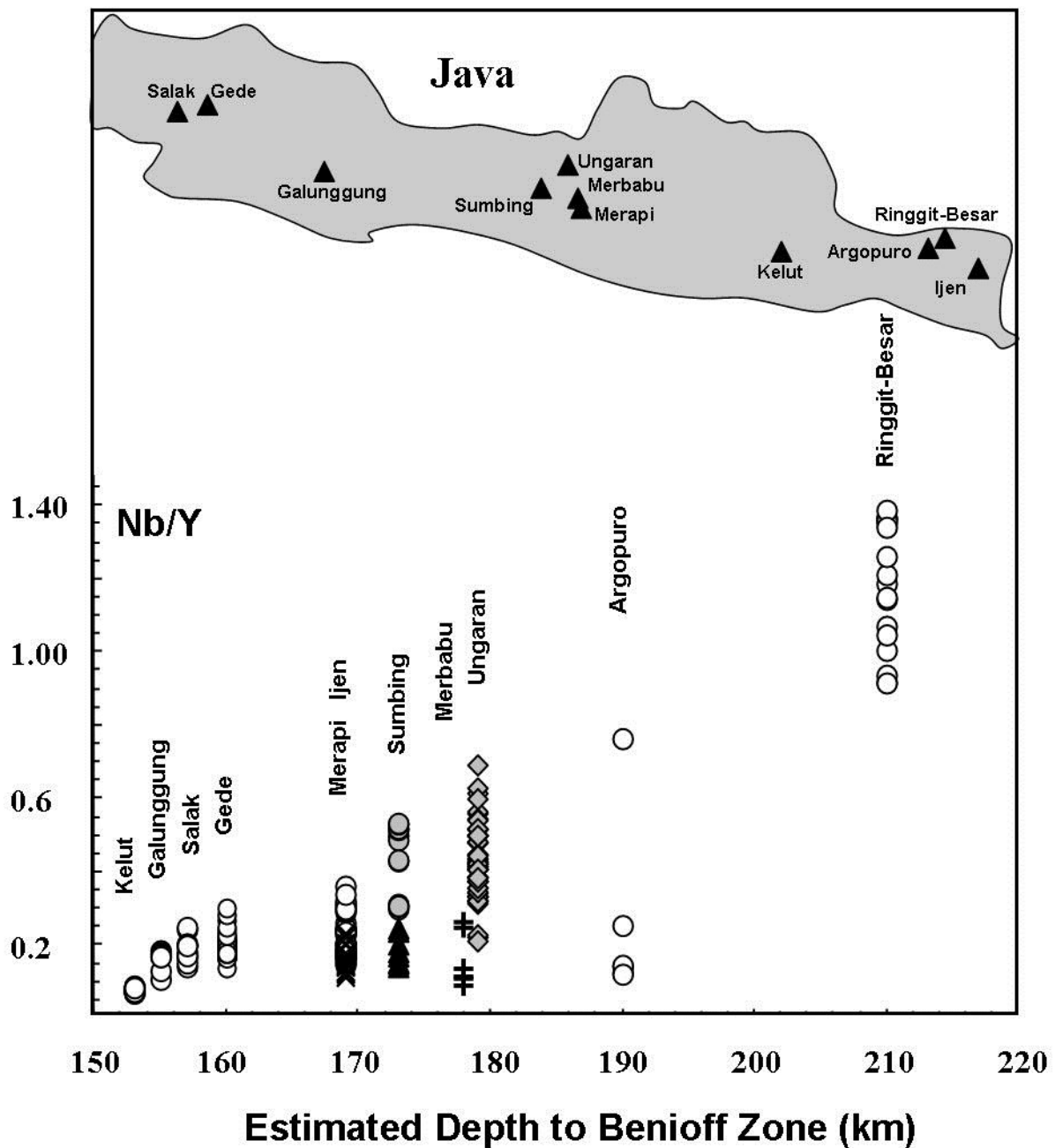
Fig. 3.23. Nb/Y against estimated depths to the Benioff Zone (after Hutchinson,1982). Lower depths are equilalent to closer trench positions (see schematic figure above). Data sources include Salak (Handley *et al*., 2008), Gede (Handley *et al.,* 2010), Merapi (Gertisser & Keller 2003), Ijen (Handley et al., 2007), Merbabu (Handley *et al.,* 2011), Ungaran (Claproth, 1989), Argopuro (Edwards *et al.,* 1994), Ringgit-Besar (Edwards *et al.,* 1994). Note the lower Nb/Y of the Sumbing pyroclastic deposits, Merapi and Merbabu. See text for details.

that this is caused by significant carbonate assimilation in these rocks, which has lowered Nb preferentially over Y. An alternative explaination might be that the additional CO_2 fluxes inherited from carbonate-bearing contaminants may have increased the degree of melting within these samples (Chadwick *et al.,* 2007; Deegan *et al.,* 2010; Troll *et al.*, in press).

3.6. Summary and Conclusions

The pyroclastic deposits show convincing evidence for crustal contamination in the upper crust with carbonate-bearing lithologies. These rocks contain a highly porphyritic character, with abundant plagioclase and clinopyroxene phenocrysts. Modelling suggests that carbonate assimilation may have favoured the crystallisation of these Ca-rich phases in magmas which become progressively silica undersaturated and elevated in Sr, Sr/HFSE and $^{87}Sr/^{86}Sr$. The high-An plagioclase phenocrysts not present in the lavas suggest that these may have been inherited from calc-silicates, similar to those at Merapi, (e.g. Chadwick *et al.,* 2007).

Significant similarities between element and isotope geochemistry between the pyroclastic deposits and Merapi suggest very similar processes are happening at both volcanoes, which may account for the explosive nature of these rocks at Sumbing from CO_2 fluxing (e.g. Deegan *et al.,* 2010; Troll *et al.,* in press). Isotopic systematics suggest that Hf ratios are not modified from MORB compositions. However, Nd/Hf isotopic ratios are significantly elevated.

The Sumbing lavas are more heterogenous in character and chemistry compared to the pyroclastic deposits. Physical mingling between magmas of different compositions are apparent in some of the lavas. However, lower Sr, $^{87}Sr/^{86}Sr$, and plagioclase An-contnent suggests that the lavas (with the exception of one sample) have probably not had sufficient interaction with the upper crust to inherit the signatures described for the pyroclastic samples.

Isotopic ratios show that they are better representations of the MORB source compositions beneath Sumbing. Nevertheless, major and trace element modelling, element-element variations and isotopic modelling suggest that these magmas were not produced entirely by closed-system processes. The nature of the open system behavior is not entirely obvious. There are two possibly explainations:

1) The lavas represent melts which have partially mixed with the pyroclastic magmas.

2) The smaller degree melts have not assimilated as much crust. Evidence from Nb/Y ratios suggest that the latter might provide the strongest argument.

Two additional implications have arison from this study. Firstly, that subducted sedimentary material is not required to satisfy the elemental and isotopic variations along the segment of the Sunda arc. This supports the study in Chapter 2, which shows that the source character of Javan magmas are related to enrichments what appear to be more pronounced towards the back of the arc, the degree of melting (or previous melting), and the degree to which the mantle has been fluxed by the subducting plate.

The second implication involves differentiation, and particularly carbonate assimilation. Many previous studies have discounted differentiation on the basis of poor correlations of element concentrations and isotope ratios with SiO_2, or MgO, particularly when the observational evidence often provides excellent evidence for open-system processes. On this basis, an assuption is often made about the nature of subduction and mantle source components which are invalid. In the case of carbonate, or calc-silicate assimilation using SiO_2, or MgO provides very little benefit other than for the most extreme cases which may have suffered large degrees of desilification. Therefore, caution must be expressed prior to overlooking crustal processes.

Chapter 4

Magma Evolution by Fractional Crystallisation at Agung Volcano, Bali, Indonesia: Insights into Mantle Source Compositions beneath the Western Lesser Sunda Islands (WLSI).

4.1. Introduction

Geochemical models produced for subduction zones rely significantly on information from primitive compositions (e.g. Woodhead *et al.,* 1993, 2012). These melts provide valuable information about their source, without which, contributions from the arc crust or the subducting plate cannot be accurately measured (McCulloch and Gamble, 1991; Plank and Langmuir, 1998; Pearce *et al.,* 1995; Turner and Hawkesworth, 1997; Straub and Zellmer, 2012). However, source compositions are rarely reflected in arc magmas, particularly in continental arcs where the crust is thick. In these settings differentiation of primary source compositions are commonly accompanied by open-system processes such as magma mixing, magma-cumulate mixing or crustal contamination (Nicholls and Whitford, 1976; Conrad *et al.,* 1983; Thirlwall and Graham, 1984; Tepley *et al.,* 2000; Davidson *et al.,* 2005; Handley *et al.,* 2008). These processes will act to alter trace element compositions and isotope ratios from their parent magmas.

Differentiation controlled by closed- system processes such as fractional crystallisation can be a useful indicator of source compositions. Removal of a particular sequence of minerals in a magma chamber will alter concentrations of major and trace elements with differentiation, but the magmas will retain their incompatible trace element and isotope ratios. Therefore, in volcanoes where magmas differentiate through fractional crystallisation without magma mixing or crustal contamination, the rocks will retain trace-element and isotope ratios inherited from source compositions (Handley *et al.,* 2007).

In the Sunda Arc, and its eastward continuation into the Banda Arc, the arc magmas commonly show evidence for significant open-system behavoir throughout (Wirakusumah, 1993; Vroon *et al.,* 1993; Reubi *et al.,* 2002; Turner *et al.,* 2003; Handley, 2006; Debaille *et al.,* 2006). Even beneath volcanoes where whole-rock element and isotope ratios show no obvious signs of crustal contamination or magma mixing, phenocrysts often provide evidence of mineral-magma disequilibrium (Chadwick *et al.,* 2007; Deegan *et al.,* 2010; Troll *et al.,* in press). In addition, cumulates collected from mid- to lower sections of the crust can be collected by rising magmas, which can act to alter their composition (e.g. chapters 2 and 3; and; Beard, 1986; Beard *et al.,* 2005; Davidson *et al.,* 2007; Larocque and Canil, 2010; Tiepolo *et al.,* 2011). Source compositions beneath the Sunda Arc are still poorly known, and a number of different mantle fertilities are often invoked; including, depleted mid-ocean ridge

basalt (N-MORB), enriched mid-ocean ridge basalt (I-MORB), and ocean island basalt (OIB) compositions (Wheller *et al.,* 1987).

Agung volcano is situated on Bali, one of a group of small islands in the western part of Lesser Sunda which include Lombok and Sumbawa. Unlike most other sections of the arc, active volcanoes from these islands contain basalt-andesite-dacite associations with near-mantle-like values for radiogenic isotopes $^{87}Sr/^{86}Sr$, $^{143}Nd/^{144}Nd$, $^{206}Pb/^{204}Pb$, $^{207}Pb/^{204}Pb$, $^{208}Pb/^{204}Pb$ and $^{3}He/^{4}He$, and strong evidence for closed-system, polybaric differentiation in the arc crust (Foden and Varne, 1980; Foden, 1983; Hilton and Craig, 1989; Rubin *et al.,* 1989; Gasparon *et al.,* 1994; Gasparon and Varne, 1998; Reubi and Nicholls, 2004, 2005). They should, therefore, provide the best insights into mantle source compositions beneath the Sunda Arc. A significant amount of data exists for the Quaternary volcanoes Batur, Rindjani, Tambora, and Sangean Api (e.g. Foden and Varne, 1980; Foden 1983, 1986; Varne and Foden, 1986; Wheller and Varne, 1986; Hilton and Craig, 1989; Rubin *et al.,* 1989; Gasparon *et al.,* 1994; Turner and Foden, 2001; Turner *et al.,* 2003; Elburg *et al.,* 2004*;* Reubi and Nicholls, 2004, 2005); however, relatively little has been published from Agung. This work presents a combined major and trace element and Sr-Nd-Pb-Hf study of Agung volcano; which, in combination with previously published data, will help to address the uncertainty regarding mantle compositions beneath the Sunda arc. In turn, it will provide a reference by which contributions from the arc and the subducting plate can be more readily quantified.

4.2. Geological Background and Chapter Aims

The Lesser Sunda Islands are situated in central and eastern sections of the Sunda Arc between Java and the Banda arc. These small volcanic islands are locally subdivided into Bali, West Nusa Tenggara (Lombok and Sumbawa) and East Nusa Tenggara (Flores and Wetar). The focus of this chapter involves volcanoes from Bali, and Agung in particular; but also include volcanoes from the West Nusa Tenggara which will be collectively referred to as the western Lesser Sunda Islands, or WLSI (see figure 4.1). The reason for a regional study here is because these volcanoes are situated north of a subduction trench free of collision. Therefore, magmas influenced by subduction-related processes avoid the additional complexities associated with seamount-arc and continent-arc collisions; such as the Roo Rise in central and east Java, and the NW Australian continental shelf in East Nusa Tenggara and

the Banda arc (Hall and Wilson, 2000; Audley-Charles, 2004; Elburg et al., 2005; Kopp *et al.,* 2006; Kopp, 2011).

4.2.1. Volcanism in the WLSI

The volcanoes and their locations on Bali, Lombok and Sumbawa are shown in figure 4.1b. Previous studies show that the volcanic rocks have basalt-andesite-dacite associations which range from medium-K to high-K calc-alkaline at Batur and Rindjani, through to high-K and shoshonitic at Tambora and Sangean Api (Foden and Varne, 1980; Foden 1983, 1986; Varne and Foden, 1986; Wheller and Varne, 1986; Turner *et al.,* 2003; Reubi and Nicholls, 2004, 2005). Sangenes and Soromundi are extinct volcanoes which have erupted some highly silica-undersaturated, leucite-bearing lithologies, similar to those discovered at Muriah, Ringgit-Besar and Batu Tara (Foden and Varne, 1980; Stolz et *al.,* 1988; Edwards *et al.,* 1991; van Bergen *et al.,* 1992; Edwards *et al.,* 1994). This is unusual because, all of the other highly alkaline volcanoes are all situated behind the Quaternary volcanic arc at positions > 200 km above the Benioff Zone, and so provides a significant argument against generalised arc-trench spatial models (Arculus and Johnson, 1978; Foden and Varne, 1980). These rocks are discussed briefly later in this chapter. On Bali, the oldest volcanic rocks are Late Pliocene in age. These rocks, represented by the extinct volcanoes of Bratan, Batukau and Seraja volcanoes, are located west of the currently active centres of Agung and Batur. The volcanism had re-commenced by ~ 500 ka BP at Batur volcanic field (Wheller and Varne, 1986; Reubi and Nicholls, 2004).

4.2.2. The Indian Ocean Plate

The ocean crust being subducted beneath the WLSI is some of the oldest in the Indian Ocean. This crust increases in age from Early Cretaceous at ~ 110°E to Late Jurassic at 120°E (Hamilton, 1979; Kopp, 2011). The closest ocean drilling site to the trench is DSDP site 261 on the Argo Abyssal Plain; a deep basin situated between the Java-Sunda trench and Australia (e.g. Plank and Langmuir, 1998). Here the basement is 160 Ma and covered by Cretaceous claystones and Miocene- to Quaternary nannofossil oozes and radiolarian clays (Gasparon and Varne, 1998; Plank and Langmuir, 1998; Kopp, 2011). Sediment thickness is on average higher in the Argo Abyssal Plain (~ 500 m) than along the Java trench (200 m –
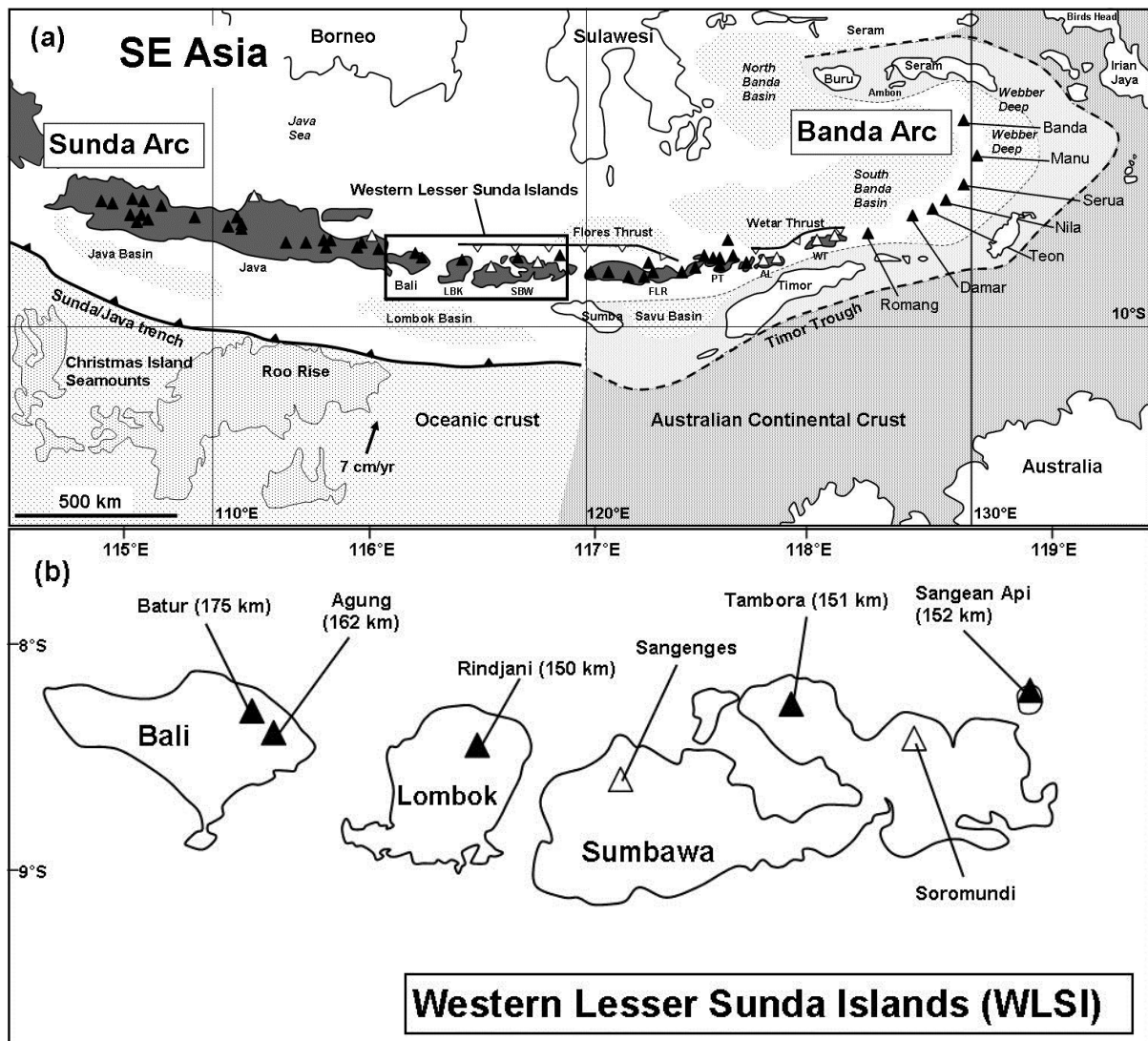
Fig. 4.1. (a) A schematic illustration of Southern SE Asia and the volcano locations from west Java to the Banda arc. The Islands associated with the modern arc are shaded in dark grey. Active volcanoes are represented by a black triangle and extinct volcanism is shown with a black circle. Only volcanoes which include some published data are included here. Features highlighted on the subducting plate include the changes from predominantly oceanic crust in the west (represented by light grey shading and white subduction contours), the collision of the Roo Rise with the trench south of central and east Java, and the collision of the NE Australian shelf in the eastern part of the arc (represented by dark grey shading and black subduction contours). Partial subduction of the Roo Rise has deflected the trench ~ 50 km north of its normal curvature and caused deformation to the fore-arc between the longitudes of 109°E and 115°E (e.g. Kopp *et al.,* 2006). Note the developed fore-arc basins either side of this area. From Flores eastwards the trench is deflected to the south and a number of continental fragments such as Timor and Seram are situated in a non-volcanic outer arc (marked in light grey and by the dashed line). From ~ 3-4 Ma this arc has been colliding with the NW Australian margin (e.g. Hall, 2009) and is most advanced beneath the volcanically extinct islands of Alor and Wetar (see Audley-Charles, 2004; Hall and Wilson, 2000 for details). Note the position of the WLSI sandwiched between these collisions. Plate vector after Tregoning *et al (*1994). Abbreviations include: LBK = Lombok, SBW = Sumbawa, FLR = Flores, PT = Pantar, AL = Alor, and WT = Wetar. The Banda arc volcanoes are located east of Wetar. **(b)** Shows the volcanoes from the WLSI included in this study. Black triangles show active Quaternary volcanoes and white triangles show extinct volcanoes. WBZ depths using the criteria of Syracuse and Geoffrey (2006).

400 m). Refrection seismic profiles of the deep structure beneath Nusa Tenggara suggest that the abrupt change from oceanic subduction to continent- arc collision occurs at the eastern edge of the Java trench, south of Sumba at ~ 121°E. The effects of collision are most pronounced in the Timor region where collision between Australian and eastern parts of the Sunda arc started ~ 3 Ma ago (Audley-Charles *et al.,* 1979; Hall, 2002) From this point eastwards the progressive influence of continental material is evident in arc magma compositions from Flores to the Banda arc (e.g. Elburg *et al.*, 2002, 2004; Elburg and Kamenetsky, 2008; Hoogewerff *et al*., 1997; Vroon *et al.,* 1993, 1995).

4.2.3. Arc Basement

The nature of the basement beneath the WLSI is still poorly known. Early studies using seismic data suggested that most of the Islands were built on thin a basement of oceanic crust and that the north and south are flanked by oceanic crust (Curray *et al.,* 1977; Foden and Varne, 1980). However, this idea has recently been challenged by suggestions that large parts of the east Sunda Arc may be underlain by fragments of Australian continental crust separated by suture zones (Hall, 2009, 2012; Hall and Sevastjanova 2012). The character of such such a transition, between continental and ophiolitic accretionary fragments, should therefore be evident in chemistry of rocks from the WLSI volcanoes, assuming that the melts have either been derived from such a source, or inherited its signature during differentiation (e.g. Davidson *et al.,* 2005).

4.2.4. Agung, Bali

Agung is the highest volcano on Bali at 3142 m and is located ~ 18 km SE of Batur caldera on the east coast (fig. 4.2). It is located ~ 160 km above a north-dipping Benioff Zone and 300 km from the trench; which is similar to the calc-alkaline volcanoes of Batur and Rindjani (Hutchison, 1982; Syracuse and Geoffrey, 2006). Samples were collected during a 2009 field season to Java and Bali. Most of the samples were collected from several quarries along the east and north east flanks, and from exposures close to the volcano summit. Table 4A details sample localities for samples discussed. The samples collected from Agung include a number of highly vesicular mafic clasts from the lahar deposits at the base of the volcano, lava flows from higher up on the volcano flank, and a dacite ignimbrite. The temporal behavoir of

Volcanoes on Bali
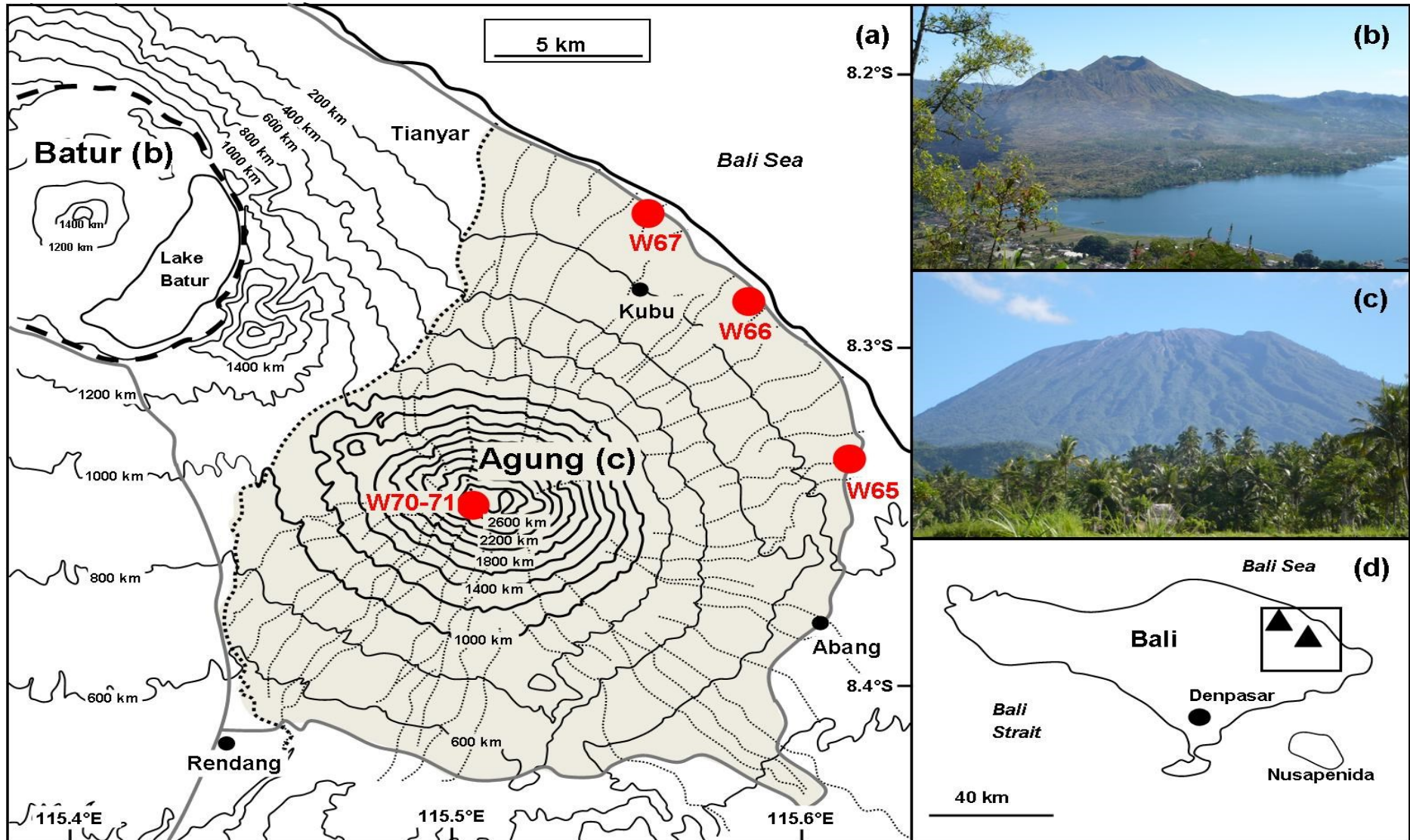
Fig. 4.2. (a) A schematic diagram of Agung volcano (grey shading), and its approximation to Batur volanic field. The red circles illustrate locations where samples used in this study were collected from. Topographic contours are marked with contiued black lines and flank streams and river cuttings with dotted lines. The approximate division between volcanic products from Agung and those from Batur is marked with a thick dotted line. The caldera rim at Batur is marked with a thick dashed line. Photos of Batur **(b)**, Agung **(c)**, and a location map **(d)** are inserted to the right of the main figure. Sample details from each waypoint are included in the table below.

Sample Descriptions for Agung Magmas

Region	Waypoint	Altitude	Age	Lat.	Long.	Benioff depth	Sample	Rock type	SiO_2 (wt.%)	mg#
East Flank - Dukat Bangke River, Labe Sari	65	81 m	Recent	-8.328610	115.615710	160km	**agu03**	andesite	58.01	42.83
Northeast Flank - Kubu	66	44 m	Recent	-8.257870	115.577770	160km	**agu06**	basaltic andesite	55.64	44.70
	66	44 m	Recent	-8.257870	115.577770	160km	**agu07**	andesite	58.21	42.27
	66	44 m	Recent	-8.257870	115.577770	160km	**agu10**	basalt	50.31	48.35
	66	44 m	Recent	-8.257870	115.577770	160km	**agu12**	basaltic andesite	54.92	42.97
	66	44 m	Recent	-8.257870	115.577770	160km	**agu13**	basalt	49.97	46.98
	66	44 m	Recent	-8.257870	115.577770	160km	**agu15**	andesite	62.41	37.78
Northheast Flank - Quarry north of Kubu	67	65 m	Recent	-8.235640	115.542790	160km	**agu16**	andesite	59.93	40.32
	67	65 m	Recent	-8.235640	115.542790	160km	**agu18**	basalt	52.02	46.64
	67	65 m	Recent	-8.235640	115.542790	160km	**agu20**	andesite	62.69	37.52
	67	65 m	Recent	-8.235640	115.542790	160km	**agu21**	basaltic andesite	54.08	46.96
	67	65 m	Recent	-8.235640	115.542790	160km	**agu22**	basaltic andesite	53.63	41.75
	67	65 m	Recent	-8.235640	115.542790	160km	**agu23**	basaltic andesite	56.42	41.77
	67	65 m	Recent	-8.235640	115.542790	160km	**agu24**	basaltic andesite	52.50	44.92
	67	65 m	Recent	-8.235640	115.542790	160km	**agu25**	dacite	65.16	36.15
Southern Flank - close to crater	70	2375 m	Recent	-8.353520	115.504760	160km	**agu30**	basaltic andesite	56.35	43.72
	70	2375 m	Recent	-8.353520	115.504760	160km	**agu31**	basaltic andesite	53.84	48.06
Southern Flank	71	2355 m	Recent	-8.353790	115.504750	160km	**agu33**	basaltic andesite	53.74	47.08

Table 4A. Details of the rocks collected from Agung at each waypoint corresponding to figure 4.2 (a). Estimated Benioff Zone depth after Hutchinson (1982). SiO_2 (wt.%) and Mg# measured and calculated from XRF data analysed at RHUL. Details of analyses are available in Appendix F.

magmatism can not be examined during this study because the lavas have not been dated so assumptions are made regarding magmatic relatonships.

4.3. Petrology and Geochemistry of Agung lavas

In terms of petrology and geochemistry, two groups can be distinguished from Agung; a high scandium (high-Sc) group and a low scandium (low-Sc) group (see fig. 4.6d).The reason for these divisions are discussed throughout the following sections.

In terms of classification, the high-Sc group comprises of medium- K basalts and basaltic andesites and the low-Sc group comprises medium-K basaltic-andesites, andesites and a dacite (fig. 4.3a-b). Compared to other volcanic rocks in the WLSI, Agung contain lower total alkalis than most other volcanoes: these include medium- to high-K rocks at Batur and Rindjani, shoshonitic rocks at Tambora and Sangean Api, and Leucititic rocks at Soromundi and Sangenes. Furthermore, many volcanoes show a wide range of compositions, with Rindjani and Batur comprising basaltic- through to trachytic compositions.

4.3.1. The high-Sc group

These samples include three basalts and two basaltic andesites with an essential mineral assemblage of plagioclase, olivine, orthopyroxene, titanomagnetite and very minor clinopyroxene, which is absent in a few samples. Samples are moderately to highly porphyritic with a fine-grained to glassy groundmass. Plagioclase phenocrysts show a wide range in compositions from An_{31} to An_{87} mol.% (fig. 4.4a), where the anorthite contents of a particular phenocryst shows decreasing concentrations with increasing FeO wt.%. Many of these phenocrysts display melt inclusions, oscillatory zoning and resorption in the centre and rims of the minerals. Orthopyroxene phenocryst contents also show a wide range from $En_{56.8}$ to $En_{70.7}$, $Fs_{26.4}$ to $Fs_{34.0,}$ and $Wo_{2.9}$ to $Wo_{9.2}$ mol.% (fig. 4.4b).

The geochemistry of the high-Sc group is distinct from the low-Sc group, but they do show many similar characteristics to the plagioclase and olivine suite from Batur (figures 4.5-4.7) (Reubi and Nicholls, 2004, 2005). MgO in the high-Sc group ranges from 2.94 to 5.77 wt.%

Classification Diagrams
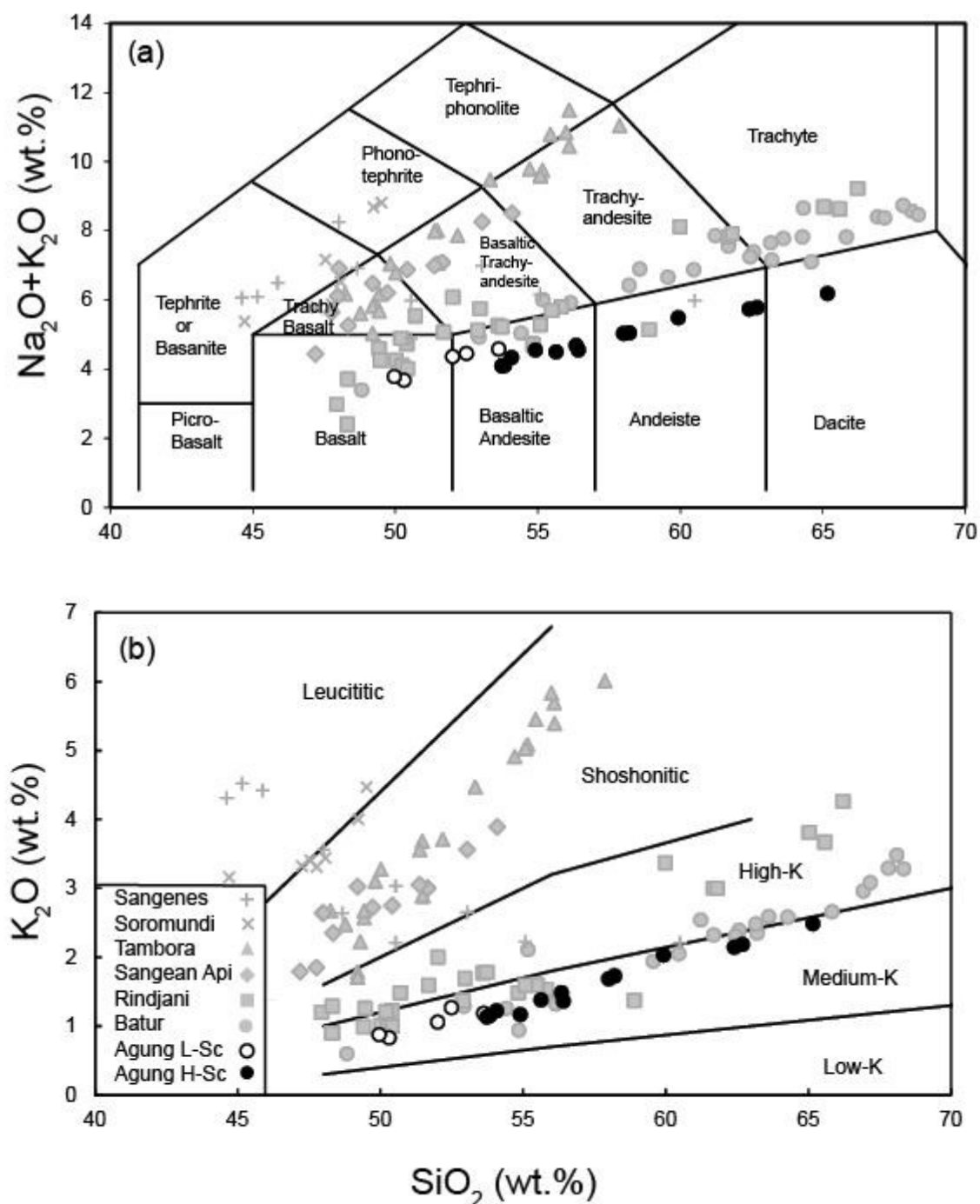
Fig. 4.3. (a) The Total Alkali-Silica (TAS) and **(b)** K$_2$O against SiO$_2$ classification schemes for east Java volcanic rocks, after Le Bas *et al*. (1986), Peccerillo & Taylor (1976) and Wheller *et al*. (1987). Agung high-Sc samples are highlighted as white circles and low-Sc samples by black circles. Additional data after Foden & Varne (1980); Foden (1983), (1986); Varne& Foden (1986); Wheller & Varne (1986); Turner & Foden (2001); Turner *et al*. (2003); Reubi & Nicholls (2005). See text for details.

Mineral Compositions
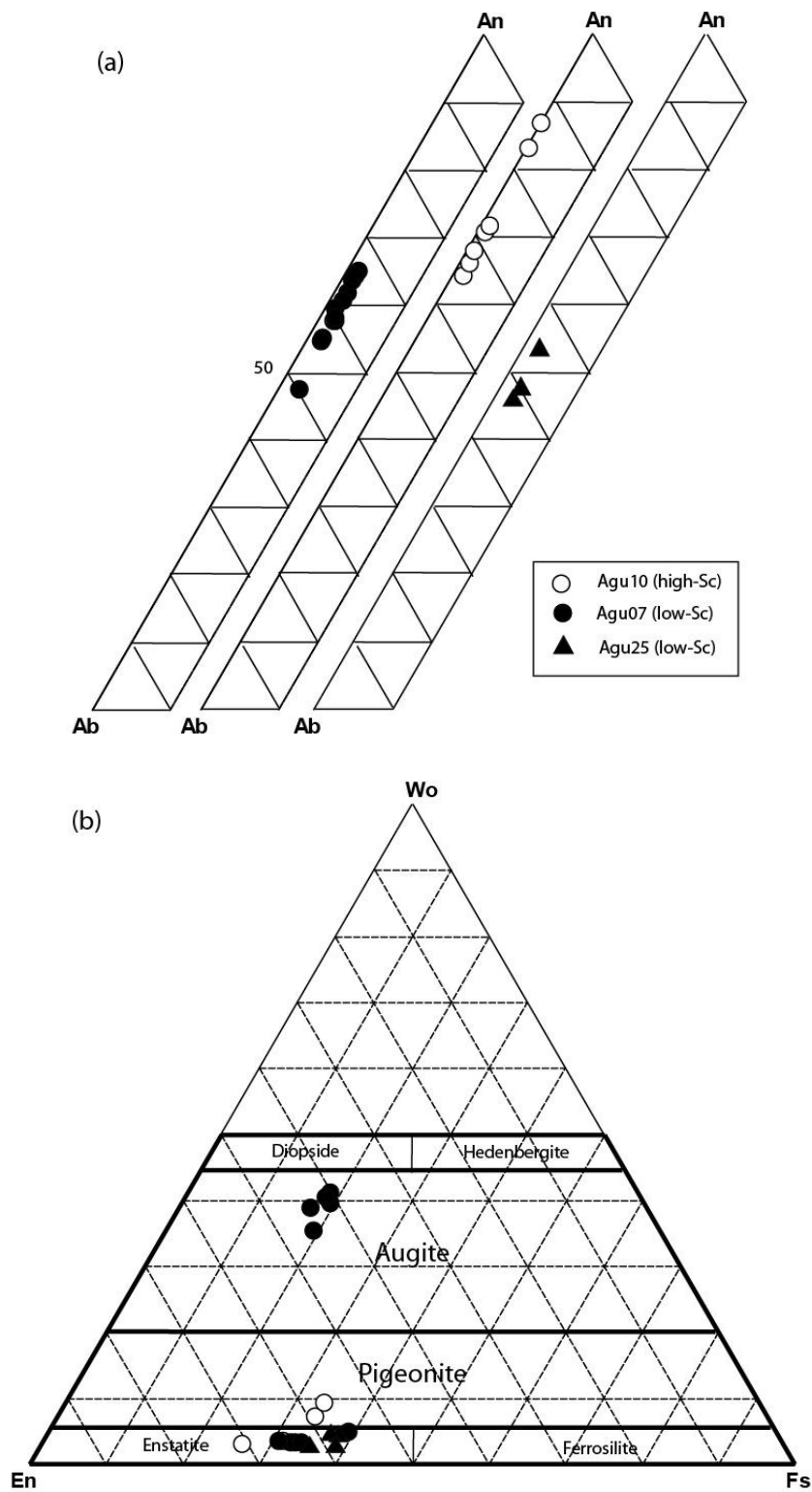
Fig. 4.4. Analyses of **(a)** plagioclase phenocrysts and **(b)** pyroxene phenocrysts, in three of the Agung samples. The high-Sc group are shown by black symbols and the low-Sc by white symbols. Dashed lines represent 10% increments. An = Anorthite, Ab = Albite, En = Enstatite, Fs = Ferrosilite, Wo = Wollastonite. See text for details.

and is used as the index for differentiation here because it more clearly distinguishes between groups compared with SiO_2. The samples show higher TiO_2, Al_2O_3, Fe_2O_3, CaO, and Na_2O and lower SiO_2, K_2O and P_2O_5 wt.% than equivalents from the low-Sc group. All major elements show limited variations against MgO. The greatest difference between the two groups of rocks at Agung is shown for concentrations of Sc, Ti, and and to a lesser extent, V. These elements are significantly higher in the high-Sc (plag+ol+opx) samples. Concentrations of most incompatible trace elements, except for Sr, which mirrors the behavior of CaO, remains constant with MgO and is generally lower than for the high-Sc group samples.

4.3.2. The low-Sc group

Most samples belong to the low-Sc group, in which rock compositions range from basaltic andesite to dacite. It is useful to subdivide this group into rocks with < 55 wt.% SiO_2 and those with > 55% wt.% SiO_2, as this highlights variations between the mafic compositions from this group and those from the high-Sc group. Furthermore, there are subtle distinctions in chemistry between the higher and lower silica samples from the low-Sc group which will be discussed later in the chapter.

The basaltic andesites with < 55 wt.% SiO_2 are composed primarily of plagioclase, orhopyroxene and titanomagnetite phenocrysts. Clinopyroxene is slightly more abundant in these samples, and it commonly forms mantling rims around the orthopyroxene phenocrysts. The textures of these samples vary between fine-grained and porphyritic to microcrystalline, porphyritic aphanitic, where amorphous glassy patches are common. One sample contains minor olivine showing irregular rims of orthopyroxene which appears to be replacing it. Other than that olivine is absent. The plagioclase phenocrysts show similar textures to those of the high-Sc group.

Samples containing > 55 wt.% SiO_2 are commonly vesicular to highly vesicular, showing abundant glassy fragments. The andesites have a basic mineralogy of plagioclase, orthopyroxene, clinopyroxene and titanomagnetite. Mineral analyses of plagioclase phenocrysts shows An-contents of between 47 and 64 mol.% (fig. 4.4*a*). In addition to the more restricted range in An-contents, they show less extensive mineral resorption compared to the high-Sc and other low-Sc samples. Orthopyroxene phenocrysts also display a more

Major Element Geochemical Plots against MgO
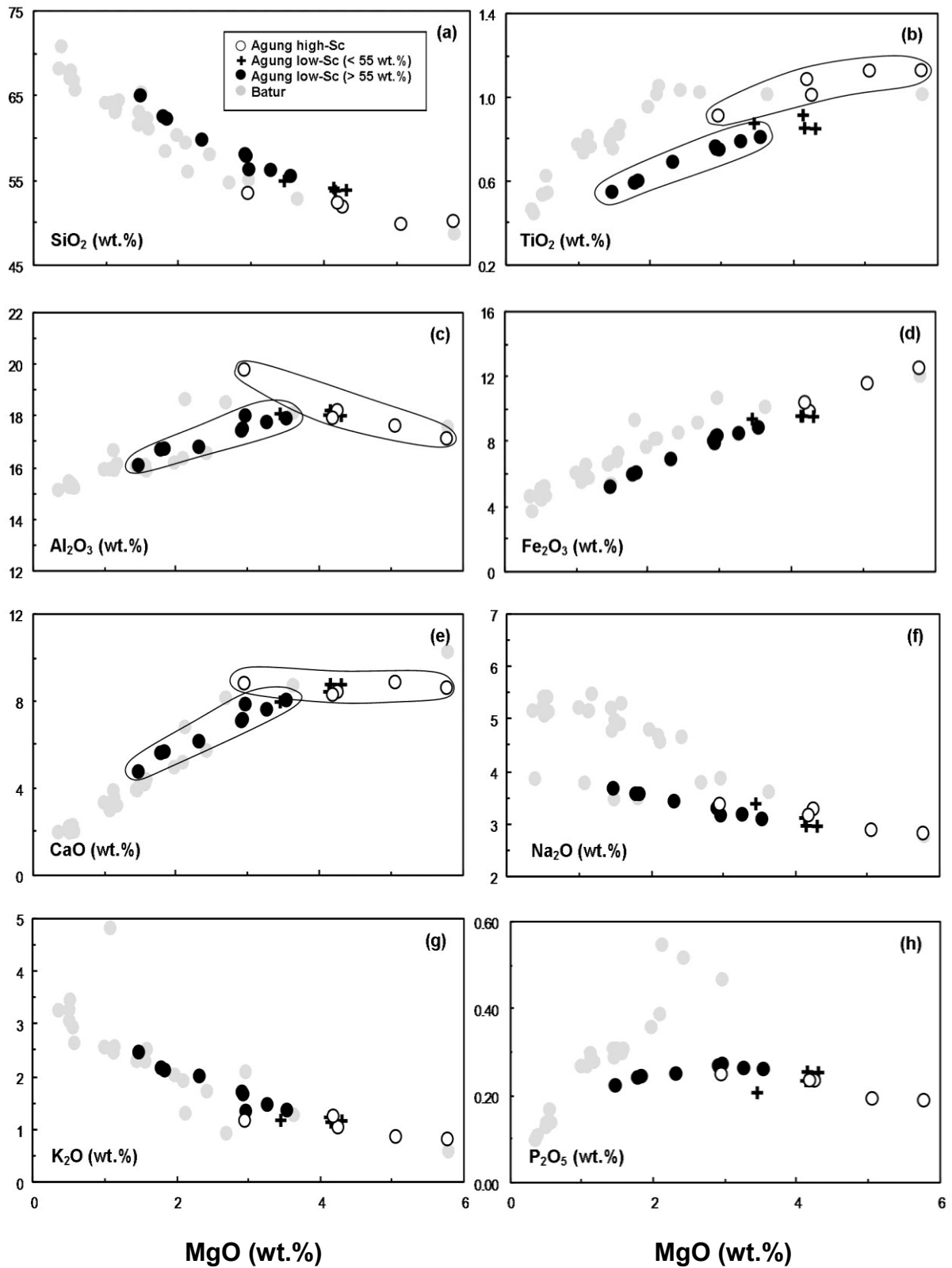
Fig. 4.5. (a-h) Major element data plotted against MgO (wt.%). Includes data from Batur (after Reubi and Nicholls, 2005; Wheller and Varne, 1986).

Compatible and LILE Trace Element Geochemical Plots against MgO
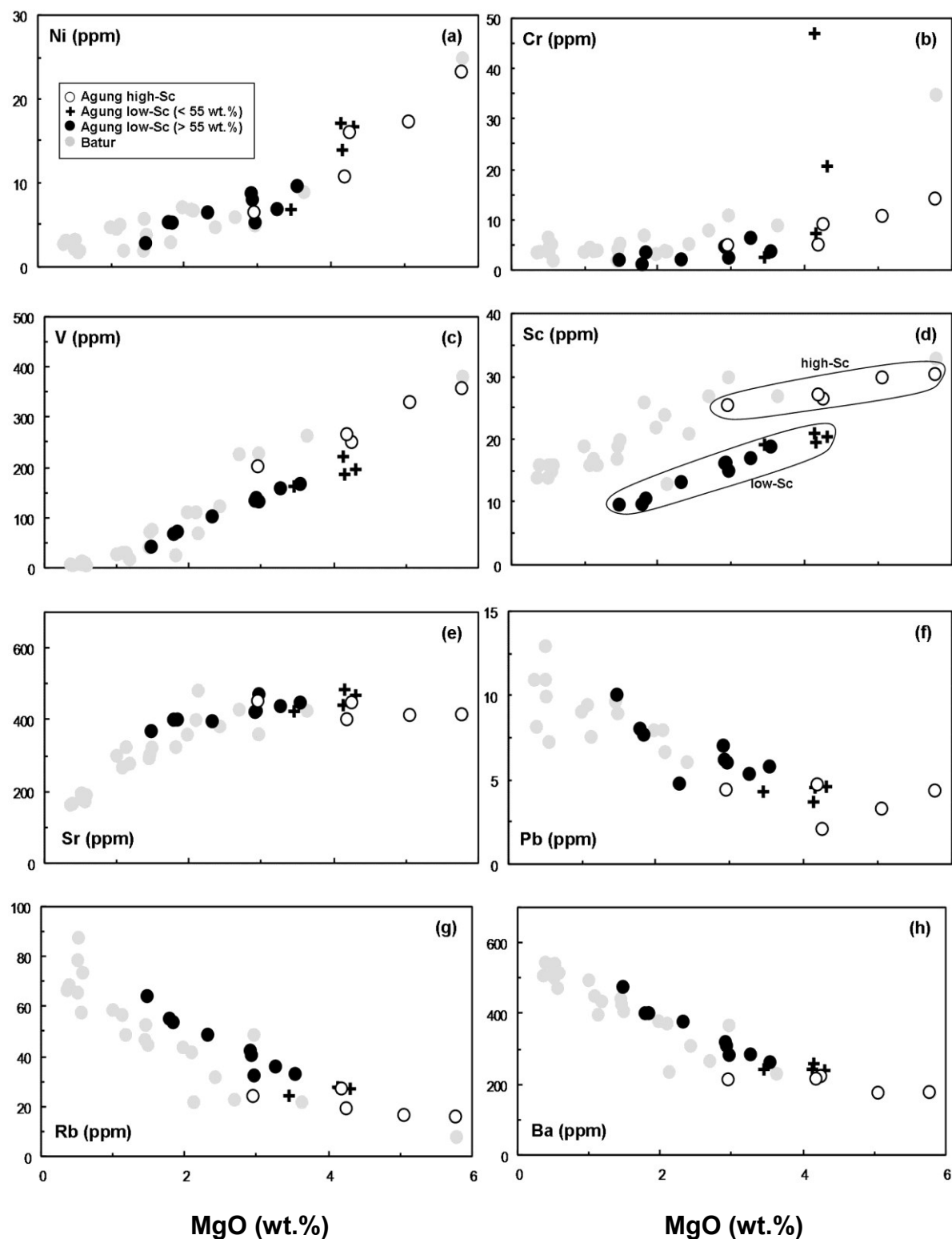
Fig. 4.6. (a-h) Trace element data plotted against MgO (wt.%). Trace elements used include those which show compatible behavoir in the magmas, and those which are considered to be incompatible and more fluid mobile (e.g. Tatsumi *et al*., 1986; Kogiso *et al*.,1997). Includes data from Batur (after Reubi and Nicholls, 2005; Wheller and Varne, 1986).

HFSE and REE Trace Element Geochemical Plots against MgO
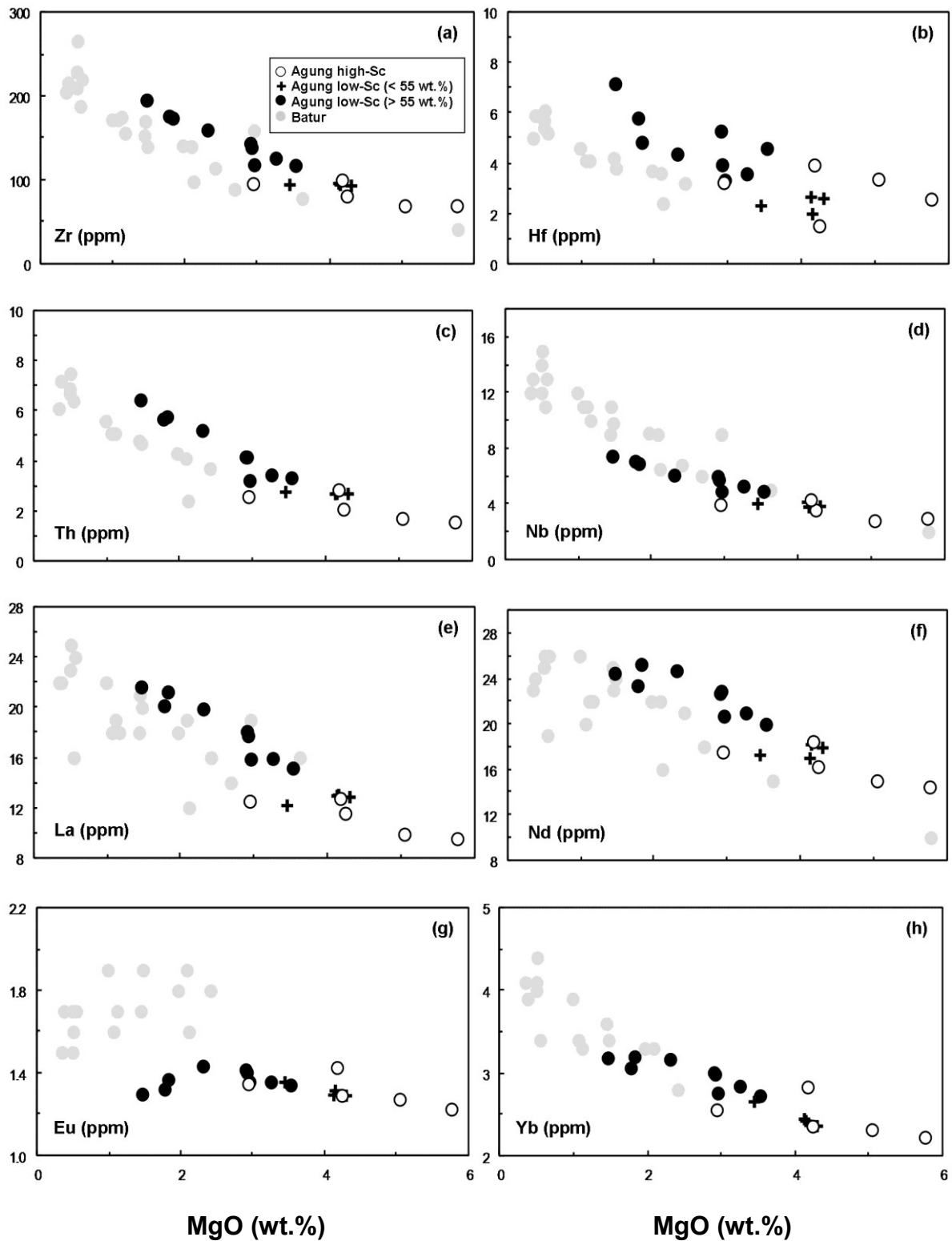
Fig. 4.7. (a-h) Trace element data plotted against MgO (wt.%). Trace elements used include high-field strength elements and rare-earth elements. Includes data from Batur (after Reubi and Nicholls, 2005; Wheller and Varne, 1986).

restricted range of compositions (En = 55.8-65.7, Fs = 30.8-39.4 and Wo = 3.2-4.8 mol.%) but are also less abundant (fig. 4.4b). The dacite is a vitrophyre ignimbrite composed primarily of glass, plagioclase, orthopyroxene and titanomagnetite. Only a few phenocrysts could be analysed for their mineral chemistry but show plagioclase An-contents between 46 and 54 mol.% and orthopyroxene En = 57.4 to 61.9, Fs = 35.1 to 38.4, and Wo = 3.0 to 4.9 mol.%.

The MgO contents of the low-Sc group range from 4.31 to 1.46 wt.%, which produce linear variations against other major and trace elements. These samples display increasing SiO_2, Na_2O, K_2O and incompatible trace elements , and decreasing TiO_2, Al_2O_3, Fe_2O_3, CaO, P_2O_5, Ni, Cr, V, Sc, Sr and Eu against MgO. Samples with < 2.5 wt.% MgO show the most significant variations for major and trace elements with significant drops in P_2O_5, Eu, and to a lesser extent Sr; and elevations in Pb and Hf. The Harker plots show a number of similarities

in the major and trace element configurations of Agung and Batur, the latter including rocks of a more evolved composition (figures 4.5- 4.7). However, there are a number of significant differences between the two volcanoes. Of the major elements, TiO_2, Na_2O and P_2O_5 are more elevated in samples of similar MgO content at Batur and show different differentiation paths against MgO. Sc and Eu are also more elevated at Batur; although Eu shows a continuation of the high-Sc differentiation path. Most of the incompatible trace elements show similar concentrations at similar MgO contents at the two volcanoes.

4.3.3. Incompatible trace elements normalised to N-MORB

The incompatible trace elements for high-Sc and low-Sc groups have been normalised to a reference of normal Mid-Ocean Ridge Basalt (N-MORB after Sun and McDonough, 1989) in figure 4.8 (*a-d*). Figures *(a)* and *(b)* also show Agung relative to Batur (Reubi and Nicholls, 2004, 2005), and *(c)* and *(d)* show Agung relative to the lavas at Kelut. The patterns produced show a typical subduction-zone pattern of high Large-Ion Lithophile Elements (LILE) and Light-Rare Earth Elements (LREE) compared to low High-Field Strength Elements (HFSE) and Heavy-Rare Earth Elements (HREE).

A number of first-order observations can also be made; firstly, with the exception of anomalies at Pb, K, Nb, Ta and Ti concentrations of elements broadly increase with

increasing incompatiblity; secondly, that the magmas with the highest MgO (in the high-Sc group) contain HFSE and HREE closest to N-MORB which beome progressively elevated in the samples with the lowest MgO. This observation is also true of Batur. Furthermore, all of these profiles remain relatively parallel in the different samples. In figures 4.8 *(c)* and *(d)*, the two groups from Agung are compared to the Kelut LHR series. The most notable differences between the most primitive rocks from Kelut and those from the high-Sc group are the high Ba and Pb and low HFSE and HREE of the latter. These observations are discussed further in section 4.5.

4.3.4. Chondrite-normalised rare-earth elements

Chondrite-normalised REE plots are displayed in figure 4.9. Figures *(a)* and *(b)* show the high-Sc and low-Sc groups, respectively, against other rocks from the WLSI and MORB. It is apparent from these plots that, typical of most arc-related magmas, the LREE are enriched with respect to MORB. The high-Sc group contain lower enrichments in LREE compared to most other volcanic rocks in the WLSI and the Agung low-Sc group, with values generally between 40 and 50 times Chondrite for La. The HREE are also less elevated in the high-Sc magmas compared to most other volcanoes, with Lu values between 14 and 18 times Chondrite. As observed in the previous chapters, the volcanoes which are more enriched in potassium contents (e.g. the shoshonites and leucitites) are also more enriched in light-medium REE.

Figures 4.9 (c) and (d) show more detailed plots of the Agung high-Sc and low-Sc magma groups. These plots show that more evolved compositions become progressively enriched in LREE, which are greatest in the low-Sc dacite with 91 times Chondrite for Lu. The HREE only become slightly more enriched in the more evolved magmas, with the dacite containing 21 times Chondrite values for Lu. There are no other discriminating variations in chemistry between the high-Sc and Low-Sc groups, other than a progressively prominent Eu-negative anomaly in the latter.

Fig. 4.8. (a-d) Incompatible trace elements normalised to N-MORB (after Sun and McDonough, 1989). A range of I-MORB compositions have also been included (after Chauvel and Blichert-Toft, 2001; Janney *et al.,* 2005) to show the extreme variation in these basalts which are commonly envoked as mantle source compositions. Figures **(a)** and **(b)** show the high-Sc and Low-Sc groups against samples from Batur (after Reubi and Nicholls, 2005; Wheller and Varne, 1986). Figures **(c)** and **(d)** show the high-Sc and Low-Sc groups against samples from Kelut in order to compared these forntal- rear-arc lavas with front-arc lavas. Note the high Ba and Pb concentrations and lower HFSE and HREE of the Kelut lavas. Observations are discussed in the text.

N-MORB Normalised Diagrams
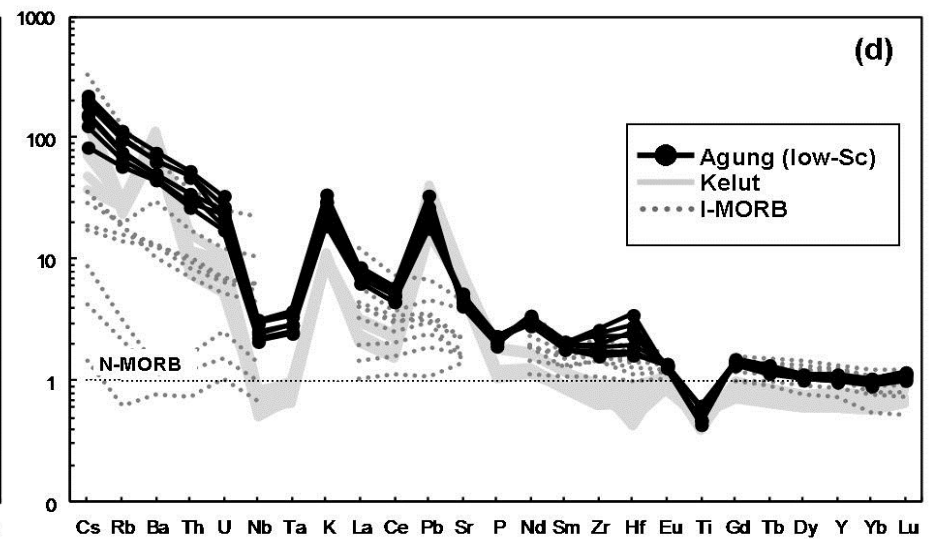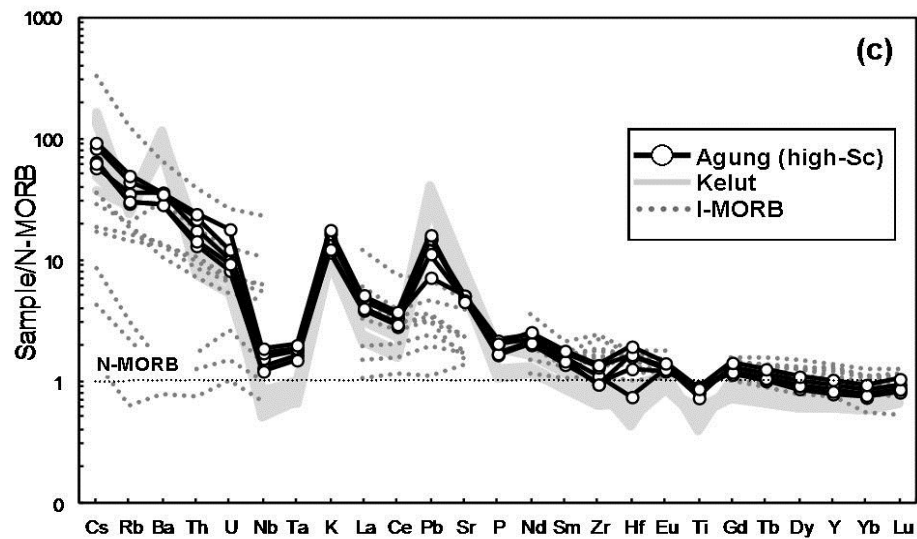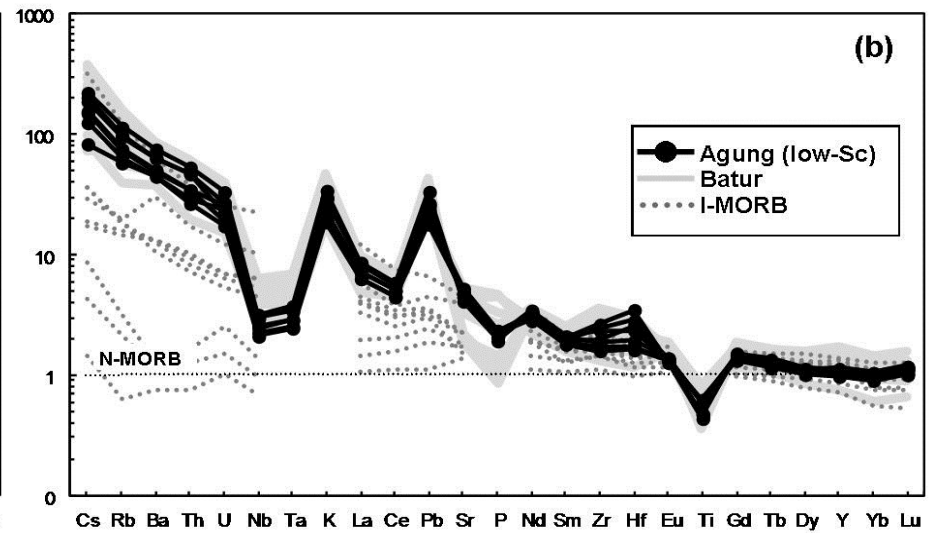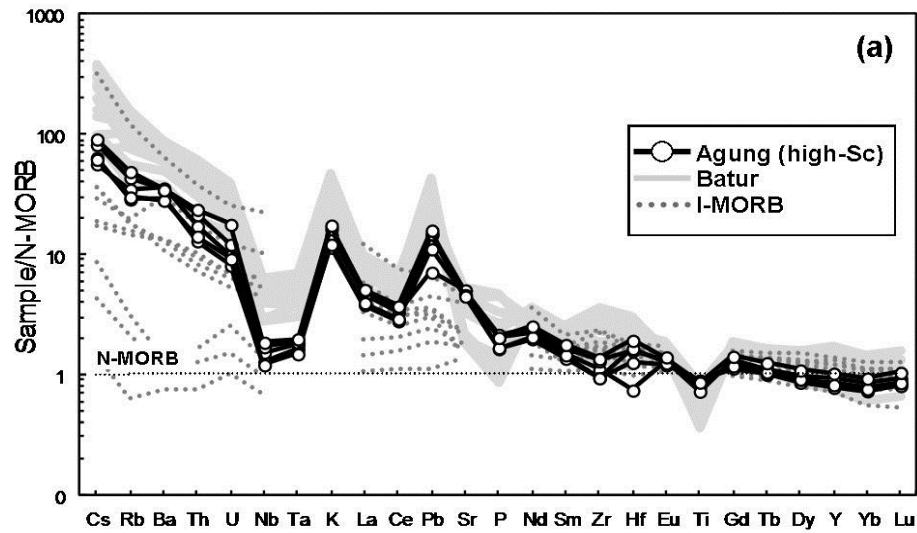
Chondrite-Normalised REE Diagrams
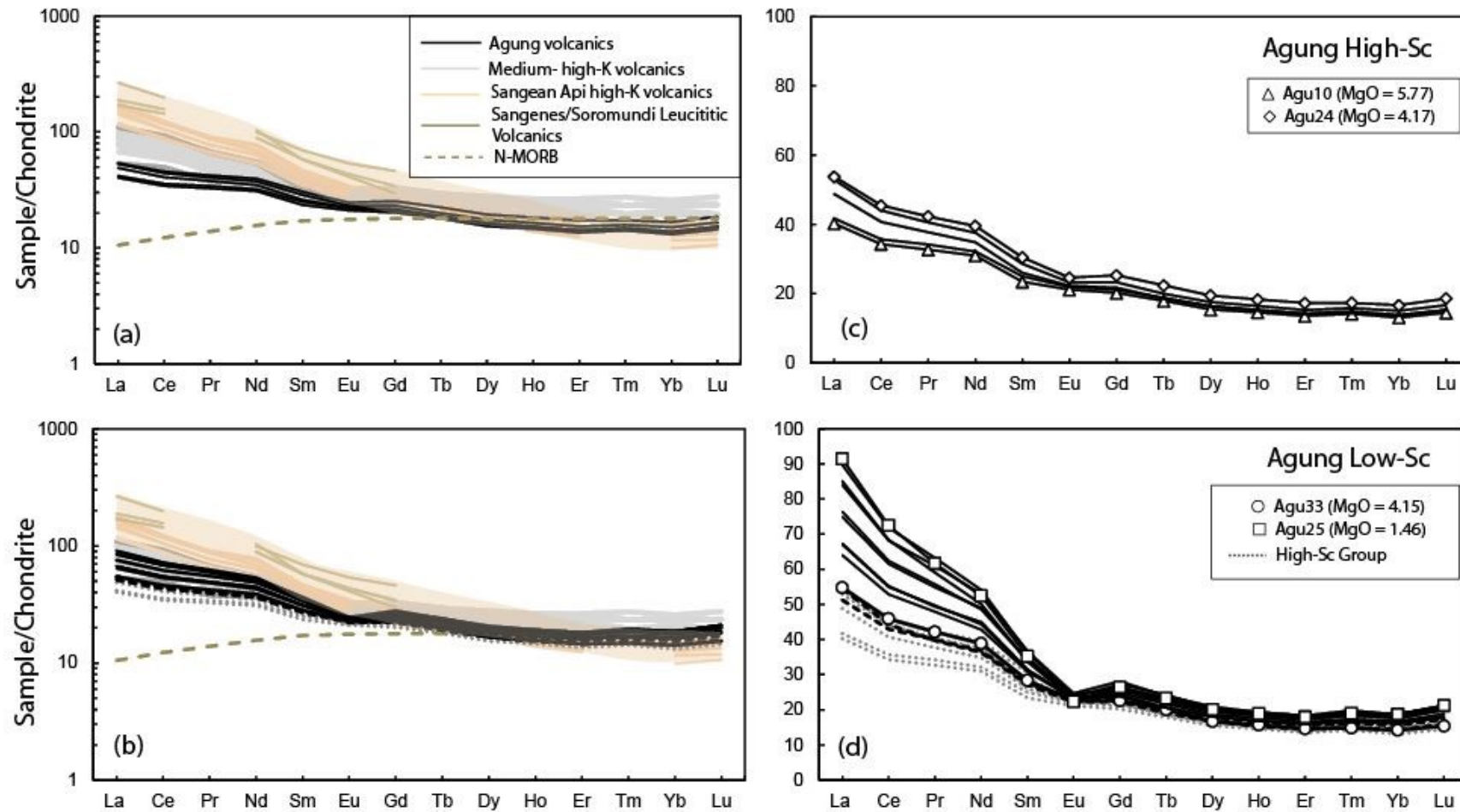
Fig. 4.9. Chondrite-normalised REE plots for **(a)** and **(c)**, the high-Sc group; and **(b)** and **(d)** the low-Sc group. Figures **(a)** and **(b)** include other data from the WLSI (references as for figure 4.3). The symbols in figures **(c)** and **(d)** show the most primitive and most evolved samples within the groups.

Radiogenic Isotope Geochemical Plots against MgO
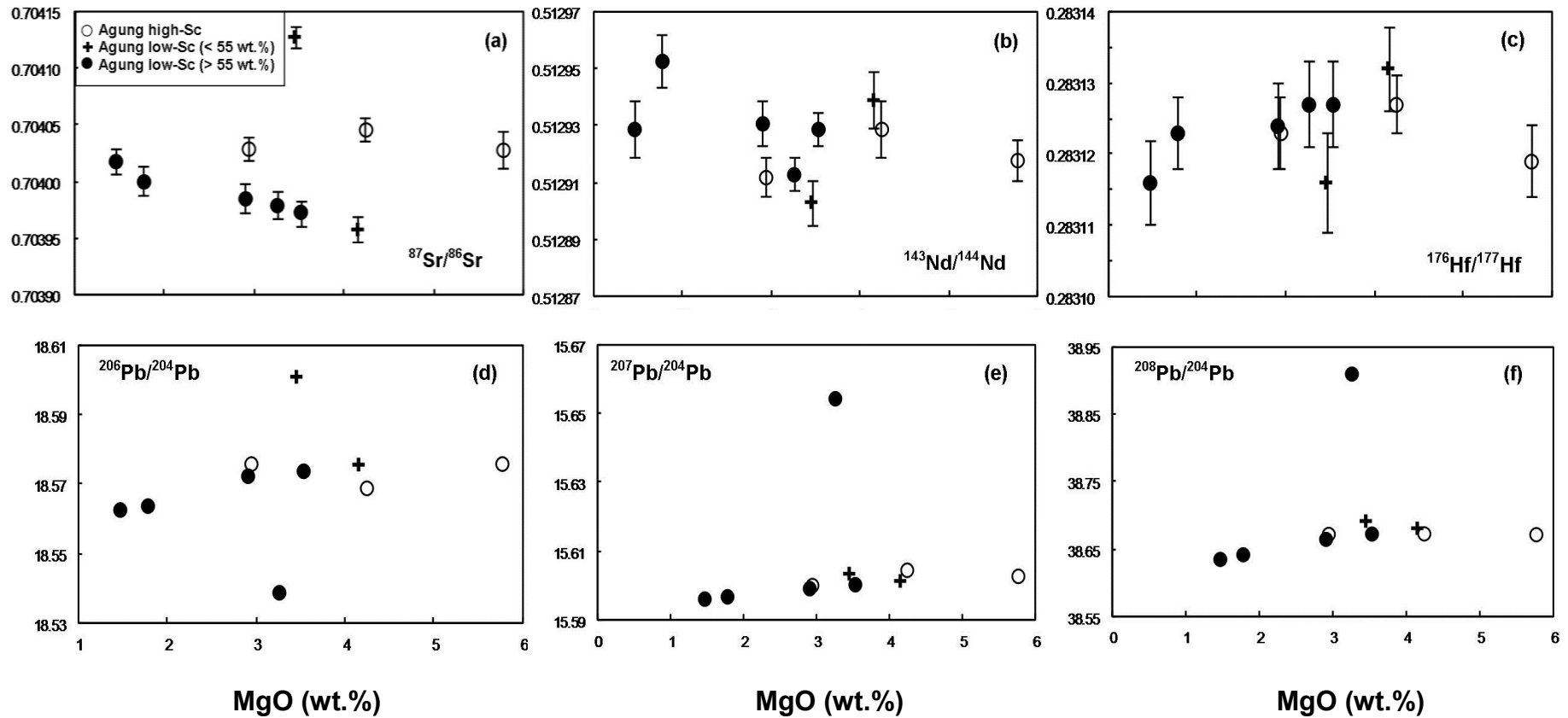
Fig. 4.10. (a-f) Isotopic compositions against MgO wt.% for the Agung lavas. The 2SE internal errors for Sr, Nd and Hf on individual lavas are shown with a solid bar. The 2SE for Pb data is not shown because error bars are smaller than symbols. External reproducibilities are provided in appendix E.

4.4. Isotope Geochemistry

In this section isotope ratios are discussed in terms of differentiation. Isotope-isotope and isotope- trace element characteristics are discussed in section 4.5. Isotope ratios against MgO are shown in figure 4.10 (*a-f*) together with 2SE internal error bars.

In general isotope ratios show very little variation in all of the samples. For $^{87}Sr/^{86}Sr$, the difference between all samples is in the low-Sc and high-Sc (> 55 wt.% SiO_2) groups are within error. Therefore, trends must be interpreted cautiously. The high-Sc group are all slightly more radiogenic than the low-Sc samples. For the latter, there is a minor increase in $^{87}Sr/^{86}Sr$ in samples with lower MgO. $^{143}Nd/^{144}Nd$ and $^{176}Hf/^{177}Hf$ ratios for the all of the samples are also within analytical error of each other. For isotopes of Pb, there is one anomalous sample which plots to lower $^{206}Pb/^{204}Pb$ and higher $^{207}Pb/^{204}Pb$ and $^{208}Pb/^{204}Pb$ otherwise the remaining samples show little variation for these isotopes. The consequences of such isotopic trends will be discussed in the next section.

4.5. Discussion

The first objective of this section is to identify how many of the chemical characteristics shown by the Agung lavas have been inherited in the crust; and further, whether crustal processes are capable of creating the variations between the high-Sc and low-Sc groups.

From the lavas analysed, the olivine basalts of the high-Sc group represent those which are potentially the least differentiated from a mantle source. However, these 'parental' rocks contain ~ 5 wt. % MgO, 20 ppm Ni and 15 ppm Cr, with an Mg# of ~ 48; which suggests they may have already been significantly differentiated from a primitive source. Some key observations were made in section 4.3, which suggest that fractional crystallisation may have a strong control over magma compositions.

4.5.1. Fractional Crystallisation

If fractional crystallisation is the dominant process operating in magma chambers beneath Agung, there should be some evidence for the removal of particular minerals during

differentiation. The petrography of the samples identified mineral variations between the high-Sc group and low-Sc group. This suggests that either:

1. The two groups were derived from a single source where removal of minerals (e.g. olivine) from the high-Sc melt produces magma compositions in the low-Sc group.

2. The two groups were derived from a single source and differentiate independently at different temperature and pressure conditions.

3. The groups were derived from different sources and differentiate independently.

Figures 4.5 to 4.7 show that most of the elements in both groups can be projected back to a single point at higher MgO values. Therefore, all of the magmas are potentially derived from the same, or at least a geochemically similar source. A particularly useful mineral to identify mineral fractionation trends is plagioclase. This is because firstly, it is ubiquitous in all of the samples; and secondly, it is the most abundant mineral phase in all of the samples. Therefore, the removal of other minerals can be compared against it.

The Harker diagrams show that elements expected to be influenced by plagioclase (e.g. Al_2O_3, CaO, Sr and Eu) exhibit different behavoir in the high-Sc group and the low-Sc group. In the former, Al_2O_3 and Eu increases while CaO and Sr remains at similar concentrations. This suggests that plagioclase removal is not sufficient to lower concentrations of these elements. The more differentiated samples in the low-Sc group show significant depletion of these elements which implies that the magmas are more strongly influenced by plagioclase removal.

Figure 4.11 (*a-f*) show plausible fractionation vectors for the low-Sc and high-Sc groups based on elements compatible in plagioclase. In these figures, MgO (wt.%) and Sr (ppm) are used as the index for differentiation and show that in the high-Sc group, Al_2O_3 and CaO either increase, or remain the same, while the europium anomaly (Eu/Eu*) becomes slightly more negative with differentiation. This suggests that the removal of plagioclase is less significant than removal of the other minerals such as olivine and clinopyroxene.

The low-Sc group contain two types of patterns. The samples containing $SiO_2 < 55$ wt.% display little change in CaO, Al_2O_3 or Eu/Eu* with MgO or Sr. For these magmas it is likely that removal of plagioclase is at a similar rate to the removal of olivine and clinopyroxene.

Plagioclase compatible elements against MgO and Sr
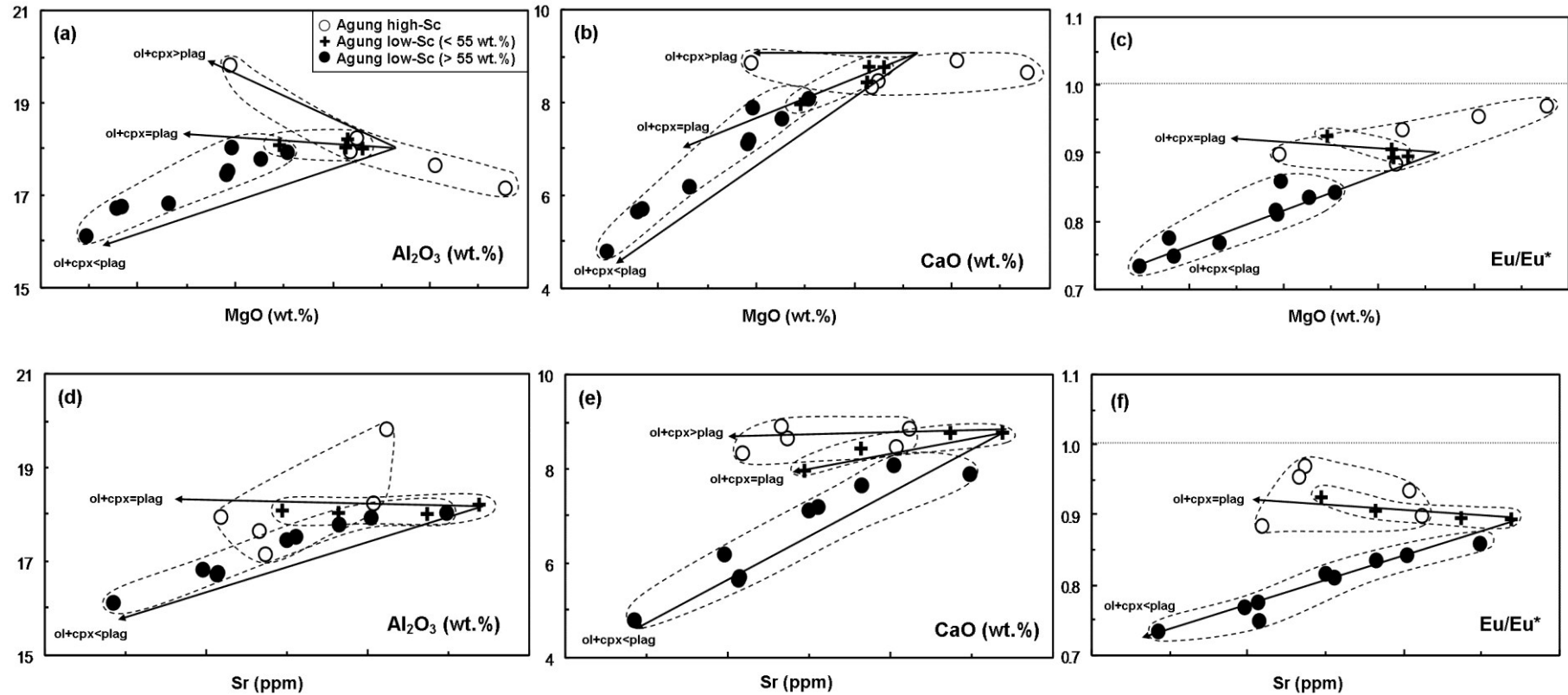
Fig. 4.11. (a-f) Fractionation vectors based upon the influence of plagioclase relative to olivine and clinopyroxene using plagioclase-compatible elements.

Therefore, there are no relative increases or decreases in these elements. The high-Sc group samples > 55 wt.%, in contrast, are significantly depleted in Al_2O_3, CaO and Eu/Eu* with decreasing MgO and Sr. This provides strong evidence that the chemistry of these magmas contain a significant plagioclase control and therefore, a strong fractional crystallisation control.

4.5.1.1. Least Squares Modelling

In order to quantify the observations made above, major and trace element modelling can be applied by utilising the Least Squares Modelling XLFRAC program by Stormer and Nicholls (1978). This program has been described in Chapters 2 and 3, and works by determining the probability of producing a final (daughter) from an intial (parent) magma composition using major element concentrations and mineral data for the phases being added or removed. Results of the modelling are shown in Table 4B (*a*). Three models are displayed, one for the high-Sc group, one for the low-Sc group where samples are < 55 wt.% SiO_2, and one for the low-Sc group where samples are > 55 wt.% SiO_2. To comply with the vectors, a mineral assemblage of plagioclase, clinopyroxene, olivine and Fe-Ti oxide were used in the models. orthopyroxene was not used because it produces a similar result to olivine and makes little difference to the models.

The results strongly support the fractionation vectors in figure 4.11. All three models produce very acceptable reults of < 0.042 and show that plagioclase removal is less than clinopyroxene and olivine for the high-Sc group (*model 1*), is roughly equal in the low-Sc (< 55 wt.%) (*model 2*), and significantly higher in the low-Sc group (> 55 wt.%) (model3). tianomagnetite fractionation in the low-Sc (> 55 wt.%) samples is also slightly higher than for the high-Sc group.

4.5.1.2. Trace element Modelling

Trace element modelling for the same three groups using the results from Least Square modelling and the Raleigh fractionation equation (where cl/co = $F^{(D-1)}$) are shown in Table 4B *(b)*. Distribution coefficients were selected from the GERM database (http://earthref.org /GERM/) for a typical basalt-andeiste-dacite magmas associations. While these values can be ambiguous, this currently provides the best way of determining trace element concentrations

(a) Major Element XLFRAC Modelling

Plag+cpx+ol+Fe-Ti oxide

Model No.	Group Daughter	Parent (initial) MgO (wt%)	Daughter (final) MgO (wt.%)	$\sum r^2$	Phases removed plag	cpx	ol	Fe-Ti oxide	Removed (%)	Added (%)	Total (%)
1	High-Sc	Agu10 (5.77)	Agu22 (2.94)	0.0316	-1.83	-5.47	-7.52	-2.89	-17.71	0.00	-17.71
2	Low-Sc (< 55 wt.%)	Agu31 (4.31)	Agu12 (3.45)	0.0419	-6.05	-4.56	-1.66	-0.12	-12.39	0.00	-12.39
3	Low-Sc (> 55 wt.%)	Agu06 (3.53)	Agu25 (1.46)	0.0152	-32.41	-7.73	-5.16	-3.56	-48.86	0.00	-48.86

(b) Trace Element Modelling

Element	Calculated Daughter compositions Model no.				Measured Daughter compositions Model no.				%Error Model no.		
	1	2	3		1	2	3		1	2	3
Rb	19.44	30.08	56.33		24.49	24.19	64.59		20.64	24.36	12.79
Ba	211.91	261.19	390.66		216.05	241.69	478.28		1.92	8.07	18.32
Th	1.85	3.01	6.23		2.58	2.74	6.45		28.30	9.96	3.44
K	8353.03	10875.78	21524.84		9826.27	9689.22	20631.56		14.99	12.25	4.33
Sr	465.83	443.38	273.38		455.49	423.52	370.96		2.27	4.69	26.30
Y	22.37	24.97	38.77		25.88	25.76	31.74		13.57	3.09	22.16
Yb	2.35	2.42	4.02		2.56	2.65	3.19		8.10	8.68	26.32
U	0.46	0.64	1.42		0.57	0.75	1.57		20.25	13.88	9.60
La	11.07	14.05	24.29		12.53	12.15	21.66		11.65	15.70	12.16
Nb	3.49	4.21	8.43		3.96	3.98	7.45		11.89	5.66	13.27
Zr	80.95	102.15	197.56		95.75	93.79	195.57		15.46	8.91	1.02
Hf	3.02	2.89	8.36		3.24	2.29	7.17		6.88	26.45	16.62
Ta	0.25	0.28	0.57		0.24	0.27	0.50		4.09	3.24	14.36
Ti	4756.17	5564.28	3990.92		5501.85	5247.26	3313.98		13.55	6.04	20.43

Table 4B (a) Major and (b) trace element modelling results. See text for discussion.

through modelling (e.g. Davidson and Wilson, 2011). The results show trace element concentrations calculated by the models in the first three columns; the second three columns show the measured trace element concentrations; and the final three columns show the errors between calcaulated and measured values. While the results do not provide the same support as major element modelling, most of the errors are within 20%, which is acceptable.

4.5.1.3.   The role of plagioclase during fractional crystallisation

Having identified that plagioclase has a significant influence on the variations in major and trace element concentrations in the high- and low-Sc groups, it is important to discuss the potential processes by which this happens.

Experiment studies show that plagioclase crystallisation is primarily dependent on water contents, temperature and pressure (Housh and Luhr, 1991; Sisson and Grove, 1993, Grove *et al.,* 2003; Parman *et al.,* 2011). During differentiation, this means that plagioclase fractionation can be suppressed (or delayed) if the magmas are either stored at higher pressures, or contain a higher concentration of water (e.g. Sisson and Grove, 1993; Parman *et al.,* 2011). This provides two mechanisms which can potentially explain the variations between the high-Sc magmas and low-Sc magmas.

Figure 4.12 shows the Agung groups compared to a number of magmas from neibouring volcanoes, all of which are suggested to be strongly influenced by fractional crystallisation during differentiation. These include, data from Batur, Bali (Reubi and Nicholls, 2004, 2005), Ijen, east Java (Handley *et al.,* 2007), and Rindjani, Lombok (Foden, 1983). These magmas provide a good comparison to Agung because they are sitauted within a close proximity and are to suggested to have a structural control on different magmatic suites (i.e. polybaric crystallisation associated with magma storage at different pressures).

Figure 4.12 *(a)* shows Al_2O_3 against MgO for these volcanoes and includes two possible liquid lines of decent, one where plagioclase fractionation is suppresed (to higher Al_2O_3) and the other in which plagioclase starts to crystallise (to lower Al_2O_3). These vectors are based on varying pre-eruptive water contents in arc magmas and are described in Parman *et al.* (2011). In figures *(b)* and *(c)*, Al_2O_3 and Eu/Eu* against MgO highlights the similarity between the low-Sc group magmas from Agung and the low-Ca group at Ijen, and also the

Comparison between Agung, Batur, Rindjani and Ijen groups
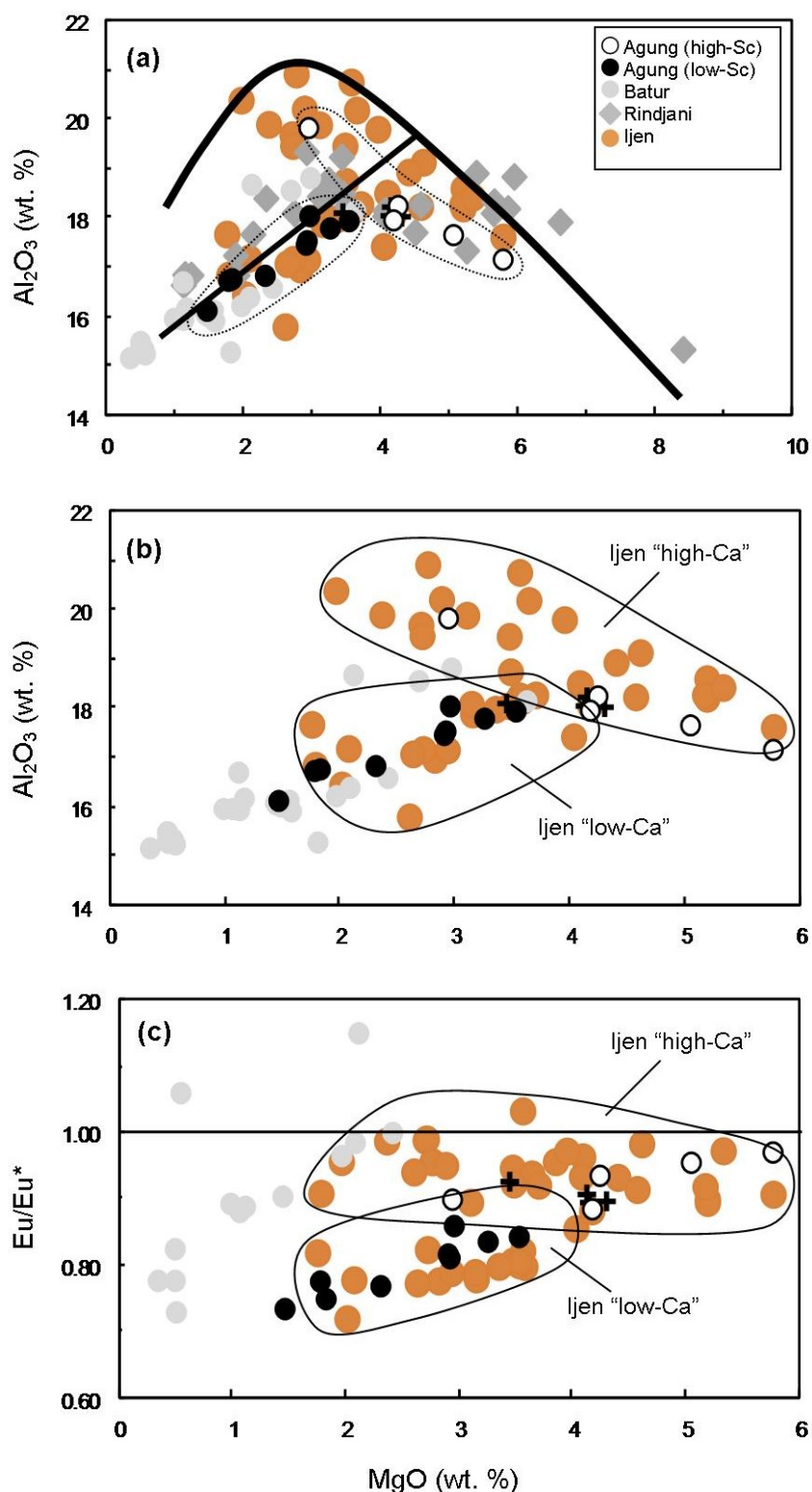
Fig. 4.12. (a) Al_2O_3 against MgO for the groups described at Agung against Batur (Reubi and Nicholls, 2004, 2005), Ijen (Handley *et al.,* 2007) and Rindjani (Foden, 1983). The bold black lines are two hypothetical liquid lines of decent which could be influenced by pre-eruptive H_2O concentrations (after Parman *et al.,* 2011). The dotted black lines outline high-Sc and low-Sc groups. **(b)** shows Al_2O_3 against MgO for the same volcanoes, but where high-Ca and low-Ca groups from Ijen are highlighted by a black line. **(c)** shows the same as before for Eu/Eu* against MgO. See text for discussion.

high-Sc magmas from Agung with the high-Ca group at Ijen. This suggests that differentiation was driven by a similar process at both volcanoes. Handley *et al.* (2007) suggest that the variation between the low- and high- Ca at Ijen are controlled by deep and shallow reservoirs, where the latter has experienced more extensive fractionation of plagioclase. A similar conclusion is plausible beneath Agung volcano. However, a role for different water contents in the high-Sc and low-Sc groups cannot be precluded.

4.5.2. Open-system processes: Magma mixing and AFC

Very modest variations in isotope ratios suggest that mixing between two compositionally different sources or contamination of magmas during asent through the crust is unlikely. If these processes do occur, they involve isotopically indistinguishable components. However, behaviour of magmas beneath Agung and Batur provide important information about differentiation in the arc crust. They display, to some extent, behavior which could be described as closed-system, or as near to closed-system as arc magmatism can be in reality. However, in many of the volcanoes from Java and the Lesser Sunda Islands, such trends are not apparent, and yet they are still commonly used to identify source processes and contributions from the subducting plate.

It is increasingly clear that many, if not most, of the magmas erupted from these volcanoes have been significantly modified by open-system behavior that is not always accompanied by fractional crystallisation, or ultimately acts to overprint it. Mixing and contamination continue to be advocated or dismissed on the basis of trace-element and isotope correlations with SiO_2 and MgO. This assumes that fractional crystallistion is still the dominant process controlling the chemistry during assimilation, and that mixed magmas have reached a state of equilibrium; therefore resulting in linear trends on x-y plots. Furthermore, it assumes that the two components have detectably different concentrations of SiO_2 and MgO and/or the trace element and isotopes measured against them.

Some of the most compelling evidence for crustal contamination now comes from central Java, where for years source processes where evaluated using rocks contaminated by calc-silicates at the surface (e.g. Gertisser and Keller, 2003; Chadwick *et al.,* 2007; Deegan *et al.,* 2010; Troll *et al.,* in press). These contributions were previously overlooked because of the lack of correlation between isotopes and major elements. However, is hardly suprising that

mixing between mafic magmas of varying composition and heterogenous calc-silcate crust does not produce such trends.

The following conclusions can be drawn from this section:

1. Fractional crystallisation was the dominant process controlling differentiation beneath Agung. A similar conclusion has been suggest for nearby volcanoes Batur, Kelut and Rindjani.

2. Two magma types are identified and are associated with different suites of minerals; a high Sc group, composed primarily of plagioclase, olivine, orthopyroxene and titanomagnetite, and a low-Sc group, composed of plagioclase, orthopyroxene, clinopyroxene and titanomagnetite.

3. Modelling suggests that the high-Sc group can be explained by the removal of ~ 2% plagioclase, 5% clinopyroxene and 7% olivine (or orthopyroxene). In this group plagioclase removal is less significant than olivine and clinopyroxene.

4. The low-Sc group can be subdivided into samples with < 55 wt.% SiO_2 and > 55 wt.% SiO_2. Modelling shows that the former is can be produced by the removal of ~ 6% plagioclase, 5% clinopyroxene and 2% olivine, where plagioclase fractionation is roughly equal to that of clinopyroxene and olivine. The latter show evidence for significant plagioclase removal (~32%), this is significantly higher than removal of clinopyroxene (~ 8%) and olivine (~5%).

5. Major and trace element concentrations against MgO show similar characteristics to nearby volcanoes Batur, Kelut and Rindjani which also show a strong influence by fractional crystallisation

6. There is no evidence to suggest that magmas at Agung have had their isotope ratios modified in the arc crust, and they should therefore provide a good estimate of their source composition/s.

4.5.3. The pre-subduction mantle wedge

The pre-subduction mantle wedge is something of a hypothetical component, because it assumes the composition of mantle before subduction contributions are added to it. However, it is a fundamental constraint with which to quantify fluid and/or sediment slab contributions that are added to it (Woodhead, 1989; McCulloch and Gamble, 1991; Pearce *et al.,* 1995; Elliot *et al.,* 1997; Turner and Hawkesworth, 1997; Dorendorf *et al.,* 2000; Hochstaedter *et al.,* 2000, 2001; Churikova *et al.,* 2001; Handley *et al.,* 2007; Trollstrup *et al.,* 2010). An examination of the pre-subduction mantle usually involves the trace elements and isotopes shown to be less readily transported in aqueous fluids (Tatsumi *et al.,* 1986; Brenan *et al.,* 1994, 1995; Keppler, 1996; Ayers *et al.,* 1997; Kogiso *et al.,* 1997; Tatsumi and Kogiso, 1997; Ayers, 1998; Hermann *et al.,* 2006). These include the HFSE and HREE, which are significantly less enriched than LILE and LREE in a metasomatised mantle (McCulloch and Gamble, 1991; Saunders *et al.,* 1991. In primitive arc magmas or those not suspected of significant contamination in the arc crust, ratios of HFSE and HREE such as Zr/Nb are then used to identify the character of this mantle wedge (Woodhead *et al.,* 1993; Elliot *et al.,* 1997; Macpherson *et al.,* 2003; Handley *et al.,* 2007).

According to the criteria described above three types of mantle wedge are frequently postulated beneath island arcs in SE Asia; N-type MORB (N-MORB), I, or E-type MORB (E-MORB, I-MORB) and Ocean island basalt (OIB) (Wheller *et al.,* 1987; Elburg and Foden, 1998; Gertisser and Keller, 2003; Turner *et al.,* 2003; Reubi and Nicholls, 2004; Handley *et al.,* 2008; Sendjaja *et al.,* 2009; Macpherson *et al.,* 2010). These terms essentially describe the fertility of the mantle composition prior to melting. For example, N-type MORB which is characteristic of a depleted mantle will typically have lower Nb and Ta and higher Zr/Nb than I-MORB and OIB, which are progressively more enriched.

Detailed studies on a number of oceanic arcs have provided particularly useful information on mantle melting and fertility beneath arc volcanoes (Woodhead *et al.,* 1993; Hochstaedter *et al.,* 2000). In essence they show that mantle melting is generally higher towards the front of an arc and mantle fertility is higher toward the back of the arc (e.g. Pearce and Parkinson, 1993). Furthermore, the arcs with the most-developed back-arc spreading centres are generally the ones with the most depleted fore-arcs e.g. Tonga (Ewart and Hawkesworth, 1987; Turner *et al.,* 1997; Turner and Hawkesworth, 1997) and Izu-Bonin (Hochstaedter et al. 2000).

The link between melting and mantle fertility is an obvious one, although there can be a number of different triggers. Essentially, when a small degree of partial melt is extracted from a fertile source, it preferentially concentrates the most incompatible elements; therefore any subsequent melting events of the same source will be melting progressively refractory material (e.g. Foley, 1992). Ultimately higher degrees of melting will act as a diluent producing progressively depleted melts.

Above subduction zones, once a melt has been extracted in the back-arc, convection can drive the residual towards the front of the arc where melts can continue to be extracted from a progressively depleted source (McCulloch and Gamble, 1991; Pearce and Parkinson, 1993). This process is likely to be exaggerated towards the front of the arc, where the low pressure introduction of fluids from the slab into the mantle wedge can induce more melting resulting in the production of refractory tholeiitic magmas (Hermann *et al.*, 2006).

As a first approach here, the model of Pearce and Parkinson (1993) has been adopted, as it was in Chapter 2. This method uses a number of elements thought not to be modified by subduction-related processes and ranks them in order of their compatibility. For this model only rocks with > 5 wt.% are used as they are more likely to represent magma source compositions prior to significant amounts differentiation. The expception to this rule is Kelut, which has slightly less than 5 wt.% MgO. However, for this sample crustal contamination and magma mixing is not an issue. In theory, enriched sources will have higher concentrations of very highly incompatible elements (VHI), and become progressively lower with less enriched sources.

The model categorises all of volcanoes in accordance to their location across the arc and subdivides them between front-arc, rear-arc and back-arc positions. In compliance with Chapter 2, front-arc volcanoes are defined here as situated < 160 km, rear-arc 160 – 200 km, and back-arc > 200 km. There is clearly some degree of overlap between estimated Benioff-Zone volcano depths (e.g. Whitford 1975; Hutchinson, 1982; England *et al.*, 2004; Syracuse and Geoffrey, 2006), but in most cases the volcanoes remain in similar relative positions to each other and the variation in estimated depths are small. For this purpose, it is the position of each volcano relative to each other and a fixed point that is important. Therefore, the values shown in figure 4.13 (*a-f*) are in accordance to the calculated Benioff Zone depths of Hutchinson (1982) for consistency with previous studies (e.g. Turner *et al.*, 2003), but the

Source and Melting Variations across the Lesser Sunda Arc
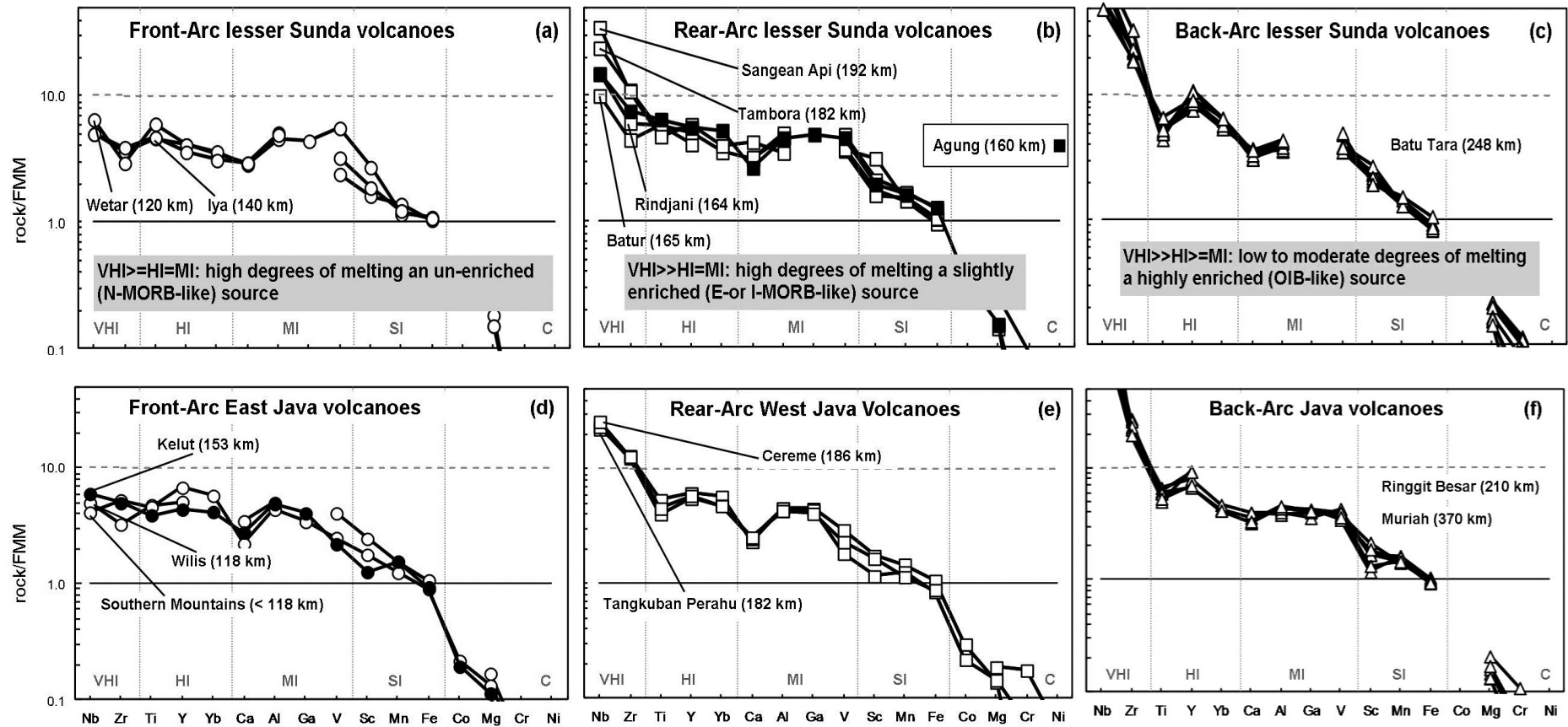
Fig. 4.13. (a-f) Source melting models after (Pearce and Parkinson, 1993). Front-arc volcanoes are represented by circles, rear-arc volcanoes by squares, and back-arc by triangles. Model shows that the nature of the sub-arc manlte contains similar concentrations at similar positions from west Java to East Sunda. See text for discussion. VHI = very highly incompatible elements (during mantle melting), HI = highly incompatible, MI = Moderately incompatible, SI = slightly incompatible, C = compatible. Degree of enrichment or depletion is largely shown by behavior of VHI. Interpretations in grey boxes after (Pearce and Parkinson, 1993). Volcano data for a-c in Table 4C. Other data includes: (d) Kelut and Southern Mountains (this study), Willis (Hartono, 1996); (e) Tangkuban Perahu (Sendjaja *et al.,* 2009), Cereme (Edwards, 1990); (f) Ringgit-Besar, Muriah (Edwards, 1990).

Lesser Sunda Rocks used in Modelling

Author	Elburg et al., (2005)	Stolz et al (1990)	This study	Foden (1983)	Wheller and Varne (1986)	Foden (1986)	Turner et al., (2003)		Stolz et al ., (1988, 1990)		
Island	Wetar	Flores	Bali	Lombok	Bali	Sumbawa	Sumbawa	Alor	Alor	Alor	Alor
Volcano	Intrusive	Iya	Agung	Rindjani	Batur	Tambora	Sangeang Api	Batu Tara	Batu Tara	Batu Tara	Batu Tara
Lat.	7.88	8.88	8.26	8.42	8.24	8.25	8.18	7.79	7.79	7.79	7.79
Long.	126.40	121.63	115.58	116.47	115.38	118.00	119.06	123.58	123.58	123.58	123.58
BZD (km)	120	140	160	164	165	182	248	248	248	248	248

(wt.%)

SiO_2	50.55	52.19	50.31	47.95	48.83	49.21	47.20	47.76	47.68	48.14	49.74
TiO_2	1.05	0.82	1.13	0.83	1.02	0.98	0.83	0.90	0.90	0.93	0.78
Al_2O_3	17.14	17.69	17.17	13.78	17.62	17.07	13.16	13.48	13.58	13.76	15.68
Fe_2O_3	10.68	9.71	12.62	10.33	12.12	9.94	10.33	8.65	8.51	8.59	8.12
MnO	0.15	0.15	0.21	0.17	0.22	0.18	0.19	0.17	0.17	0.17	0.17
MgO	7.01	6.12	5.77	10.61	5.78	6.88	9.45	8.38	8.28	7.68	6.40
Mg#	57.36	56.36	48.35	67.79	49.43	58.65	65.21	66.50	66.60	64.69	61.76
CaO	9.28	9.75	8.67	13.14	10.33	10.65	13.91	12.24	12.08	12.05	10.28
Na_2O	3.24	2.73	2.84	1.78	2.79	3.25	2.64	1.48	2.79	1.87	2.24
K_2O	0.84	0.46	0.83	1.20	0.60	1.78	1.79	4.69	3.42	4.51	4.97
P_2O_5	0.06	0.12	0.19	0.21	0.14	0.35	0.39	0.87	0.84	0.85	0.78
Total	100.12	99.38	99.76	100.00	99.40	100.29	100.02	99.27	99.71	99.55	99.79

(ppm)

Ni	20.00	60.00	23.39	125.00	25.00	43.00	49.00	81.00	79.00	68.00	51.00
Cr	24.00	161.00	14.35	307.00	35.00		232.00	287.00	272.00	244.00	194.00
V	434.00	250.00	360.04		383.00	307.00	294.00	276.00	302.00	307.00	278.00
Sc	42.10	31.00	30.53	36.00	33.00	33.90	49.00	36.00	37.00	42.00	32.00

Table 4C. Major element and compatible trace-element data for the samples used in model 4.13 (*a-c*). BZD = Benioff Zone depth (after Hutchinson, 1982).

modelling can be equally replicated using data from Syracuse and Geoffrey (2006), using different limits.

Variations in magma source compositions may be linked to a particular volcano's position relative to the subducting plate (i.e. the Benioff Zone); however, they may also be linked to their position on the upper plate itself. For instance, if the back-arc volcanoes are controlled by rifting, opposed to subduction fluxes, their depth to the subducting plate may be irrelivent. For these volcanoes it may be the upper plate rather than the lower plate which controls their magmatism through localised decompression. Further towards the trench, subduction is likely to become increasingly influential. Therefore, a volcano's relative position on the upper plate is just as important as its position from the subducting plate for a model such as this where the tectonic controls on mantle composition are poorly known.

The first three models include volcanoes from the Lesser Sunda region (Table 4C). The WLSI do not contain volcanoes in front-arc or back-arc positions so the model has been expanded to the entire Lesser Sunda region. The front-arc volcanoes used here (figure 4.13*a*) are represented by an intrusive rock from Wetar (MgO =7 wt.% , Ni = 20 ppm and Cr = 24 ppm, after Elburg *et al.,* 2005) and a tholeiitic basalt from Iya, Flores (MgO = 6 wt.%, Ni = 60 ppm and Cr = 161 ppm, after Stolz *et al.,* 1990). The back-arc volcano (figure 4.10c) is represented by alkaline basalts from Batu Tara (MgO = 6.4 – 8.3 wt.%, Ni = 51 – 81 ppm, Cr = 194 – 287 ppm, after Stolz *et al.* 1990, and van Bergen *et al.,* 1992). Figure 4.13 *(b)* shows the volcanoes from the western Lesser Sunda Islands, while these are restricted to rear-arc positions, they span a range of estimated depths and compositions from medium-K rocks at Agung to shoshonites at Sangean Api (e.g. Turner *et al.,* 2003).

The second set of three models (figure 4.13*d-f*) include equivalent volcanic rocks from Java based on their composition and position relative to the top of the Benioff Zone and on the arc. The source compositions of these rocks have been discussed in Chapter 2. Rather than include all of the volcanoes which qualify for the model, examples from particular regions have been used here (e.g. east Java and west Java). The modelling shows that despite the changing environment along the arc, the elements thought to represent source compositions prior to subduction display systematic variations from the front of the arc to the back. This suggests that there is a generic relationship between the pre-subduction source composition of a particular volcano and its relative position on the arc, or relative to the Benioff Zone. Furthermore, this type of mantle variation can be modelled in the most primitive rocks from

west Java to the most eastern section of Lesser Sunda, where the arc is colliding with Australia.

The concept of spatial variations in Sunda Arc magmas is not a new one. During the 70's and 80's Whitford and Nicholls published a series of papers (e.g. Whitford, 1975; Nicholls and Whitford, 1976; Whitford and Nicholls, 1976; Whitford *et al.,* 1979; Nicholls *et al.,* 1980; Whitford *et al.,* 1981; Whitford and Jezek, 1982) discussing what they termed as 'normal island-arc associations' and 'high-K alkaline associations', and their positions from the trench. This early work identified that tholeiitic magmas are found closest to the trench at depths of 100-150 km, calc-alkaline and high-K calc-alkaline magmas are located at depths of 150-250 km, and high-K alkaline magmas are situated most distal from the trench at depths > 300 km. Their work established a number of important conclusions:

1. A number of incompatible trace elements appear to correlate with position on the arc.
2. Low Mg#, Ni and Cr concentrations in magmas indicate that few represent primary, mantle-derived compositions.
3. Spatial variations in the lavas are best explained by melting of a chemically zoned mantle source with smaller degrees of partial melting at greater depths.

However, this type of idealised model has been challenged on the basis that a number of volcanoes on the arc do not comply to such a model (Arculus and Johnson, 1978; Foden and Varne, 1980). In the Sunda arc this argument includes the extinct volcanoes of Sangenes and Soromundi on Sumbawa which contain highly nepheline-normative alkaline magmas similar to the back-arc volcanoes advocated in model 4.13 (Foden and Varne, 1980). These volcanoes occupy a position on the arc similar to Agung, Rindjani and Batur and so cannot be explained by this type of hypothesis. The nature of these volcanoes are discussed later in this chapter, and in Chapter 5. The remainder of this section will focus on the majority of volcanoes which do identify these type of spatial variations.

The idea of melting chemically zoned mantle sources beneath island arcs is now well recognised, particulary in some oceanic arcs where there is less influence from the arc crust (Woodhead *et al.,* 1993; Elliot et al., 1997; Hochstaedter *et al.,* 2000; Stracke and Bourdon, 2009). A number of fractional and dynamic melting models have been devised in order to try and replicate the loss of a melt fraction from a residue beneath volcanic arcs and spreading ridges (e.g. Wood, 1979; Johnson and Dick ,1992; Phipps Morgan and Morgan, 1999; Pearce

2005). As previously mentioned, this idea suggests that a partial melt can be extracted from a source and leave behind a depleted residue. The ultimate expression of such a process is shown in ultrapotassic melts. Highly alkaline magmas such as lamproites and kimberlites are often associated with highly depleted harzburgite residues, where over long periods of time small degree melts in the lithopshere have formed enriched veins surrounded by a depleted residue (Foley *et al.,* 1987; Foley, 1992; Pilet *et al.,* 2008; Prelevic *et al.,* 2012). It is suggested that at small degrees of partial melting in such environments, the vien will be preferentially melted and concentrate high quantities of incompatible elements into the magma. As melting continues, the refractory material will start to melt creating hybrid magmas as an expression of the enriched vien being progressively diluted by the surrounding refractory wallrock (e.g. Foley, 1992; Pearce, 2005). Therefore in theory, the more contrast there is between enriched and depleted mantle end-members the more compositional variation that can be produced during melting of such material.

The most widely used expression of this type of enrichment or depletion in a mafic magma is its potassium contents relative to a particular value of SiO_2. At island arcs and spreading centres the magmas associated with the lowest potassium concentrations (i.e. tholeiitic compositions) are usually found closest to the trench or at the ridge, where lower pressures produce higher degrees of melting (Whitford *et al.,* 1979; Fitton *et al.,* 2003). Moving progressively away from the trench, or the ridge, magma compositions can become progressively more alkaline in response to higher pressures and lower degrees of partial melting. Over time this can result in the heterogeneous mantle compositions discussed above. However, this process is incompatible with the idea of metasomatism in which potassium, being highly mobile in aqueous fluids should readily re-enrich magmas at the front of the arc. Indeed, most of the early spatial variations discovered across volcanic arcs were of incompatible trace elements such as K, Rb, Cs and Ba (e.g. Kuno, 1959; Jakes and White, 1969, 1970, 1972; Jakes and White, 1969; Whitford and Nicholls, 1976), all of which are thought to be significantly transported during slab dehyration (Tatsumi *et al.,* 1986; Tatsumi and Kogiso, 1997). Many of these elements behave in a similar manner to the more fluid immobile elements such as HFSE and HREE in Sunda magmas across the arc.

Figure 4.14 *(a)* shows a plot of K_2O against *Zr/Nb* for a range of samples from Java and the WLSI. As for the previous model, all the samples shown here are from volcanoes where crustal contamination is minimal and MgO concentrations exceed 5 wt.%. The exception to

Across-Arc Geochemical Trends
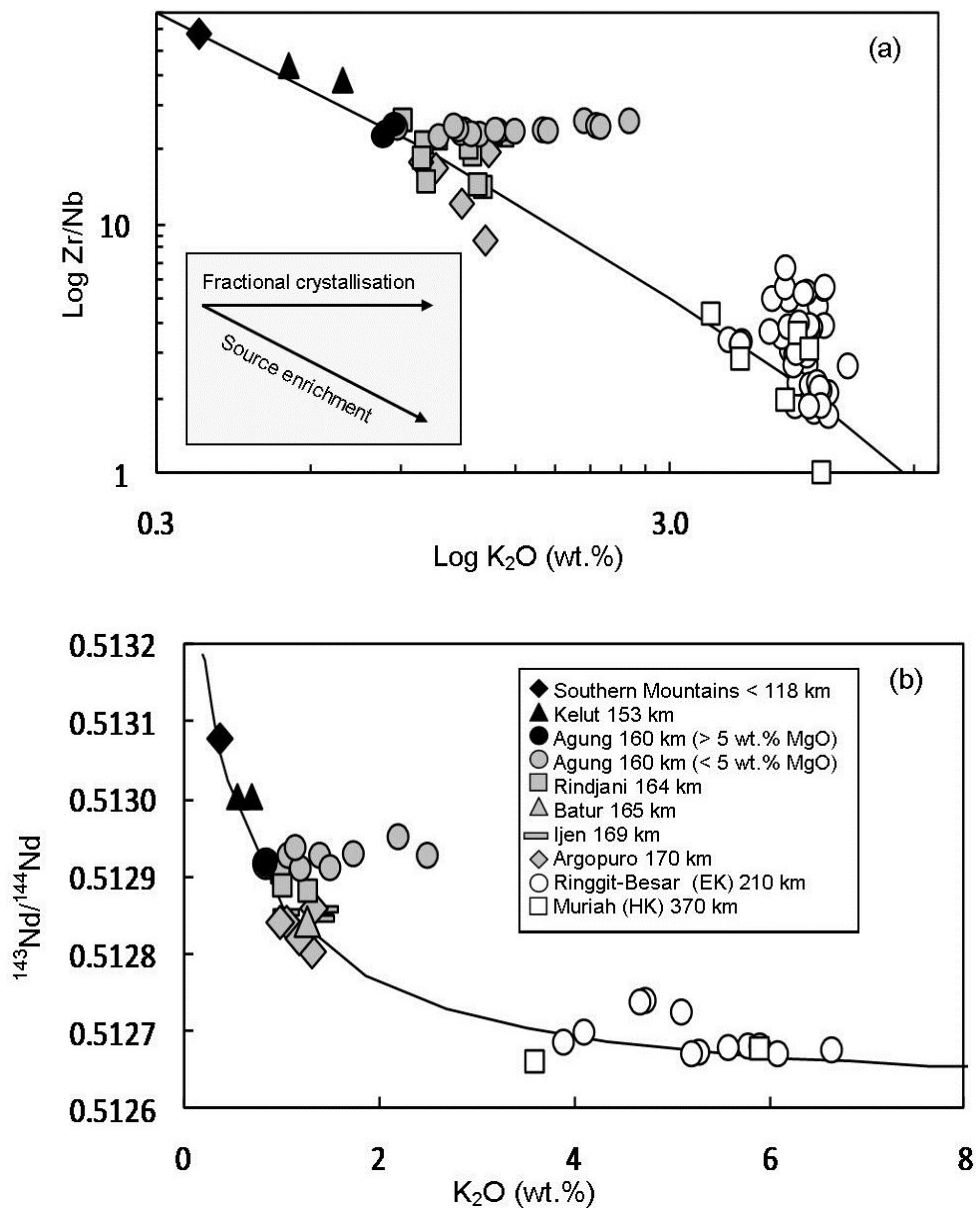
Fig. 4.14. (a) Shows Zr/Nb against K2O (wt.%) for the rocks used in model 4.13. Front-arc volcanoes are shown in black, except for Agung, which is situated towards the front of the rear-arc. For Agung, black symbols have been used to differentiate rocks containing > 5 wt.% MgO from those with progressive lower MgO (grey circles) which have been modified through fractional crystallisation. Other Grey symbols show rear-arc volcanoes and white symbols show back-arc volcanoes. **(b)** Show the same rocks for [143]Nd/[144]Nd against K2O (wt.%). Data sources as for 4.13, plus Ijen (Handley *et al.,* 2007) and Argopuro (Edwards, 1990). Lines represent mixing a depleted source (such as MORB) with low K_2O, high Zr/Nb and [143]Nd/[144]Nd and enriched end-member such as a Lamproite with high K_2O (wt.%), low Zr/Nb and low [143]Nd/[144]Nd.

this is Agung, where all of the samples have been included to show the effects of fractional crystallisation. The plot shows that both K_2O and Zr/Nb are systematically elevated in magmas which are progressively further from the Benioff Zone. The most primitive samples at Agung (i.e. the high-Sc samples with MgO > 5 wt.%) plot on the mixing line, while progressive fractional crystallisation enriches samples in K_2O but not Zr/Nb as would be expected from this process.

In figure 4.14b K_2O is plotted against $^{143}Nd/^{144}Nd$. It was shown in Chapter 2 that $^{143}Nd/^{144}Nd$ and $^{176}Hf/^{177}Hf$ are particularly good isotopic indicators of source compositions in uncontaminated magmas, and these results support that observation. Again, the differentiated magmas at Agung show no change in $^{143}Nd/^{144}Nd$ with increasing K_2O which strengthens the case for closed-system differentiation discussed in section 4.4 as crustal contamination would be expected to modify K_2O and $^{143}Nd/^{144}Nd$. Overall, most incompatible trace elements show this type of systematic behavoir in these magmas which suggests that the previous model cannot be restricted to HFSE and HREE.

4.5.4. A mixing-melting model for Agung

It has been established that the most primitive magmas beneath Agung are best represented by melting a front to rear arc type mantle composition which has largely been metasomatised by AOC fluids opposed to sediment. Therefore, it should be possible to model such a process for the rocks > 5 wt.% MgO. The olivine basalt Agu10 was chosen for this purpose. In order to replicate the composition of the pre-subduction mantle, ratios such as Zr/Nb should be broadly similar to Agu10 (i.e. 23.39) and not be as depleted as sources from the front of the arc (> 30). However, most I-MORB compositions are highly heterogeneous in there Zr/Nb ratios and too elevated in Nb and Ta to be suitable for this purpose. Therefore, an enriched-depleted MORB mantle (E-DMM) was used with a Zr/Nb of 24 (Workman and Hart, 2005).

For the fluid composition, element mobility data from (Kogiso *et al.,* 1997) was applied to AOC data from Staudigel *et al* (1996). For elements not included in the dehydration experiments (e.g. Zr and Hf) mobility values were estimated according to the elements which have similar mobility values in fluids (e.g. Nb and Ta). Figure 4.15a shows the result of adding 1.5 wt% of this fluid to the E-DMM. For the final part of the model, a batch melt has been produced for 10 % melting of this hybrid mantle. This is a conservative estimate for

mantle melting beneath arcs (e.g. Pearce and Parkinson, 1993; Plank and Langmuir, 1998); but within the range suggested for intra-continental arcs, where melting may be siginfcantly less than some oceanic equivalents. The distribution coefficients, mineral assemblages and other components used in the modelling are shown in Table 4D. There is little evidence of a garnet residual, therefore the melting behavoir was modelled for a spinel lherzolite composition.

Results of the modelling generally produce a good fit of the data. The HREE concentrations are slighly low, but this could easily be rectified by adjusting the starting composition of the mantle, using different distribution coefficients, or applying other types of melting models such as fractional or dynamic melting. Neverthess, the aim of producing such a model was not necessarily to provide a perfect match of the data, as this can easily be achieved by changing the aforementioned parameters which are highly variable. It is more to show that using experimentally determined fluid mobility data from dehydration experiments of altered basaltic crust it is possible to easily replicate the trace element data for Agung. It is not essential here to envoke a number of different mechanisms associated with different types of sediment melts, sediment fluids, or AOC fluid-sediment mixtures.

4.5.5. The nature of basement and magma sources

In the tectonic reconstruction of Hall and Sevastjanova (2012), they show that Island of Sumbawa is underlain by Australian continental crust, while Bali and Lombok may be situated above a suture zone which continues into south Sulawesi. Should this be accurate, the magmas in the southern part of Sulawesi may have genetic relationship with those from Agung. In figure 4.15b, a number of samples from Lompobetang have been included in the mixing-melting model. This Quaternary volcano is situated on the southwest arm of Sulawesi referred to by Elburg and Foden (1999b) as post-collisional. Lompobetang contain a similar basalt-andesite-dacite rocks association to Agung; however, the lavas tend to be more K_2O and incompatible element enriched. In this case, it is clear that the magmatism from Lompobetang was not triggered by subduction, as no subduction exists beneath the western arm of Sulawesi. The mantle beneath this arm may; however, have been metasomatised by previous subduction events (Hall, 1996, 2002, 2012; Elburg and Foden, 1999b).

Mixing and Melting Models
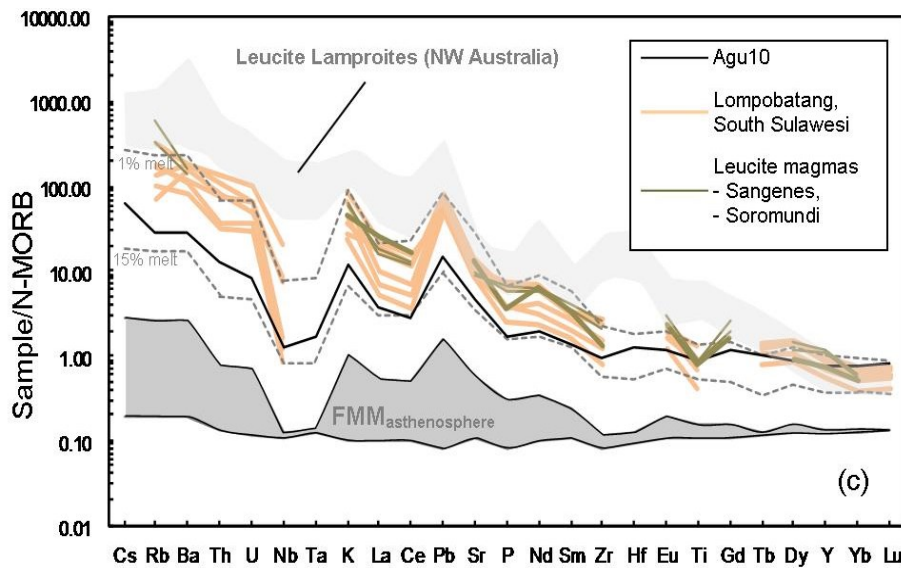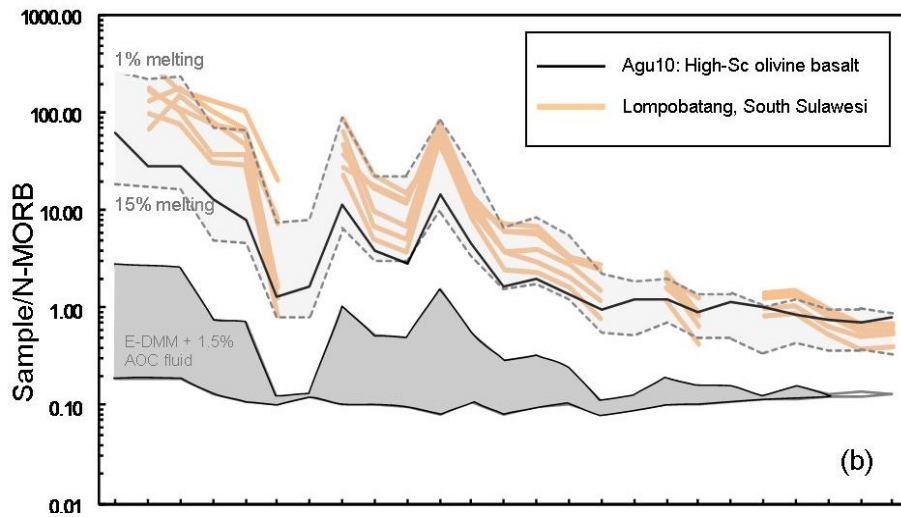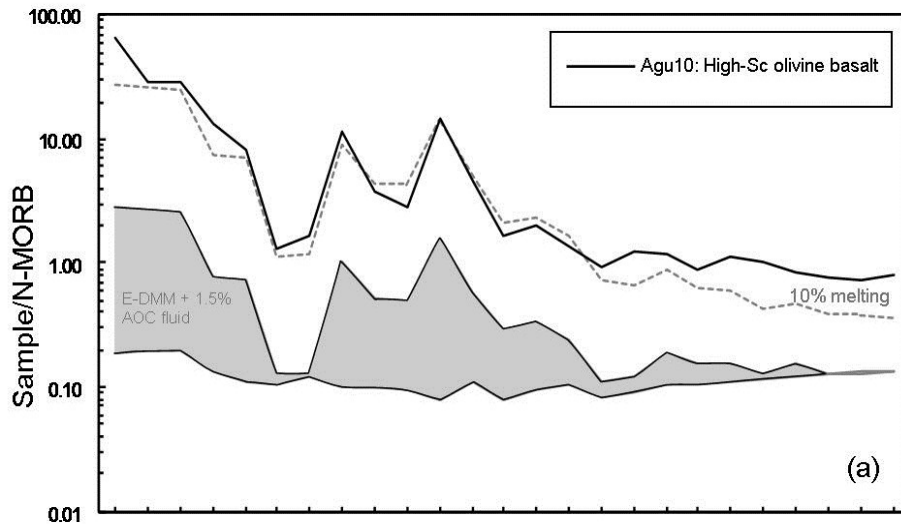
	Model components			kd values			
	E-DMM (Zr/Nb = 24)	AOC	AOC fluid	ol	opx	cpx	sp
Cs	0.001	0.04	1.20	0.0000	0.0000	0.0000	0.0000
Rb	0.11	2.21	92.82	0.0002	0.0006	0.0110	0.0001
Ba	1.22	100.00	999.93	0.0001	0.0010	0.0058	0.0010
Th	0.02	0.20	5.07	0.0001	0.0001	0.0060	0.0010
U	0.01	0.10	1.93	0.0001	0.0001	0.0070	0.0010
Nb	0.25	1.30	3.12	0.0006	0.0049	0.0350	0.0010
Ta	0.02	0.10	0.10	0.0006	0.0049	0.0350	0.0010
K	60.00	1079.26	35975.33	0.0000	0.0001	0.0070	0.0000
La	0.25	3.69	69.44	0.0005	0.0090	0.0800	0.0100
Ce	0.73	6.36	204.68	0.0005	0.0050	0.0800	0.0100
Pb	0.02	0.54	30.60	0.0001	0.0010	0.0720	0.0010
Sr	9.72	102.00	2788.00	0.0002	0.0070	0.0670	0.0001
P	40.70	523.68	6982.40	0.0001	0.0090	0.1780	0.0006
Nd	0.70	6.58	114.05	0.0010	0.0100	0.1900	0.0100
Sm	0.27	2.51	23.43	0.0002	0.0270	0.1800	0.0100
Zr	6.09	63.40	152.16	0.0033	0.0360	0.2040	0.0010
Hf	0.19	1.91	4.58	0.0010	0.0360	0.3440	0.0100
Eu	0.11	0.94	5.95	0.0016	0.1410	0.2960	0.0100
Ti	798.00	6772.09	26185.41	0.0400	0.0240	0.4500	0.1500
Gd	0.40	3.72	12.40	0.0011	0.0065	0.3500	0.0100
Tb	0.08	0.73	0.68	0.0040	0.0600	0.3800	0.0015
Dy	0.54	4.61	11.06	0.0017	0.0600	0.6900	0.0100
Y	3.55	28.20	9.40	0.0010	0.0600	0.7380	0.0010
Yb	0.38	2.87	2.68	0.0015	0.0920	0.7130	0.0100
Lu	0.06	0.44	0.09	0.0015	0.1190	0.7180	0.0100
Mineral Mode				0.50	0.30	0.12	0.08
Melt contribution				0.25	0.25	0.36	0.14

Table 4D. Parameters used in mixing-melting modelling.

Fig. 4.15. Mixing-melting models for: **(a)** an Agung primitive composition; **(b)** primitive magmas from Agung and Lompobatang (south Sulawesi), and; **(c)** primitive magmas from Agung, Lompobatang (south Sulawesi), Sangenes, and Soromundi (Sumbawa). A hypothetical fluid-modified mantle asthenosphere is modelled using a E-DMM composition, after (Workman & Hart, 2005) and adding 1.5 wt.% AOC-derived fluid. The fluid composition is calculated using element mobility data from Kogiso *et al.* (1997) and an initial AOC composition from Staudigel *et al.* (1996), shown in table 4D. Batch melting of the modified mantle was calculated using kd values and mineral-melt contributions for an olivine-orthopyroxene-clinopyroxene-spinel lherzolie, either by calculated or interpolated values used by Pearce and Parkinson (1993); McDade et al. (2003); Salters and Stracke (2004), Janney et al. (2005) and references therin. Partition coefficients used in modelling are shown in table 4D. Data for Lompobetang after Elburg and Foden (1999b), Sangenes and Soromundi after Varne and Foden (1986), and the field for leucite Lamproites from the Fitzroy Basin, NW Australia after Fraser *et al.* (1986) and Jaques *et al.* (1984). See text for discussion.

In their study, Elburg and Foden (1999b) reached a similar conclusion for the southern Sulawesi volcanics to the ones described above for the Banda arc system; namely that pre-collisional subduction related magmas are dominated by a fluid-rich metasomatism (similar to the WLSI), syn-collisional magmas reflect a larger sedimentary signature, intoduced to the mantle as a partial melt (similar to collisional east Sunda-Banda), and post-collisional reflects melting of a subduction-modified source with a contribution from the lithospheric mantle. This latter example refers to the Quaternary lavas of Lompobetang.

Low $^{87}Sr/^{86}Sr$ (0.7038-0.7061) and high $^{143}Nd/^{144}Nd$ (0.5129-0.5127) at Lompobetang are suggested to reflect a young lithosphere, and the lower limits are within isotope values for the Agung lavas. Model 4.15*b* shows that incompatible trace element concentrations in the high-K and shoshonitic rocks at Lompobetang could be produced from a similar source to those at Agung through lower degrees of melting. Considering these magmas are related to lithospheric thinning and decopression, it follows that the degree of melt would be less than for Agung.

In the largely absent evidence for direct melting of continental crust (other that in western Sulawesi, Wetar and Alor, e.g. Elburg and Foden, 1999a; Polve *et al.,* 2001; Elburg *et al.,* 2004, 2005), contributions from enriched parts of the subcontinental lithosphere provide the best evidence for regions in SE Asia which are underlain by old continental material (Foden and Varne, 1980; Varne, 1985; Wheller *et al.,* 1987; Housh and McMahon, 2000; Elburg *et al.,* 2003; Hoernle *et al.,* 2011). Some time before modern tectonic reconstructions, which suggest that a large part of Sunda Arc may be underlain by Gondwanan continental fragments. Varne (1985) identified a notable resemblance between the Sunda arc Leucititic lavas and Leucite-bearing Lamproites and Kimberlites from the Kimberly Craton in NW Australia. In this work, he also suggested that terranes of Gondwanan affinity are located

The Origin of Ultrapotassic Magmatism in the WLSI
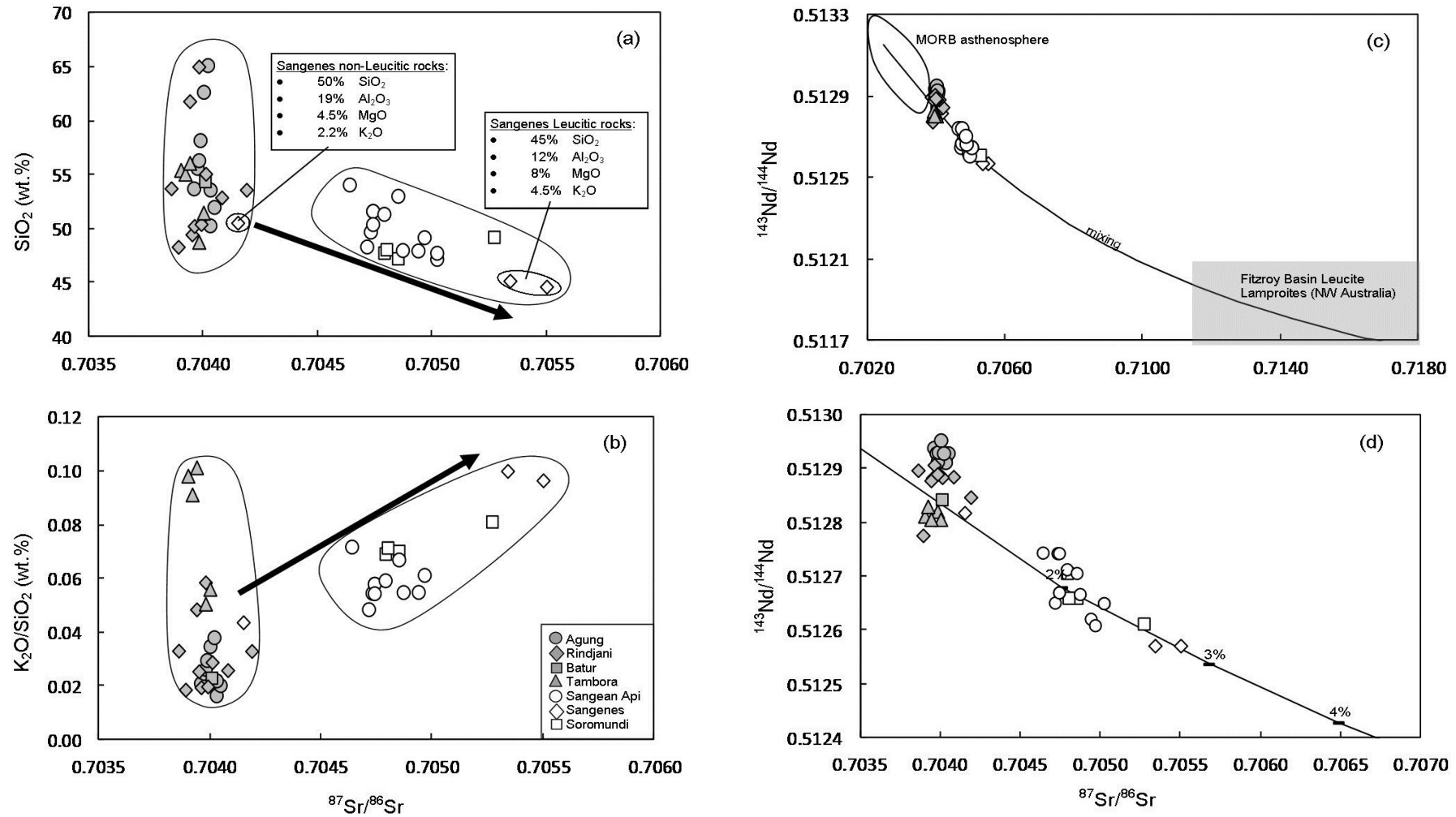
Fig. 4.16. Shows **(a)** $^{87}Sr/^{86}Sr$ against SiO_2; **(b)** $^{87}Sr/^{86}Sr$ against K_2O/SiO_2 and; **(c and d)** calculated mixing lines between MORB and the Fitzroy Basin Leucite Lamproites. Data sources as for figures 4.13 and 4.17.

beneath the east Sunda arc and that the highly alkaline and potassic magmas were a result of melting this old lithospheric mantle. Similar 'enriched' mantle reservoirs have since been identified in Western New Guinea and western Sulawesi (Housh and McMahon, 2000; Elburg *et al.,* 2003;).

There is now a considerable amount of evidence that the lithospheric mantle has a important role in the genesis of ultrapotassic mafic rocks, particularly beneath old continental regions, or where continents may have been fragmented and dispersed (Cebria and Lopez-Ruiz, 1995; McCulloch *et al.,* 1983; Lloyd *et al.,* 1985; Bergman, 1987; Fitton, 1987; McDonough, 1990; Duggen *et al.,* 2005; Mirnejad and Bell, 2006; Pilet *et al.,* 2008; Kamenov *et al.,* 2011;). Furthermore, these rocks are generally conspicuous by thier abasence in most oceanic arcs, far from continents, where the mantle asthenosphere drives variations in rock compositions (Pearce and Parkinson, 1993).

In southwest Anatolia, Turkey, the large spectrum of rocks from ultrapotassic through to calc-alkaline are thought to be a result of the progressive 'asthenospherization' of such enriched lithosphere (Prelevic *et al.,* 2012). It is plausible that this type of asthenosphere-lithosphere interaction is significant beneath continental arcs such as Sunda, where the widest compositional variation including Leucititic-alkaline-shoshonitic-calcalkaline-tholeiitic associations are found worldwide. This process could potentially be driven by any tectonic process which enabled the enriched signature of the mantle lithosphere (where present) to be progressively depleted by mixing with the asthenosphere. In theory, would produce much the same effect as the melt extraction processes described in section *4.5.3*, but could be distinguished by their isotope ratios. The mechanics and nature of this concept will be discussed in greater detail during the final Chapter.

The WLSI volcanoes provide an ideal location with which to examine such enrichment. While the volcanoes on Bali and Rindjani show typically calc-alkaline compositions, volcanoes on Sumbawa contain potassic (shoshonitic) and ultrapotassic (leucititic) magmas. Figure 4.16 *a* shows a plot of $^{87}Sr/^{86}Sr$ against SiO_2 (wt.%) for these volcanoes. It shows that two groups can be established; those which show no change in $^{87}Sr/^{86}Sr$ with SiO_2, such as Agung, Batur, Rindjani and Tambora; and those which show increasing $^{87}Sr/^{86}Sr$ with decreasing SiO_2. Figure 4.16 *b* shows the same distinction, but this time for $^{87}Sr/^{86}Sr$ against K_2O/SiO_2. It is not unsurprising that Agung, Batur, Rindjani and Tambora show no change in $^{87}Sr/^{86}Sr$ with SiO_2 or K_2O/SiO_2 because they are all differentiated through fractional

crystallisation, where the elevations in major elements are not accompanied by elevations in $^{87}Sr/^{86}Sr$. For these volcanoes, the higher-K nature of Tambora relative to the others is inherently a source feature. In contrast, the other volcanoes on Sumbawa all show decreasing SiO_2 and increasing K_2O/SiO_2 with $^{87}Sr/^{86}Sr$. This cannot be accounted for by assimilation of I-MORB-type crust as proposed by Turner *et al.* (2003), because that would act to lower $^{87}Sr/^{86}Sr$ with SiO_2. Rather contamination must involve assimilation or mixing with a source enriched in $^{87}Sr/^{86}Sr$ with low SiO_2 and high K_2O/SiO_2. This provides considerable support for an old lower crust- lithospheric mantle contribution to these magmas, without which it would be difficult to explain such a feature.

The Leucititic magmas from extinct volcanoes Sangenes and Soromundi are plotted on the melting-mixing diagram in figure 4.15*c*, along with some of the Miocene Leucite lamproites from the Fitzroy Region of NW Australia. The lamproites typically contain low SiO_2 (generally between 40 and 50 wt.%), high K_2O/SiO_2 (up to 0.21) and extremely high concentrations of incompatible trace elements (e.g. Jaques *et al.,* 1984). The leucititic magmas from Sumbawa contain similar properties and would require partial melting far too low for an arc magma to explain such incompatible trace element enrichment.

As an alternative, figure 4.16 *(c)* and *(d)* shows that mixing 2-3% of an enriched mantle composition from NW Australian with a typical asthesonsphere composition such as MORB can readily satisfy major and trace element and isotope criteria. This makes the assumption that the lamproites from NW Australia represent melts directly the lithopsheric mantle (which is not an unreasonable assumption to make, e.g. Graham *et al.,* 1999); and therefore, this mixing curve essential shows the quantity of enriched- Australian-derived lithosphere incorporated into an asthenospheric melt beneath some of the volcanoes on Sumbawa. The Sangenes sample which is not Leucititic plots back into the uncontaminated field. This sample shows that not all of the lavas on Sumbawa reflect such enrichment, and therefore have either not been derived from such a source, or have not inherited its signature through assimilation deep in the lower crust- upper lithosphere.

It was noted that earlier in the chapter that this type of enrichment in these rear-arc volcanoes has been used to has been used to argue against spatial variations in the Sunda arc. This is because all of the other nephaline normative, incompatble element-enriched ultrapotassic rocks are situated in back-arc positions (e.g. Stolz *et al.,* 1988; Edwardset *al.,*1991, 1994). To the contrary, this argues against the subducting plate being the cause of such enrichment

through sedimentary melts at higher pressures. If this were the case, enrichments would have to be situated at particular depths to the benioff zone. If however, enriched parts of the lithopshere in the upper plate are only evident in magmas which have undergone decompression, for example, this would be most common at the back of the arc, but could also be localised in other regions. It may be more relevent that the volcanoes which show enriched signatures are now extinct, this implies a link between melting of such an enriched source and a termination in melting. Nevertheless, excluding volcanoes which have been contaminated in the upper plate (which includes Sangenes, Soromundi and Sangean Api), the spatial variations in mantle sources can be applied to Sunda Arc.

4.6. Conclusions

From this Chapter, the following conclusions can be made:

1. Agung, like Batur and Rindjani, shows strong evidence for fractional crystallisation in the arc crust. Two magmatic suites represented by the high-Sc group and the low-Sc group show that independent differentiation of a similar source can explain all of the chemical features beneath Agung.

2. The lack of open-system behavoir in this part of the Sunda arc provides a good insight into the nature of the mantle source compositions, which relates to the volcanoes position on the arc and degree of melting. Source enrichment towards the back arc is reflected in systematic variations trace element concentrations, trace-element ratios and ^{143}Nd/^{144}Nd and ^{176}Hf/^{177}Hf ratios, but only in volcanoes which have not been contaminated in the arc crust.

3. Along-arc isotopic ratios show that dominant subduction component is fluid in sections of the arc not in collision.

4. The enriched alkaline nature of some volcanoes in the WLSI support tectonic and provenance studies for the presence of an Australian-derived lithopshere beneath Sumbawa, but there is no evidence for such a feature beneath Bali and Lombok. Here the magmas either did incorporate this signature (i.e. such as Tambora in Sumbawa), or it

simply is not there beneath these islands. They may instead be above one of ophiolitic suture zones which separate the continental fragments. The age of zircons in east Java and compositional similarity between mafic leucite magmas in the Sunda arc and those in the Fitzroy area of the Kimberly Craton, NW Australia, provide a very persuasive argument for this provenance (e.g. Varne, 1985; Smyth *et al.,* 2007; Hall and Sevastjanova, 2012).

Chapter 5

A regional and tectonic framework for magmatism in the Sunda Arc, SE Asia: A Summary and Conclusions.

5.1. Chapter outline

During each of the preceding chapters, a detailed study was conducted on three volcanoes for which little data has previously been published. The volcanoes were then discussed in the context of their regional setting with the aid of previously published data for other volcanoes. As a result, a general framework for magma petrogenesis along the Sunda Arc has been established in terms of crustal contributions, source character, and the influences of subduction. The objective of this chapter is synthesise and built on the previous chapters by integrating the geochemical data with modern tectonic reconstructions in order to assess the limitations, or otherwise, of using geochemical proxies as a tool for basement reconstruction in SE Asia.

5.2. Magmas with a continental signature

The volcanoes studied in Chapters 2, 3 and 4, all show different chemical characteristics related to their particular tectonic region. However, none of them show evidence for having a truly continental character like other parts of SE Asia such as Sumatra, eastern sections of the Banda Arc or west Sulawesi (Vroon *et al.,* 1993; Gasparon and Varne, 1995; Bergman *et al.,* 1996; Polve *et al.,* 2001).

A continental signature in volcanic rocks is typically considered to be of an evolved composition (i.e. felsic in character) and contain enriched isotope ratios. The most obvious way for the geochemistry of a volcanic rock to provide information about the character of lithologies beneath the arc is for the magma to assimilate some of the material on its way to the surface (e.g. Davidson *et al.,* 1987; Davidson *et al.,* 2005). However, in order to use this process as a reliable informant of basement composition the contributions inherited in the arc crust must be distinguished from those inherited from the subducting plate. Traditionally this is done by plotting trace-element and isotope ratios against an index for differentiation (e.g. SiO_2 or MgO) and if correlations are recorded it is usually attributed to crustal contamination in association with fractional crystallisation (AFC).

West Java is one of the few areas in the Sunda arc, between Sumatra and Flores, which show evidence for having incorporated continental-derived material (Whitford and Jezek, 1982; Gasparon and Varne, 1998). However, it is still unclear whether this reflects the arc crust or

subducted sediment. The reason for this dispute is because west Java is situated within a distal range of the Himalayan deep sea fans depositing terrigneous turbiditic material around the Java trench (Plank and Langmuir, 1998; Handley *et al.,* 2011). Around 1 km of sedimentary material is proposed be in the West Java trench, compared to ~ 5 km in the Sumatran trench (Plank and Langmuir, 1998), although Kopp (2011) suggests that the majority of this is added to the forearc through accretion. This section will attempt to address the ambiguity regarding the continental signature in west Java by evaluating a number of the volcanic rocks and potential contaminants.

5.2.1. Continental contributions in west Java

New major and trace element and isotopic Sr-Nd-Hf-Pb data is presented here for Galunggung, Patuha and Papandayan which can be found in sections *B* and *C* of the appendix. These provide a good contrast of samples by which to examine the effects of contamination because Galunggung contains some primitive olivine basalts, with MgO > 10 wt. %, Ni > 150 ppm and Cr > 500 ppm, while Patuha and Papandayan largely consist of dacites with low MgO, Ni and Cr.

Figure 5.1 shows a map of the volcanoes in west Java. These broadly define two volcanic chains situated toward the front of the arc and behind the front. The focus here will be of the five volcanoes in the southern section of west Java; namely, Patuha, Papandayan, Cikuray, Guntur and Galunggung. A list of depths to the WBZ is presented in Chapter 1 (see table 1A). By selecting these volcanoes it removes the uncertainty associated with long distances between volcanic centres as they are all located within ~ 50 km of each other at similar distances from the trench.

It is evident from figure 5.1 that the volcanoes are situated very close to a proposed suture zone which marks the eastern edge of Sundaland and the accreted arc and ophiolitic lithologies which transect west Java and run up into SE Borneo (e.g. Hamilton, 1979). Four Eocene and Oligocene Formations have been included as these probably represent the sedimetary cover which the volcanoes are built on. The Ciletuh and Ciemas represent the oldest sequences above the basement and largely consist of volcaniclastic turbidite sandstones and breccias (Clements *et al.,* 2012). These Formations are interpreted by
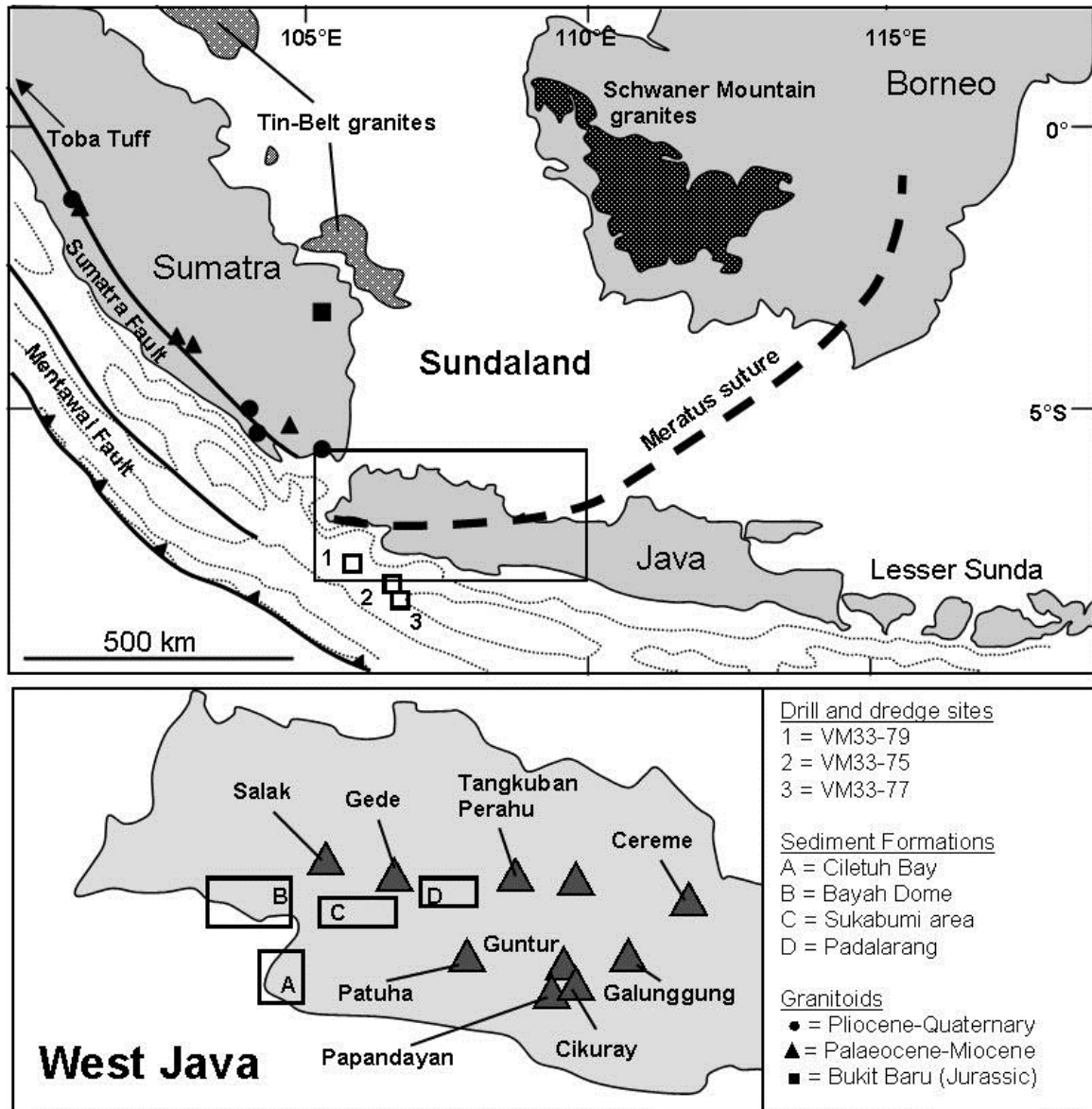
Fig. 5.1. *(Top)* Shows a section of the western Sunda Arc containing west Java and Sumatra. The map includes the location of the Meratus suture (after Hamilton, 1979); dredge sediments from the forearc basin which include terrigneous biogenic (VM33-75), biocalcareous sand (VM33-77) and terrigneous mud (VM33-79), after Gasparon and Varne (1998); and Sumatran granitoids (after Gasparon and Varne, 1995). Fault positions after Hall (2012). *(Bottom)* A location map for west Java showing the volcano positions relative to Eocene and Oligocene quartz-rich and volcanogenic sandstone Formations (after Clements *et al.,* 2012).

Clements *et al.* (2012) to be detritus from Cretaceous and early Palaeogene volcanic arcs. The remaining Formations are proposed to be siliciclastic material derived from Sundaland.

The sediments analysed from the west Java forearc basin (i.e. VM33-75, 77, 79; after Gasparon and Varne, 1998) all contain a strong terrigneous character and are likely to derived from the arc itself, either directly, or from the recycled quartz-rich sandstones and turbidite sequences. Some of the young Quaternary granitoids of wesetrn Sumatra are included in this discussion because they are thought to represent post-Gondwanan Sumatran lithosphere (Gasparon and Varne, 1995), while the Toba Tuff contains considerably more enriched isotope ratios and is probably derived from older parts of the Sundaland basement.

Figure 5.2. shows the five volcanoes from southen west Java for a number of elements and element ratios against SiO_2, which show two distinct trends. The first includes Galunggung, Cikuray, and the Guntur tholeiitic (IAT) magmas (marked in grey), and the second includes Papandayan, Patuha and the Guntur calc-alkaline (CA) magmas (in white). The first group of volcanoes generally contain rocks with lower SiO_2 contents and display minor enrichments of K_2O, Rb, Th and Rb/Sr. In contrast, the second group contain very few magmas with < 55 wt.% SiO_2 and become distinctively more enriched in K_2O, Rb, Th and Rb/Sr.

Papandayan, Patuha and the Guntur calc-alkaline (CA) magmas show similarities to the Sumatran granitoids and the Toba Tuff. There are a number of lines of evidence which suggest that these variations were caused by crustal contamination the arc rather than sediment being subducted at the trench many of which have already been argued by (Gasparon and Varne, 1998). The evidence will be presented during this section.

The plots in figure 5.2 suggest that all of the west Java volcanoes used are derived from the same source as they all project back to the same point at a lower SiO_2 contents. They also suggest that they may have been contaminated by a similar type of material as the felsic Sumatran rocks. To highlight this, figure 5.3 shows the same rocks against the Sumatran granitoids and the Toba Tuff for trace elements normalised to N-MORB (Sun and McDonough, 1989). In addition to a general enrichment in incompatible elements, the most obvious difference between Papandayan, Patuha and Guntur (CA) compared to Guntur (IAT) and Galunggung is the enrichment of Th relative to Ba. This is a characteristic of upper continental crust (see fig 5.3*b* and Rudnick and Fountain, 1995; Rudnick and Gao, 2003). In contrast, the Guntur (IAT) have trace element characteristics closer to that of lower continental crust.

Differentiation Plots for West Java Arc Volcanoes, Sumatran Granitoids and the Toba Tuff
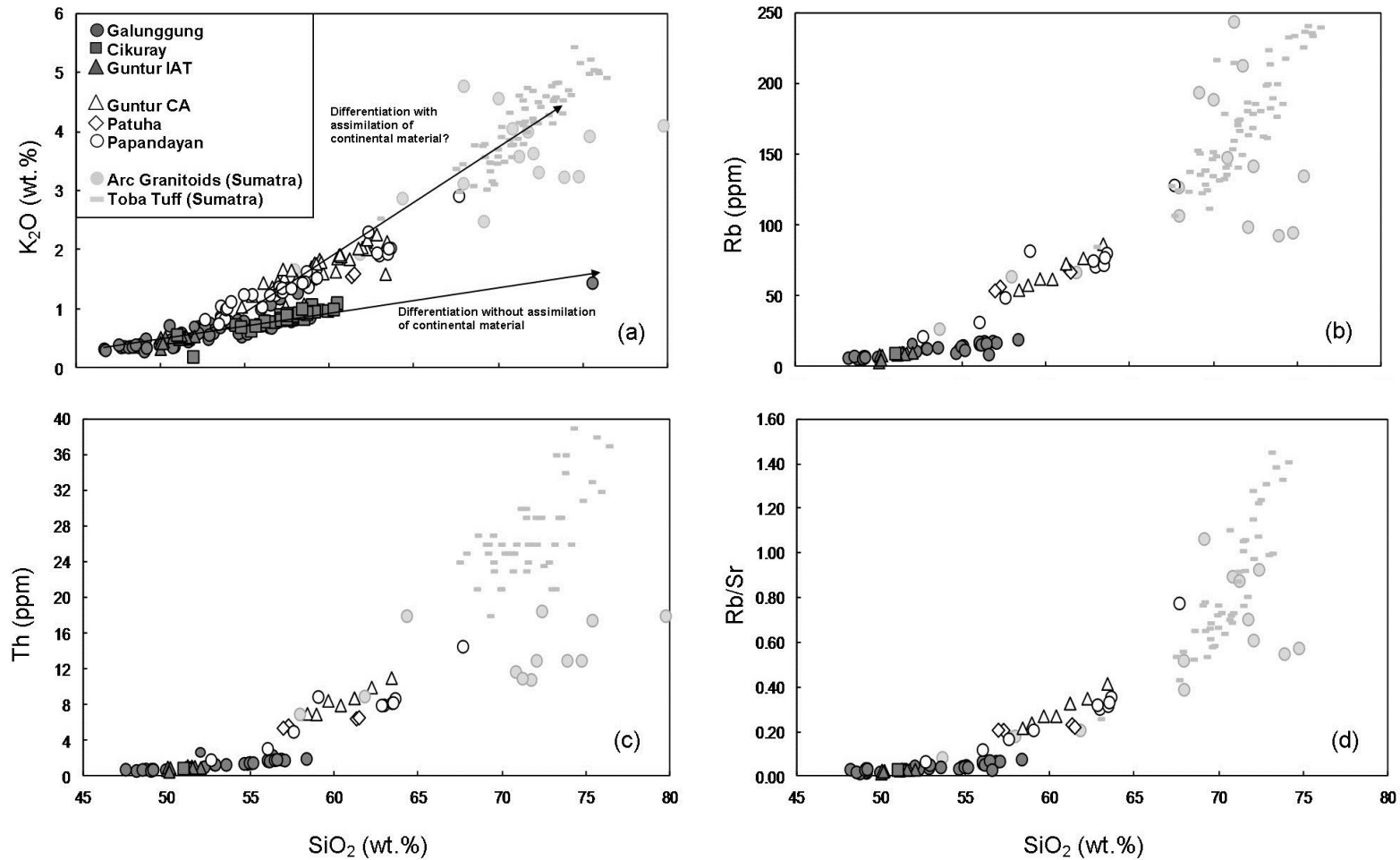
Fig. 5.2. (a-d) K_2O, Rb, Th and Rb/Sr against SiO_2 for west Java volcanoes, Sumatran Granitoids and the youngest Toba Tuff. Data sources after Jones (1989); Edwards (1990); Gerbe *et al.* (1992); Gasparon and Varne (1995); de Hoog *et al.* (2001); Sendjaja *et al.* (2009)**;** and this study.

Normalised Diagrams for West Java Arc Volcanoes, Sumatran felsic rocks and Continental Crust
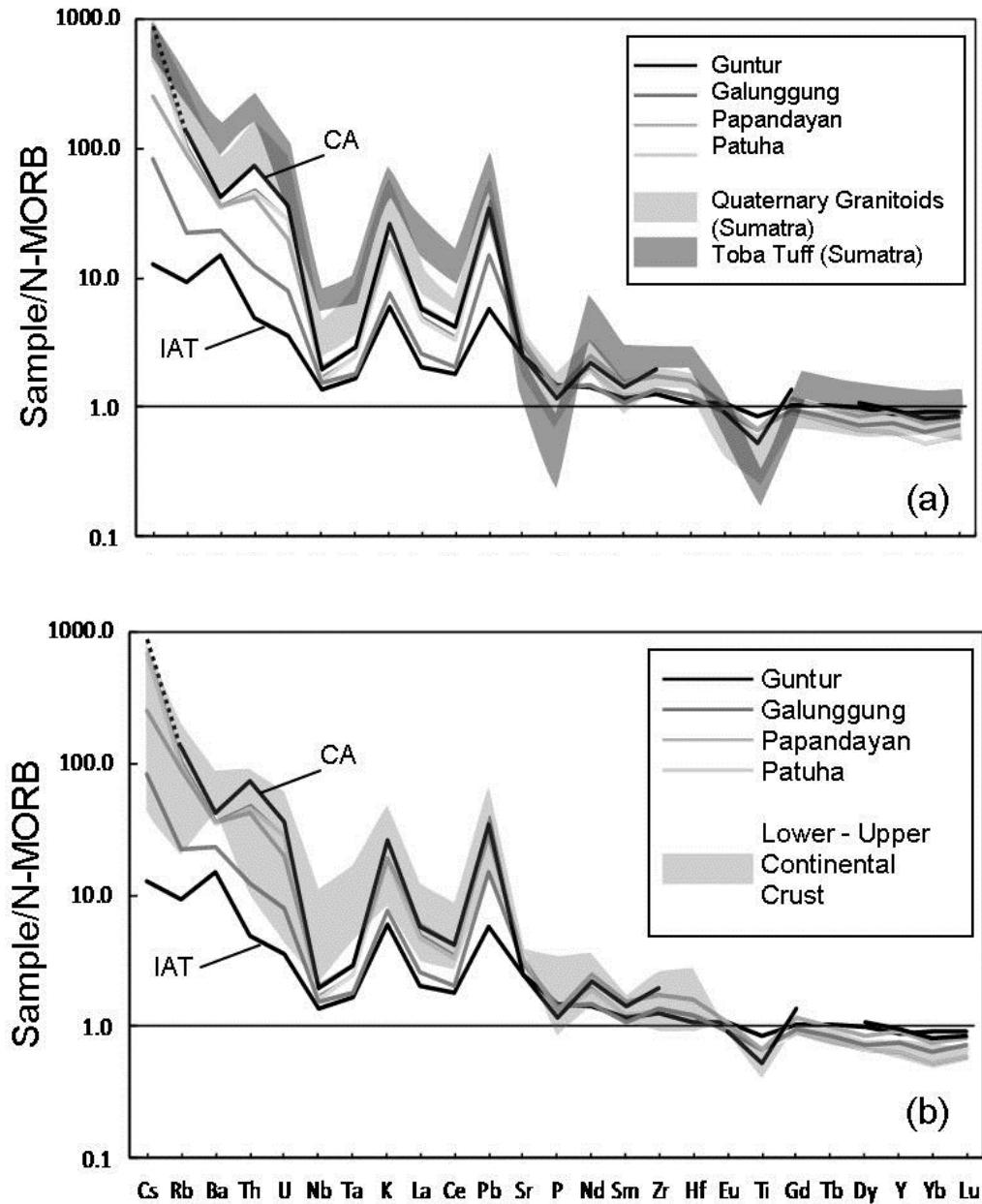
Fig. 5.3. N-MORB normalised diagrams for the contaminated arc magmas and including **(a)** The Quaternary granitoids and Youngest Toba Tuff, **(b)** including values for upper and lower continental crust. Values for continental crust after Rudnick and Fountain (1995) and Rudnick and Gao (2003). Other data sources as for fig. 5.2.

Guntur provides quite a persuasive argument that this continental signature is not derived from terrigneous material from the slab into the mantle wedge (e.g. Plank and Langmuir 1998; Handley, 2006) because it is difficult to explain the contrasting magma compositions in the same volcanic centre by source processes alone. Furthermore Oxygen isotope data also suggest that potentially both groups of magma has been modified by contamination in the arc crust (Macpherson *et al.,* 2008).

Figure 5.4. shows the $^{87}Sr/^{86}Sr$ isotope ratios of the magmas from Guntur (CA), Papandayan and Patuha. The isotope ratios in the magmas from Papandayan and Patuha (0.706 – 0.707) are some of the most radiogenic found in Java (Gertisser and, Keller, 2003; Handley ,2006; Sendjaja *et al.,* 2009) and similar to those of the the Quaternary Sumatran Granitoids (Gasparon and Varne, 1995). Terrigenous sediments from the west Java forearc basin are only slightly higher (~ 0.708) which supports the suggestion that they may have been derived from the arc. Bengal Fan sediments typically of the compositions which might be on the Indian Ocean floor are significantly higher than any of these ratios.

At papandayan a few samples contain inclusions of quartz-rich material (see fig. 5.5). On this basis it is plausible to assume that some of the quartz-rich sands and volcanogenic sedimentary Formations may have been assimilated, or mixed with the magmas at Papandayan, Patuha and Guntur (CA). It would explain the very obvious crustal signature that is associated with these rocks including significant enrichments SiO_2, Th, and the HFSE. The quartz-rich xenocryst in the Papandayan sample appears to contain a number of platy minerals and some Fe-Ti oxides and could plausibly represent a thermally altered sandstone. The presence of tridymite (shown in fig. 5.5*c*) would suggest so. To speculate, if the siliciclastic sedimentary material was derived from Sundaland the crustal contribution in Sumatra may not be to dissimilar. However, for Toba the melt was probably anatectic opposed to assimilating or incorporating the sedimentary material (Jones, 1989; Gasparon and Varne, 1995).

To dermine a provenance, εHf, εNd and $^{87}Sr/^{86}Sr$ are used in combination in figure 5.6. εHf against εNd can be used to identify 'zircon-bearing sediment' because its preference for Hf (Vervoort *et al.,* 1999; Bayon *et al.,* 2009). Therefore most continental sediment will form an array which is distinct from zircon free sediment with lower εHf with respect to εNd. Figure 5.6 *(a)* shows that the west Java volcanic rocks fit an array between MORB and terrigneous sediment as previously noted by Handley *et al.* (2011). However, a mixing curve has been

⁸⁷S/⁸⁶Sr Isotope Data from Potential Sources Associated with Contaminated Volcanic Rocks
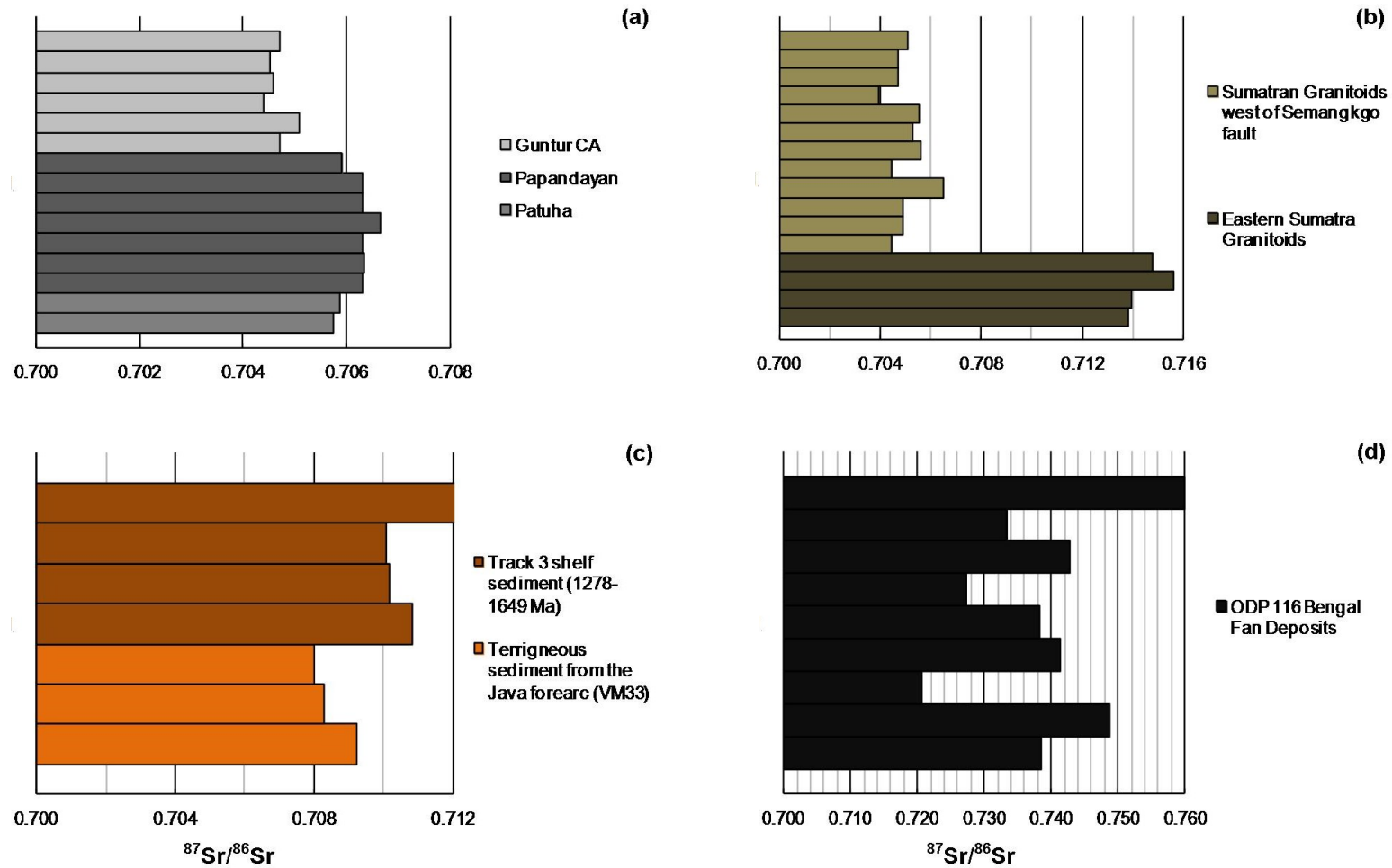
Fig. 5.4. $^{87}Sr/^{86}Sr$ for **(a)** west Java contaminated volcanic rocks, **(b)** Sumatran Granitoids from west and east of the Semangkgo fault, **(c)** track 3 sediment: includes Proterozoic shelf sediment from the Timor region and terrigneous sediment from the West Java forearc basin, **(d)** Bengal Fan deposits from ODP site 116. Data sources after Bouquillon *et al.* (1990); Gasparon and Varne (1995); Vroon *et al.* (1995); Gasparon and Varne (1998).

Photomicrographs of Papandayan rock sample (Pap11)
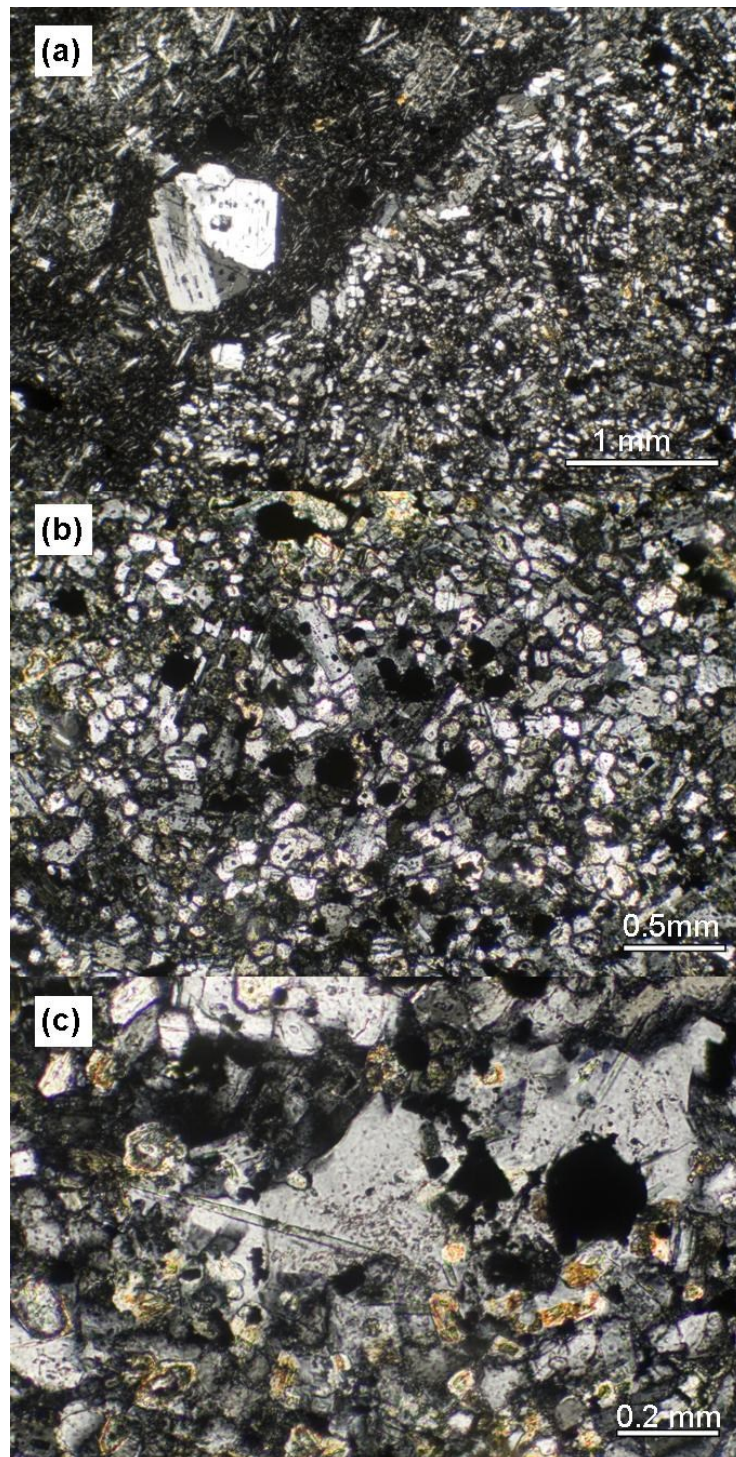
Fig. 5.5. Photomicrographs showing quartz-rich inclusions in magma. **(a)** shows the boundary between the dacite groundmass and the second lithology. Note the plagioclase crystallisation around the rim of the xenocrystic material. **(b)** Shows the texture of the quartz-rich lithology which includes highly rounded grains and platy minerals. **(c)** Shows what appears to be detrital quartz and platy mineral textures.

Quantifying Crustal Contributions

(a)

(b)
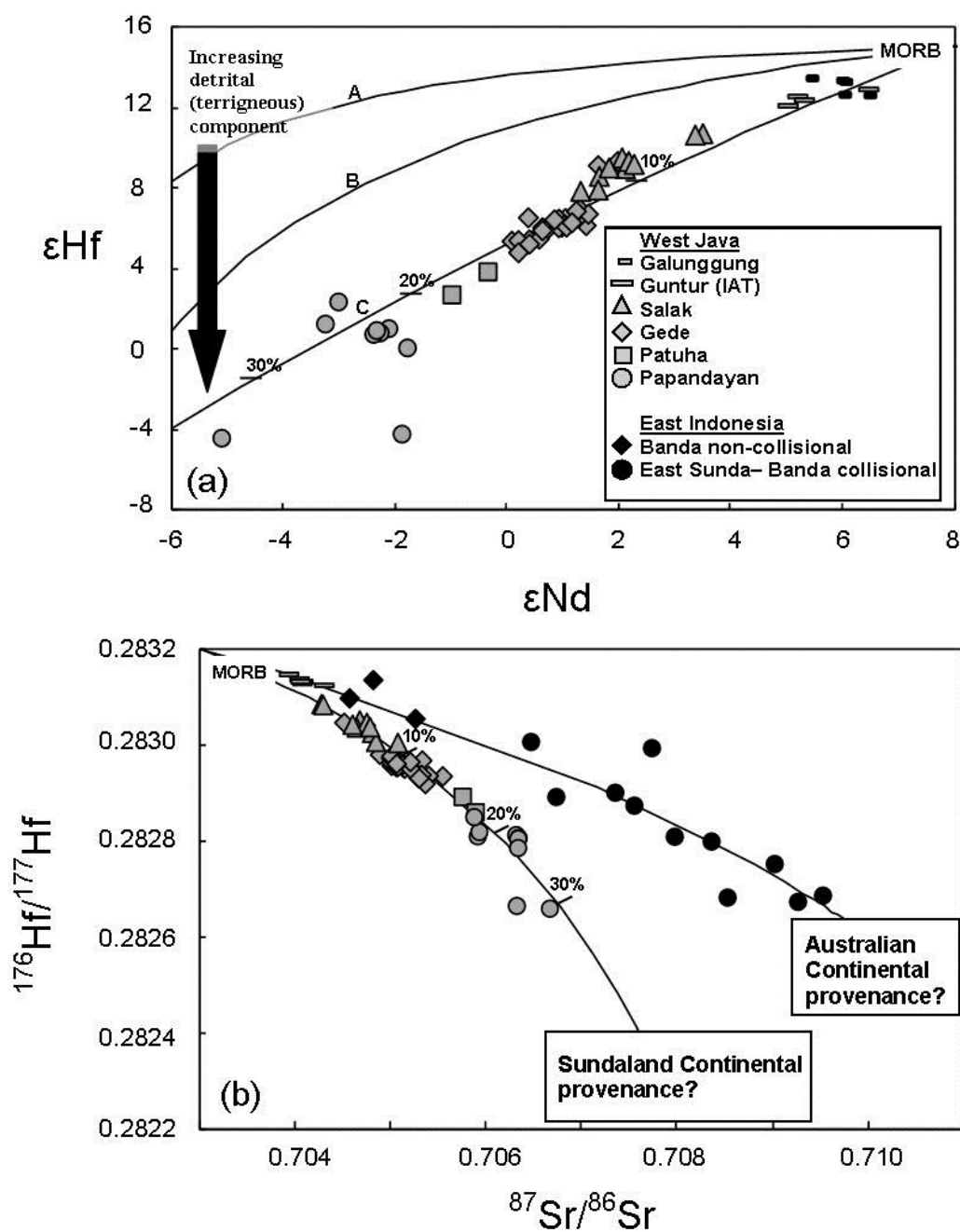
Table 5A. Mixing Parameters

		εHf	εNd	$^{176}Hf/^{177}Hf$	$^{87}Sr/^{86}Sr$	Hf	Nd	Sr
(a)	MORB	14	8.04			2.5	9.7	
A	Turbidite	-19.63	-14.05			5.58	31.3	
B	Pelagic clay	-2.58	-6.87			3.67	55.26	
C	Mn-nodule	1.52	-7.69			2	50	
(b)	MORB			0.283203	0.703	1.92		98.10
	Terrigneous sand			0.282230	0.708	5.5		700
	Track 3 sediment			0.282580	0.710180	16.3		1346

Fig. 5.6. (a) εNd against εHf for the west Java arc rocks **(b)** $^{87}S/^{86}Sr$ against $^{176}Hf/^{177}Hf$ for the west Java rocks and magmas from the Banda arc. Note the difference between the profile of west Java and that of Banda. Volcanoes and data sources used in figures include; West Java: Galunggung (this study), Guntur (Edwards, 1990), Salak (Handley *et al.,* 2008), Gede (Handley *et al.,* 2010); Patuha and Papandayan (this study); Banda Arc: Romang, Damar, Teon, Nila, Serua (black circles), Manuk and Banda Api (black diamonds), data after Nebel *et al.* (2011). Mixing curves created by using the parameters in Table. Tick marks on mixing curves represent percentage of sediment mixed with magma. Data sources for the sediment used in modelling after (White *et al.,* 1986; Vroon *et al.,* 1995; Gasparon and Varne, 1998; Vervoort *et al.,* 1999; Nebel *et al.,* 2011).

applied to this model on the basis that the sediment was assimilated in the arc crust using the parameters in table 5A. The model suggests that it would require between 20 and 30 % of the terrigneous end-member to be mixed with a MORB source to achieve the isotope ratios shown in Papandayan. The final model (fig. 5.6*b*) uses $^{176}Hf/^{177}Hf$ against $^{87}Sr/^{86}Sr$. This clearly distinguishes between the continental signature in west Java and the continental signature in the Banda Arc.

The terrigneous sediments used here include sand from the west Java forearc basin (for the west Java mixing curve) and Australian-derived Proterozoic sand from the Timor Trough (Gasparon and Varne, 1998; Vroon *et al.,* 2001; Vroon, 1992). The mixing curve for west Java volcanoes suggest a similar value of terrigneous sediment is required to be incorporated into a MORB source as in fig. 5.6*a*. These results suggest that the continental signature in some arc magmas from west Java is derived in the shallow (upper crust) by some of the Sundaland derived siliciclastic sands that overlay the basement. More work is required to identify a more specific source.

5.2.2. Crustal contamination in Java

Having identified which volcanoes have been contaminated in the arc crust using the data analysed hitherto, a model for Java can start to be produced. Figure 5.7 shows the $^{87}Sr/^{86}Sr$ isotope ratios from a representative selection of volcanoes along the arc. $^{87}Sr/^{86}Sr$ is particularly useful in this respect because the buffering effects from fluids, derived from the subducting plate, are relatively constant across Java (~ 0.7042, see Chapter 2). Enrichments can thus, be easily identified. Figure 5.7 clearly shows the volcanoes affected by contamination in the arc crust. These include, Papandayan, Patuha and Guntur from west Java, which have assimilated terrigneous material and Sumbing (pyroclastic deposits), Merapi and Merbabu, from central Java which have assimilated calc-silicate lithologies.

Elevations in ^{87}Sr/^{86}Sr in Java volcanoes: Crustal Contamination
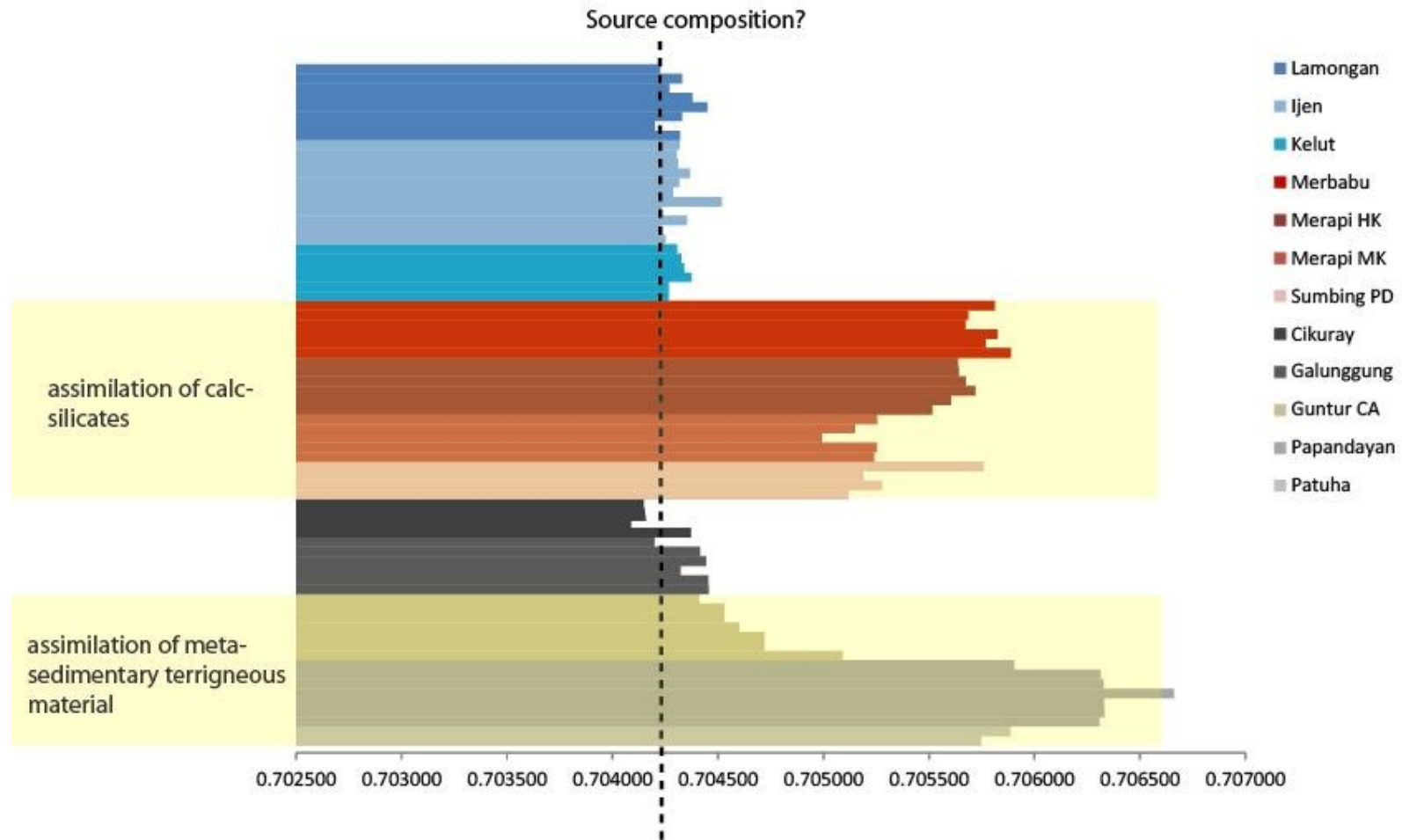
Fig. 5.7. ^{87}Sr/^{86}Sr for selected volcanoes along Java. Papandayan, Patuha, Galunggung and Kelut (LZR) from this study. Other data after Edwards (1990); Carne &Pyle (2001); Gertisser & Keller (2003); and Handley *et al*. (2007), (2011).

5.3. Isotopic changes across the Sunda Arc

Having identified which magmas from west Java, central Java, east Java and WLSI volcanoes have had their chemical signature influenced in the upper crust, and which have not (thereby providing reliable source compositions); it should be possible clarify the major controls on isotope ratios Sunda across the arc.

Radiogenic isotopes such as $^{87}Sr/^{86}Sr$, $^{143}Nd/^{144}Nd$, $^{206}Pb/^{204}Pb$, $^{207}Pb/^{204}Pb$, $^{208}Pb/^{204}Pb$ and $^{176}Hf/^{177}Hf$ are frequently used as particular slab tracers because they are commonly displaced away from mantle values in arc magmas. However, from the detailed studies conducted here, it is clear that much of the isotopic displacement in volcanoes on Java and the WLSI can be attributed to processes that occur in the crust. This is particularly evident for Kelut and Sumbing, which contain two suites of magmas; one which shows evidence for isotopic change with differentiation (i.e. contaminated in the crust), and another where isotopes are not modified during differentiation. When the data is combined for each volcano it can provide a clearer picture of how the subducting slab and upper crust influence magma genesis.

To address along-arc petrogenesis, the chemical data must be discussed in the context of tectonic changes along the arc which may directly, or indirectly, effect the compositon of the volcanic rocks. Figure 5.8*a* shows a recent reconstruction of tectonic units, or terrains, and their possible derivation throughout SE Asia (Hall and Sevastjanova, 2012). As previously mentioned, this interpretation suggests that Australian (i.e. mature) continental crust is widespread beneath the Sunda arc. For this reason, Banda arc geochemical data has also been included in this part of the discussion because there are more obvious signs for the involvement of Austrian-derived continental material in the magma compositions (e.g. Vroon *et al*., 1993, 1995; Nebel *et al*., 2010, 2011). It must be stressed that the inclusion of Banda volcanic data is used here as a reference and not in terms of a discussion about the petrogeneis, for which there are numerous studies (e.g. Vroon *et al*., 1993, 1995; Hoogewerff *et al*., 1996; Elburg *et al*., 2004, 2005, 2008; Nebel *et al*., 2010, 2011).

Each region across the arc has been split into a number of sections which relate to volcano distribution, the volcanoes tectonic setting and the previous chapters (see figure 5.8*b*). A similar approach was used by (Elburg *et al.,* 2004, 2005) to identify the effects of continental collision in the east Sunda and Banda arc. Some of their divisions have been adopted here.

Basement Reconstructions of SE Asia and NW Australia
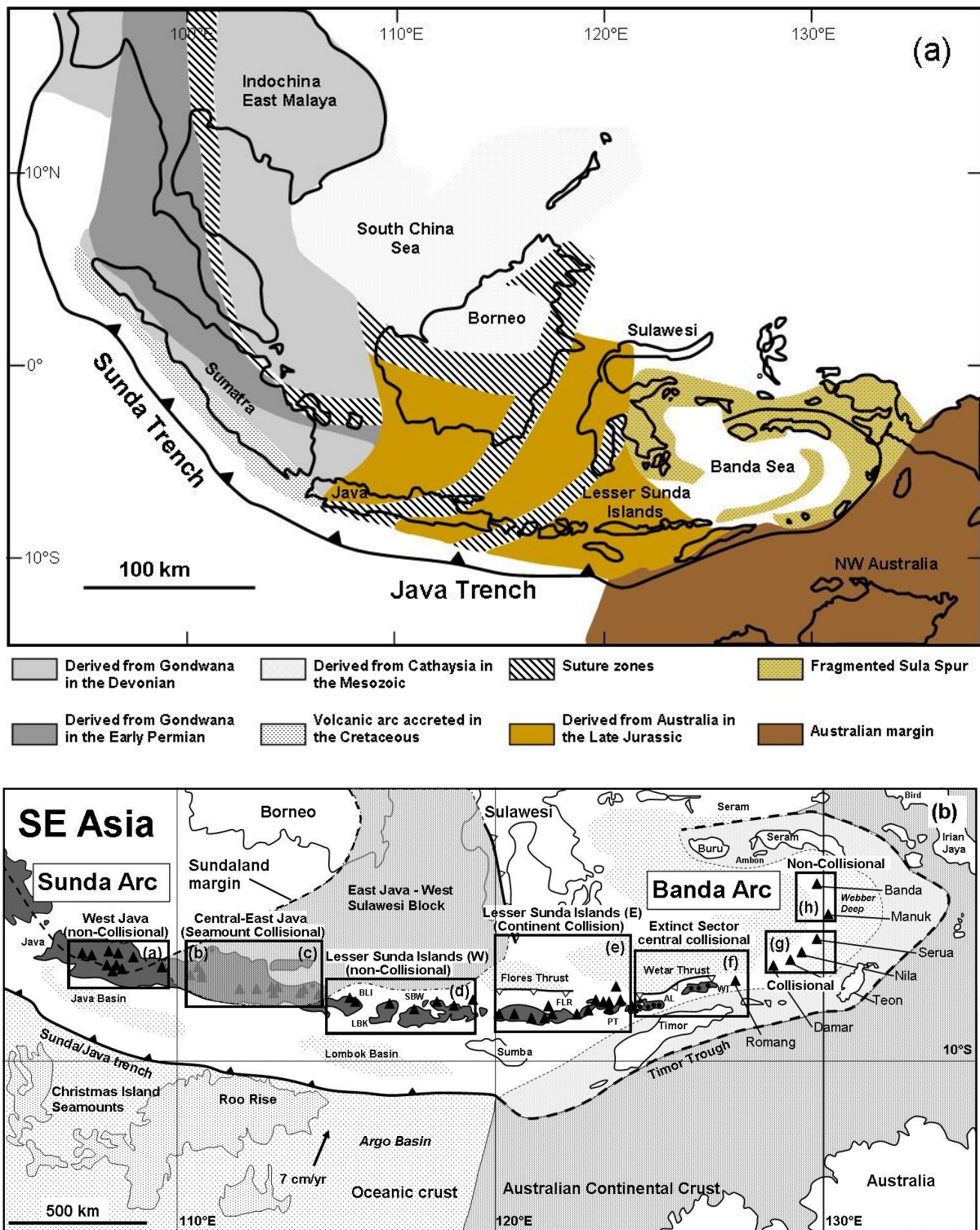
Fig. 5.8. (a) A recent reconstruction of continental fragments and ophiolite sutures in SE Asia, after Hall and Sevastjanova (2012); Metcalfe (2011a,b), and references therein. The Australian continental fragments are interpreted to have rifted from the Australian margin during the Mesozoic and accreted progressively to the Sundaland margin via the closure of numerous oceans. (b) A subdivision of regions based upon the tectonic feature discussed in the text. The region proposed to be underlain by the east Java- west Sulawesi block in this figure is after (Granath et al., 2011), who consider a single block opposed to numerous fragments.

Regional Isotope Variations from West Java to the Banda Arc
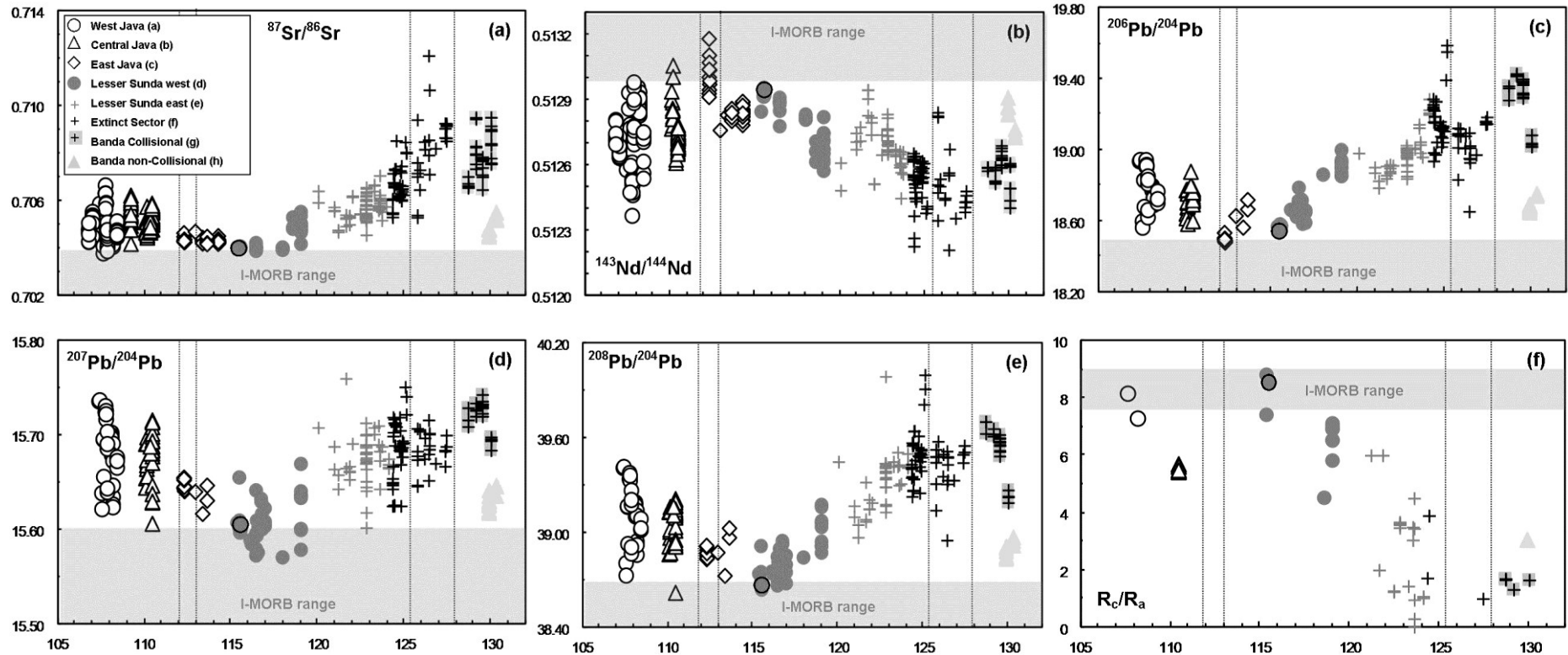
Fig. 5.9. (a-f) Sr-Nd-Pb-He Isotope changes in volcanoes from west Java to the Banda arc. Data sources and volcanoes as follows; West Java: Papandayan (Sendjaja *et al.,* 2009; this study), Patuha (this study), Galunggung (Gerbe *et al.,* 1992; Turner and Foden, 2001; Woodhead *et al.,* 2001; Sendjaja *et al.,* 2009; this study), Tangkuban Perahu (Sendjaja *et al.,* 2009; this study), Gede (Handley, 2006), Salak (Handley, 2006; Handley et al., 2008), Guntur (Edwards, 1990; Sendjaja *et al.,* 2009), Cereme (Edwards, 1990). Central Java: Sumbing (this study), Merapi (Gertisser and Keller, 2003; Turner and Foden, 2001; Woodhead *et al.,* 2001), Slamet (Vukadinovic and Sutawidjaja, 1995), Ungaran (Claproth, 1989), Merbabu (Handley *et al.,* 2011). East Java: Kelut (this study), Ijen (Handley *et al.,* 2007), Lamongan (Carn and Pyle, 2001; Woodhead *et al.,* 2001), Argopuro (Edwards 1990). WLSI: Agung (this study), shown with black circle; Batur (Woodhead *et al.,* 2001; Elburg *et al.,* 2004), Rindjani (Varne and Foden, 1983; Turner and Foden, 2001; Elburg *et al.,* 2004), Tambora (Varne and Foden, 1983; Turner and Foden, 2001), Sangean Api (Varne and Foden, 1986; Turner and Foden, 2001; Turner *et al.,* 2003), Sangenes and Soromundi (Varne and Foden, 1986). Lesser Sunda (east): Flores (Wheller *et al.,* 1987; Edwards 1990; Stolz *et al.,* 1990; Turner and Foden, 2001), Batu Tara (Stolz *et al.,* 1988, 1990), Pantar (Elburg *et al.,* 2004). Central collisional sector: Pantar Strait, Alor, Wetar (Elburg *et al.,* 2004), Romang (Vroon *et al.,* 1993; Elburg *et al.,* 2004, 2005). Banda volcanics (collisional and non-collisional) (Vroon *et al.,* 1993). [3]He/[4]He after Hilton and Craig (1989); Hilton *et al* (1992); Gasparon *et al.* (1994). I-MORB ranges after (Price *et al.,* 1986; Ito *et al.,* 1987; Dosso *et al.,* 1988; Rehkamper and Hofmann, 1997; Chauvel and Blichert-Toft, 2001; Janney et al., 2005). Vertical lines represent gaps in the subducting plate which correspond to central areas of collision (Widiyantoro *et al.,* 2011).

Figure 5.9 (*a-f*) shows the corresponding isotope ratios for each of the regions identified in figure 5.8. The volcanoes used in these diagrams, and the data sources are detailed in the figure caption. For each isotope ratio an I-MORB range is included as an arbitrary indicator of mantle compositions, although, as discussed in chapters 2-4 this is not necessarily applicable (or representative) for all magmas. However, because the alkaline volcanoes of Muriah, Ringgit-Besar and Batu Tara are not included in figure 5.9, it should provide a reasonable estimate for most source compositions. ^{176}Hf/^{177}Hf ratios have been excluded due to the lack of sufficient data and been replaced by a helium isotope study across the arc (after Hilton and Craig, 1989; Gasparon *et al.,* 1994). The lines between 112°E - 113°E and 125°E - 128°E highlight the central sections of collision at the trench. They also show areas where seismic gaps occur on the subducting plate.

The following can be concluded from each area of part of the arc:

(a) West Java:

This is perhaps the most complicated and heterogeneous section of arc for the reasons explained above. While there is strong evidence that isotopic enrichments in magmas from Papandayan, Patuha, Guntur and Salak have been obtained in the arc crust (see section 5.2.1 and Handley *et al*., 2008), not all volcanoes in west Java show such evidence for crustal contamination. Gede for example, has isotope ratios elevated above MORB (see fig. 5.6) which do not show any correlation with SiO_2 or MgO. As a result some authors have postulated that lower ratios of ^{143}Nd/^{144} and ^{176}Hf/^{177}Hf in the arc magmas reflect a terrigneous slab contribution opposed to any influence from the upper crust (see Handley *et al*., 2010 and references therein). Other volcanoes such as Galunggung and Cikuray show less evidence for crustal contamination, or a terrigneous input from the subducting plate, and are more likely to provide reasonable estimates of mantle source composition/s not influenced by sediment (see figure 5.2).

(b) Central Java:

Other than Slamet, all of the volcanoes in central Java are located in the two SSE-NNW chains of volcanoes discussed in Chapter 2. Figure 5.8*b* shows that these volcanoes are within a part of the arc which is being deformed at the trench by the collision of the Roo Rise. Furthermore, figure 5.9 shows that similar to many of the west Java volcanoes these a number of these magmas are displaced away from I-MORB. There is now strong evidence to

suggest that this displacement is the result of assimilation of calc-silicate lithologies in the mid to upper crust at Sumbing, Merapi and Merbabu (see Chapter 2 and Chadwick *et al.*, 2007; Deegan *et al.*, 2010).

The Sumbing lava deposits (and where available Ungaran) show the least evidence for crustal contamination and less enriched isotopic ratios, which are most likely to reflect a magma source in this region. However, at this stage, the evidence suggests that, in agreement with Gasparon and Varne (1998), the enriched isotope ratios in central and west Java are best explained by upper crustal processes.

(c) East Java:

The volcanoes and tectonic environment of east Java are extensively discussed in Chapter 2. An evaluation of Kelut volcano showed that contamination in the upper crust had displaced isotope ratios in the high-Zr group away from the low-Zr group, and that they correlated very well with indices of differentiation. The low-Zr group, together with Ijen and Argopuro provide good information about source processes because of the limited influence of crustal contamination. These volcanoes show very similar $^{87}Sr/^{86}Sr$ ratios (fig. 5.9a) with variable $^{143}Nd/^{144}Nd$, which reflects the addition of fluids into a variably depleted-enriched mantle source (see Chapter 2 for details). The most depleted mantle and elevated fluid signatures correspond with a section of the Sunda arc where the influence of the Roo Rise is most prominent (fig. 5.9*b*). This may suggest some cause and effect.

(d) The WLSI:

This section of the arc represents the easternmost part before the collision of the Australian continent begins to disrupt the trench (and possibly the composition of the magmas). Similar to east Java, many of these volcanoes produce a wider range of magma compositions which are produced by fraction crystallisation. As a result, this part of the arc provides a particularly good area to study source compositions. It is clear from figure 5.9, that isotope ratios are similar to those in east Java (other than $^{207}Pb/^{204}Pb$ and $^{208}Pb/^{204}Pb$ which are particularly low in some of the WLSI volcanoes). Agung and Batur produce the most mantle-like $^{3}He/^{4}He$ values in the Sunda or Banda arc, which supports the tectonic reconstruction in figure 5.8*a* and the suggestion that they are not influenced by continental material (Hilton and Craig, 1989; Hilton *et al.,* 1992; Gasparon *et al.,* 1994).

(e-h) The eastern Sunda and Banda arc

These sections are based on the criteria of Elburg *et al*. (2004, 2005) who subdivided sections of the east Sunda and Banda arc on their 'collisional' locations with respect to Australia. Lesser Sunda east *(e)* corresponds broadly with west collisional arc magmas and includes Flores and the Pantar Strait volcanoes; the extinct sector *(f)* corresponds broadly to the central collisional section and includes Alor, Wetar, Lirang and Romang; the Banda collisional section *(g)* includes Damar, Teon and Nila and corresponds to the east collisional section; and the Banda non-collisional section (*h*) contains Banda, Manuk and Serua, and is the equivalent of the east non-collisional section of Elburg *et al*. (2004).

As previously mentioned, the idea of including this section of the arc is not to discuss the viability of previous models, rather to use as a comparison with the other Sunda arc magmas. It is clear that the eastern Indonesian arc magmas are more enriched in $^{87}Sr/^{86}Sr$, $^{143}Nd/^{144}Nd$, $^{208}Pb/^{204}Pb$, $^{208}Pb/^{204}Pb$, $^{208}Pb/^{204}Pb$, and contain crustal values for $^{3}He/^{4}He$ which suggests an influence of continental material, which most authors believe to be from the Australian continent (e.g. Vroon *et al*. 1993; 1995; Hoogewerff *et al*., 1996; Elburg *et al.,* 2004, 2005). The only magmas on Java which show similar isotopic characteristics to those in eastern Indonesia are those from west Java. However, model 5.6 suggests that the continental material influencing these isotopic compositions is not derived from Australia, and more likely has a Sundaland provenance.

5.4. The nature of alkaline magmatism in SE Asia

From the results in chapters 2-4, and the discussion so far in Chapter 5; it is evident that crustal contamination has a significant effect on the composition of some Sunda arc magmas. This is particularly true for many of the volcanoes located in west and central Java, where contamination is either more obvious than in east Java and the WLSI, or more likely that differentiation is controlled predominently by fractional crystallisation in the latter. As a result, any discussion about source compositions, or processes which occur deeper in crust, beneath volcanoes in west and central Java come with considerable degrees of uncertainty and ambiguity. So, while they are useful for studying 'open' system differentiation at shallow depths and detecting the nature of local sediment they are less useful for identifying the

194

presence of older continental material which, if as suggested, was added to Sundalnd during the Cretaceous, would have a deeper root.

It is not clear why the volcanoes in east Java and the WLSI appear to contain a greater number of magmas which are not contaminated in the shallow arc crust. However, they are more useful for identfying processes and components deeper beneath the arc. Chapters 2 and 4 discuss spatial variations at some length and highlight how, in general, the most depleted magmas (i.e. Kelut LZR) are located at the front of the arc and most enriched 'alkaline', or ultrapotassic assocaitions (Muriah and Ringgit-Besar) are at the back. In between these two extremes are a range of medium- to high-K magmas which broadly become more incompatible element enriched and unradiogenic in $^{143}Nd/^{144}Nd$ and $^{176}Hf/^{177}Hf$ towards the back of the arc. This spectrum in rock compositions is the widest known from any arc worldwide (e.g. Wheller *et al.*, 1997). The question is why? what causes the variation? and is it related to the involvement of Australian-derived continental lithosphere as eluded to in Chapter 4?

In a detailed study of the alkaline Sunda arc magmas, Edwards (1990) concluded that the Muriah (HK Series) and Ringgit-Besar (EK Series) are from similar sources which are not inherited from a subduction zone component. Their similarity with alkaline magmas from Batu Tara in east Indonesia and a number of alkaline magmas from the western arm of Sulawesi support this argument. Edwards (1990) also advocated the presence of a phlogopite-rich metasomatic layer at the base of the lithosphere, in which melting may have been triggered by mixing with MORB-like asthopshere and/or decompression related to extension. A number of other authors have also advcoted the presence of a lithopsheric, or subcontinental, manlte component in alkaline magmas from the Sunda arc (e.g. Varne, 1985; Wheller *et al.*, 1997; Leterrier *et al.*, 1990) and west Sulawesi (e.g. Polve *et al.*, 1997; Elburg *et al.*, 2003). However, most were inconclusive about the exact origin and drivation of such a component.

The combined studies of Smyth *et al.* (2005), (2007); Granath *et al.* (2011) and Hornle *et al.* (2011); Hall (2012); and Hall and Sevastjanova (2012) may provide an answer to why (and how) enriched continental lithosphere is present beneath parts of the Sunda arc and west Sulawesi. They all suggest, through different methods, that parts of SE Asia are underlain by continental material derived from Australian, which was rifted from the NW margin during the Jurassic. Hornle *et al.* (2011) used supporting isotope data to show that this type of

ancient metasomatised continental lithosphere is present in the Christmas Island seamounts south of the Java trench. They suggest that both recycled continental lithopshere and young asthenosphere (similar to OIB and/or MORB) are important in the magmatism which produced the seamounts south of the Java trench.

Applying a similar logic to Hornle *et al*. (2011) and using the theorectical the melting models of Foley (1992) and Pearce (2005) it is possible to propose a model which accounts for the wide compositional range of mafic arc rocks in the Sunda arc. If the mantle beneath the Sunda arc contains enriched fragments of delaminated continental lithosphere which have been present since the rifting of the Australian margin, it would create highly homogenous mantle compositions composed of unmelted lithosphere, residual lithosphere and MORB-like asthenosphere. Assuming that melting is greatest at the front of the arc, most of the melting would involve residual lithosphere or young asthenosphere mantle with a depleted signature. At lower degrees of melting towards the back of the arc, more enriched parts of the lithosphere would be preferentially incorporated (see Chapter 4). Therfore, from front to back, this would provide the spectrum of compositions observed in the Sunda arc magmas which have not be subsequently modified by crustal contamination during differentiation.

There are a number of pieces of evidence which support this idea. Firstly, leucite-bearing alkaline magmas are located in NW Australia, the Sunda arc and west Sulawesi (see fig. 5.10) which suggests that they are not associated with modern subdctuion processes. Furthermore, it provides a chemical link between Australia and the Sunda arc, which was first noticed by Varne (1985). Secondly, these type of alkaline magmas are commonly assciated with continental provinces such as those from Italy and North America (e.g. Mirnejad & Bell, 2006; Nikogosian & van Bergen, 2010) and are not found in regions removed from continental lithosphere.

In order to highlight this observation figure 5.11 shows (*a*) ^{143}Nd/^{144}Nd against ^{87}Sr/^{86}Sr and (*b*) ^{208}Pb/^{204}Pb against ^{206}Pb/^{204}Pb for the alkaline rocks from NW Australia (Fitzroy Trough, Kimberly Block), the Sunda arc and west Sulawesi against a number of oceanic arc magmas in the west Pacific (Mariana, Tonga, Izu-Bonin and Kermadec) and MORB. These figures clearly show that the oceanic arcs are associated with MORB, because they are presumably the result of melting in asthenospheric mantle devoid of continental (lithospheric) material. In contrast, the alkaline magmas from the Sunda arc and Sulawesi become much more enriched isotope ratios and project towards the alkaline rocks (lamproites) from NW Australia.

Locations of Leucite-Bearing Alkaline Magmas
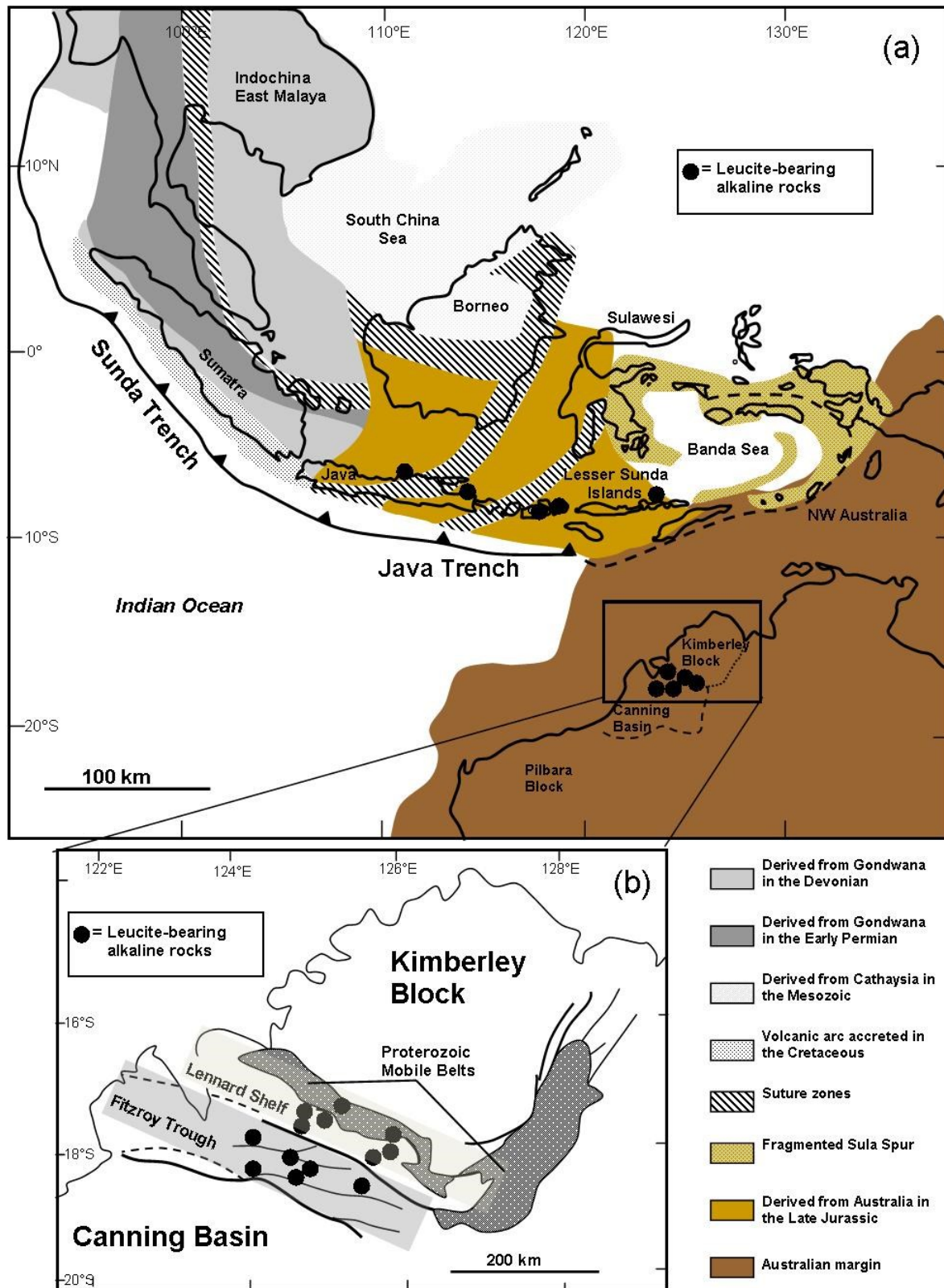
Fig. 5.10. (a) Reconstruction of continental fragments in SE Asia, after (Hall and Sevastjanova, 2012) and **(b)** the Fitzroy Trough, after (Allsopp *et al.,* 1985). Black circles represent the areas in the Sunda arc and NW Australia which have erupted leucititic magma compositions.

197

Alkaline Magmas in the Sunda arc and Sulawesi
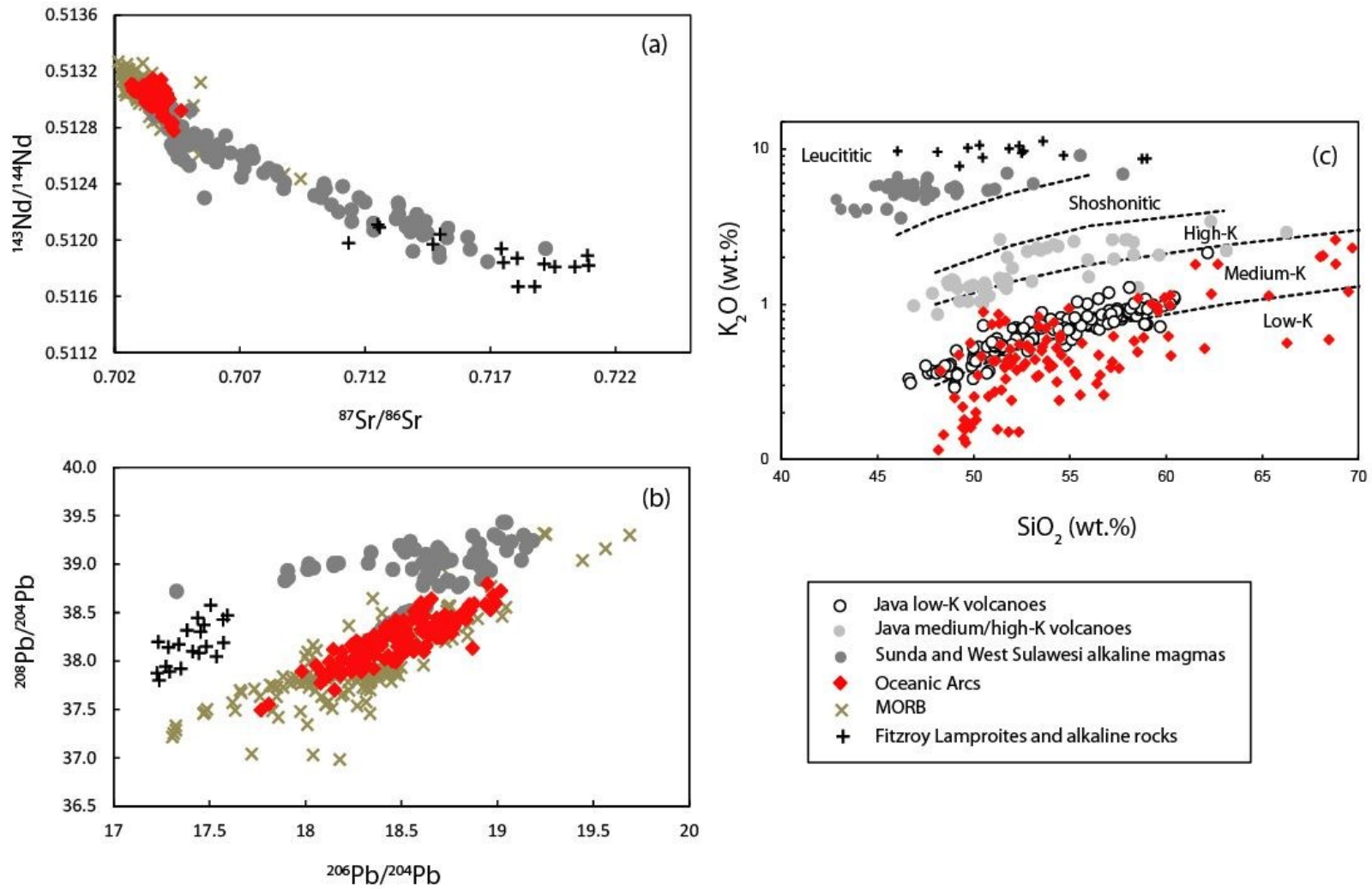
Fig. 5.11. (a) $^{143}Nd/^{144}Nd$ against $^{87}Sr/^{86}Sr$ and **(b)** $^{208}Pb/^{204}Pb$ against $^{206}Pb/^{204}Pb$ for alkaline and ultrapotassic associations in the Sunda arc and west Sulawesi. Data sources for alkaline volcanoes after Stolz *et al*. (1988), (1990); Edwards *et al*. (1991), (1994); van Bergen *et al*. (1992); Bergman *et al*. (1996); Elburg and Foden (1999a); Elburg *et al*. (2002), (2003). Also includes data for oceanic arcs (Tonga, Kermadec, Mariana, New Britain, Kamchatka, South Sandwich, and Izu Bonin): after Pearce *et al*. (1995); Elliot *et al*. (1997); Turner *et al*. (1997); Taylor & Nesbit (1998); Churikova *et al*. (2001); Straub *et al*. (2010); Lamproites from the Fitzroy Trough: after Frazer *et al*. (1986) and Nelson *et al*. (1986); and MORB after Price *et al*. (1986); Ito *et al*. (1987); Dosso *et al*. (1988); Rehkamper & Hofmann (1997); Chauvel & Blichert-Toft (2001); and Janney *et al*. (2005). **(c)** shows the range of potassium contents in Java volcanoes which have not been contaminated in the arc crust (e.g. Low-K: Galunggung, Cikuray and Kelut; medium/high-K: Ijen and Argopuro; Leucititic: Muriah HK and Ringgit-Besar EK) and includes oceanic arc volcanoes used in *(a)* and *(b)* and the leucite lamproites after Jaques *et al*. (1984). Data sources for Java volcanoes after figure 2.18 and 5.2. See text for details.

The latter are assumed to be direct melts from the lithosphere, without the involvement of asthenosphere.

Figure 5.11 (*c*) shows K_2O against SiO_2 for Muriah (HK) and Ringgit Besar (EK) (leucititic compositions), Argopuro and Ijen (high-K compositions), and Galunggung, Cikuray and Kelut (low-medium-K) compositions against the oceanic arcs mentioned above. Again, it shows that K_2O enrichment is not extended beyond medium-K in any of the oceanic arc magmas. This suggests that the elevations in K_2O above low- medium-K compositions may also be related to the involvement of the lithosphere. The most depleted rocks from Java, Kelut, show MORB-like isotope ratios and trace element patterns very similar to these oceanic equivalents (see Chapter 2). This supports the idea that magmas at the front of the arc (at least in east Java) involves the mantle asthenosphere and excludes any enrichment from the lithosphere.

A similar model has been suggested for by Prelevic *et al*. (2012), in a process they term 'asthenospherisation'. In their study, Prelevic *et al*. (2012) suggests that the spectrum of composicompotions found in southwestern Anatolia, Turkey which range from calc-alkaline to ultrapotassic are produced by the progressive interaction between the asthenoshere and the lithosphere. Interestingly, they advocate an important role for the asthenosphere in triggering melting within, the lithosphere. A comparable conclusion was reached by Mirnejad & Bells (2006) for the emplacement of the Leucite Hills Lamproites in Wyoming USA. These leucite-bearing ultrapotassic rocks are also associated with an Archaean province and the ancient metasomatism of the lithosphere as suggested for NW Australia (e.g. Graham *et al.,* 1999).

To conclude, there are many lines of evidence which suggest that parts of the lithosphere, seperated from the NW Australian margin during rifting plays an important role in the chemical budget of the magmas in the Sunda arc. The degree of melting is likely is likely to create the same chemical zonation that is present in many oceanic arcs, but the presence of ancient mantle lithosphere creates a wider range of mama compositions.

5.5. Thesis Conclusions and suggestions for future work

There are a number of important aspects to come out of this work. Firstly, mantle source compositions have a more important role in the geochemistry than previously thought. This can be best observed in volcanoes from east Java and the WLSI where contamination in the arc crust in less extensive than in west Java and central Java. The range in magma compositions from tholeiitic through to leucititic largely reflects the changing source compositions and broadly correlates with the distance away from the trench. This probably reflects the change in degrees of melting in which any enriched contributions the mantle contain are swamped by more refractory material closer to the front of the arc where melting is higher.

In west Java some rocks contain a distinct continental signatutre (e.g. Patuha, Papandayan and Guntur). It is proposed that this signature is derived from the the large quantity of quartz-rich detrital and volcanogeneic material, possibly with a Sundaland provenance. Many volcanoes in central Java also show strong evidence for contamination in the arc crust, but by carbonate rich lithologies. This is highlighted by the strong presence of Ca-rich mineral phases, progressive silica undersaturation and elevations in Sr (ppm) and $^{87}Sr/^{86}Sr$ compared to magmas with less obvious assimilation of carbonate-rich crust.

Kelut and Agung have provided an excellent opportunity to examine and compare source compositions in the Sunda arc. Kelut in particular, provides a new 'depleted' end-member for Java, with MORB like $^{143}Nd/^{144}Nd$ and $^{176}Hf/^{177}Hf$ and low concentrations of incompatible trace elements, similar to Pacific oceanic arcs. A change is mantle source compositions between Lesser Sunda and east Java can be related to a volcanoes position on the trench, but more likely the impact of collision at the Java trench by the Roo Rise. The imact of this collsion is still poorly known as is a particular area for future reseach.

In terms of using geochemistry as a tool for examining unseen basement rocks, the active arc is potentially of less benefit that in regions removed from the arc. Alkaline igneous rocks provide the key to understanding about the nature of enriched basement. However, the involvement of the lithosphere is likely to be a signifcant contribution toward the enrichment of some arc magmas. The subduction contribution, at least across Java, appears to be a homogeneous, dominently fluid, component with $^{87}Sr/^{86}Sr$ of ~ 0.7042. This contribution is most strongly observed in the most depleted rocks (e.g. Kelut) for which ratios such as Ba/La and Zr/Nb are significantly elevated above magmas which are more enriched (by the progessive involvement of the lithosphere).

Additional work should focus on those volcanoes which are poorly understood along the Sunda arc, as there are still significant gaps in the chemical dataset. The Tenggar Caldera looks like a particulalry intersesting volcano to investigate the nature of melt extraction as limited data suggest that it contains Zr/Nb ratios higher than Kelut and therefore a potentially more 'depleted' nature.

Finally, more work still needs to be done on the link between alkaline igneous rocks from the Sunda arc, Sulawesi and NW Australia. The role of the lithosphere clearly has a significant effect on the composition of these magmas, but more clarity is required about the mechanisms involved.

References

Allsopp, H. L., Bristow, J. W., Skinner, E. M., Scott Smith, B. H., & Danchin, R. V. (1985). Rb-Sr Geochronology of some Miocene West Australian Lamproites. *Trans. geol. S. Afr., 88*, 341-345.

Alonzo-Perez, R., Muntener, O., & Ulmer, P. (2009). Igneous garnet and amphibole fractionation in the roots of island arcs: experimental constraints on andesitic liquids. *Contrib Mineral Petrol, 157*, 541-558.

Arculus, R. J., & Johnson, R. W. (1978). Criticism of the generalised models for magmatic evolution of the arc-trench systems. *Earth and Planetary Science Letters, 39*, 118-126.

Audley-Charles, M. G. (2004). Ocean Trench blocked and obliterated by Banda forearc collision with Australian proximal continental slope. *Tectonophysics, 389*, 65-79.

Audley-Charles, M. G., Carter, D. J., Barber, A. J., Norvick, M. S., & Tjokrosapeotro, S. (1979). Reinterpretation of the geology of Seram: implications for the Banda Arcs and northern Australia. *Journal Geological Society London, 136*, 547-568.

Ayers, J. (1998). Trace element modelling of aqueous fluid - peridotite interaction in the mantle wedge of subduction zones. *Contrib Mineral Petrol, 132*, 390-404.

Ayers, J. C., Dittmer, S. K., & Layne, G. D. (1997). Partitioning of elements between peridotite and H2O at 2.0-3.0 Gpa and 900-1100 degrees celcius, and application to models of subduction zone processes. *Earth and Planetary Science Letters, 150*, 381-398.

Baker, J., Peate, D., Waight, T., & Meyzen, C. (2004). Pb isotopic analysis of standards and samples using a 207Pb- 204Pb double spike and thallium to correct for mass bias with a double-focusing MC-ICP-MS. *Chemical Geology, 211*(3-4), 275-303.

Barber, A. J., Crow, M. J., & Milsom, J. S. (2005). Sumatra Geology, Resources and Tectonic Evolution. *Geological Society Memoir., 31*, 290.

Barling, J., & Goldstein, S. L. (1990). Extreme isotopic variations in Heard Island lavas and the nature of mantle reservoirs. *Nature, 348*, 59-62.

Barnes, C. G., Dumond, G., Yoshinobu, A. S., & Prestvik, T. (2004). Assimilation and crystal accumulation in a mid-crustal magma chamber: the Sausfjellet pluton, north-central Norway. *Lithos, 75*, 389-412.

Barnes, C. G., Prestvik, T., Sundvoll, B., & Surratt, D. (2005). Pervasive assimilation of carbonate and silicate rocks in the Hortavaer igneous complex, north-central Norway. *Lithos, 80*, 179-199.

Bayon, G., Burton, K. W., Soulet, G., Vigier, N., Dennielou, B., Etoubleau, E., et al. (2009). Hf and Nd isotopes in marine sediments: Constraints on global silicate weathering. *Earth and Planetary Science Letters, 3-4*(277), 318-326.

Beard, J. S. (1986). Characteristic mineralogy of arc-related cumulate gabbros: Implications for the tectonic setting of gabbro plutons and for andesite genesis. *Geology, 14*, 848-851.

Beard, J. S., Ragland, P. C., & Crawford, M. L. (2005). Reactive bulk assimilation: A model for crust-mantle mixing in silicic magmas. *Geological Society of America, 33*(8), 681-684.

Ben Othman, D., White, W. M., & Patchett, J. (1989). The geochemistry of marine sediments, island arc magma genesis and crust-mantle recycling. *Earth and Planetary Science Letters, 94*, 1-21.

Bergman, S. C. (1987). Lamproites and other potassium-rich igneous rocks: a review of their occurence, mineralogy and geochemistry. *Geological Society, London, Special Publications, 30*, 103-190.

Bergman, S. C., Coffield, D. Q., Talbot, J. P., & Garrad, R. A. (1996). Tertiary tectonic and magmatic evolution of western Sulawesi and the Makassar Strait, Indonesia: evidence for a Miocene continent-continent collision. In R. Hall, & D. Blundell (Eds.), *Tectonic evolution of Southeast Asia*, 391-429. Geological Society Special Publications. Geological Society of London.

Best, M. G. (2003). *Igneous and Metamorphic Petrology* (second edition ed.). Blackwell Science Ltd.

Borisova, A. Y., Belyatsky, B. V., Portnyagin, M. V., & Sushchevskaya, N. A. (2001). Petrogenesis of Olivine-phyric Basalts fro the Aphanasey Nikitin Rise: Evidence for Contamination by Cratonic Lower Continental Crust. *Journal of Petrology, 42*(2), 277-319.

Bouquillon, A., France-Lanord, C., Michard, A., & Tiercelin, J.-J. (1990). Sedimentary and isotopic chemistry of the Bengal Fan sediments: The denudation of the Himalaya. *Proceedings of the Ocean Drilling Program, Scientific Results, 116*, 43-58.

Brenan, J. M., Shaw, H. F., Phinney, D. L., & Ryerson, F. J. (1994). Rutile-aqueous fluid partitioning of Nb, Ta, Hf, Zr, U and Th: implications for high field strength element depletions in island-arc basalts. *Earth and Planetary Science Letters, 128*, 327-339.

Brenan, J. M., Shaw, H. F., Ryerson, F. J., & Phinney, D. L. (1995). Mineral-aqueous fluid partitioning of trace-elements at 900 degrees and 2.0 GPa: constraints on the trace element chemistry of mantle and deep crustal fluids. *Geochim. Cosmochim. Acta, 59*, 3331-3335.

Carn, S. A., & Pyle, D. M. (2001). Petrology and Geochemistry of the Lamongan Volcanic Field, East Java, Indonesia: Primitive Sunda Arc Magmas in an Extensional Tectonic Setting? *Journal of Petrology, 42*(9), 1643-1683.

Cebria, J. M., & Lopez-Ruiz, J. (1995). Alkali basalts and leucitites in an extensional intracontinental plate setting: The late Cenozoic Calatrava Volcanic Province (Central Spain). *Lithos, 35*(1), 27-46.

Chadwick, J. P., Troll, V. R., Ginibre, C., Morgan, D., Gertisser, R., Waight, T. E., et al. (2007). Carbonate Assimilation at Merapi Volcano, Java, Indonesia: Insights from Crystal Isotope Stratigraphy. *Journal of Petrology, 9*, 48.

Chakhmouradian, A. R. (2006). High-field-strength elements in carbonatitic rocks: crystal chemistry and significance for constraining sources of carbonatites. *Chemical Geology, 235*, 138-160.

Chauvel, C., & Blichert-Toft, J. (2001). A hafnium isotope and trace element perspective on melting of the depleted mantle. *Earth and Planetary Science Letters, 190*, 137-151.

Churikova, T., Dorendorf, F., & Worner, G. (2001). Sources and fluids in the mantle wedge below Kamchatka, evidence from across-arc geochemical variation. *Journal of Petrology, 8*, 1567-1593.

Claproth, R. (1989). Magmatic affinities of volcanic rocks from Ungaran, Central Java. *Geol. Indon., 12*(1), 511-562.

Clements, B., Hall, R., Smyth, H. R., & Cottam, M. A. (2009). Thrusting of a volcanic arc: a new structural model for Java. *Petroleum Geoscience, 15*, 159-174.

Clements, B., Sevastjanova, I., Hall, R., Belousova, E. A., Griffin, W. L., & Pearson, N. (2012). Detrital zircon U-Pb age and Hf-isotope perspective on sediment provenance and tectonic models in SE Asia. *The Geological Society of America Special Paper, 487*, 37-61.

Clift, P. D., Vannucchi, P., & Phipps Morgan, J. (2009). Crustal redistribution, crust-mantle recycling and Phanerozoic evolution of the continental crust. *Earth and Planetary Science reviews, 97*, 80-104.

Collerson, K. D., & Palacz, Z. (1999). Accurate and precise isotope ratio measurements of NBS 981 lead by multiple collector inductively coupled plasma mass spectrometry. Why are the ratios different from TIMS measurements? *Ninth Annual V. M. Goldschmidt Conference, Harvard University.*, 21-27. Cambridge, Massachuetts.

Coltorti, M., Bonadiman, C., O'Reilly, S. Y., Griffin, W. L., & Pearson, N. J. (2010). Buoyant ancient continetal mantle embedded in oceanic lithosphere (Sal Island, Cape Verde Archipelago). *Lithos, 120*, 223-233.

Conrad, W. K., Kay, S. M., & Kay, R. W. (1983). Magma mixing in the Aleutian Arc: Evidence from cognate inclusions and composite xenoliths. *Journal of Volcanology and Geothermal Research, 18*, 279-295.

Cottam, M. A., Hall, R., Froster, M. A., & Boudagher-Fadel, M. K. (2011). Basement character and basin formation in Gorontalo Bay, Sulawesi, Indonesia: new observations from the Togian Islands. In R. Hall, M. A. Cottam, & M. E. Wilson, *The SE Asian Gateway: History and Tectonics of the Australia-Asia Collision* (Vol. 355, pp. 177-202). Geological Society, London, Special Publications.

Curray, J. R., Shor Jr, G. G., Raitt, R. W., & Henry, M. (1977). Seismic Refraction and Reflection Studies of Crustal Structure of the Eastern Sunda and Western Banda Arcs. *Journal of Geophysical Research, 82*(17), 2479-2489.

Dallai, L., Freda, C., & Gaeta, M. (2004). Oxygen isotope geochemistry of pyroclastic clinopyroxene monitors carbonate contributions to Roman-type ultrapotassic magmas. *Contrib Mineral Petrology, 148*, 247-263.

Davidson, J. P. (1987). Crustal contamination versus subduction zone enrichment: Examples from the Lesser Antilles and implications for mantle source compositions of island arc volcanic rocks. *Geochim. Cosmochim. Acta, 51*, 2185-2198.

Davidson, J. P., Dungan, M. A., Ferguson, K. M., & Colucci, M. T. (1987). Crust-magma interactions and the evolution of arc magmas: The San Pedro-Pellado Volcanic Complex, southern Chilean Andes. *Geology, 15*, 443-446.

Davidson, J. P., Hora, J. M., Garrison, J. M., & Dungan, M. A. (2005). Crustal forensics in arc magmas. *J. Volcanol. Geotherm. Res, 140*, 157-170.

Davidson, J., & Wilson, M. (2011). Differentiation and Source Processes at Mt Pelee and the Quill; Active Volcanoes in the Lesser Antilles Arc. *Journal of Petrology, 52*(7 & 8), 1493-1531.

Davidson, J., Turner, S., & Plank, T. (in Press). Dy/Dy*: variations arising from mantle sources and petrogenetic processes.

Davidson, J., Turner, S., Handley, H., Macpherson, C., & Dosseto, A. (2007). Amphibole "sponge" in arc crust? *Geology, 35*, 787-790.

Dawson, J. B. (1998). Peralkaline nephalinite-natrocarbonatite relationships at Oldoinyo Lengai, Tanzania. *Journal of Petrology, 39*, 2077-2094.

de Genevraye, P., & Samuel, L. (1972). The geology of the Kendeng Zone (East Java). *Proceedings of Indonesian Petroleum Association 1st Annual Convention*, (pp. 17-30).

de Hoog, J. C., Koetsier, G. W., Bronto, S., Sirwana, T., & van Bergen, M. J. (2001). Sulfur and chlorine degassing from primitive arc magmas: temporal changes during the

1982-1983 eruptions of Galunggung (West Java, Indonesia). *Journal of Volcanology and Geothermal Research, 108*, 55-83.

Debaille, V., Doucelance, R., Weis, D., & Schiano, P. (2006). Multi-stage mixing in subduction zones: Application to Merapi volcano (Java Island, Sunda arc). *Geochimica et Cosmochimica Acta, 70*, 723-741.

Deegan, F. M., Troll, V. R., Freda, C., Misiti, V., Chadwick, J. P., McLeod, C. L., et al. (2010). Magma-Carbonate Interaction Processes and Associated CO2 Release at Merapi Volcano, Indonesia: Insights from Experimental Petrology. *Journal of Petrology, 51*(5), 1027-1051.

Del Moro, A., Fulignati, P., Marianelli, P., & Sbrana, A. (2001). Magma contamination by direct wall rock interaction: constraints from xenoliths from the walls of a carbonate-hosted magma chamber (Vesuvius 1944 eruption). *Journal of Volcanology and Geothermal Research, 112*, 15-24.

Dorendorf, F., Wiechert, U., & Worner, G. (2000). Hydrated sub-arc mantle: a source for the Kluchevskoy volcano, Kamchatka/Russia. *Earth and Plantetary Science Letters, 175*, 69-86.

Dosso, L., Bougault, P., Beuzart, P., Calvez, J.-Y., & Joron, J.-L. (1988). The geochemical structure of the South-East Indian Ridge. *Earth and Planetary Science Letters, 88*, 47-59.

Dowall, D. P., Nowell, G. M., & Pearson, D. G. (2003). Chemical pre-concentration procedures for high-precision analysis of Hf-Nd-Sr isotopes in geological materials by plasma ionisation multi-collector mass spectrometry (PIMMS) techniques. *Plasma Source Mass Spectrometry. Spec. Pub. Royal Society of Chemistry.*, 321-337.

Duggen, S., Hoernle, K., van den Bogaard, P., & Garbe-Schonberg, D. (2005). Post-collisional Transition from Subduction- to Intraplate-type Magmatism in the Westernmost Mediterranean: Evidence for Continental-Edge Delamination of Subcontinental Lithosphere. *Journal of Petrology, 46*(6), 1155-1201.

Dupre, B., & Allegre, C. J. (1983). Nd and Sr isotope variation in Indian Ocean basalts and mixing phenomena. *Nature, 303*, 142-146.

Edwards, C. M. (1990). Petrogenesis of tholeiitic, calc-alkaline and alkaline volcanic rocks, Sunda Arc, Indonesia. *Ph.D Thesis, Royal Holloway, University of London*.

Edwards, C. M., Menzies, M. A., & Thirlwall, M. F. (1991). Evidence from Muriah, Indonesia, for the Interplay of Supra-Subduction Zone Intraplate Processes in the Genesis of Potassic Alkaline Magmas. *Journal of Petrology, 32*(2), 556-590.

Edwards, C. M., Menzies, M. A., Thirlwall, M. F., Morris, J. D., Leeman, W. P., & Harmon, R. S. (1994). The Transition to Potassic Alkaline Volcanism in Island Arcs: The

Ringgit-Besar Complex, East Java, Indonesia. *Journal of Petrology, 35*(6), 1558-1595.

Edwards, C. M., Morris, J. D., & Thirlwall, M. F. (1993). Separating mantle from slab signatures in arc lavas using B/Be and radiogenic isotope systematics. *Nature, 362*, 530-533.

Elburg, M. A., & Foden, J. (1998). Temporal changes in arc magma geochemistry, Northern Sulawesi, Indonesia. *Earth and Planetary Science Letters*, 381-398.

Elburg, M. A., & Foden, J. (1999a). Sources for magmatism in Central Sulawesi: Geochemical and Sr-Nd-Pb constraints. *Earth and Planetary Science Letters, 156*, 67-93.

Elburg, M. A., & Foden, J. (1999b). Geochemical response to varying tectonic settings: an example from Southern Sulawesi (Indonesia). *Geochimica et Cosmochimica Acta, 63*(7/8), 1155-1172.

Elburg, M. A., Foden, J., van Bergen, M., & Zulkarnain, I. (2005). Australia and Indonesia in collision: geochemical sources of magmatism. *Journal of Volcanology and Geothermal Research, 140*, 25-47.

Elburg, M. A., van Bergen, M. J., & Foden, J. D. (2004). Subducted upper and lower continental crust contributes to magmatism in the collision sector of the Sunda-Banda arc, Indonesia. *Geology, 32*, 41-44.

Elburg, M. A., van Bergen, M., Hoogewerff, J., Foden, J., Vroon, P., Zulkarnain, I., & Nasution, A. (2002). Geochemical trends across an arc-continent collision zone: magma sources and slab-wedge transfer processes below the Pantar Strait volcanoes, Indonesia. *Geochimica et Cosmochimica Acta, 66*(15), 2771-2789.

Elburg, M. A., van Leeuwen, T. M., Foden, J., & Muhardjo. (2003). Spatial and temporal isotopic domains of contrasting igneous suites in Western and Northern Sulawesi, Indonesia. *Chemical Geology, 199*, 243-276.

Elburg, M. A., van Leeuwen, T., Foden, J., & Murhardjo. (2002). Origin of Geochemical Variability by Arc-Continent Collision in the Biru Area, Southern Sulawesi (Indonesia). *Journal of Petrology, 43*(4), 581-606.

Elburg, M., & Kamenetsky, V. S. (2008). Limited influence of subducted continental material on mineralogy and elemental geochemistry of primitive magmas from Indonesia-Australia collision zone. *Lithos, 105*, 73-84.

Ellam, R. M., & Harmon, R. S. (1990). Oxygen isotope constraints on the crustal contribution to the subduction-related magmatism of the Aeolian Islands, southern Italy. *J. Volcanol. and Geotherm. Res., 44*, 105-122.

207

Elliot, T., Plank, T., Zindler, A., White, W., & Bourdon, B. (1997). Element transport from slab to volcanic front at the Mariana arc. *Journal of Geophysical Research, 102*, 14991-15019.

England, P., Engdahl, R., & Thatcher, W. (2004). Systematic variation in the depths of slabs beneath arc volcanoes. *Geophys. J. Int., 156*, 377-408.

Ewart, A., & Hawkesworth, C. J. (1987). The Pleistocene-Recent Tonga-Kermadec arc lavas: Interpretation of new isotopic and rare earth data in terms of a depleted mantle source model. *Journal of Petrology, 28*, 495-530.

Falloon, T. J., Berry, R. F., Robinson, P., & Stolz, A. J. (2006). Whole-rock geochemistry of the Hili Manu peridotite, East Timor: implications for the origin of Timor ophiolites. *Australian Journal of Earth Sciences, 53*, 637-649.

Fitton, G. J., Saunders, A. D., Kempton, P. D., & Hardarson, B. S. (2003). Does depleted mantle form an intrinsic part of the Iceland plume? *Geochemistry. Geophysics. Geosystems., 4*(3), 1525-2027.

Fitton, J. G. (1987). The Cameroon line, West Africa: a comparison between oceanic and continental alkaline volcanism. *Geological Society, London, Special Publications., 30*, 272-291.

Flood, T. P., Schuraytz, B. C., & Vogel, T. A. (1989). Magma Mixing due to Disruption of a Layered Magma Body. *Journal of Volcanology and Geothermal Research*, 36.

Foden, J. D. (1983). The petrology of calcalkaline lavas of Rindjani volcano, East Sunda Arc: a model for island arc petrogenesis. *Journal of Petrology, 24*, 98-130.

Foden, J. D. (1986). The Petrology of Tambora Volcano, Indonesia: a model for the 1815 eruption. *Journal of Volcanology and Geothermal Research., 27*, 1-41.

Foden, J. D., & Varne, R. (1980). The petrology and tectonic setting of the Quaternary-Recent volcanic centres of Lombok and Sumbawa. *Chemical Geology, 30*, 201-226.

Foley, S. (1992). Vein-plus-wall-rock melting mechanisms in the lithosphere and the origin of potassic magmas. *Lithos, 28*, 435-453.

Foley, S. F., Venturelli, D. H., Green, D. H., & Toscani, L. (1987). The ultrapotassic rocks: characteristics, classification, and constraints for petrogenetic models. *Earth-Science Reviews, 24*, 81-134.

Foley, S. F., Venturelli, G., Green, D. H., & Toscani, L. (1987). The ultrapotassic Rocks: Characteristics, Classification, and Constraints for Petrogenetic models. *Earth and Planetary Science Reviews, 24*, 81-134.

Fraser, K. J., Hawkesworth, C. J., Erlank, A. J., Mitchell, R. H., & Scott-Smith, B. H. (1986). Sr, Nd and Pb isotope and minor element geochemistry of lamproites and kimberlites. *Easrth and Planetary Science Letters, 76*, 57-70.

Freda, C., Gaeta, M., Misiti, V., Mollo, S., Dolfi, D., & Scarlato, P. (2008). Magma-carbonate interaction: An experimental study on ultrapotassic rocks from Alban Hills (Central Italy). *Lithos, 101*, 397-415.

Fryer, P., & Smoot, C. N. (1985). Processes of seamount subduction in the Mariana and Izu-Bonin Trenches. *Marine Geology, 64*, 77-90.

Gaeta, M., Di Rocco, T., & Freda, C. (2009). Carbonate Assimilation in Open Magmatic Systems: the Role of Melt-bearing Skarns and Cumulate-forming Processes. *Journal of Petrology, 50*(2), 361-385.

Gasparon, M., & Varne, R. (1995). Sumatran granitoids and their relationship to Southeast Asian terranes. *Tectonophysics, 251*, 277-299.

Gasparon, M., & Varne, R. (1998). Crustal assimilation versus subducted sediment input in west Sunda arc volcanics: an evaluation. *Mineralogy and Petrology, 64*, 89-117.

Gasparon, M., Hilton, D. R., & Varne, R. (1994). Crustal contamination processes traced by helium isotopes: Examples from the Sunda arc, Indonesia. *Earth and Planetary Science Letters, 126*, 15-22.

Gerbe, M.-C., Gourgaud, A., Sigmarsson, O., Harmon, R. S., Joron, J.-L., & Provost, A. (1992). Mineralogical and geochemical evolution of the 1982-1983 Galunggung eruption (Indonesia). *Bull. Volcanol., 54*, 284-298.

Gertisser, R., & Keller, J. (2003). Temporal variations in magma composition at Merapi volcano (Central Java, Indonesia): magmatic cycles during the past 2000 years of explosive activity. *Journal of Volcanology and Geothermal Research, 123*, 1-23.

Gertisser, R., & Keller, J. (2003). Trace Elemenet and Sr, Nd, Pb and O Isotopic Variations in the Medium-K and high-K Volcanic Rocks from Merapi Volcano, Central Java, Indonesia: Evidence for the Involvement of Subducted Sediments in the Sunda Arc Magma Genesis. *Journal of Petrology, 44*, 457-489.

Gilg, H. A., Lima, A., Somma, R., Belkin, H. E., De Vivo, B., & Ayuso, R. A. (2001). Isotope geochemistry and fluid inclusion study of skarns from vesuvius. *Mineralogy and Petrology, 73*, 145-176.

Gill, J. B. (1981). *Orogenic Andesites and Plate Tectonics.* Berlin: Springer.

Goff, F., Love, S. P., Warren, R. G., Counce, D., Obenholzner, J., Siebe, C., et al. (2001). Passive infrared remote sensing evidence for large, intermittent CO2 emmisions at Popocatepetl volcano, Mexico. *Chemical Geology, 177*, 133-156.

Graham, S., Lambert, D. D., Shee, S. R., Smith, C. B., & Reeves, S. (1999). Re-Os isotooic evidence for Archaean lithospheric mantle beneath the Kimberly block, Western Australia. *Geology, 27*(5), 431-434.

Granath, J. W., Christ, J. M., Emmet, P. A., & Dinkelman, M. G. (2011). Pre-Cenozoic sedimentary section and structure as reflected in the JavaSPAN crustal-scale PSDM seismic survey, and its implcations regarding the basement terranes in the East Java Sea. *Geological Society, London, Special Publications, 355*, 53-74.

Gregoire, M., Bell, D. R., & Le Roex, A. P. (2003). Garnet Lherzolites from the Kaapvaal Craton (South Africa): Trace Element Evidence for a Metasomatic History. *Journal of Petrology, 44*(4), 629-657.

Grove, T. L., Elkins-Tanton, L. T., Parman, S. W., Chatterjee, N., Muntener, O., & Gaetani, G. A. (2003). Fractional crystallization and mantle-melting controls on the calc-alkaline differentiation trends. *Contrib. Mineral. Petrol., 145*, 515-533.

Hall, R. (1996). Reconstructing Cenozoic SE Asia. In R. Hall, & D. J. Blundell (Eds.), *Tectonic Evolution of SE Asia*, 153-184. London: Geological Society Special Publication.

Hall, R. (2002). Cenozoic geological and plate tectonic evolution of SE Asia and the SW Pacific: Computer-based reconstructions, model and animations. *Journal of Asian Earth Sciences, 20*(4), 354-398.

Hall, R. (2008). Continental growth at the Indonesian margins of southeast Asia. In J. E. Spencer, & S. R. Titley, *Ores and orogenesis: Circum-Pacific tectonics, geological evolution, and ore deposits*, 22, 245-258. Arizona Geoloical Society Digest.

Hall, R. (2009). The Eurasian SE Asian margin as a modern example of an accretionary orogen. In P. A. Cawood, & A. Kroner (Eds.), *Earth Accretionary Systems in Space and Time*, 351-372. London: Geological Society, Special Publications.

Hall, R. (2011). Australia-SE Asia collision: plate tectonics and crustal flow. In R. Hall, M. A. Cottam, & M. E. Wilson (Eds.), *The SE Asian Gateway: History and Tectonics of the Australi-Asia Collision,* 75-109. London: Geological Society, London, Special Publications.

Hall, R. (2012). Late Jurassic-Cenozoic reconstructions of the Indonesian region and the Indian Ocean. *Tectonophysics*, in press.

Hall, R., & Sevastjanova, I. (2012). Australian Crust in Indonesia. *Australian Journal of Earth Sciences*, 59, 827-844.

Hall, R., & Smyth, H. (2008). Cenozoic arc processes in Indonesia: identification of the key influences on the stratigraphic record in active volcanic arcs. *Geological Society of London, Special Publication, 436*, 27-54.

Hall, R., & Wilson, M. E. (2000). Neogene sutures in eastern Indonesia. *Journal of Asian Earth Sciences*, *18*, 781-808.

Hall, R., Clements, B., & Smyth, H. R. (2009). Sundaland: Basement structure and plate tectonic development. (pp. 1-26). Jakarta: Proceedings Indonesian Petroleum Association, 33rd Annual Convention, IPA09-G-134.

Hall, R., Clements, B., Smyth, H. R., & Cottam, M. A. (2007). A new interpretation of Java's structure. *Proceedings, Indonesian Petroleum Association.*

Hall, R., Cross, L., Clements, B., & Spakman, W. (2009). Neogene subduction beneath Java: slab tearing, arc deformation and arc magmatism, and their causes. In: *Southeast Asian Gateway Evolution Conference (abstract)*. Royal Holloway University of London, United Kingdom.

Hamilton, W. (1979). Tectonics of the Indonesia region. *US Geol. Surv. Prof. Paper, 1078*, 345.

Hammer, J. E., Cashman, K. V., & Voight, B. (2000). Magmatic processes revealed by textural and compositional trends in Merapi dome lavas. *Journal of Volcanology and Geothermal Research, 100*, 165-192.

Handley, H. K. (2006). Geochemical and Sr-Nd-Hf-O isotopic constraints on volcanic petrogenesis at the Sunda Arc, Indonesia. *Ph.D thesis, Durham University.*

Handley, H. K., Davidson, J. P., Macpherson, C. G., & Stimac, J. A. (2008). Untangling differentiation in arc lavas: Constraints from unusual minor and trace element variations at Salak Volcano, Indonesia. *Chemical Geology, 255*, 360-376.

Handley, H. K., Macpherson, C. G., & Davidson, J. P. (2010). Geochemical and Sr-O isotopic constraints on magmatic differentiation at Gede Volcanic Complex (GVC), West Java, Indonesia. *Contributions to Mineralogy and Petrology, 159*(6), 885-908.

Handley, H. K., Macpherson, C. G., Davidson, J. P., Berlo, K., & Lowry, D. (2007). Constraining Fuid and Sediment Contributions to Subduction-Related Magmatism in Indonesia: Ijen Volcanic Complex. *Journal of Petrology, 48*(6), 1155-1183.

Handley, H. K., Turner, S., Macpherson, C. G., Gertisser, R., & Davidson, J. P. (2011). Hf-Nd isotope and trace element constraints on subduction inputs at island arcs: Limitations of Hf anomalies as sediment input indicators. *Earth and Planetary Science Letters, 304*, 212-223.

Hart, S. R. (1984). A large-scale isotopic anomaly in the Southern Hemisphere mantle. *Nature, 309*, 753-757.

Hart, S. R. (1984). The DUPAL anomaly: a large-scale isotopic anomaly in the southern hemisphere. *Nature, 309*, 753-756.

Hartono, U. (1996). Stratigraphic geochemical trends of the Wilis Volcanic Complex, Eastern Sunda Arc: Implication for the magma evolution. *GRDC Bulletin, 19*, 97-133.

Hassler, D. R., & Shimizu, N. (1998). Osmium Isotopic Evidence for Ancient Subcontinental Lithospheric Mantle Beneath the Kerguelen Islands, Southern Indian Ocean. *Science, 280*, 418-420.

Hawkesworth, C. J., Gallagher, K., Hergt, J. M., & McDermott, F. (1993). Mantle and slab contributions in arc magmas. *Annual Review of Earth and Planetary Science, 21*, 175-204.

Hemming, S. R., & McLennan, S. M. (2001). Pb isotope compositions of modern deep sea turbidites. *Earth and Planetary Science Letters, 184*, 489-503.

Hermann, J., Spandler, C., Hack, A., & Korsakova, A. V. (2006). Aqueous fluids and hydrous melts in high-pressure and ultra-high pressure rocks: Implications for element transfer in subduction zones. *Lithos, 92*, 399-417.

Hidayati, S., Basuki, A., Kristianto, & Mulyana, I. (2009). Emergence of Lava Dome from the Crater Lake of Kelut Volcano, East Java. *Jurnal Geologi Indonesia, 4*(4), 229-238.

Hildreth, W., & Moorbath, S. (1988). Crustal contributions to arc magmatism in the Andes of Central Chile. *Contrib. Mineral Petrol, 98*, 455-489.

Hilton, D. R., & Craig, H. (1989). A helium isotope transect along the Indonesian archipelago. *Nature, 342*, 906-908.

Hilton, D. R., Hoogewerff, J. A., van Bergen, M. J., & Hammerschmidt, K. (1992). Mapping magma sources in the east Sunda-Banda arcs, Indonesia: Constraints from helium isotopes. *Geochimica et Cosmochimica, 56*, 851-859.

Hochstaedter, A. G., Gill, J. B., Taylor, B., Ishizuka, O., Yuasa, M., & Morita, S. (2000). Across-arc geochemical trends in the Izu-Bonin arc: Constraints on the source composition and mantle melting. *Jounal of Geophysical Research, 105*(B1), 495-512.

Hochstaedter, A., Gill, J., Peters, R., Broughton, P., Holden, P., & Taylor, B. (2001). Across-arc geochemical trends in the Izu-Bonin arc: Contributions from the subducting slab. *Geochemistry Geophysics Geosystems, 2*, 1525-2027.

Hoernle, K. (1998). Gerochemistry of Jurassic Oceanic Crust beneath Gran Canaria (Canary Islands): Implications for Crustal Recycling and Assimilation. *Journal of Petrology, 39*(5), 859-880.

Hoernle, K., HauffF, Werner, R., Bogaard, P., Gibbons, A. D., Conrad, S., et al. (2011). Origin of Indian Ocean Seamount Province by shallow recycling of continental lithosphere. *Nature Geoscience, 4*, 883-886.

Hoogewerff, J. A., van Bergen, M. J., Vroon, P. Z., Hertogen, J., Wordel, J., Sneyers, A., et al. (1997). U-Series, Sr-Nd-Pb isotope and trace element systematics across an active island arc-continent collision zone: Implications for element transfer at the slab-wedge interface. *Geochimica et Cosmochimica Acta, 61*(5), 1057-1072.

Housh, T. B., & Luhr, J. F. (1991). Plagioclase-melt equilibria in hydrous systems. *American Mineralogist, 76*, 477-492.

Housh, T., & McMahon, T. P. (2000). Ancient isotopic characteristics of Neogene potassic magmatism in Western New Guinea (Irian Jaya, Indonesia). *Lithos, 50*, 217-239.

Hutchison, C. S. (1982). Indonesia. In R. S. Thorpe (Ed.), *Andesites: Orogenic Andesites and Related Rocks* (pp. 207-224). J.Wiley & Sons Ltd.

Hutchison, C. S. (1977). Banda sea volcanic arc: some comments on the Rb, Sr and cordierite contents. *Warta Geologi, 3*(2), 27-35.

Ishikawa, T., & Tera, F. (1999). Two isotopically distinct fluid components involved in the Mariana arc: Evidence from Nb/B ratios and B, Sr, Nd, and Pb isotope systematics. *Geology, 27*(1), 83-86.

Ishikawa, T., & Tera, F. (1999). Two isotopically distinct fluid components involved in the Mariana arc: Evidence from Nb/B ratios and B, Sr, Nd, and Pb isotope systematics. *Geology, 27*, 83-86.

Ito, E., White, W., & Gopel, C. (1987). The O, Sr, Nd, and Pb isotope geochemistry of MORB. *Chemical Geology, 62*, 157-176.

Jakes, P., & Gill, J. B. (1970). Rare earth elements and the island arc tholeiitic series. *Earth and Planetary Science Letters, 9*, 17-28.

Jakes, P., & White, A. J. (1969). Structure of Melanesian arcs and correlation with distribution opf magma types. *Tectonophysics, 8*, 222-236.

Jakes, P., & White, A. J. (1970). K/Rb ratios of rocks from island arcs. *Geochim. Cosmochim. Acta., 34*, 849-856.

Jakes, P., & White, A. R. (1972). Major and trace element abundances in volcanic rocks of orogenic areas. *Geological Society of Ameriaca Bulletin, 83*, 29-40.

Janney, P. E., Le Roex, A. P., & Carlson, R. W. (2005). Hafnium Isotope and Trace Element Constraints on the Nature of Mantle heterogeneity beneath the Central Southwest Indian Ridge (13E to 47E). *Journal of Petrology, 46*(12), 2427-2464.

Jaques, A. L., Lewis, J. D., Smith, C. B., Gregory, G. P., Ferguson, J., Chappel, B. W., et al. (1984). The diamond-bearing ultrapotassic (lamproitic) rocks of the west Kimberley region, Western Australia. In J. Kornprobst (Ed.), *Kimberlites I: Kimberlites and related rocks.* (pp. 222-254). Amsterdam: Elsiver.

Johnson, K. T., & Dick, H. J. (1992). Open system melting and temporal and spatial variation of peridotite and basalt at the Atlantis II fracture zone. *J. Geophys. Res., 97*, 9219-9241.

Jones, S. (1989). *Mechanisms of Large Silicic Magma Chamber Zonation: the Youngest Toba Tuff, Sumatra.* PhD thesis, The Open University.

Kamenov, G. D., Perfit, M. R., Lewis, J. F., Goss, A. R., Arevalo Jr, R., & Shuster, R. D. (2011). Ancient lithospheric source for Quaternary lavas in Hispaniola. *Nature Geoscience, 4*, 554-557.

Kelly, K. A., & Cottrell, E. (2009). Water anf the Oxidation State of Subduction Zone Magmas. *Science, 325*, 605-607.

Kelly, K. A., Plank, T., Ludden, J., & Staudigel, H. (2003). Composition of altered oceanic crust at ODP sites 801 and 1149. *Geochemistry Geophysics Geosystems, 4*(6), 1-21.

Keppler, H. (1996). Constraints from partitioning experiments on the composition of subduction zone fluids. *Nature, 380*, 237-240.

Kogiso, T., Tatsumi, Y., & Nakano, S. (1997). Trace element transport during dehydration processes in the subducted oceanic crust 1. Experiments and implications for the origin of ocean island basalts. *Earth and Planetary Science Letters., 148*, 193-205.

Kopp, H. (2011). The Java convergent margin: structure, seimogenesis and subduction processes. In R. Hall, M. A. Cottam, & M. E. Wilson (Eds.), *The SE Asian Gateway: History and Tectonics of the Australia-Asia Collision* (pp. 111-137). London: Geological Society, Special Publications.

Kopp, H., Flueh, E. R., Wittwer, A., Klaeschen, D., & Scientists, M. (2006). Subduction of Basement Relief off Central Java: Geological Indications for Subduction Erosion. *Earth and Planetary Science Letters, 242*, 130-142.

Kundu, B., & Gahalaut, V. K. (2011). Slab detachment of subducted Indo-Australian plate beneath Sunda arc, Indonesia. *J. Earth Syst. Sci, 120*(2), 192-204.

Kuno, H. (1959). Origin of Cenozoic petrographic provinces of Japan and surrounding areas. *Bull. Volcan., 20*, 37-76.

Langmuir, C. H., Vocke, R. D., Hanson, G. N., & Hart, S. R. (1978). A general mixing equation with applications to Icelandic basalts. *Earth and Planetary Science Letters, 37*, 380-392.

Larocque, J., & Canil, D. (2010). The role of amphibole in the evolution of arc magmas and crust: the case from Jurassic Bonanza arc section, Vancouver Island, Canada. *Contrib Mineral Petrol, 159*, 475-492.

Le Bas, M. J., Le Maitre, R. W., & Streckeisen, A. (1986). A chemical classification of volcanic rocks based on the Total Alkali-Silica diagram. *Journal of Petrology, 27*(1984), 745-750.

Leterrier, J., Yuwono, Y. S., Soeria-Atmadja, R., & Maury, R. C. (1990). Potassic volcanism in central Java and South Sulawesi, Indonesia. *Journal of Southeast Asian Earth Sciences., 4*, 171-187.

Liew, T. C., & McCulloch, M. T. (1985). Genesis of the granitoid batholiths of Peninsular Malaysia and implications for models of crustal evolution: Evidence from a Nd-Sr isotopic zircon study. *Geochimica et Cosmochimica Acta, 49*, 587-600.

Liew, T. C., & Page, R. W. (1985). U-Pb zircon dating of granitoid plutons from the west Coast of Peninsular Malaysia. *Geological Society London, 142*, 515-526.

Lin, P. N., Stern, R. J., Morris, J., & Bloomer, S. H. (1990). Nd- and Sr-iostopic compositions of the lavas from the northern Mariana and southern volcano arcs: implications for the origin of island arc melts. *Contrib Mineral Petrol, 105*, 381-392.

Liu, C.-Z., Snow, J. E., Hellebrand, E., Brugmann, G., von der Handt, A., Buchl, A., et al. (2008). Ancient, highly heterogenous mantle beneath Gakkel ridge, Arctic Ocean. *Nature, 452*, 311-316.

Lloyd, F. E., Arima, M., & Edgar, A. D. (1985). Paritial melting of a phlogopite-clinopyroxenite nodule from south-west Uganda: an experimental study bearing the origin of highly potassic continental rift volcanics. *Contrib Mineral Petrol, 91*, 321-329.

Luhr, J. F., & Haldar, D. (2006). Barren Island Volcano (NE Indian Ocean): Island-arc high-alumina basalts produced by troctolite contamination. *Journal of Volcanology and Geothermal Research, 146*, 177-212.

Macpherson, C. G. (2008). Lithosphere erosion and crustal growth in subduction zones: Insights from initiation of the nascant East Philippine Arc. *Geology, 36*(4), 311-314.

Macpherson, C. G., & Hall, R. (1999). Tectonic controls of the Geochemical Evolution in Arc Magmatism of SE Asia. Bali, Indonesia: Proceedings 4th PACRIM Congress, Australian Institute of mining and Metallurgy.

Macpherson, C. G., & Hall, R. (2002). Timing and controls in the evolving orogen of SE Asia and the western Pacific and some implications for ore generation. In D. J. Blundell, & et al. (Eds.), *The Timing and Location of Major Ore Deposits in an Evolving Orogen* (pp. 49-67). London: Geological Society, Special Publications.

Macpherson, C. G., Chiang, K. K., Hall, R., Nowell, G. M., Castillo, P. R., & Thirlwall, M. F. (2010). Plio-Pleistocene intraplate magmatsim for the Sulu Arc, Semporna Peninsula, Sabah, Borneo: Implications for high-Nb basalt in subduction zones. *Journal of Volcanology and Geothermal Research, 190*, 25-38.

Macpherson, C. G., Dreher, S. T., & Thirlwall, M. F. (2006). Adakites without slab melting: High pressure differentiation of island arc magma, Mindanano, the Philippines. *Earth & Planetary Science Letters, 243*, 581-593.

Macpherson, C. G., Forrde, E. J., Hall, R., & Thirlwall, M. F. (2003). Geochemical evolution of magmatism in an arc-arc collision: the Halmahera and Sangihe arcs, eastern Indonesia. *Geological Society, London, Special Publications, 219*, 207-220.

Macpherson, C. G., Gamble, C. G., & Mattey, D. P. (1998). Oxygen isotope geochemistry of lavas from an oceanic to continental arc transition, Kermadec-Hikurangi margin, SW Pacific. *Earth and Planetary Science Letters, 160*, 609-621.

Macpherson, C. G., Handley, H. K., & Edwards, C. M. (2008). Oxygen isotope fractionation in tholeiitic and calc-alkaline magma, Gunnung Guntur, west Java, Indonesia. Geophysical Research Abstracts.

Mamani, M., Worner, G., & Sempere, T. (2010). Geochemical variations in igneous rocks of the Central Andean orocline (13 degrees S to 18 degrees S): Tracing crustal thickening and magma generation through time and space. *GSA Bulletin, 122*(1/2), 162-182.

Marziano, G. I., Gaillard, F., & Pichavant, M. (2008). Limestone assimilation by basaltic magmas: an experimental re-assessment and application to Italian volcanoes. *Contributions to Mineralogy and Petrology, 155*(6), 719-738.

Masson, D. G., Parson, L. M., Milsom, J., Nichols, G., Sikumbang, N., Dwiyanto, B., et al. (1990). Subduction of seamounts at the Java Trench: a view with long-range sidescan sonar. *Tectonophysics, 185*, 51-65.

McCourt, W. J., Crow, M. J., Cobbing, E. J., & Amin, T. C. (1996). Mesozoic and Cenozoic plutonic evolution of SE Asia: Evidence from Sumatra, Indonesia. In R. Hall, & D. J. Blundell (Eds.), *Tectonic Evolution of SE Asia.* (pp. 161-178). London: Geological Society Special Publication.

McCulloch, M. T., & Gamble, J. A. (1991). Geochemical and Geodynamical constraints on subduction zone magmatism. *Earth and Planetary Science Letters, 102*, 358-374.

McCulloch, M. T., Jaques, A. L., Nelson, D. R., & Lewis, J. D. (1983). Nd and Sr isotopes in Kimberlites and lamproites from Western Australia: an enriched mantle origin. *Nature, 302*, 400-403.

McDade, P., Blundy, J. D., & Wood, B. J. (2003). Trace element partitioning between mantle peridotite and hydrous MgO-rich melt. *American Mineralogist, 88*, 1825-1831.

McDonough, W. F. (1990). Constraints on the Composition of the continental lithospheric mantle. *Earth and Planetary Science Letters, 101*, 1-18.

McDonough, W. F. (1990). Contraints on the composition of the continetal lithospheric mantle. *Earth and Planetary Science Letters, 101*, 1-18.

Menzies, M., & Murthy, V. R. (1980). Nd and Sr isotope geochmeistry of hydrous mantle nodules and their host alkali basalts: implications for local heterogeneities in metasomatically veined mantle. *Earth and Planetary Science Letters, 46*, 323-332.

Metcalfe, I. (1996). Pre-Cretaceous evolution of SE Asian terranes. In R. Hall, & D. J. Blundell, *Tectonic Evolution of SE Asia* (pp. 97-122). Geological Society London Special Publication.

Metcalfe, I. (2011a). Tectonic framework and Phanerozoic evolution of Sundaland. *Gondwana Research, 19*, 3-21.

Metcalfe, I. (2011b). Palaeozoic-Mesozoic History of SEAsia. In R. Hall, M. A. Cottam, & M. E. Wilson, *The SE Asian Gateway: History anf the Tectonics of the Australia-Asia collision.* (Vol. 355, pp. 7-35). Geological Society London Special Publication.

Miller, D. M., Goldstein, S. L., & Langmuir, C. H. (1994). Cerium/lead and lead isotope ratios in arc magmas and the enrichment of lead in the continents. *Nature, 368*, 514-520.

Mirnejad, H., & Bell, K. (2006). Origin and Source Evolution of the Leucite Hills Lamproites: Evidence from Sr-Nd-Pb-O Isotopic Compositions. *Journal of Petrology, 47*(12), 2463-2489.

Mitchell, R. H. (2009). Peralkaline nephalinite-natrocarbonatite immiscibility and carbonate assimilation at Oldoinyo Lengai, Tanzania. *Contrib Mineral Petrol, 158*, 589-598.

Mollo, S., Gaeta, M., Freda, C., Di Rocco, T., Misiti, V., & Scarlato, P. (2010). Carbonate assimilation in magmas: A reappraisal based on experimental petrology. *Lithos, 114*, 503-514.

Nebel, O., Vroon, P. Z., Westrenen, v. W., Lizuka, T., & Davies, G. R. (2011). The effect of sediment recycling in subduction zones on the Hf isotope character of new arc crust, Banda arc, Indonesia. *Earth and Planetary Science Letters, 303*, 240-250.

Nebel, O., Vroon, P. Z., Wigger, d., Jenner, F. E., & Mavrogenes, J. A. (2010). Tungsten isotopes as tracers of core-mantle interactions: The influence of subducted sediments.*Geochimica et Cosmochimica Acta, 74*, 751-762.

Nelson, D. R., Chivas, A. R., Chappell, B. W., & McCulloch, M. T. (1998). Geochemical and isotopic systematics in carbonatites and implications for the evolution of ocean island sources. *Geochimica et Cosmochimica, 52*, 1-17.

Nelson, D. R., McCulloch, M. T., & Sun, S.-S. (1986). The origins of ultrapotassic rocks as inferred from Sr, Nd and Pb isotopes. *Geochimica et Cosmochimica Acta, 50*, 231-245.

Nicholls, I. A., & Whitford, D. J. (1976). Primary magmas associated with Quaternary volcanism in the western Sunda Arc, Indonesia. (R. W. Johnson, Ed.) *Volcanism in Australasia*, 77-89.

Nicholls, I. A., Whitford, D. J., Harris, K. L., & Taylor, S. R. (1980). Variation in the geochemistry of mantle sources for tholeiitic and calc-alkaline mafic magmas, western Sunda volcanic arc, Indonesia. *30*, 177-199.

Nikogosian, I. K., & van Bergen, M. J. (2010). Heterogeneous mantle sources of potassium-rich magmas in central-southern Italy: Melt inclusion evidence from Roccamonfina and Ernici (Mid Latina Valley). *Journal of Volcanology and Geothermal Research, 197, 279-302.*

Ninkovich, D. (1979). Distribution, age and chemical composition of tephra layers in deep-sea sediments off western Indonesia. *Journal of Volcanology and Geothermal Research., 5*, 67-86.

Nowell, G. M., & Parish, R. R. (2002). Simultaneous acquisition of isotope compositions and parent/daughter ratios by non-isotope dilution solution-mode Plasma ionisation Multi-collector Mass Spectrometry (PIMMS). *Plasma Source Mass Spectrometry The New Millenium*, 298-310.

Nowell, G. M., Kempton, P. D., Noble, S. R., Fitton, J. G., Saunders, A. D., Mahoney, J. J., et al. (1998). High-precision Hf isotope measurements of MORB and OIB by thermal ionisation mass spectrometry: insights into the depleted mantle. *Chemical Geology, 149*, 211-233.

Nowell, G. M., Pearson, D. J., Ottley, C. J., & Schweiters, J. (2003). Long-term performance characteristics of a plasma ionisation multi-collector mass spectrometer (PIMMS): the ThermoFinnigan Neptune. *Plasma Source Mass Spectrometry. Spec. Pub. Royal Society of Chemistry*, 307-320.

Nuru, S., & Kerrich, R. (2010). Mgnesian dyke suites of the 2.7 Ga Kambalda Sequence, Western Australia: Evidence for coeval melting of plume asthenosphere and metasomatised lithospheric mantle. *Precambrian Research, 180*, 183-203.

O'Reilly, S. Y., & Zhang, M. (1995). Geochemical characteristics of lava-field basalts from eastern Australia and inferred sources: connections with the subcontinental lithospheric mantle? *Contib. Mineral Petrol., 121*, 148-170.

Othman, D. B., White, W. M., & Patchett, J. (1989). The geochemistry of marine sediments, island arc magma genesis, and crust-mantle recycling. *Earth and Planetary Science Letters, 94*, 1-21.

Ottley, C. J., Pearson, D. G., & Irvine, G. J. (2003). A routine method for the dissolution of geological samples for the analysis of REE and trace elements via ICP-MS. *Plasma Source Mass Spectrometry. Spec. Pub. Royal Society of Chemistry*, 221-230.

Parkinson, C. D., Miyazaki, K., Wakita, K., Barber, A. J., & Carswell, D. A. (1998). An overview and tectonic synthesis of the pre-Tertiary very-high-pressure metamorphic and associated rocks of Java, Sulawesi and Kalimantan, Indonesia. *The Island Arc, 7*, 184-200.

Parman, S. W., Grove, T. L., Kelly, K. A., & Plank, T. (2011). Along-Arc Variations in the Pre-Eruptive H2O Contents of Mariana Arc Magmas Inferred from Fractionation Paths. *Journal of Petrology, 52*(2), 257-278.

Pearce, J. A. (2005). Mantle Preconditioning by Melt Extraction during Flow: Theory and Petrogenetic Implications. *Journal of Petrology*, *46*(5), 973-997.

Pearce, J. A., & Parkinson, I. J. (1993). Trace element models for mantle melting: application to volcanic arc petrogenesis. *Geological Society Special Publications, 76*, 373-403.

Pearce, J. A., Baker, P. E., Harvey, P. K., & Luff, I. W. (1995). Geochemical evidence for subduction fluxes, mantle melting and fractional crystallisation beneath the South Sandwich Island Arc. *Journal of Petrology, 36*(4), 1073-1109.

Pearce, J. A., Stern, R. J., Bloomer, S. H., & Fryer, P. (2005). Geochemical mapping of the Mariana arc-basin system: Implications for the nature and distribution of subduction components. *Geochemistry Geophysics Geosystems, 6*(7), 1-27.

Peccerillo, A., & Taylor, S. R. (1976). Geochemistry of Eocene calc-alkaline volcanic rocks from the Kastamonu area, northern Turkey. *Contributions to Mineralogy and Petrology, 58*, 63-81.

Peccerillo, A., Dallai, L., Frezzotti, M. L., & Kempton, P. D. (2004). Sr-Nd-Pb-O isotopic evidence for decreasing crustal contamination with ongoing magma evolution at Alicudi volcano (Aeolian arc, Italy): implications for style of magma-crust interaction and for mantle source compositions. *Lithos, 78*, 217-233.

Phipps Morgan, J., & Morgan, W. J. (1999). Two-stage melting and geochemical evolution of the mantle: a recipe for mantle plum-pudding. *Earth and Planetary Science Letters, 170*, 215-239.

Pichavant, M., & Macdonald, R. (2007). Crystallization of primitive basaltic magmas at crustal pressures and genesis of the calc-alkaline igneous suite: experimental evidence from St Vincent, Lesser Antilles arc. *Contrib Mineral Petrol, 154*, 535-558.

Pilet, S., Baker, M. B., & Stolper, E. M. (2008). Metasomatized Lithosphere and the origin of Alkaline Lavas. *Science, 320*, 916-919.

Plank, T., & Langmuir, C. H. (1993). Tracing trace elements from sediment input to volcanic output at subduction zones. *Nature, 362*, 739-743.

Plank, T., & Langmuir, C. H. (1998). The chemical composition of subducting sediment and its consequences for the crust and mantle. *Chemical Geology, 145*, 325-394.

Plank, T., & Ludden, J. N. (1992). Geochemistry of sediments in the Aro Abyssal plain at site 765: A continental margin reference section for sediment recycling in subduction zones. *Proceedings of the Ocean Drilling Program, Scientific Results, 23*, 167-189.

Polve, M. M., Maury, R. C., Bellon, H., Priadi, B., Yuwono, S., Joron, J. L., et al. (1997). Magmatic evolution of Sulawesi (Indonesia): constraints on the Cenozoic geodynamic history of the Sundaland active margin. *Tectonophysics, 272*, 69-92.

Polve, M., Maury, R. C., Vidal, P., Priadi, B., Bellon, H., Soeria-Atmadja, R., et al. (2001). Melting of lower continental crust in a young post-collision setting: A geochemical study of Plio-Quaternary acidic magmatism from central Sulawesi (Indonesia). *Bull. Soc. Geol. Fr., 172*, 333-342.

Potts, P. J., Tindle, A. G., & Webb, P. C. (1992). Geochemical reference material compositions: rocks, minerals, sediments, soils, carbonates, refractories and ores used in research and industry. *Whittles Publishing, Caithness, UK*.

Prelevic, D., Akal, C., Foley, S. F., Romer, R. L., Stracke, A., & van den Bogaard, P. (2012). Ultrapotassic Mafic Rocks as Geochemical Proxies for Post-collisional Dynamics of Orogenic Lithospheric Mantle: the Case of Southwestern Anatolia, Turkey. *Journal of Petrology, 53*(5), 1019-1055.

Priadi, B., Polve, M., Maury, R. C., Bellon, H., Soeria-Atmadja, R., Joron, J. L., et al. (1994). Tertiary and Quaternary magmatism in central Sulawesi: chronological and petrological constraints. *Journal of Southeast Asia Earth Sciences, 9*, 81-93.

Price, R. C., Kennedy, A. K., Riggs-Sneeringer, M., & Frey, F. A. (1986). Geochemistry of basalts from the Indian Ocean triple junction: implications for the generation and evolution of Indian Ocean ridge basalts. *Earth and Planetary Science Letters, 78*, 379-396.

Ray, J. S. (2009). Radiogenic Isotope Ratio Variations in Carbonatites and Associated Alkaline Silicate Rocks: Role of Crustal Assimilation. *Journal of Petrology, 50*(10), 1955-1971.

Rehkamper, M., & Hofmann, A. W. (1997). Recycled ocean crust and sediment in Indian Ocean MORB. *Earth and Planetary Science Letters, 147*, 93-106.

Reubi, O., & Nicholls, I. A. (2004). Magmatic evolution at Batur volcanic field, Bali, Indonesia: petrological evidence for polybaric fractional crystallisation and implications for caldera-forming eruptions. *Journal of Volcanology and Geothermal Research, 138*, 345-369.

Reubi, O., & Nicholls, I. A. (2005). Structure and Dynamics of a Silicic Magmatic System Associated with Caldera-Forming Eruptions at Batur Volcanic Field, Bali. *Journal of Petrology, 46*(7), 1367-1391.

Reubi, O., Nicholls, I. A., & Kamenetsky, V. S. (2002). Early mixing and mingling in the evolution of basaltic magmas: evidence from phenocryst assemblages, Slamet Volcano, Java, Indonesia. *Journal of Volcanology and Geothermal Research, 119*, 255-274.

Rittmann, A. (1953). Magmatic character and tectonic position of the Indonesian volcanoes. *Bull. Volcan., 14*, 45-58.

Rogers, N. W., Hawkesworth, C. J., Mattey, D. P., & Harmon, R. S. (1987). Sediment subduction and the source of potassium in orogenic leucitites. *Geology, 15*, 451-453.

Royse, K., Kempton, P. D., & Darbyshire, D. P. (1998). *NERC Isotope Geosciences Laboratory Report Series.*

Rubin, K. H., Wheller, G. E., Tanzer, M. O., Macdougall, J. D., Varne, R., & Finkel, R. (1989). 238U decay series systematics of young lavas from Batur volcano, Sunda Arc. *Journal of Volcanology and Geothermal Research, 38*, 215-226.

Rudnick, R. L., & Fountain, D. M. (1995). Nature and composition of the contental crust: a lower crustal perspective. *Reviews of Geophysics, 33*(3), 267-309.

Rudnick, R. L., & Gao, S. (2003). Composition of the Continental Crust. *Treatise on Geochemistry, 3*, 1-64.

Ruellan, E., Deltiel, J., Wright, I., & Matsumoto, T. (2003). From rifting to active arc spreading in the Lau Basin - Havre trough backarc system (SW Pacific): Locking/Unlocking induced by seamount chain subduction. *Geochemistry Geocphysics Geosystems, 4*(5), 1-21.

Salters, V. J., & Hart, S. R. (1991). The mantle sources of Ocean ridges, islands and arcs: the Hf-isotope connection. *Earth and Planetary Science Letters, 104*, 364-380.

Salters, V. J., & Stracke, A. (2004). Composition of the depleted mantle. *Geochemistry Geophysics Geosystems, 5*, doi: 10.1029/2003GC000597.

Salters, V. J., & White, W. M. (1998). Hf constraints on mantle evolution. *Chemical Geology, 145*, 447-460.

Saunders, A. D., Norry, M. J., & Tarney, J. (1991). Fluid influence on the trace element compositions of subduction zone magmas. *Philosophical Transactions of the Royal Society of London, 335*, 377-392.

Schaaf, P., Stimac, J., Siebe, C., & Macias, J. L. (2005). Geochemical evidence for mantle origin and crustal processes in volcanic rocks from Popocatepetl and surrounding monogenetic volcanoes, Central Mexico. *Journal of Petrology, 46*, 1243-1282.

Sendjaja, Y. A., Kimura, J.-I., & Sunardi, E. (2009). Across-arc geochemical variation of Quaternary lavas in West Java, Indonesia: Mass-balance elucidation using arc basalt simulator model. *Island Arc, 18*, 201-224.

Setijadji, L. D. (2010). Segmented Volcanic Arc and its Association with Geothermal Fields in Java Island, Indonesia. *Proceedings World Geothermal Congress*, (pp. 1-12).

Shulgin, A., Kopp, H., Mueller, C., Lueschen, E., Planert, L., Engels, M., et al. (2009). Sunda-Banda arc transition: Incipient continent-island arc collision (northwest Australia). *Geophysical Research Letters*, *36*, 1-6.

Shulgin, A., Kopp, H., Muller, C., Planert, L., Lueschen, E., Flueh, E. R., et al. (2011). Structural architecture of oceanic plateau subduction offshore Eastern Java and the potential implications for geohazards. *Geophysical Journal International, 184*, 12-28.

Sisson, T. W., & Grove, T. L. (1993). Experimental investigations of the role of H2O in calc-alkaline differentiation and subduction zone magmatism. *Contrib. Mineral Petrol, 113*, 143-166.

Sisson, T. W., & Grove, T. L. (1993b). Temperatures and H2O contents of low MgO high-alumina basalts. *Contrib Mineral Petrol, 113*, 167-184.

Smyth, H. (2005). Eocene to Miocene Basin Histroy and volcanic activity in East Java, Indonesia. *P.hD thesis. Royal Holloway University of London*.

Smyth, H. R., Hall, R., & Nicholls, G. J. (2008). Early Cenozoic volcanic arc history of East Java, Indonesia: The stratigraphic record of eruptions on an active continental margin. *The Geological Society of America Special Paper, 436*, 199-222.

Smyth, H. R., Hamilton, P. J., Hall, R., & Kinny, P. D. (2007). The deep crust beneath island arcs: Inherited zircons reveal a Gondwana continental fragment beneath East Java. *Earth and Planetary Science Letters, 258*, 269-282.

Smyth, H., Hall, R., Hamilton, J., & Kinny, P. (2005). East Java: Cenozoic basins, volcanoes and ancient basement. *Proceedings, Indonesian Petroleum Association*, (pp. 251-266).

Soeria-Atmadja, R., Maury, R. C., Bellon, H., Pringgoprawiro, H., Polve, M., & Priadi, B. (1994). Tertiary magmatic belts in Java. *Journal of Southeast Asian Earth Sciences, 9*(1/2), 13-27.

Southgate, P., Sircombe, K., & Lewis, C. (2011). Identifying potential provenance and sediment transport pathways for reservoir facies on the North West Shelf using SHRIMP zircon ages. *APPEA Conference.*

Staudigel, H., Davies, G. R., Hart, S. R., Marchant, K. M., & Smith, B. M. (1995). Large scale Sr, Nd and O anatomy of altered oceanic crust: DSDP/ODP sites 417/418. *Earth and Planetary Science Letters, 130*, 169-185.

Staudigel, H., Plank, T., White, B., & Schimincke, H.-U. (1996). Geochemical fluxes during seafloor alteration of the basaltic upper oceanic crust: DSDP Sites 417 and 418. In G. E. Bebout, D. W. Scholl, S. H. Kirby, & J. P. Platt (Eds.), *Subduction: Top to Bottom* (pp. 19-36). Geophysical Monograph, American Geophysical Union 96.

Stolz, A. J., Varne, R., Davies, G. R., Wheller, G. E., & Foden, J. D. (1990). Magma source components in an arc-continent collision zone: the Flores-Lembata sector, Sunda arc, Indonesia. *Indonesia. Contrib. Mineral. Petrol, 4*(2), 143-159.

Stolz, A. J., Varne, R., Wheller, G. E., Foden, J. D., & Abbott, M. J. (1988). The geochemistry and petrogenesis of K-rich alakline volcanics from Batu Tara volcano, eastern Sunda Arc. *Contrib. Mineral. Petrol., 98*, 374-389.

Stormer, J. C., & Nicholls, J. (1978). XLFRAC; a program for the interactive testing of magmatic differentiation models. *Computers and Geoscience, 4*, 143-159.

Stracke, A., & Bourdon, B. (2009). The importance of melt extraction for tracing mantle heterogeneity. *Geochimica et Cosmochimica Acta, 73*, 218-238.

Straub, S. M., & Zellmer, G. F. (2012). Volcanic arcs as archives of plate tectonic change. *Gondwana Research, 21*, 495-516.

Straub, S. M., Goldstein, S. L., Class, C., Schmidt, A., & Gomez-Tuena, A. (2010). Slab and Mantle Controls on the Sr-Nd-Pb-Hf Isotope Evolution of the Post 42 Ma Izu-Bonin Volcanic Arc. *Journal of Petrology, 51*(5), 993-1026.

Sudradjat, A. (1991). A Preliminary Account of the 1990 Eruption of the Kelut Volcano. In A. Sudradjat (Ed.), *The Dynamics of Indonesian Volcanoes* (pp. 447-462). Hannover: Padjadjaran University, Bandung, Indonesia.

Sukhyar, R. (1990). Geochemistry and petrogenesis of arc rocks from Dieng, Sundoro and Sumbing volcanic complexes central Java, Indonesia. *Ph.D Thesis, Bandung Institute of Technology*.

Sun, S., & McDonough, M. F. (1989). Chemical and isotopic systematics of oceanic basalts: implications for mantle composition and processes. In A. D. Saunders, & M. J. Norry (Eds.), *Magmatism in the Ocean Basisns* (pp. 313-345). Geological Society Special Publication.

Syracuse, E. M., & Geoffrey, A. A. (2006). Global compliation of variations in slab depth beneath arc volcanoes and implications. *Geochemistry, Geophysics, Geosystems, 7*(5), 1-18.

Tatsumi, Y., & Kogiso, T. (1997). Trace element transport during dehydration processes in the subducted oceanic crust: 2. Origin of chemical and physical characteristics in arc magmas. *Earth and Planetary Science Letters., 148*, 207-221.

Tatsumi, Y., Hamilton, D. L., & Nesbit, R. W. (1986). Chemical characteristics of fluid phase released from a subducted lithosphere and origin of arc magmas: evidence from high-pressure experiments and natural rocks. *J. Volcanol. Geotherm. Res., 29*, 239-309.

Taylor, R. N., & Nesbitt, R. W. (1998). Isotopic characteristics of subduction fluids in an intra-oceanic setting, Izu-Bonin Arc, Japan. *Earth and Planetary Science Letters, 164*, 79-98.

Tepley, F. J., Davidson, J. P., Tilling, R. I., & Arth, J. G. (2000). Magma Mixing, Recharge and Eruption Histories Recorded in Plagioclase Phenocrysts from El Chichon Volcano, Mexico. *Journal of Petrology, 41*(9), 1397-1411.

Thirlwall, M. F. (1991). Long-term reproducibility of multicollector Sr and Nd isotope ratio analysis. *Chemical Geology; Isotope Geoscience Section., 94*(2), 85-104.

Thirlwall, M. F., & Graham, A. M. (1984). Evolution of high-Ca, high-Sr C-series basalts from Grenada, Lesser Antilles: the effects of intra-crustal contamination. *Journal of the Geological Society, London, 141*, 427-445.

Thirlwall, M. F., Graham, A. M., Arculus, R. J., Harmon, R. S., & Macpherson, C. G. (1996). Resolution of the effects of crustal assimilation, sediment subduction, and fluid transport in island arc magmas: Pb-Sr-Nd-O isotope geochemistry of Grenada, Lesser Antilles. *Geochim. Cosmochim. Acta, 60*, 4785-4810.

Tiepolo, M., Oberti, R., & Zanetti, A. (2007). Trace-Element Partitioning Between Amphibole and Silicate Melt. *Reviews in Mineralogy & Geochemistry, 67*, 417-452.

Tiepolo, M., Tribuzio, R., & Langone, A. (2011). High-Mg Andesite Petrogenesis by Amphibole Crystallisation and Ultramafic Crust Assimilation: Evidence from Adamello Hornblendites (Central Alps, Italy). *Journal of Petrology, 52*(5), 1011-1045.

Tingey, D. G., Christiansen, E. H., Best, M. G., Ruiz, J., & Lux, D. R. (1991). Tertiary Minette and Melanephelinite Dikes, Wasatch Plateau, Utah: Records of Mantle Heterogeneities and Changing Tectonics. *Journal of Geophysical Research, 96*(B8), 13,529-13,544.

Tregoning, P., Brunner, F. K., Bock, Y., Puntodewo, S. S., McCaffrey, R., Genrich, J. F., et al. (1994). First geodetic measurement of convergence across the Java Trench. *Geophysical Research Letters, 21*(19), 2135-2138.

Troll, V. R., Hilton, D. R., Jolis, E. M., Chadwick, J. P., Blythe, L. S., Deegan, F. M., et al. (in press). Crustal CO2 liberation at Merapi volcano, Indonesia during the 2006 eruption and earthquake events. *Geophysical Research Letters,* doi:10.1029/2012GL051307.

Trollstrup, D., Gill, J., Kent, A., Prinkey, D., Williams, R., Tamura, Y., et al. (2010). Across-arc geochemical trends in the Izu-Bonin arc: Contributions from the subducting slab, revisited. *Geochemistry Geophysics Geosystems, 11*(1), 1525-2027.

Turner, S., & Foden, J. (2001). U, Th and Ra disequilibria, Sr, Nd and Pb isotope and trace element variations in Sunda arc lavas: predominance of a subducted sediment component. *Contrib Mineral Petrol, 142*, 43-57.

Turner, S., & Hawkesworth, C. (1997). Constraints on flux rates and mantle dynamics beneath island arcs from Tonga-Kermadec lava geochemistry. *Nature, 389*, 568-573.

Turner, S., Foden, J., George, R., Evens, P., Varne, R., Elburg, E., et al. (2003). Rates and Processes of Potassic Magma Evolution beneath Sangean Api Volcano, East Sunda Arc, Indonesia. *Journal of Petrology, 44*(3), 491-515.

Turner, S., Handler, M., Bindeman, I., & Suzuki, K. (2009). New insights into the origin of O-Hf-Os isotope signatures in arc lavas from Tonga-Kermadec. *Chemical Geology, 266*, 187-193.

Turner, S., Hawkesworth, C., Rogers, N., Bartlett, J., Worthington, T., Hergt, J., et al. (1997). 238U-230Th disequilibria, magma petrogenesis, and flux rates beneath the depleted Tonga-Kermadec island arc. *Geochimica et Cosmochimica Acta, 61*(22), 4855-4884.

van Bemmelen, R. W. (1949). The Geology of Indonesia. *Martinus Nijhoff, The Hague., 1*, 732.

van Bergen, M. J., Vroon, P. Z., Varekamp, J. C., & Poorter, R. P. (1992). The origin of the potassic rock suite from Batu Tara volcano (East Sunda Arc, Indonesia). *Lithos, 28*, 261-282.

van Gerven, M., & Pichler, H. (1995). Some aspects of the volcanology and geochemistry of the Tengger Caldera, Java, Indonesia: eruption of a K-rich tholeiitic series. *Journal of Southeast Asian Earth Scieneces, 11*(2), 125-133.

van Leeuwen, M. T., & Muhardjo. (2005). Stratigraphic and tectonic setting of the Cretaceous and Paleogene volcanic-sedimentary successions in north-west Sulawesi, Indonesia: Implications for the Cenozoic evolution of Western and Northern Sulawesi. *Journal of Asian Earth Sciences, 25*, 481-511.

van Leeuwen, T. M., Allen, C. M., Kadarusman, A., Elburg, M., Michael Palin, J., Muhardjo, et al. (2007). Petrologic, isotopic, and radiometric age constraints on the origin and tectonic history of the Malino Metamorphic Complex, NW Sulawesi, Indonesia. *Journal of Asian Earth Sciences, 29*, 751-777.

Varne, R. (1985). Ancient subcontinental mantle: A source for K-rich orogenic volcanics. *Geology, 13*, 405-408.

Varne, R., & Foden, J. D. (1986). Geochemical and isotopic systematics of eastern Sunda arc volcanics: implications for mantle sources and mantle mixing processes. *The Origin of Arcs*, 159-189.

Varne, R., & Foden, J. D. (1986). Geochemical and isotopic systematics of eastern Sunda arc volcanics: implications for mantle sources and mantle mixing processes. In F. C. Wezel (Ed.), *The Origin of Arcs.* (pp. 159-189). Amsterdam: Elsevier.

Veksler, I. V., Petibon, C., Jenner, G. A., Dorfman, A. M., & Dingwell, D. B. (1998). Trace Element Partitioning in Immiscible Silicate-Carbonate Liquid Systems: and Initial Experiemtal Study using a Centrifuge Autoclave. *Journal of Petrology, 39*(11 & 12), 2095-2104.

Vervoort, J. D., Patchett, P. J., Blichert-Toft, J., & Albarede, F. (1999). Relationships between Lu-Hf and Sm-Nd isotopic systems in the global sedimentary system . *Earth and Planetary Science Letters, 168*, 79-99.

Vogel, T. A. (1982). Magma Mixing in the Acidic-Basic Complex of Ardnamurchan: Implications on the Evolution of Shallow Magma Chambers. *Contrib Mineral Petrol, 79*, 411-423.

Vroon, P. Z. (1992). *Subduction of continental material in the Banda Arc, Eastern Indonesia: Sr-Nd-Pb isotope and trace-element evidence from volcanics and sediments.* Utrecht: Ph.D. thesis University of Utrecht.

Vroon, P. Z., Lowry, D., van Bergen, M. J., Boyce, A. J., & Mattey, D. P. (2001). Oxygen isotope systematics of the Banda Arc: Low delta18O despite involvement of subducted continental material in magma genesis. *Geochimica et Cosmochimica Acta, 65*(4), 589-609.

Vroon, P. Z., van Bergen, M. J., Klaver, G. J., & White, W. M. (1995). Strontium, neodymium, and lead isotopic and trace-element signatures of the east Indonesian sediments: Provenance and implications for Banda Arc magma petrogenesis. *Geochim. Cosmochim. Acta, 59*, 2573-2598.

Vroon, P. Z., van Bergen, M. J., White, W. M., & Varekamp, J. C. (1993). Sr-Nd-Pb Isotope Systematics of the Banda Arc, Indonesia: Combined Subduction and Assimilation of Continental Material. *Journal of Geophysical Research, 98*(B12), 349-366.

Vukadinovic, D., & Sutawidjaja, I. (1995). Geology, mineralogy and magma evolution of the Gunung Slamet Volcano, Java, Indonesia. *Journal of Southeast Asian Earth Sciences, 11*(2), 135-164.

Wakita, K. (2000). Cretaceous accretionary-collision complexes in central Indonesia. *Journal of Asian Earth Sciences, 18*, 739-749.

Waltham, D., Hall, R., Smyth, H. R., & Ebinger, C. J. (2008). Basin formation by volcanic arc loading. In A. E. Draut, P. D. Clift, & D. W. Scholl (Eds.), *Formation and*

Applications of the Sedimentary Record in Arc Collision Zones. (Vol. 436, pp. 11-26). The Geological Society of America Special Papaer.

Watson, S., & McKenzie, D. (1991). Melt generation by plumes: A study of Hawaiian volcanism. *Journal of Petrology*, *32*, 501-537.

Wheller, G. E., & Varne, R. (1986). Genesis of dacitic magmatism at Batur volcano, Bali, Indonesia: implications for the origins of stratovolcano calderas. *Journal of Volcanology and Geothermal Research., 28*, 363-378.

Wheller, G. E., Varne, R., Foden, J. D., & Abbot, M. J. (1987). Geochemistry of Quaternary volcanism in the Sunda-Banda arc, Indonesia, and three-component genesis of island-arc basaltic magmas. *Journal of Volcanology and Geothermal Research, 32*, 137-160.

White, R. S. (1993). Melt production rates in mantle plumes. *Phil. Trans. R. Soc. Lond. A, 342*, 137-153.

White, W. M., & Patchett, J. (1984). Hf-Nd-Sr isotopes and incompatible element abundances in island arcs: implications for magma origins and crust-mantle evolution. *Earth and Planetary Science Letters*, 167-185.

White, W. M., Patchett, J., & BenOthman, D. (1986). Hf isotope ratios of marine sediments and Mn nodules: evidence for a mantle source of Hf in seawater. *Earth and Planetary Science Letters, 79*, 46-54.

Whitford, D. J. (1975). Strontium isotopic studies of the volcanic rocks of the Sunda arc, Indonesia, and their petrogenetic implications. *Geochimica et Cosmochimica Acta, 39*, 1287-1302.

Whitford, D. J. (1975). Strontium isotopic studies of volcanic rocks of the Sunda arc, Indonesia, and their petrogenetic implications. *Geochimca et Cosmchimica Acta, 39*.

Whitford, D. J., & Jezek , P. A. (1982). Isotopic constraints on the role of subducted sialic material in Indonesian island-arc magmatism. *Geological Society of America Bulletin, 93*, 504-513.

Whitford, D. J., & Nicholls, I. A. (1976). Potassium variation in lavas across the Sunda Arc in Java and Bali. (R. W. Johnson, Ed.) *Volcanism in Australasia*, 63-75.

Whitford, D. J., Nicholls, I. A., & Taylor, S. R. (1979). Spatial Variations in the Geochemistry of Quaternary Lavas Across the Sunda Arc in Java and Bali. *Contrib. Mineral. Petrol., 70*, 341-356.

Whitford, D. J., White, W. M., & Jezek, P. A. (1981). Neodymium isotopic composition of Quaternary island arc lavas from Indonesia. *Geochimica et Cosmochimica Acta, 45*, 989-995.

Widiyantoro, S., Pesicek, J. D., & Thurber, C. H. (2011). Subducting slab structure below the eastern Sunda arc inferred from non-linear seismic tomographic imaging. *Geological Society, London, Special Publications, 355*, 139-155.

Wirakusumah, A. D. (1993). Geology of and magma mixing process at Mt. Kelut, East Java. Proceedings of The 22nd Annual Convention of the Indonesian Association of Geologists.

Wood, D. A. (1979). Dynamic partial melting: its application to the petrogenesis of basalts erupted in Iceland, the Faeroe Islands, the Isle of Skye (Scotland) and the Troodos Massif (Cyprus). *Geochimica et Cosmochimica Acta, 43*, 1031-1046.

Woodhead, J. (1989). Geochemistry of the Mariana arc (western Pacific): Source compositions and processes. *Chemical Geology, 76*, 1-24.

Woodhead, J. D., Eggins, S. M., & Johnson, W. (1998). Magma genesis in the New Britain Island Arc: Further insights into the melting and mass transfer processes. *Journal of Petrology, 39*(9), 1641-1668.

Woodhead, J. D., Hergt, J. M., Davidson, J. P., & Eggins, S. M. (2001). Hafnium isotopic evidence for 'consrvative' element mobility during subduction zone processes. *Earth and Planetary Science Letters, 192*, 331-346.

Woodhead, J., Eggins, S., & Gamble, J. (1993). High field strength transition element systematics in island arc and back-arc basin basalts: evidence for multi-stage extraction and a depleted mantle wedge. *Earth and Planetary Science Letters, 114*, 491-504.

Woodhead, J., Stern, R. J., Pearce, J., Hergt, J., & Vervoort, J. (2012). Hf-Nd isotope variation in Mariana Trough basalts: The importance of "ambient mantle" in the interpretation of subduction zone magmas. *Geology*, in press.

Workman, R. K., & Hart, S. R. (2005). Major and trace element composition of the depleted MORB mantle (DMM). *Earth and Planetary Science Letters, 231*, 53-72.

Yang, H.-J., Frey, F. A., Weis, D., Giret, A., Pyle, D., & Michon, G. (1998). Petrogenesis of the Flood Basalts Forming the Northern Kerguelen Archipelago: Implications for the Kerguelen Plume. *Journal of Petrology, 39*(4), 711-748.

Yuwono, Y. S., Maury, R. C., Soeria-Atmadja, R., & Bellon, H. (1988). Tertiary and Quaternary geodynamic evolution of South Sulawesi: contraints from the study of volcanic units. *Geologi Indonesia, Jakarta, 13*, 32-48.

Zhang, L., Han, B.-F., Wei, C.-J., & Shu, G.-M. (2011). Cumulate hornblendite enclaves in diorite-porphyrite intrusions from the Shuangyashan, Northeast hina, and implications for the transition from lower crust to upper mantle in subduction setting. *Int J Earth Sci, 100*, 63-79.

Zindler, A., & Hart, S. (1986). Chemical Geodynamics. *Annu. rev. Earth Planet. Sci., 14*, 493-571.

Appendices

Appendix A. Sample localities and descriptions

Table A.1. West Java volcanoes

Table A.2. Sumbing volcano (Central Java)

Table A.3. Kelut volcano (East Java)

Table A.4. Agung volcano (Bali)

Appendix B. Whole-rock major- and trace-element data

Table B.1. West Java volcanoes

Table B.2. Sumbing volcano (Central Java)

Table B.3. Kelut volcano (East Java)

Table B.4. Agung volcano (Bali)

Appendix C. Whole-rock isotope data

Table C.1. West Java volcanoes

Table C.2. Sumbing volcano (Central Java)

Table C.3. Kelut volcano (East Java)

Table C.4. Agung volcano (Bali)

Appendix D. Mineral data

Table D.1. Plagioclase mineral data for Sumbing volcano (Central Java)

    Table D.1.1. Clinopyroxene mineral data

    Table D.1.2. Orthopyroxene mineral data

    Table D.1.3. Ti-Fe oxide mineral data

    Table D.1.4. Amphibole mineral data

Table D.2. Plagioclase mineral data for Kelut volcano (East Java)

    Table D.2.1. Clinopyroxene mineral data

    Table D.2.2. Orthopyroxene mineral data

Appendix E. CIPW normative calculations

Appendix F. Analytical techniques

Figure F.1. ICP-MS against XRF element concentrations

F.2.3. Isotopic analysis

F.2.4. Data quality

Table F.7 (a) Reproducibility and accuracy for Sr-isotope analysis

(b) Reproducibility and accuracy for Nd-isotope analysis

(c) Reproducibility and accuracy for Pb-isotope analysis

(d) Reproducibility and accuracy for Hf-isotope analysis

Appendix A

Sample localities and descriptions

Table A.1. Sample summary for west Java volcanoes.

Sample	volcano	Grid Ref. (S)	Grid Ref. (E)	Locality Description	Deposit	Rock Type	Texture/comments
Pat04	Patuha	-7.164360	107.35805	Lake Patuha	lava	andesite	Porphyritic with minor olivine. Some alteration
Pat05	Patuha	-7.165610	107.36033	Lake Patuha	lava	basaltic andesite	Porphyritic with minor olivine. Some alteration
Pat07	Patuha	-7.167650	107.40114	Kawah Putih	lava	andesite	Porphyritic, fine-grained
Pat09	Patuha	-7.167650	107.40114	Kawah Putih	lava	andesite	Porphyritic, with minor amphibole. Some alteration
Pap10	Papandayan	-7.315030	107.73178	Crater	lava	dacite	Porphyritic. Contains Cumulophyric clots
Pap11	Papandayan	-7.314820	107.73137	Crater	lava	andesite	Porphyritic, with some alteration. Calcite and clays common
Pap14	Papandayan	-7.312320	107.73557	Crater	lava	dacite	
Pap15	Papandayan	-7.312320	107.73557	Crater	lava	basaltic andesite	Porphyritic, with some alteration.
Pap16	Papandayan	-7.312320	107.73557	Crater	lava	andesite	Porphyritic, with some alteration.
Pap17	Papandayan	-7.312320	107.73557	Crater	lava	dacite	
Pap18	Papandayan	-7.305770	107.76698	Riverside exposure	lava	andesite	Vitrophyre.
Gal32(a)	Galunggung	-7.257510	108.08020	Crater rim	lava	basalt	Porphyritic. Contains moderate olivine
Gal32(b)	Galunggung	-7.257510	108.08020	Crater rim	lava	basalt	Porphyritic. Contains moderate olivine
Gal33	Galunggung	-7.257510	108.08020	Crater rim	lava	basaltic andesite	Porphyritic, with cumulophyric clots
Gal34	Galunggung	-7.257510	108.08020	Crater rim	lava	basaltic andesite	Porphyritic, with cumulophyric clots
Gal35	Galunggung	-7.253620	108.07700	Crater	lava	basaltic andesite	Porphyritic, with cumulophyric clots
Gal36	Galunggung	-7.253620	108.07700	Crater	lava	basaltic andesite	Porphyritic, with cumulophyric clots
Gal37(a)	Galunggung	-7.278810	108.16392	Crater	lava	basaltic andesite	Porphyritic, with cumulophyric clots
Gal37(b)	Galunggung	-7.278810	108.16392	Crater	lava	basaltic andesite	Porphyritic, with cumulophyric clots
Tan01	Tangkuban Perahu	-6.761310	107.60882	Kawah Domas	lava	andesite	Porphyritic, contains vesicles. Some alteration
Tan02	Tangkuban Perahu	-6.761430	107.60868	Kawah Domas	lava	basaltic andesite	Porphyritic, contains vesicles. Some alteration
Tan03	Tangkuban Perahu	-6.761490	107.60844	Kawah Domas	lava	basaltic andesite	Porphyritic, with minor olivine

Sample mineralogy includes plagioclase, clinopyroxene, orthopyroxene and Fe-Ti oxide unless stated.

234

Sample	volcano	Grid Ref. (S)	Grid Ref. (E)	Locality Description	Deposit	Rock Type	Texture/comments
Tan19	Tangkuban Perahu	-6.965050	107.52769	Paseban Quarry	lava	andesite	Porphyritic, with some alteration
Tan20	Tangkuban Perahu	-6.965050	107.52769	Paseban Quarry	lava	andesite	Porphyritic, with minor amphibole. Some alteration
Tan21(a)	Tangkuban Perahu	-6.965050	107.52769	Paseban Quarry	lava	dacite	Porphyritic, with minor amphibole and quartz? Some alteration
Tan22(a)	Tangkuban Perahu	-6.921500	107.53554	Lagadar Quarry	lava	dacite	Porphyritic, with minor amphibole. Highly altered
Tan22(b)	Tangkuban Perahu	-6.921500	107.53554	Lagadar Quarry	lava	dacite	
Tan22(c)	Tangkuban Perahu	-6.921500	107.53554	Lagadar Quarry	lava	dacite	
Tan23	Tangkuban Perahu	-6.921500	107.53554	Lagadar Quarry	lava	andesite	Microcrystalline
Tan24(a)	Tangkuban Perahu	-6.921500	107.53554	Lagadar Quarry	lava	dacite	Porphyritic, with minor amphibole. Moderately altered
Tan24(b)	Tangkuban Perahu	-6.921500	107.53554	Lagadar Quarry	lava	dacite	
Tan24(c)	Tangkuban Perahu	-6.921500	107.53554	Lagadar Quarry	lava	dacite	
Tan25	Tangkuban Perahu	-6.921500	107.53554	Lagadar Quarry	lava	basaltic andesite	Phaneritic. Diorite, containing amphibole and biotite
Tan31	Tangkuban Perahu	-6.830380	107.63503	Gunung Batu	lava	basaltic andesite	Porphyritic, with minor amphibole. Highly altered
Ged26(a)	Gede	-6.897300	106.98354	Crater rim	lava	andesite	Highly porphyritic, with cumulophyric clots
Ged26(b)	Gede	-6.897300	106.98354	Crater rim	lava	andesite	
Ged26(c)	Gede	-6.897300	106.98354	Crater rim	lava	andesite	
Ged26(d)	Gede	-6.897300	106.98354	Crater rim	lava	andesite	
Ged27(a)	Gede	-6.897300	106.98354	Crater rim	lava	andesite	Phaneritic, diorite. Contains xenoliths
Ged27(b)	Gede	-6.897300	106.98354	Crater rim	lava	basaltic andesite	
Ged28(a)	Gede	-6.897300	106.98354	Crater rim	lava	andesite	Phaneritic, diorite. Contains irregular xenoliths
Ged28(b)	Gede	-6.897300	106.98354	Crater rim	lava	andesite	
Ged30	Gede	-6.738830	106.98667	Volcano flank	lava	andesite	Vitrophyre.

Table A.2. Sample summary for Sumbing volcano.

Sample	Grid Ref. (S)	Grid Ref. (E)	Altitude (m)	Locality Description	Deposit	Rock Type	Texture/comments
Sumb69	-7.316370	110.058180		North volcano flank, Kwandungan quarry	pyroclastic	basaltic andesite	vitrophyre, with cumulophyric clots
Sumb71	-7.316370	110.058180		North volcano flank, Kwandungan quarry	pyroclastic	basaltic andesite	vitrophyre, with cumulophyric clots
Sumb72	-7.340920	110.062730	1505	North volcano flank, Kruwisan	lava	andesite	porphyritic, containing hornblende and biotite-rich cumulate
Sumb73	-7.340920	110.062730	1505	North volcano flank, Kruwisan	lava	andesite	porphyritic, containing hornblende and biotite-rich cumulate
Sumb74	-7.340920	110.062730	1505	North volcano flank, Kruwisan	lava	andesite	porphyritic, containing hornblende and biotite-rich cumulate
Sumb76	-7.347200	110.061560	1623	North volcano flank, near Kruwisan	lava	basaltic andesite	microcrystalline, containing feldspar microlites
Sumb77	-7.347200	110.061560	1623	North volcano flank, near Kruwisan	lava	basaltic andesite	microcrystalline, containing feldspar microlites
Sumb78	-7.305310	110.115300	851	North volcano flank, Kruas river	lava	basaltic andesite	vitrophyre
Sumb80	-7.305310	110.115300	851	North volcano flank, Kruas river	lava	andesite	Porphyritic, containing diorite cumulate
Sumb81	-7.305310	110.115300	851	North volcano flank, Kruas river	lava	basaltic andesite	
Sumb83	-7.305310	110.115300	851	North volcano flank, Kruas river	lava	andesite	Porphyritic, with minor hornblende
Sumb85	-7.304280	110.117190	826	North volcano flank, Kruas river	lava	andesite	porphyritic, with minor hornblende
Sumb91	-7.416180	110.145300	964	East volcano flank, Windu Sari	lava	andesite	porphyritic/vitrophyre, containing hornblende
Sumb92	-7.416180	110.145300	964	East volcano flank, Windu Sari	lava	andesite	porphyritic/vitrophyre, containing hornblende
Sumb94	-7.568620	110.128930	338	South volcano flank, Jebengsari	pyroclastic	basaltic andesite	vitrophyre, with minor amphibole
Sumb95	-7.568620	110.128930	338	South volcano flank, Jebengsari	pyroclastic	basaltic andesite	porphyritic, medium-grained
Sumb96	-7.568620	110.128930	338	South volcano flank, Jebengsari	pyroclastic	basaltic andesite	porphyritic, medium-grained
Sumb97	-7.568620	110.128930	338	South volcano flank, Jebengsari	pyroclastic	basaltic andesite	porphyritic, medium-grained with minor hornblende
Sumb98	-7.568620	110.128930	338	South volcano flank, Jebengsari	pyroclastic	basaltic andesite	porphyritic, medium-grained with minor hornblende
Sumb99	-7.568620	110.128930	338	South volcano flank, Jebengsari	pyroclastic	basaltic andesite	porphyritic, medium-grained with minor hornblende

Sample mineralogy includes plagioclase, clinopyroxene, orthopyroxene and Fe–Ti oxide unless stated.

236

Table A.3. Sample summary for Kelut volcano.

Sample	Grid Ref. (S)	Grid Ref. (E)	Altitude (m)	Locality Description	Deposit	Rock Type	Texture/comments
Kel12	-7.864710	112.262350	471	North volcano flank, near Satak	lava	andesite	porphyritic/vitrophyre, with large xenocrystic plagioclase and quartz
Kel14	-7.864710	112.262350	471	North volcano flank, near Satak	lava	andesite	microcrystalline
Kel22	-7.864710	112.262350	471	North volcano flank, near Satak	lava	andesite	porphyritic/vitrophyre, with abundant hornblende
Kel23	-7.864710	112.262350	474	North volcano flank, near Satak	lava	andesite	microcrystalline, with some cumulophyric clots
Kel25	-7.881420	112.278490	586	North flank quarry, near Satak	lava	basaltic andesite	porphyritic/vitrophyre, with cumulophyric clots
Kel26	-7.881420	112.278490	586	North flank quarry, near Satak	lava	basaltic andesite	porphyritic, with minor hornblende
Kel27	-7.881420	112.278490	586	North flank quarry, near Satak	lava	basaltic andesite	porphyritic, with minor hornblende
Kel34	-7.881420	112.278490	586	North flank quarry, near Satak	lava	basaltic andesite	porphyritic, with large xenocrystic hornblende
Kel37	-7.881420	112.278490	586	North flank quarry, near Satak	cumulate	gabbro	
Kel38	-7.881420	112.278490	586	North flank quarry, near Satak	cumulate	hornblende gabbro	
Kel40	-7.932590	112.266710	892	West volcano flank	lava	basaltic andesite	porphyritic/vitrophyre, includes cumulophyric clots
Kel43	-7.932590	112.266710	892	West volcano flank	lava	andesite	porphyritic, with minor hornblende
Kel45	-7.932590	112.266710	892	West volcano flank	lava	basaltic andesite	seriate, with irregular gas bubbles
Kel48	-7.937760	112.296990	1255	Crater	lava	basaltic andesite	porphyritic/vitrophyre, includes cumulophyric clots
Kel50	-7.938740	112.298150	1242	Crater	lava	basaltic andesite	porphyritic, with irregular gas bubbles
Kel51	-7.939930	112.301590	1214	New lava dome	lava	basaltic andesite	porphyritic/vitrophyre
Kel53	-7.939340	112.299880	1236	Crater	cumulate	hornblendite	
Kel56	-7.936700	112.270220	946	West flank, roadside outcrop	lava	basaltic andesite	porphyritic, with minor olivine
Kel59	-7.936700	112.270200	946	West flank, roadside outcrop	lava	andesite	microcrystalline
Kel60	-7.936700	112.270220	946	West flank, roadside outcrop	lava	andesite	microcrystalline
Kel61	-7.936700	112.270220	946	West flank, roadside outcrop	lava	andesite	porphyritic
Kel64	-7.936700	112.270220	946	West flank, roadside outcrop	lava	andesite	microcrystalline, with cumulophyric clots

Sample mineralogy includes plagioclase, clinopyroxene, orthopyroxene and Fe-Ti oxide unless stated.

Table A.4. Sample summary for Agung volcano.

Sample	Grid Ref. (S)	Grid Ref. (E)	Altitude (m)	Locality Description	Deposit	Rock Type	Texture/comments
Agu03	-8.328610	115.615710	81	East volcano flank, Dukat Bangke River, Labe Sari	pyroclastic	andesite	vitrophyre, highly vesicular
Agu06	-8.257870	115.577770	44	Northeast volcano flank, north of Kubu	pyroclastic	basaltic andesite	vitrophyre, highly vesicular
Agu07	-8.257870	115.577770	44	Northeast volcano flank, north of Kubu	pyroclastic	andesite	vitrophyre, highly vesicular
Agu10	-8.257870	115.577770	44	Northeast volcano flank, north of Kubu	lava	basalt	porphyritic, fine-grained, with minor olivine
Agu12	-8.257870	115.577770	44	Northeast volcano flank, north of Kubu	lava	basaltic andesite	porphyritic, fine-grained, cpx commonly mantles opx
Agu13	-8.257870	115.577770	44	Northeast volcano flank, north of Kubu	lava	basalt	porphyritic, fine-grained, with minor olivine
Agu15	-8.257870	115.577770	44	Northeast volcano flank, north of Kubu	lava	andesite	vitrophyre, including cumulophyric clots
Agu16	-8.235640	115.542790	65	Northeast volcano flank, Kubu quarry	lava	andesite	microcrystalline, fine-grained
Agu18	-8.235640	115.542790	65	Northeast volcano flank, Kubu quarry	lava	basalt	
Agu20	-8.235640	115.542790	65	Northeast volcano flank, Kubu quarry	lava	andesite	vitrophyre, including cumulophyric clots
Agu21	-8.235640	115.542790	65	Northeast volcano flank, Kubu quarry	lava	basaltic andesite	
Agu22	-8.235640	115.542790	65	Northeast volcano flank, Kubu quarry	lava	basaltic andesite	vitrophyre, with minor olivine
Agu23	-8.235640	115.542790	65	Northeast volcano flank, Kubu quarry	lava	basaltic andesite	microcrystalline, fine-grained
Agu24	-8.235640	115.542790	65	Northeast volcano flank, Kubu quarry	lava	basaltic andesite	
Agu25	-8.235640	115.542790	65	Northeast volcano flank, Kubu quarry	pyroclastic	dacite	ignimbrite
Agu30	-8.353520	115.504760	2375	South volcano flank, close to crater	lava	basaltic andesite	vitrophyre
Agu31	-8.353520	115.504760	2375	South volcano flank, close to crater	lava	basaltic andesite	
Agu33	-8.353790	115.504750	2355	South volcano flank	lava	basaltic andesite	medium-grained, with minor olivine

Sample mineralogy includes plagioclase, clinopyroxene, orthopyroxene and Fe-Ti oxide unless stated.

Appendix B

Whole-rock major- and trace-element data

Table B.1. Major- and trace-element data for selected west Java volcanoes.

Sample	SiO_2	TiO_2	Al_2O_3	Fe_2O_3	MnO	MgO	CaO	Na_2O	K_2O	P_2O_5	LOI	TOT	Ni	Cr	V	Sc	Co	Ga	Rb	Ba	Cs	Sr
Pat04	57.22	0.85	16.89	7.88	0.14	5.02	7.49	2.90	1.37	0.15	0.31	100.08	46.30	137.7	155.70	20.40	-	18.50	56.70	225.30	4.84	272.00
Pat05	56.91	0.84	16.70	7.85	0.14	5.35	7.64	2.90	1.31	0.15	0.43	99.95	58.00	176.8	163.10	20.50	-	17.20	54.00	213.10	4.80	258.00
Pat07	61.28	0.77	17.49	6.41	0.12	3.01	6.38	3.00	1.56	0.16	1.14	100.33	14.40	23.70	143.00	14.90	-	18.60	69.30	251.10	5.70	296.50
Pat09	61.44	0.75	17.38	6.45	0.12	3.10	6.50	3.24	1.61	0.16	0.98	100.94	10.60	19.50	122.80	14.00	-	18.20	67.20	253.40	5.85	302.20
Pap10	63.60	0.73	16.59	5.73	0.11	1.99	5.41	3.51	2.04	0.16	0.09	100.00	5.70	9.40	93.60	18.40	-	16.30	80.40	330.90	2.36	225.30
Pap11	62.92	0.73	16.89	5.70	0.10	2.19	5.64	3.18	1.92	0.16	0.84	99.60	6.00	9.90	98.00	20.00	-	16.40	71.00	305.70	2.18	233.10
Pap14	63.42	0.74	16.80	5.53	0.10	1.97	5.43	3.33	1.94	0.15	1.14	99.56	6.00	9.20	103.90	19.30	-	16.00	72.10	315.00	1.99	227.30
Pap15	55.98	0.95	18.03	9.04	0.15	3.81	8.03	2.73	1.04	0.12	-0.10	100.06	6.90	11.10	227.20	32.50	-	18.10	31.70	230.90	0.96	262.40
Pap16	62.79	0.73	16.90	6.39	0.14	2.11	5.76	3.33	1.96	0.15	0.47	100.40	5.70	11.40	111.10	19.10	-	17.10	75.10	316.60	2.10	233.60
Pap17	63.48	0.72	16.80	6.02	0.12	2.06	5.58	3.35	2.03	0.16	0.44	100.47	6.60	10.10	94.10	19.30	-	10.10	77.40	321.40	2.55	323.00
Pap18	57.53	0.83	18.78	7.52	0.13	2.77	7.97	3.01	1.36	0.15	0.09	100.21	7.60	12.80	180.70	23.20	-	18.00	49.10	229.10	1.73	290.70
Gal32a	49.14	0.83	15.93	10.32	0.17	10.33	11.19	2.23	0.36	0.10	-0.51	100.84	163.1	541.0	269.30	39.70	-	15.30	7.50	85.20	0.58	208.20
Gal32b	49.06	0.84	15.93	10.18	0.17	10.14	11.15	2.19	0.36	0.10	-0.49	100.35	157.8	521.5	265.60	39.00	-	16.10	7.50	88.10	0.63	207.40
Gal33	56.27	0.89	19.87	7.47	0.14	2.35	8.09	4.04	0.81	0.22	-0.26	100.29	5.70	5.70	139.00	21.80	-	19.80	18.10	186.70	0.63	284.10
Gal34	56.79	0.71	18.22	7.74	0.16	3.62	7.99	3.64	0.77	0.16	-0.16	99.95	14.40	35.20	148.10	19.10	-	17.80	18.20	186.00	1.56	266.10
Gal35	55.99	0.74	18.73	8.13	0.17	3.57	8.23	3.72	0.73	0.17	-0.40	100.29	8.20	9.80	152.60	18.70	-	18.60	16.10	186.00	0.86	275.10
Gal36	55.98	0.74	17.88	8.17	0.16	4.35	8.36	3.49	0.73	0.15	-0.27	100.16	25.00	70.30	162.10	21.00	-	17.70	17.70	175.60	1.49	259.60
Gal37a	54.77	0.84	18.94	8.35	0.15	4.31	8.63	3.66	0.54	0.16	-0.13	100.48	14.90	25.40	177.10	25.00	-	19.30	12.50	147.70	0.58	277.10
Gal37b	54.58	0.84	18.95	8.47	0.14	4.30	8.66	3.67	0.60	0.16	-0.17	100.51	16.10	25.40	178.40	24.80	-	18.60	10.00	148.10	0.69	279.00
Tan01	57.11	1.24	15.36	10.91	0.20	2.12	5.71	3.09	3.46	0.46	0.87	99.96	4.90	2.10	166.20	23.20	-	17.50	137.40	498.70	5.14	221.60
Tan02	54.30	0.93	17.32	9.90	0.18	3.78	8.19	2.81	2.29	0.31	0.74	100.23	22.50	52.30	177.80	22.10	-	18.80	99.50	359.20	2.68	312.50
Tan03	54.52	0.95	17.41	9.93	0.18	3.45	7.92	2.98	2.36	0.32	0.79	100.22	22.60	57.40	182.30	23.00	-	18.00	102.50	367.70	2.36	314.00

Cs, Ta, Hf, Th, U and REE analysed by ICP-MS. Remaining elements analysed by XRF.

Sample	La	Ce	Pr	Nd	Sm	Eu	Gd	Tb	Dy	Ho	Er	Tm	Yb	Lu	Y	Nb	Ta	Zr	Hf	Th	U	Pb
Pat04	12.45	26.26	3.52	14.51	3.26	1.01	3.38	0.52	2.95	0.58	1.62	0.25	1.59	0.26	17.90	4.00	0.33	97.20	2.56	5.71	1.37	11.70
Pat05	11.73	24.68	3.33	13.99	3.19	0.99	3.42	0.53	3.01	0.58	1.63	0.25	1.61	0.27	18.00	3.80	0.32	95.80	2.52	5.45	1.34	9.90
Pat07	14.57	03.57	4.11	17.00	3.89	1.07	3.95	0.59	3.19	0.60	1.66	0.26	1.60	0.27	19.80	4.30	0.39	116.00	2.76	6.50	1.62	13.40
Pat09	13.24	27.35	3.62	14.54	3.21	0.98	3.18	0.48	2.70	0.53	1.47	0.24	1.44	0.23	16.10	4.30	0.39	114.90	2.76	6.62	1.66	13.30
Pap10	20.66	43.60	5.79	23.44	5.03	1.18	5.25	0.84	5.02	1.06	2.93	0.47	2.93	0.49	32.20	6.80	0.55	179.70	4.64	8.73	1.71	8.90
Pap11	20.05	42.67	5.69	23.02	5.08	1.26	5.35	0.86	5.05	1.05	2.89	0.46	2.95	0.48	31.50	6.80	0.53	177.10	4.50	8.01	1.55	10.00
Pap14	24.14	51.29	6.93	28.51	6.33	1.61	7.04	1.08	6.25	1.31	3.52	0.55	3.44	0.56	38.60	7.10	0.55	178.70	4.61	8.25	1.58	11.40
Pap15	13.23	27.88	3.80	15.80	3.60	1.09	4.14	0.67	4.03	0.90	2.25	0.35	2.22	0.37	24.00	5.30	0.39	117.70	3.06	3.15	0.55	6.80
Pap16	19.61	41.35	5.51	22.18	4.93	1.18	5.13	0.83	4.85	1.00	2.84	0.45	2.91	0.48	32.00	6.90	0.55	178.00	4.53	8.00	1.58	9.50
Pap17	19.81	41.62	5.60	22.90	4.96	1.20	5.45	0.85	5.09	1.07	2.97	0.48	3.07	0.51	34.80	7.20	0.54	182.50	4.53	8.27	1.61	10.30
Pap18	15.16	31.66	4.35	17.91	4.06	1.08	4.29	0.67	3.90	0.80	2.31	0.37	2.28	0.38	25.30	4.80	0.38	129.40	3.33	5.04	0.93	8.50
Gal32a	4.03	9.60	1.49	7.15	2.05	0.78	2.71	0.45	2.69	0.55	1.61	0.25	1.58	0.26	16.90	1.80	0.13	46.00	1.23	0.82	0.19	3.80
Gal32b	4.12	9.65	1.49	7.16	2.05	0.80	2.75	0.45	2.72	0.54	1.62	0.25	1.57	0.26	16.90	2.20	0.13	46.50	1.23	0.82	0.20	3.90
Gal33	9.65	21.83	3.20	14.68	3.63	1.19	4.41	0.70	4.19	0.87	2.52	0.41	2.52	0.41	26.50	4.90	0.33	125.00	3.02	2.36	0.56	6.70
Gal34	8.29	17.88	2.50	11.00	2.64	0.92	3.28	0.52	2.97	0.60	1.80	0.29	1.84	0.31	18.90	3.40	0.25	91.20	2.22	1.95	0.46	6.80
Gal35	7.85	17.16	2.43	10.86	2.73	1.00	3.30	0.53	3.10	0.63	1.89	0.29	1.98	0.33	19.90	3.50	0.24	86.40	2.18	1.77	0.42	6.50
Gal36	7.99	17.25	2.44	10.61	2.71	0.92	3.20	0.53	3.04	0.61	1.81	0.29	1.85	0.32	19.00	3.30	0.24	85.90	2.16	1.86	0.43	6.50
Gal37a	6.55	15.22	2.31	10.76	2.82	0.96	3.52	0.57	3.30	0.68	1.97	0.31	2.00	0.33	21.40	3.60	0.24	101.30	2.52	1.45	0.36	4.50
Gal37b	6.64	15.55	2.35	10.89	2.85	0.97	3.53	0.56	3.37	0.71	1.98	0.32	2.02	0.34	20.80	3.50	0.23	102.00	2.53	1.46	0.38	5.30
Tan01	38.72	81.18	10.39	42.66	8.78	1.52	8.26	1.32	7.54	1.57	4.27	0.67	4.29	0.70	47.20	12.40	0.83	322.10	7.72	22.07	4.69	20.70
Tan02	26.64	55.06	7.03	28.60	5.99	1.23	5.61	0.88	5.00	1.05	2.86	0.45	2.87	0.47	31.30	7.30	0.51	198.10	4.81	13.85	2.93	11.70
Tan03	27.99	58.02	7.48	30.42	6.40	1.29	5.85	0.93	5.26	1.09	3.01	0.48	3.08	0.49	33.30	7.40	0.53	203.10	5.03	14.63	3.05	12.80

Sample	SiO$_2$	TiO$_2$	Al$_2$O$_3$	Fe$_2$O$_3$	MnO	MgO	CaO	Na$_2$O	K$_2$O	P$_2$O$_5$	LOI	TOT	Ni	Cr	V	Sc	Co	Ga	Rb	Ba	Cs	Sr
Tan19	61.41	0.59	17.32	5.85	0.09	3.02	6.60	3.39	1.11	0.13	1.07	99.61	10.30	24.10	127.40	18.00	-	17.70	34.50	197.20	0.63	249.70
Tan20	62.66	0.61	17.97	5.15	0.04	2.22	6.36	3.63	1.17	0.13	1.10	100.06	10.70	27.80	139.20	18.90	-	18.80	37.70	209.50	0.77	260.50
Tan21a	64.14	0.61	18.68	3.83	0.03	0.98	6.39	3.75	1.19	0.13	1.61	99.85	8.30	26.20	135.80	18.60	-	18.90	36.40	213.70	0.84	263.30
Tan22a	63.99	0.66	16.85	5.28	0.12	1.95	5.83	3.66	1.42	0.17	2.82	100.05	7.70	20.50	67.20	10.10	-	18.10	47.00	238.30	2.87	260.40
Tan22b	63.83	0.65	16.70	5.13	0.13	1.79	6.17	3.62	1.56	0.16	3.78	99.85	7.40	22.60	73.20	12.00	-	17.60	51.40	259.10	3.39	244.40
Tan22c	63.68	0.67	16.91	5.30	0.09	2.35	5.61	3.62	1.43	0.17	2.13	99.94	8.80	22.20	70.00	10.80	-	18.10	46.00	240.80	2.07	258.90
Tan23	57.82	1.15	18.66	7.76	0.12	2.36	7.08	3.91	0.82	0.23	0.67	100.05	3.10	5.00	83.50	10.20	-	20.50	21.30	149.00	1.16	299.50
Tan24a	64.80	0.67	17.44	5.72	0.11	1.08	4.62	3.46	1.37	0.16	3.38	99.53	11.90	36.40	89.40	13.10	-	18.30	41.60	211.40	1.73	261.90
Tan24b	64.80	0.67	17.44	5.72	0.11	1.08	4.62	3.46	1.37	0.16	3.38	99.52	13.10	46.50	90.70	13.90	-	18.50	45.90	226.80	1.70	215.60
Tan24c	64.48	0.66	17.49	6.08	0.12	1.24	4.83	3.54	1.34	0.17	3.31	100.06	13.80	46.00	90.60	13.80	-	18.80	45.00	226.30	1.58	225.70
Tan25	55.75	0.99	19.44	8.40	0.16	3.32	7.41	2.96	0.77	0.16	6.24	99.54	125.6	125.2	228.20	31.00	-	19.70	24.00	129.30	1.30	241.90
Tan31	55.37	0.71	17.04	8.25	0.16	5.46	7.97	3.27	1.54	0.30	-0.09	100.26	119.3	154.0	142.10	17.90	-	17.50	59.80	205.70	1.33	459.50
Ged26a	59.30	0.73	17.48	7.10	0.14	3.13	7.15	3.25	1.75	0.15	-0.03	100.36	6.50	5.80	136.70	17.40	-	17.90	65.20	306.40	4.09	306.10
Ged26b	59.06	0.73	17.69	7.28	0.14	3.07	7.32	3.28	1.72	0.15	-0.03	100.64	6.10	6.30	141.00	17.10	-	18.50	64.80	307.90	4.05	308.90
Ged26c	58.47	0.74	17.78	7.31	0.14	3.16	7.40	3.17	1.70	0.15	-0.09	100.17	6.10	5.10	146.90	17.20	-	17.80	63.90	298.80	4.15	306.50
Ged26d	58.74	0.73	17.60	7.32	0.14	3.12	7.41	3.17	1.70	0.15	-0.06	100.26	6.50	6.80	153.40	19.10	-	18.70	63.00	297.70	4.14	306.10
Ged27a	59.02	0.72	17.64	7.13	0.14	3.09	7.29	3.21	1.72	0.14	-0.09	100.23	6.90	6.20	151.00	18.30	-	18.80	63.10	305.80	2.80	305.20
Ged27b	54.18	0.86	18.74	8.79	0.17	4.14	8.88	3.06	1.12	0.16	-0.09	100.25	8.90	8.90	197.70	23.10	-	19.90	36.90	219.80	2.00	357.10
Ged28a	58.43	0.75	17.66	7.36	0.14	3.17	7.36	3.22	1.69	0.15	-0.17	100.09	6.00	5.00	141.90	17.60	-	19.40	62.50	310.70	2.81	310.60
Ged28b	57.99	0.75	17.78	7.46	0.14	3.27	7.55	3.18	1.64	0.15	-0.11	100.06	5.90	6.90	148.70	17.50	-	19.10	61.10	297.60	3.84	311.90
Ged30	58.60	0.77	17.72	7.31	0.14	3.23	7.34	3.08	1.73	0.16	0.71	100.27	5.70	10.90	154.00	19.60	-	18.40	69.40	285.00	4.47	289.90

Sample	La	Ce	Pr	Nd	Sm	Eu	Gd	Tb	Dy	Ho	Er	Tm	Yb	Lu	Y	Nb	Ta	Zr	Hf	Th	U	Pb
Tan19	11.33	23.12	2.94	11.95	2.61	0.86	2.63	0.41	2.40	0.49	1.31	0.21	1.34	0.23	15.40	3.10	0.26	100.10	1.82	3.95	1.16	6.90
Tan20	11.54	23.64	2.99	12.21	2.52	0.86	2.47	0.37	2.07	0.41	1.09	0.18	1.08	0.18	12.90	3.10	0.28	103.30	2.04	4.19	1.20	8.30
Tan21a	12.03	24.26	3.11	12.64	2.57	0.87	2.47	0.36	1.94	0.38	0.93	0.14	0.83	0.13	12.50	3.10	0.28	108.40	1.97	4.29	1.00	7.60
Tan22a	13.25	27.51	3.51	14.75	3.13	0.99	2.94	0.42	2.03	0.37	0.90	0.13	0.80	0.12	13.30	3.90	0.35	130.80	0.63	2.78	0.49	6.70
Tan22b	12.97	27.02	3.46	14.51	3.13	0.97	2.89	0.43	2.07	0.37	0.92	0.14	0.84	0.13	13.50	3.90	0.34	126.90	0.65	2.97	0.51	7.20
Tan22c	13.11	24.47	3.50	14.57	3.12	0.97	2.81	0.40	2.03	0.36	0.89	0.13	0.83	0.13	13.50	3.90	0.34	131.20	0.72	3.21	0.60	7.10
Tan23	11.06	26.09	3.77	17.55	4.34	1.39	4.69	0.68	3.20	0.53	1.12	0.15	0.83	0.13	16.20	5.50	0.41	154.30	3.73	2.65	0.66	5.20
Tan24a	12.05	25.49	3.30	13.65	3.01	0.99	2.80	0.40	2.07	0.37	0.92	0.14	0.85	0.14	12.60	4.50	0.33	128.50	1.72	4.63	1.07	6.50
Tan24b	13.47	27.79	3.58	14.99	3.19	1.03	3.10	0.47	2.47	0.46	1.22	0.18	1.17	0.19	15.50	4.30	0.35	133.60	1.72	4.61	1.06	6.50
Tan24c	12.69	26.18	3.37	13.85	3.01	0.98	3.00	0.44	2.34	0.46	1.15	0.18	1.13	0.18	15.50	4.10	0.32	128.00	1.68	4.40	1.00	7.10
Tan25	7.92	17.82	2.56	11.75	3.04	1.06	3.57	0.58	3.29	0.66	1.78	0.27	1.72	0.28	20.60	3.10	0.22	100.80	2.22	1.96	0.63	7.00
Tan31	28.26	56.38	7.10	28.25	5.26	1.41	4.14	0.62	3.46	0.70	1.88	0.31	2.02	0.33	21.50	4.70	0.33	114.60	2.68	10.44	1.96	4.50
Ged26a	16.74	34.51	4.47	18.68	4.08	1.05	4.07	0.65	3.77	0.78	2.15	0.35	2.19	0.36	23.60	5.10	0.39	143.80	3.55	7.07	1.62	13.10
Ged26b	15.84	32.61	4.26	17.53	3.83	1.00	3.96	0.63	3.62	0.76	2.04	0.32	2.12	0.35	23.80	5.00	0.39	144.10	3.48	6.82	1.56	13.20
Ged26c	15.87	32.84	4.29	17.63	3.96	1.05	4.08	0.64	3.68	0.78	2.10	0.34	2.15	0.36	23.60	5.00	0.40	138.60	3.52	6.87	1.56	10.60
Ged26d	16.33	33.82	4.39	18.32	4.39	18.32	4.00	1.06	4.06	0.64	2.13	0.35	2.15	0.36	23.40	4.70	0.39	139.80	3.60	6.89	1.57	12.60
Ged27a	15.06	31.65	4.15	17.33	3.89	1.01	3.76	0.62	3.57	0.72	1.98	0.32	2.04	0.33	22.90	4.90	0.38	139.30	3.01	6.22	1.45	9.70
Ged27b	12.06	25.28	3.44	14.70	3.44	1.06	3.71	0.59	3.38	0.70	1.90	0.30	1.90	0.31	21.10	3.90	0.28	97.40	2.02	3.91	0.85	5.10
Ged28a	14.68	30.49	4.00	16.85	3.78	1.06	3.83	0.61	3.53	0.74	1.97	0.33	2.03	0.34	22.80	4.90	0.38	139.60	3.48	6.74	1.55	11.30
Ged28b	15.36	31.74	4.16	17.35	3.85	1.03	3.98	0.63	3.60	0.75	2.04	0.32	2.04	0.33	23.10	4.70	0.38	131.90	3.22	6.36	1.42	11.00
Ged30	17.07	36.26	4.81	20.42	4.49	1.12	4.69	0.74	4.28	0.89	2.41	0.38	2.41	0.39	27.20	5.30	0.42	158.90	3.97	7.50	1.72	12.10

Table B.2. Major- and trace-element data for Sumbing volcano.

Sample	SiO$_2$	TiO$_2$	Al$_2$O$_3$	Fe$_2$O$_3$	MnO	MgO	CaO	Na$_2$O	K$_2$O	P$_2$O$_5$	LOI	TOT	Ni	Cr	V	Sc	Co	Ga	Rb	Ba	Cs	Sr
Sumb69	56.71	0.71	18.31	8.27	0.19	2.78	7.27	3.61	2.10	0.31	-0.11	100.30	6.47	2.04	131.38	12.19	15.87	18.81	53.60	590.42	3.57	573.38
Sumb71	56.21	0.72	18.15	8.25	0.19	2.80	7.26	3.60	2.06	0.31	-0.17	99.61	6.67	4.04	126.44	11.96	15.13	18.51	53.44	576.98	3.65	574.01
Sumb72	61.47	0.59	17.88	5.69	0.14	2.20	5.54	4.01	2.12	0.20	1.24	99.89	5.86	5.52	83.94	9.77	8.18	18.25	56.49	508.07	3.69	317.84
Sumb73	61.65	0.59	17.76	5.66	0.14	2.18	5.48	4.02	2.15	0.19	1.08	99.88	6.02	6.41	81.82	9.53	8.99	18.34	57.85	500.00	3.82	308.36
Sumb74	60.29	0.62	18.53	5.98	0.15	2.29	5.65	3.96	1.98	0.20	1.32	99.66	6.42	7.40	89.65	10.40	11.12	18.84	52.12	530.85	3.63	326.68
Sumb76	55.16	0.94	19.64	8.28	0.17	2.75	7.16	3.92	1.74	0.26	0.09	100.09	5.78	3.06	157.52	16.91	17.09	21.15	32.12	359.86	1.68	348.79
Sumb77	55.01	0.94	19.71	8.25	0.17	2.75	7.03	3.90	1.75	0.27	0.14	99.82	5.51	1.94	154.53	15.81	17.07	21.25	31.50	361.78	1.66	348.96
Sumb78	56.45	0.71	18.23	8.20	0.19	2.74	7.22	3.61	2.08	0.31	-0.01	99.81	7.47	6.33	116.84	13.32	13.08	20.17	65.24	420.20	3.21	322.99
Sumb80	58.13	0.75	18.21	7.19	0.15	3.07	6.63	3.53	1.96	0.21	0.77	99.85	11.12	22.87	123.44	14.12	15.64	19.08	58.78	555.51	4.64	393.32
Sumb81	53.65	1.01	18.63	8.84	0.16	3.93	8.32	3.31	1.51	0.22	-0.42	99.63	8.01	9.19	207.22	24.52	18.39	19.42	39.44	354.12	1.48	356.56
Sumb83	61.70	0.61	17.21	5.64	0.14	2.14	5.56	3.72	2.32	0.22	0.84	99.34	5.49	4.17	78.25	9.58	6.86	17.95	74.62	514.07	5.04	397.42
Sumb85	58.81	0.77	17.91	7.01	0.15	2.49	6.45	3.80	2.09	0.24	0.23	99.73	5.77	6.43	114.53	12.10	13.25	19.29	61.68	414.09	4.04	305.18
Sumb91	60.27	0.74	17.09	6.45	0.15	2.64	6.92	3.54	1.80	0.15	0.26	99.76	8.26	8.53	134.14	14.38	10.61	18.23	45.60	642.68	3.50	288.69
Sumb92	60.35	0.72	17.24	6.31	0.14	2.60	6.95	3.55	1.80	0.15	0.39	99.84	8.66	8.76	130.05	13.67	11.66	17.90	45.86	640.95	3.57	291.08
Sumb94	54.49	0.83	18.80	8.11	0.18	2.80	8.62	3.64	2.19	0.25	0.24	99.97	7.94	6.60	195.38	15.24	16.89	18.80	52.04	550.43	4.40	558.17
Sumb95	54.50	0.92	18.53	8.70	0.16	3.09	8.43	3.66	1.58	0.30	0.06	99.93	9.02	5.32	155.97	15.25	17.68	19.45	38.35	375.02	2.15	564.18
Sumb96	53.08	0.83	19.26	8.50	0.20	2.88	9.14	3.49	2.00	0.30	-0.27	99.73	8.02	5.16	169.88	13.12	14.72	19.46	43.75	528.41	2.06	605.90
Sumb97	55.07	0.76	19.01	7.71	0.19	2.42	8.36	3.71	2.15	0.30	-0.26	99.71	7.95	4.13	132.22	9.80	11.34	20.53	54.01	527.40	4.05	609.50
Sumb98	54.87	0.79	18.79	8.14	0.18	2.76	8.55	3.62	1.73	0.26	-0.13	99.75	8.28	6.57	152.18	11.52	13.91	19.87	45.36	487.09	1.66	592.80
Sumb99	53.28	0.81	18.83	8.70	0.20	3.18	9.09	3.41	2.03	0.30	0.10	99.90	10.54	9.68	181.39	13.84	15.81	19.57	53.05	550.86	2.78	615.08

Cs, Ta, Hf, Th, U and REE analysed by ICP-MS. Remaining elements analysed by XRF.

Sample	La	Ce	Pr	Nd	Sm	Eu	Gd	Tb	Dy	Ho	Er	Tm	Yb	Lu	Y	Nb	Ta	Zr	Hf	Th	U	Pb
Sumb69	24.50	49.29	6.20	25.16	5.30	1.45	5.08	0.78	4.37	0.90	2.47	0.40	2.62	0.44	27.17	6.70	0.40	138.82	3.40	7.88	1.66	17.67
Sumb71	25.15	50.17	6.53	26.16	5.56	1.46	5.39	0.79	4.51	0.94	2.54	0.41	2.75	0.44	27.27	6.49	0.41	137.92	3.30	7.63	1.60	17.37
Sumb72	18.53	35.80	4.43	17.01	3.51	1.03	3.40	0.55	3.29	0.69	1.92	0.33	2.22	0.36	21.04	10.51	0.76	189.06	3.89	7.11	1.67	14.86
Sumb73	19.91	37.67	4.73	18.50	3.81	1.08	3.64	0.58	3.50	0.75	2.06	0.34	2.26	0.38	21.33	10.39	0.77	187.25	3.89	6.92	1.61	14.99
Sumb74	19.53	39.06	4.79	18.71	3.85	1.16	3.72	0.61	3.55	0.75	2.10	0.35	2.29	0.39	21.08	10.87	0.81	193.45	4.11	7.22	1.65	15.55
Sumb76	21.05	42.35	5.80	24.50	5.41	1.55	5.75	0.92	5.55	1.18	3.20	0.51	3.20	0.55	31.29	13.45	0.88	196.92	4.49	5.31	1.23	12.57
Sumb77	21.11	42.96	5.87	24.56	5.51	1.53	5.74	0.94	5.49	1.15	3.19	0.52	3.24	0.54	31.56	13.66	0.88	197.55	4.51	5.27	1.23	12.15
Sumb78	24.74	49.85	6.47	25.97	5.60	1.53	5.24	0.76	4.48	0.94	2.53	0.42	2.71	0.44	27.26	14.47	0.40	216.33	3.46	7.91	1.64	13.06
Sumb80	20.33	40.81	5.20	20.62	4.29	1.19	4.24	0.67	3.87	0.80	2.22	0.36	2.29	0.38	21.84	11.33	0.80	173.55	3.97	8.04	1.87	16.10
Sumb81	15.83	33.34	4.61	19.87	4.76	1.40	5.11	0.80	4.76	0.97	2.69	0.42	2.63	0.44	25.83	7.73	0.54	133.55	3.31	5.06	1.18	8.42
Sumb83	30.09	60.06	7.57	29.79	5.87	1.47	5.04	0.81	4.70	0.99	2.76	0.45	2.94	0.50	26.61	8.17	0.61	194.62	4.67	11.60	2.50	17.48
Sumb85	25.87	51.64	6.62	25.91	5.42	1.50	4.94	0.79	4.65	0.97	2.65	0.42	2.70	0.47	25.63	13.66	0.97	203.73	4.32	7.46	1.78	12.67
Sumb91	17.58	33.92	4.33	17.61	3.94	1.16	3.99	0.66	3.72	0.78	2.12	0.34	2.18	0.37	20.77	6.36	0.54	132.48	3.36	5.75	1.30	10.44
Sumb92	17.41	33.42	4.29	17.06	3.77	1.13	3.77	0.59	3.57	0.74	2.04	0.33	2.12	0.36	20.49	6.39	0.50	130.89	3.23	5.58	1.25	9.90
Sumb94	21.13	41.27	5.41	22.85	5.12	1.53	4.86	0.74	4.27	0.89	2.41	0.38	2.44	0.41	23.28	3.49	0.23	89.66	2.44	6.63	1.48	19.81
Sumb95	21.11	43.31	5.85	25.01	5.64	1.76	5.36	0.80	4.69	0.97	2.63	0.40	2.53	0.43	25.65	5.21	0.35	116.24	2.42	4.80	1.07	11.39
Sumb96	21.28	42.85	5.74	24.78	5.57	1.66	5.27	0.80	4.71	0.96	2.62	0.41	2.53	0.42	25.18	3.88	0.27	90.89	2.28	5.70	1.25	13.46
Sumb97	23.93	47.79	6.26	26.15	5.66	1.68	5.11	0.81	4.67	0.97	2.69	0.43	2.67	0.44	25.59	4.66	0.31	110.24	2.78	7.04	1.53	19.37
Sumb98	19.90	39.87	5.32	22.48	5.05	1.50	4.62	0.71	4.15	0.86	2.32	0.37	2.32	0.39	22.85	3.91	0.26	96.09	2.31	5.08	1.22	14.27
Sumb99	21.82	42.96	5.63	23.69	5.36	1.61	5.00	0.77	4.35	0.89	2.41	0.38	2.41	0.40	23.50	3.32	0.23	81.96	2.19	6.37	1.38	15.79

245

Table B.3. Major- and trace-element data for Kelut volcano.

Sample	SiO2	TiO2	Al2O3	Fe2O3	MnO	MgO	CaO	Na2O	K2O	P2O5	LOI	TOT	Ni	Cr	V	Sc	Co	Ga	Rb	Ba	Cs	Sr
Kel12	59.04	0.55	18.18	7.23	0.19	2.79	7.56	3.24	0.93	0.18	0.21	99.91	7.50	2.65	90.40	12.19	21.02	20.38	22.45	720.24	1.39	527.23
Kel14	59.69	0.50	19.00	6.02	0.26	1.80	7.98	3.34	0.72	0.21	0.19	99.53	5.03	3.55	46.47	6.89	8.01	16.61	15.97	724.77	1.11	719.91
Kel22	57.14	0.69	18.51	7.71	0.18	3.07	8.42	2.94	0.86	0.14	0.52	99.68	7.99	6.82	140.44	18.04	15.30	17.90	19.64	584.43	1.28	517.82
Kel23	58.90	0.54	18.95	6.76	0.24	2.07	7.81	3.36	0.75	0.22	-0.11	99.62	5.65	3.46	64.18	8.98	9.45	16.79	15.02	687.74	0.26	687.66
Kel25	53.53	0.74	19.03	9.16	0.21	3.58	9.71	2.75	0.73	0.120	0.34	99.56	7.54	4.69	174.90	19.24	16.64	15.71	13.93	515.47	0.90	537.70
Kel26	55.91	0.65	18.73	8.32	0.19	3.48	8.78	2.91	0.83	0.14	0.46	99.99	8.74	3.90	133.85	15.60	15.66	17.84	19.18	647.43	1.26	596.70
Kel27	56.66	0.63	18.56	8.02	0.19	3.33	8.54	2.94	0.86	0.14	0.57	99.90	8.27	2.90	140.92	15.98	15.62	17.72	19.60	628.61	1.29	580.67
Kel34	56.99	0.61	18.76	7.81	0.20	2.83	8.76	2.91	0.75	0.14	0.11	99.83	7.57	6.09	121.21	13.29	12.57	16.00	16.36	620.03	0.55	584.06
Kel37	41.68	0.29	27.31	8.35	0.09	5.84	16.03	0.49	0.02	0.01	-0.23	100.17	24.41	9.90	207.28	12.94	33.48	14.93	b.d.	45.21	0.03	626.89
Kel38	43.66	0.84	21.26	11.58	0.20	6.33	14.31	1.19	0.09	0.01	0.11	99.52	22.80	26.47	381.75	41.97	34.22	18.34	0.38	79.75	0.04	585.58
Kel40	54.43	0.67	18.76	9.00	0.20	3.89	9.14	2.90	0.69	0.14	0.36	99.86	10.91	10.88	165.25	18.48	18.10	15.98	13.24	479.60	1.00	608.06
Kel43	57.29	0.61	18.62	7.59	0.20	2.64	8.68	3.04	0.77	0.15	0.09	99.64	8.03	13.52	105.48	10.62	9.73	16.15	16.07	628.09	1.04	594.82
Kel45	55.25	0.71	18.75	8.77	0.21	3.39	8.70	2.90	0.82	0.12	0.14	99.66	7.16	7.52	171.39	17.30	15.65	15.14	17.79	582.80	0.53	467.32
Kel48	54.92	0.67	18.59	8.85	0.20	3.77	9.01	2.91	0.68	0.14	0.14	99.79	11.26	11.90	154.20	18.35	17.01	16.01	13.47	530.48	0.96	604.29
Kel50	55.38	0.64	18.63	8.28	0.21	3.63	8.53	2.74	1.03	0.13	0.54	99.25	11.17	8.18	174.79	23.36	22.42	17.60	18.34	637.97	1.10	547.48
Kel51	54.98	0.66	18.70	8.83	0.20	3.80	8.99	2.93	0.69	0.14	-0.14	100.00	10.79	11.98	151.12	17.31	16.95	16.04	13.49	499.55	0.98	606.47
Kel53	41.03	1.75	15.05	17.17	0.16	11.91	10.61	1.54	0.21	0.02	0.04	99.54	46.27	51.33	724.54	90.24	66.45	15.05	0.61	132.94	0.02	311.32
Kel56	54.16	0.69	18.36	9.12	0.20	4.31	9.04	2.90	0.69	0.14	-0.24	99.68	17.95	26.23	171.72	19.59	20.34	16.26	13.14	457.60	0.99	603.59
Kel59	58.89	0.54	19.00	6.76	0.25	2.12	7.92	3.40	0.75	0.21	-0.13	99.85	4.91	1.09	63.80	9.29	7.70	16.82	16.66	687.75	0.51	691.12
Kel60	59.01	0.54	18.96	6.77	0.25	2.11	7.97	3.40	0.74	0.21	-0.36	99.99	5.50	2.43	65.57	8.56	8.54	16.82	15.12	672.87	0.33	689.02
Kel61	57.03	0.65	18.56	7.70	0.18	3.23	8.38	3.01	0.83	0.14	-0.26	99.76	8.63	5.57	132.29	15.96	14.55	18.51	20.83	656.45	1.04	571.64
Kel64	58.96	0.55	19.04	6.84	0.25	2.11	7.95	3.42	0.74	0.22	-0.19	100.10	5.09	1.02	65.85	8.74	8.22	16.87	16.65	671.41	0.50	690.74

Cs, Ta, Hf, Th, U and REE analysed by ICP-MS. Remaining elements analysed by XRF.

Sample	La	Ce	Pr	Nd	Sm	Eu	Gd	Tb	Dy	Ho	Er	Tm	Yb	Lu	Y	Nb	Ta	Zr	Hf	Th	U	Pb
Kel12	10.27	21.54	3.00	12.72	2.95	0.98	3.30	0.49	2.99	0.64	1.82	0.31	2.03	0.34	19.34	3.01	0.23	102.53	2.64	2.60	0.65	12.20
Kel14	7.94	17.67	2.65	12.12	3.15	1.11	3.61	0.57	3.44	0.73	2.10	0.35	2.35	0.41	22.25	1.86	0.13	69.96	1.87	1.41	0.48	12.12
Kel22	8.31	17.82	2.47	10.99	2.83	0.96	3.27	0.52	3.16	0.67	1.91	0.30	2.05	0.35	20.06	2.79	0.21	86.59	2.34	2.05	0.54	9.95
Kel23	8.27	17.86	2.54	12.37	3.12	1.15	3.60	0.57	3.43	0.75	2.12	0.35	2.33	0.41	22.06	1.95	0.12	65.90	0.87	1.93	0.50	9.13
Kel25	5.15	11.50	1.75	8.33	2.29	0.85	2.97	0.47	2.93	0.62	1.78	0.28	1.89	0.32	18.29	1.37	0.09	56.03	1.53	1.06	0.38	4.68
Kel26	7.48	16.01	2.24	9.95	2.49	0.88	2.91	0.45	2.71	0.57	1.63	0.27	1.76	0.30	17.59	2.06	0.15	69.17	1.83	1.75	0.55	10.27
Kel27	7.67	16.19	2.30	10.10	2.47	0.88	2.80	0.45	2.75	0.58	1.64	0.28	1.79	0.30	17.77	2.19	0.15	70.92	1.84	1.69	0.54	10.40
Kel34	5.74	12.50	1.87	8.81	2.34	0.86	2.79	0.47	2.89	0.62	1.73	0.29	1.87	0.31	18.06	1.52	0.11	60.19	1.67	1.10	0.39	9.13
Kel37	0.26	0.52	0.10	0.52	0.13	0.15	0.26	0.04	0.26	0.06	0.14	0.02	0.13	0.02	1.61	0.01	0.02	0.31	0.11	0.01	0.01	0.97
Kel38	1.33	3.67	0.70	4.15	1.42	0.67	2.07	0.35	2.16	0.46	1.24	0.19	1.18	0.19	12.50	0.39	0.03	8.87	0.43	0.04	0.01	1.80
Kel40	5.54	12.16	1.85	8.69	2.22	0.86	2.69	0.44	2.68	0.58	1.63	0.26	1.72	0.30	16.56	1.20	0.09	46.02	1.33	0.96	0.37	9.13
Kel43	6.07	13.23	2.00	9.47	2.43	0.89	3.02	0.50	2.99	0.65	1.82	0.30	1.95	0.33	18.83	1.75	0.12	64.08	1.77	1.16	0.38	10.08
Kel45	5.64	12.63	1.87	8.70	2.30	0.86	2.94	0.48	2.99	0.64	1.80	0.30	1.87	0.32	18.87	1.52	0.12	57.51	0.97	0.87	0.25	8.01
Kel48	5.52	12.25	1.84	8.78	2.26	0.84	2.71	0.43	2.66	0.57	1.60	0.26	1.72	0.29	16.75	1.45	0.09	47.32	1.32	0.90	0.34	9.23
Kel50	7.79	16.96	2.45	11.23	2.88	0.97	3.30	0.53	3.19	0.66	1.85	0.31	1.92	0.33	18.88	1.96	0.14	62.56	1.75	1.47	0.50	8.22
Kel51	5.64	12.46	1.85	8.82	2.32	0.89	2.64	0.44	2.72	0.58	1.61	0.27	1.74	0.29	16.70	1.15	0.09	47.80	1.34	0.91	0.34	8.09
Kel53	1.73	4.81	0.93	5.71	2.24	0.87	3.58	0.62	3.90	0.83	2.13	0.32	1.88	0.28	21.55	0.56	0.05	21.46	0.93	0.21	0.08	1.85
Kel56	5.79	12.57	1.91	8.94	2.30	0.90	2.76	0.46	2.78	0.60	1.66	0.27	1.76	0.30	17.15	1.20	0.09	45.95	1.32	0.89	0.35	8.45
Kel59	7.61	16.81	2.55	11.98	3.03	1.15	3.55	0.56	3.41	0.73	2.05	0.33	2.24	0.38	21.27	1.48	0.12	63.31	1.12	1.04	0.31	9.44
Kel60	7.94	17.47	2.62	12.17	3.06	1.13	3.55	0.56	3.46	0.74	2.12	0.35	2.33	0.40	21.78	1.66	0.12	65.14	1.62	1.21	0.41	10.02
Kel61	8.73	18.41	2.54	11.23	2.72	0.94	2.99	0.49	2.84	0.59	1.66	0.27	1.74	0.29	17.81	2.54	0.19	77.90	0.71	1.64	0.40	9.94
Kel64	7.70	17.03	2.54	11.90	3.07	1.14	3.52	0.59	3.49	0.74	2.07	0.34	2.22	0.38	21.66	1.59	0.13	62.94	1.20	1.05	0.33	9.08

Table B.4. Major- and trace-element data for Agung volcano.

Sample	SiO$_2$	TiO$_2$	Al$_2$O$_3$	Fe$_2$O$_3$	MnO	MgO	CaO	Na$_2$O	K$_2$O	P$_2$O$_5$	LOI	TOT	Ni	Cr	V	Sc	Co	Ga	Rb	Ba	Cs	Sr
Agu03	58.01	0.76	17.55	7.98	0.18	2.92	7.22	3.34	1.69	0.27	0.09	99.92	8.11	4.61	140.68	16.41	16.65	19.06	40.93	311.67	1.06	427.44
Agu06	55.64	0.82	17.95	8.94	0.19	3.53	8.10	3.11	1.38	0.26	-0.06	99.97	9.73	3.85	168.74	18.97	19.86	19.42	33.34	264.80	0.87	450.71
Agu07	58.21	0.77	17.47	8.12	0.17	2.90	7.14	3.32	1.73	0.27	0.16	100.15	8.87	4.82	135.42	16.32	16.11	18.90	42.69	322.03	1.10	424.62
Agu10	50.31	1.13	17.17	12.62	0.21	5.77	8.67	2.84	0.83	0.19	-0.73	99.76	23.39	14.35	360.04	30.53	35.85	19.71	16.25	180.10	0.45	418.00
Agu12	54.92	0.88	18.09	9.39	0.20	3.45	7.97	3.38	1.17	0.21	-0.56	99.66	6.80	2.45	161.77	19.12	20.83	19.33	24.19	241.69	0.42	423.52
Agu13	49.97	1.13	17.67	11.67	0.21	5.04	8.93	2.90	0.88	0.20	-0.43	98.62	17.44	10.91	332.24	30.00	32.68	19.68	16.87	178.36	0.44	416.12
Agu15	62.41	0.61	16.77	6.15	0.16	1.82	5.73	3.59	2.14	0.25	-0.21	99.68	5.36	3.64	73.40	10.68	9.07	17.92	54.11	403.87	1.33	403.31
Agu16	59.93	0.70	16.84	6.99	0.16	2.30	6.21	3.45	2.03	0.25	-0.36	98.93	6.58	2.23	103.98	13.31	12.50	18.29	49.08	379.82	0.59	398.65
Agu18	52.02	1.02	18.26	9.94	0.18	4.24	8.49	3.30	1.06	0.24	-0.54	98.77	16.17	9.28	252.49	26.61	26.35	19.88	19.55	225.46	0.40	451.45
Agu20	62.69	0.60	16.74	6.04	0.15	1.77	5.67	3.59	2.19	0.24	0.07	99.72	5.41	1.28	68.89	9.79	8.27	17.95	55.53	403.61	1.44	402.96
Agu21	54.08	0.92	18.03	9.57	0.19	4.13	8.44	3.11	1.22	0.23	-0.03	99.98	17.12	47.02	221.50	20.93	22.50	20.21	27.62	241.80	0.56	440.91
Agu22	53.63	0.92	19.84	8.40	0.16	2.94	8.88	3.39	1.18	0.25	-0.29	99.68	6.61	5.10	204.02	25.59	18.73	19.59	24.49	216.05	0.58	455.49
Agu23	56.42	0.76	18.06	8.43	0.19	2.95	7.92	3.18	1.36	0.28	-0.29	99.58	5.38	2.58	133.68	15.11	15.96	19.11	32.72	285.13	0.59	474.08
Agu24	52.50	1.09	17.97	10.48	0.20	4.17	8.36	3.18	1.27	0.24	-0.20	99.52	10.88	5.20	268.07	27.28	27.27	19.60	27.50	218.17	0.64	404.22
Agu25	65.16	0.55	16.13	5.28	0.14	1.46	4.81	3.70	2.49	0.23	0.99	100.01	2.90	2.15	43.39	9.71	6.03	17.52	64.59	478.28	1.57	370.96
Agu30	56.35	0.80	17.81	8.58	0.18	3.25	7.68	3.20	1.49	0.27	-0.13	99.64	6.97	6.53	160.03	17.12	19.38	19.34	36.32	286.90	0.88	440.82
Agu31	53.84	0.85	18.01	9.54	0.19	4.31	8.77	2.95	1.16	0.25	-0.36	99.88	16.70	20.59	195.80	20.38	21.40	19.53	26.99	238.74	0.52	468.35
Agu33	53.74	0.85	18.21	9.57	0.19	4.15	8.77	2.96	1.13	0.25	-0.49	99.87	13.92	7.19	185.95	19.47	21.07	20.47	27.40	257.79	0.50	484.41

Cs, Ta, Hf, Th, U and REE analysed by ICP-MS. Remaining elements analysed by XRF.

Sample	La	Ce	Pr	Nd	Sm	Eu	Gd	Tb	Dy	Ho	Er	Tm	Yb	Lu	Y	Nb	Ta	Zr	Hf	Th	U	Pb
Agu03	17.76	37.67	5.21	22.90	5.25	1.40	5.32	0.86	5.01	1.05	2.86	0.47	2.99	0.51	29.13	5.75	0.39	138.99	3.94	4.16	1.22	6.25
Agu06	15.18	32.34	4.55	19.99	4.73	1.34	5.00	0.77	4.59	0.95	2.65	0.43	2.73	0.46	27.26	4.92	0.31	117.59	4.59	3.33	0.86	5.84
Agu07	18.10	38.18	5.30	22.72	5.21	1.42	5.39	0.88	5.08	1.07	2.94	0.48	3.01	0.51	29.79	5.99	0.38	143.87	5.29	4.17	0.90	7.09
Agu10	9.54	20.99	3.11	14.46	3.58	1.23	4.15	0.67	3.91	0.83	2.24	0.36	2.22	0.37	21.82	2.97	0.22	69.44	2.58	1.56	0.38	4.41
Agu12	12.15	26.28	3.79	17.22	4.23	1.35	4.72	0.76	4.51	0.93	2.58	0.41	2.65	0.44	25.76	3.98	0.27	93.79	2.29	2.74	0.75	4.29
Agu13	9.90	21.83	3.25	15.01	3.82	1.27	4.34	0.70	4.16	0.87	2.34	0.37	2.32	0.39	22.95	2.80	0.20	69.34	3.37	1.70	0.43	3.34
Agu15	21.26	41.81	5.61	23.39	5.16	1.32	5.25	0.83	4.93	1.04	2.88	0.47	3.06	0.52	30.95	6.91	0.48	174.05	4.84	5.77	1.28	7.74
Agu16	19.90	41.72	5.80	24.71	5.62	1.43	5.78	0.90	5.31	1.09	3.04	0.51	3.17	0.54	30.47	6.08	0.45	159.88	4.37	5.23	1.50	4.83
Agu18	11.57	24.89	3.58	16.26	3.99	1.29	4.47	0.70	4.14	0.86	2.35	0.38	2.36	0.39	23.69	3.57	0.23	81.03	1.51	2.07	0.46	2.13
Agu20	20.15	41.81	5.61	23.39	5.16	1.32	5.25	0.83	4.93	1.04	2.88	0.47	3.06	0.52	30.41	7.08	0.45	176.38	5.80	5.68	1.00	8.09
Agu21	12.92	27.11	3.77	16.95	4.14	1.29	4.58	0.71	4.22	0.86	2.40	0.38	2.44	0.40	24.93	4.09	0.26	95.45	2.63	2.66	0.77	3.68
Agu22	12.53	26.95	3.85	17.55	4.38	1.35	4.78	0.75	4.46	0.93	2.53	0.40	2.56	0.42	25.88	3.96	0.24	95.75	3.24	2.58	0.57	4.47
Agu23	15.89	33.61	4.72	20.71	4.76	1.36	4.89	0.77	4.61	0.95	2.67	0.42	2.76	0.46	27.32	4.91	0.33	118.36	3.33	3.22	0.82	6.08
Agu24	12.75	27.82	4.02	18.46	4.67	1.43	5.20	0.84	4.95	1.04	2.86	0.44	2.83	0.47	28.62	4.31	0.26	100.09	3.93	2.85	0.84	4.78
Agu25	21.66	44.33	5.85	24.49	5.38	1.30	5.42	0.87	5.08	1.07	2.97	0.48	3.19	0.54	31.74	7.45	0.50	195.57	7.17	6.45	1.75	10.11
Agu30	15.94	33.78	4.69	20.99	4.81	1.36	5.11	0.81	4.74	1.01	2.75	0.44	2.84	0.48	28.29	5.29	0.34	126.23	3.58	3.45	1.10	5.41
Agu31	12.81	27.47	3.91	17.87	4.19	1.29	4.62	0.71	4.14	0.85	2.34	0.37	2.35	0.39	24.73	3.80	0.25	92.55	2.57	2.67	0.58	4.58
Agu33	12.98	28.11	4.01	18.15	4.34	1.31	4.65	0.75	4.23	0.89	2.42	0.38	2.41	0.39	25.04	3.74	0.25	93.72	1.96	2.67	0.66	4.54

Appendix C

Whole-rock isotope data

Table C.1. Sr- Nd- Hf and Pb-isotope data for select west Java volcanoes.

Sample	$^{87}Sr/^{86}Sr_m$	2SE	$^{143}Nd/^{144}Nd_m$	2SE	$^{176}Hf/^{177}Hf_m$	2SE	$^{206}Pb/^{204}Pb_m$	2SE	$^{207}Pb/^{206}Pb_m$	2SE	$^{208}Pb/^{206}Pb_m$	2SE
Pat04												
Pat05	0.705748[c]	0.000011	0.512612[e]	0.000006	0.282896[j,m]	0.000007	18.9381[g]	0.0011	15.7362	0.0011	39.4128	0.0041
Pat07												
Pat09	0.705883[a]	0.000016	0.512579[e]	0.000006	0.282863[j]	0.000008	18.9455[g]	0.0012	15.7374	0.0014	39.4192	0.0056
Pap10	0.706307[a]	0.000013	0.512521[b]	0.000007	0.282816[n]	0.000005	18.9098[g]	0.0012	15.7251	0.0014	39.3428	0.0050
Pap11	0.706332[a]	0.000012	0.512513[b]	0.000010	0.282810[n]	0.000005	18.9119[g]	0.0009	15.7256	0.0010	39.3443	0.0032
Pap14	0.706328[a]	0.000012	0.512507[b]	0.000006	0.282808[n]	0.000005	18.9117[g]	0.0008	15.7247	0.0010	39.3418	0.0040
Pap15	0.706660[c]	0.000015	0.512368[e]	0.000009	0.282662[j]	0.000009	18.9451[g]	0.0015	15.7312	0.0017	39.3805	0.0059
Pap16	0.706327[a]	0.000009	0.512538[b]	0.000008	0.282789[n]	0.000010	18.9113[g]	0.0010	15.7238	0.0011	39.3389	0.0044
Pap17	0.706314[a]	0.000010	0.512533[b]	0.000009	0.282668[n]	0.000009	18.9097[g]	0.0010	15.7239	0.0013	39.3394	0.0049
Pap18	0.705904[c]	0.000011	0.512510[e]	0.000007	0.282813[j]	0.000006	18.9180[g]	0.0009	15.7261	0.0012	39.3561	0.0048
Gal32a	0.704455[c]	0.000014	0.512906[e]	0.000008	0.283165[m]	0.000008	18.7998[g]	0.0029	15.7030	0.0030	39.1947	0.0103
Gal32b	0.704453[c]	0.000016	0.512903[e]	0.000009		0.000009	18.7973[g]	0.0021	15.7004	0.0022	39.1890	0.0069
Gal33	0.704320[c]	0.000015	0.512934[e]	0.000009	0.283162[m]	0.000008	18.7999[g]	0.0009	15.6969	0.0008	39.1724	0.0032
Gal34	0.704443[c]	0.000013	0.512959[e]	0.000008	0.283141[m]	0.000007	18.7936[g]	0.0016	15.6979	0.0019	39.1816	0.0071
Gal35	0.704414[c]	0.000015	0.512936[e]	0.000008	0.283142[m]	0.000008	18.7944[g]	0.0011	15.6976	0.0012	39.1779	0.0042
Gal36												
Gal37a	0.704198[c]	0.000015	0.512937[e]	0.000010	0.283160[m]	0.000007	18.7808[g]	0.0010	15.6915	0.0010	39.1425	0.0036
Gal37b												
Tan01	0.705077[c]	0.000014	0.512724[e]	0.000007	0.283119[j]	0.000006	18.8317[g]	0.0010	15.6956	0.0013	39.1665	0.0039
Tan02												
Tan03	0.704924[c]	0.000016	0.512713[e]	0.000007	0.283121[j,m]	0.000006	18.8315[g]	0.0009	15.6963	0.0012	39.1708	0.0044

Superscript letter refers to the respective analytical session. Two letters indicate a rerun sample. m = measured, 2SE = 2 x standard error. All ratios are corrected to an average internal standard.

Table C.2. Sr- Nd- Hf and Pb-isotope data for Sumbing volcano.

Sample	$^{87}Sr/^{86}Sr_m$	2SE	$^{143}Nd/^{144}Nd_m$	2SE	$^{176}Hf/^{177}Hf_m$	2SE	$^{206}Pb/^{204}Pb_m$	2SE	$^{207}Pb/^{206}Pb_m$	2SE	$^{208}Pb/^{204}Pb_m$	2SE
Sumb69	0.705118[d]	0.000011	0.512769[f]	0.000006	0.283139[j]	0.000007	18.7750[h]	0.0012	15.6911	0.0012	39.1336	0.0034
Sumb71												
Sumb72												
Sumb73												
Sumb74	0.704789[d]	0.000012	0.512902[f]	0.000007	0.283143[j]	0.000006	18.6434[h]	0.0012	15.6548	0.0012	38.9148	0.0042
Sumb76	0.704673[d]	0.000010	0.512940[f]	0.000008	0.283124[j]	0.000007	18.6167[h]	0.0013	15.6448	0.0013	38.8656	0.0043
Sumb77												
Sumb78	0.705108[d]	0.000009	0.512814[f]	0.000008	0.283134[j]	0.000004	18.7778[h]	0.0014	15.6915	0.0016	39.1373	0.0052
Sumb80												
Sumb81	0.704636[d]	0.000013	0.512890[f]	0.000008	0.283113[j]	0.000005	18.6784[h]	0.0012	15.6646	0.0012	38.9702	0.0038
Sumb83	0.704674[d]	0.000012	0.512851[f]	0.000008	0.283142[j]	0.000006	18.7104[i]	0.0013	15.6742	0.0014	39.0215	0.0040
Sumb85	0.704720[d]	0.000011	0.512861[f]	0.000005	0.283096[j]	0.000005	18.7045[i]	0.0012	15.6686	0.0012	39.0078	0.0042
Sumb91	0.704458[d]	0.000008	0.513059[f]	0.000009	0.283147[j]	0.000005	18.6852[i]	0.0013	15.6726	0.0012	39.0132	0.0040
Sumb92												
Sumb94												
Sumb95	0.705278[d]	0.000010	0.512825[f]	0.000006	0.283169[j]	0.000011	18.7601[i]	0.0010	15.6934	0.0011	39.1395	0.0040
Sumb96												
Sumb97												
Sumb98	0.705187[d]	0.000012	0.512855[f]	0.000007	0.283135[j]	0.000005	18.7557[i]	0.0013	15.6920	0.0012	39.1333	0.0048
Sumb99	0.705759[d]	0.000008	0.512784[f]	0.000007	0.283131[j]	0.000010	18.7753[i]	0.0011	15.6982	0.0010	39.1649	0.0041

Superscript letter refers to the respective analytical session. m = measured, 2SE = 2 x standard error. All ratios are corrected to an average internal standard.

Table C.3. Sr- Nd- Hf and Pb-isotope data for Kelut volcano.

Sample	$^{87}Sr/^{86}Sr_m$	2SE	$^{143}Nd/^{144}Nd_m$	2SE	$^{176}Hf/^{177}Hf_m$	2SE	$^{206}Pb/^{204}Pb_m$	2SE	$^{207}Pb/^{206}Pb_m$	2SE	$^{208}Pb/^{204}Pb_m$	2SE
Kel12	0.704643[c]	0.000016	0.512914[e,o]	0.000010	0.283140[m]	0.000006	18.5346[g]	0.0013	15.6554	0.0012	38.9144	0.0039
Kel14	0.704306[c]	0.000015	0.513182[e]	0.000018	0.283180[m]	0.000008	18.4971[g]	0.0011	15.6541	0.0012	38.9192	0.0041
Kel22	0.704492[k]	0.000008	0.512930[l]	0.000013	0.283152[n]	0.000011						
Kel23												
Kel25	0.704374[c]	0.000015	0.513106[e]	0.000010	0.283171[m]	0.000007	18.5026[g]	0.0015	15.6548	0.0015	38.8916	0.0057
Kel26	0.704325[k]	0.000010	0.512947[l]	0.000011	0.283163[n]	0.000009						
Kel27												
Kel34	0.704339[d]	0.000012	0.513073[e]	0.000011	0.283190[m]	0.000008	18.4927[h]	0.0015	15.6457	0.0016	38.8718	0.0057
Kel37	0.704369[d]	0.000011	0.512931[e]	0.000005	0.283206[m]	0.000004	18.4824[h]	0.0085	15.6563	0.0077	38.9012	0.0214
Kel38												
Kel40												
Kel43			0.513133[e]	0.000009	0.283188[m]	0.000007	18.4916[h]	0.0011	15.6449	0.0012	38.8563	0.0042
Kel45												
Kel48	0.704265[d]	0.000012	0.513038[e]	0.000011	0.283181[m]	0.000007	18.4801[h]	0.0013	15.6426	0.0014	38.8412	0.0047
Kel50	0.704378[k]	0.000008	0.512973[l]	0.000012	0.283166[n]	0.000009						
Kel51	0.704265[d]	0.000010	0.512988[e]	0.000013	0.283192[m]	0.000007	18.4864[h]	0.0012	15.6457	0.0013	38.8566	0.0047
Kel53	0.704339[d]	0.000011	0.512933[e]	0.000009	0.283158[m]	0.000007	18.4857[h]	0.0030	15.6488	0.0031	38.8611	0.0097
Kel56	0.704261[k]	0.000007	0.513005[l]	0.000012	0.283172[n]	0.000007						
Kel59												
Kel60	0.704325[d]	0.000011	0.513041[e]	0.000008	0.283187[m]	0.000008	18.4959[h]	0.0012	15.6527	0.0014	38.9101	0.0050
Kel61												
Kel64												

Superscript letter refers to the respective analytical session. Two letters indicate a rerun sample. m = measured, 2SE = 2 x standard error. All ratios are corrected to an average internal standard.

Table C.4. Sr- Nd- Hf and Pb-isotope data for Agung volcano.

Sample	$^{87}Sr/^{86}Sr_m$	2SE	$^{143}Nd/^{144}Nd_m$	2SE	$^{176}Hf/^{177}Hf_m$	2SE	$^{206}Pb/^{204}Pb_m$	2SE	$^{207}Pb/^{206}Pb_m$	2SE	$^{208}Pb/^{204}Pb_m$	2SE
Agu03												
Agu06	0.703972[d]	0.000011	0.512929[e]	0.000006	0.283127[m]	0.000006	18.5690[h]	0.0012	15.6004	0.0012	38.6738	0.0044
Agu07	0.703985[d]	0.000013	0.512931[e]	0.000008	0.283124[m]	0.000006	18.5676[h]	0.0012	15.5993	0.0013	38.6658	0.0045
Agu10	0.704028[d]	0.000017	0.512918[e]	0.000007	0.283119[m]	0.000005	18.5711[h]	0.0009	15.6029	0.0010	38.6728	0.0038
Agu12	0.704128[d]	0.000009	0.512903[e]	0.000008	0.283116[m]	0.000007	18.5960[h]	0.0012	15.6034	0.0011	38.6916	0.0041
Agu13												
Agu15												
Agu16												
Agu18	0.704046[d]	0.000010	0.512929[e]	0.000010	0.283127[m]	0.000004	18.5641[h]	0.0014	15.6046	0.0017	38.6740	0.0066
Agu20	0.704000[d]	0.000013	0.512953[e]	0.000009	0.283123[m]	0.000005	18.5590[h]	0.0010	15.5969	0.0013	38.6429	0.0044
Agu21												
Agu22	0.704029[d]	0.000011	0.512912[e]	0.000007	0.283123[m]	0.000005	18.5711[h]	0.0008	15.6002	0.0008	38.6732	0.0032
Agu23												
Agu24												
Agu25	0.704018[d]	0.000011	0.512929[e]	0.000010	0.283116[m]	0.000006	18.5578[h]	0.0012	15.5962	0.0012	38.6360	0.0048
Agu30	0.703979[d]	0.000012	0.512913[e]	0.000006	0.283127[m]	0.000006	18.5339[h]	0.0013	15.6547	0.0012	38.9118	0.0039
Agu31												
Agu33	0.703957[d]	0.000011	0.512939[e]	0.000010	0.283132[m]	0.000006	18.5707[h]	0.0014	15.6012	0.0015	38.6809	0.0048

Superscript letter refers to the respective analytical session. m = measured, 2SE = 2 x standard error. All ratios are corrected to an average internal standard.

Appendix D

Mineral data

Sumbing mineral data

Table D.1. Plagioclase mineral data for Sumbing volcano

Sample	Grain	Position	SiO₂	TiO₂	Al₂O₃	FeO	MgO	CaO	Na₂O	K₂O	Total	Si	Ti	Al	Fe2	Mg	Ca	Na	K	Total	An	Ab	Or
Sumb69	G	C	46.00	0.01	33.32	0.56	0.00	17.82	1.52	0.04	99.30	8.56	0.00	7.31	0.09	0.00	3.55	0.55	0.01	20.07	86.44	13.35	0.22
	P	C	46.89	0.00	32.85	0.64	0.03	16.78	1.92	0.08	99.26	8.70	0.00	7.19	0.10	0.01	3.34	0.69	0.02	20.06	82.47	17.05	0.48
	P	R	52.07	0.00	28.62	0.56	0.00	12.72	4.24	0.23	98.45	9.63	0.00	6.24	0.09	0.00	2.52	1.52	0.06	20.04	61.51	37.14	1.34
	P	C	51.60	0.05	29.61	0.70	0.01	13.15	3.89	0.21	99.22	9.48	0.01	6.41	0.11	0.00	2.59	1.38	0.05	20.03	64.37	34.42	1.21
	P	C	50.84	0.02	29.93	0.63	0.07	13.59	3.52	0.19	98.79	9.38	0.00	6.51	0.10	0.02	2.69	1.26	0.04	20.01	67.35	31.53	1.12
	P	C	52.63	0.05	28.91	0.55	0.00	12.23	4.20	0.26	98.83	9.66	0.01	6.26	0.08	0.00	2.41	1.50	0.06	19.98	60.72	37.75	1.53
	CC	C	49.78	0.00	31.03	0.66	0.05	14.94	2.78	0.15	99.41	9.16	0.00	6.73	0.10	0.01	2.95	0.99	0.04	19.99	74.14	24.96	0.90
	CC	C	50.56	0.00	30.33	0.73	0.08	13.93	3.37	0.19	99.21	9.31	0.00	6.58	0.11	0.02	2.75	1.20	0.04	20.02	68.76	30.10	1.14
	P	C	45.60	0.00	33.88	0.57	0.03	17.97	1.03	0.05	99.17	8.49	0.00	7.43	0.09	0.01	3.58	0.37	0.01	19.99	90.37	9.34	0.29
	P	C	51.24	0.09	29.83	0.58	0.04	13.34	3.59	0.24	99.00	9.43	0.01	6.47	0.09	0.01	2.63	1.28	0.06	19.99	66.32	32.28	1.40
	P	C	45.37	0.00	34.08	0.51	0.00	18.02	1.12	0.04	99.14	8.45	0.00	7.48	0.08	0.00	3.60	0.40	0.01	20.02	89.69	10.06	0.25
	P	R	52.96	0.00	28.43	0.49	0.05	12.15	4.15	0.25	98.54	9.74	0.00	6.17	0.08	0.01	2.39	1.48	0.06	19.94	60.85	37.64	1.51
	CC	C	53.38	0.06	28.74	0.60	0.00	12.00	4.04	0.31	99.14	9.75	0.01	6.19	0.09	0.00	2.35	1.43	0.07	19.89	61.02	37.14	1.84
Sumb74	G	C	53.68	0.00	28.19	0.29	0.00	11.15	4.58	0.24	98.13	9.87	0.00	6.11	0.04	0.00	2.20	1.63	0.06	19.92	56.55	42.01	1.44
	G	C	53.18	0.00	28.31	0.40	0.01	11.37	4.72	0.23	98.25	9.80	0.00	6.15	0.06	0.00	2.24	1.69	0.05	20.00	56.32	42.34	1.34
	G	C	58.61	0.01	24.97	0.39	0.00	7.48	6.57	0.47	98.55	10.63	0.00	5.34	0.06	0.00	1.45	2.31	0.11	19.91	37.53	59.66	2.81
	G	C	52.38	0.02	28.88	0.36	0.00	12.01	4.41	0.19	98.28	9.66	0.00	6.28	0.06	0.00	2.38	1.58	0.06	20.00	59.42	39.43	1.14
	G	C	54.96	0.00	27.34	0.42	0.03	10.38	5.44	0.31	98.95	10.03	0.00	5.88	0.06	0.01	2.03	1.92	0.07	20.02	50.41	47.80	1.80
	G	C	55.69	0.00	26.84	0.36	0.03	9.74	5.49	0.33	98.49	10.17	0.00	5.78	0.05	0.01	1.91	1.94	0.08	19.95	48.53	49.51	1.96
	G	C	56.02	0.01	26.51	0.34	0.02	9.39	5.55	0.42	98.33	10.24	0.00	5.71	0.05	0.01	1.84	1.97	0.10	19.95	47.12	50.40	2.48
Sumb94	P	C	53.23	0.06	28.55	0.59	0.07	11.92	4.15	0.30	98.93	9.75	0.01	6.16	0.09	0.02	2.34	1.48	0.07	19.93	60.22	37.98	1.80
	P	R	51.69	0.04	29.09	0.52	0.04	12.58	3.84	0.32	98.19	9.57	0.01	6.35	0.08	0.01	2.50	1.38	0.08	19.97	63.20	34.89	1.90
	CC	C	50.79	0.00	29.70	0.57	0.05	13.57	3.52	0.28	98.48	9.41	0.00	6.48	0.09	0.01	2.69	1.26	0.06	20.02	66.95	31.44	1.62
	P	C	52.85	0.00	28.46	0.60	0.02	12.19	4.00	0.32	98.46	9.74	0.00	6.18	0.09	0.01	2.41	1.43	0.08	19.93	61.54	36.53	1.93
	P	C	46.79	0.00	32.36	0.54	0.00	16.44	1.98	0.12	98.28	8.76	0.00	7.14	0.08	0.00	3.30	0.72	0.03	20.04	81.50	17.80	0.70
	P	R	52.34	0.06	28.61	0.54	0.02	12.10	4.02	0.34	98.03	9.69	0.01	6.24	0.08	0.01	2.40	1.44	0.08	19.95	61.17	36.79	2.04
	P	R	52.97	0.00	28.78	0.55	0.02	12.14	4.04	0.33	98.87	9.71	0.00	6.22	0.08	0.01	2.38	1.44	0.08	19.93	61.17	36.85	1.98
	P	C	45.84	0.01	32.98	0.53	0.00	17.20	1.61	0.09	98.28	8.60	0.00	7.29	0.08	0.01	3.46	0.59	0.02	20.05	85.02	14.44	0.54
	P	C	57.66	0.05	24.09	0.59	0.00	7.12	5.69	1.55	96.76	10.69	0.01	5.26	0.09	0.00	1.41	2.05	0.37	19.88	36.98	53.46	9.55
	P	C	52.03	0.09	28.91	0.51	0.01	12.52	3.82	0.34	98.26	9.62	0.01	6.30	0.08	0.00	2.48	1.37	0.08	19.94	63.14	34.83	2.03
	CC	C	55.46	0.06	26.56	0.88	0.01	9.68	5.05	0.55	98.25	10.18	0.01	5.75	0.13	0.00	1.90	1.80	0.13	19.90	49.73	46.93	3.34
	G	C	52.94	0.03	28.28	0.53	0.02	11.66	4.16	0.38	98.05	9.78	0.00	6.16	0.08	0.01	2.31	1.49	0.09	19.93	59.40	38.30	2.31
	P	C	44.36	0.00	34.08	0.53	0.00	18.45	0.82	0.05	98.36	8.35	0.00	7.56	0.08	0.00	3.72	0.30	0.01	20.03	92.35	7.38	0.27
	P	R	52.85	0.02	28.25	0.46	0.02	12.04	4.07	0.38	98.11	9.77	0.00	6.15	0.07	0.01	2.38	1.46	0.09	19.93	60.64	37.10	2.26

D.1.1 Clinopyroxene mineral data for Sumbing volcano

Sample	Grain	Position	SiO₂	TiO₂	Al₂O₃	Fe₂O₃	FeO	MgO	CaO	Na₂O	K₂O	Total	Si	Ti	Al	Fe2	Fe3	Mg	Ca	Na	K	Total	En	Fs	Wo
Sumb69	P	C	52.30	0.39	2.40	1.47	8.08	15.67	19.69	0.26	0.00	100.70	1.93	0.01	0.10	0.25	0.04	0.86	0.78	0.02	0.00	4.00	44.34	15.63	40.04
	CC	C	50.97	0.55	2.65	3.49	7.95	13.83	20.27	0.46	0.04	100.84	1.90	0.02	0.12	0.25	0.10	0.77	0.81	0.03	0.00	4.00	39.55	18.79	41.66
	CC	C	52.10	0.32	1.87	2.20	6.91	16.13	19.82	0.21	0.00	100.17	1.93	0.01	0.08	0.21	0.06	0.89	0.79	0.01	0.00	4.00	45.22	14.85	39.93
	G	C	49.56	0.60	4.40	3.02	7.08	14.24	19.89	0.26	0.07	99.60	1.85	0.02	0.19	0.22	0.08	0.79	0.80	0.02	0.00	4.00	41.53	16.76	41.71
	P	C	51.62	0.30	2.18	2.42	7.18	15.76	19.60	0.22	0.07	99.86	1.92	0.01	0.10	0.22	0.07	0.87	0.78	0.02	0.00	4.00	44.51	15.70	39.79
	P	C	51.25	0.42	2.47	2.89	7.44	15.24	19.56	0.31	0.00	100.13	1.90	0.01	0.11	0.23	0.08	0.84	0.78	0.02	0.00	4.00	43.24	16.87	39.88
	CC	C	51.38	0.27	1.73	3.27	7.69	14.51	20.17	0.34	0.01	100.03	1.92	0.01	0.08	0.24	0.09	0.81	0.81	0.02	0.00	4.00	41.07	17.92	41.01
	CC	C	51.56	0.34	1.43	3.14	7.43	14.33	20.52	0.41	0.00	99.92	1.93	0.01	0.06	0.23	0.09	0.80	0.82	0.03	0.00	4.00	40.64	17.52	41.84
	CC	R	52.25	0.28	1.53	1.35	9.25	14.10	20.26	0.37	0.00	100.06	1.95	0.01	0.07	0.29	0.04	0.79	0.81	0.03	0.00	4.00	40.40	17.88	41.72
Sumb74	P	C	51.05	0.18	1.04	3.42	6.44	14.20	21.56	0.25	0.00	98.80	1.93	0.01	0.05	0.20	0.10	0.80	0.87	0.02	0.00	4.00	40.09	16.13	43.78
	P	C	51.42	0.34	1.32	2.59	7.08	14.46	21.04	0.27	0.00	99.28	1.93	0.01	0.06	0.22	0.07	0.81	0.85	0.02	0.00	4.00	40.99	16.11	42.90
Sumb94	P	C	51.04	0.44	2.21	3.03	5.39	15.15	20.98	0.35	0.00	99.10	1.91	0.01	0.10	0.17	0.09	0.84	0.84	0.03	0.00	4.00	43.19	13.83	42.98
	P	C	51.07	0.50	2.60	2.88	5.76	14.88	21.44	0.29	0.00	99.84	1.90	0.01	0.11	0.18	0.08	0.82	0.85	0.02	0.00	4.00	42.26	13.97	43.77
	P	C	50.68	0.47	2.71	3.85	5.44	14.90	21.06	0.33	0.00	99.99	1.88	0.01	0.12	0.17	0.11	0.83	0.84	0.02	0.00	4.00	42.18	14.97	42.85
	CC	C	51.55	0.49	2.51	2.50	6.34	15.11	20.60	0.30	0.01	100.34	1.91	0.01	0.11	0.20	0.07	0.83	0.83	0.02	0.00	4.00	42.80	14.47	42.73
	P	C	51.12	0.40	2.28	3.11	5.56	15.20	21.07	0.27	0.00	99.59	1.90	0.01	0.10	0.17	0.09	0.84	0.84	0.02	0.00	4.00	43.00	14.14	42.86
	P	C	50.91	0.42	2.01	3.39	5.47	15.12	20.88	0.31	0.01	99.13	1.91	0.01	0.09	0.17	0.10	0.84	0.84	0.02	0.00	4.00	42.91	14.49	42.60
	P	C	51.56	0.35	2.03	2.33	6.31	15.21	20.81	0.28	0.01	99.43	1.92	0.01	0.09	0.20	0.07	0.85	0.83	0.02	0.00	4.00	43.20	14.29	42.50
	P	C	50.59	0.58	2.65	3.17	5.96	14.83	20.88	0.30	0.00	99.45	1.89	0.02	0.12	0.19	0.09	0.83	0.84	0.02	0.00	4.00	42.30	14.89	42.81
	P	C	51.33	0.35	1.96	2.89	6.20	15.21	20.64	0.29	0.00	99.45	1.92	0.01	0.09	0.19	0.08	0.85	0.83	0.02	0.00	4.00	43.08	14.91	42.01
	P	C	51.49	0.37	1.88	2.45	6.05	15.20	21.02	0.26	0.00	99.32	1.92	0.01	0.08	0.19	0.07	0.85	0.85	0.02	0.00	4.00	43.08	13.89	43.03
	P	C	50.94	0.39	2.58	2.83	6.37	15.21	20.25	0.27	0.00	99.41	1.90	0.01	0.11	0.20	0.08	0.85	0.81	0.02	0.00	4.00	43.33	15.19	41.48
	P	C	51.09	0.49	2.48	3.65	5.40	15.27	20.93	0.33	0.01	100.20	1.89	0.01	0.11	0.17	0.10	0.84	0.83	0.02	0.00	4.00	43.02	14.59	42.39
	P	C	50.59	0.51	2.81	2.70	6.76	14.79	19.81	0.37	0.02	99.00	1.90	0.01	0.12	0.21	0.08	0.83	0.80	0.03	0.00	4.00	42.80	15.81	41.39
	P	C	51.41	0.45	2.03	2.58	6.29	15.27	20.64	0.28	0.00	99.56	1.92	0.01	0.09	0.20	0.07	0.85	0.82	0.02	0.00	4.00	43.29	14.66	42.05
	P	C	51.19	0.35	2.16	3.20	5.79	15.21	20.84	0.29	0.00	99.58	1.91	0.01	0.09	0.18	0.09	0.85	0.83	0.02	0.00	4.00	43.02	14.61	42.36
	P	C	50.48	0.45	2.61	3.93	5.41	14.86	21.02	0.31	0.00	99.59	1.89	0.01	0.11	0.17	0.11	0.83	0.84	0.02	0.00	4.00	42.12	15.06	42.82

D.1.2 Orthopyroxene mineral data for Sumbing volcano

Sample	Grain	Position	SiO₂	TiO₂	Al₂O₃	Fe₂O₃	FeO	MgO	CaO	Na₂O	K₂O	Total	Si	Ti	Al	Fe2	Fe3	Mg	Ca	Na	K	Total	En	Fs	Wo
Sumb69	CC	C	52.35	0.20	1.40	2.87	18.74	22.79	1.85	0.00	0.00	101.23	1.92	0.01	0.06	0.58	0.08	1.25	0.07	0.00	0.00	4.00	62.15	34.23	3.62
	CC	R	52.35	0.14	1.39	2.95	17.65	23.61	1.48	0.03	0.00	100.54	1.93	0.00	0.06	0.54	0.08	1.30	0.06	0.00	0.00	4.00	64.50	32.59	2.91
Sumb74	P	C	53.30	0.08	0.40	0.49	19.86	22.73	1.22	0.05	0.05	99.67	1.98	0.00	0.02	0.62	0.01	1.26	0.05	0.00	0.00	4.00	63.43	34.12	2.45
	P	C	53.25	0.22	0.74	1.62	18.05	24.17	1.31	0.02	0.00	100.33	1.96	0.01	0.03	0.55	0.04	1.32	0.05	0.00	0.00	4.00	66.08	31.34	2.58
	P	C	53.01	0.18	0.58	1.58	19.11	23.35	1.25	0.01	0.01	100.22	1.96	0.00	0.03	0.59	0.04	1.29	0.05	0.00	0.00	4.00	64.10	33.43	2.47
	P	C	52.88	0.11	0.71	1.37	21.37	21.96	1.30	0.00	0.00	100.84	1.96	0.00	0.03	0.66	0.04	1.21	0.05	0.00	0.00	4.00	60.65	36.76	2.59
	P	C	52.06	0.14	1.00	2.08	19.81	21.81	1.58	0.03	0.03	99.98	1.95	0.00	0.04	0.62	0.06	1.22	0.06	0.00	0.00	4.00	60.71	36.13	3.16
	P	C	52.71	0.09	0.44	1.50	19.91	22.39	1.21	0.00	0.04	99.90	1.97	0.00	0.02	0.62	0.04	1.25	0.05	0.00	0.00	4.00	62.06	35.53	2.41
	P	C	52.58	0.12	0.70	1.74	20.00	22.12	1.33	0.04	0.02	100.24	1.96	0.00	0.03	0.62	0.05	1.23	0.05	0.00	0.00	4.00	61.36	35.99	2.65
	CC	C	52.52	0.09	0.76	2.86	16.88	23.82	1.94	0.01	0.00	99.87	1.94	0.00	0.03	0.52	0.08	1.31	0.08	0.00	0.00	4.00	64.91	31.29	3.79
	CC	C	52.51	0.16	0.78	2.53	17.17	23.98	1.61	0.01	0.03	99.57	1.94	0.00	0.03	0.53	0.07	1.32	0.06	0.00	0.00	4.00	65.69	31.13	3.18
	CC	C	52.58	0.19	1.09	2.29	17.76	23.71	1.49	0.00	0.00	100.21	1.94	0.01	0.05	0.55	0.06	1.30	0.06	0.00	0.00	4.00	64.94	32.12	2.94

D.1.3. Fe-Ti oxide mineral data for Sumbing volcano

Sample	Grain	Position	SiO$_2$	TiO$_2$	Al$_2$O$_3$	Fe$_2$O$_3$	FeO	MgO	CaO	Na$_2$O	K$_2$O	Total	Si	Ti	Al	Fe3	Fe2	Mg	Ca	Na	K	Total	Ti	Fe3	Fe2
Sumb69	P	C	0.00	8.92	3.78	47.62	35.27	2.06	0.02	0.10	0.00	98.37	0.00	0.25	0.17	1.34	1.10	0.12	0.00	0.01	0.00	3.00	0.10	0.52	0.38
	CC	C	0.45	8.34	4.50	48.06	35.03	2.90	0.02	0.00	0.02	99.96	0.02	0.23	0.19	1.32	1.07	0.16	0.00	0.00	0.00	3.00	0.09	0.53	0.38
	CC	C	0.00	8.54	4.46	50.24	34.75	2.82	0.00	0.14	0.00	101.52	0.00	0.23	0.19	1.36	1.04	0.15	0.00	0.01	0.00	3.00	0.09	0.54	0.37
	CC	C	0.03	8.49	4.35	47.84	36.70	1.52	0.01	0.00	0.00	99.45	0.00	0.24	0.19	1.33	1.14	0.08	0.00	0.00	0.00	3.00	0.09	0.51	0.39
Sumb74	CC	C	0.04	10.83	2.43	46.25	38.46	1.57	0.07	0.00	0.00	100.38	0.00	0.30	0.11	1.29	1.19	0.09	0.00	0.00	0.00	3.00	0.11	0.48	0.40
	CC	C	0.00	10.76	2.34	45.92	38.85	1.11	0.06	0.00	0.02	99.76	0.00	0.30	0.10	1.29	1.22	0.06	0.00	0.00	0.00	3.00	0.11	0.48	0.41
	CC	C	0.00	10.76	2.36	46.71	38.72	1.49	0.00	0.00	0.00	100.79	0.00	0.30	0.10	1.30	1.20	0.08	0.00	0.00	0.00	3.00	0.11	0.49	0.40
	P	C	0.02	9.75	1.83	48.64	37.86	1.04	0.00	0.05	0.00	99.97	0.00	0.27	0.08	1.37	1.19	0.06	0.00	0.00	0.00	3.00	0.10	0.51	0.39
	P	C	0.11	10.66	1.99	46.64	38.61	1.33	0.04	0.00	0.03	100.12	0.00	0.30	0.09	1.31	1.20	0.07	0.00	0.00	0.00	3.00	0.11	0.49	0.40
	P	C	0.02	9.92	1.90	47.90	38.07	1.11	0.02	0.00	0.00	99.73	0.00	0.28	0.08	1.35	1.19	0.06	0.00	0.00	0.00	3.00	0.10	0.50	0.40
	P	C	0.01	10.45	1.90	47.93	38.32	1.46	0.02	0.00	0.01	100.87	0.00	0.29	0.08	1.33	1.19	0.08	0.00	0.00	0.00	3.00	0.11	0.50	0.40
Sumb94	P	C	0.00	8.98	3.84	49.84	34.14	3.40	0.06	0.05	0.00	101.12	0.00	0.24	0.16	1.35	1.03	0.18	0.00	0.00	0.00	3.00	0.10	0.54	0.37
	P	C	0.00	9.64	4.41	46.80	36.63	2.26	0.00	0.03	0.00	100.47	0.00	0.26	0.19	1.28	1.12	0.12	0.00	0.00	0.00	3.00	0.10	0.50	0.39
	P	C	0.05	10.10	4.15	45.64	37.26	1.97	0.02	0.01	0.00	100.17	0.00	0.28	0.18	1.26	1.14	0.11	0.00	0.00	0.00	3.00	0.11	0.49	0.40
	P	C	0.00	9.68	3.82	47.04	36.98	1.81	0.02	0.04	0.00	100.25	0.00	0.27	0.17	1.30	1.14	0.10	0.00	0.00	0.00	3.00	0.10	0.50	0.39

D.1.4. Amphibole mineral data for Sumbing volcano

Sample	Grain	Position	SiO$_2$	TiO$_2$	Al$_2$O$_3$	FeO	MgO	CaO	Na$_2$O	K$_2$O	Total	Si	Ti	Al	Fe2	Mg	Ca	Na	K	Total	(Na+k)$_A$	classification
Sumb74	P	C	42.40	2.73	11.43	12.28	14.24	11.08	2.38	0.60	97.33	6.28	0.30	1.99	1.52	3.14	1.76	0.68	0.11	15.82	0.80	Pargasite
	P	R	42.59	2.89	11.45	12.21	13.97	10.97	2.21	0.57	97.07	6.31	0.32	2.00	1.51	3.08	1.74	0.64	0.11	15.74	0.74	Pargasite
	P	C	41.35	2.80	12.02	12.41	13.48	11.24	2.25	0.59	96.47	6.19	0.32	2.12	1.55	3.01	1.80	0.65	0.11	15.81	0.77	Pargasite
	P	C	41.22	1.99	12.19	13.93	12.45	11.72	2.30	0.62	96.72	6.21	0.23	2.16	1.75	2.80	1.89	0.67	0.12	15.88	0.79	Pargasite
	P	C	41.15	1.98	12.21	13.86	12.47	11.82	2.32	0.57	96.69	6.20	0.22	2.17	1.75	2.80	1.91	0.68	0.11	15.88	0.79	Pargasite

Grain: P = Phenocryst, G = Groundmass, CC = Cumulophyric clot. Position: C = Core, R = Rim. Mineral end-members: An = Anorthite, Ab = Albite, Or = Orthoclase, En = Enstatite, Fs = Ferrosilite, Wo = Wollastonite.

Kelut mineral data

Table D.2. Plagioclase mineral data for Kelut volcano

Sample	Grain	Position	SiO2	TiO2	Al2O3	FeO	MgO	CaO	Na2O	K2O	Total	Si	Ti	Al	Fe2	Mg	Ca	Na	K	Total	An	Ab	Or
Kel12	CC	C	47.78	0.00	32.91	0.54	0.00	16.68	1.90	0.01	99.81	8.79	0.00	7.14	0.08	0.00	3.29	0.68	0.00	19.98	82.89	17.05	0.06
	CC	C	48.69	0.01	31.50	0.46	0.00	15.21	2.67	0.04	98.61	9.04	0.00	6.89	0.07	0.00	3.02	0.96	0.01	20.00	75.70	24.03	0.26
	CC	C	53.66	0.04	28.37	0.44	0.01	11.49	4.78	0.17	98.97	9.81	0.00	6.12	0.07	0.00	2.25	1.70	0.04	19.99	56.45	42.53	1.01
	P	C	51.99	0.00	29.56	0.41	0.02	13.10	3.94	0.09	99.18	9.53	0.00	6.39	0.06	0.01	2.57	1.40	0.02	19.99	64.42	35.03	0.54
	P	C	52.24	0.00	28.92	0.43	0.04	12.38	3.96	0.12	98.10	9.65	0.00	6.30	0.07	0.01	2.45	1.42	0.03	19.92	62.90	36.40	0.71
	CC	C	50.00	0.04	31.04	0.54	0.00	14.56	3.12	0.06	99.38	9.19	0.01	6.73	0.08	0.00	2.87	1.11	0.01	20.00	71.79	27.85	0.36
	G	C	55.59	0.00	27.16	0.49	0.00	10.09	5.32	0.25	98.94	10.12	0.00	5.83	0.07	0.00	1.97	1.88	0.06	19.93	50.43	48.10	1.47
	P	R	53.38	0.00	28.11	0.47	0.00	11.09	5.11	0.27	98.46	9.82	0.00	6.10	0.07	0.00	2.19	1.82	0.06	20.07	53.69	44.77	1.55
	CC	C	51.06	0.00	29.69	0.60	0.00	13.54	3.59	0.06	98.67	9.43	0.00	6.46	0.09	0.00	2.68	1.28	0.01	19.98	67.34	32.29	0.37
	G	C	51.18	0.00	28.73	1.00	0.27	13.03	3.87	0.10	98.27	9.51	0.00	6.29	0.15	0.08	2.59	1.39	0.02	20.05	64.67	34.74	0.58
Kel51	P	C	47.07	0.03	32.85	0.56	0.02	16.83	1.87	0.06	99.32	8.72	0.00	7.18	0.09	0.01	3.34	0.67	0.01	20.03	82.96	16.71	0.33
	G	C	49.58	0.02	31.11	0.55	0.02	15.14	2.77	0.06	99.31	9.14	0.00	6.76	0.08	0.01	2.99	0.99	0.01	19.99	74.84	24.80	0.35
	G	C	48.06	0.00	31.77	0.62	0.01	15.85	2.48	0.06	98.85	8.93	0.00	6.96	0.10	0.01	3.15	0.89	0.02	20.05	77.63	22.00	0.37
	P	C	49.35	0.00	31.21	0.53	0.02	15.28	2.81	0.05	99.30	9.10	0.00	6.78	0.08	0.01	3.02	1.00	0.01	20.01	74.85	24.86	0.30
	G	C	49.35	0.00	31.06	0.56	0.03	14.87	2.88	0.08	98.86	9.13	0.00	6.77	0.09	0.01	2.95	1.03	0.02	20.01	73.68	25.84	0.48
	G	C	50.41	0.00	30.41	0.57	0.01	14.29	3.21	0.08	98.97	9.30	0.00	6.61	0.09	0.00	2.82	1.15	0.02	19.98	70.80	28.74	0.46
	G	C	50.10	0.02	31.11	0.54	0.00	14.78	2.88	0.03	99.46	9.20	0.00	6.73	0.08	0.00	2.91	1.02	0.01	19.95	73.79	26.01	0.20
	P	C	48.37	0.04	31.52	0.58	0.00	15.44	2.60	0.02	98.62	8.99	0.01	6.91	0.09	0.00	3.07	0.94	0.00	20.02	76.55	23.35	0.10
	P	C	50.06	0.00	30.66	0.88	0.03	14.37	3.22	0.05	99.32	9.22	0.00	6.66	0.14	0.01	2.84	1.15	0.01	20.03	70.95	28.76	0.30
	G	C	45.51	0.00	34.00	0.46	0.00	18.23	1.08	0.03	99.36	8.46	0.00	7.45	0.07	0.00	3.63	0.39	0.01	20.02	90.11	9.70	0.19
Kel60	G	C	50.85	0.01	29.68	0.77	0.00	13.41	3.49	0.21	98.44	9.42	0.00	6.48	0.12	0.00	2.66	1.25	0.05	19.99	67.16	31.62	1.22
	G	C	50.87	0.00	29.41	0.76	0.03	13.22	3.66	0.22	98.20	9.45	0.00	6.44	0.12	0.01	2.63	1.32	0.05	20.02	65.76	32.93	1.30
	P	C	45.14	0.00	33.56	0.53	0.00	17.82	1.27	0.02	98.46	8.47	0.00	7.42	0.08	0.00	3.58	0.46	0.00	20.05	88.52	11.38	0.10
	P	R	49.49	0.00	30.16	0.72	0.02	14.26	3.27	0.15	98.13	9.23	0.00	6.63	0.11	0.00	2.85	1.18	0.04	20.06	70.03	29.10	0.87
	P	C	58.10	0.08	24.29	0.72	0.01	7.39	6.41	0.79	97.83	10.65	0.01	5.25	0.11	0.00	1.45	2.28	0.19	19.95	37.06	58.20	4.73
	P	C	45.64	0.00	33.90	0.53	0.00	17.63	1.13	0.03	98.94	8.50	0.00	7.45	0.08	0.00	3.52	0.41	0.01	19.98	89.41	10.39	0.20
	P	R	50.91	0.00	29.78	0.65	0.04	13.64	3.36	0.15	98.63	9.41	0.00	6.49	0.10	0.01	2.70	1.21	0.04	19.96	68.52	30.58	0.90
	P	C	46.53	0.00	32.20	0.67	0.01	16.53	2.00	0.07	98.02	8.75	0.00	7.13	0.11	0.00	3.33	0.73	0.02	20.06	81.72	17.90	0.38
	P	C	50.61	0.00	29.56	0.77	0.00	13.54	3.49	0.22	98.21	9.41	0.00	6.47	0.12	0.00	2.70	1.26	0.05	20.01	67.34	31.38	1.28
	P	C	47.42	0.00	31.96	0.58	0.01	16.25	2.17	0.08	98.51	8.85	0.00	7.03	0.09	0.00	3.25	0.78	0.02	20.03	80.20	19.35	0.45
	P	C	45.16	0.00	33.43	0.44	0.03	17.90	1.17	0.01	98.18	8.49	0.00	7.41	0.07	0.01	3.61	0.43	0.00	20.02	89.41	10.56	0.03
	P	C	45.66	0.00	33.01	0.60	0.01	17.30	1.54	0.00	98.17	8.58	0.00	7.31	0.09	0.00	3.48	0.56	0.00	20.04	86.11	13.87	0.02
	P	R	50.55	0.00	29.73	0.78	0.00	13.78	3.41	0.20	98.48	9.37	0.00	6.50	0.12	0.00	2.74	1.23	0.05	20.01	68.25	30.55	1.20
	P	C	45.81	0.08	33.01	0.66	0.01	17.20	1.58	0.06	98.43	8.59	0.01	7.29	0.10	0.00	3.46	0.57	0.01	20.05	85.45	14.21	0.34
	P	R	49.25	0.08	30.14	0.77	0.00	14.49	3.02	0.15	97.94	9.21	0.01	6.64	0.12	0.00	2.90	1.10	0.04	20.02	71.97	27.14	0.89

D.2.1 Clinopyroxene mineral data for Kelut volcano

Sample	Grain	Position	SiO2	TiO2	Al2O3	Fe2O3	FeO	MgO	CaO	Na2O	K2O	Total	Si	Ti	Al	Fe2	Fe3	Mg	Ca	Na	K	Total	En	Fs	Wo
Kel12	CC	C	51.68	0.42	2.47	1.72	8.06	14.38	20.97	0.23	0.00	100.47	1.92	0.01	0.11	0.25	0.05	0.80	0.83	0.02	0.00	4.00	40.90	16.21	42.89
	CC	C	51.78	0.37	2.02	2.35	7.31	14.97	20.81	0.21	0.01	100.40	1.92	0.01	0.09	0.23	0.07	0.83	0.83	0.02	0.00	4.00	42.12	15.80	42.09
	CC	C	51.41	0.29	1.84	3.16	6.41	15.03	20.73	0.29	0.00	99.78	1.92	0.01	0.08	0.20	0.09	0.84	0.83	0.02	0.00	4.00	42.41	15.54	42.05
	CC	C	50.82	0.37	2.34	3.08	6.39	14.76	20.85	0.25	0.00	99.35	1.90	0.01	0.10	0.20	0.09	0.82	0.84	0.02	0.00	4.00	41.97	15.41	42.62
	CC	C	49.38	0.73	3.32	3.90	6.48	12.94	22.51	0.19	0.00	99.85	1.86	0.02	0.15	0.20	0.11	0.73	0.91	0.01	0.00	4.00	37.03	16.67	46.30
	P	C	51.87	0.24	1.39	2.45	7.47	14.92	20.93	0.17	0.00	100.01	1.93	0.01	0.06	0.23	0.07	0.83	0.84	0.01	0.00	4.00	41.78	16.10	42.11
	P	C	51.35	0.24	2.55	2.44	6.07	15.05	21.61	0.15	0.00	99.82	1.91	0.01	0.11	0.19	0.07	0.83	0.86	0.01	0.00	4.00	42.50	13.63	43.87
	P	R	51.47	0.23	1.66	3.08	7.41	14.45	20.63	0.32	0.01	99.92	1.93	0.01	0.07	0.23	0.09	0.81	0.83	0.02	0.00	4.00	40.87	17.19	41.93
	P	C	51.80	0.29	1.64	2.51	7.51	14.41	21.13	0.27	0.00	100.27	1.93	0.01	0.07	0.23	0.07	0.80	0.84	0.02	0.00	4.00	40.67	16.45	42.88
	P	C	51.15	0.28	2.06	3.15	6.82	14.35	21.16	0.28	0.01	99.83	1.91	0.01	0.09	0.21	0.09	0.80	0.85	0.02	0.00	4.00	40.65	16.26	43.09
Kel51	P	C	51.56	0.33	1.82	3.40	6.82	15.05	20.71	0.28	0.00	100.45	1.91	0.01	0.08	0.21	0.10	0.83	0.82	0.02	0.00	4.00	42.10	16.26	41.64
	P	C	51.42	0.33	1.90	3.83	6.08	15.12	21.09	0.27	0.00	100.52	1.91	0.01	0.08	0.19	0.11	0.84	0.84	0.02	0.00	4.00	42.13	15.65	42.22
	P	C	51.13	0.32	2.14	3.30	7.35	14.48	20.49	0.34	0.00	100.03	1.91	0.01	0.09	0.23	0.09	0.81	0.82	0.02	0.00	4.00	41.09	17.14	41.77
	P	C	52.14	0.36	1.93	1.88	7.87	15.14	20.38	0.26	0.01	100.44	1.93	0.01	0.08	0.24	0.05	0.84	0.81	0.02	0.00	4.00	42.74	15.91	41.34

D.2.2 Orhopyroxene mineral data for Kelut volcano

Sample	Grain	Position	SiO2	TiO2	Al2O3	Fe2O3	FeO	MgO	CaO	Na2O	K2O	Total	Si	Ti	Al	Fe2	Fe3	Mg	Ca	Na	K	Total	En	Fs	Wo
Kel12	CC	C	53.32	0.13	1.00	1.94	17.47	24.42	1.22	0.03	0.02	100.62	1.95	0.00	0.04	0.53	0.05	1.33	0.05	0.00	0.00	4.00	66.57	31.04	2.39
	CC	R	53.48	0.15	0.77	1.19	19.50	23.25	1.39	0.05	0.02	100.85	1.97	0.00	0.03	0.60	0.03	1.27	0.05	0.00	0.00	4.00	63.92	33.33	2.75
	CC	C	53.15	0.08	0.64	2.21	17.85	23.72	1.66	0.04	0.02	100.46	1.96	0.00	0.03	0.55	0.06	1.30	0.07	0.00	0.00	4.00	64.73	32.01	3.26
	CC	C	52.60	0.15	1.15	1.83	18.76	23.31	1.19	0.00	0.02	100.13	1.95	0.00	0.05	0.58	0.05	1.29	0.05	0.00	0.00	4.00	64.30	33.33	2.37
	P	C	52.93	0.09	0.73	2.12	18.60	23.58	1.16	0.01	0.00	100.44	1.95	0.00	0.03	0.57	0.06	1.30	0.05	0.00	0.00	4.00	64.43	33.29	2.28
	P	C	54.17	0.06	0.47	0.36	20.17	23.40	1.21	0.00	0.02	101.04	1.98	0.00	0.02	0.62	0.01	1.28	0.05	0.00	0.00	4.00	64.07	33.54	2.39
	P	C	52.48	0.16	1.07	1.70	18.93	23.04	1.34	0.01	0.01	99.87	1.95	0.00	0.05	0.59	0.05	1.28	0.05	0.00	0.00	4.00	63.85	33.48	2.67
	P	C	52.93	0.12	0.67	2.69	17.20	24.22	1.35	0.05	0.03	100.24	1.95	0.00	0.03	0.53	0.07	1.33	0.05	0.00	0.00	4.00	65.92	31.44	2.64
	P	C	52.26	0.23	1.05	2.53	18.59	23.01	1.28	0.06	0.00	100.18	1.94	0.01	0.05	0.58	0.07	1.27	0.05	0.00	0.00	4.00	63.38	34.09	2.53
Kel60	P	C	53.35	0.14	0.72	1.47	18.84	23.59	1.41	0.01	0.02	100.68	1.96	0.00	0.03	0.58	0.04	1.29	0.06	0.00	0.00	4.00	64.53	32.70	2.77
	P	C	53.17	0.14	1.11	1.99	18.11	24.00	1.47	0.00	0.02	100.87	1.95	0.00	0.05	0.55	0.05	1.31	0.06	0.00	0.00	4.00	65.38	31.75	2.87
	P	C	52.91	0.21	0.86	2.58	17.66	24.09	1.36	0.04	0.00	100.66	1.94	0.01	0.04	0.54	0.07	1.32	0.05	0.00	0.00	4.00	65.47	31.88	2.65
	P	C	54.12	0.14	0.63	1.08	18.01	24.73	1.42	0.00	0.00	101.06	1.97	0.00	0.03	0.55	0.03	1.34	0.06	0.00	0.00	4.00	67.01	30.22	2.77
	P	C	53.10	0.20	1.20	2.07	17.82	24.23	1.37	0.00	0.00	100.89	1.94	0.01	0.05	0.54	0.06	1.32	0.05	0.00	0.00	4.00	65.90	31.41	2.69
	P	R	53.24	0.14	1.06	1.76	17.73	24.39	1.28	0.00	0.00	100.52	1.95	0.00	0.05	0.54	0.05	1.33	0.05	0.00	0.00	4.00	66.50	30.99	2.51
	P	C	53.76	0.09	0.45	1.65	18.22	24.25	1.40	0.02	0.01	100.83	1.97	0.00	0.02	0.56	0.05	1.32	0.05	0.00	0.00	4.00	65.78	31.50	2.72

D.2.3. Fe-Ti oxide mineral data for Kelut volcano

Sample	Grain	Position	SiO2	TiO2	Al2O3	Fe2O3	FeO	MgO	CaO	Na2O	K2O	Total	Si	Ti	Al	Fe3	Fe2	Mg	Ca	Na	K	Total	Ti	Fe3	Fe2
Kel12	CC	C	0.00	8.04	2.37	50.72	34.84	1.89	0.01	0.00	0.01	98.60	0.00	0.23	0.11	1.44	0.80	0.11	0.00	0.00	0.00	3.00	0.09	0.54	0.37
	CC	C	0.00	1.44	3.79	62.31	25.58	3.43	0.00	0.00	0.01	98.11	0.00	0.04	0.17	1.75	0.80	0.19	0.00	0.00	0.00	3.00	0.02	0.70	0.29
	CC	C	0.00	12.72	2.07	41.35	39.65	1.40	0.04	0.03	0.02	97.87	0.00	0.36	0.09	1.18	1.26	0.08	0.00	0.00	0.00	3.00	0.14	0.44	0.42
	CC	C	0.05	11.94	2.05	42.43	39.58	1.09	0.00	0.00	0.00	97.82	0.00	0.34	0.09	1.22	1.26	0.06	0.00	0.00	0.00	3.00	0.13	0.45	0.42
	CC	C	0.18	3.47	5.78	57.03	29.62	2.73	0.00	0.11	0.00	100.21	0.01	0.09	0.25	1.56	0.90	0.15	0.00	0.01	0.00	3.00	0.04	0.63	0.33
Kel51	P	C	0.00	8.98	2.98	50.08	36.15	2.24	1.00	0.00	0.00	101.16	0.00	0.25	0.13	1.38	1.10	0.12	0.00	0.00	0.00	3.00	0.09	0.53	0.38
	P	C	0.01	9.00	2.94	49.91	36.81	1.75	0.00	0.02	0.00	101.11	0.00	0.25	0.13	1.38	1.10	0.10	0.00	0.00	0.00	3.00	0.09	0.52	0.38
	P	C	0.00	8.47	3.13	50.78	35.51	2.36	0.00	0.00	0.01	101.23	0.00	0.23	0.13	1.39	1.08	0.13	0.00	0.00	0.00	3.00	0.09	0.54	0.37
	P	C	0.00	8.31	3.42	50.91	35.06	2.57	0.00	0.00	0.01	100.90	0.00	0.23	0.15	1.40	1.07	0.14	0.00	0.00	0.00	3.00	0.09	0.54	0.37
	P	C	0.01	8.98	2.92	49.54	36.33	2.44	0.00	0.00	0.00	100.44	0.00	0.25	0.13	1.37	1.12	0.11	0.00	0.00	0.00	3.00	0.09	0.52	0.38
	P	C	0.00	8.99	2.81	50.04	36.27	2.20	0.00	0.00	0.00	100.89	0.00	0.25	0.12	1.38	1.11	0.12	0.00	0.00	0.00	3.00	0.09	0.53	0.38
Kel60	P	C	0.66	11.77	0.72	43.95	39.09	0.84	0.63	0.06	0.05	98.93	0.03	0.34	0.03	1.25	1.24	0.05	0.03	0.00	0.00	3.00	0.12	0.46	0.41
	P	C	0.04	10.57	1.01	47.92	38.29	0.92	0.00	0.00	0.01	99.90	0.00	0.30	0.04	1.36	1.21	0.05	0.00	0.00	0.00	3.00	0.11	0.50	0.40
	P	C	0.00	11.53	0.55	46.16	39.71	0.60	0.00	0.02	0.00	99.58	0.00	0.33	0.02	1.32	1.26	0.03	0.00	0.00	0.00	3.00	0.12	0.47	0.41

Grain: P = Phenocryst, G = Groundmass, CC = Cumulophyric clot. Position: C = Core, R = Rim. Mineral end-members: An = Anorthite, Ab = Albite, Or = Orthoclase, En = Enstatite, Fs = Ferrosilite, Wo = Wollastonite.

Agung mineral data

Table D.3. Plagioclase mineral data for Agung volcano

Sample	Grain	Position	SiO$_2$	TiO$_2$	Al$_2$O$_3$	FeO	MgO	CaO	Na$_2$O	K$_2$O	Total	Si	Ti	Al	Fe2	Mg	Ca	Na	K	Total	An	Ab	Or
Agu07	P	C	52.64	0.03	28.77	0.59	0.02	12.27	4.04	0.29	98.72	9.68	0.00	6.24	0.09	0.01	2.42	1.44	0.07	19.95	61.60	36.68	1.71
	P	C	54.03	0.00	27.51	0.56	0.04	10.93	4.75	0.33	98.20	9.95	0.00	5.97	0.09	0.01	2.16	1.70	0.08	19.95	54.85	43.17	1.98
	P	C	53.72	0.04	28.00	0.54	0.04	11.55	4.50	0.33	98.75	9.85	0.01	6.05	0.08	0.01	2.27	1.60	0.08	19.95	57.52	40.55	1.94
	P	C	52.70	0.05	29.55	0.51	0.01	12.56	3.85	0.23	99.46	9.61	0.01	6.35	0.08	0.00	2.45	1.36	0.05	19.92	63.44	35.15	1.41
	P	R	53.53	0.05	28.02	0.77	0.07	11.76	4.06	0.30	98.53	9.84	0.00	6.07	0.12	0.02	2.32	1.45	0.07	19.88	60.41	37.76	1.83
	CC	C	51.86	0.02	29.14	1.02	0.12	12.72	3.63	0.26	98.77	9.56	0.00	6.33	0.16	0.03	2.51	1.30	0.06	19.95	64.91	33.52	1.57
	P	C	51.97	0.00	29.44	0.53	0.02	12.92	3.81	0.23	98.95	9.55	0.00	6.38	0.08	0.01	2.54	1.36	0.05	19.97	64.28	34.33	1.38
	P	R	54.56	0.04	27.61	0.56	0.00	10.91	4.82	0.34	98.88	9.97	0.01	5.95	0.09	0.00	2.14	1.71	0.08	19.94	54.45	43.50	2.05
	P	C	53.13	0.00	28.55	0.64	0.07	11.89	4.37	0.23	98.93	9.74	0.00	6.17	0.10	0.02	2.34	1.55	0.05	19.98	59.24	39.40	1.36
	P	R	54.17	0.04	28.33	0.63	0.02	11.55	4.44	0.38	99.60	9.85	0.01	6.07	0.10	0.01	2.25	1.57	0.09	19.94	57.62	40.11	2.27
	P	C	54.07	0.00	28.61	0.61	0.03	11.71	4.47	0.32	99.83	9.81	0.00	6.12	0.09	0.01	2.28	1.57	0.07	19.96	58.00	40.09	1.91
	P	R	56.61	0.05	25.78	0.65	0.02	9.38	5.46	0.46	98.42	10.35	0.01	5.55	0.10	0.01	1.84	1.93	0.11	19.89	47.35	49.87	2.78
Agu10	P	C	49.95	0.00	30.52	0.89	0.03	14.16	3.13	0.19	98.94	9.24	0.00	6.65	0.14	0.01	2.81	1.12	0.05	20.02	70.62	28.24	1.14
	G	C	51.68	0.06	28.88	1.05	0.07	12.86	3.80	0.24	98.68	9.55	0.01	6.29	0.16	0.02	2.55	1.36	0.06	20.00	64.22	34.35	1.43
	G	C	62.92	0.17	20.32	1.17	0.15	5.48	4.30	3.79	98.32	11.46	0.02	4.36	0.18	0.04	1.07	1.52	0.88	19.54	30.83	43.77	25.40
	P	C	46.38	0.00	32.91	0.66	0.04	17.26	1.43	0.03	98.75	8.66	0.00	7.24	0.10	0.01	3.45	0.52	0.01	19.99	86.79	13.02	0.19
	P	C	46.96	0.03	32.71	0.69	0.03	16.74	1.83	0.08	99.08	8.73	0.00	7.16	0.11	0.01	3.33	0.66	0.02	20.03	83.10	16.44	0.45
	P	R	49.83	0.00	30.38	0.80	0.06	14.27	3.02	0.18	98.53	9.25	0.00	6.64	0.12	0.02	2.84	1.09	0.04	20.00	71.53	27.38	1.09
	G	C	51.25	0.02	29.46	1.12	0.09	13.23	3.61	0.25	99.08	9.45	0.00	6.40	0.17	0.03	2.61	1.29	0.06	20.02	66.00	32.54	1.45
	G	C	50.44	0.06	29.36	0.92	0.06	13.48	3.42	0.17	97.94	9.40	0.01	6.45	0.14	0.02	2.69	1.24	0.04	20.00	67.82	31.16	1.02
Agu25	P	C	56.36	0.00	26.12	0.44	0.00	9.39	5.37	0.41	98.14	10.32	0.00	5.63	0.07	0.00	1.84	1.91	0.10	19.87	47.91	49.57	2.51
	P	C	56.28	0.00	25.98	0.35	0.00	9.18	5.65	0.39	97.86	10.33	0.00	5.62	0.05	0.00	1.81	2.01	0.09	19.91	46.22	51.47	2.31
	G	C	54.16	0.00	27.18	0.45	0.02	10.68	4.86	0.34	97.71	10.01	0.00	5.92	0.07	0.01	2.11	1.74	0.08	19.94	53.71	44.24	2.05

D.3.1 Clinopyroxene mineral data for Sumbing volcano

Sample	Grain	Position	SiO$_2$	TiO$_2$	Al$_2$O$_3$	Fe$_2$O$_3$	FeO	MgO	CaO	Na$_2$O	K$_2$O	Total	Si	Ti	Al	Fe2	Fe3	Mg	Ca	Na	K	Total	En	Fs	Wo
Agu07	CC	C	50.87	0.36	2.07	3.25	8.66	14.32	19.33	0.32	0.01	99.91	1.91	0.01	0.09	0.27	0.09	0.80	0.78	0.02	0.00	4.00	40.80	19.63	39.58
	CC	R	50.45	0.64	4.28	0.57	9.47	14.68	18.15	0.23	0.16	99.06	1.89	0.02	0.19	0.30	0.02	0.82	0.73	0.02	0.01	4.00	43.73	17.40	38.87
	CC	C	51.62	0.41	2.18	1.83	9.36	14.10	20.07	0.24	0.00	100.57	1.92	0.01	0.10	0.29	0.05	0.78	0.80	0.02	0.00	4.00	40.16	18.76	41.08
	P	C	50.26	0.73	3.70	1.93	9.71	15.59	16.95	0.22	0.02	99.57	1.88	0.02	0.16	0.30	0.05	0.87	0.68	0.02	0.00	4.00	45.25	19.38	35.37
	P	C	50.64	0.51	2.59	3.24	8.21	14.36	19.68	0.32	0.00	100.04	1.89	0.01	0.11	0.26	0.09	0.80	0.79	0.02	0.00	4.00	41.01	18.59	40.40

D.3.2 Orthopyroxene mineral data for Agung volcano

Sample	Grain	Position	SiO$_2$	TiO$_2$	Al$_2$O$_3$	Fe$_2$O$_3$	FeO	MgO	CaO	Na$_2$O	K$_2$O	Total	Si	Ti	Al	Fe2	Fe3	Mg	Ca	Na	K	Total	En	Fs	Wo
Agu07	P	R	52.91	0.08	0.87	2.47	17.48	23.80	1.76	0.04	0.03	100.30	1.95	0.00	0.04	0.54	0.07	1.31	0.07	0.00	0.00	4.00	65.02	31.53	3.45
	P	C	53.38	0.17	0.96	1.39	19.14	23.45	1.63	0.02	0.02	100.98	1.96	0.00	0.04	0.59	0.04	1.28	0.06	0.00	0.00	4.00	64.23	32.57	3.20
	P	R	52.31	0.21	1.86	2.18	17.43	23.65	1.67	0.03	0.06	100.14	1.93	0.01	0.08	0.54	0.06	1.30	0.07	0.00	0.00	4.00	65.46	31.23	3.31
	P	C	50.81	0.43	0.63	3.56	20.80	20.04	2.41	0.05	0.03	99.96	1.93	0.01	0.03	0.66	0.10	1.13	0.10	0.00	0.00	4.00	55.79	39.38	4.83
	P	C	53.17	0.12	0.75	2.10	17.56	24.17	1.77	0.00	0.00	100.39	1.95	0.00	0.03	0.54	0.06	1.32	0.07	0.00	0.00	4.00	65.71	30.83	3.46
	P	C	52.85	0.14	0.88	1.97	18.78	23.23	1.61	0.00	0.00	100.51	1.95	0.00	0.04	0.58	0.05	1.28	0.06	0.00	0.00	4.00	63.68	33.15	3.17
	P	C	52.89	0.13	1.07	1.37	19.71	22.66	1.63	0.07	0.00	100.36	1.96	0.00	0.05	0.61	0.04	1.25	0.06	0.01	0.00	4.00	62.90	33.85	3.25
Agu10	P	R	50.96	0.41	0.72	4.54	17.12	21.57	3.60	0.08	0.02	99.72	1.91	0.01	0.03	0.54	0.13	1.21	0.14	0.01	0.00	4.00	59.18	33.72	7.10
	CC	C	51.92	0.24	2.50	3.41	13.69	25.91	1.49	0.01	0.00	99.67	1.89	0.01	0.11	0.42	0.09	1.41	0.06	0.00	0.00	4.00	70.71	26.37	2.91
	P	R	51.40	0.34	1.76	1.55	18.35	19.18	4.32	0.55	0.11	98.34	1.95	0.01	0.08	0.58	0.04	1.09	0.18	0.04	0.01	4.00	56.76	34.04	9.19
Agu25	P	C	53.68	0.14	1.20	0.00	19.42	20.51	1.38	0.47	0.46	98.57	2.02	0.00	0.05	0.67	0.00	1.15	0.06	0.03	0.02	4.00	61.95	35.07	2.98
	P	C	51.07	0.18	0.74	2.42	20.49	20.37	2.25	0.03	0.01	98.95	1.94	0.01	0.03	0.65	0.07	1.16	0.09	0.00	0.00	4.00	57.45	37.99	4.56
	P	C	51.04	0.12	0.48	3.44	19.27	20.90	2.45	0.02	0.00	99.07	1.94	0.00	0.02	0.61	0.10	1.18	0.10	0.00	0.00	4.00	58.12	36.98	4.90
	P	C	51.74	0.20	0.99	1.70	21.49	20.86	1.47	0.02	0.01	99.87	1.95	0.01	0.04	0.68	0.05	1.17	0.06	0.00	0.00	4.00	58.63	38.41	2.96

D.3.3. Fe-Ti oxide mineral data for Agung volcano

Sample	Grain	Position	SiO$_2$	TiO$_2$	Al$_2$O$_3$	Fe$_2$O$_3$	FeO	MgO	CaO	Na$_2$O	K$_2$O	Total	Si	Ti	Al	Fe3	Fe2	Mg	Ca	Na	K	Total	Ti	Fe3	Fe2
Agu07	P	C	0.06	9.42	3.39	47.22	33.10	2.09	2.53	0.01	0.03	98.36	0.00	0.26	0.15	1.32	1.03	0.12	0.10	0.00	0.00	3.00	0.10	0.53	0.37
	P	C	0.12	10.30	3.11	44.43	37.22	1.55	0.40	0.00	0.00	97.68	0.00	0.29	0.14	1.27	1.18	0.09	0.02	0.00	0.00	3.00	0.11	0.48	0.40
	CC	C	0.00	11.54	2.13	44.06	38.50	1.59	0.00	0.04	0.00	98.46	0.00	0.33	0.09	1.25	1.22	0.09	0.00	0.00	0.00	3.00	0.12	0.47	0.41
	P	C	0.22	11.33	1.59	44.75	34.84	1.17	3.46	0.02	0.02	98.03	0.01	0.32	0.07	1.27	1.10	0.07	0.14	0.00	0.00	3.00	0.12	0.49	0.38
	P	C	0.04	11.60	1.37	45.11	39.33	1.29	0.00	0.00	0.02	99.39	0.00	0.33	0.06	1.28	1.24	0.07	0.00	0.00	0.00	3.00	0.12	0.47	0.41
	P	C	0.00	10.99	2.72	45.27	36.77	2.63	0.02	0.00	0.02	98.88	0.00	0.31	0.12	1.27	1.14	0.15	0.00	0.00	0.00	3.00	0.12	0.49	0.40
Agu10	P	C	0.23	7.84	6.62	45.69	34.06	3.00	0.00	0.00	0.00	98.00	0.01	0.22	0.29	1.26	1.05	0.16	0.00	0.00	0.00	3.00	0.09	0.52	0.39
	CC	C	0.03	9.49	4.84	45.97	35.31	3.07	0.00	0.00	0.01	99.22	0.00	0.26	0.21	1.27	1.08	0.17	0.00	0.00	0.00	3.00	0.10	0.51	0.39
	P	C	0.00	8.29	6.19	47.44	35.24	2.82	0.00	0.00	0.00	100.40	0.00	0.22	0.26	1.29	1.06	0.15	0.00	0.00	0.00	3.00	0.09	0.52	0.39
Agu25	P	C	0.00	9.60	2.05	47.54	33.42	1.18	2.87	0.02	0.00	97.45	0.00	0.27	0.09	1.36	1.06	0.07	0.12	0.00	0.00	3.00	0.11	0.52	0.37

D.3.4. Olivine mineral data for Agung volcano

Sample	Grain	Position	SiO$_2$	TiO$_2$	Al$_2$O$_3$	FeO	MgO	CaO	Na$_2$O	K$_2$O	Total	Si	Ti	Al	Fe2	Mg	Ca	Na	K	Total	Fo	Fa
Kel10	P	C	36.03	0.00	0.02	32.78	30.43	0.21	0.00	0.01	100.27	0.99	0.00	0.00	0.75	1.25	0.01	0.00	0.00	3.01	62.33	37.67
	P	C	36.80	0.00	0.01	32.11	31.38	0.16	0.03	0.00	101.15	0.99	0.00	0.00	0.73	1.26	0.00	0.00	0.00	3.01	63.53	36.47
	P	C	36.09	0.00	0.00	32.91	30.90	0.22	0.08	0.00	100.92	0.98	0.00	0.00	0.75	1.26	0.01	0.00	0.00	3.02	62.59	37.41
	P	C	35.25	0.00	0.08	32.01	29.62	0.25	0.03	0.03	97.96	0.99	0.00	0.00	0.75	1.24	0.01	0.00	0.00	3.01	62.26	37.74
	P	C	36.81	0.00	0.00	29.89	33.20	0.15	0.01	0.00	100.80	0.99	0.00	0.00	0.67	1.33	0.00	0.00	0.00	3.01	66.44	33.56
	P	C	35.95	0.00	0.03	34.02	29.79	0.16	0.00	0.00	100.74	0.99	0.00	0.00	0.78	1.22	0.00	0.00	0.00	3.01	60.95	39.05
	P	C	36.26	0.00	0.00	32.27	31.02	0.19	0.00	0.00	100.53	0.99	0.00	0.00	0.74	1.26	0.01	0.00	0.00	3.01	63.15	36.85
	P	C	37.02	0.00	0.00	32.48	30.60	0.21	0.00	0.00	101.00	1.00	0.00	0.00	0.74	1.24	0.01	0.00	0.00	3.00	62.67	37.33
	P	R	36.17	0.02	0.00	32.72	31.06	0.16	0.00	0.02	100.99	0.98	0.00	0.00	0.74	1.26	0.00	0.00	0.00	3.01	62.85	37.15

Grain: P = Phenocryst, G = Groundmass, CC = Cumulophyric clot. Position: C = Core, R = Rim. Mineral end-members: An = Anorthite, Ab = Albite, Or = Orthoclase, En = Enstatite, Fs = Ferrosilite, Wo = Wollastonite, Fo = Forsterite, Fa = Fayalite.

Appendix E

CIPW normative calculations

Table E. CIPW norm calculations for Sumbing volcano.

Sample	Quartz	Zircon	K_2SiO_3	Anorthite	Na_2SiO_3	Acmite	Diopside	Sphene	Hypersthene	Albite	Orthoclase	Wollastonite	Olivine	Perovskite	Nepheline	Leucite	Larnite
Sumb69	5.97	0.03	0.00	27.39	0.00	0.00	5.79	0.00	12.77	30.63	12.92	0.00	0.00	0.00	0.00	0.00	0.00
Sumb71	5.78	0.03	0.00	27.30	0.00	0.00	5.97	0.00	12.84	30.72	12.80	0.00	0.00	0.00	0.00	0.00	0.00
Sumb72	12.91	0.04	0.00	24.41	0.00	0.00	1.68	0.00	10.56	34.10	13.02	0.00	0.00	0.00	0.00	0.00	0.00
Sumb73	13.13	0.04	0.00	23.97	0.00	0.00	1.85	0.00	10.39	34.19	13.20	0.00	0.00	0.00	0.00	0.00	0.00
Sumb74	11.64	0.04	0.00	26.88	0.00	0.00	0.12	0.00	11.91	33.76	12.25	0.00	0.00	0.00	0.00	0.00	0.00
Sumb76	3.64	0.04	0.00	30.89	0.00	0.00	2.64	0.00	13.97	33.34	10.63	0.00	0.00	0.00	0.00	0.00	0.00
Sumb77	3.69	0.04	0.00	31.21	0.00	0.00	1.93	0.00	14.33	33.25	10.69	0.00	0.00	0.00	0.00	0.00	0.00
Sumb78	6.02	0.04	0.00	27.43	0.00	0.00	5.65	0.00	12.81	30.80	12.77	0.00	0.00	0.00	0.00	0.00	0.00
Sumb80	9.09	0.03	0.00	28.04	0.00	0.00	3.19	0.00	13.49	30.04	12.08	0.00	0.00	0.00	0.00	0.00	0.00
Sumb81	3.11	0.03	0.00	31.68	0.00	0.00	7.19	0.00	15.27	28.35	9.33	0.00	0.00	0.00	0.00	0.00	0.00
Sumb83	14.52	0.04	0.00	23.41	0.00	0.00	2.63	0.00	9.92	31.82	14.32	0.00	0.00	0.00	0.00	0.00	0.00
Sumb85	9.48	0.04	0.00	25.67	0.00	0.00	4.21	0.00	11.33	32.41	12.77	0.00	0.00	0.00	0.00	0.00	0.00
Sumb91	13.01	0.03	0.00	25.35	0.00	0.00	6.85	0.00	9.77	30.12	11.20	0.00	0.00	0.00	0.00	0.00	0.00
Sumb92	13.01	0.03	0.00	25.69	0.00	0.00	6.69	0.00	9.59	30.21	11.20	0.00	0.00	0.00	0.00	0.00	0.00
Sumb94	1.68	0.01	0.00	28.48	0.00	0.00	10.89	0.00	9.97	30.97	13.44	0.00	0.00	0.00	0.00	0.00	0.00
Sumb95	3.36	0.03	0.00	29.51	0.00	0.00	9.01	0.00	12.15	31.22	9.69	0.00	0.00	0.00	0.00	0.00	0.00
Sumb96	0.48	0.01	0.00	31.03	0.00	0.00	10.78	0.00	10.75	29.79	12.37	0.00	0.00	0.00	0.00	0.00	0.00
Sumb97	3.01	0.03	0.00	28.92	0.00	0.00	9.20	0.00	9.56	31.65	13.20	0.00	0.00	0.00	0.00	0.00	0.00
Sumb98	3.76	0.01	0.00	29.97	0.00	0.00	9.40	0.00	10.73	30.89	10.70	0.00	0.00	0.00	0.00	0.00	0.00
Sumb99	0.72	0.01	0.00	30.09	0.00	0.00	11.29	0.00	11.49	29.02	12.55	0.00	0.00	0.00	0.00	0.00	0.00

Sample	Kalsilite	Apatite	Halite	Fluorite	Anhydrite	Thenardi	Pyrite	Magnesi	Chromite	Ilmenite	Calcite	Na_2CO_3	Corundur	Rutile	Magnetite	Hematit	Total
Sumb69	0.00	0.72	0.00	0.00	0.00	0.00	0.00	0.00	0.00	1.37	0.00	0.00	0.00	0.00	2.41	0.00	99.99
Sumb71	0.00	0.74	0.00	0.00	0.00	0.00	0.00	0.00	0.00	1.39	0.00	0.00	0.00	0.00	2.41	0.00	99.98
Sumb72	0.00	0.46	0.00	0.00	0.00	0.00	0.00	0.00	0.00	1.14	0.00	0.00	0.00	0.00	1.65	0.00	99.98
Sumb73	0.00	0.44	0.00	0.00	0.00	0.00	0.00	0.00	0.00	1.12	0.00	0.00	0.00	0.00	1.65	0.00	99.98
Sumb74	0.00	0.46	0.00	0.00	0.00	0.00	0.00	0.00	0.00	1.18	0.00	0.00	0.00	0.00	1.74	0.00	99.99
Sumb76	0.00	0.63	0.00	0.00	0.00	0.00	0.00	0.00	0.00	1.79	0.00	0.00	0.00	0.00	2.41	0.00	99.98
Sumb77	0.00	0.63	0.00	0.00	0.00	0.00	0.00	0.00	0.00	1.79	0.00	0.00	0.00	0.00	2.41	0.00	99.96
Sumb78	0.00	0.72	0.00	0.00	0.00	0.00	0.00	0.00	0.00	1.35	0.00	0.00	0.00	0.00	2.39	0.00	99.98
Sumb80	0.00	0.49	0.00	0.00	0.00	0.00	0.00	0.00	0.00	1.42	0.00	0.00	0.00	0.00	2.09	0.00	99.96
Sumb81	0.00	0.51	0.00	0.00	0.00	0.00	0.00	0.00	0.00	1.94	0.00	0.00	0.00	0.00	2.58	0.00	99.98
Sumb83	0.00	0.51	0.00	0.00	0.00	0.00	0.00	0.00	0.00	1.18	0.00	0.00	0.00	0.00	1.65	0.00	100.00
Sumb85	0.00	0.56	0.00	0.00	0.00	0.00	0.00	0.00	0.00	1.46	0.00	0.00	0.00	0.00	2.04	0.00	99.98
Sumb91	0.00	0.35	0.00	0.00	0.00	0.00	0.00	0.00	0.00	1.41	0.00	0.00	0.00	0.00	1.88	0.00	99.97
Sumb92	0.00	0.35	0.00	0.00	0.00	0.00	0.00	0.00	0.00	1.39	0.00	0.00	0.00	0.00	1.84	0.00	99.99
Sumb94	0.00	0.58	0.00	0.00	0.00	0.00	0.00	0.00	0.00	1.60	0.00	0.00	0.00	0.00	2.36	0.00	99.98
Sumb95	0.00	0.70	0.00	0.00	0.00	0.00	0.00	0.00	0.00	1.77	0.00	0.00	0.00	0.00	2.54	0.00	99.97
Sumb96	0.00	0.70	0.00	0.00	0.00	0.00	0.00	0.00	0.00	1.60	0.00	0.00	0.00	0.00	2.48	0.00	99.98
Sumb97	0.00	0.72	0.00	0.00	0.00	0.00	0.00	0.00	0.00	1.44	0.00	0.00	0.00	0.00	2.25	0.00	99.97
Sumb98	0.00	0.60	0.00	0.00	0.00	0.00	0.00	0.00	0.00	1.52	0.00	0.00	0.00	0.00	2.38	0.00	99.97
Sumb99	0.00	0.70	0.00	0.00	0.00	0.00	0.00	0.00	0.00	1.56	0.00	0.00	0.00	0.00	2.54	0.00	99.97

Calculated assuming $Fe_2O_3/(FeO+Fe_2O_3) = 0.2$.

Appendix F

Analytical techniques

F.1.1. Preparation of whole-rock powders

A total of 103 volcanic rocks were prepared for analysis by crushing into fine powders. Initially, the weathered edges were removed using a Junior Clipper Saw in a rock preparation room and cleaned using de-ionised water. For the second stage of preparation, fresh sample blocks were broken into smaller fragments and crushed into centimetre-sized gravel using the fly-press machine. Before, and between each use, the equipment was thoroughly cleaned using ethanol and any loose fragments swept up to minimise contamination. To ensure that the powders were as homogenous as possible, the 'cone and quartering technique' was applied to every sample and larger volumes of coarser-grained material were crushed, and mixed, prior to milling.

For the final part of rock preparation, the gravel samples were powdered using the agate ball mill. Each gravelled sample was placed in an agate jar, together with four agate balls. One half of a sample was powdered in the mill for approximately 30 minutes, followed by the second half. The total powder volume produced for each sample was approximately 20g. Following each session, the agate jars and balls were cleaned by adding sand and milling for five minutes. The sand was then disposed of and jars and balls cleaned using hot water and fairy liquid. Each jar was blown dry using compressed air and wiped with ethanol.

F.1.2. XRF sample preparation

Major and trace element analysis was conducted at Royal Holloway University of London using the 2010 PANalytical Axios sequential X-ray fluorescence spectrometer.

F.1.2.1 Major Element Preparation

Major element concentrations were determined on fused glass discs and prepared in batches of six. Approximately 5g of sample powder was placed into a pre-cleaned glass vial and left to dry at 110°C overnight. 0.7g of the dried powder was then transferred to a pre-cleaned and accurately weighed platinum crucible. The combined weight of the powder and the crucible was recorded. To calculate the loss on ignition, each sample was covered with a lid and ignited at 1100°C for 20 minutes. After cooling the combined weight of the crucible and

powder was then reweighed and noted. Transferring crucibles to and from the furnace was done using platinum-tipped tongs and a safety glove.

The flux required for each sample was calculated at six times the weight of the ignited sample plus an additional 0.04g to compensate for the loss of volatiles. The flux (Spectroflux 105 lithium tetraborate) is transferred using a clean stainless steel spatula. The samples and flux were then fused in a furnace at 1100°C for 20 minutes and allowed to cool for 10 minutes with the lids on (preventing cross-contamination from hot spitting samples). Prior to casting, an additional flux is added to make up a calculated total of a 6:1 flux to sample ratio.

Casting of the fusion bead was done using a Bunsen burner and hotplate set at 220°C. To ensure that the additional flux had dissolved, it was swirled above a Bunsen burner for ~ 3 minutes. The disc was cast using an Al-Platten and plunger on the hotplate and left to anneal under a glass beaker. Once cool each disc was removed from the hotplate, trimmed with pliers and stored in labelled polythene bags. The discs were stored in a dessicator overnight before analysis.

The crucibles were cleaned between each batch in hot 50% HCL for ~ 60 minutes. They were then transferred into a clean vial of de-ionised water and dried using the Bunsen burner.

F.1.2.2 Trace Element Preparation

Trace element concentrations were determined on pressed powdered pellets, using approximately 7g of sample. 7g (± 0.2%) of sample powder was weighed out onto clean paper and transferred to a clean plastic vial. Between six and eight drops of Mowiol PVA solution was mixed to powder as a binding agent and stirred thoroughly using a clean glass rod. The die apparatus consisted of an external mould cylinder, and a tungsten carbide platten, which was inserted into the mould. These were thoroughly cleaned with acetone prior to use.

The sample-PVA mixture was transferred to an aluminium tube, placed inside the mould and hand-pressed using a Perspex plunger until the die was compressed. The inner tube was then carefully removed, leaving the plunger in place to avoid damaging the pellet. The pellet and the plunger were removed together and one- to- two tablespoons of boric acid placed inside the mould until the sample is well covered. The apparatus was then placed in a hydraulic

press and pressed under10 ton/cm^2 for 1 minute. Once removed, the base of the die assembly was removed, and the pellet extracted pressing down firmly on the cylindrical mould. Each pellet was labelled on the boric acid side and placed in a vacuum dessicator for 30 minutes.

A second session of XRF was conducted using 10g (±0.1) sample, mixed with 1 ml of 20% araldite solution, using the technique outlined above.

F.1.3. ICP-MS sample preparation

Trace element concentrations were also determined on the PerkinElmer ELAN 6000 quadrupole ICP-MS at Durham University. Full details of this technique are explained in Handley (2006) and Ottley et al (2003). A summary of the preparation is given below.

Weighing samples

Samples were processed in batches of 30, including 3 internal standards and 3 blanks. 0.1g (± 0.001) of sample was weighed onto a clean piece of paper and then transferred into a Teflon vial. A record of the sample name, number and weight was recorded.

Acid Digestion

1 ml of Romil-grade HNO_3 and 4 ml of HF were added to each vial and placed on a hotplate at 150°C for a minimum of 24 hours. The acid was then evaporated until a few µl remained and repeated adding 1ml of HNO_3 until all traces of HF was removed. 2.5 ml of Aristar 16N HNO_3 and 10-15 ml of MQ H_2O was added to each vial and left overnight at 100°C. The samples were then spiked with 1 ml of 1 ppm Re- 1ppm Rh solution and transferred to a 50 ml pre-cleaned polypropylene volumetric flask and made up to 50 ml with MQ H_2O.

Cleaning Procedure

Each of the Teflon vials were cleaned by removing marker numbers with ethanol and placing them into the dishwasher for 1½ hours. The vials were rinsed with MQ H_2O and dried, before adding 2 ml of Analar Nitric acid and leaving on a hotplate for 24 hours at 150°C. After cooling the acid was discarded and the vials rinsed with MQ H_2O ready for the next analysis.

F.1.4. MC-ICP-MS sample preparation

Radiogenic isotope analysis of Sr, Nd, Hf and Pb was conducted using the ThermoElectron Neptune Multi-collector Plasma Mass Spectrometer at the Arthur Holmes Isotope Geology Laboratory (AHIGL), University of Durham. The instrument operations for MC-ICP-MS are detailed in Nowell et al (2003) and Dowall et al (2003). The following describes sample dissolution procedures for Sr, Pb, Nd and Hf fractions.

F.1.4.1. Sample dissolution

The dissolution procedure was the same for all analyses. Samples where generally run in batches of 20, which included one standard and one blank. For the first run, a batch of 10 included 5 samples, 2 sandards and 3 blanks. Approximately 0.1g of sample powder was added to a 7 ml teflon beaker. 1 ml of 16N HNO_3 and 3 ml of 29N HF was then added to each beaker and left on the hotplate at 120°C for 24 hours to dissolve. Once dissolved the lids were removed and the solution evaporated under clean air extraction at 120°C, taking care not to bake out the samples. An additional 1 ml of 16N HNO_3 was added to the residues and left on the hotplate at 120°C overnight. The HNO_3 was evaporated , and the process repeated to ensure that any remaining HF was removed. For the final stage, 0.5 ml of 3N HNO_3 was added to each sample and left in sealed beakers on the hotplate at 100°C.

F.1.4.2. Sr and Pb sample dissolution

Before separating the fractions of Sr and Pb, the samples (in 3N HNO_3) were transferred to pre-cleaned, labelled, microcentifuge tubes and centrifuged for 15 minutes. The supernatant acid solution was carefully removed from residue with an automated pipette and loded to a series of cation and anion exchange columns in order to separate the appropriate isotope fractions. Sr-Spec column chemistry for collecting Sr and Pb fractions is tabulated below.

Table F.1(a) Procedure used for cleaning and preconditioning of Sr- Spec. resin.

Column Setup

Step	Reagent	Volume
Cleaning	MQ H_2O	1CV
Cleaning	TD 6N HCl	1CV
Cleaning	MQ H_2O	1CV
Loading resin	Sr-Spec Resin	2 Drops (~60µl)
Resin Cleaning	TD 6N HCl	1 CV
Resin Cleaning	MQ H_2O	2CV
Preconditioning	3N HNO_3	200µl

Table F.1(b) Procedure used for fraction separation and collection of Sr and Pb.

Elution Procedure

Step	Reagent	Volume	Collect
Sample Loading	TD 3N HNO_3	100-500 µl	YES
Waste Elution	TD 3N HNO_3	2 × 250 µl	YES
Sr Collection	MQ H_2O	2 × 200 µl	YES
Waste Elution	TD 2.5N HCl	2 × 100 µl	NO
Pb Collection	TD 8N HCl	2 × 50 µl	YES

Grey bands indicate collected solutions

The columns were prepared using 1 ml pipette tips which were cut at ~ 45° below a filter, which was inserted gently using a T-bar tool. The coulmns were pre-cleaned by sitting in a storage box filled with 6N HCL. Colunm stands and shelves were also pre-cleaned with MQ H_2O and 6N HCL prior to use. The cleaning stage was conducted using the reagents listed above, 1 CV refers to a column volume. The Sr spec. resin was aggitated before adding to the colunms to ensure it was well mixed and loaded onto the columns at approimately the same thickness as the filter and cleaned using the reagents detailed. The Nd-Hf, Sr and Pb fractions were all collected during a series of elution procedures. Details of the fractions collected are shown in table F.1(b). The first two steps are collected back into the 7 ml teflon vials and used for additional colunm chemistry for Nd and Hf. The Sr was collected into a pre-cleaned microcentrifuge tube with 200 µl of MQ H_2O. An additional 20 µl of 16n HNO_3 was added before analysis.

The Pb fractions were seperated and collected into a microcentrifuge tubes using 100 µl of 8N HCL. The solutions were then evaporated on a hotplate at 100°C and 0.5 ml of 3% HNO_3 added to each. The samples were tested for their intensities on the Neptune and all normalised to 10 V and spiked with 3.5 µl of Tl in order to identify isobaric interference. Details of the use of Tl as an internal mass bias monitor is detailed in Baker et al (2004). All samples were then made up to 0.5 ml of solution before analysing.

F.1.4.3. Nd and Hf separation

Before separating the Nd and Hf fractions using column chemistry, the 3N HNO$_3$ solution
was evaporated and 1 ml of 1N HCl added to each vial. Collection of Nd and Hf was
achieved using 10 ml cation resin (AG50 X-8) columns using the procedure tabulated below.

Table F.2 (a) Procedure used for cleaning and preconditioning of the AG50 X-8 cation exchange.

Pre-Procedure Cleaning

Step	Reagent	Volume
Cleaning	TD 29N HF	5 ml
Cleaning	MQ H$_2$O	10 ml
Preconditioning	TD 1N HF – 1N HCl	10 ml

Table F.2 (b) Procedure used for Nd collection and Hf-Ti elution.

Hf and Nd Elution Procedure

Step	Reagent	Volume	Collect
Sample Loading	1N HCl	1 ml	YES
Hf Collection	TD 1N HF - 1N HCl	3 ml	YES
Waste Elution	TD 2.5N HCl	14 ml	NO
Ba Elution	TD 2N HNO3	10 ml	NO
Nd Collection	TD 6N HCl	12 ml	YES

Grey bands indicate collected solutions.

Table F.2 (c) Procedure for post-sample cleaning of the AG50 X-8 cation exchange columns.

Post-Procedure Cleaning

Step	Reagent	Volume
Cleaning	TD 29N HF	5 ml
Cleaning	MQ H$_2$O	10 ml
Cleaning	TD 6N HCl	10 ml

The columns are stored in 6N HCl before and after use, and apparatus thoroughly cleaned
with MQ H2O and 6N HCl. Following the post-procedure cleaning and preconditioning
detailed in F.2 (a); the sample solution of 1N HCL was loaded onto the column and
immediately collected in the same Teflon beaker. An additional 3 ml of 1N HF – 1NHCl is
additionally loaded to the column which acted to elute the Hf fraction. The Teflon beaker was

then transferred to the hotplate and solution evaporated at 100°C. 1 ml of 0.52N H_2SO_4 – 5% H_2O_2 was added to the dried residue and stored, ready for a final Hf elution procedure.

The Nd fraction was collected with 12 ml of 6N HCl into pre-cleaned 15 ml vials and immediately evaporated at 120°C. To get the sample back into solution, 0.5 ml of 3% HNO3 was added to each Teflon beaker and the contents were transferred to pre-cleaned microcentrifuge tubes ready for analysis.

The final stage of column chemistry was to separate the Hf fraction from Ti. This procedure used 10 ml anion-exchange resin columns and is detailed below.

Table F.3 (a) Procedure used for cleaning and preconditioning of the anion exchange.

Cleaning and Preconditioning

Step	Reagent	Volume
Cleaning	TD 29N HF	5 ml
Cleaning	MQ H2O	5 ml
Cleaning	12N H2SO4	4 ml
Cleaning	MQ H2O	5 ml
Preconditioning	0.52N H_2SO_4 – 5% H_2O_2	5 ml

Table F.3 (b) Procedure used for Hf collection.

Hf Elution Procedure

Step	Reagent	Volume	Collect
Sample Loading	0.52N H_2SO_4 – 5% H_2O_2	1 ml	NO
Ti Elution	0.52N H_2SO_4 – 5% H_2O_2	5 ml	NO
Ti Elution	0.52N H_2SO_4 – 5% H_2O_2	5 ml	NO
Hf Collection	TD 1N HF – 2N HCl	4 ml	YES

Grey band indicates collected solution.

Following collection of the Hf fraction, the solution was placed on a hotplate at 200°C to evaporate the concentrated H_2SO_4. A small amount (20 µl) of 30% H_2O_2 was added to samples which became discoloured, as this may have leaked from the anion resin. This process was used to oxidise and remove the organic resin beads. After evaporation, a drop of 29N HF was added to each sample to help it back into solution. Finally, 0.5 ml of 3% HNO3 was added to each sample and the solutions transferred to pre-cleaned microcentrifuge tubes ready for analysis, details of which are provided in Nowell et al (1998), Nowell & Parish (2002) and Nowell et al (2003).

F.1.5. SEM analysis

Three samples from Sumbing, Kelut and Agung were analysed by a Scanning Electron Microprobe at Leicester University to examine the mineral constituents of phenocrysts. The analyses were obtained on 9 polished sections that were carbon coated prior to loading into the machine. The data was generated by VB Plum system Version 1.09 using 15 kV and a 10 μm beam with a current of 33 nA.

F.2. Analysis, accuracy, precision and reproducibility

For each session a series of standard reference materials and blank samples were run to access the quality and reproducibility of the data for all types of analyses. The different methods used for analysing trace element concentrations also provided a means for which the data could be tested.

F.2.1. Major Element analysis

Major elements were analysed by XRF using the preparation techniques described above. The analyses were made using a 2010 PANalytical Axios sequential X-ray fluorescence spectrometer with a 4 Kw Rh-anode X-ray tube at Royal Holloway University of London. The precision of analysis and machine calibration was achieved by running a number of in-house rock standards (I516, I629 and I107). Sample Sumb80 was prepared by the fusion bead technique on six separate occasions to test the precision and reproducibility of both preparation and analysis. The reproducibility of sample Sumb80 produced excellent results for major element and trace element concentration (see table F.4), yielding 2sd values of 0 wt.% and < 3 ppm. Most samples have LOI values < 1 (see appendix B); however, any rocks with LOI > 3 where not discussed during the discussion of chapters.

F.2.2. Trace Element analyses

Trace element analyses were analysed by XRF (using the machine calibration described above) and ICP-MS. The latter was conducted on the PerkinElmer ELAN 6000 quadrupole ICP-MS at the University of Durham, where instrument operating procedures are detailed by Ottley *et al.* (2003). Data quality was controlled by a number of methods used in combination which are listed below.

1) Blank analyses
2) Standard Reference Materials
3) Duplicates and re-analyses
4) Rh/Re concentrations
5) Standard Deviations
6) ICPMS against XRF concentrations

Calibration of the ELAN 6000 was achieved using six in-house standards (BE-N, W2, AGV1, BHVO, BIR1and NBS688) which were run at the beginning and end of each session. A select standard was analysed continuously on four occasions before the samples to the reproducibility. Blanks were also run before, during and after analysis. All of the samples were pre-spiked with 1 ppm of a Re-Rh solution to test for intensity drift. In such circumstances a correction would be applied. This was not necessary during the six batches of samples.

Table F.5 shows that analytical accuracy was excellent for most elements, and in good agreement with those of internal standards. This was also evaluated by calculating the relative standard deviations (RSD%) for each element after the analysis. Samples with an RSD lower than 5% were generally considered to be acceptable. Elements for which errors where generally higher than for XRF (e.g. Cr, Ni and Sr) where not used during the course of this study. Table F.6 highlights the elements which show a good reproducibility during ICP-MS, these include Cs, Th, U, Ta and the REE which were all incorporated from this technique. The remaining trace elements (Ni, Cr, Co, Ga, V, Sc, Rb, Ba, Nb, Sr, Pb, Zr, Nb and Y were used from XRF data.

Table F.4. Reproducibility for XRF analysis of major and trace elements.

(wt.%)	Duplicate major element analyses for Sumb80						2SD
SiO_2	58.13	58.13	58.13	58.13	58.13	58.13	0.00
Al_2O_3	18.21	18.21	18.21	18.21	18.21	18.21	0.00
Fe_2O_3	7.19	7.19	7.19	7.19	7.19	7.19	0.00
MgO	3.07	3.07	3.07	3.07	3.07	3.07	0.00
CaO	6.63	6.63	6.63	6.63	6.63	6.63	0.00
Na_2O	3.53	3.53	3.53	3.53	3.53	3.53	0.00
K_2O	1.96	1.96	1.96	1.96	1.96	1.96	0.00
TiO_2	0.75	0.75	0.75	0.75	0.75	0.75	0.00
MnO	0.15	0.15	0.15	0.15	0.15	0.15	0.00
P_2O_5	0.21	0.21	0.21	0.21	0.21	0.21	0.00
Total	99.85	99.85	99.85	99.85	99.85	99.85	

(ppm)	Duplicate trace element analyses for Sumb80						2SD
Ni	11.12	11.33	11.53	11.83	11.29	10.87	0.61
Co	15.64	14.65	15.32	15.32	15.21	15.18	0.59
Cr	22.87	20.77	21.24	23.77	20.72	20.72	2.40
V	123.44	123.90	124.87	126.06	125.13	123.05	2.08
Sc	14.12	14.86	14.47	14.34	14.50	14.48	0.44
Ga	19.18	19.08	19.24	19.39	19.00	18.83	0.36
Cs	4.64	3.81	4.73	5.25	5.77	3.90	1.38
Rb	58.78	59.02	58.50	58.35	58.21	58.63	0.54
Ba	555.51	554.73	556.50	555.95	552.57	553.73	2.69
Th	8.82	8.86	8.71	8.90	8.75	9.10	0.25
U	2.24	2.07	2.02	2.13	1.98	2.19	0.18
Nb	11.33	11.19	11.21	11.23	11.07	11.22	0.15
Ta	1.57	0.44	0.99	1.02	0.25	0.23	0.97
Pb	16.10	16.20	16.23	16.18	16.15	16.29	0.12
Sr	393.32	393.96	393.59	392.67	391.98	392.32	1.41
La	18.63	18.67	19.10	18.41	17.56	19.68	1.29
Ce	37.92	39.55	39.49	41.05	41.23	37.91	2.64
Sm	6.97	4.66	4.47	6.32	3.48	2.85	2.90
Nd	17.30	17.61	18.10	18.65	16.35	17.33	1.43
Zr	173.55	173.58	173.55	172.40	171.80	172.74	1.36
Hf	4.71	4.50	4.33	3.90	4.45	4.11	0.53
Y	21.84	21.84	21.93	21.99	21.97	21.70	0.20
Yb	2.61	2.39	2.04	3.11	2.66	1.58	0.97

Table F.5. Standard and blank reproducibility during ICP-MS analysis.

Standard or Blank	Standard Deviations	Sc (ppm)	Ti (wt.%)	V (ppm)	Cr (ppm)	Mn (wt.%)	Co (ppm)	Ni (ppm)	Cu (ppm)	Zn (ppm)	Ga (ppm)	Rb (ppm)	Sr (ppm)	Y (ppm)	Zr (ppm)	Nb (ppm)	Cs (ppm)	Ba (ppm)	La (ppm)
BE-N	1SD (n = 25)	1.21	0.08	5.96	7.89	0.01	1.08	4.87	1.15	19.45	0.35	0.68	88.26	0.27	2.23	0.96	0.03	25.44	1.76
	mean (n = 25)	23.77	2.70	240.41	374.47	0.21	65.02	312.43	73.14	130.20	17.83	48.40	1234.94	30.69	274.04	118.27	0.72	1030.77	81.55
	Accepted Value	22.00	2.61	235.00	360.00	0.20	61.00	267.00	72.00	120.00	17.00	47.00	1370.00	30.00	265.00	100.00	0.80	1025.00	82.00
	1SD*	0.88	0.05	2.70	7.23	0.00	2.01	22.71	0.57	5.10	0.42	0.70	67.53	0.34	4.52	9.13	0.04	2.88	0.23
W2	1SD (n = 11)	1.60	0.05	10.44	3.75	0.01	1.14	2.04	1.40	1.73	0.29	0.17	2.03	0.27	0.93	0.08	0.02	3.15	0.15
	mean (n = 11)	36.37	1.06	267.17	92.73	0.17	45.08	80.25	103.45	75.07	17.43	19.84	194.50	22.39	89.87	7.64	0.87	170.14	10.44
	Accepted Value	35.00	1.06	262.00	93.00	0.16	44.00	70.00	103.00	77.00	20.00	20.00	194.00	24.00	94.00	7.90	0.99	182.00	11.40
	1SD*	0.69	0.00	2.58	0.13	0.00	0.54	5.13	0.22	0.96	1.29	0.08	0.25	0.80	2.07	0.13	0.06	5.93	0.48
BHVO-1	1SD (n = 10)	1.00	0.12	10.36	6.77	0.01	1.04	3.45	1.61	2.05	0.33	0.12	3.27	0.18	1.07	0.15	0.01	3.66	0.33
	mean (n = 10)	32.15	2.77	322.27	295.56	0.17	45.67	136.00	139.10	110.24	21.36	9.42	401.74	27.59	173.87	19.34	0.09	133.55	15.39
	Accepted Value	31.80	2.71	317.00	289.00	0.17	45.00	121.00	136.00	105.00	21.00	11.00	403.00	27.60	179.00	19.00	0.13	139.00	15.80
	1SD*	0.18	0.03	2.64	3.28	0.00	0.34	7.50	1.55	2.62	0.18	0.79	0.63	0.00	2.56	0.17	0.02	2.72	0.20
BIR1	1SD (n =14)	2.12	0.05	16.16	12.87	0.01	1.66	4.70	3.06	1.80	0.41	0.02	4.54	0.52	0.54	0.06	0.01	0.37	0.03
	mean (n = 14)	46.14	0.98	336.67	413.43	0.18	54.67	201.12	120.94	72.30	15.43	0.21	109.11	16.50	14.85	0.60	0.01	6.61	0.61
	Accepted Value	44.00	0.96	313.00	382.00	0.17	51.40	166.00	126.00	71.00	16.00	0.27	108.00	16.00	2.00	2.00	0.45	7.70	0.88
	1SD*	1.07	0.01	11.83	15.72	0.00	1.64	17.56	2.53	0.65	0.29	0.03	0.56	0.25	6.43	0.70	0.22	0.54	0.14
NBS688	1SD (n = 11)	1.31	0.04	6.37	5.41	0.00	0.72	2.70	0.52	1.41	0.24	0.05	2.13	0.21	0.63	0.08	0.01	4.81	0.14
	mean (n = 11)	38.79	1.19	258.08	337.35	0.17	49.38	176.56	89.21	74.75	16.30	1.95	170.30	21.37	55.67	4.35	0.03	180.55	5.16
	Accepted Value	38.00	1.17	242.00	332.00	0.17	49.00	158.00	96.00	84.00	17.00	1.91	169.20	17.00	61.00	5.00	0.24	200.00	5.30
	1SD*	0.40	0.01	8.04	2.67	0.00	0.19	9.28	3.39	4.62	0.35	0.02	0.55	2.18	2.67	0.32	0.10	9.72	0.07
Blank	1SD (n = 48)	12.15	0.00	14.99	61.70	0.00	0.70	56.96	3.76	131.24	0.31	0.15	1.43	0.04	0.29	0.12	0.06	1.22	0.09
	mean (n = 48)	1.23	0.00	1.99	14.06	0.00	0.08	32.77	0.42	41.58	0.03	0.04	0.29	0.01	0.04	0.01	0.01	0.25	0.02
	Accepted Value	0.00	0.00	0.00	0.00	0.00	0.00	0.00	0.00	0.00	0.00	0.00	0.00	0.00	0.00	0.00	0.00	0.00	0.00
	1SD*	0.61	0.00	1.00	7.03	0.00	0.04	16.38	0.21	20.79	0.02	0.02	0.15	0.01	0.02	0.01	0.00	0.12	0.01

1SD (n) refers to the standard deviation of a particular element from the standard analysed during six batches of ICP-MS between 12/01/10 and 07/09/10. The mean refers to the mean average concentration of the number of samples *n*. Accepted values for the standards are taken after Potts et al (1992). ISD* shows the standard deviation between the mean concentrations and accepted standard concentrations.

Table F.5 continued.

Standard or Blank	Standard Deviations	Ce (ppm)	Pr (ppm)	Nd (ppm)	Sm (ppm)	Eu (ppm)	Gd (ppm)	Tb (ppm)	Dy (ppm)	Ho (ppm)	Er (ppm)	Tm (ppm)	Yb (ppm)	Lu (ppm)	Hf (ppm)	Ta (ppm)	Pb (ppm)	Th (ppm)	U (ppm)
BE-N	1SD (n = 25)	3.05	0.37	1.40	0.22	0.08	0.19	0.03	0.11	0.02	0.05	0.01	0.03	0.01	0.15	0.06	0.58	0.31	0.08
	mean (n = 25)	147.90	17.89	69.45	12.28	3.70	9.84	1.31	6.31	1.09	2.39	0.33	1.83	0.27	5.77	6.12	4.10	10.57	2.38
	Accepted Value	152.00	16.90	70.00	12.00	3.60	9.00	1.30	6.29	1.03	2.48	0.37	1.80	0.24	5.40	5.50	4.00	11.00	2.40
	1SD*	2.05	0.50	0.28	0.14	0.05	0.42	0.00	0.01	0.03	0.04	0.02	0.01	0.01	0.18	0.31	0.05	0.22	0.01
W2	1SD (n = 11)	0.33	0.05	0.25	0.06	0.02	0.09	0.01	0.09	0.02	0.03	0.00	0.03	0.00	0.07	0.01	0.17	0.05	0.01
	mean (n = 11)	22.39	3.10	13.49	3.31	1.12	3.90	0.65	3.81	0.79	2.12	0.33	2.05	0.33	2.43	0.50	7.65	2.18	0.49
	Accepted Value	24.00	5.90	14.00	3.25	1.10	3.60	0.63	3.80	0.76	2.50	0.38	2.05	0.33	2.56	0.50	9.30	2.20	0.53
	1SD*	0.80	1.40	0.26	0.03	0.01	0.15	0.01	0.00	0.01	0.19	0.03	0.00	0.00	0.07	0.00	0.82	0.01	0.02
BHVO-1	1SD (n = 10)	0.76	0.11	0.57	0.11	0.05	0.10	0.02	0.11	0.02	0.04	0.01	0.04	0.01	0.08	0.01	0.07	0.03	0.01
	mean (n = 10)	37.12	5.62	26.08	6.25	2.14	6.68	0.99	5.35	1.00	2.43	0.34	2.01	0.30	4.44	1.26	2.09	1.24	0.41
	Accepted Value	39.00	5.70	25.20	6.20	2.06	6.40	0.96	5.20	0.99	2.40	0.33	2.02	0.29	4.38	1.23	2.60	1.08	0.42
	1SD*	0.94	0.04	0.44	0.02	0.04	0.14	0.01	0.07	0.00	0.01	0.01	0.00	0.01	0.03	0.01	0.25	0.08	0.00
BIR1	1SD (n =14)	0.08	0.02	0.11	0.04	0.03	0.09	0.02	0.10	0.02	0.07	0.01	0.05	0.01	0.03	0.01	0.09	0.00	0.00
	mean (n = 14)	1.93	0.39	2.48	1.11	0.53	2.05	0.38	2.57	0.58	1.62	0.26	1.66	0.27	0.59	0.05	3.15	0.04	0.01
	Accepted Value	2.50	0.50	2.50	1.08	0.54	1.90	0.41	2.40	0.50	1.80	0.27	1.70	0.26	0.58	0.06	3.20	0.03	0.01
	1SD*	0.28	0.06	0.01	0.02	0.01	0.07	0.01	0.09	0.04	0.09	0.00	0.02	0.01	0.00	0.01	0.03	0.00	0.00
NBS688	1SD (n = 11)	0.32	0.04	0.20	0.06	0.03	0.08	0.01	0.07	0.02	0.05	0.01	0.05	0.01	0.04	0.01	0.07	0.01	0.01
	mean (n = 11)	11.73	1.82	8.89	2.44	1.02	3.25	0.55	3.45	0.75	2.08	0.33	2.13	0.35	1.52	0.29	2.77	0.35	0.30
	Accepted Value	13.00	2.40	9.60	2.50	1.01	3.20	0.52	3.40	0.81	2.10	0.29	2.05	0.35	1.55	0.31	3.30	0.33	0.31
	1SD*	0.64	0.29	0.35	0.03	0.00	0.03	0.02	0.03	0.03	0.01	0.02	0.04	0.00	0.01	0.01	0.26	0.01	0.00
Blank	1SD (n = 48)	0.16	0.02	0.09	0.17	0.01	0.04	0.01	0.04	0.02	0.01	0.01	0.01	0.00	0.04	0.01	9.04	0.02	0.00
	mean (n = 48)	0.04	0.01	0.02	0.01	0.00	0.01	0.00	-0.01	-0.01	0.00	0.00	0.00	0.00	0.00	0.00	2.00	0.01	0.00
	Accepted Value	0.00	0.00	0.00	0.00	0.00	0.00	0.00	0.00	0.00	0.00	0.00	0.00	0.00	0.00	0.00	0.00	0.00	0.00
	1SD*	0.02	0.00	0.01	0.01	0.00	0.00	0.00	0.00	0.00	0.00	0.00	0.00	0.00	0.00	0.00	1.00	0.00	0.00

Table F.6. Sample reproducibility during ICP-MS analysis.

	30/04/2010	13/08/2010	07/09/2010			30/04/2010	13/08/2010	07/09/2010			30/04/2010	13/08/2010	07/09/2010		
	sumb78	sumb78	sumb78	Mean	1SD	kel12	kel12	kel12	Mean	1SD	kel22	kel22	kel22	Mean	1SD
Ni	*-2.41*	*2.39*	*1.18*	*0.39*	*2.04*	*-2.25*	*26.42*	*16.60*	*13.59*	*11.89*	*-1.04*	*70.36*	*407.48*	*158.93*	*178.15*
Cr	*1.27*	*2.26*	*3.74*	*2.42*	*1.02*	*1.26*	*9.35*	*4.31*	*4.97*	*3.34*	*4.81*	*19.02*	*462.20*	*162.01*	*212.35*
V	*145.22*	*159.97*	*114.82*	*140.00*	*18.80*	*107.62*	*125.27*	*90.59*	*107.83*	*14.16*	*153.77*	*168.83*	*140.89*	*154.50*	*11.42*
Sc	*13.30*	*15.82*	*9.98*	*13.03*	*2.39*	*14.41*	*17.08*	*11.32*	*14.27*	*2.35*	*18.58*	*20.50*	*29.31*	*22.80*	*4.67*
Cs	**3.75**	**3.61**	**3.21**	**3.52**	**0.23**	**1.39**	**1.51**	**1.28**	**1.39**	**0.09**	**1.28**	**1.32**	**1.07**	**1.22**	**0.11**
Rb	*52.10*	*53.39*	*45.01*	*50.16*	*3.68*	*21.13*	*21.94*	*18.39*	*20.49*	*1.52*	*19.62*	*19.48*	*16.20*	*18.43*	*1.58*
Ba	*683.09*	*603.50*	*628.62*	*638.40*	*33.22*	*850.10*	*660.68*	*706.05*	*738.95*	*80.75*	*737.40*	*560.26*	*609.63*	*635.76*	*74.64*
Th	**7.43**	**8.35**	**7.91**	**7.90**	**0.37**	**2.51**	**2.69**	**2.60**	**2.60**	**0.07**	**2.00**	**2.05**	**2.05**	**2.03**	**0.02**
U	**1.54**	**1.78**	**1.64**	**1.65**	**0.10**	**0.63**	**0.67**	**0.65**	**0.65**	**0.02**	**0.54**	**0.57**	**0.54**	**0.55**	**0.02**
Nb	*6.34*	*6.49*	*5.18*	*6.00*	*0.58*	*3.23*	*3.25*	*2.62*	*3.03*	*0.29*	*2.86*	*2.87*	*2.35*	*2.69*	*0.24*
Ta	**0.41**	**0.40**	**0.40**	**0.41**	**0.00**	**0.23**	**0.22**	**0.23**	**0.22**	**0.00**	**0.21**	**0.20**	**0.20**	**0.20**	**0.01**
La	**27.20**	**24.74**	**25.34**	**25.76**	**1.05**	**12.84**	**10.27**	**10.85**	**11.32**	**1.10**	**10.69**	**8.31**	**8.84**	**9.28**	**1.02**
Ce	**54.62**	**49.85**	**50.02**	**51.50**	**2.21**	**27.07**	**21.54**	**22.51**	**23.71**	**2.41**	**23.22**	**17.82**	**18.91**	**19.98**	**2.33**
Pb	*14.90*	*16.28*	*16.25*	*15.81*	*0.64*	*10.35*	*10.98*	*11.11*	*10.81*	*0.33*	*8.88*	*9.41*	*21.37*	*13.22*	*5.77*
Sr	*564.34*	*581.16*	*474.10*	*539.87*	*47.01*	*508.21*	*529.34*	*434.74*	*490.77*	*40.55*	*523.02*	*523.75*	*431.73*	*492.83*	*43.21*
Nd	**28.83**	**25.97**	**25.65**	**26.82**	**1.43**	**16.16**	**12.72**	**13.10**	**13.99**	**1.54**	**14.50**	**10.99**	**11.58**	**12.35**	**1.54**
Sm	**5.92**	**5.60**	**5.41**	**5.64**	**0.21**	**3.58**	**2.95**	**2.99**	**3.17**	**0.28**	**3.53**	**2.83**	**2.87**	**3.08**	**0.32**
Zr	*134.74*	*140.20*	*111.80*	*128.91*	*12.30*	*97.35*	*103.20*	*82.92*	*94.49*	*8.52*	*82.94*	*84.05*	*69.06*	*78.68*	*6.82*
Hf	*3.41*	*3.43*	*3.46*	*3.43*	*0.02*	*2.64*	*2.61*	*2.66*	*2.64*	*0.02*	*2.34*	*2.24*	*2.26*	*2.28*	*0.04*
Eu	**1.62**	**1.53**	**1.47**	**1.54**	**0.06**	**1.14**	**0.98**	**0.99**	**1.04**	**0.07**	**1.18**	**0.96**	**0.99**	**1.04**	**0.10**
Gd	**5.48**	**5.24**	**5.10**	**5.27**	**0.16**	**3.49**	**3.30**	**3.24**	**3.34**	**0.11**	**3.65**	**3.27**	**3.32**	**3.42**	**0.17**
Tb	**0.84**	**0.76**	**0.77**	**0.79**	**0.03**	**0.57**	**0.49**	**0.51**	**0.53**	**0.03**	**0.60**	**0.52**	**0.54**	**0.55**	**0.04**
Dy	**4.76**	**4.48**	**4.37**	**4.54**	**0.16**	**3.41**	**2.99**	**3.08**	**3.16**	**0.18**	**3.60**	**3.16**	**3.19**	**3.32**	**0.20**
Y	*27.45*	*28.11*	*21.82*	*25.79*	*2.82*	*19.00*	*19.92*	*15.54*	*18.15*	*1.89*	*20.66*	*20.51*	*16.61*	*19.26*	*1.88*
Yb	**2.77**	**2.71**	**2.66**	**2.71**	**0.04**	**2.11**	**2.03**	**2.01**	**2.05**	**0.04**	**2.25**	**2.05**	**2.07**	**2.12**	**0.09**
Lu	**0.46**	**0.44**	**0.45**	**0.45**	**0.01**	**0.35**	**0.34**	**0.35**	**0.35**	**0.01**	**0.39**	**0.35**	**0.35**	**0.37**	**0.02**

Samples re-analysed on the dates shown above. The bold black fonts highlight which elements were used in the study from ICP-MS analysis.

As a final test of data quality, the ICP-MS trace element concentrations were plotted against XRF trace element concentrations. Figure F.1 shows that even for elements with slightly higher standard deviations, a good solution is produced with most elements showing an r^2 value > 0.9.

Fig. F.1. ICP-MS against XRF element concentrations.
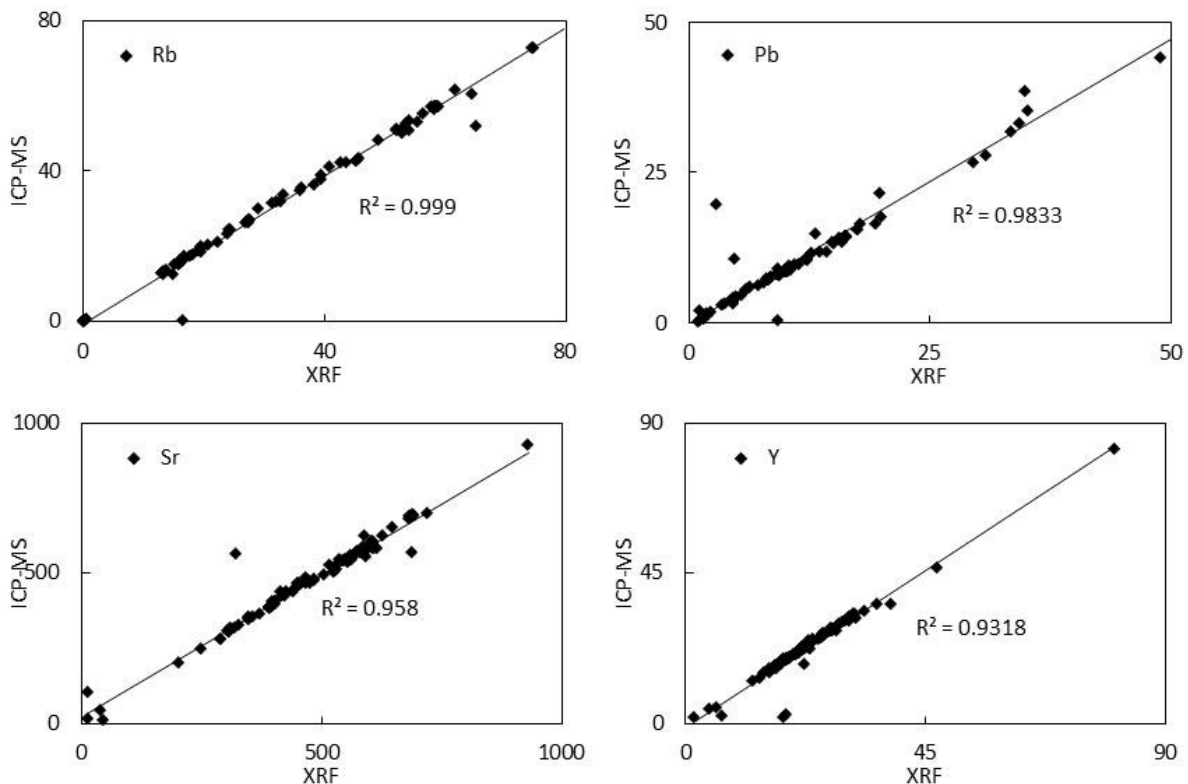
F.2.3. Isotopic analysis

All isotope data was measured using the AHIGL ThermoElectron Neptune Multi-Collector Plasma Mass Spectrometer (MC-ICP-MS) by the operating conditions detailed in Dowall et al (2003) and Nowell et al (2003).

Sr-analysis

Strontium isotope ratios were analysed in ~ 0.5 ml of 3% HNO_3. This solution was introduced into the Neptune through a PFA-50 nebuliser and cinnabar spray chamber. The

Neptune runs one block of 50 cycles per sample which meant that each sample took 3.5 minutes to analyse. This was followed by a wash cycle which resumed until background intensity levels were reached. The sensitivity for Sr varied between 60 and 80 V per ppm and a standard uptake of 90 µl/min^{-1}. Beam intensities for ^{88}Sr were typically ~ 20 volts. Samples with significantly higher intensities were diluted down with 3% HNO$_3$. Instrmental mass bias corrections were applied using a ^{88}Sr/^{86}Sr ratio of 8.375209 (the reciprocal of conventionally used 0.1194) and an exponential law.

Nd-analysis

Neodymium isotope ratios were analysed in a similar approach to strontium. Each sample was introduced in ~ 0.5 ml of 3% HNO$_3$ through a ESI PFA microflow nebuliser and cinnabar spray chamber. The signal size varied between 80 and 160 V per pmm between different batches, all with an uptake of 100 µl/min^{-1}. Beam intensities for ^{146}Nd were ~ 10 V, although some samples contained significantly lower Nd than this. Instrmental mass bias corrections were applied using a ^{146}Nd/^{145}Nd ratio of 2.079143 (the reciprocal of 0.7219) and an exponential law. Isobaric interference on ^{144}Nd, ^{148}Nd and ^{150}Nd by Sm were corrected for using the approach of Nowell & Parish (2002).

Hf-analysis

Samples containing hafnium were introduced into the Neptune vial a 3% HNO$_3$ – 1N HF (0.5 ml) solution. This method used a PFA 50 or TIH nebuliser with Aridus or cinnebar spray chamber and a high sensitivity X skimmer cone. The sensitivity was between 320 and 450 V per Hf ppm^{-1} at an uptake rate of 100 µl/min^{-1}. ^{179}Hf sample intensities were typically lower than 10 V, and in some cases as low as 1 V. Standard intensities for Hf-analysis was ~ 4 V. A mass bias correction was applied using a ^{179}Hf/^{177}Hf ratio of 0.7325 and isobaric corrections from Yb and Lu after Nowell & Parish (2002).

Pb-analysis

Isotopes of lead (^{206}Pb/^{204}Pb, ^{207}Pb/^{204}Pb and ^{208}Pb/^{204}Pb) were run in 0.5 ml of 3% HNO3 using a PFA-50 nebuliser and cinnabar spray chamber. Sensitivity was 100 V per ppm^{-1} with an uptake rate of 90 100 µl/min^{-1}. Beam intensity values for ^{208}Pb were typically ~ 10 V.

Each sample was normalised to a beam intensity for ^{208}Pb of 10 V and spiked with 3.5 µl of a 1ppm Tl solution to mitigate for isobaric interference. A mass bias correction was applied using a ^{205}Tl/^{203}Tl ratio of 2.38846 and an exponential law.

F.2.4.Data quality

Data control was particularly important for the analysis because isotope ratios were obtained throughout a number of different sessions (see appendix C).Internal reference standards were analysed before and after each session. In addition, standards were run after every five samples to test for data quality and reproducibly. Table F.7 shows the number of standards and samples analysed during each session, together with reported values for the former. The reproducibility for all sessions is generally good. ^{87}Sr/^{86}Sr ratio standard solutions are < 34 ppm, ^{143}Nd/^{144}Nd <30 ppm, ^{206}Pb/^{204}Pb < 53 ppm, ^{207}Pb/^{204}Pb < 67 ppm, ^{208}Pb/^{204}Pb < 61 ppm and ^{176}Hf/^{177}Hf < 33 ppm. The average solution for each standard is mostly within error for all sessions. At least one blank sample was prepared during each sample batch to test for traces of contamination during preparation. The blanks were analysed at the beginning of session (b) and (n). Nd blanks (b) range from192 pg to 2 pg, producing a mean concentration of 85 pg and 1SD of 97.The blank Hf samples range from 559 pg to 67 pg, producing a mean of 244 pg and 1SD of 171. These values represent insignificant quantities compared with those values measured for the rock samples, and are within the errors noted in appendix C.

Table F.7 (a). Reproducibility and accuracy for Sr-isotope analyses

$^{87}Sr/^{86}Sr$	15-06-10 (a)	29-03-11 (c)	19-04-11(d)	30-09-11 (k)
Number of samples run	14	19	38	17
Number of standards run	8	9	13	8
Std Average (NBS987)	0.710262	0.710265	0.710265	0.710283
Reported Sr (NBS 987)	0.710240[i]	0.710240[i]	0.710240[i]	0.710240[i]
Measured Av. – Reported Sr	0.000022	0.000025	0.000025	0.000043
2SD abs	0.000011	0.000006	0.000019	0.000024
2SD ppm	15.5	7.8	27.2	33.9

Table F.7 (b). Reproducibility and accuracy for Nd-isotope analyses

$^{143}Nd/^{144}Nd$	01-03-11 (b)	21-04-11 (e)	22-04-11(f)	06-10-11 (l)
Number of samples run	14	40	19	14
Number of standards run	11	21	13	11
Std Average (J&M*)	0.511111	0.511114	0.511115	0.511107
Reported Nd (J&M*)	0.511110[ii]	0.511110[ii]	0.511110[ii]	0.511110[ii]
Measured Av. – Reported Nd	0.000001	0.000004	0.000005	-0.000003
2SD abs	0.000015	0.000014	0.000006	0.000007
2SD ppm	29.8	26.6	11.9	14.0

J&M* refers to J&M – pure and J&M – Sm doped

Table F.7 (c) Reproducibility and accuracy for Pb-isotope analyses

$^{206}Pb/^{204}Pb$	05-05-11 (g)	13-06-11 (h)	14-06-11(i)
Number of samples run	26	24	14
Number of standards run	11	11	9
Std Average $^{206}Pb/^{204}Pb$ (NB 981)	16.94060	16.94056	16.94047
Reported (NBS981)[iii]	16.94050	16.94050	16.94050
Measured Av. – Reported Pb	0.00010	0.00006	-0.00003
2SD abs	0.00088	0.00061	0.00089
2SD ppm	51.78	35.7	52.5
$^{207}Pb/^{204}Pb$			
Std Average (NBS981)	15.49785	15.49766	15.49790
Reported $^{207}Pb/^{204}Pb$ (NBS981)[iii]	15.49630	15.49630	15.49630
Measured Av. – Reported Pb	0.001550	0.00136	0.00160
2SD abs	0.001033	0.00069	0.00054
2SD ppm	66.62	44.7	34.7
$^{208}Pb/^{204}Pb$			
Std Average (NBS981)	36.71261	36.71548	36.71702
Reported $^{208}Pb/^{204}Pb$ (NBS981)[iii]	36.72190	36.72190	36.72190
Measured Av. – Reported Pb	-0.00569	-0.00642	-0.00488
2SD abs	0.002253	0.00141	0.00160
2SD ppm	61.36	38.4	43.7

Table F.7 (d) Reproducibility and accuracy for Hf-isotope analyses

$^{176}Hf/^{177}Hf$	23-06-11 (i)	25-10-11 (m)	26-10-11(n)
Number of samples run	25	34	20
Number of standards run	12	12	8
Std Average (JMC475)	0.282142	0.282150	0.282146
Reported Hf (JMC475)[iv]	0.282160	0.288160	0.282160
Measured Av. – Reported Hf	-0.000018	-0.000010	-0.000015
2SD abs	0.000009	0.000004	0.000009
2SD ppm	30.9	15.3	32.8

References: i = Thirlwall (1991), ii = Royse et al (1998), iii = Nowell et al (1998), iv = Collerson & Palacz (1999).